The University of Liverpool

Proteomic study of the CD40 stimulation-induced pro-survival effect on chronic lymphocytic leukaemia cells

Thesis submitted in accordance with the requirements of the University of Liverpool for the degree of Doctor in Philosophy by Chang Su

Word count: 109,990

(except the words in the bibliography)

March 2021

Contents

Chapter 3 CD40 stimulation protects primary CLL cells from drug-induced cell death

Chapter 5 DDX3X potentially plays a role in the CD40 stimulation-induced pro-survival signals in CLL cells

Chapter 6 General discussion

Appendix

Abstract

The interactions between chronic lymphocytic leukaemia (CLL) cells and the CLL microenvironment play an important role in the disease progression and development of resistance to therapies. CD40 stimulation of CLL cells by T cells represents a major interaction *in vivo*, contributing to the survival and proliferation of CLL cells. However, the molecular mechanisms mediating these effects of CD40 stimulation are not fully understood. Through the proteomics approach, this project aimed to identify molecules/pathways associated with the pro-survival effect of CD40 stimulation by studying the global changes in protein expression in CD40 stimulated CLL cells. Herein, it was independently confirmed that CD40 stimulation protected CLL cells from spontaneous and drug-induced cell death, which are in accordance with the previously published work. Mass spectrometry-based proteomic study identified 552 proteins that were differentially expressed in the CD40 stimulated CLL cells in comparison with their unstimulated counterparts. Bioinformatics analysis showed that these differentially expressed proteins were involved in a variety of biological processes. The functional enrichment analysis of the significantly up-regulated proteins identified the 'cell-cell adhesions' at the top of a list of the most enriched functional clusters. This cluster included 38 differentially expressed proteins, 17 of them with over 2-fold changes in protein expression. Among the proteins with over 2-fold changes in expression was the ATP-dependent RNA helicase DDX3X. The preliminary functional study suggested that DDX3X potentially plays a role in the CD40 stimulation-mediated survival of CLL cells. Taken together, these data indicated that CD40 stimulation produced the pro-survival effect by enhancing the cell adhesion properties of CLL cells. Therefore, the findings from this study have provided a reasonable foundation for future studies to investigate the molecular mechanisms responsible for the CD40 stimulation-mediated survival of CLL cells, which could help identify potential targets for therapeutic intervention to overcome the CD40 stimulation-induced drug resistance in CLL.

Declaration

Unless stated otherwise, all of the work presented in this thesis is my own.

Acknowledgements

I would like to thank all the help and support from my three supervisors, Dr. Jack Zhuang, Dr. Rosalind Jenkins, and Professor Andrew Pettitt, during my four-year PhD study. I would like to thank Dr. Jack Zhuang for introducing me to the new research environment in the lab and for his scrupulous guidance in every aspect of scientific research during my four-year study. His patience helped me to survive several difficult periods during my study. I would like to thank Dr. Rosalind Jenkins for developing my understanding of the principles and techniques of mass spectrometry-based proteomic study and for her generous help in the completion of the entire proteomic study in this project. Her professional manner at work influenced me a lot and her encouragement did help me at times when I felt lost. I would like to thank Professor Andrew Pettitt for gathering and providing such a great research group for us and for all the wise suggestions he gave me during this study. His wisdom in conducting research and in everyday life makes him a role model for me.

I would like to thank the post-doctor researcher Gina Eagle in the research group for her kind help in the proteomic study in this project. I felt grateful for the help from all the members of the research group. The communication and friendship with all of them are so important to me during the four years.

I would like to thank the members of my family. I cannot manage and complete my PhD study without the understanding and support from them.

Last but not least, I would like to thank the China Scholarship Council and the University of Liverpool for giving me the opportunity to study overseas and providing joint funding for this study.

Figures

Tables

Abbreviations

ACN	acetonitrile
ADCC	antibody-dependent cellular cytotoxicity
amu	atomic mass unit
ANOVA	analysis of variance
APCs	antigen-presenting cells
APRIL	a proliferation-inducing ligand
ATM	ataxia telangiectasia mutated
BAFF	B cell activating factor
BAFFR	BAFF receptor
BCL-2	B cell lymphoma 2
BCMA	B cell maturation antigen
BCR	B cell receptor
BIRC3	baculoviral IAP repeat containing 3
BMSCs	bone marrow stromal cells
BSA	bull serum albumin
BTK	Bruton tyrosine kinase
Cas9	CRISPR-associated protein 9
CCD	charged-coupled device
CD40 ligand	CD40L
cDNA	complementary DNA
cIAP	the cellular inhibitor of apoptosis
CID	collision-induced dissociation
CLL	chronic lymphocytic leukaemia
CRISPRs	clustered regularly interspaced short palindromic repeats
DAVID	Database for Annotation, Visualization, and Integrated Discovery
DCs	dendritic cells
DMSO	dimethyl sulfoxide
ELISA	enzyme-linked immunosorbent assay

EASE score	Fisher Exact Statistics in DAVID system, referring to one-tail Fisher Exact Probability Value used for gene-enrichment analysis
FACS	flow cytometry
FADD	Fas-associated death domain
FBS	fetal bovine serum
FDR	false discovery rate
FITC	fluorescein isothiocyanate
FSC	forward-scattered light
GC	germinal centre
HA	hemagglutinin
HGP	Human Genome Project
HPLC	high-performance liquid chromatography
HRP	horseradish peroxidase
HSCs	haematopoietic stem cells
HSP	heat shock protein
HSPCs	haematopoietic stem and progenitor cells
Ig	immunoglobulins
IGHV	immunoglobulin heavy chain variable region
IGHV-M	IGHV-mutated
IGHV-UM	IGHV-unmutated
IgM	immunoglobulin M
IHC	immunohistochemistry
IL	interleukin
iTRAQ	isobaric tags for relative and absolute quantitation
JAK3/STAT5	Janus family kinase 3-phosphorylation of signal transducer and activator of transcription 5
LC-MS	liquid chromatography mass spectrometry
LC_{50}	lethal concentration, the concentration that causes the death of 50% test object
MAPKs	mitogen-activated protein kinases
MBL	monoclonal B cell lymphocytosis

MEFs	mouse embryonic fibroblasts
miR	microRNA
MMP-9	matrix metalloproteinase-9
MMTS	methyl methanethiosulfate
mRNA	messenger RNA
MS	mass spectrometry
MYD88	myeloid differentiation primary response 88
m/z	mass-to-charge
NF-κB	nuclear factor κB
NFKBIE	NFκ light polypeptide gene enhancer in B cells inhibitor-ε
NGS	next-generation sequencing
NIK	NF-κB-inducing kinase
NK cells	natural killer cells
NLCs	nurse-like cells
ODNs	oligodeoxynucleotides
PANTHER	Protein Analysis Through Evolutionary Relationships
PBMCs	peripheral blood mononuclear cells
PCA	Principal Component Analysis
PCR	polymerase chain reaction
PDCD4	programmed cell death factor 4
PE	phycoerythrin
PECAM1	the platelet endothelial cell adhesion molecule-1
PI	propidium iodide
PI3K	phosphoinositide-3-kinase
PKC-β	protein kinase C – β
PLCγ	phospholipase Cγ
PS	phosphatidylserine
PTMs	post-translational modifications
PVDF	polyvinylidene difluoride
rh	recombinant human
RISC	RNA-induced silencing complex

RNA-seq	RNA sequencing
RNAi	RNA interference
ROS	reactive oxygen species
RPS15	ribosomal protein S15
SD	standard deviation
SDS	sodium dodecyl sulphate
SDS-PAGE	sodium dodecyl sulphate polyacrylamide gel electrophoresis
SF3B1	splicing factor 3b subunit 1
shRNAs	short hairpin RNAs
siRNA	small interfering RNA
SLIAC	stable isotope labelling by amino acids in cell culture
SLL	small lymphocytic lymphoma
SSC	side-scattered light
STAT-1	signal transducer and activator of transcription-1
TACI	transmembrane activator and Ca^{2+} modulator and CAML (calcium-modulating cyclophilin ligand) interactor
TBS-T	Tris Buffered Saline plus 0.1% detergent Tween-20
TCEP	tris(2-carboxyethyl)phosphine
TEAB	triethylammonium bicarbonate
TFA	trifluoroacetic acid
TNF	tumour necrosis factor
TNF-R	tumour necrosis factor receptor
TOF	time-of-flight
TRAFs	TNFR-associated factors
VCAM1	vascular cell adhesion protein 1
VLA-4	very late activation antigens-4
WB	Western blotting
WHO	the World Health Organization
WT	wild type
7-AAD	7-aminoactiniomycin

Chapter 1. Introduction

1.1 Chronic lymphocytic leukaemia

1.1.1 Epidemiology

Chronic lymphocytic leukaemia, CLL for short, is the most common leukaemia in adults in the Western world with 4.9/100,000 newly diagnosed cases every year in the United Kingdom (UK) and the United States of America (USA) (von Tresckow et al., 2019, Milne et al., 2020, Bosch and Dalla-Favera, 2019). It tends to affect the older adults with a median age of 74 at diagnosis and a male to female ratio of 1.3:1 (Bosch and Dalla-Favera, 2019). In comparison with Western countries, the incidence of CLL is relatively lower in Asian, African, and Caribbean countries, which indicates a racial disparity of CLL (Wu et al., 2010, Wu et al., 2016). It has been reported that exposure to herbicides and pesticides, reduced recreational sun exposure, medical history of atopic health conditions, exposure to hepatitis C virus, and common infections may increase the risk of CLL (Slager et al., 2014, Landgren et al., 2007). Meanwhile, around 10% of the patients diagnosed with CLL have a family history of the disease, indicating CLL as one of the inherited haematological malignancies (Cerhan and Slager, 2015).

1.1.2 The clinical features

CLL is now defined as a malignancy of clonal expansion of B lymphocytes accumulating in the peripheral blood, bone marrow, lymph nodes, and other lymphoid tissues (Fabbri and Dalla-Favera, 2016). The diagnostic criteria of CLL require the presence of ≥ 5000 clonal B lymphocytes per microlitre in the peripheral blood persisting for more than 3 months (Hallek et al., 2018, Hallek, 2019). Together with small lymphocytic lymphoma (SLL), CLL is classified as the mature B cell neoplasm by the World Health Organization (WHO) and CLL is preceded by monoclonal B cell lymphocytosis (MBL) with a rate of 1-2% every year (Rossi and Gaidano, 2013). Based on the mutation status of the immunoglobulin heavy chain variable region (IGHV) genes, CLL is clinically classified into two subtypes, known as the IGHV-mutated (IGHV-M) and unmutated (IGHV-UM) CLL (Vardi et al., 2014). The clinical outcomes of patients with IGHV-M CLL are usually better than those with IGHV-UM CLL

(Damle et al., 1999, Hamblin et al., 1999). Currently, there are two staging systems, the Rai staging system (Rai et al., 1975) and the Binet staging system (Binet et al., 1981), which are used to clinically stratify CLL patients to direct therapy and predict survival. The Rai staging system (Table 1.1), together with the revised edition (Table 1.2), is commonly used in the USA, whereas the Binet staging system (Table 1.3) is widely applied in Europe (Eichhorst et al., 2015).

Table 1.1 Rai staging system

Stage	Characteristics	Median survival
0	Only lymphocytosis in the peripheral blood and bone marrow infiltration	> 150 months
I	Presence of lymphadenopathies	101 months
II	Presence of hepatosplenomegaly	71 months
III	Presence of anemia (defined as Hb < 11 g/dl)	19 months
IV	Presence of thrombocytopenia (Plt < 100,000/mm^3)	19 months

Table 1.2 Revised Rai staging system

Stage	Characteristics
Low risk	Only lymphocytosis in the peripheral blood and bone marrow infiltration (same as stage 0)
Intermediate risk	Presence of lymphadenopathies (same as stage I) and/or hepatosplenomegaly (same as stage II)
High risk	Presence of anemia (same as stage III) and/or thrombocytopenia (same as stage IV)

Table 1.3 Binet staging system

Stage	Characteristics
A	No anemia (Hb > 10 g/dl) or thrombocytopenia (Plt > 100,000/mm3) and up to 2 lymphoid sites involved
B	No anemia (Hb > 10 g/dl) or thrombocytopenia (Plt > 100,000/mm3) and more than 2 lymphoid sites involved
C	Presence of anemia (Hb < 10 g/dl) or thrombocytopenia (Plt < 100,000/mm3) regardless of the number of lymphoid sites involved

Since the beginning of the 21st century, several genomic aberrations have been used as independent risk factors to direct the choice of therapy and briefly predict survival. The most frequent genetic lesions detected in the patients with CLL include the deletion of the long arm of chromosome 13 (del13q14), trisomy 12 (+12), the deletion of the long arm of

chromosome 11 (del11q22-q23), and the deletion of the short arm of chromosome 17 (del17p13) (Hallek et al., 2018).

Del13q14 has been found in 50-60% of patients with CLL and it is more frequently in patients with IGHV-M CLL (Döhner et al., 2000). Del13q14 is usually associated with a favourable prognosis compared with other genomic aberrations. It has been shown that the acquisition of del13q14 leads to the loss of microRNA (miR) clusters 15 and 16, both of which regulate the expression of the B cell lymphoma 2 (*BCL-2*) gene (Calin et al., 2002). The loss of miR15 and miR16 results in the upregulation of anti-apoptotic BCL-2 protein, which contributes to the proliferation and expansion of CLL B cells and the development of the disease (Calin et al., 2002, Klein et al., 2010).

Trisomy 12 has been found in 10-20% of patients with CLL, which is indiscriminate among patients with IGHV-M CLL or IGHV-UM CLL (Döhner et al., 2000). Patients with trisomy 12 are considered to have an intermediate prognosis but they are more likely to have the Richter transformation (Strati et al., 2015).

Del11q22-23 can be detected in up to 20% of patients with CLL at diagnosis (Stankovic and Skowronska, 2014) and it frequently occurs the IGHV-UM CLL patients with the nodal disease (Döhner et al., 1997). Del11q22-23 disrupts the ataxia-telangiectasia mutated (ATM) gene encoding a kinase involved in DNA damage response (Shiloh and Ziv, 2013) and the disruption of the baculoviral IAP repeat-containing 3 (BIRC3) gene, a negative regulator of the non-canonical NF-κB pathway (Rossi et al., 2012). The prognosis of the patients with del11q22-23 is worse than the patients with del13q14 or trisomy 12 (Stankovic and Skowronska, 2014).

Del17p13 occurs in less than 10% of the patients with CLL at diagnosis and more frequently in patients with IGHV-UM CLL (Döhner et al., 2000). It has reported that Del17p13 may lead to the loss of the *TP53* gene, a tumour suppressor gene associated with the initiation of cell cycle arrest and apoptosis in cells with DNA damages (Chen, 2016). The frequency of Del17p13 increases in chemotherapy-resistant and refractory CLL patients (Gaidano et al., 1991, Landau et al., 2015). The presence of del17p13 represents a poor prognosis and directly impacts the clinical choice of therapy (Zenz et al., 2008). TP53 mutations have been found in most of the CLL patients with Del17p13 and taken as an independent factor for the

poor prognosis resulting from the impaired p53 pathway (Scarfò et al., 2016). TP53 mutations show preference in the IGHV-UM CLL patients (Campo et al., 2018). Studies have demonstrated that TP53 mutations play a role in the pathogenesis and progression of CLL and its incidence is increased with the progression of the disease (Rossi et al., 2014, Scarfò et al., 2016).

Recently, several novel gene mutations have been identified including NOTCH1, Splicing factor 3b subunit 1 (SF3B1), BIRC3, myeloid differentiation primary response 88 (MYD88), and NFκ light polypeptide gene enhancer in B cells inhibitor-ε (NFKBIE).

NOTCH1 mutations have been found in around 10-15% of CLL patients at diagnosis with a higher preference in the patients with IGHV-UM CLL (Fabbri et al., 2011, Landau et al., 2015). It has been reported that one-third of the CLL patients with NOTCH1 mutations also have trisomy 12 and that the presence of those two aberrations leads to poor prognosis (Del Giudice et al., 2012, Riches et al., 2014). The biological significance of NOTCH1 mutations in CLL Cells has not been fully understood but the preliminary investigation demonstrates that it may play a role in regulating the survival, proliferation, and migration of CLL cells (Rosati et al., 2009, López-Guerra et al., 2019). Clinically, it has been reported that CLL patients with NOTCH1 mutations exhibit unsatisfactory responses to the anti-CD20 monoclonal antibody (Stilgenbauer et al., 2014). Later, researchers found that patients with NOTCH1 mutated CLL have low expression levels of CD20 (Pozzo et al., 2016), which may be the reason for the poor response to the therapy with the anti-CD20 antibody.

SF3B1 mutations have been found in 10-15% CLL patients, with a higher incidence in the patients of IGHV-UM CLL (Quesada et al., 2012). *SF3B1* gene encodes an RNA-protein complex, U2 snRNP, and it is involved in the initial stage of RNA splicing (Quesada et al., 2012, Landau et al., 2015, Allen and Parsons, 2015). SF3B1 mutations are associated with Del11q22-23 in CLL patients who have a poor prognosis (Wang et al., 2011a). It has been reported that SF3B1 mutated CLL cells without ATM and TP53 aberrations show impaired ATM/p53 transcriptional responses when they are treated by DNA damaging agents such as fludarabine (Te Raa et al., 2015).

Mutations of the BIRC3 gene have been found in 4% of CLL patients at diagnosis (Rossi et al., 2012). BIRC3 mutations have been more frequently found in patients with fludarabine-

refractory CLL but it seems that BIRC3 mutations are independent of the TP53 aberration (Rossi et al., 2012). It has been shown that BIRC3 mutations result in an elimination of the C-terminal RING domain of the BIRC3 protein, leading to a loss of its function for the degradation of a negative regulator of the non-canonical NF-κB signalling pathway, which causes sustained activation of this pathway (Keats et al., 2007). The age at diagnosis of the patients with BIRC3 mutated CLL is lower than the average age of CLL patients at diagnosis (Puente et al., 2015).

MYD88 mutations have been found in around 5% of CLL patients with a higher prevalence in IGHV mutated CLL (Puente et al., 2011, Puente et al., 2015). MYD88 protein is a cytosolic adaptor protein participating in the Toll-like receptor pathway, which can further activate the NF-κB signalling pathway in normal B cells (Rawlings et al., 2012). Further studies are needed to establish the role of MYD88 mutations in CLL (Maleki et al., 2019).

Besides BIRC3 and MYD88, NFKBIE mutations have been found as one more aberration involved in the aberrant activation of NF-κB signalling in CLL. *NFKBIE* gene encodes IκBε, a negative regulator of the NF-κB signalling pathway, in normal B cells (Mansouri et al., 2015). It has been reported that NFKBIE mutations are accumulated during the pathogenesis and progression of CLL (Damm et al., 2014, Mansouri et al., 2015, Alves et al., 2014). These genetic aberrations related to the NF-κB signalling pathway may explain the constitutive activation of this pathway in CLL but the precise mechanisms and their functions in CLL remain to be fully characterized.

1.1.3 Current treatment

Despite the impressive advances in the understanding of the pathophysiology of the disease and the introduction of novel molecularly-targeted therapeutics in recent years, CLL remains an incurable disease (Bosch and Dalla-Favera, 2019, Milne et al., 2020).

Chlorambucil with or without the steroid was used as the preferred drug for the treatment of patients with CLL in early time (Han et al., 1973, Knospe and Loeb, 1980). At the beginning of the 21st century, the combination of fludarabine (F) and cyclophosphamide (C) plus rituximab (R), an anti-CD20 monoclonal antibody, (the so-called FCR), became the front-line therapy, as it significantly improves the outcome of the patients with CLL

comparing with the previous management (Eichhorst et al., 2006, Catovsky et al., 2007, Hallek et al., 2010). This combination is still a front-line therapy for the untreated, del(17p) negative, TP53 unmutated, IGHV-mutated patients, with age less than 65 years old and without any significant comorbidities, according to the National Comprehensive Cancer Network (NCCN) Guidelines version 2.2021.

A better understanding of the pathogenesis of CLL does lead to a new era and tremendously change the clinical management of this disease. A group of small molecular inhibitors have become the preferred regimens for CLL patients. With the understanding of the signalling induced by the B cell receptor (BCR) in CLL cells, small molecule inhibitors targeting the components of the BCR signalling pathway have been introduced in the clinical management for CLL patients (Burger, 2012b). It has been shown that the inhibitor of Bruton tyrosine kinase (BTK) including ibrutinib and acalabrutinib, and the inhibitor of phosphatidylinositol-3-kinase (PI3K-δ) including idelalisib and duvelisib, display impressive efficacy in the treatment of CLL patients, including those with high-risk CLL such as deletion/mutation in *TP53* (O'Brien et al., 2016, Ghia et al., 2020). As monotherapy (reported by the RESONATE2 study), ibrutinib exhibited a significantly higher overall response rate (ORR) and longer progress-free survival (PFS) rate, compared to that of chlorambucil (Burger et al., 2015; Burger et al., 2020). In the ELEVATE-TN phase III study, acalabrutinib both as monotherapy and a combination with anti-CD20 antibody resulted in better ORR compared with the combination of chlorambucil and anti-CD20 antibody (Sharman et al., 2019). Those two types of inhibitors have been used as the first-line therapies for previously untreated patients with/without del(17p)/TP53 mutation, according to the latest version of NCCN Guidelines. The discovery of the abnormal expression status of the proteins belonging to the BCL-2 family in CLL cells contributed to creation of the inhibitors targeting these proteins (Kang and Reynolds, 2009, Balakrishnan and Gandhi, 2013). Venetoclax, known as ABT-199, is a highly selective BCL-2 inhibitor and it has been approved to be used for the treatment of CLL patients with 17p deletion since 2016 (Lampson and Davids, 2017). These inhibitors become the main treatment options for patients with CLL according to the NCCN Guidelines version 2.2021.

Figure 1.1 is a flow chart providing general guidelines on the preferred choice of therapies for medical professionals treating patients with CLL.

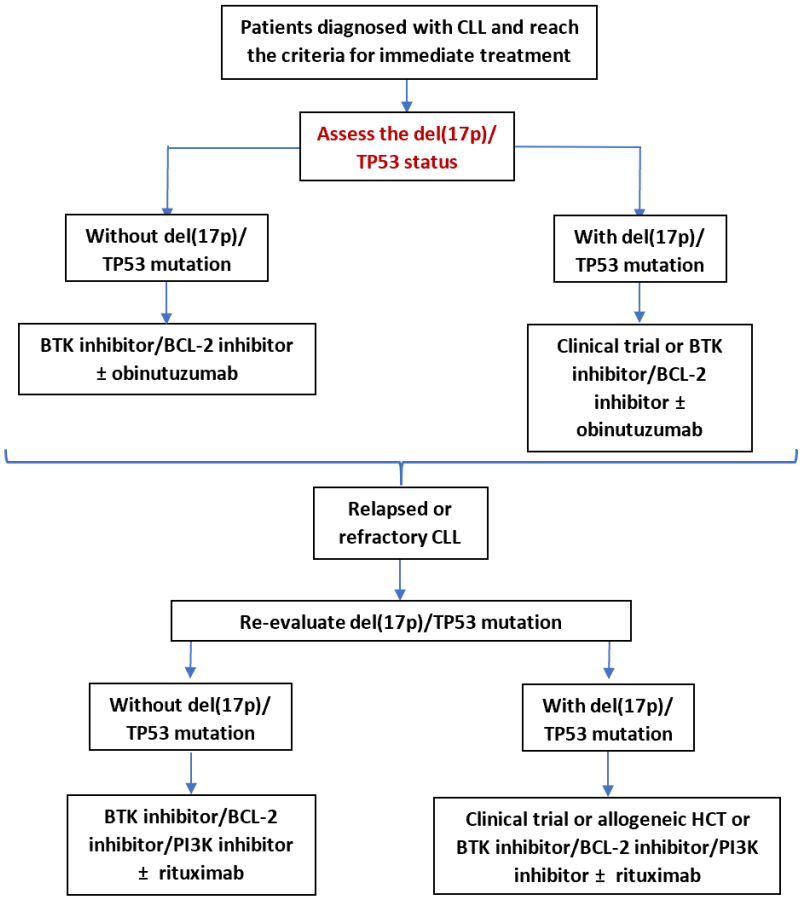

Figure 1.1 Clinical management of CLL and the preferred regimens. This flow chart shows the clinical options for the previously untreated CLL patients. The workflow and corresponding preferred therapy are recommended by NCCN Guidelines version 2.2021.

1.2 The pathogenesis of CLL

As mentioned above, the improved clinical management of CLL depends heavily on a better understanding of the pathogenesis of this disease. Below I will provide an overview of the current understanding of the pathogenesis of CLL.

1.2.1 The origin of CLL cells

Although the understanding of CLL pathogenesis has been improved drastically over the last decades, the origin of CLL cells is still a matter of debate.

In the earlier days, CLL B cells were thought to derive from the B1 lineage of B cells weakly secreting immunoglobulin M (IgM), which was based on the observation that many phenotypic properties of this type of B cells were shared by CLL B cells (Caligaris-Cappio et

al., 1982, Stall et al., 1988). Recently, an alternative theory has emerged that the cellular origin of CLL could be linked to the haematopoietic stem cells (HSCs) (Husby and Grønbæk, 2017). In 2011, Yoshikane Kikushige and colleagues reported that immunodeficient mice transplanted with purified HSCs from patients diagnosed with CLL generate clonal B cells with CLL-like phenotype (Kikushige et al., 2011), supporting the theory that the presence of genetic and epigenetic alterations in HSCs can lead to the occurrence of CLL. In 2014, Frederik Damm and colleagues reported that the genetic and epigenetic lesions related to CLL, such as NOTCH1, SF3B1, could be found in the pluripotent HSCs in patients with CLL (Damm et al., 2014). These reports indicate that the genetic abnormalities leading to the onset of CLL may have occurred in the multipotent HSCs, which further supports the HSCs theory.

The clonal rearrangements of immunoglobulin genes together with cell surface markers on CLL B cells lead to the theory that CLL cells come from the mature B cells which express a low amount of surface membrane immunoglobulins (Ig), CD19, CD20, and co-express CD23, CD5, CD200 (Swerdlow et al., 2017). With the identification of the mutation status of the IGHV genes, it has been proposed that the IGHV-M CLL cells and the IGHV-UM CLL cells have different cell origins (Figure 1.2). In 2001, it was reported by Klein and colleagues that the gene expression profile of CLL cells showed a certain amount of homogeneity with that of $CD27^+$ memory B cells (Klein et al., 2001). In humans, the $CD27^+$ memory B cells have been found to possess both IGHV-M and IGHV-UM genes (Klein et al., 1998). Basing on those findings, the IGHV-M CLL cells were considered to derive from the post-germinal centre B cells that have experienced antigen-presenting process, and they are CD5 and CD27 positive (Klein et al., 2001, Seifert et al., 2012). The situation about the origin of the IGHV-UM CLL cells is more complicated and there are currently two proposals. One is that the IGHV-UM CLL cells derive from the naïve B cells which are pre-GC B cells expressing CD5, but not CD27. Another one is that the IGHV-UM CLL cells originate from the GC- and T cell-independent, antigen-experienced B cells which may directly derive from a lineage of precursor B cells (Klein et al., 2001, Seifert et al., 2012). Over the last decade, evidence emerges that antigen selection plays a role in the pathogenesis of CLL (Stamatopoulos et al., 2017). It is reported that both IGHV-UM and IGHV-M CLL cells showed a highly restricted expression of certain immunoglobulin genes (Agathangelidis et al., 2012, Vardi et al., 2014).

In 2012, a study showed that IGHV-UM CLL cells express low-affinity, poly-reactive, and self-reactive BCRs, and the IGHV-M CLL cells express oligo-reactive and mono-reactive BCRs (Agathangelidis et al., 2012). Meanwhile, another study reported that IGHV-UM and IGHV-M CLL cells may rely on antigen-independent, cell-autonomous BCR signalling (Dühren-von Minden et al., 2012).

Collectively, the origin of CLL cells is still uncertain and further studies are needed to characterize the cell origin of CLL. Figure 1.2 summarises a briefly current consensus regarding the origin of CLL cells.

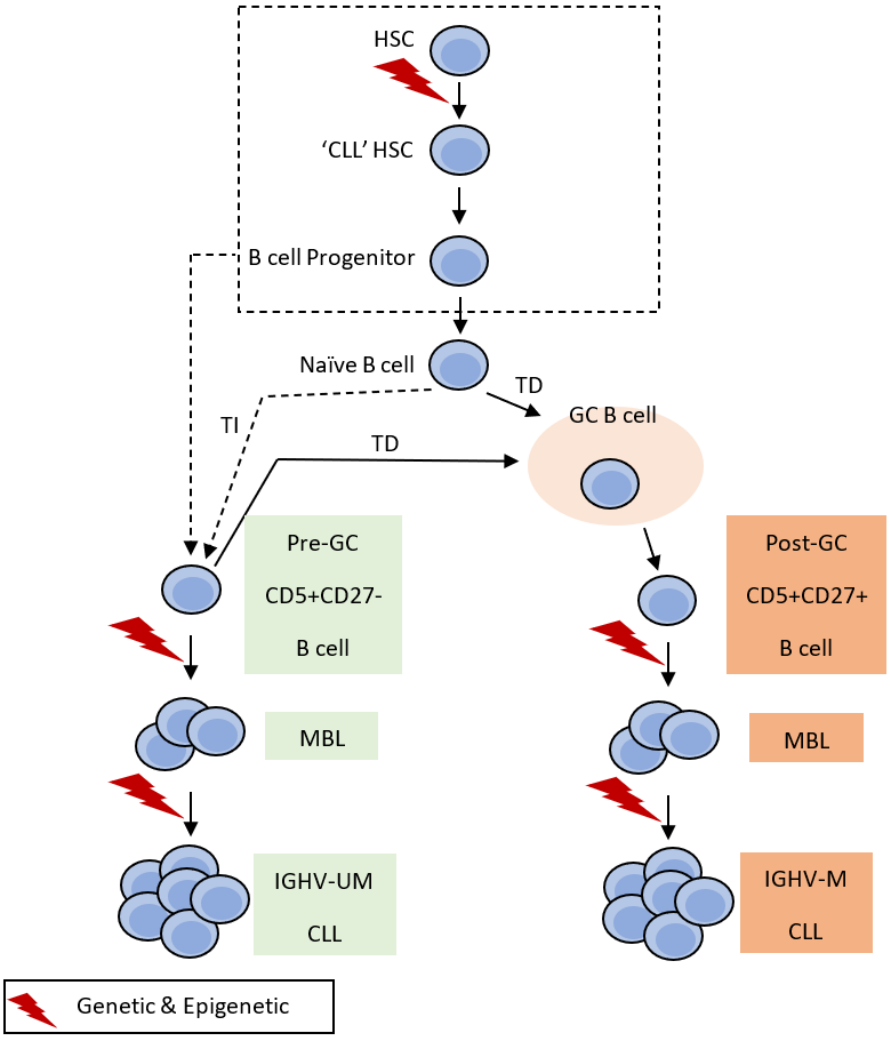

Figure 1.2 The cellular origin of CLL. Based on the evidence published in the literature so far, one theory suggests that CLL cells may derive from the haematopoietic stem cells (HSCs). The accumulation of certain genetic and epigenetic lesions may lead to the transformation of the HSCs to 'CLL' HSCs and further expansion of polyclonal B cell progenitors. However, this theory is still debatable. IGHV-M CLL cells seem to derive from the post-GC CD5+ CD27+ B cells. The IGHV-UM CLL cells may originate from the pre-GC CD5+ CD27- B cells, which could arise from the naïve B cells or from a lineage of B cells that have experienced antigens independently of T cells. With the further accumulation of genetic and epigenetic lesions, these progenitor cells transform and expand, developing monoclonal B-cell lymphocytosis (MBL) and finally resulting in the occurrence of CLL. GC: germinal centre; TD: T cell-dependent antigen; TI: T cell-independent antigen. This figure is modified from the paper published by Giulia Fabbri et al. (2016).

1.2.2 CLL microenvironment

The tumour microenvironment is known to be critically involved in establishing many hallmarks of cancers and is important in the pathogenesis of cancers (Hanahan and

Weinberg, 2011). Emerging evidence also indicates that the microenvironment plays an important role in the survival and expansion of CLL cells.

Firstly, it has been observed that CLL cells isolated from patients cannot survive alone *ex vivo* unless they were co-cultured with bone marrow stromal cells (BMSCs) or nurse-like cells (NLCs) (Panayiotidis et al., 1996, Lagneaux et al., 1998, Burger et al., 2000), which indicates that the extracellular signals from the microenvironment support the survival of CLL cells. Then, it has been noticed that there are various chemokine receptors expressed on CLL cells, which helps the cell trafficking and homeostasis in-between the bone marrow, lymphoid tissues, and peripheral blood in response to cytokines/chemokines secreted by the accessory cells within the microenvironment (Burger and Kipps, 2002). Later, a seminal study published in 2005 reinforced the role of the microenvironment in the development of CLL (Messmer et al., 2005). Before 2005, based on the observation that CLL cells were non-dividing, cell-cycle arrested cells, CLL was considered as an accumulative disease as the leukaemia cells failed to undergo the programmed cell death and accumulated in the bone marrow, lymphoid tissues, and peripheral blood in patients (Dameshek, 1967). However, by using the deuterated water to measure the DNA replication in CLL cells *in vivo*, Bradley Messmer and colleagues demonstrated that CLL cells proliferated at a rate of 0.1% to 1% of the entire clone every day in the patients with CLL (Messmer et al., 2005). The higher the proliferation rate the CLL patients had, the more aggressive the disease became (Messmer et al., 2005). This report redefined CLL as a proliferative disease and, from then on, CLL researchers have become more interested in the study of the compartments where CLL cells proliferate. Further studies have confirmed that CLL cells proliferate mainly in the lymph node microenvironment (Calissano et al., 2011).

It is now established that the microenvironment plays a significant role in the pathogenesis and the disease progression of CLL (Burger, 2012b, Ramsay and Rodriguez-Justo, 2013, Burger and Gribben, 2014, Fabbri and Dalla-Favera, 2016).

The CLL microenvironment consists of the bone marrow and secondary lymphoid organs, where CLL cells are interacting with groups of accessory cells including bone marrow stromal cells (BMSCs), monocyte-derived nurse-like cells (NLCs), and T cells (Burger, 2012b), as shown in Figure 1.3.

The BMSCs is the first type of accessory cells that have been found to rescue CLL cells from spontaneous apoptosis when those two types of cell are co-cultured *in vitro* (Lagneaux et al., 1998). It has also been reported that co-culturing with BMSCs also protects CLL cells from drug-induced cell death, which seems to rely on the increased expression of MCL-1 (Kurtova et al., 2009). The interaction between CLL cells and BMSCs activates the NF-κB signalling pathway through protein kinase C – β (PKC-β) in BMSCs themselves, which further makes BMSCs indispensable for the survival of CLL cells (Lutzny et al., 2013). The high affinity of CLL cells for BMSCs relies on the CXCR4-CXCL12 axis. It has been found that the chemokine (C-X-C motif) receptor 4 (CXCR4) (also known as CD184) is expressed at a high level on the surface of CLL cells that circulates in the peripheral blood (Burger et al., 1999, Burger and Bürkle, 2007, Pasikowska et al., 2016). CLL cells with high expression of CXCR4 are attracted to the corresponding ligand (CXCL12) that are expressed by BMSCs and migrate to the bone marrow (Burger et al., 1999, Möhle et al., 1999). Once there, the expression level of CXCR4 in CLL cells decreases, enabling the retention of CLL cells within the bone marrow and promoting the survival and expansion of the leukaemia cells (Burger and Bürkle, 2007, Pasikowska et al., 2016). CLL cells express the very late activation antigens-4 (VLA-4), also termed as CD49d, which interacts with the vascular cell adhesion protein 1 (VCAM1) expressed by BMSCs (Fabbri and Dalla-Favera, 2016).

NLCs has been found in the secondary lymphoid tissues and spleen of the CLL patients (Burger et al., 2000, Tsukada et al., 2002) and NLCs can be developed *in vitro* by culturing the peripheral blood mononuclear cells (PBMCs) isolated from patients with CLL for one to two weeks (Burger et al., 2000). Similar to BMSCs, co-culturing with the NLCs protect CLL cells from spontaneous apoptosis (Burger et al., 2000). Co-culturing with the NLCs also activates the BCR signalling and the NF-κB pathways in CLL cells and the gene expression profile of CLL cells co-cultured with NLCs is similar to that of CLL cells isolated from the lymph nodes of CLL patients (Burger et al., 2009). NLCs secret CXCL12 and CXCL13 to attract CLL cells and induce pro-survival signals to support the survival of CLL cells by binding to many receptors expressed on CLL cells with their corresponding ligands (Burger et al., 2000, Bürkle et al., 2007). Co-culturing with NLCs can activate the BCR signalling pathways and stimulate the interaction between CD100 on CLL cells and plexin B1 expressed by NLCs and activate NOTCH1 signalling in CLL cells as well (Fabbri and Dalla-Favera, 2016).

In the meantime, the role of T cells in the development of CLL has long been documented. It has been shown that co-culturing CLL cells with activated $CD4^+$ T cells can reverse the cell cycle resting status of the CLL cells from peripheral blood to proliferation status *in vitro* and induced the differentiation of CLL cells into IgM secreting cells (Tretter et al., 1998, Os et al., 2013). It has also been observed that CD40 stimulated CLL cells can secrete CCL22 that attracted $CD4^+$, $CD154^+$ T cells in the microenvironment of CLL such as lymph nodes and bone marrow (Ghia et al., 2002). Definitive evidence for T cell involvement in CLL was provided by a seminal study employing an adoptive transfer model. In the study, the authors transplanted purified human CLL cells alone into the immunodeficient mice and the animals did not develop CLL; however, when CLL cells and autologous T cells were co-transplanted, the transplanted mice develop CLL-like leukaemia (Bagnara et al., 2011). They also showed that eliminating $CD4^+$ T cells in the transfer model abrogated the survival and proliferation of CLL cells (Bagnara et al., 2011). This proves that the autologous T cells were necessary for the survival and expansion of CLL cells in the transplanted mice. The successful induction of CLL in the adoptive transfer model shows that the components of the microenvironment including T cells are crucial for the development of CLL. It is also reported that the $CD4^+$ and $CD8^+$ T cells isolated from the patients with CLL are dysfunctional with impaired synapse formation and this abnormal formation can be induced by CLL cells on T cells from healthy persons (Ramsay et al., 2008). T cells from the patients with CLL display the characteristics of T-cell exhaustion with increased expression of exhaustion markers CD244, CD160, and PD1, especially on $CD8^+$ T cells, resulting in the functional defects in cytotoxicity (Riches et al., 2013). Oligoclonal expansion of T cells that express activation marker CD57 in the patients with CLL indicates that these T cells may undergo chronic activation during their development (Burger and Gribben, 2014). It has also been shown that the migration, immunological synapse signalling, and interactions with tumour cells of autologous $CD4^+$ T cells can be enhanced by exposure to the extracellular vesicles secreted by CD40/IL-4 stimulated CLL cells (Smallwood et al., 2016).

Based on the evidence, it is reasonable to suggest that the interaction between CLL cells and T cells mutually influences each other. On one hand, it supports the survival and proliferation of CLL cells. On the other hand, it alters the function of T cells amenable to the development of the disease. Although the exact underlying mechanisms are still not fully

understood, it is accepted that the interaction between CLL cells and T cells is mainly mediated by the ligation of CD40 on CLL cells by CD154 on T cells (Caligaris-Cappio, 2003, Burger and Gribben, 2014, Fabbri and Dalla-Favera, 2016). Studies have also shown that the gene expression profile of CLL cells stimulated by CD40L is highly similar to that of CLL cells stimulated by autologous T cells and that gene expression of such stimulated CLL cells closely resemble that of the CLL cells isolated from lymph nodes of CLL patients (Herishanu et al., 2011, Pascutti et al., 2013). Therefore, it is the study of the interaction between CLL cells and T cells mediated by CD40-CD154 crosstalk that will form the main topic for this study.

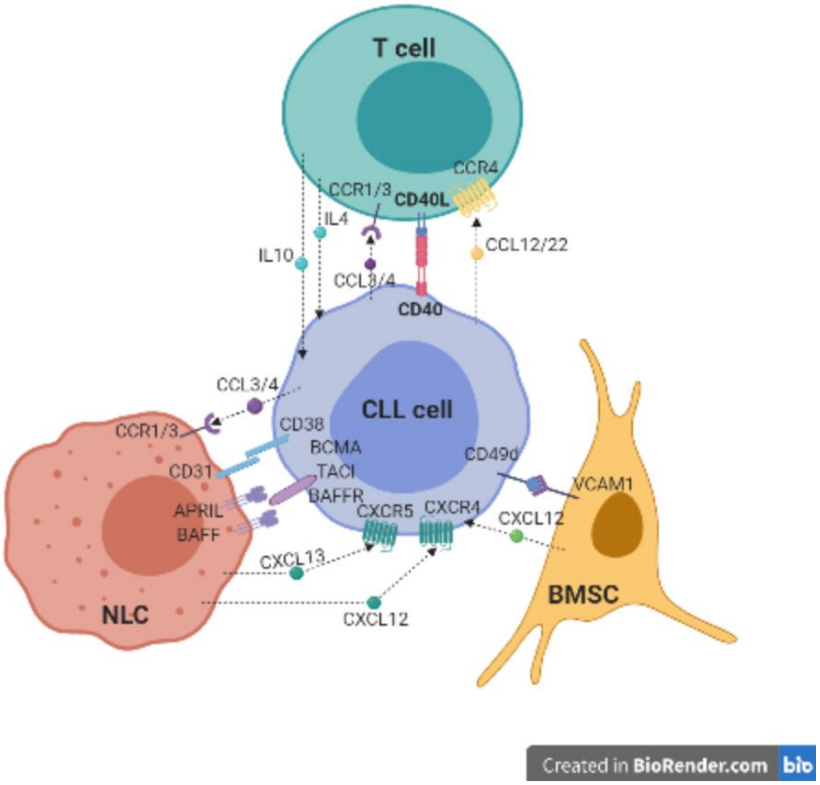

Figure 1.3 Main components of the microenvironment of CLL. Bone marrow stromal cells (BMSCs), monocyte-derived nurse-like cells (NLCs) and T cells are the main components within the microenvironment of CLL. CLL cells express VLA-4, also termed as CD49d, which interacts with VCAM1 expressed by BMSCs. Besides, CLL cells also interact with BMSCs through the CXCR4-CXCL12 axis. NLCs secret CXCL12 and CXCL13 to attract CLL cells and induce pro-signals to support the survival of CLL cells by the ligation of CD38 with CD31, binding to the BCMA/TACI/BAFFR receptors on CLL cells via ligands including APRIL/BAFF on NCLs. The interaction between CLL cells and T cells is mainly mediated by the ligation of CD40 with CD154 (also known as CD40L). CD40 stimulated CLL cells secret CCL22 that attracted $CD4^+$, $CD154^+$ T cells. This figure was modified from a review paper by Fabbri and Dalla-Favera (2016). APRIL, a proliferation-inducing ligand; BAFF, B cell activating factor; BAFFR, BAFF receptor; BCMA, B cell maturation antigen; TACI, transmembrane activator, and Ca^{2+} modulator and CAML (calcium-modulating cyclophilin ligand) interactor; VLA-4, very late activation antigens-4; VCAM1, vascular cell adhesion protein 1.

1.3 CD40-CD154 interaction

1.3.1 CD40 signalling in normal B cells

As mentioned above, CD40-CD154 interaction is regarded as the main mode of communication between CLL cells and T cells. CD40 is a 43-50kDa transmembrane protein, a cell surface receptor of the tumour necrosis factor receptor (TNF-R) family (van Kooten and Banchereau, 2000). CD40 is first identified on B lymphocytes and it is shown to play an important role in the humoral immune system (van Kooten and Banchereau, 2000, Qu,

2009). CD40 is widely expressed on B lymphocytes, monocytes, dendritic cells (DCs), endothelial cells (van Kooten and Banchereau, 1997). CD40 ligand, also termed as CD40L or CD154, is a 39 kDa type II transmembrane protein that belongs to the tumour necrosis factor (TNF) family (Smith et al., 1994). CD40 ligand is expressed not only on activated $CD4^+$ T cells but also on different types of cells such as B cells, DCs, basophils, monocytes, macrophages, natural killer (NK) cells, fibroblasts (van Kooten and Banchereau, 1997, van Kooten and Banchereau, 2000).

When CD154 binds to CD40, CD40 needs to form a trimer and the acidic domain in the receptor interacts with the basic domain of CD154 (Schonbeck and Libby, 2001). The signals induced by the engagement of CD40 by CD154 need to be transduced via the recruitment of adapter proteins, TNFR-associated factors (TRAFs) (Bishop et al., 2007). So far, six proteins have been identified, which constitute the TRAF family, and they are named from TRAF1 to TRAF6, which can be directly and indirectly recruited upon the CD40-CD154 ligation transducing signals for cellular biological processes (Elgueta et al., 2009) (Figure 1.4). The signalling pathways which can be activated by CD40-CD154 engagement include the canonical and non-canonical nuclear factor κB (NF-κB)-signalling pathways, the mitogen-activated protein kinases (MAPKs), phosphoinositide-3-kinase (PI3K), phospholipase Cγ (PLCγ) pathway, and Janus family kinase 3 (JAK3)-phosphorylation of signal transducer and activator of transcription 5 (STAT5) pathways (Bishop et al., 2007, Säemann et al., 2003, Säemann et al., 2002).

It has been reported that TRAF1 deficient B cells exhibit an increasing degradation of TRAF2 and TRAF3 (Xie et al., 2006) and this phenomenon can be found in the antigen-presenting cells (APCs) (Arron et al., 2002). The recruitment of TRAF1 together with TRAF2 transduces signalling leading to the activation of the canonical NF-κB pathway, as deficiency of those two TRAF proteins abolishes the activation of the NF-κB signalling pathway and this abolishment cannot be achieved by the deletion of TRAF1 and TRAF2 individually (Xie et al., 2006). The recruitment of TRAF2 upon CD40-CD40L ligation plays a role in the activation of p38, JNK, and Akt signalling, as CD40-CD40L ligation is unable to activate these in TRAF2 deficient B cells and mouse embryonic fibroblasts (Hostager et al., 2003, Yeh et al., 1997, Lee et al., 1997).

Together with TRAF3, TRAF2 has also been shown to negatively regulate the non-canonical NF-κB signalling pathway in B cells (Gardam et al., 2008, Vallabhapurapu et al., 2008, Zarnegar et al., 2008). To be specific, CD40-CD40L ligation leads to the recruitment of TRAF2 and TRAF3 together with the cellular inhibitor of apoptosis (cIAP) to the cytoplasmic tail of CD40 transmembrane receptor and the NF-κB-inducing kinase (NIK). NIK is usually degraded by the cIAP, which, following interacting with TRAR2 and TRAF3, loses its degradation function, resulting in the accumulation of NIK and the activation of the non-canonical NF-κB signalling pathway (Zarnegar et al., 2008, Vallabhapurapu et al., 2008, Bishop et al., 2007).

The role of TRAF3 in the NF-κB signalling appears to be a negative one, at least in B cells (He et al., 2007). Thus, CD40 signalling is almost intact in TRAF3 deficient B cells (He et al., 2007, Xie et al., 2004). Reinforced expression and recruitment of TRAF3 upon CD40-CD154 ligation has been shown to suppresses the canonical NF-κB signalling pathway in B cells (He et al., 2007). However, contrasting results are observed in epithelial cells where TRAF3 is essential for the CD40-mediated activation of NF-κB signalling (Urbich et al., 2001, Propst et al., 2002). It indicates a distinct function of TRAF3 in different types of cells.

The role of TRAF5 in positively regulating CD40 signalling has been reported. It has been shown that the recruitment of TRAF5 to the cytoplasmic domain of CD40 upon receptor ligation is indirect as it requires the presence of TRAF3 (Bishop et al., 2007, Hauer et al., 2005). However, knocking down TRAF5 in B cells disables the activation of the canonical and non-canonical NF-κB signalling pathways, down-regulates the expression of co-stimulators and decreases the proliferation, and the production of antibodies in B cells (Nakano et al., 1999, Elgueta et al., 2009).

TRAF6 has been shown to bind directly and indirectly to the cytoplasmic domain of the CD40 receptor upon CD40-CD40L engagement (Davies et al., 2005, Rowland et al., 2007). When directly recruited upon CD40-CD40L ligation, TRAF6 induces Akt phosphorylation by forming a complex with Casitas B-lineage lymphoma b (Cbl-b), Casitas B-lineage lymphoma (c-Cbl), and PI3K (Arron et al., 2001, Davies et al., 2004) (Figure 1.4). When indirectly recruited, TRAF6 interacts with TRAF2 to complete the signalling transduction induced by CD40-CD40L ligation (Bishop et al., 2007, Elgueta et al., 2009).

The signalling transduction activated by CD40-CD40L engagement through TRAFs has yet to be fully understood, which still needs further study to fully characterize the biological functions of individual TRAFs.

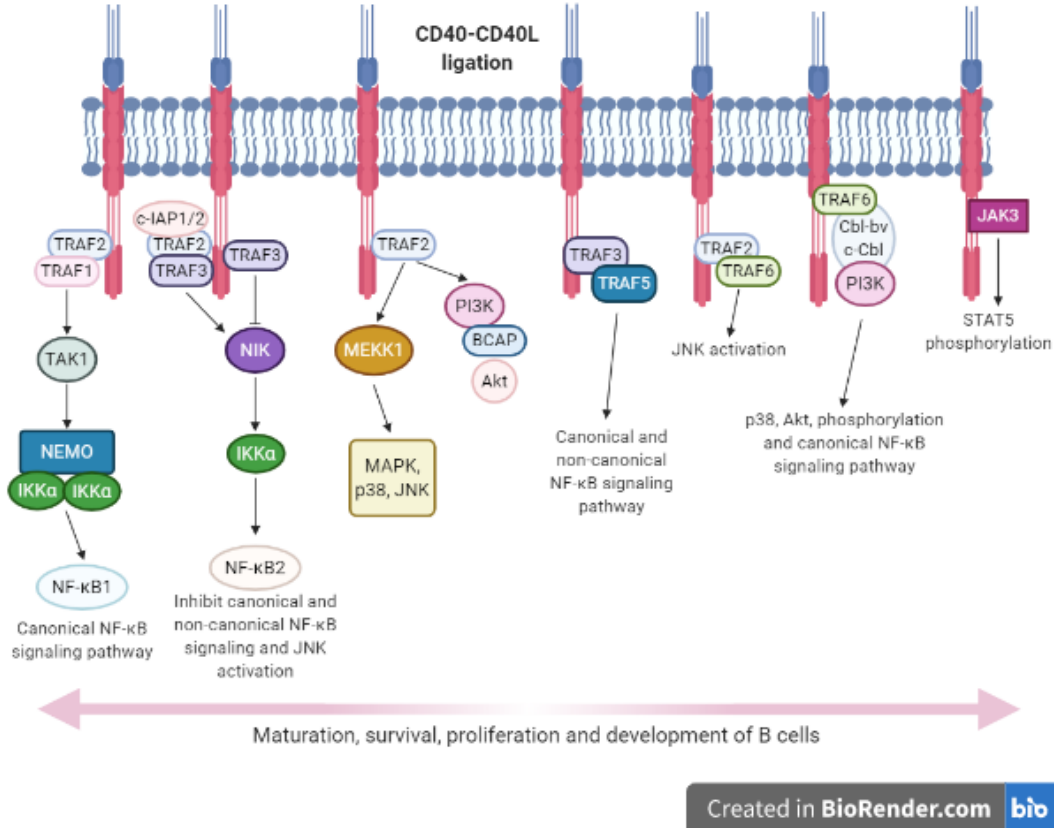

Figure 1.4 CD40 signalling in B cells. CD40-CD40L ligation recruits TRAFs to the cytoplasmic domain of CD40 transmembrane receptor in B cells and transduces signalling through individual TRAFs or the combination of TRAFs. TRAF1 together with TRAF2 transduces the signals in the canonical NF-κB signalling pathway. The recruitment of TRAF2 upon CD40-CD40L ligation plays a role in the activation of p38, JNK, and Akt signalling. TRAF2 and TRAF3 together with cIAP regulate the non-canonical NF-κB signalling pathway by controlling the degradation of NIK. The recruitment of TRAF3 upon CD40-CD40L ligation suppresses the canonical NF-κB signalling pathway. The recruitment of TRAF5 with the combination of TRAF3 transduces the activation of the canonical and non-canonical NF-κB signalling pathways. Directly recruited TRAF6 induces the signalling for the Akt phosphorylation by forming a complex with Casitas B-lineage lymphoma b (Cbl-b), Casitas B-lineage lymphoma (c-Cbl), and PI3K. Indirectly recruited TRAF6 interacts with TRAF2 to complete the signalling transduction induced by CD40-CD40L ligation. This figure is modified from two papers published by Elgueta et al. (2009) and Hobeika et al. (2015).

CD40-CD154 interaction has attracted intense interest from researchers due to its significant role in the haematopoiesis and the immune system. CD40 signalling induced upon CD40-CD154 engagement is crucial for the differentiation, apoptosis, proliferation,

and isotype switching for B lymphocytes (Kehry, 1996, Greiner et al., 1997, Seijkens et al., 2010). The differentiation of B lymphocytes is regulated not only by the signal from surface immunoglobulins but also by the signals induced by activated T cells. The signal induced by T cells is mainly based on the engagement of the CD40 receptor expressed on B lymphocytes with the CD154 expressed on activated T cells (Bishop and Hostager, 2003). CD40-mediated signalling is also important for the differentiation from germinal centre B cells to memory B cells, as abrogating CD40 ligand cancels the differentiate from germinal centre B cells into the cells with the features of plasma cells (Arpin et al., 1995). It has been reported that CD40-mediated signalling can rescue B cells from surface Ig-induced apoptosis (Wang et al., 1995, Choi et al., 1995, Merino et al., 1995). Via CD40-CD154 engagement, activated $CD4^+$ T cells stimulate the precursor of B cells to proliferate *in vitro* (Renard et al., 1994). The inhibition of the CD40-CD154 interaction abolishes the proliferation and production of Ig by B cells (Clark and Ledbetter, 1994, Marshall et al., 1993).

In addition, CD40-CD154 interaction is also indispensable for the development and functions of other types of cells including T lymphocytes, DCs, NK cells (Seijkens et al., 2010). For the differentiation of T lymphocytes, CD40-CD154 interaction plays important role in the development of T-help cells including the T-helper 1, T-helper 2, and T-helper 17 (Pilon et al., 2009, Straw et al., 2003, Jenkins et al., 2008, Iezzi et al., 2009). Knocking out respective genes encoding CD40 and CD154 in mice leads to an obvious reduction of CD4 and CD25 double-positive T regulatory cells in the peripheral blood, spleen, and thymus (Guiducci et al., 2005, Smook et al., 2005). CD40-CD154 ligation in the haematopoietic stem and progenitor cells (HSPCs) recruits TRAF6 and activates NF-κB signalling pathway resulting in the formation of mature DCs (Ouaaz et al., 2002, Kobayashi et al., 2003). *In-vitro* studies show that CD40-mediated signalling up-regulates the level of Flt3 ligand and thrombopoietin secreted by bone marrow stromal cells, which facilitates the differentiation of HSPCs towards NK cells (Fu et al., 2002). CD40-CD154 engagement between the NK cells and APCs promotes the cytotoxicity of NK cells (Sartorius et al., 2003, Tomihara et al., 2007).

Accumulating evidence supports the notion that CD40-CD154 interaction plays a critical role in the immune system. It has been known for a long time that CD40-CD154 engagement is important for the formation of the germinal centre (Foy et al., 1994). Abolishment of CD40-mediated signalling leads to a loss of GC activity, while restoration of the CD40-mediated

signalling enables the initiation and maturation of the GC activity (Elgueta et al., 2009). Inhibition of the CD40-CD154 interaction either by using the blocking antibodies or genetically abrogating the genes encoding CD40 or CD154 results in the deletion of thymus-dependent humoral immunity (Banchereau et al., 1994). It is now known that the interaction between T cells and B cells constitutes an essential part of humoral immunity (Mitchison, 2004). In addition to its role in the differentiation and mediating interaction of these two types of cells, CD40-CD154 engagement is involved in the differentiation and functions of the APCs such as DCs (described above). Meanwhile, evidence exhibits the significant role of CD40-CD154 crosstalk in cellular immunity, especially its role in the donor-specific transfusion tolerance (Quezada et al., 2003). It has been reported that CD40-CD154 engagement induces the activation of $CD8^+$ T cells, which leads to allograft rejection (Larsen et al., 1996, Jones et al., 2000). Blocking this engagement results in T cell tolerance by suppressing the $CD4^+$ and $CD8^+$ T cells (Honey et al., 1999, Jones et al., 2000). It, in turn, helps the persistence of allograft tolerance (Parker et al., 1995, Zheng et al., 1999, Lehnert et al., 2001, Jarvinen et al., 2003, Chalermskulrat et al., 2006). These observations together highlight the therapeutic potential in targeting or activating CD40-CD154 interaction in immunotherapy.

1.3.2 Activation of the CD40 signalling pathway in CLL cells

The CD40-CD154 crosstalk between CLL cells and activated $CD4^+$ $CD154^+$ T cells constitutes one of the major forms of communication between cells within the CLL microenvironment. The functional effects of CD40 stimulation have been studied by many research groups, especially its pro-survival role in CLL. In 1998, using an agonistic anti-CD40 monoclonal antibody (G28-5), Maria Romano and colleagues reported that the activation of CD40 receptors on CLL cells can reduce the amount of apoptosis induced by fludarabine and that this pro-survival effect was due to the activation of NF-κB signalling pathway in CD40 stimulated CLL cells (Romano et al., 1998a). In line with this observation, Richard Furman and colleagues reported that, comparing with normal B cells, CLL cells exhibit a higher level of NF-κB activity which can be further activated by CD40 stimulation and that blocking the CD40-CD154 engagement on CLL inhibited the activity of NF-κB and induced apoptosis (Furman et al., 2000). Furthermore, there is no difference between M-CLL and UM-CLL cells

in terms of the activation of the NF-κB signalling pathway and proliferation induced by CD40-CD154 ligation (Tromp et al., 2010). Later, it has been found that CD40-CD154 engagement can induce the expression of both anti-apoptotic and pro-apoptotic proteins in CLL cells. CD40 stimulation regulates the expression profile of a group of the apoptosis-regulatory proteins, including the members of the BCL-2 superfamily, in CLL cells (Willimott et al., 2011, Smit et al., 2007, Kater et al., 2004). The proteins of the BCL-2 family can be classified into three groups: the anti-apoptotic proteins including BCL-2, BCL-XL, MCL-1, BCL-W, and Bfl-1; the pro-apoptotic proteins including BAX, BAK, and BOK; the BH3-only pro-apoptotic proteins such as BAD, BID, BIK, BIM, BMF, HRK, Noxa, Puma, and so on (Kale et al., 2018).

Although the overall influence induced by CD40 activation in CLL cells is pro-survival and the inhibition of cell death, CD40 stimulation also produces seemingly contradictory effects in the expression of the individual proteins involved in apoptosis. For example, CD40 stimulation induces the expression of anti-apoptotic proteins such as BCL-XL, MCL-1, Bfl-1 and down-regulates the expression of pro-apoptotic proteins like BH3-only proteins Noxa and Harakiri in CLL cells; at the same time, it also upregulates the expression of the protein BID that is a pro-apoptotic BH3-only protein (Kater et al., 2004, Smit et al., 2007). Besides, CD40 stimulation increases the expression of CD95, a death receptor belonging to the TNF-R superfamily (Nagata and Golstein, 1995), but it does not sensitize CLL cells to death-receptor-induced cell death (Wang et al., 1997, Kater et al., 2004). Although it does not sensitize CLL cells to CD95-induced cell death immediately, the up-regulation of the expression of CD95 induces the up-regulation of the Fas-associated death domain protein (FADD) and DAP3 (a FADD-binding molecule) 5 days after CD40 stimulation and consequently the CD40-stimulated CLL cells respond to CD95-induced apoptosis (Chu et al., 2002).

Besides its influences on survival, CD40 activation seems to help CLL cells interact with other bystander cells within the microenvironment. CD40 stimulated CLL cells produce chemokines including CCL2, CCL3, CCL4, CCL5, CCL7, CCL24, CXCL5, CXCL10, and IL4, and those chemokines can attract monocytes (van Attekum et al., 2017). Also, it has been found that CD40-CD154 engagement increases the level of CD44 in CLL cells and enhances the binding of CD44 to its extracellular matrix ligand hyaluronan present on stromal cells (Girbl

et al., 2013). As a result, CD44-HA adhesion restrains the motility of CLL cells, thus retaining the leukemic cells within the lymph node microenvironment (Girbl et al., 2013).

CD40 stimulation also works together with other co-stimulators to induce the proliferation of CLL cells. CD40 stimulation, in the presence of BMSCs and CpG-oligodeoxynucleotides (ODNs), activated the non-cycling CLL cells to enter into the cell cycle and induces proliferation as measured by the expression of Ki-67 (Purroy et al., 2015). It was also shown that the proliferation effect was more pronounced in cells induced by the combined stimuli than by individual stimulus (Purroy et al., 2015). Moreover, the co-stimulation induced by the combined stimuli increases the expression of ZAP-70 and causes the resistance of stimulated cells to the induction of apoptosis by fludarabine and bendamustine (Purroy et al., 2015). It was reported that compared with IL-2, IL-15, anti-IgM, and CpG-ODNs, the IL-21 produced by activated T cells shows the highest potency to work synergistically with CD40 stimulation to induce proliferation on CLL cells (Pascutti et al., 2013). The co-stimulation by CD40 and IL-4 has been shown to promote DNA damage repair by up-regulating the expression of ATM and increasing the phosphorylation of the downstream targets of ATM (Lezina et al., 2018). Those data indicate that CD40 activation induces a range of biological effects including the induction of the expression of many genes and altering signal transduction pathways, ultimately promoting the survival and proliferation of CLL cells. The clinical significance of the *in-vitro* response of CLL cells to CD40 stimulation has also been highlighted by the observation that not all CLL cells isolated from patients with CLL respond to CD40 stimulation by CD40 ligand (Scielzo et al., 2011). Significantly, CLL patients with CLL cells not responding to the CD40 stimulation tends to lead a more aggressive disease course than the patients whose CLL cells respond to the CD40 stimulation (Scielzo et al., 2011). It further indicates that CD40-CD154 interaction is likely involved in the pathogenesis and progress of the disease course of CLL.

In the meanwhile, *in-vitro* studies employing inhibitors to inhibit CD40 stimulation also show that they can overcome the pro-survival effect induced by CD40 stimulation on CLL cells. It is shown that HCD122, an antagonist anti-CD40 monoclonal antibody, abrogates the pro-survival signals induced by CD40 stimulation and inhibits the secretion of IL-6, IL-8, IL-10, TNF-α, and GM-CSF by CLL cells (Luqman et al., 2008). It also induces cell death of CLL cells possibly by targeting antibody-dependent cellular cytotoxicity (ADCC) (Luqman et al., 2008).

It has also been reported that the c-Abl inhibitors, dasatinib, and imatinib, abolish the pro-survival effect induced by CD40 stimulation on CLL cells and restores the sensitivity of CLL cells to the killing of cytotoxic drugs (Hallaert et al., 2008). The treatment of CLL cells with chlorambucil cancels the pro-survival effect induced by CD40 stimulation, which can be further enhanced by the combination of bezafibrate and medroxyprogesterone acetate through generating reactive oxygen species (ROS) and mitochondrial superoxide (Hayden et al., 2009, Calissano et al., 2011). Besides, treating CLL cells with NVP-AUY922 (a heat shock protein-90 inhibitor) together with fludarabine overcomes the fludarabine-resistance induced by CD40 stimulation (Best and Mulligan, 2012).

Given the critical role of CD40-CD154 interaction in the immune system, it is important to characterize the effect of inhibiting CD40 signalling on other immune cells before the clinical application of therapeutics targeting pro-survival signals induced by CD40 stimulation in CLL. A comprehensive understanding of the influence induced by CD40 stimulation on the immune system as well as on CLL cells is required so that more precise targets can be identified for therapeutic intervention in the clinical management of CLL patients in the future.

1.4 Proteomics study in CLL

The accomplishment of the Human Genome Project (HGP) provides us a blueprint for the entire genetic information of human beings (Gannett, 2008). However, HGP also reveals a further biological complexity involving the transmission processes of the genetic information within the human organism as there are only about 20,000 protein-coding genes identified (Moraes and Góes, 2016), whereas the number of proteins within the human organism is estimated to be as many as 500,000 (Pray, 2008). The wide difference makes the multi-omics studies, especially at the protein level, significant in the investigation of biological activities of individual genes in a human body. The DNAs carry the genetic information and direct the development of different types of cells, while the proteins are the executors to perform the function of the individual genes. Following the concept of ‘genome’, the ‘proteome’ is defined as the entire constituent of proteins expressed by a specific cell or organism (Wasinger et al., 1995, Poon and Johnson, 2001). As mentioned above, compared with the genome, the proteome is more complex and deserves further

investigations. This is because, first of all, the number of genes for a specific cell or organism is constant and relative stable (Ermini et al., 2008), whereas the number of proteins is different from cell to cell due to the different biological function (Walsh, 2002, Elguoshy et al., 2017). Secondly, even for a specific cell within an organism, the number of proteins is changeable from time to time, which is influenced not only by the changes in gene expression but also by the environmental factors such as changes in the pH, exposure to stimuli, and inflammatory condition (Walsh, 2002, Lundberg and Borner, 2019). Thirdly, working as the bridging molecules, messenger RNA (mRNA) can be transcribed from the same gene by different transcription starting locus or alternative splicing resulting in more than one peptides being translated, which leads to the diversity of proteoforms (Sperling et al., 2008). In addition, the existence of the post-translational modifications (PTMs) including the methylation, ubiquitylation, phosphorylation, and glycosylation magnifies the difference between the number of genes and the number of proteoforms in a cell or organism (Niall, 1973, Walsh, 2006). These phenomena indicate that the proteome provides more accurate and up-to-date information on the functional status of a cell or organism, although technical challenges have held back researchers from investigating a large number of proteins simultaneously.

The techniques such as genome microarrays, *in situ* hybridization, polymerase chain reaction (PCR), and RNA sequencing (RNA-seq) have been comprehensively applied in research (Griffiths et al., 2018), which all depends on the complementary characteristics of the paired purine base: guanine to cytosine and adenine to thymine (A-T) for DNA (Pullman and Pullman, 1959), guanine to cytosine and adenine to uracil (A-U) for RNA (Tobias et al., 2011). However, proteins are comprised of chains of the 20 common amino acids linked via peptide bonds and there has been no technology so far that exist to amplify these chains directly. One traditional technique relies on electrophoresis to separate proteins based on their molecular weight (O'Farrell, 1975, Hames, 1998). The proteins separated are then transferred onto nitrocellulose membrane and probed with enzyme-conjugated antibodies; the relative abundance of the identified proteins is then measured against the relatively stable proteins such as β-actin and GAPDH (Kurien and Scofield, 2006). These processes are term as '*Western blotting*'. So far, Western blotting is still a useful method for in-cell protein analysis but the number of proteins that can be investigated simultaneously is limited by its

principle (Moritz, 2020). Later on, the emerging techniques for protein characterization such as enzyme-linked immunosorbent assay (ELISA), immunohistochemistry (IHC), and immunofluorescence are all based on the interaction between a specific protein or epitope of interest and the corresponding antibodies (Engvall et al., 1971, Lequin, 2005, Ramos-Vara and Miller, 2014, Odell and Cook, 2013). Like Western blotting, the number of proteins that can be studied simultaneously by these methods is limited as well. Attempts have been made to use antibodies to construct the protein microarray, also termed as the 'protein chips', which is based on the ideas of the genome microarrays (MacBeath et al., 1999, MacBeath, 2002, Templin et al., 2003). Now protein microarray techniques can be divided into the following categories: analytical protein microarray, reverse-phase protein microarray, and functional protein microarray (Sutandy et al., 2013). Similar to the genome microarrays, protein microarrays essentially assemble thousands of miniaturized assays on a small plate to detect many proteins simultaneously from the same sample (Sutandy et al., 2013). The analytic protein microarrays are widely used for protein quantification, in which the plate contains different antibodies that capture the proteins in a sample and the bound proteins are then detected by reporter antibodies directly or indirectly (Gupta et al., 2016). The reverse-phase protein microarrays are opposite to the steps involved in the analytic protein microarrays, in which protein samples are immobilized on the plate and then detected by antibodies (Gupta et al., 2016). As the analytic protein microarrays are performed in the so-called sandwich way (antibodies in plates; proteins in samples; antibodies added further for detection), the reverse-phase protein microarrays involve immobilizing proteins from samples onto the plates, following which antibodies are used for detection. The functional protein microarrays are mainly applied in the study of protein interactions and useful to detect binding between protein-protein, protein-DNA, protein-RNA, and so on, with the plate containing known proteins or peptides which are then mixed with to be analysed samples with any binding molecules detected as a result of the interaction (Gupta et al., 2016). Although the technique of protein microarrays increases the number of proteins detected simultaneously, the results are strongly influenced by the specificity and sensitivity of the corresponding antibodies (Gupta et al., 2016). The limited number of miniaturized assays and the number of antibodies or samples that can be immobilized on one plate restricts the number of proteins to be identified (MacBeath, 2002,

Templin et al., 2003, Gupta et al., 2016), which makes this type of technique suitable for the study of targeted proteins.

The application of mass spectrometry (MS) techniques provides a new opportunity for proteomics studies (Aebersold and Mann, 2003). Instead of using antibodies to detect proteins, MS identifies proteins by measuring the mass-to-charge (m/z) ratio of the peptides from a protein, from which the specific molecular weight can be accurately calculated and ultimately the sequence of the specific amino acids of the peptide chain or chains that form the protein can be obtained (Koomen et al., 2005). With the rapid development, MS-based techniques can be applied not only to accurately measure the level of proteins in samples but also to detect the PTMs of the proteins (Kirkpatrick et al., 2005, Nita-Lazar et al., 2008, Pan et al., 2011, Mischerikow and Heck, 2011, Afjehi-Sadat and Garcia, 2013). The classic procedures of MS-based proteomics study have now been well established concerning the extraction of proteins from cell/tissue samples, digesting proteins into peptides, separating the peptides by high-performance liquid chromatography (HPLC), detecting peptides by mass spectrometers, searching on database and data analysis (Walker, 2005).

Over the last two decades, MS-based proteomic techniques have also been applied in CLL research including the studies of the distinct expression of proteins by CLL cells from patients of different CLL subgroups. In 2003, a study using two-dimensional gel electrophoresis followed with MS showed that the pattern of PTMs of nucleophosmin was different between M-CLL and UM-CLL and that the expression levels of F-actin-capping protein β subunit, 14-3-3 β protein, laminin-binding protein precursor were significantly up-regulated in M-CLL cells comparing with that in UM-CLL cells (Cochran et al., 2003). The difference in expression and localization of proteins between M-CLL and UM-CLL has also been reported by others employing various proteomic approaches (Barnidge et al., 2005, Rees-Unwin et al., 2010, Admoni-Elisha et al., 2016). The proteomic study from our research group has also identified migration defects as a feature associated with UM-CLL cells (Eagle et al., 2015). In that study, among a total number of 3521 identified proteins, 274 proteins were found to be differentially expressed between UM-CLL and M-CLL cells. The functional enrichment analysis of the differentially expressed proteins showed that the migration/adhesion pathways were significantly enriched by 39 differentially expressed proteins, 35 of them were significantly under-expressed in UM-CLL, thus indicating a

migration defect and/or enhanced adhesive capacity in these cells. Clinical correlation analysis also confirmed that patients with UM-CLL are likely to develop bulky lymph nodes, a well-known indicator for poor prognosis of the disease (Eagle et al., 2015).

Meanwhile, MS-based proteomics techniques have been used to investigate novel biomarkers as well as the pathogenetic factors for CLL. In 2003, Boyd and colleagues used plasma-membrane-based proteomic analysis to identify new prognostic and therapeutic targets and found that two novel proteins (MIG2B and B-cell novel protein#1, BCNP1) were expressed preferentially in CLL B cells (Boyd et al., 2003). In a separate study, by comparing CLL B cells to the B cells from young and elderly healthy donors, Rupert Mayer and colleagues reported that CLL cells share protein expression profile of B cells from elderly healthy donors, thus suggesting that aging may predispose B cells to CLL cells (Mayer et al., 2018). In another study, by comparing CLL B cells from 14 patients with CLL to B cells from healthy donors, authors identified a total number of 8694 proteins with 544 of them significantly up-regulated in CLL B cells including some established markers such as BCL-2, CD5, CD23 and several previously unreported proteins that are involved in B-cell receptor signalling (e.g. LAX1, CLEC17A, APT2B4) (Johnston et al., 2018). A recent study using a quantitative label-free proteomics technique showed that the activities of metabolic pathways of CLL B cells were different from healthy B cells with the overexpression of proteins involved in the metabolism of lipid and cholesterol in CLL cells (Thurgood et al., 2019). Studies of histone proteome in CLL cells also revealed a distinct expression and diverse post-translation modifications of histone proteins. Thus, comparing to normal B cells, the expression of histone H2A variants (H2AFL and H2AFA/M) was significantly decreased in CLL cells (Su et al., 2009). However, the expression of a histone H2A variant with a molecular mass of 14,063 Da was associated with a significantly shorter time to treatment (Singh et al., 2015). Another study investigated the proteomic profile of plasma-derived exosomes from patients with CLL and found that CLL cells from patients with progressive disease secreted exosomes with high levels of S100-A9 which in turn activated the NF-κB pathway during CLL progression (Prieto et al., 2017).

MS-based proteomics techniques have also been used to investigate activities of specific signalling pathways. A study investigating the signalosomes of BCR reported that the activation of BCR led to the phosphorylation and ubiquitylation of the receptor-proximal

signalling components and that two novel components of BCR signalling, RAB7A, and BCL10, were identified (Satpathy et al., 2015). It is also showed that the ubiquitylation of BCL10 was required for the BCR-mediated activation of the NF-κB signalling pathway (Satpathy et al., 2015). Another study reported that a protein known as kininogen was up-regulated upon BCR activation and that its expression was associated with shorter median survival (Kashuba et al., 2013). MS-based proteomic techniques have also been used to explore the alteration of CXCR4/CXCL12 signalling pathways of CLL cells. Morgan O'Hayre and colleagues reported that the activation of CXCR4 by CXCL12 induced phosphorylation and degradation of programmed cell death factor 4 (PDCD4), which functions as a tumour suppressor (O'Hayre et al., 2010). CXCL12 stimulation also led to phosphorylation of heat shock protein 27 (HSP27), an anti-apoptosis protein (O'Hayre et al., 2010). In addition, a study employing the quantitative MS technique revealed that mutations in ribosomal protein S15 (RPS15) led to an alteration in global protein synthesis and translational fidelity in CLL cells (Bretones et al., 2018).

MS-based proteomic techniques have also been used to investigate the on/off-target effects of kinase inhibitors and other therapeutic agents in CLL. In 2013, Yiping Che and colleagues reported that SNX-7081, an HSP90 inhibitor, decreased the expression of proteins involved in cell cycle and DNA replication and repair in CLL cells, demonstrating an on-target effect of SNX-7081 (Che et al., 2013). Later, they showed that SNX7081 induced cell death synergistically with fludarabine by inhibiting the DNA repair and increasing the expression of pro-apoptotic molecules such as BID in CLL cells lacking functional p53 (Kaufman et al., 2015). In another study, Chiara Agnoletto and colleagues reported that cell death induced by a mitochondria-targeting small molecule, sodium dichloroacetate, in p53 mutated CLL cells was associated with the activation of transcription factor interleukin enhancer binding factor 3 (IEF3) and p21 (Agnoletto et al., 2015). By screening protein-protein interaction using MS-based techniques together with co-immunoprecipitation, Zhuojun Liu and colleagues reported that the receptor tyrosine kinase-like orphan receptor 1 (ROR1) interacted with HSP90 to promote the survival of CLL cells and that targeting HSP90 led to the degradation of ROR1 through ubiquitin-proteasome pathway, resulting in improved cytotoxicity of ibrutinib in CLL cells (Liu et al., 2020). Therefore, MS-based proteomic techniques help us achieve a better understanding of the effects of drugs in the protein

expression at a global level and the precise mechanism of drugs, which will benefit the development and synergistic study of drugs.

MS-based proteomic techniques provide us a way to investigate the pathogenesis of CLL at a global protein expression level. So far, there has not been any proteomic study in the CD40 stimulation on CLL cells.

1.5 The rationale underlying this project

Although novel therapeutic agents such as inhibitors of BCR or BCL-2 significantly improve the clinical management of patients, CLL remains an incurable disease. One major challenge in the clinical management of CLL is that almost all patients receiving therapies eventually develop drug resistance, resulting in mortalities (Hallek, 2019). In addition to the intrinsic factors such as certain genetic mutations that cause drug resistance, the extrinsic signals from the microenvironment also protect CLL cells from drug-induced cell death, resulting in resistance to therapy (Ramsay and Rodriguez-Justo, 2013, Arruga and Deaglio, 2017). Therefore, over the past decades, understanding how CLL cells interact with the microenvironment has been the focus of the CLL research community worldwide to find a novel therapeutic strategy to overcome the microenvironment-mediated drug resistance (Burger, 2012b, Ramsay and Rodriguez-Justo, 2013, Crassini et al., 2015). T cells are one of the major components in the CLL microenvironment and their significant role in the pathogenesis and development of CLL has been well documented. The interaction between CLL cells and T cells is mainly mediated via CD40-CD154 crosstalk (Caligaris-Cappio, 2003, Burger and Gribben, 2014). *In vitro* simulating the interactions of CLL cells with the microenvironment by co-culturing or stimulating CLL cells with the components from the microenvironment provides a useful model to study the pro-survival signals induced by the microenvironment (Purroy et al., 2015, Boissard et al., 2017, Pascutti et al., 2013, Crassini et al., 2017). Previous work in this research group has shown that co-culturing CLL cells with transfected mouse fibroblasts expressing human CD154 protected CLL cells not only from spontaneous cell death but also from drug-induced cell death (Zhuang et al., 2014, Chapman et al., 2017). Despite the clear cytoprotective effects observed at the cellular level by us and others, the underlying molecular mechanisms are still not well characterized. In addition,

there has been no published MS-based proteomic studies of the CD40 stimulation in CLL. Since MS-based proteomic techniques have the potential to unravel the changes in protein expression at a global level, this project was initiated to investigate the molecular mechanisms mediating pro-survival effects induced specifically by CD40 stimulation in CLL cells through the proteomics approach.

1.6 Hypothesis and aims

The hypothesis of this project was that CD40 stimulation alters the protein expression at a global level, resulting in the survival and drug resistance of CLL cells.

The aim of this study was therefore to investigate the molecular mechanisms underlying the CD40 stimulation-mediated cytoprotective effect in CLL cells by studying the global changes in protein expression induced by CD40 stimulation through the MS-based proteomic approach. Ultimately, it was hoped that the protein(s)/pathways that are critically involved in mediating the pro-survival effect of CD40 stimulation in CLL can be identified and that the therapeutic strategy of intervention can subsequently be developed to overcome CD40 stimulation-induced drug resistance in CLL.

Chapter 2. Methodology

2.1 Introduction

This chapter contains information about the techniques applied in this project and consists of two parts. The first part includes the description of the principles of the techniques and explains the reasons why they were selected for this project. These techniques include flow cytometry, mRNA sequencing, mass spectrometry, and RNA interference (Figure 2.1). Western blotting has been commonly used throughout this project to investigate individual protein targets, so it is included in this chapter. The second part is the description of the operational procedures of the methods used throughout the project.

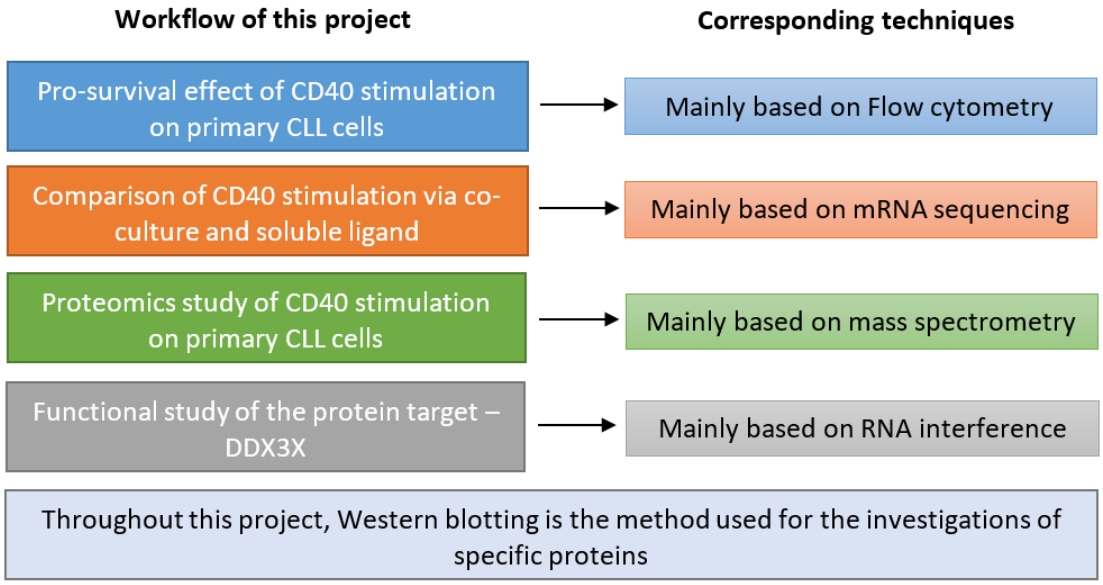

Figure 2.1 Main techniques applied in this project to measure the biological outcomes

2.2 The principles of the key techniques applied in this project

2.2.1 Flow cytometry

In this project, flow cytometry has been applied for the cell death analysis and the cell surface marker assay (to test the phenotype of fibroblasts and the percentage of primary CLL cells co-expressing CD5 and CD19). With flow cytometry, it is possible to simultaneously measure and analyse (even sorting) the multiple physical characteristics of the single cell in a mixture of a sample (Givan, 2001). The flow cytometer generally consists of three

components, the fluidics system, the optics system, and the electronics system (Biosciences, 2000). The fluidics system transports analytes to the laser beam for interrogation. The optics system includes the lasers to illuminate the analytes and optical filters to direct the resulting light signals to the correlated detectors (DaC, 2000). The electronics system then converts the detected light signals into electronic signals for further analysis. The analytes for flow cytometry should be in a fluid stream and the suitable size of analytes ranges from 0.2 to 150µm (Biosciences, 2000). All the analytes in the fluid stream will pass through the laser intercept and scatter laser light, and the fluorescent molecules presenting on the analytes will fluoresce. The scattered laser light is collected by appropriately positioned lenses and finally detected with the help of beam splitters and filters. The scattering light travels in two directions, namely the forward-scattered light (FSC) and the side-scattered light (SSC) (Figure 2.2). FSC is mainly affected by the size of analytes and the SSC is mainly affected by the internal complexity of analytes. SSC is collected at approximately 90 degrees to the FSC (Biosciences, 2000).

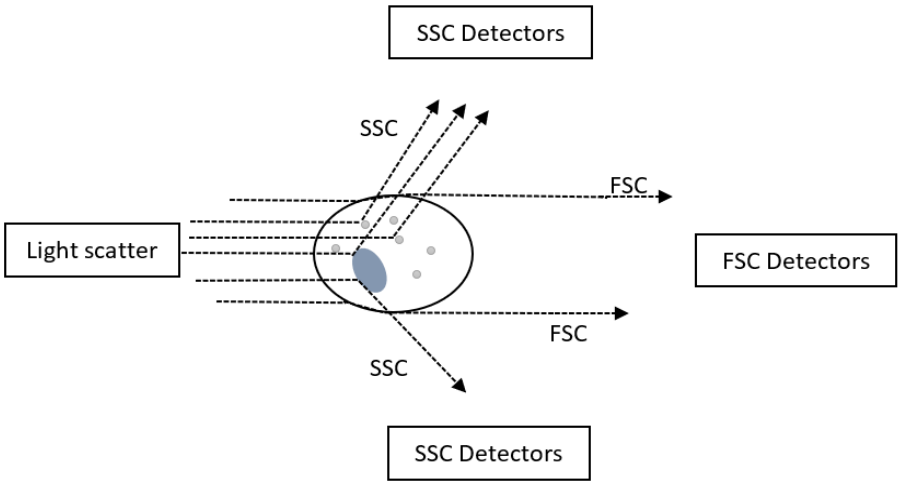

Figure 2.2 Simple schematic diagram of the optics system of a flow cytometer
FSC: forward-scattered light; SSC: side-scattered light.

Fluorescent compounds absorb light energy, and the absorbed energy raises the fluorescent compound to a higher energy level. The excited electron quickly decays to its original status and emits excess energy in the form of a photon of light (Givan, 2011). This transition of energy gives out fluorescence (Givan, 2011). Based on this principle, labelling analytes with different fluorochromes can help to identify and quantify targets on the analytes for

biological analysis on the condition that the combination of the fluorochromes will emit distinguishable wavelengths for individual identification. The most commonly used laser is the argon-ion laser as its light of 488 nm wavelength can excite versatile fluorochromes. The most popular fluorochrome for individual applications is the fluorescein isothiocyanate (FITC) which usually works in the combination with another fluorochrome phycoerythrin (PE) (Shapiro, 2005). With the fast development of the flow cytometer, the maximum number of fluorochromes in combination can reach eighteen.

Here in this project, the fluorochrome combination used for cell death detection was FITC Annexin V together with propidium iodide (PI) or 7-aminoactinomycin (7-AAD). Annexin V is a 35-36 kDa $Ca2^{+}$ dependent phospholipid-binding protein and has a high affinity for phosphatidylserine (PS) (Pharmingen). In a healthy cell, PS residues are usually retained in the inner leaflet of the cell membrane. When cells undergo apoptosis, the PS will translocate to the outer side of the cell membrane and the Annexin V can bind to the exposed PS to identify the apoptotic cells at an early stage (Abedin et al., 2007, Turcotte et al., 1994). PI is used as a fluorescent reagent to stain the nucleic acids (DNA) of the cells (Ormerod, 1998). PI is cell membrane impermeant and thus excluded from viable cells with intact membranes. However, when the cell membrane becomes permeabilised or disrupted during late apoptosis or necrosis, PI will enter the cells and bind to DNA with high affinity. PI is used together with Annexin V to identify apoptotic cells in the late stage. Alternatively, 7-AAD is also used as a fluorescent dye to identify apoptotic cells in the late stage. 7-AAD has a high binding affinity with DNA when the cell membrane becomes permeabilized or disrupted by apoptosis or necrosis (Zimmermann and Meyer, 2011). In this way, the combination of FITC Annexin V with PI/7-AAD works together to identify cells that undergo early and late-stage apoptosis. The FITC Annexin V positive and PI/7-AAD negative cells are under the early apoptotic stage. The FITC Annexin V and PI/7-AAD double-positive cells are under the late apoptotic stage whereas cells double negative for FITC Annexin V and PI/7-AAD are considered to be viable (Figure 2.3).

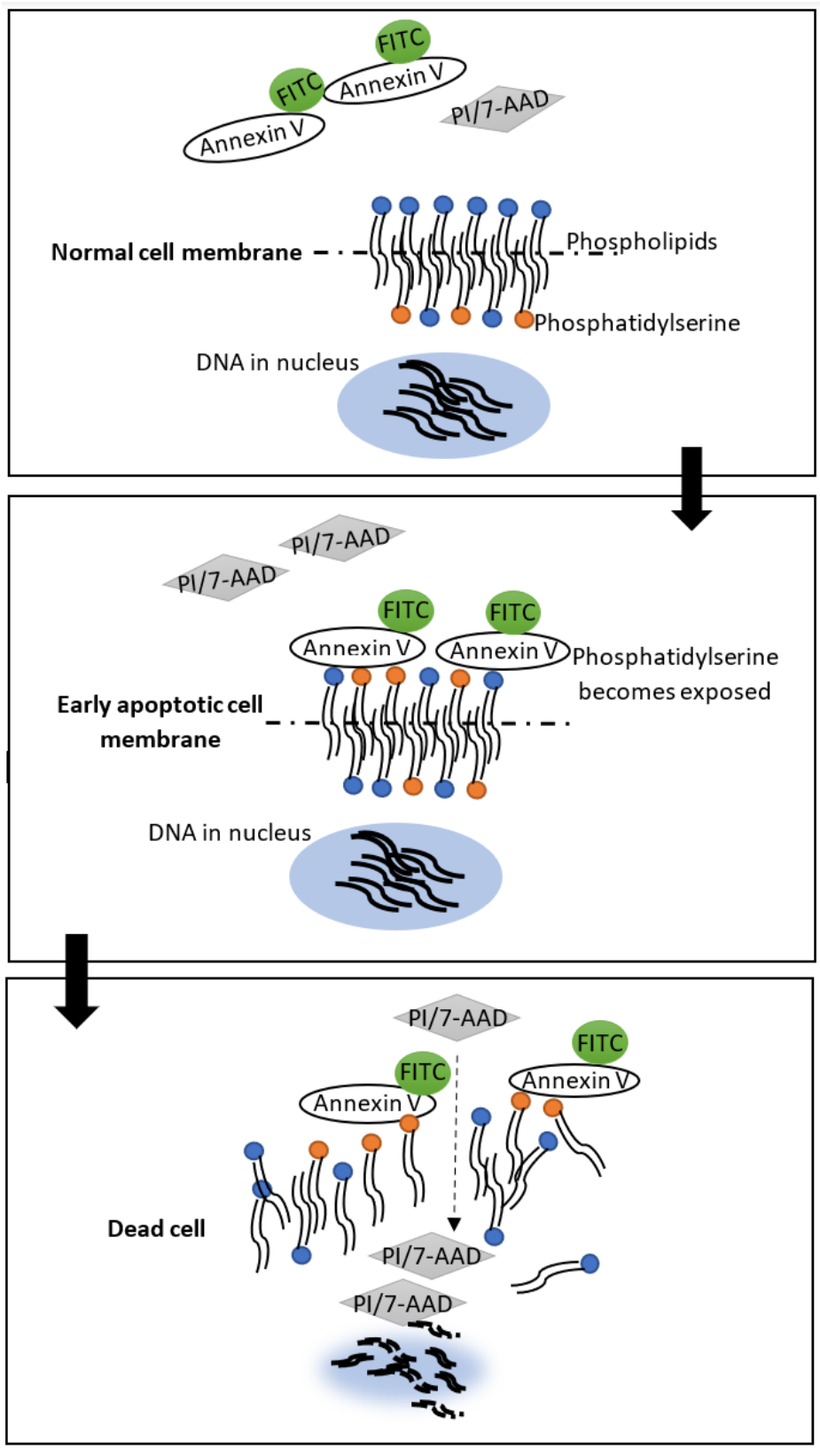
FITC
Annexin V
FITC
Annexin V
PI/7-AAD
Normal cell membrane
Phospholipids
Phosphatidylserine
DNA in nucleus
PI/7-AAD
PI/7-AAD
FITC
Annexin V
FITC
Annexin V
Phosphatidylserine
becomes exposed
Early apoptotic cell
membrane
DNA in nucleus
PI/7-AAD
FITC
Annexin V
FITC
Annexin V
Dead cell
PI/7-AAD
PI/7-AAD

A.

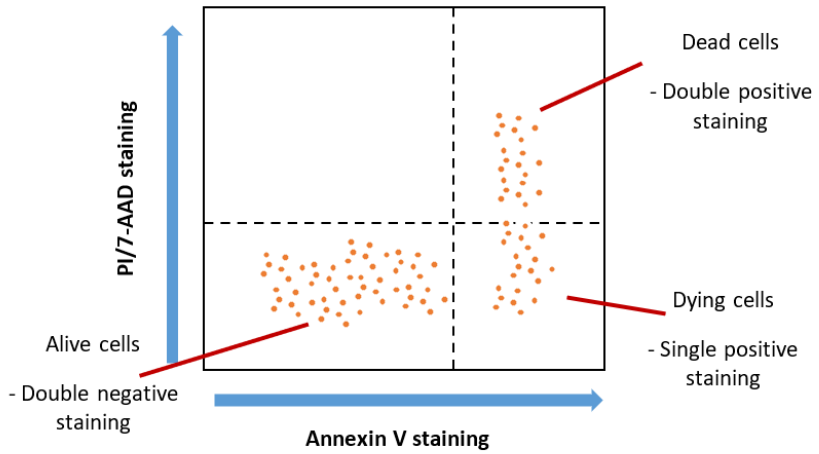

B.

Figure 2.3 Schematic diagram of cell death detection by flow cytometry using Annexin V and PI/7-AAD. (A) shows how the Annexin V and PI/7-AAD binding to the dying and dead cells. PS residues are usually retained in the inner leaflet of the healthy cell membrane. When cells undergo apoptosis, the PS translocates to the outer side of the cell membrane and the Annexin V can bind to the exposed PS to identify the apoptotic cells at an early stage. When the cell membrane becomes permeabilised or disrupted during the late apoptosis or necrosis, PI will enter the cells and bind to DNA with high affinity. 7-AAD also has a high binding affinity with DNA and it works like PI. (B) shows an example of the results of cell death detection using the combination of FITC Annexin V with PI/7-AAD works together to identify cells that undergo early and late-stage apoptosis. The FITC Annexin V positive and PI/7-AAD negative cells are under the early apoptotic stage as shown in the lower-right corner. The FITC Annexin V and PI/7-AAD double-positive cells are under the late apoptotic stage as shown in the upper-right corner. Cells double negative for FITC Annexin V and PI/7-AAD are considered to be viable as shown in the lower-left corner.

Comparing with other techniques to identify the apoptotic cells, flow cytometry is quicker and more efficient with the minimum amount of cells needed (Olson et al., 1993). It is particularly suitable in assays where the aim of the experiments is to quickly measure the percentage of cell death in response to drug treatment.

Flow cytometry was also applied in this project for monitoring the surface expression of human CD154 in the transfected mouse fibroblasts and the percentage of CLL cells co-expressing CD5 and CD19 among the peripheral blood mononuclear cells (PBMCs) samples from individual patients with CLL. In the former case, stably transfected mouse embryonic fibroblasts expressing human CD154 were used in the co-culture experiments for CD40 stimulation of CLL cells. The parental mouse fibroblasts which were also stably transfected with an empty vector were used as a control in co-culture experiments. The phenotypes of

the fibroblasts were thus regularly checked by flow cytometry to ensure that the correct fibroblasts were used for CD40 stimulation. In the case of CLL samples, as the proportion of CD5 and CD19 double-positive CLL cells among the PBMC samples varies from individual patients, the percentage of CLL cells co-expressing CD5 and CD19 in every PBMC samples used in the study was monitored by flow cytometry to ascertain the level of contamination from other types of cells such as T cells and monocytes.

2.2.2 mRNA sequencing

The mRNA sequencing technique applied in this project was the RNA-seq, a next-generation sequencing (NGS) technique that has become the method of choice for RNA sequencing analysis after 2012. The entire process for sequencing applied in this project consisted of preparation of biological samples, RNA extraction, RNA sample quality, and quantity test, library construction, sequencing, data processing (quality control, mapping, quantification), and data analysis (Conesa et al., 2016). To be specific, biological sample preparation and RNA extraction together with the quantification and purity tests for all the RNA samples were conducted in this laboratory before sending them to a commercial company (NOVOGENE plc, Hong Kong, China) for sequencing. The sequencing data analysis was supported by the bioinformatics group at the Computational Biology Facility at the University of Liverpool.

For the NGS technique, the mRNA isolated from the whole RNA extracted from biological samples is fragmented and converted to the complementary DNA (cDNA). The cDNA is then combined with adaptors and further amplified. The adaptor ligated to the cDNA includes the sequencing primer binding site, the index, and the region complementary to the flow cell oligo. Each part has two types that fit the two ends of cDNA separately. The following process is the cluster generation where prepared cDNA binds to the oligos within the flow cell and generates the correlated complementary strand. The original strand cDNA is washed away leaving the complementary strand for bridge amplification. During the bridge amplification, the left strand bends over, binds to the complementary oligo, and works as the template to generate the double-stranded cDNA with each of the strands attached to the flow cell with their different end oligo. The double strands denature and generate one forward strand and one reverse strand. The bridge amplification is repeated with millions of

clusters simultaneously resulting in the clonal amplification for all the clusters. After the bridge amplification, the reverse strands are washed off leaving only the forward strands in the flow cell and all the forward strands work as the template for sequencing synthesis and paired-end sequencing synthesis to read out the forward and reverse strands. The whole process description was derived from the online information provided by Illumina and the schematic of the process is shown in Figure 2.4.

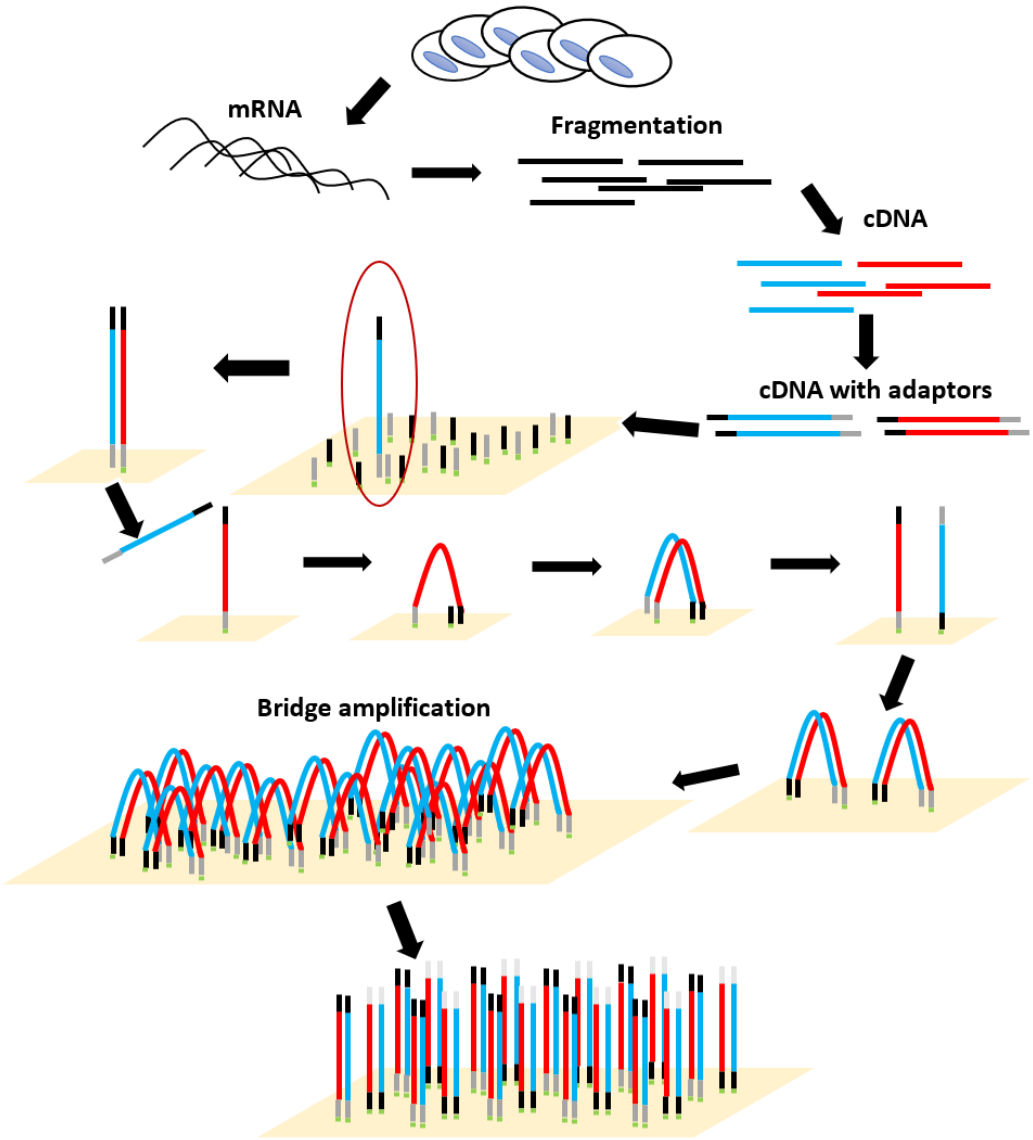

Figure 2.4 Schematic diagram of the NGS principle. mRNA isolated from the whole RNA extracted from biological samples is fragmented and converted to cDNA. The cDNA is then added with adaptors and amplified. The original strand cDNA is washed away leaving the complementary strand for bridge amplification. During the bridge amplification, the left strand bends over, binds to the complementary oligo, and works as the template to generate the double strands cDNA. The double strands denature and generate one forward strand and one reverse strand. The bridge amplification is repeated with millions of clusters simultaneously resulting in the clonal amplification for all the clusters. Then, the reverse strands are washed off leaving only the forward strands in the flow cell and all the forward strands work as the template for sequencing synthesis and paired-end sequencing synthesis to read out the forward and reverse strands.

NGS is the latest sequencing technique that has been commonly used nowadays. Comparing with the microarray sequencing, NGS does not need prior knowledge for the design of probe sets, which makes it more economic and efficient.

2.2.3 Mass spectrometry-based proteomic approaches

Liquid chromatography mass spectrometry (LC-MS/MS) technique provides a sensitive and efficient way to analyse proteins both qualitatively and quantitatively. The key aim of this project was to investigate the CD40 stimulation-induced pro-survival effect on primary CLL cells mediated through changes in protein expression. To identify the changes in protein expression induced by CD40 stimulation at a global level, the protein expression of CD40 stimulated primary CLL cells was compared with that of their unstimulated counterparts.

Mass spectrometry (MS)-based proteomics is an advanced technique, and its application leads to comprehensive identification and quantification of proteins expressed in a cell/tissue-specific manner. The advantage of MS-based discovery proteomics techniques is that they require no prior knowledge of what proteins are presenting in a particular cell/tissue sample and that they can identify and quantify hundreds and thousands of proteins simultaneously (Schulze and Usadel, 2010). MS-based approaches have been shown to detect the changes in protein expression associated with different stages of a disease or different treatments (Han, 2010, Zhang et al., 2019).

Basically, there are two forms of proteomics study which are also called the ‘top-down’ and the ‘bottom-up’ approaches (Chait, 2006). The ‘top-down’ type of proteomics study refers to identifying and quantifying proteins by analysing the intact proteins, such as analysing the intact proteins using a mass spectrometer, tandem mass spectrometry, and two-dimensional gel electrophoresis in combination with tandem mass spectrometry (Kelleher, 2004, Sze et al., 2002, Wright et al., 2014). This is a relatively slow process and it requires proteins to be presented to the mass spectrometer in a semi-pure state. In contrast, the ‘bottom-up’ type of proteomics study means identifying and quantifying proteins by analysing the sequence of amino acids of peptides that are generated from digested proteins (Chait, 2006, Aebersold and Mann, 2003). In this project, we use a bottom-up proteomics approach to identify and relatively quantify proteins: the complexity of samples

from the CD40 stimulated and unstimulated primary CLL cells makes this relatively high throughput approach more suitable.

The entire process performed by a mass spectrometer consists of three parts which are the sample ionisation, ion selection, and ion/mass detection (Gross, 2006). In this project, the instrument of mass spectrometry used was the TripleTOF6600 (Sciex) (Figure 2.5). Specifically, samples of mixed peptides are suspended in solution and these in-solution peptides are sprayed into the instrument by electrospray ionisation (Klein et al., 1997, Hopfgartner et al., 2004). During the spray, the peptides are heated and ionised, from which the peptides adopt 1 or more protons (Awad et al., 2015, Koomen et al., 2005). The ionised peptides then enter the instrument and via a mini-quadrupole (QJet) and a slightly larger quadrupole Q zero (Q0), they reach the chamber of Q1 that has four parallel metal rods arranged in a circle. By adjusting the voltages of the device of Q1, it is manageable to select the range of mass-to-charge ratio (m/z) for analytes (Hunter and Seymour, 2015). Generally speaking, researchers will set the voltage to cover the entire range firstly. Then, if the researchers will target at any special analytes, they will adjust the settings of Q1 with specific m/z range to select analytes of interest (Chernushevich et al., 2001, Chernushevich and Thomson, 2003). The ionised peptides coming out from the Q1 enter the next chamber, linear accelerator (LINAC), in which the collision-induced dissociation (CID) happens to further fragment the peptides for the purpose of amino acid sequencing read out. In the chamber of LINAC, ionised peptides are bombarded with high energy nitrogen for further fragmentation and the sequence of amino acids can be determined due to the places of breakage induced by CID on the peptide backbone can be reasonably predictable (Koomen et al., 2005). The last part of the TripleTOF6600 is the time-of-flight (TOF) tube where the m/z of peptides are measured based on the principle that the time an ion takes to travel the reflected distance in the instrument is proportional to its m/z (Cotter, 1999, Koomen et al., 2005). When it comes to the calculation of the mass of peptides from its m/z, it can be explained by taking the positive ion mode as an example. The charge is conferred by the adoption of a proton or protons H^+ and an H^+ has a mass of amu (atomic mass unit, 1 amu = 1 Da = 1g/mol). Taking a peptide of 1529.8204 Da as an example, the singly charged ion of this peptide will have an m/z of (1529.8204+1)/1 = 1530.8204; the doubly charged ion of this peptide will have an m/z of (1529.8204+2)/2 = 765.9102; the triply charged ion of this

peptide will have an m/z of (1529.8204+3)/3 = 510.9401. When the MS presents the spectrum results as Figure 2.6, the first peak in Figure 2.6 A will be identified as the doubly charged ion of the peptide 1529.8204 Da and the first peak in Figure 2.6 B will be identified as the triply charged ion of the peptide 1529.8204 Da. The mass spectrometer can identify the isotopic series as well. Taken the ^{12}C and ^{13}C as an example, it has been known that 99% of the carbon atoms occur as ^{12}C and only 1% of the carbon atoms occur as ^{13}C in nature and ^{13}C is 1 amu heavier than ^{12}C (O'Leary, 1988). If all the carbon atoms in the peptide of 1529.8204 Da turn out to be ^{12}C, the doubly charged ion of this peptide will have an m/z of 765.9102 as the first peak from the left in Figure 2.7. If one of the carbon atoms in this peptide turns out to be ^{13}C, the doubly charged ion of this peptide will have an m/z of 766.4116 as the second peak from the left in Figure 2.7. If two of the carbon atoms in this peptide turn out to be ^{13}C, the doubly charged ion of this peptide will have an m/z of 766.9118 as the third peak from the left in Figure 2.7. The proteins can be identified using a mass spectrometer by searching the peptide and fragment ion m/z values against a publicly available database such as SwissProt.

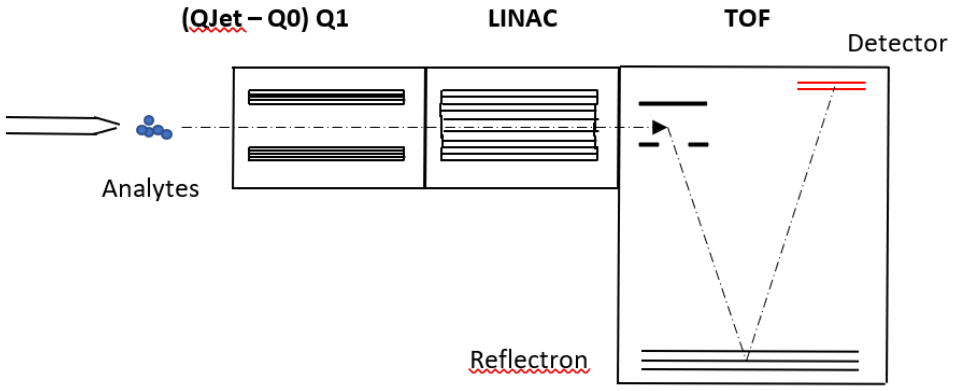

Figure 2.5 Schematic diagram of the QqTOF process of the Triple TOF® 6600 machine. Peptides in solution are sprayed through a very fine needle and are heated and ionised at the same time. Via the QJet and the Q0, ions enter the Q1. The voltages can be adjusted to select the range of mass or m/z according to the aim of the study. Then, ions enter the chamber of LINAC where the process of collision-induced dissociation (CID) takes place. The ionised peptides are bombarded with high energy nitrogen gas for fragmentation. The last part of the TripleTOF6600 is the time-of-flight (TOF) tube where the m/z of peptides are measured based on the principle that the time an ion takes to travel the reflected distance in the instrument is proportional to its m/z

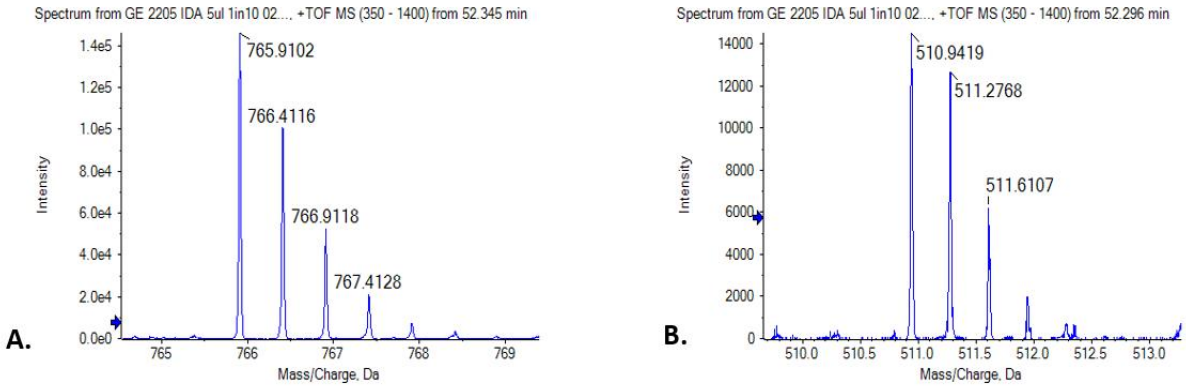

Figure 2.6 An example of the spectrum result of MS. The x-axis represents the number of m/z; the y-axis represents the intensity of peptides. (A) The spectrum is identified as the doubly charged ion of the peptide of 1529.8024. (B) The spectrum is identified as the triply charged ion of the peptide of 1529.8204.

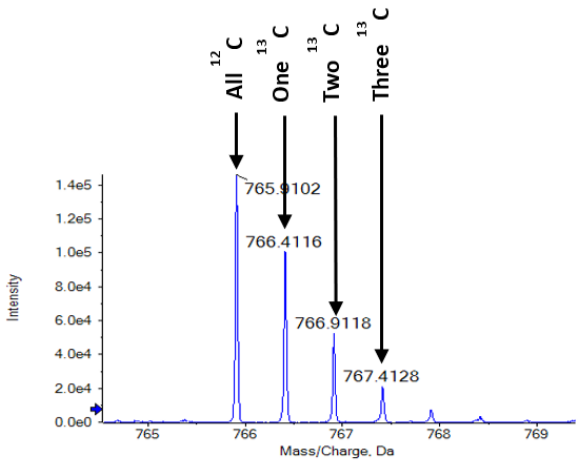

Figure 2.7 An example of the identification of isotopic series results of MS. The x-axis represents the number of m/z; the y-axis represents the intensity of peptides. The first peak from the left side is identified as the doubly charged ion of the peptide of 1529.8204 Da in which all the carbon atoms in it occur as ^{12}C and it is a monoisotopic peptide. The second peak from the left side is identified as the doubly charged ion of this peptide in which one of the carbon atoms in it occurs as ^{13}C. The third peak from the left side is identified as the doubly charged ion of this peptide in which two of the carbon atoms in it occur as ^{13}C.

The method of quantitative MS-based proteomics applied in this project was the isobaric tags for relative and absolute quantification (iTRAQ). The protein quantification methods based on mass spectrometry can be divided into two forms, label-free and label-based approaches (Patel et al., 2009). The labelling techniques depending on cell division, such as stable isotope labelling by amino acids in cell culture (SLIAC), are not appropriate for this

project because the primary CLL cells obtained from the peripheral blood of the patients are in cell-cycle arrest and they do not proliferate *in vitro*. Meanwhile, the limitation of the numbers and amount of primary CLL samples makes the label-free approaches such as SWATH (Sequential Windowed Acquisition of All Theoretical fragments) inappropriate as they require a certain amount of samples to establish a specific library for the global protein expression of the tissue in question (for example the protein expression profiles of the CD40-stimulated and unstimulated primary CLL cells) (Pham et al., 2012). Also, the statistical power of these types of approaches requires analysing a large number of samples. The iTRAQ labelling approach allows proteins/peptides from different samples to be analysed simultaneously and it increases the sensitivity of peptides detection by its additive effect in the mass spectrometer. Generally speaking, the same liquid chromatography mass spectrometry (LC-MS) method can be run to achieve reliable data across a cohort of samples. However, in reality, the more times of running the samples, the more variations will generate (Musenga and Cowan, 2013, Nováková, 2013). The multiplexed labelling principle of iTRAQ decreases the number of LC-MS acquisitions, which further reduces the technical-generated variations. Considering the minimum number of biological replicates (referring to the number of primary CLL cases) required, as suggested by bioinformaticians to achieve statistical confidence with the data generated, iTRAQ 8-plex was selected as the suitable option for this project.

The principle of iTRAQ was established by Thompson et al. in 2003. iTRAQ is a tandem mass spectrometry-based quantification technique that requires the peptides to be fragmented before being quantified. iTRAQ-labelled peptides from several samples are pooled and analysed simultaneously, and this process provides information on peptide amino acid sequence and the relative abundance across labelled samples (Thompson et al., 2003). The 4-plex version of iTRAQ was further described by Ross PL and colleagues in 2004 (Ross et al., 2004) and three years later, iTRAQ was developed into the 8-plex version, which increases the utility of this technique. The 8-plex multiplexing labelling technique is very efficient when studying the protein expression in different biological conditions simultaneously and it enhances the accuracy of statistical analysis (Choe et al., 2007).

All of the iTRAQ labelling tags have the same mass, that is they are isobaric, and they consist of three parts (Figure 2.8): a reporter group, a mass balance group, and an amine reactive

group (Thompson et al., 2003). The reactive group binds to peptides through the N-terminus and lysine side chains. The mass of the balance group varies depending on the different mass of the corresponding reporter group in order to keep the overall mass of the tags the same. The reporter and the balance groups will be released from peptides during the fragmentation process in the mass spectrometer (labelled with red arrows in Figure 2.8), and the difference in abundance of the reporter ions provides relative quantitation of that peptide across all the samples. The relative quantitation of proteins is extrapolated from the average ratio of the released reporter ions from all the peptides derived from an individual protein. At the same time, the spectra detected by the tandem mass spectrometry process provide the information of the amino acid sequence of peptides, which reveals the identity of the peptide/protein (Ross et al., 2004).

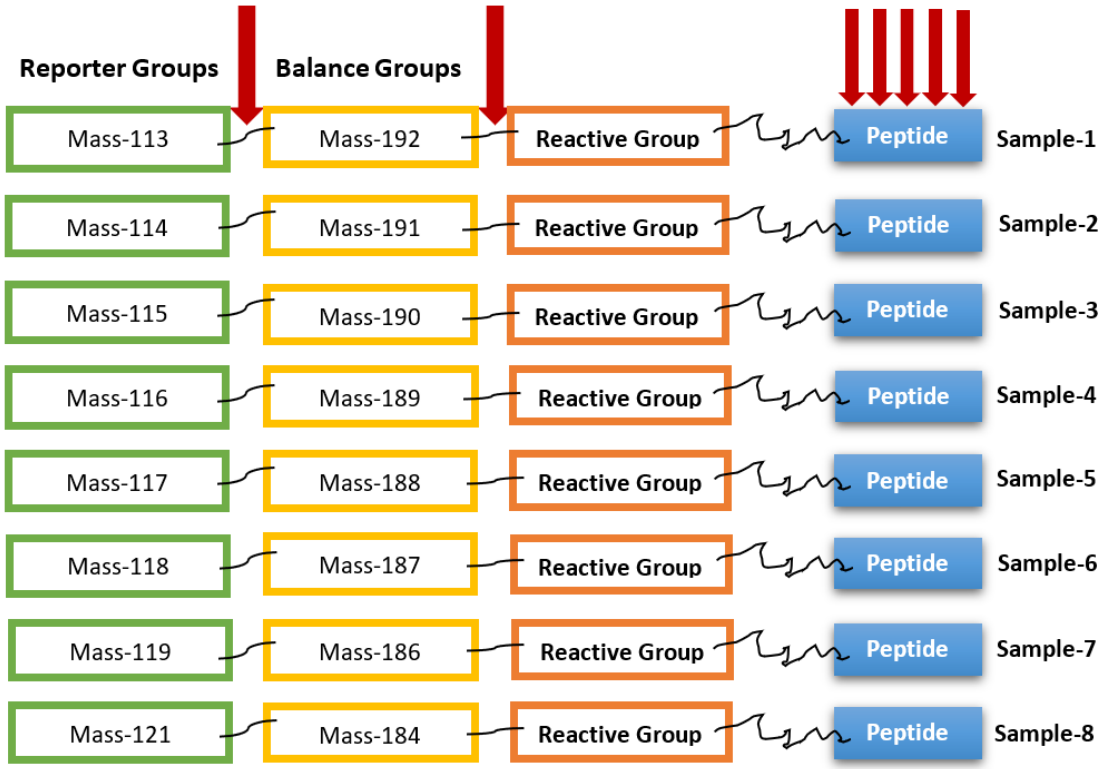

Figure 2.8 Schematic diagram of the iTRAQ 8-plex labelling tags. The isobaric mass tags of iTRAQ consist of three parts: a reporter group, a mass balance group, and an amine reactive group. They label peptides at the N-terminus and lysine side chains by the reactive groups. During the fragmentation, the reporter and the balance groups will be released from peptides (labelled with red arrows) and the relative abundance of the reporter is used to extrapolate the relative abundance of corresponding proteins.

After labelling samples using iTRAQ 8-plex, two stages of pre-fractionation were performed on the labelled peptides to increase proteome coverage and accuracy of the analysis. The principles for the pre-fractionation applied in this project were the high-performance liquid chromatography (HPLC), the ion exchange chromatography, and the gradient analysis.

HPLC is a commonly used automatic technique with high efficiency and sensitivity and it usually consists of four parts, the pump with high pressure, the injection and loading system, the separation process by running through the column, and the detection (Snyder et al., 2012). There are three major modes of HPLC separation that are based on polarity, charge, or size. For the separation based on polarity, there is the normal phase (Figure 2.9 A) and the reverse phase (Figure 2.9 B) HPLC. The column plays the role of the stationary phase and the molecules in the mobile phase run through the column to be separated. In the normal phase, the column is polar hydrophilic, which delays the polar molecules and helps the non-polar molecules run through faster. In contrast, in the reverse phase, the column is non-polar hydrophobic, which delays the non-polar molecules and helps the polar molecules run faster from the column (Gilar et al., 2005). Comparing with the normal phase, the reverse phase HPLC has a wider range of molecule applications and is more commonly applied in organic analytes.

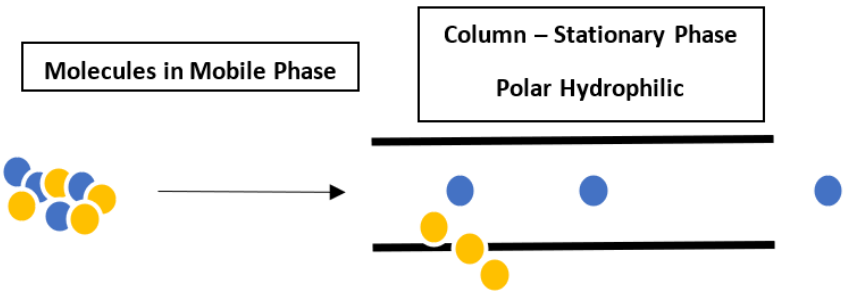

A. Normal phase

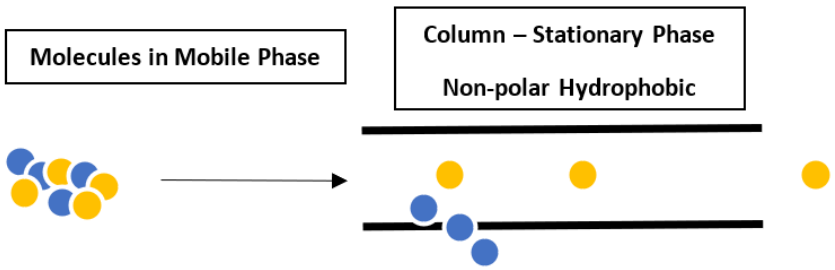

B. Reverse phase

Figure 2.9 Schematic diagrams of the normal and reverse phase separation. Blue spots: the non-polar molecules. Yellow spots: the polar molecules. (A) the normal phase column is polar hydrophilic, which delays the polar molecules and helps the non-polar molecules run through faster. (B) the reverse phase column is non-polar hydrophobic, which delays the non-polar molecules and helps the polar molecules run faster from the column.

Cation exchange chromatography is one type of ion exchange chromatography. Ion exchange chromatography is a process that separates or purifies ions and polar molecules based on their affinity to the ion exchanger applied and it has been widely applied in the charged molecules including proteins, peptides, nucleic acids, and nucleotides (Acikara, 2013, Yamamoto et al., 1988). The cation exchange chromatography contains a negatively charged stationary phase and positively charged molecules in the mobile phase will be attracted (Cummins et al., 2017), which makes it usually applied in the molecules of interest that are positively charged (Figure 2.10 A). The other type of ion exchange chromatography is the anion exchange chromatography. Inversely to cation exchange, the anion exchange chromatography contains a positively charged stationary phase and negatively charged molecules will be attracted (Cummins et al., 2017), which makes this type of ion exchange chromatography applied in the molecules of interest are negatively charged (Figure 2.10 B). Here in this project, we used the cation exchange chromatography (column: 200×4.6mm, 5µm, 300A, Poly LC, Columbia, MD) resulting from the fact that we used trypsin to digest

proteins. Trypsin is a commonly used protease that hydrolyzes proteins by cleaving the peptides on the C-terminal side of the amino acid residues lysine and arginine (Olsen et al., 2004) and fully tryptic peptides are usually positively charged under acidic conditions, which makes cation exchange chromatography appropriate for this project.

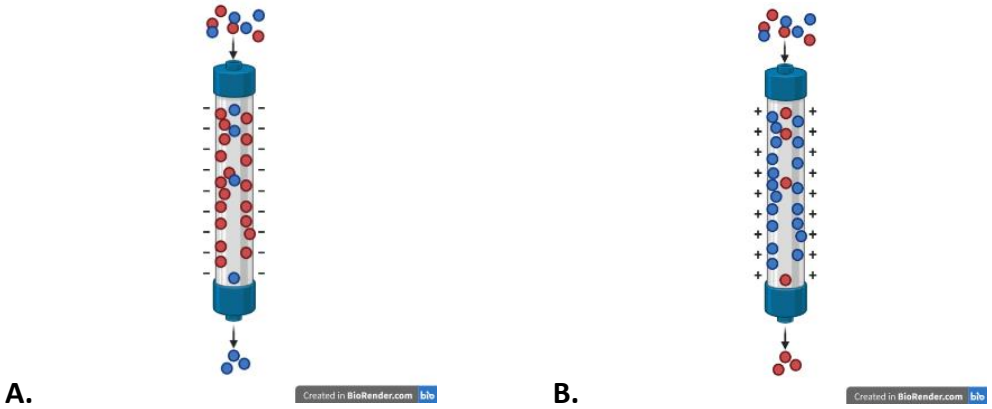

Figure 2.10 Schematic diagrams of the two types of ion exchange chromatography. Red spots: positively charged molecules; blue spots: negatively charged molecules. (A) shows the process of cation exchange chromatography. The stationary phase, the column, of cation exchange chromatography is negatively charged. Positively charged molecules in the mobile phase will be attracted and the negatively charged molecules will pass through. (B) shows the process of anion exchange chromatography. The stationary phase of anion exchange chromatography is positively charged. Negatively charged molecules in the mobile phase will be attracted and positively charged molecules will pass through.

Another key principle commonly applied in the separation is the gradient analysis. The gradient analysis is the process that using buffers consist of two or more solvents and the composition of the components in the buffers are programmed to change during the elution, which manages to further separate a specific type of molecules (the polar/non-polar molecules, the positively/negatively charged molecules) (Schoenmakers, 1986, Patil, 2017). Taking cation exchange as an example, firstly, the positively charged molecules are attracted by the negatively charged column and the negatively charged molecules pass through the column directly. The application of the gradient analysis can further separate the positively charged molecules binding to the column by eluting with the special buffer increasing the concentration of the positively charged components sequentially (Figure 2.11). The positively charged components in the buffer will displace the positively charged

molecules binding to the column. The higher the concentration of the positively charged components, the more positively charged molecules can be eluted from the column.

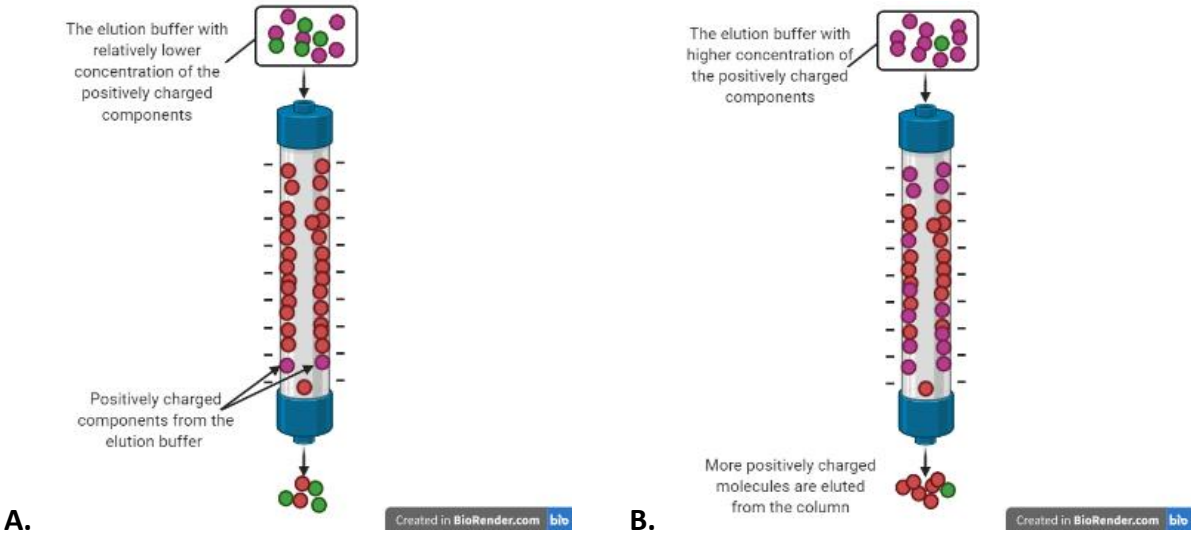

Figure 2.11 Schematic diagrams of the gradient analysis. The red spots represent the positively charged molecules from the samples to be analysed and they are binding to the negatively charged column of the cation exchange chromatography. The purple spots represent the positively charged components from the elution buffer. The green spots represent the negatively charged components in the elution buffer. (A) With relatively lower concentrations of the positively charged components in the elution buffer, the positively charged molecules binding to the column are eluted with the positively charged components from the elution buffer taking place in the column. (B) With a higher concentration of the positively charged components in the elution buffer, more positively charged molecules are eluted from the column.

Due to the complexity of the organic analytes in biology study, using only one simple separation is absolute not enough to separate the abundant mixture of peptides. As mentioned above, there were two stages of the pre-fractionation of the peptides applied in this project. The iTRAQ labelled protein samples were digested by using trypsin. The first stage peptides separation was performed by using cation exchange chromatography. When loaded the mixture samples of the positively charged tryptic peptides into the column of cation exchange chromatography, they were first attracted to the column with the negatively charged passing through the stationary phase. The elution buffer applied here was a gradient buffer with different levels of positively charged ions that took place the positively charged peptides in the column during the elution. With the increasing concentration of the positively charged ions in the elution buffer, the positively charged

peptides binding to the column were gradually eluted from the column based on their charges. The fractions of peptides obtained from the first stage separation were then desalted by a reversed phase cartridge and dried. The second stage of separation was performed by using the Eksigent NANO LC 415 (Eksigent) in-line with the mass spectrometer. The dried fragments of peptides were resuspended and submitted to the Eksigent NanoLC 415. The Eksigent NanoLC 415 automatically separated the analysed the peptides with gradient analysis together with the reverse phase HPLC processes. The sequential separation reduces the complexity of the peptide mixture presented to the MS at any one time, which increases the number and dynamic range of the peptides that can be captured.

The LC-MS/MS-based iTRAQ technique is selected for the proteomics study in this project as it can accommodate the characteristics of primary CLL cells and fulfil the aims and design of the proteomics study for this project. However, the LC-MS/MS-based iTRAQ technique still has limitations. As described above, the entire procedure of this LC-MS/MS-based iTRAQ technique consists of multiple steps, and the operation of each step influences the final proteomics analysis. The condition of sample preparation is fundamental for MS-based proteomics study. Primary CLL cells are mostly non-proliferative cells and the high level of spontaneous apoptosis of these cells in culture conditions affects the repertoire of proteins extracted. The efficiency of iTRAQ labelling is a significant factor for the quality of the proteomics data. During the iTRAQ labelling in this study, a manufacturing issue with the iTRAQ reagents was encountered, which leads to the consequence that a group of samples was unlabelled. It was unpredictable and this step was redone after the manufacture provided a new kit. The LC-MS/MS-based iTRAQ technique cannot capture all the proteins expressed in samples. The quality of the protein samples to be analysed was checked by two-dimensional peptide separation before mass spectrometry processes to avoid the loss of protein identification due to the complexity of samples. Special types of proteins may be poorly captured and identified by mass spectrometry, such as membrane proteins (protein solubility), cytokines and chemokines (protein abundance), and protein expelled from cells. The degradation during every step of the entire procedure is another issue affecting the proteomics analysis. It is necessary to point out that the design of the LC-MS/MS-based iTRAQ technique applied in this project is not appropriate to capture the post-translationally

modified proteins. With prudent design and carefully operating in all steps, it was confident that obtaining a comprehensive understanding of the influences induced by CD40-stimulation in primary CLL cells at the translational level was reliable by using the LC-MS/MS-based iTRAQ technique.

2.2.4 siRNA knockdown

The knockdown technique applied in this project was small interfering RNA (siRNA) knocking down which is one of the RNA interference (RNAi) techniques. Upon entering cells, the long dsRNA will be processed by DICER (a dsRNA-specific RNase III enzyme) which produces the double-strand RNA of 21-23 bases (JAGLA et al., 2005). These RNAs then incorporate into the RNA-induced silencing complex (RISC) where one of the strands will be removed (Birmingham et al., 2007). The remaining strand of the RNA binds to the mRNA of the target gene through the complementary sequence and induces its degradation, effectively stopping the mRNA from being translated into proteins (Carthew and Sontheimer, 2009). The main processes of siRNAs knockdown have been summarised in Figure 2.12.

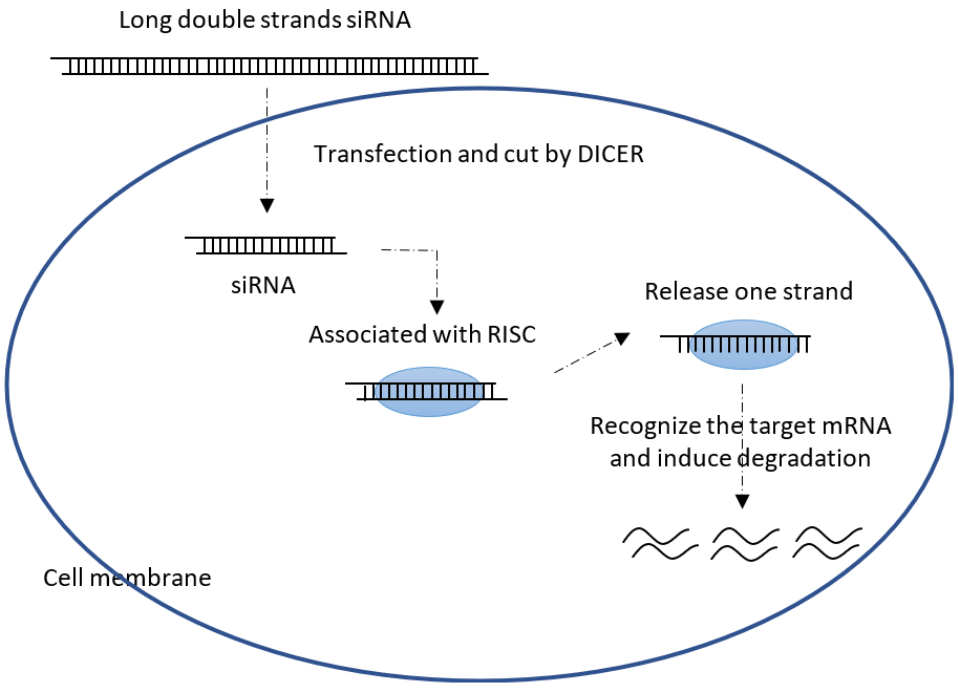

Figure 2.12 Schematic diagram of the siRNA knockdown process. The long double-strand (ds) RNA firstly enters the cells through the cell membrane. The long dsRNA is then cut by DICER, which produces siRNAs of 21-23 bases. These siRNAs then incorporate into RISC with one of the strands removed. The remaining strand of siRNA binds to the mRNA of the target gene through the complementary sequence and induces its degradation, effectively stopping the mRNA from being translated into proteins.

With the rapid development of the RNAi techniques, there are many other tools which can be used for gene silencing experiment such as short hairpin RNAs (shRNAs) and clustered regularly interspaced short palindromic repeats (CRISPRs). shRNA is an artificial RNA molecule that has a hairpin turn (Paddison et al., 2002, Brummelkamp et al., 2002). When it is delivered into targeted cells, it will generate siRNAs stably to silence target gene expression (Brummelkamp et al., 2002). Using shRNAs to silence target gene expression requires help with plasmids or viral/bacterial vectors to deliver the shRNAs into cells (Brummelkamp et al., 2002, Wang et al., 2011b). CRISPR is a family of DNA sequences that have been found in the genomes of prokaryotic organisms such as bacteria and it can detect and destroy DNA from similar bacteriophages during infections (Barrangou, 2015). Together with an enzyme, CRISPR-associated protein 9 (Cas9), CRISPR is now applied in scientific research to edit genes in organisms (Zhang et al., 2014, Hsu et al., 2014). Using shRNA or CRISPR-Cas9 to silence target gene expression may achieve a long-term effect but to

produce the specific constructs and generate cells consistently not expressing the target gene take a lot of time (Boettcher and McManus, 2015). Considering the experimental design, the cost, and benefit effectiveness, siRNAs knockdown is selected for this project.

2.2.5 Western blotting

So far, Western blotting is still the most frequently used method for the identification of specific in-cell proteins and relative quantification because of its relatively low cost and easy to use. It has been used through all this project to investigate the expression level of specific proteins. The basic process of Western blotting analysis (Figure 2.13) consists of protein extraction from biological samples, protein quantification, separation by sodium dodecyl sulphate polyacrylamide gel electrophoresis (SDS-PAGE), protein transfer to the membrane, antibodies probing detection, visualized detection, imaging, and densitometry analysis.

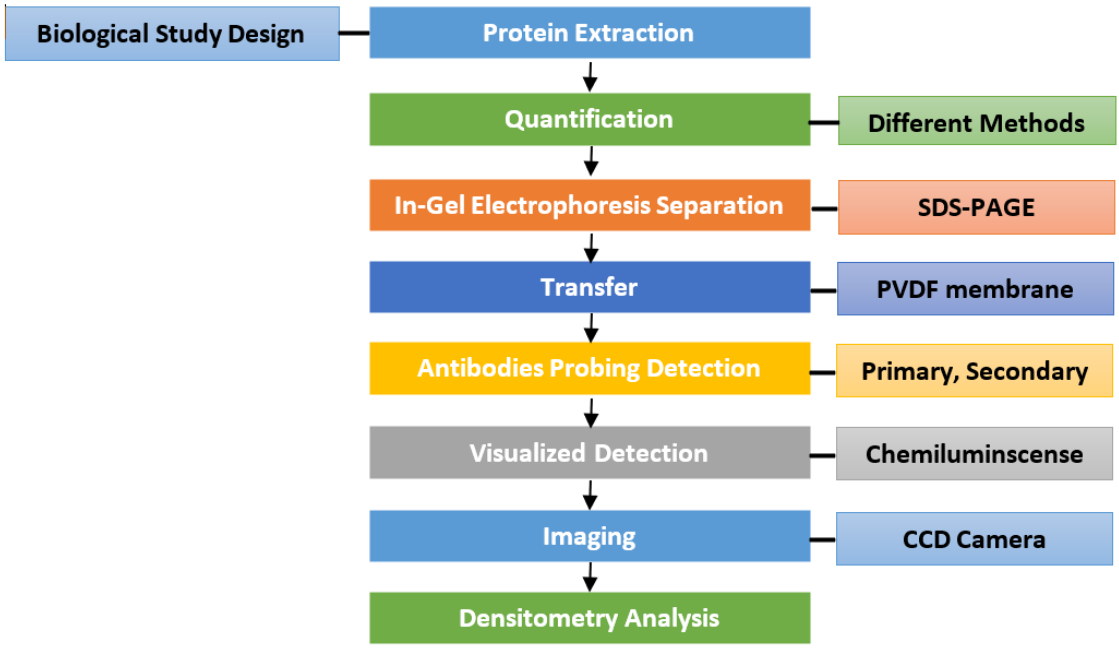

Figure 2.13 The workflow of the process of Western blotting. Proteins are extracted from the targeted cellular samples and quantified to calculate the same amount of proteins for SDS-PAGE separation. The proteins separated in gels are then transferred to PVDF membranes and be detected for visualization. The relative amount of the expression of targeted proteins is concluded by analysing the densitometry of the protein bands.

In practice, cells are first lysed for protein extraction. Protein samples are quantified by different biochemical methods to work out the concentrations of protein for individual samples. A set amount of proteins from each sample are loaded on the pre-set gel usually made of an acrylamide solution.

In-gel protein separation by electrophoresis is the key process in which proteins can be separated according to their molecular weight and be identified with the help of the pre-stained protein marker. Usually, the polyacrylamide gels with different concentrations are used as the supporting medium and sodium dodecyl sulphate (SDS) is used to denature the proteins, a process known as SDS-PAGE (sodium dodecyl sulphate polyacrylamide gel electrophoresis) (Kurien and Scofield, 2006). When the gel is placed under an electric field, the charged molecules within the gel will run from one end to the other. The SDS within the gel binds to proteins and form a negatively charged layer around proteins regardless of their inherent charge (Kurien and Scofield, 2006). In this way, when proteins travel on the gel under electrophoresis, they will be separated depending only on their molecular weight (Figure 2.14).

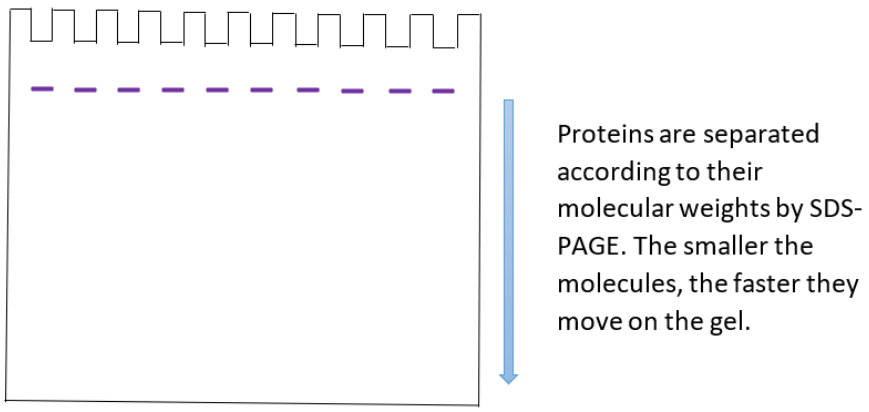

Figure 2.14 Schematic diagram of SDS-PAGE. A set amount of proteins from each sample (the purple lines) are loaded on the pre-set gel made of an acrylamide solution. The wells for loading protein samples are made by a comb. When gel loaded with protein samples is placed under an electric field, the charged molecules within the gel will run from one end to the other end, and then the proteins will be separated depending on their molecular weight.

Separated proteins in gels need to be transferred to supporting membranes for further probing using an antibody specific to the protein of interest. The membrane commonly used is the polyvinylidene difluoride (PVDF) membrane. Comparing with other types of

membranes such as nitrocellulose and nylon, the PVDF membrane is more stable, thus less brittle and the hydrophobic nature of PVDF provides higher protein binding capacity (Gorr and Vogel, 2015). By placing the gel with PVDF membrane in-between the sponges and filter papers (Figure 2.15), proteins in the gel transfer from the gel to the PVDF membrane under electrophoresis. Wet transfer with all the components completely submersing in transfer buffer usually provides higher resolution and more distinct bands in final image acquisition (Mahmood and Yang, 2012).

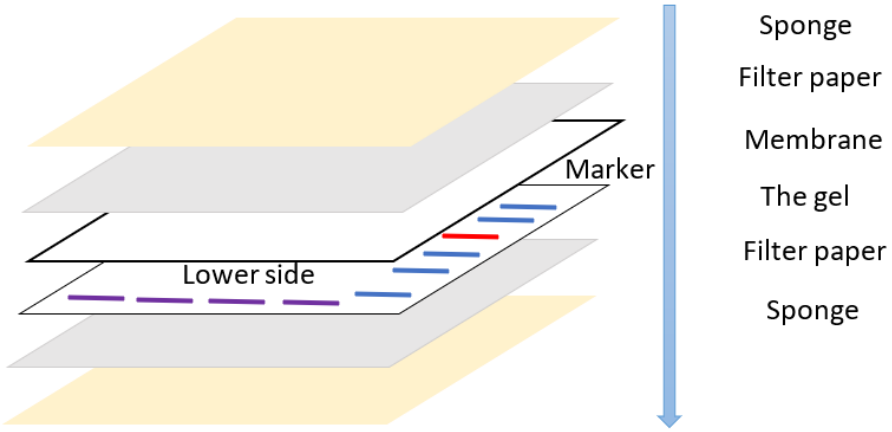

Figure 2.15 Schematic diagram of the transfer. The transferring usually uses a 'sandwich style' unit, which consists of a sponge on the top, a filter paper, a PVDF membrane, the gel, a filter paper, and a sponge at the bottom. This unit will be put in a cassette submersing in the transfer buffer to transfer the proteins from the gel to the PVDF membrane.

Proteins transferred onto the membrane are further probed with primary antibody and corresponding secondary antibody in blocking solution to block the non-specific bindings. The blocking solution is usually comprised of an unrelated protein such as non-fat milk or bovine serum albumin in Tris Buffered Saline plus 0.1% detergent Tween-20 (TBS-T). Finally, after the membrane is incubated with the secondary antibody conjugated with horseradish peroxidase (HRP), the protein-primary antibody-secondary antibody complex is visualised using the commercially available HRP substrates such as Immobilon^{TM} Western Chemiluminescent HRP substrate (catalogue number P36599, Merck/MILLIPORE, UK). Chemiluminescent detection uses an enzyme to catalyse a chemical reaction that results in the generation of visible light (Stewart et al., 2015). The HRP chemiluminescent reaction is based on the catalysed oxidation of luminol by peroxide. Oxidized luminol emits light as it

decays to its ground state (User Guide for Immobilon™ Western, MILLIPORE). This process has been shown in Figure 2.16. The imaging is then acquired by using a charged-coupled device (CCD) to capture the emitted light.

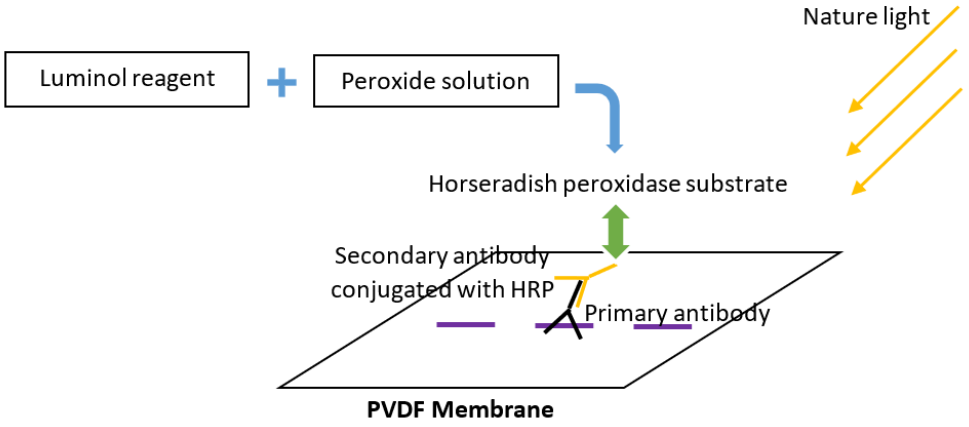

Figure 2.16 Schematic diagram of protein identification and exposure. The protein-primary antibody-secondary antibody complex is detected by Chemiluminescent HRP substrates which then catalyse a reaction resulting in the generation of visible light.

Western blot is an inexpensive and established method for protein identification and relative quantification. So far, the parallel techniques for protein identification and relative quantification are flow cytometry, immunofluorescence, enzyme-linked immunosorbent assay (ELISA), and immunohistochemistry. As described earlier, flow cytometry is an efficient technique for detecting proteins expresses on the surface of cells but is not the best option for analysing the molecules inside cells (Falkmer, 1992, Nüsse and Marx, 1997). Immunofluorescence and immunohistochemistry are better choices for analysis of protein expression *in situ* (Rojo et al., 2009, Sullivan and Chung, 2008). Those two techniques can identify and provide relative quantification of the expression of target proteins in tissue but are not the appropriate methods for protein identification in suspension cells. ELISA has a relatively easier process comparing with the complex process of Western blot and is the choice of methods for detecting the molecules suspended in supernatant such as chemokines and cytokines (Yolken, 1980). Therefore, for the in-cell protein analysis, Western blot still has its irreplaceable place.

2.3 Methods used throughout this project

2.3.1 Cell culture

2.3.1.1 Primary CLL cells culture

The majority of the work in this project was based on the use of primary CLL cells. The process to prepare primary CLL cells for the experiment consists of isolation and cryopreservation, recovery of frozen cells, and cell culture. The following part will describe in this order.

2.3.1.1.1 Isolation of CLL cells from blood samples and storage

The peripheral blood samples from patients with CLL were obtained with informed consent and approval from Liverpool (Adult) Local Research Ethics Committee and transferred to the Liverpool Blood Disease Biobank. The procedure to isolate CLL cells was immediately carried out in a class II bio-safety tissue culture cabinet to maintain the sterile condition.

Blood samples were slowly poured on top of the Lymphoprep (catalogue number 1114544, Axis-Shield PoC AS, Oslo, Norway), as shown in Figure 2.17. The samples were spun at 800g at room temperature for 30 minutes and the mononuclear cells layer was collected into new tubes. The mononuclear cells were washed with pre-warmed RPMI-1640 medium (catalogue number 22409015, Gibco/Life Technologies, UK) and centrifuged 550g for 10 minutes. The supernatant was then removed and the cells were resuspended. Following the cell count, 20 million cells in 1ml freezing medium were aliquoted into the labelled cryotube and stored at -80℃ freezer initially and transferred to -150℃ freezer for long-term storage.

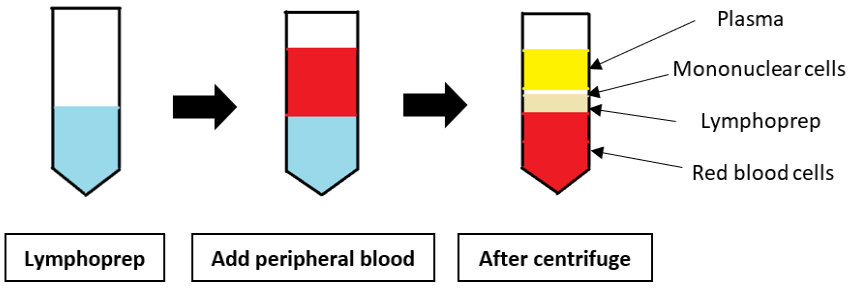

Figure 2.17 The process of lymphocyte extraction using Lymphoprep. Blood samples will be slowly flowed onto the top of the Lymphoprep and then centrifuged at 800g, room temperature, for 30 minutes. After the centrifuge, the sample in the tube will be separated into four layers, the plasma, the mononuclear cells, the lymphoprep, and the red blood cells.

2.3.1.1.2 Recovery of frozen primary CLL cells

The frozen sample was thawed in 37℃ water-bath firstly and transferred into a 20ml universal tube on ice. Ice-cold RPMI-1640 medium with 10% heat-inactivated qualified fetal bovine serum (FBS) (catalogue number 16000044, Gibco/Life Technologies, UK), 1% L-Glutamine (catalogue number G7513, Sigma-Aldrich, UK) and 1% Penicillin/Streptomycin (catalogue number P4333, Sigma-Aldrich, UK) were added drop by drop until it reached 10ml for one vial of cells thawed. Then, the sample was centrifuged at 550g, 4℃ for 5 minutes. The supernatant was removed and the pellet was washed with the ice-cold medium. The sample was centrifuged again in the same setting and the supernatant was removed. The pellet was resuspended with the ice-cold medium in appropriate volumes depending on the size of the cell pellet. The sample was then incubated in an incubator with the atmosphere containing 5% CO_2 at 37℃ for 1h to recover. After the recovery, the number of cells was counted using an automated cell counter (Cellometer) and the initial viability of the sample was tested by flow cytometer before the further experiment.

2.3.1.1.3 The analysis of the percentage of CD5 and CD19 double-positive primary CLL cells by flow cytometry

The analysis of the percentage of CD5 and CD19 double-positive primary CLL cells for each primary sample is performed in order to determine the level of contamination of other types of blood cells in each CLL PBMC samples. Therefore, CD5 and CD19 antibodies and the corresponding isotype-control antibodies (Table 2.1) were used for staining. The stained primary CLL cells were analysed by flow cytometry.

Table 2.1 Antibodies used for purity test using flow cytometry

	Company	Catalogue No.	Description
CD5 (FITC)	BD	345781	Monoclonal mouse anti-human reagent for identification of cells expressing CD5 antigen
Mouse IgG1 (FITC)	BD	345815	Fluorescence controls for use with human cells
CD19 (PE)	BD	345777	Monoclonal mouse anti-human reagent for identification of cells expressing CD19 antigen
Mouse IgG1 (PE)	BD	345816	Fluorescence controls for use with human cells

2 million primary CLL cells were collected and transferred into 1.5ml Eppendorf tubes with 1 million cells for test antibodies and 1 million for corresponding control antibodies. Each sample was centrifuged at 500rcf, room temperature, for 5min. The medium was removed and the cell pellet was washed with PBS. Then, the sample was centrifuged again in the same setting. The supernatant was removed and the pellet was resuspended with Staining Buffer (PBS with 0.1% BSA), 100µl per 1 million cells.

20µl of CD5 antibody (FITC) and 20µl of CD19 antibody (PE) were added into the test group tubes and mixed well. 20µl of the mouse IgG1 (FITC) and 20µl of the mouse IgG1 (PE) were added into the control group tubes and mixed well. The detailed information about the antibodies used for the purity test by flow cytometry has been listed in Table 2.1. The testing samples were incubated in the dark for 10min. Then, samples were centrifuged at the previous setting and the supernatants of the samples were removed. The cell pellets were resuspended with 350-400µl Staining Buffer and analysed on the flow cytometer.

The diagrams in Figure 2.18 are an example of the results showed by the flow cytometer.

Isotype control antibodies

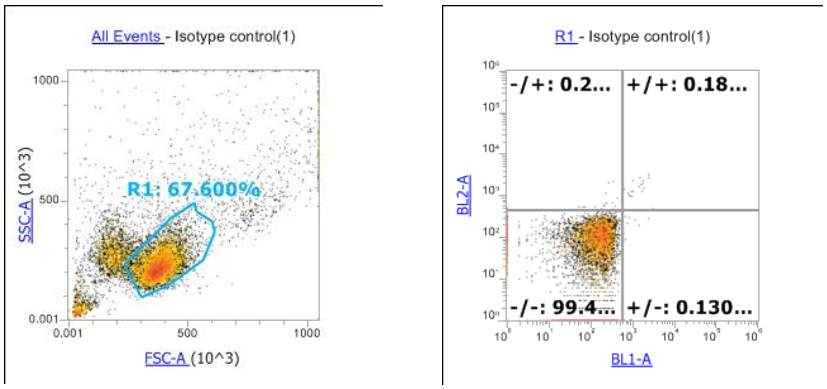

A.

CD5, CD19 antibodies

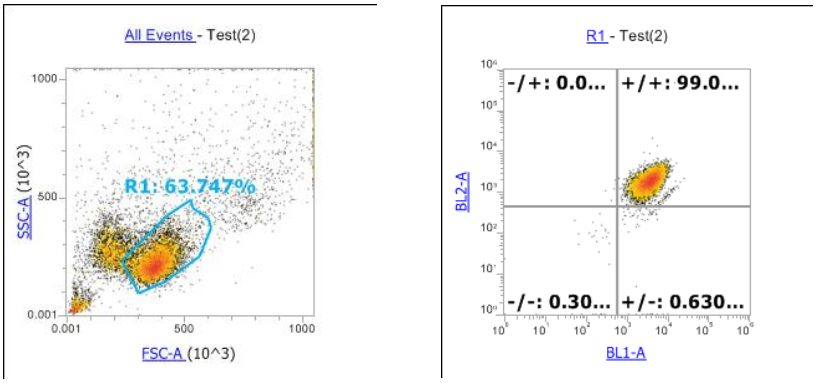

B.

Figure 2.18 An example of the results of the purity test of primary CLL sample by flow cytometer A. CLL cells were stained with negative control antibodies; B. CLL cells were stained with both FITC-labelled CD5 and PE-labelled CD19 antibodies. The BL1-A channel is for FITC (CD5) and the BL2-A channel is for PE (CD19).

2.3.1.1.4 Culture of primary CLL cells

For the standard cell culture condition, primary CLL cells were cultured in the RPMI medium with 10% heat-inactivated FBS, 1%L-Glutamine, and 1% Penicillin/Streptomycin at the density of 4×10^6 cells/ml in tissue culture plates (Falcon, BD Biosciences, UK).

For the co-culture cell condition, primary CLL cells were resuspended in the DMEM medium (catalogue number D6546, Sigma-Aldrich, UK) with 10% heat-inactivated FBS and 1% Penicillin/Streptomycin at the density of 3×10^6 cells/ml. Primary CLL cells were then co-cultured with adherent mouse fibroblasts that were γ-irradiated and seeded at 3×10^5 cells/ml the day before the co-culture experiment.

2.3.1.2 MEFs used for the co-culture CD40 stimulation system

Mouse embryonic fibroblasts (MEFs) stably transfected with the expression vector containing human CD154 cDNA were expressing human CD154 on the plasma membrane, which were used to co-culture with primary CLL cells to imitate the CD40-CD154 interaction between $CD4^+$ T cells and CLL cells in the lymph nodes. The parental MEFs transfected with an empty vector, which were not expressing CD154, were used as a control. Both fibroblasts were provided by Professor Gerry Cohen within the Department at the University of Liverpool and maintained as described (Vogler et al., 2009b).

2.3.1.2.1 Maintenance of MEFs

Both the MEFs expressing CD154 and the parental control MEFs were cultured in DMEM medium with 10% heat-inactivated FBS and 1% Penicillin/Streptomycin and incubated in the incubator with an atmosphere containing 5% CO_2 at 37℃.

MEFs were routinely passaged every 3-4 days according to the density. Each time when passaged, the culture medium was removed from the adhering fibroblasts. The MEFs were trypsinised for 3-5 minutes in the incubator before being collected and centrifuged at 250g, room temperature, for 5 minutes. The cell pellet was resuspended with the pre-warmed fresh culture medium. The resuspended fibroblasts were then cultured in new flasks.

2.3.1.2.2 Preparation for co-culture experiments

Before the co-culture experiment, the MEFs need to be γ-irradiated to inhibit their proliferation. The culture medium was removed and the monolayer of the fibroblasts was trypsinised for 3-5 minutes before being collected and spun at 250g, room temperature, for 5 minutes. Then, the cell pellet was resuspended with an appropriate volume of pre-warmed culture medium to obtain the cell density of 6×10^5 cells/ml. The fibroblasts were γ-irradiated at 75Gy to inhibit the proliferation. The irradiated fibroblasts were then diluted with pre-warmed culture medium to the density of 3×10^5 cells/ml and cultured in plates in the incubator with an atmosphere containing 5% CO_2 at 37℃ for over 12h allowing them to recover and adhere. The irradiated fibroblasts were ready for co-culturing with primary CLL cells when they were confluent. After gently removing the culture medium over the

fibroblasts, primary CLL cells at the density of 3×10^6 cells/ml were plated on the top of the confluent monolayer of fibroblasts for co-culture.

2.3.1.2.3 Detection of CD154 expression on MEFs

The expression of CD154 on fibroblasts was monitored using the flow cytometer once a month to ensure that the correct type of fibroblasts was used for co-culture experiments. Thus, the culture medium was removed from the adhering fibroblasts and the monolayer was washed with pre-warmed PBS. The monolayer of fibroblasts was detached using Cell Dissociation Solution (catalogue number C5789, Sigma-Aldrich) and collected into a labelled universal tube. The fibroblasts were centrifuged at 200g, room temperature, for 5 minutes and the cell pellet was washed with PBS and spun again. The cell pellet was resuspended in 0.5ml staining buffer (PBS containing 0.1% BSA) and aliquoted 1×10^6 cells from each type of fibroblasts and divided into two 1.5ml Eppendorf tubes with each one containing 5×10^5 cells. 10µl of FITC mouse anti-human CD154 (catalogue number 555699, BD Biosciences) was added into one tube of each type of fibroblasts as a test. 10µl of FITC mouse IgG1 κ isotype control antibody (catalogue number 555748, BD Biosciences) was added into the other one tube of each type of fibroblasts as a control. The fibroblasts were incubated at room temperature in the dark for 10 minutes and analysed by flow cytometer.

The diagrams in Figure 2.19 are an example of the results of detecting CD154 expression on both CD154 expressing fibroblasts and the parental control fibroblasts by flow cytometer.

Isotype control - control fibroblasts

CD154 antibody - control fibroblasts

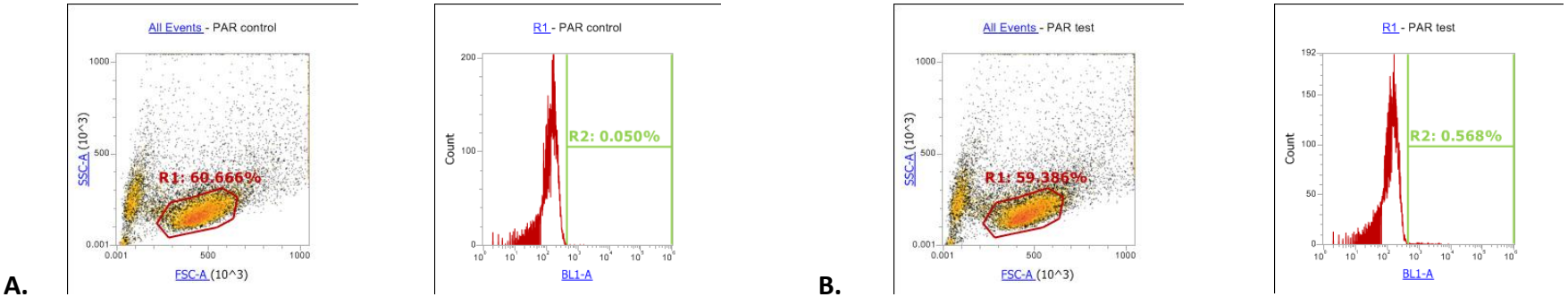

A. **B.**

Isotype control - CD154 expressing fibroblasts

CD154 antibody - CD154 expressing fibroblasts

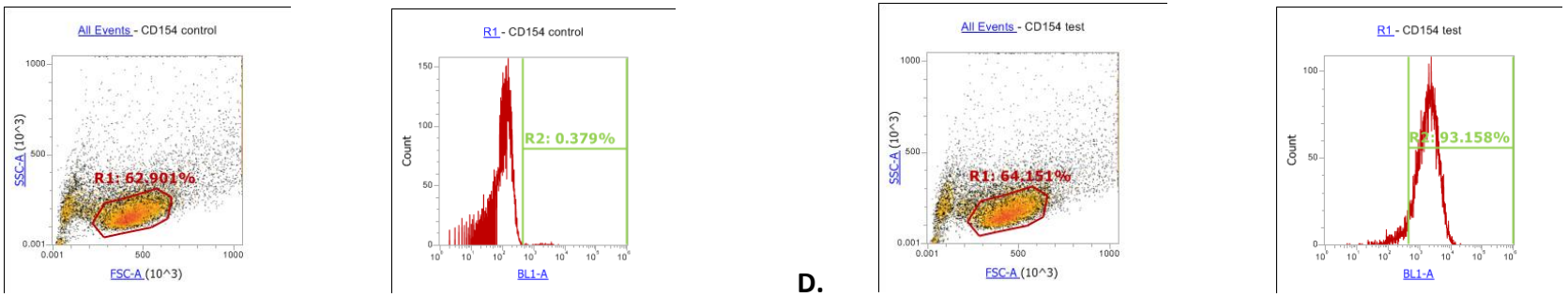

C. **D.**

Figure 2.19 An example of the results of testing the phenotype of fibroblasts. The left diagram in each paired example shows the cells selected for detection, which are the cells in the red gate. The corresponding histograms on the right show the percentage of cells expressing CD154 in all the selected cells. The threshold was set according to the results of the control antibody in each type of fibroblasts. A. The results of the parental fibroblasts stained with the negative control antibody. B. The results of the parental fibroblasts stained with CD154 antibody. C. The results of the CD154 expressing fibroblasts stained with negative control antibody. D. The results of the CD154 expressing fibroblasts stained with CD154 antibody. BL1-A channel in histograms is for FITC-CD154.

2.3.1.2.4 Cryopreservation of MEFs

The culture medium was removed from the monolayer of fibroblasts and the monolayer was trypsinised for 3-5 minutes. The fibroblasts were collected and centrifuged at 250g, room temperature for 5 minutes. The supernatant was discarded and the cell pellet was resuspended with an appropriate volume of ice-cold medium with 10% DMSO to obtain a cell density of 1×10^6 cells/ml. Then, the fibroblasts were aliquoted 1ml per vial into each cryopreservation tube and kept at -80℃.

2.3.1.3. CLL cell lines

HG-3 CLL cell line was established in 1998 from a 70-year-old Caucasian male patient with CLL (see the information of HG-3 cell line on the website: https://www.dsmz.de/collection/catalogue/details/culture/ACC-765), Rai stage II. MEC1 CLL cell line was originally established in 1993 from a 61-year-old Caucasian male diagnosed with CLL in prolymphocytoid transformation to B-PLL (Stacchini et al., 1999).

Both CLL cell lines were obtained from the Leibniz Institute (DSMZ) German Collection of Microorganisms and Cell Cultures (Braunschweig, Germany). The catalogue number of the HG-3 cell line and MEC1 cell line were ACC 765 and ACC497, respectively. The cells with a low number of passages were kept in cryopreservation.

2.3.1.3.1 Culture and passage of CLL cell lines

Both HG-3 cells and MEC1 cells were cultured in RPMI medium with 10% heat-inactivated FBS, 1%L-Glutamine, and 1% Penicillin/Streptomycin and incubated in the incubator with an atmosphere containing 5% CO_2 at 37℃.

HG-3 cells and MEC1 cells were passaged every 4-5 days depending on the cell density. Cells were collected from flasks and centrifuged at 550g, at room temperature, for 5 minutes. Then, the cell pellet was resuspended in an appropriate amount of pre-warmed culture medium and cells were cultured in new flasks in the incubator.

2.3.1.3.2 Culture of CLL cell lines for the experiment

When used for experiments, both HG-3 cells and MEC1 cells were cultured in RPMI medium with 10% heat-inactivated FBS, 1% L-Glutamine, and 1% Penicillin/Streptomycin with the cell density of 0.5×10^6 cells/ml in plates in the presence or absence of the test reagents at the indicated concentrations and kept in the incubator with an atmosphere containing 5% CO_2 at 37℃.

2.3.1.3.3 Cryopreservation of CLL cell lines

To avoid the genetic and phenotypic changes of the two CLL cell lines, I expanded the cell number in culture first after receiving them and cryopreserved a stock of vials for subsequent experiments. The two cell lines were maintained in culture for only three months before a new cryopreserved vial of cells was used.

Cells for the cryopreservation were collected from the flasks and centrifuged the cells at 550g, at room temperature, for 5 minutes. The cell pellet was resuspended with an appropriate volume of ice-cold medium to obtain a cell density of 2×10^6 cells/ml. Operating on ice, an appropriate volume of the ice-cold medium with 20% DMSO was slowly added into the tube with cells. The cells were aliquoted 1ml per vial into each cryo-tube and kept at -80℃.

2.3.1.4 Mycoplasma test of cell lines to avoid contamination in lab

To avoid contamination, the mycoplasma test has been conducting every month for all the cell lines cultured in the tissue culture room of the department. For each type of cell lines, at least 5×10^4 cells were collected from culture flasks into the correlated 1.5ml Eppendorf tube and centrifuged at 7000rpm, room temperature for 5 minutes. The cell pellet was washed twice and resuspended in 100µl sterile PBS. Each sample was heated for 10 minutes at 95℃ and vortexed for 5-10 seconds. The sample was then centrifuged at 13000rpm for 2 minutes and an aliquot (~100µl) of the heated supernatant was transferred into a fresh tube. The technician in the department tested the samples using a commercial PCR kit according to the manufacturer's instructions. Only the cell lines which passed the mycoplasma tests can be used in the tissue culture room.

2.3.2 Cell death detection

Cell death detection was analysed by flow cytometer using FITC Annexin V (catalogue number 556420, BD Pharmingen) and propidium iodide (PI) solution (catalogue number 556463, BD Biosciences) or 7-AAD (catalogue number 2032240, Invitrogen).

For each sample to be tested, 1 million cells were collected and transferred into a 1.5ml Eppendorf tube. The cells were centrifuged at 500rcf at room temperature for 5 minutes. The supernatant was removed and the cell pellet was resuspended with PBS. The cells were centrifuged again in the same setting. The supernatant was removed and the cell pellet was resuspended with 500µl Annexin V Binding Buffer (constituents of 10mM Hepes/NaOH, 140mM NaCl, 2.5mM $CaCl_2$, pH 7.4). 5µl of FITC Annexin V was added to each sample and incubated in the dark for 10 minutes. 10µl of PI or 5µl of 7-AAD was then added into the sample before analysed by flow cytometry.

2.3.3 Western blotting

2.3.3.1 Cell lysis and protein quantification

Cell samples were first washed with ice-cold PBS three times and centrifuged at 1000g, 4℃, three times, 5 minutes each. Cell pellets were then lysed with RIPA buffer containing protease inhibitor (catalogue number P8439, Sigma-Aldrich) and phosphatase inhibitor (catalogue number 524625, Millipore, UK) and kept on ice for 10 minutes. Then, the CLL samples were further sonicated for 5 cycles (30 seconds on plus 30 seconds off) on a high setting using a sonicator (Bioruptor® Standard, B01010001, Diagenode). The process of sonication was only applied to primary CLL cells. After sonication, cell debris was centrifuged at 14000rpm, 4℃, for 20 minutes and the supernatant of each sample was transferred into new 1.5mL Eppendorf tubes. Extracted protein samples were kept at -20℃ before use.

The total protein from each sample was quantified using the Bio-Rad DC™ Protein Assay Reagents Package (catalogue number 500-0116, Bio-Rad, UK) (Table 2.2). A serial dilution of BSA protein standard samples with protein concentrations from 0mg/ml to 3mg/ml were located into a multi-well plate together with samples to be tested. 5µl of lysates was collected from each sample and added into one well of a 96-well plate. The protein quantification was duplicated for each sample to avoid technical bias. After plated all the

duplicates of BSA standard samples and samples to be tested, 25µl of reagent A plus reagent S (consist of 1ml of reagent A and 20µl of reagent S) and 200µl of reagent B were added into each well. The plate was incubated for 15 minutes before placing it into a plate reader for scanning at 650nm. The protein concentrations of samples were calculated by comparing with the standard curve generated by BSA standard protein samples.

Table 2.2 Information about the reagents for protein quantification

Reagent	Company	Catalogue Number
DC™ Protein Assay Reagent A	BIO-RAD	500-0113
DC™ Protein Assay Reagent S	BIO-RAD	500-0115
DC™ Protein Assay Reagent B	BIO-RAD	500-0114
Methanol, >=99.8%	FisherChemical	1666182
PBS	Laboratory scope	-

2.3.3.2 SDS-PAGE running and transferring

The running gel and stacking gel were prepared in advance and 10µg of protein sample from each sample was calculated according to the protein quantification and collected into a 1.5ml Eppendorf tube. The rest of the samples were at -20℃. An appropriate volume of Laemmli sample buffer was added into each sample according to the protein concentrations (the maximum volume for each sample was 30µl for 15-well comb and 40µl for 10-well comb). Samples were then heated at 90℃ for 5 minutes and loaded on the gel. The electrophoresis was conducted in apparatus filling the running buffer under 115V for 90 minutes. After separation by the electrophoresis, the gel was taken out and washed with the pre-cold transfer buffer. The transfer sandwich was prepared in the order of sponge, filter paper, membrane, gel, filter paper, and sponge in a cassette (Figure 2.15). The proteins were transferred from gel to PVDF membrane under 400mA for 60 minutes.

2.3.3.3 Protein targets probing with antibodies

The PVDF membrane was taken out after transferring and washed with 1×TBST for 10 minutes. The membrane was then blocked with 5% milk/1×TBST for 30 minutes and incubated with primary antibody (1:1000 dilution) with continuous agitation at 4℃ overnight. Then the other day, the membrane was washed with 1×TBST for 10 minutes and blocked with 5% milk/1×TBST for 30 minutes. Finally, the membrane was incubated with

correlated secondary antibody (1:2000 dilution) at room temperature for 1h and visualized using an imaging machine (Bio-RAD).

Here in this project, β-actin (1:10000 dilution) was probed as the protein loading control for Western blot analysis. After the probing for the target protein, the membrane was washed with 1×TBST for 10 minutes and blocked with 5% milk/1×TBST for 30 minutes. Then, the membrane was incubated with the β-actin antibody at room temperature for 1h and washed with 1×TBST for 10 minutes and blocked with 5% milk/1×TBST for 30 minutes. Finally, the membrane was incubated with the correlated secondary antibody for 1h and visualized.

The visualization for the protein of interest or β-actin was detected by using the Immobilon^{TM} Western Chemiluminescent horseradish peroxidase (HRP) substrate (catalogue number P36599, Merck/MILLIPORE, UK). Densitometry analysis was performed by using ImageJ analysis software (National Institutes of Health, USA).

The detailed information of materials and the component of reagents used to complete the process of Western blotting have been listed in Appendix 1.

2.4 Statistical analysis

In this project, pooled data generated from the results of independent experiments were shown in the format of mean ± standard deviation (mean ± SD). The statistical significance of the difference between the two groups was determined using the Student's t-test (two-tailed, paired) by either Microsoft Excel^{TM} or GraphPad Prism 8. LC_{50} of agents was calculated using the non-linear analysis by GraphPad Prism 8.

Chapter 3. CD40 stimulation protects primary CLL cells from drug-induced cell death

3.1 Background and aims

This chapter will be divided into two parts: the first part is focused on characterizing the biological effect of CD40 stimulation on drug-induced cell death of primary CLL cells and the second part is a comparison study to find out if CLL cells stimulated by the soluble CD40 ligand system display similar biological responses to those stimulated by co-culture system. When the biological effects are confirmed, CLL cells stimulated by the soluble ligand system will be used in the proteomics study to examine the effect of CD40 stimulation on the protein expression of CLL cells at a global level, which will be described in the next chapter.

For the first part, as described in the introduction chapter, although most evidence indicates that CD40 stimulation induces the pro-survival signal that leads to chemo-resistance in CLL cells, there are still some discrepancies in reporting the effect of CD40 stimulation largely due to the differences in the methods of stimulation used in different studies (De Totero et al., 2003, Söderberg et al., 1997). Therefore, it is necessary to independently confirm the biological effect of CD40 stimulation on primary CLL cells under the experimental conditions used in this study. The method of CD40 stimulation applied in the first part of the study described in this chapter was the established co-culture system in which primary CLL cells were cultured on the monolayer of mouse embryonic fibroblasts (MEFs) that were stably transfected with an expression vector containing human CD154 cDNA so they expressed human CD154 on the cell membrane continuously (Vogler et al., 2009a). In parallel, CLL cells that were cultured with the MEFs stably transfected with the empty vector were used as controls. Such a co-culture system is a robust, reproducible model to mimic the CD40 stimulation within the microenvironment to support the survival and proliferation of CLL cells, and this system has been widely used by many CLL research groups worldwide (Patten et al., 2008, Buggins et al., 2010, Pepper et al., 2011, Hamilton et al., 2012). In addition, Pascutti and colleagues showed that the gene expression profile of CLL cells co-cultured with CD154-expressing fibroblasts was similar to that induced by autologous activated T cells, and such gene expression profile was also detected in CLL samples taken from the

lymph nodes of the patients with CLL (Pascutti et al., 2013), thus further validated the utility of the co-culture system to simulate the CD40 stimulation of CLL cells by activated T cells *in vivo* at the level of gene expression of mRNA. Previous work from this research group has shown that the CD40 stimulation induced by the co-culture system can protect CLL cells from cell death induced by cytotoxic agents that activate cell death through either death receptor (extrinsic) or mitochondrial (intrinsic) apoptosis pathway (Zhuang et al., 2014, Chapman et al., 2017). The aim of this part of the study is to independently investigate how CD40 stimulation influences the sensitivity of primary CLL cells to cell death induced by cytotoxic drugs that are currently used in CLL clinics.

Four different drugs were used to induce cell death, including fludarabine, bendamustine, ABT-199 (venetoclax), and ibrutinib. Fludarabine is an important component of chemotherapy consisting of fludarabine, cyclophosphamide, and rituximab (FCR) that is a front-line therapy for the untreated, del(17p) negative, TP53 unmutated, IGHV-mutated patients with the age of less than 65 years old and without any significant comorbidities, according to the National Comprehensive Cancer Network (NCCN) Guidelines version 2.2021. Fludarabine is a purine analogue and it induces apoptosis in cell cycle arresting cells such as CLL cells by interfering with the DNA repair process, which leads to the overloading of unrepaired DNA, triggering p53-dependent apoptosis (Pettitt, 2003). Bendamustine is a DNA damage agent as well but the cytotoxic mechanism is different in comparison with fludarabine. Bendamustine induces apoptosis by crosslinking DNA bases between the double-stranded DNA and inhibiting the replication and repair of DNA (Gandhi and Burger, 2009, Cheson and Leoni, 2011). ABT-199 and ibrutinib are relatively new therapeutics for CLL, but they already show impressive efficiency in the treatment of CLL (Itchaki and Brown, 2016, Kaur and Swami, 2017). ABT-199 is a selective inhibitor specific for BCL-2, which was developed upon improvement from ABT-737 that had a severe side-effect of causing thrombocytopenia due to its inhibition of BCL-XL (Souers et al., 2013).

The second part of this chapter is to investigate whether using the soluble CD40 ligand system can reproduce the biological effect of the CD40 stimulation using the co-culture system. This is out of the consideration that, if CD40-stimulated CLL cells via the co-culture were used for the proteomics study, the fibroblasts from the co-culture system will inevitably mix with CLL cells, thus potentially contaminating the cellular protein contents

from the CLL cells used for protein expression analysis. Consequently, CD40 stimulation induced by the soluble CD40 ligand was explored in this project to ensure that the proteins from primary CLL cells were used for proteomics analysis. CD40 stimulation induced by the soluble CD40 ligand has been applied in many studies to imitate the CD40-CD154 ligation between T cells and CLL cells (Younes et al., 1998, Jacob et al., 1998, Grdisa, 2003, Plander et al., 2009, Smallwood et al., 2016). Although it has been reported that CD40 stimulation induced by the soluble CD40 ligand together with interleukin (IL)-4 can rescue CLL cells from apoptosis (Grdisa, 2003), it is unclear how similar or different the effect of CD40 stimulation induced by the soluble ligand versus by the co-culture system is. It is thus important to compare these two methods of stimulation to link the previous work carried out using the co-culture system to the proposed proteomics study of CLL cells stimulated by the soluble CD40 ligand. The analysis of mRNA expression of CD40-stimulated CLL cells using the co-culture system has been reported (Pascutti et al., 2013), which can be used as a reference to compare the mRNA expression of CLL cells stimulated with the soluble CD40 ligand system. Therefore, in this study, the mRNA expression from the CLL cells stimulated by the soluble CD40 ligand system was analysed using RNA-seq technology. The differential gene expression profile of CLL cells stimulated by the soluble CD40 ligand was also compared to that of CLL cells isolated from bone marrow, lymph node, and peripheral blood of patients with CLL (Herishanu et al., 2011).

3.2 Materials and Methods

3.2.1 Materials

Cryopreserved primary CLL samples were obtained from the Liverpool Blood Disease Biobank. Before further experiments, the percentage of CD5 and CD19 double-positive cells (i.e. real CLL cells) of each primary CLL case was analysed by flow cytometry. The detailed procedures of the analysis have been described in Chapter 2. Primary CLL samples with less than 60% of CD5 and CD19 double-positive CLL cells were excluded from the study. The details of the percentage of the double-positive cells of each primary CLL sample applied in the study was shown in Appendix 2. The clinical information of the applied cases has been described in Appendix 3.

The source of the transfected fibroblasts expressing CD154 and the control fibroblasts has been described in Chapter 2. The phenotype of the fibroblasts expressing or not expressing CD154 was tested by flow cytometry once a month throughout the duration of experiments involving CD40 stimulation using the co-culture system.

Fludarabine (catalogue number F2773, Sigma-Aldrich), ABT-199 (catalogue number S8048-SEL, Selleck Chemicals), and bendamustine (catalogue number B5437, Sigma-Aldrich) were applied in the study for the induction of cell death experiments. All three drugs were suspended in dimethyl sulfoxide (DMSO) (catalogue number 1371913, Fisher Chemical, UK) to make the stock concentrations of 50mM, 10mM, 100mM for fludarabine, ABT-199, bendamustine, respectively. Stocks of the individual drugs were aliquoted into 0.5ml Eppendorf tubes with small quantities and stored in a -20℃ freezer to avoid repeated thaw-freeze cycles. The range of concentrations used in fludarabine treatment was based on previous studies from our research group in which time- and concentration-dependent induction of cell death in CLL cells by fludarabine were established (Zhuang et al., 2014). The choice of concentrations applied for ABT-199 treatment was based on the findings of a published study in which ABT-199 was shown to induce apoptosis in primary CLL cells with LC_{50} of 3nM (Souers et al., 2013). The concentrations of bendamustine were based on the previous study from our research group (Chapman et al., 2017).

The hemagglutinin (HA)-tagged recombinant human (rh) CD40 ligand/TNFSF5 was purchased from the R&D Systems (Oxford, UK). The lyophilised rhCD40 ligand/TNFSF5 was resuspended in PBS with 0.1% BSA at a stock concentration of 100ng/µl. The rhCD40 ligand/TNFSF5 solution was aliquoted into 0.5ml Eppendorf tubes with the aliquot size of 5µl or 10µl and kept at -80℃ before use. The lyophilised anti-HA antibody was resuspended in PBS at a stock concentration of 500ng/µl and kept at 4℃.

RNeasy Mini Kit and QIAshredder Kit were all purchased from the company of QIAGEN (Manchester, UK). The Qubit microRNA Assay kit was purchased from the company of Life Technologies/Thermo Fisher Scientific (Paisley, UK). The process of RNA extraction and purity/concentration assays was conducted according to the protocols provided by the company.

The detailed information about the suppliers of these reagents and products has been shown in Table 3.1.

Table 3.1 Products and reagents used in Chapter 3

Reagents/products	Company	Catalogue No.
HA-tagged rhCD40 Ligand/TNFSF5	R&D SYSTEMS	TFE1316121
Anti-HA Antibody	R&D SYSTEMS	CDCV0517051
RNeasy Mini Kit and QIAshredder Kit	QIAGEN	74104, 79654
Qubit microRNA Assay Kit	Life Technologies	Q32880, Q32881

3.2.2 Cell culture

3.2.2.1 Standard culture condition

Thawed primary CLL cells were re-suspended at the concentration of 4×10^6 cells/ml in complete RPMI-1640 medium and plated to multi-well plates and cultured in the incubator with an atmosphere containing 5% CO_2 at 37℃ before use.

3.2.2.2 Co-culture of primary CLL cells

The monolayers were prepared as described in the section 2.3.1.2.2 in Chapter 2 and the procedures of thawing and recovery of frozen primary CLL cells have been described in the section 2.3.1.1.2 in Chapter 2. After thawing, CLL cells were checked for viability following Trypan blue dye staining using a Cellometer. Cells were then adjusted to a density of 3×10^6 cells/ml and plated over the monolayers of the pre-prepared fibroblasts to ensure that the ratio of primary CLL cells to fibroblasts was kept at 10:1. The primary CLL cells in co-culture were kept in the incubator with an atmosphere containing 5% CO_2 at 37℃ for 24h for CD40 stimulation. The procedure of co-culture is shown in Figure 3.1.

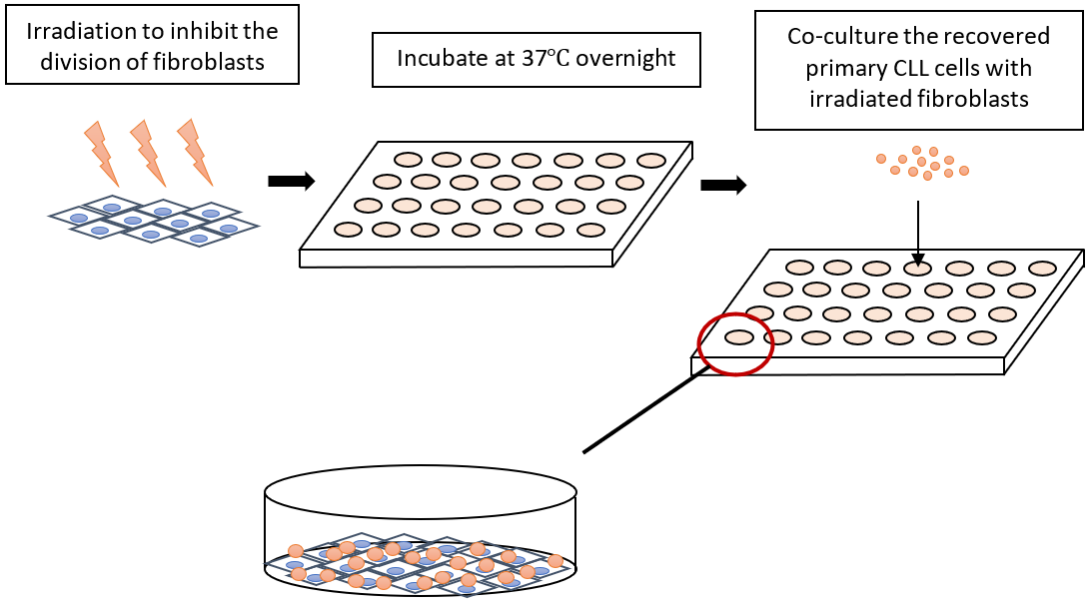

Figure 3.1 Schematic diagram of the co-culture system. The division of fibroblasts was inhibited by irradiation with a dose of 75Gy. The irradiated fibroblasts were plated at a concentration of 3×10^5 cells/ml into 24-well plates and kept in the incubator with an atmosphere containing 5% CO_2 at 37°C overnight. When the fibroblasts were confluent, the thawed primary CLL cells were plated on the top of the confluent fibroblasts at the concentration of 3×10^6 cells/ml.

3.2.2.3 CD40 stimulation induced by the soluble CD40 ligand system

The method of CD40 stimulation using the soluble HA-tagged CD40 ligand was essential as described (Lezina et al., 2018). Briefly, 0.1µg/ml HA-tagged rhCD40 ligand/TNFSF5 was incubated with 0.5µg/ml anti-HA antibody for 30 minutes. Then, the mixture was added to the culture of thawed primary CLL cells and incubated for 24h for CD40 stimulation. In parallel, thawed primary CLL cells were incubated with 0.5µg/ml anti-HA antibody alone as the unstimulated control. The density of primary CLL cells was maintained at 4×10^6 cells/ml in the 24-well plate or 5×10^6 cells/ml in the 6-well plate.

3.2.3 Drug treatments

Induction of cell death by drugs was performed on primary CLL cells that have been co-cultured with the CD154-expressing or control fibroblasts for 24h. Once CLL cells were gently collected from the monolayers, their numbers were counted on the Cellometer. The

cell density of both CD40-stimulated and unstimulated CLL cells was then adjusted to 4×10^6 cells/ml in fresh complete medium and a fixed number of CLL cells were plated into a new multi-well plate, and cultured under standard conditions with or without the cytotoxic drugs. The duration of incubation with the drugs varied according to the type of drugs (see details below). At the end of incubation, CLL cells were collected and the percentage of cell death of each sample was detected by flow cytometry. The detailed procedure of cell death detection by flow cytometer has been described in the Methodology chapter (Chapter 2).

3.2.4 Preparation of the mRNA sequencing samples

3.2.4.1 Cell preparation

To meet the minimum requirement of statistical and bioinformatics analysis, primary CLL samples from six individual patients with CLL were used as the biological replicates for the mRNA sequencing experiment. The criteria for the selection of CLL cases were that over 90% of CLL PBMCs are positive for both CD5 and CD19, which was measured by flow cytometry, and that CLL cells respond to CD40 stimulation induced by the soluble CD40 ligand method. The expression of BCL-XL measured by Western blotting was used to confirm CD40 stimulation status resulting from that CD40 stimulation has been reported to up-regulate the expression of BCL-XL in CLL cells (Vogler et al., 2009a). With these criteria in mind, six primary CLL cases had been chosen for the mRNA sequencing study (the purity information of the six CLL cases has been provided in Appendix 2 and the clinical information of the CLL cases has been provided in Appendix 3).

To generate a sufficient number of CD40 stimulated and unstimulated primary CLL cells from each CLL case for the RNA extraction and the subsequent sequencing study, thawed primary CLL cells were cultured at a concentration of 5×10^6/ml with 3ml of cell suspension per well in a 6-well plate in the presence or absence of the soluble CD40 ligand, as shown in Figure 3.2. Cells were harvested after 12h and 24h, respectively. In total, there were twenty-four mRNA samples generated from six primary CLL cases.

At each time point, in addition to cells harvested for RNA extraction, 1 million cells were collected for the viability test by flow cytometry and 4 million cells were collected for the detection of the BCL-XL expression by western blotting. The viabilities and the status of

CD40 stimulation of these samples were detected before further study (results have been shown in Figure 3.12 and 3.13).

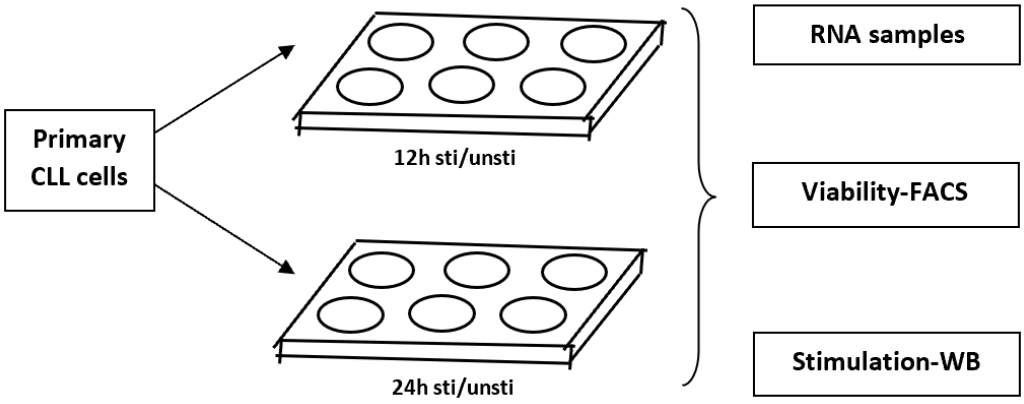

Figure 3.2 Schematic diagram of RNA sequencing sample preparation.
12h/24h sti: CD40 stimulated primary CLL cells with HA-tagged CD40 ligand + anti-HA antibody for 12h/24h; 12h/24h unsti: primary CLL cells cultured with anti-HA antibody for 12h/24h as controls. FACS: flow cytometry; WB: Western blotting.

3.2.4.2 RNA extraction

RNA extraction was conducted using the RNeasy Mini Kit and QIAshredder Kit (both from QIAGEN). During the process of RNA extraction, all the samples were kept on ice to reduce the risk of RNA degradation. Cell pellets were lysed with 700µl per sample of Buffer RLT from the commercial kit containing β-mercaptoethanol. The lysate of each sample was transferred directly into the QIAshredder column and spun for 2 minutes at room temperature. The flow-through liquids were collected and mixed with 600µl of 70% ethanol, and then transferred to the RNeasy mini-column and spun for 15-20 seconds at 11,000g. The flow-through liquids were discarded and the remaining RNeasy mini-columns were spun again for 15-20 seconds at 11,000g. Each RNeasy mini-column was loaded with 700µl of Buffer RW1 and left on the bench for 5 minutes before being spun for 15-20 seconds at 11,000g. With the flow-through discarded, the columns were loaded with 500µl Buffer RPE and centrifuged for 15 seconds at 11,000g. This step was repeated before transferring the columns to the 2ml collection tubes and centrifuged at 11,000g for 1 minute to dry the membrane. Finally, the RNeasy spin column was transferred to new 1.5ml collection tubes and loaded 30µl RNase-free water directly to the column membrane and centrifuged for 1

minute at 11,000g to elute the RNA. 5µl out of each sample was used for the purity and concentration test (diluted the sample in 1:5 with RNase-free water when the concentration was too high). All the exacted RNA samples were then stored at -80℃ before sent to NOVOGENE for RNAseq analysis.

3.2.4.3 The purity and concentration of the RNA samples

According to the requirement for sequencing from NOVOGENE, the purity of the RNA samples determined by the optical density reading at 260nm and 280nm wavelengths should be with the ratio of 260/280 over 1.8, together with the minimum quantity of 2000ng for the total RNA. The purity was also confirmed by Nanodrop using 1µl from each RNA sample.

The concentration was tested by Qubit with the Qubit® microRNA Assay Kits (catalogue number Q32880, Q32881, Molecular Probes of Life Technologies of Thermo Fisher Scientific, UK). The kits included the stock buffer, fluorescent dyes S1 and S2. The stock buffer and fluorescent dyes were mixed at the ratio of 199:1 in an appropriate volume for two standard samples and the test RNA samples. The mixed buffer should be kept in dark for 2 minutes before further steps. 190µl of the prepared mixed buffer was loaded to standard samples and 199µl of the mixed buffer was loaded to the test RNA samples. 10µl of S1 was added to the standard sample 1 and 10µl of S2 was added to the standard sample 2. 1µl from each RNA sample was added to the corresponding tube separately and mixed well with the buffer. The samples were incubated at room temperature for 2 minutes and measured the concentrations on the Qubit apparatus connecting with a computer.

The information of the RNA samples sent to NOVOGENE has been shown in Table 3.2.

Table 3.2 The information of the RNA samples

Case No.	Duration time	RNA purity (260/280)	RNA concentrations (ng/µl)	Total volume (µl)	Total amount (ng)
#3684	12h unsti	2.09	147.5	59	8702.5
	12h sti	2.1	133	59	7847
	24h unsti	1.87	284	29	8236
	24h sti	1.82	176	29	5104
#3679	12h unsti	1.91	90	29	2610
	12h sti	1.92	205	29	5945
	24h unsti	1.93	159	29	4611
	24h sti	1.86	224	29	6496
#3640	12h unsti	1.9	396	29	11484
	12h sti	1.94	680	29	19720
	24h unsti	1.98	230	29	6670
	24h sti	1.96	266	29	7714
#3564	12h unsti	1.98	92	59	5428
	12h sti	2.04	117	59	6903
	24h unsti	1.92	114	59	6726
	24h sti	1.9	176	59	10384
#3568	12h unsti	1.98	101.5	59	5988.5
	12h sti	1.96	100	59	5900
	24h unsti	1.93	116	59	6844
	24h sti	1.99	41.7	59	2460.3
#3585	12h unsti	2.02	97.5	59	5752.5
	12h sti	1.9	104	59	6136
	24h unsti	1.92	114	59	6726
	24h sti	1.91	139	59	8201

Note: 12h/24h unsti: primary CLL cells cultured with 0.5ng/ml anti-HA antibody for 12h or 24h; 12h/24h sti: primary CLL cells cultured with 0.1ng/ml HA-tagged CD40 ligand and 0.5ng/ml anti-HA antibody for 12h or 24h.

3.2.5 Data analysis

The mRNA sequencing was performed by a commercial company NOVOGENE Ltd (Cambridge, UK). The differential expression analysis of the mRNA sequencing data between the CD40 stimulated and the unstimulated samples were performed using the DESeq2 package in the R computer statistical environment. The comparison between data induced by the two CD40 stimulation methods and the comparison between the data of the soluble CD40 ligand system with the data of the primary CLL cells isolated from different *in vivo* tissues were performed by using GSEA 4.0.3. The omics data analysis was completed with help from the bioinformatician at the University of Liverpool.

3.3 Results

3.3.1 CD40 stimulation protects primary CLL cells from drug-induced cell death

3.3.1.1 CD40 stimulation protects primary CLL cells from fludarabine-induced cell death

The first drug applied in this part of the study was fludarabine. The concentrations of fludarabine used were 0μM, 1μM, 3μM, 10μM, and 30μM. This was based on the findings of a previous study from this group in which time- and concentration-dependent induction of cell death on CLL cells by fludarabine was established (Zhuang et al., 2014).

As previously stated, fludarabine is a purine analogue and it induces apoptosis in CLL cells by interfering with the DNA repair process, which leads to the overloading of unrepaired DNA, triggering p53-dependent apoptosis (Pettitt, 2003). However, CLL cells with 17p deletion or TP53 mutation exhibits resistance to fludarabine (Stilgenbauer et al., 2015). Considering there would be a certain amount samples harbouring 17p deletion and TP53 mutation, it was reasonable to screen samples to select fludarabine-response CLL samples for this part of study. Analysing the results using the drug-induced cell death formula of drug-induced cell death = [(% cell death of drug-treated cells - % cell death of untreated cells)/(100 - % cell death of untreated cells)] × 100 (Figure 3.3), the primary CLL cells from the six cases were observed to respond to fludarabine in a concentration-dependent manner when incubated for 48h at standard culture conditions.

Although the results of drug-induced cell death showed that the primary CLL cells from the six cases responded to fludarabine (Figure 3.3), this data was generated by not factoring in the basal (spontaneous) cell death observed in control CLL cells. Therefore, this figure was modified to further reflect the extent of spontaneous cell death in these cells (Figure 3.4). Using this approach, it can be found that primary CLL cells from #3637 and #3642 were not very sensitive to fludarabine, compared with the results from other cases. This may be caused by the high percentage of spontaneous cell death. The extent of spontaneous cell death was different from case to case and it reflected the heterogeneity of CLL. In order to avoid the effect caused by high spontaneous cell death, only the primary CLL cells of the cases with initial viability (after recovery from freeze-thaw) over 80% were used for fludarabine treatment (Appendix 2). However, even though the initial viability of those six cases were satisfactory, the percentage of spontaneous cell death after 48h was excessive

(as observed in #3637 and #3642), which affected the results to some degree. Results of #3640 showed that the percentage of drug-induced cell death did not increase with the escalating concentrations from 3μM to 30μM (Figure 3.3 E), which can be explained by the results of the original cell death, with almost all of the cells under these concentrations were dead (Figure 3.4 E). Results of #3396 showed a lower percentage of cell death induced by 1μM fludarabine compared with that of the untreated cells (Figure 3.3 C and 3.4 C), which could have been due to technical error. Taken together, the primary CLL cells from these cases were considered as cells responding to fludarabine.

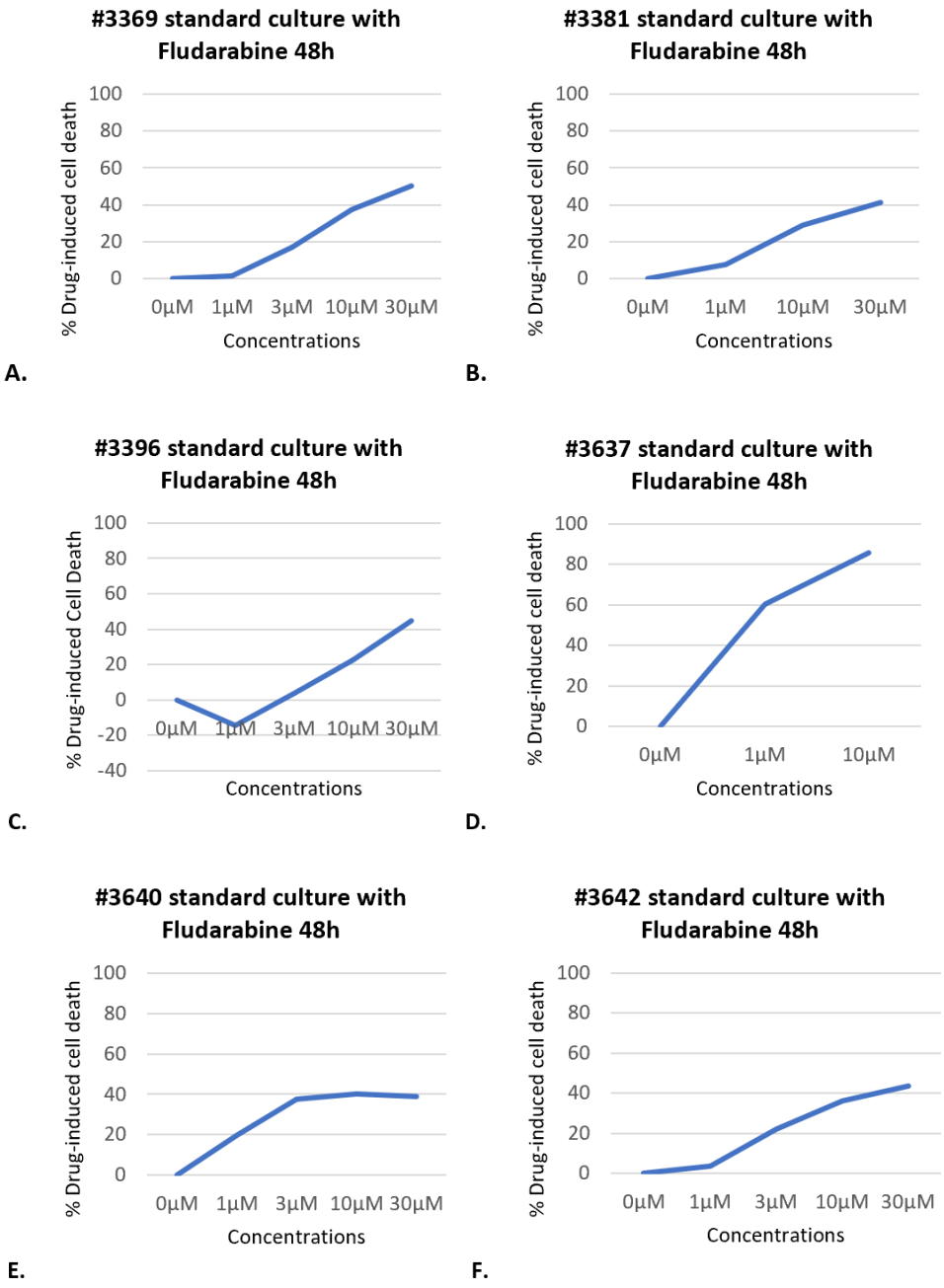

Figure 3.3 Fludarabine-induced cell death in primary CLL cells. For each CLL sample, thawed primary CLL cells were re-suspended at the concentration of 4×10^6 cells/ml in complete RPMI-1640 medium and loaded into 5 wells of a 24-well plate with 1ml per well. Fludarabine of each working concentration was diluted from the stock concentration with DMSO before the treatment. 1μl of each working concentration of fludarabine was added into one well of primary CLL cells and mixed well. One well was taken as the control and the primary CLL cells in this well were treated with 1μl of DMSO. After 48h incubation, the cells were collected and the cell death was analysed by flow cytometry following staining cells with FITC labelled annexin V and PI as described in Methods. Drug-induced cell death = [(% cell death of drug-treated cells - % cell death of untreated cells)/(100 - % cell death of untreated cells)] × 100.

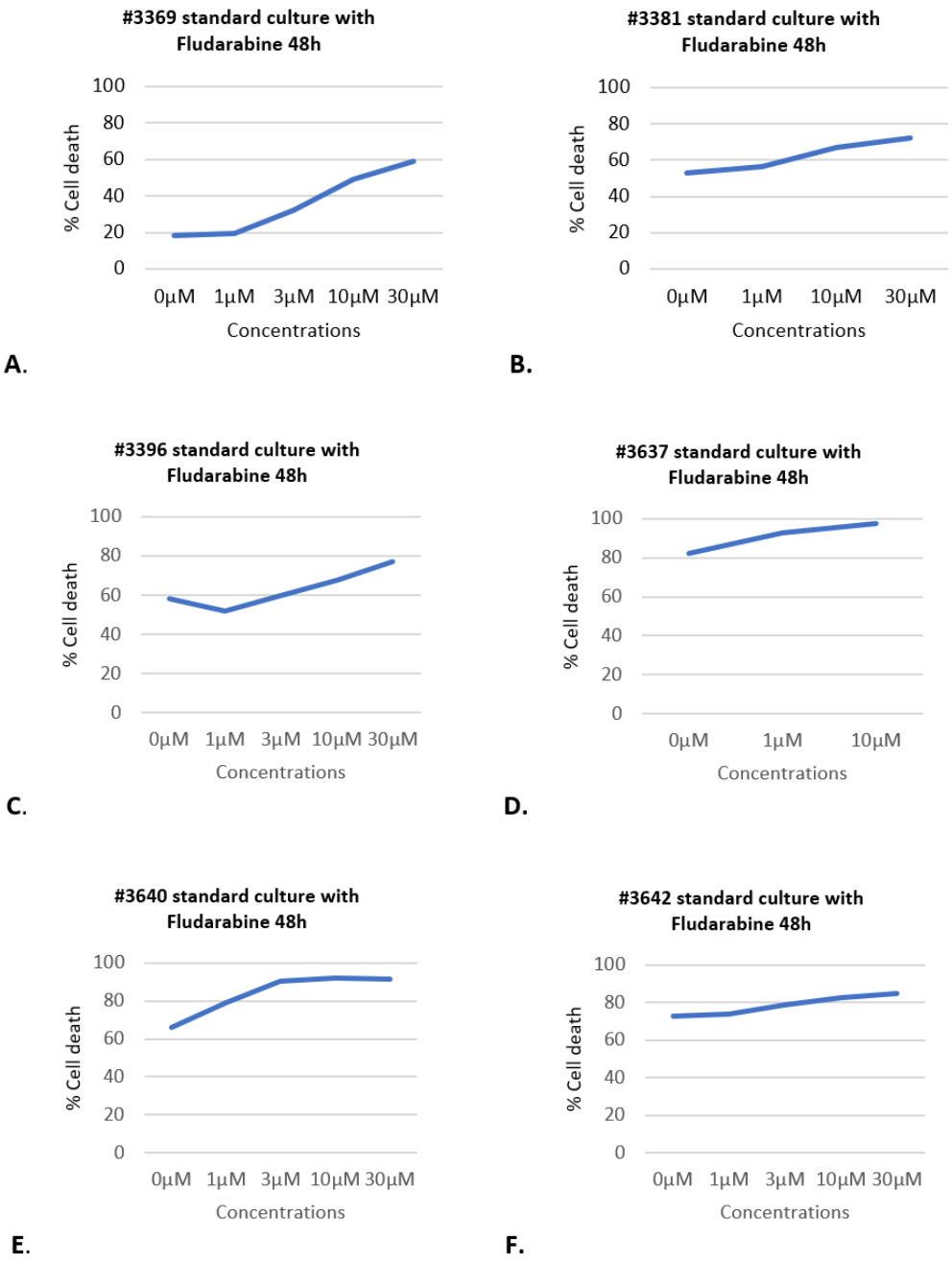

Figure 3.4 The extent of spontaneous and fludarabine-induced cell death in primary CLL cells. For each CLL sample, thawed primary CLL cells were re-suspended at the concentration of 4×10^6 cells/ml in complete RPMI-1640 medium and loaded into 5 wells of a 24-well plate with 1ml per well. Fludarabine of each working concentration was diluted from the stock concentration with DMSO before the treatment. 1μl of each working concentration of fludarabine was added into one well of primary CLL cells and mixed well. One well was taken as the control and the primary CLL cells in this well were treated with 1μl of DMSO. After 48h incubation, the cells were collected and the cell death was analysed by flow cytometry following staining cells with FITC labelled annexin V and PI as described in Methods.

These six fludarabine-responsive CLL samples were thus taken forward for the co-culture experiments. Primary CLL cells were co-cultured with CD154 expressing fibroblasts for 24h for CD40 stimulation. CLL cells co-cultured with parental fibroblasts not expressing CD154 for 24h were used as the controls. The CD40 stimulated and unstimulated primary CLL cells were then collected from the co-culture system, respectively, and incubated with fludarabine at standard culture conditions for another 48h.

The results of individual CLL samples (#3369, #3396, #3637, #3640, and #3642) treated with fludarabine showed that there were differences in the fludarabine-induced cell death between the CD40 stimulated and unstimulated cells (Figure 3.5 A, C, D, E and F). Results of case #3637 showed that both CD40 stimulated and unstimulated cells exhibited a relatively lower percentage of cell death compared with the results of other cases (Figure 3.5 D). Resulting from the same procedure of the experiment, the situation was considered due to the heterogeneous features of CLL cells from different cases. The incomplete clinical information of those cases made no address for the explanation. Comparing the results of case #3637 with the results of this case under the standard culture condition (Figure 3.4 D), it can be found that the co-culture system may greatly improve viability of the primary CLL cells. Results of CLL case #3381 showed no difference in fludarabine-induced cell death between the stimulated and unstimulated cells (Figure 3.4 B). At the same time, it can be found that primary CLL cells from case #3381 were not sensitive to fludarabine as they had been treated under the standard condition. The treatment experiment on case #3381 was repeated twice and the results were similar. These results suggested that the co-culture condition may alter the sensitivity of the CLL cells from case #3381 to fludarabine. Again, no address for the explanation can be made from the incomplete clinical information of those cases.

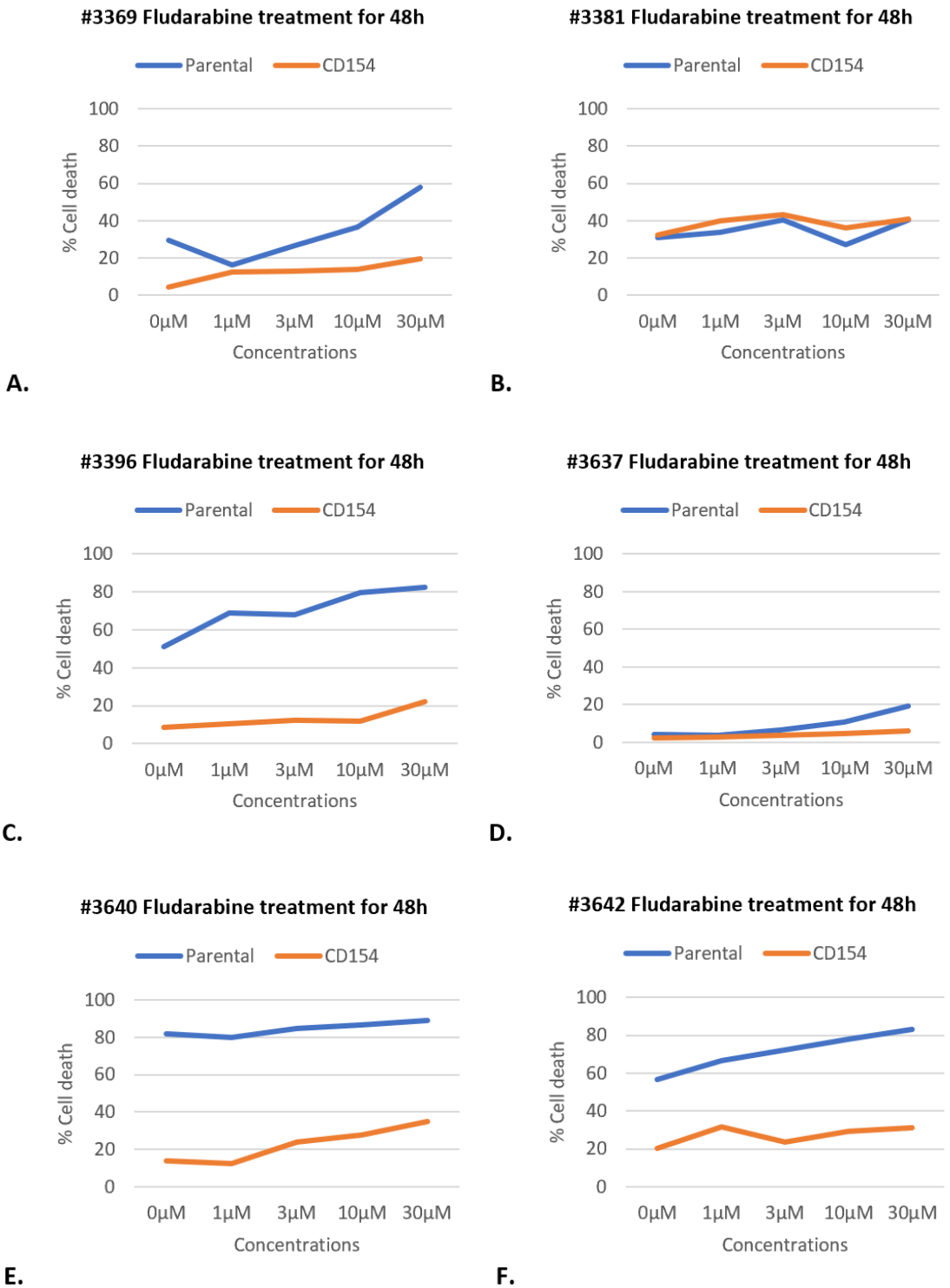

Figure 3.5 Cell death induced by fludarabine in CD40 stimulated and unstimulated CLL cells. CD154: CLL cells co-cultured with CD154 expressing fibroblasts for 24h for CD40 stimulation. Parental: CLL cells co-cultured with parental fibroblasts for 24h. CLL cells were co-cultured for 24h and collected from the co-cultures to be incubated with fludarabine for another 48h at standard culture conditions. Cell death was analysed by flow cytometry following staining cells with FITC labelled annexin V and PI as described in Methods.

When pooled the cell death data from the six cases and performed statistical analysis to determine if the difference in cell death between the CD40 stimulated and unstimulated cells, the average of those data showed that the differences were statistically significant at the concentrations of 0μM, 3μM, 10μM, 30μM, respectively. The pooled results showed that CD40 stimulation decreased the percentage of cell death induced by fludarabine on primary CLL cells (Figure 3.6) and the differences in cell death of the average data across six cases between CD40 stimulated cells and unstimulated cells were statistically significant at 3μM (with 49.83% ± 30.17 for the unstimulated and 19.97% ± 13.62 for the CD40 stimulated cells), 10μM (with 53.14% ± 32.13 for the unstimulated and 20.50% ± 12.13 for the CD40 stimulated cells), 30μM (with 62.02% ± 27.86 for the unstimulated and 25.81% ± 12.41 for the CD40 stimulated cells), respectively. Importantly, the difference in cell death between the CD40 stimulated and unstimulated cells that were treated without fludarabine was also statistically significant (Figure 3.5, average data for 0μM fludarabine with 42.34% ± 26.91 for the unstimulated and 13.66% ± 11.17 for the CD40 stimulated cells). Although the pooled data showed there were statistical significance between the cell death induced by fludarabine in CD40 stimulated and unstimulated primary CLL cells, the high standard errors indicated that there were obvious variation across the primary CLL cells from different cases, which made the results of individual cases more valuble than the pooled results.

These results thus demonstrated that CD40 stimulation protected primary CLL cells from spontaneous and fludarabine-induced cell death.

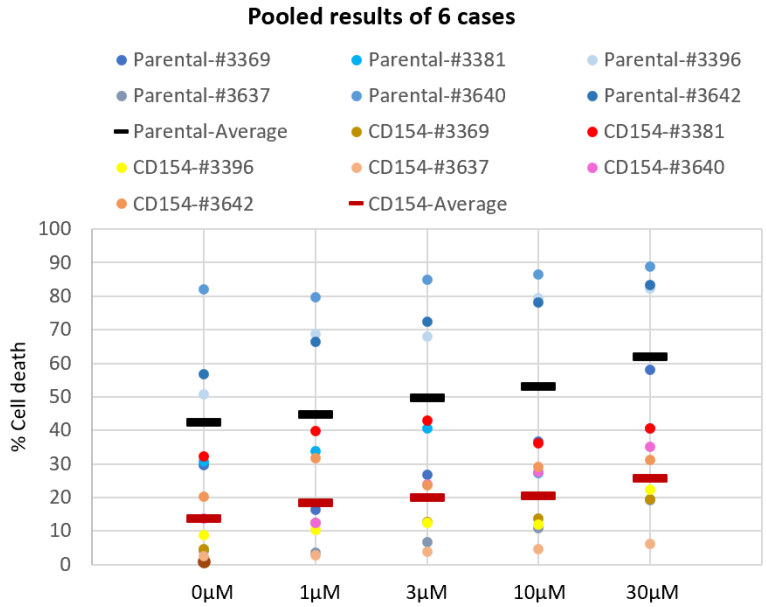

Figure 3.6 Pooled results of fludarabine-induced cell death in CD40 stimulated and unstimulated CLL cells. CD154: primary CLL cells co-cultured with CD154 expressing fibroblasts for 24h for CD40 stimulation. Parental: primary CLL cells co-cultured with parental fibroblasts for 24h. CLL cells were co-cultured for 24h and collected from the co-cultures to be incubated with fludarabine for another 48h under standard culture conditions. At the end of incubation, CLL cells were harvested and cell death was analysed by flow cytometry following staining cells with FITC labelled annexin V and PI as described in Methods.

3.3.1.2 CD40 stimulation protects primary CLL cells from ABT-199-induced cell death

The next drug tested for this part of study was ABT-199. The experiment with ABT-199 was directly taken forward under the co-culture system without the response test under standard culture condition due to the reason that the resistance to ABT-199 in CLL cells was reported to be caused by the abnormal expression of the BCL-2 family proteins induced by the signals from the CLL microenvironment (Klanova et al., 2020). The concentrations of ABT-199 used were 0nM, 1nM, 10nM, 100nM, 1000nM. The choice of the concentrations was based on the findings of a published study in which ABT-199 was shown to effectively induce apoptosis in primary CLL cells with the LC_{50} of 3nM (Souers et al., 2013). Primary CLL cells were first co-cultured with CD154 expressing fibroblasts for 24h for CD40 stimulation and the cells co-cultured with the parental fibroblasts were used as the unstimulated controls. Both CD40 stimulated cells and the unstimulated cells were then collected from

the co-cultures separately and treated with different concentrations of ABT-199 for another 6h under standard culture conditions, respectively. There were three different CLL samples applied.

The results of individual CLL samples treated with ABT-199 showed an obvious difference in ABT-199-induced cell death between CD40 stimulated and unstimulated cells (Figure 3.7). For all three CLL samples, the percentages of cell death of the CD40 stimulated cells (Figure 3.7 A-C, orange lines) were dramatically lower than those of the unstimulated cells (Figure 3.7 A-C, blue lines).

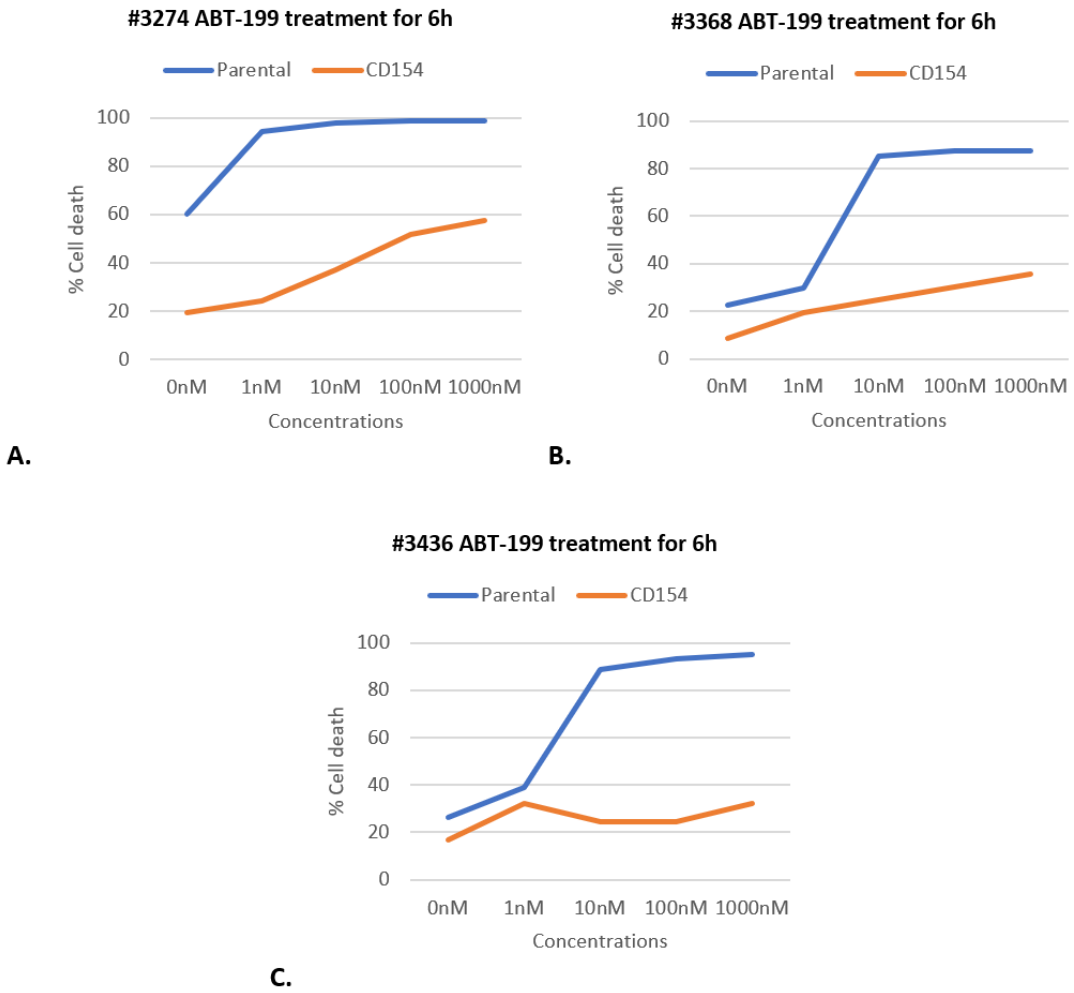

Figure 3.7 Cell death induced by ABT-199 in CD40 stimulated and unstimulated CLL cells. CD154: primary CLL cells co-cultured with CD154 expressing fibroblasts for 24h for CD40 stimulation. Parental: primary CLL cells co-cultured with parental fibroblasts that were used as unstimulated controls. CLL cells were co-cultured for 24h and collected from the co-cultures to be incubated with ABT-199 for another 6h under standard conditions. At the end of incubation, CLL cells were harvested and cell death was analysed by flow cytometry following staining cells with FITC labelled annexin V and PI as described in Methods.

The pooled data showed that the differences in ABT-199-induced cell death between CD40 stimulated and unstimulated cells were statistically significant at 10nM (with 90.72% ± 6.56 for the unstimulated and 28.76% ± 7.24 for the CD40 stimulated cells), 100nM (with 93.19% ± 5.74 for the unstimulated and 35.54% ± 14.53 for the CD40 stimulated cells), and 1000nM (with 93.76% ± 5.94 for the unstimulated and 41.78% ± 13.85 for the CD40 stimulated cells), respectively (Figure 3.8). Although the decrease was not statistically significant, the cell death of the CD40 stimulated cells without ABT-199 treatment was lower than that of the unstimulated cells without ABT-199 treatment.

These results clearly show that CD40 stimulation protects primary CLL cells from ABT-199-induced cell death.

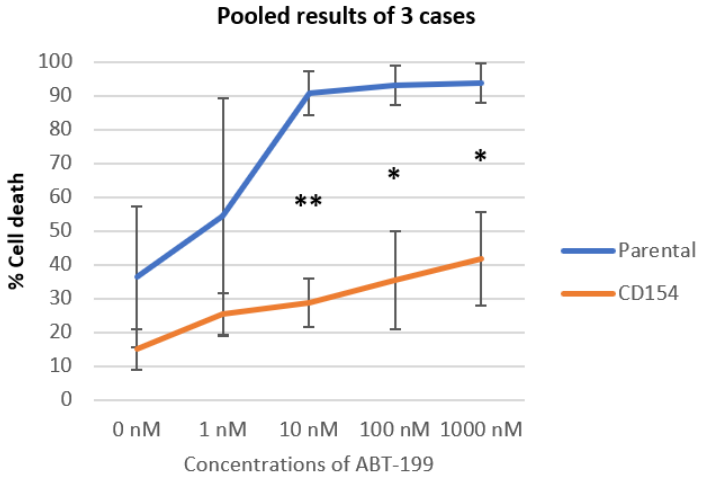

Figure 3.8 Pooled data of ABT-199-induced cell death in CD40 stimulated and unstimulated CLL cells. CD154: primary CLL cells co-cultured with CD154 expressing fibroblasts for 24h for CD40 stimulation. Parental: primary CLL cells co-cultured with parental fibroblasts that were used as unstimulated controls. Primary CLL cells were co-cultured for 24h and collected from the co-cultures to be incubated with ABT-199 at the indicated concentrations for another 6h under standard conditions. At the end of incubation, CLL cells were harvested and cell death was analysed by flow cytometry following staining cells with FITC labelled annexin V and PI as described in Methods. Mean ± SD of the results of 3 cases are shown. Statistical analysis was performed using the two-tailed, paired Student's t-test. * and ** indicate p-value < 0.05 and < 0.01, respectively.

3.3.1.3 CD40 stimulation protects primary CLL cells from bendamustine-induced cell death

The third drug tested the effect of CD40 stimulation on primary CLL cells was bendamustine. Based on the findings from a previous study by our research group (Chapman et al., 2017), the final concentrations of bendamustine used in this study were 0μM, 1μM, 3μM, 10μM, 30μM, 100μM. Primary CLL cells were first co-cultured for 24h with the CD154-expressing or parental fibroblasts, as described previously. Co-cultured CLL cells were then collected and incubated with different concentrations of bendamustine for another 24h under standard culture conditions. Three individual CLL samples were applied in this part of the study.

The results of individual CLL samples showed an obvious difference in bendamustine-induced cell death between CD40 stimulated and unstimulated CLL cells (Figure 3.9 A-C). CD40 stimulation decreased the percentage of cell death induced by bendamustine for all three CLL samples. Considering that the LC_{50} of bendamustine in primary CLL cells at standard culture condition is 27.48μM (Purroy et al. 2015), the results of case #3259 and case #3436 showed that the unstimulated CLL cells from those two cases did not as sensitive to bendamustine as reported. However, considering that the unstimulated primary CLL cells were co-cultured with the parental fibroblasts and that the cell adhesion status may alter the response pattern of primary CLL cells to some degree, those results were explicable.

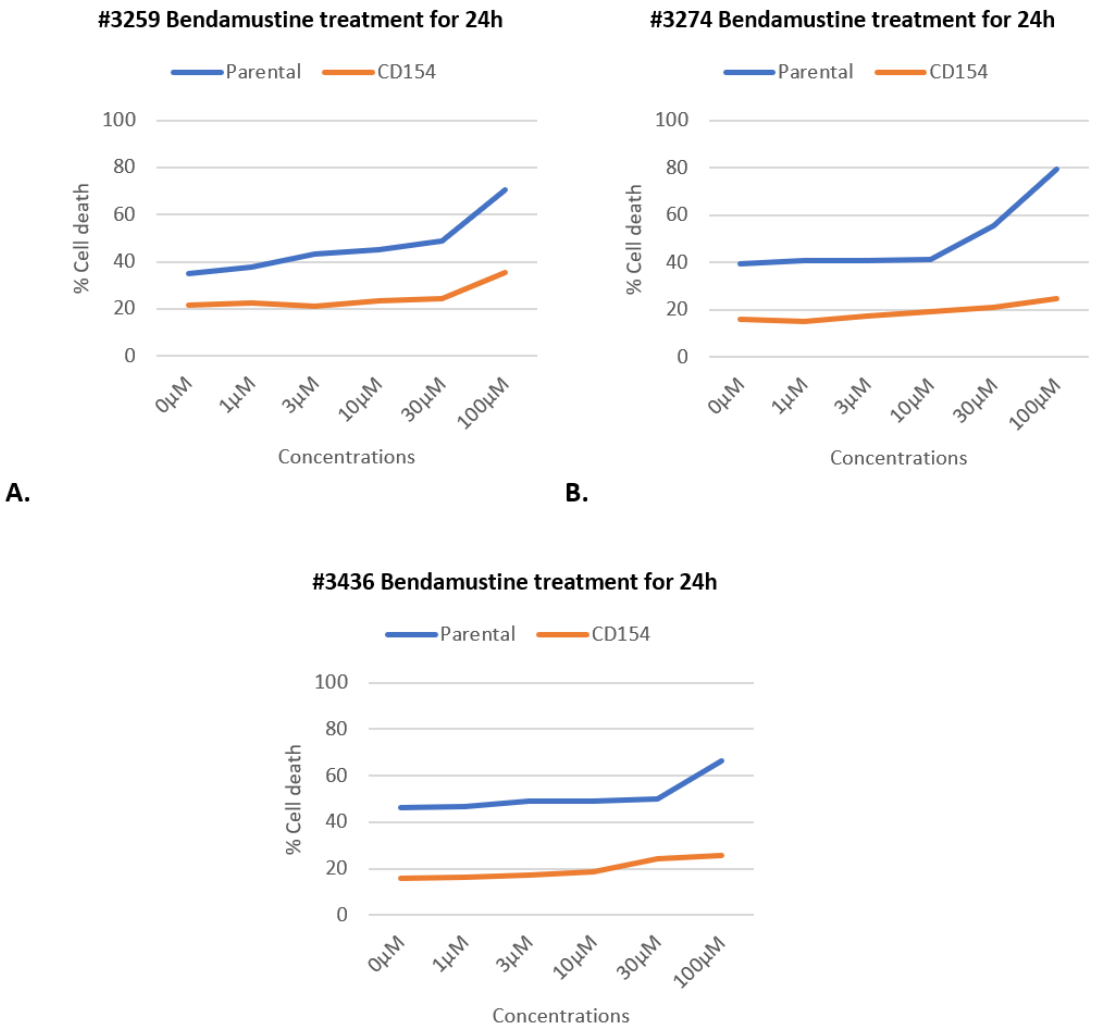

Figure 3.9 Cell death induced by bendamustine in CD40 stimulated and unstimulated CLL cells. CD154: primary CLL cells co-cultured with CD154 expressing fibroblasts for 24h for CD40 stimulation. Parental: primary CLL cells co-cultured with parental fibroblasts that were used as unstimulated controls. Primary CLL cells were co-cultured for 24h and collected from the co-cultures to be incubated with bendamustine at the indicated concentrations for another 24h under standard conditions. At the end of incubation, CLL cells were harvested and cell death was analysed by flow cytometry following staining cells with FITC labelled annexin V and PI as described in Methods.

The pooled data showed that the differences between CD40 stimulated and CD40 unstimulated cells were statistically significant at each concentration of bendamustine (Figure 3.10). The percentage of cell death at 1μM was 41.76% ± 4.58 for the unstimulated cells and 18.04% ± 4.12 for the CD40 stimulated cells. The percentage of cell death at 3μM was 43.19% ± 5.27 for the unstimulated cells and 18.52% ± 2.25 for the CD40 stimulated cells. The percentage of cell death at 10μM was 45.17% ± 3.79 for the unstimulated cells

and 20.35% ± 2.59 for the CD40 stimulated cells. The percentage of cell death at 30µM was 51.52% ± 3.64 for the unstimulated cells and 23.30% ± 2.00 for the CD40 stimulated cells. Finally, the percentage of cell death at 100µM was 72.07% ± 6.80 for the unstimulated and 28.52% ± 5.89 for the CD40 stimulated cells. The difference in cell death between the CD40 stimulated and unstimulated cells that were treated without bendamustine was also statistically significant (Figure 3.10, data for 0µM bendamustine: 40.23% ± 5.68 for the unstimulated and 17.78% ± 3.35 for the CD40 stimulated cells).

These results suggest that CD40 stimulation protects primary CLL cells from spontaneous and bendamustine-induced cell death.

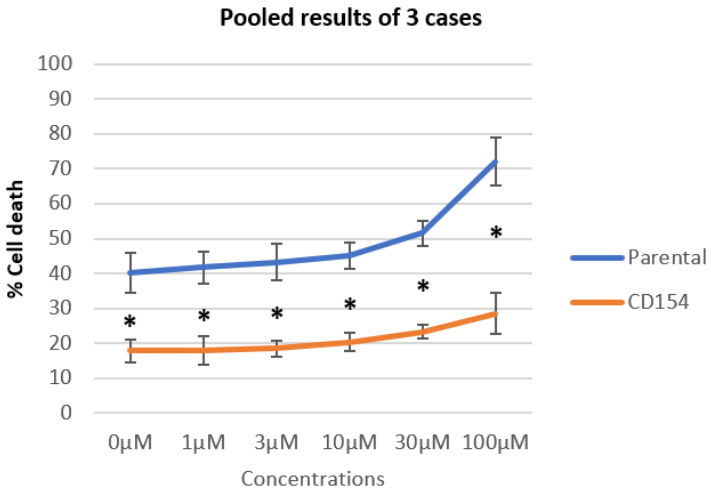

Figure 3.10 Pooled data of bendamustine-induced cell death in CD40 stimulated and unstimulated CLL cells. CD154: primary CLL cells co-cultured with CD154 expressing fibroblasts for 24h for CD40 stimulation. Parental: primary CLL cells co-cultured with parental fibroblasts that were used as unstimulated controls. Primary CLL cells were co-cultured for 24h and collected from the co-cultures to be incubated with bendamustine at the indicated concentrations for another 24h under standard conditions. At the end of incubation, CLL cells were harvested and cell death was analysed by flow cytometry following staining cells with FITC labelled annexin V and PI as described in Methods. Mean ± SD for 3 cases is shown. Statistical analysis was performed using the two-tailed, paired Student's t-test. * indicate p-value < 0.05.

The results obtained clearly showed that CD40 stimulation protected primary CLL cells from spontaneous and drug-induced cell death by fludarabine, ABT-199, and bendamustine. It has been reported that CD40 stimulation up-regulated the expression of a group of anti-apoptotic proteins such as BCL-XL and MCL-1 in CLL cells (Kater et al., 2004), which was considered one possible reason for the resistance to ABT-199 induced by CD40 stimulation

(Klanova et al., 2020). However, CD40 stimulation also up-regulates the expression of pro-apoptotic proteins such as BID in CLL cells (Kater et al., 2004, Smit et al., 2007). Considering the bi-directional effect in survival caused by CD40 stimulation, the molecular mechanism mediating the pro-survival effect and the multi-drug resistance induced by CD40 stimulation need further study to clarify. The overall aim of this study was to unravel the CD40 stimulation-induced pro-survival signals by investigating the changes in protein expression at a global level.

3.3.2 Comparison of two CD40 stimulation methods (the co-culture system versus the soluble CD40 ligand system)

As stated earlier, the soluble CD40 ligand system is a preferred method to induce CD40 stimulation in primary CLL cells for the proteomics study. Therefore, it was necessary to figure out whether the soluble CD40 ligand can reproduce the biological effect as that induced by the co-culture system on primary CLL cells. The soluble CD40 ligand stimulation method was optimised based on the published method (Lezina et al., 2018). Viability results showed that CD40 stimulation induced by the soluble CD40 ligand method protected primary CLL cells from spontaneous cell death (Figure 3.11). Considering the high level of cell death in samples that may affect the analysis, the viability tests were performed to ensure the quality of samples to be used for RNA-seq analysis. Originally, the criteria of initial viability over 70% and the 24h viability over 30% was chosen. However, since the primary CLL cells could not maintain such viability in culture, the samples used for RNA-seq were the six showed here (with the viability lower than the desired criteria).

As stated previously, the up-regulated expression of BCL-XL was chosen as the marker for the successful establishment of CD40 stimulation in primary CLL cells (Kater et al., 2004, Vogler et al., 2009a). The results of western blot of the BCL-XL expression level in primary CLL cells treated with and without the soluble CD40 ligand were showed in Figure 3.12 with the expression of BCL-XL up-regulated across all cases.

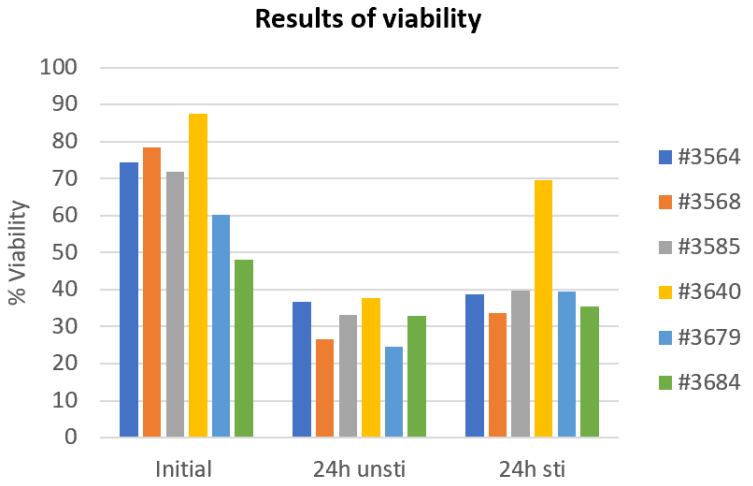

Figure 3.11 Viability of the samples used for RNA-seq. Initial: the viability detected after the recovery of the primary CLL cells from the cryopreservation. 24h unsti: the viability of the primary CLL cells incubated with 0.5ng/ml anti-HA antibody for 24h; 24h sti: the viability of the primary CLL cells incubated with 0.1ng/ml HA-tagged CD40 ligand and 0.5ng/ml anti-HA antibody for 24h.

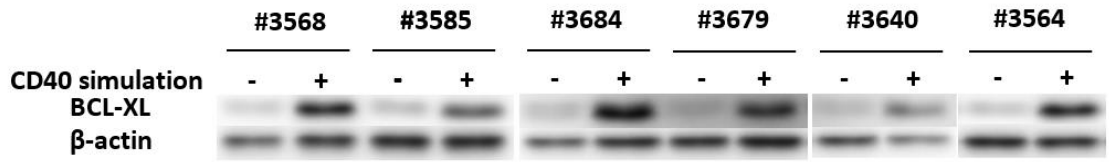

Figure 3.12 Induction of BCL-XL in CLL cells treated with or without the soluble CD40 ligand as detected by Western blotting. The plus sign '+' represents the CD40 stimulated cells of each CLL sample, in which primary CLL cells were incubated with 0.1ng/ml HA-tagged CD40 ligand and 0.5ng/ml anti-HA antibody for 24h. The minus sign '-' represents the unstimulated cells of each CLL sample, in which primary CLL cells were incubated with 0.5ng/ml anti-HA antibody for 24h.

As described previously, six primary CLL samples were used as the biological replicates, and two groups of cells were prepared from those six samples, i.e. CD40 stimulated and unstimulated CLL cells. In addition, two time points were considered for the duration of stimulation (12h and 24h). Consequently, there should be a total of twenty-four RNA samples to be sent for mRNA sequencing. After the re-examination by NOVOGENE, two of the RNA samples from the unstimulated CLL cells of case #3679 at 12h and case #3684 at 24h did not meet the requirement of the minimum amount of mRNA for sequencing. In the end, mRNA sequencing was performed on twenty-two RNA samples. 33,126 genes were identified from these samples in total. The raw sequencing data provided by NOVOGENE

was then analysed by the bioinformatics group led by Professor Francesco Falciani in the University of Liverpool, who filtered the genes and produced a new list of 33121 genes. Then, they performed a normalization in DESeq2 on the filtered data to put more emphasis on the moderately expressed genes (Anders and Huber, 2010). Further analyses were all based on the filtered and normalized data.

3.3.2.1 CD40 stimulation induced by the soluble CD40 ligand system causes changes in the gene expression in primary CLL cells

Due to missing data from unstimulated CLL cells of cases #3679 at 12h and #3684 at 24h, the sequencing data from the corresponding CD40 stimulated samples at the 12h and 24h had to be excluded from the data analysis of the paired samples between the CD40 stimulated and unstimulated cells. The principal component analysis (PCA) of all the genes basing on the filtered and normalised data showed that the CD40 stimulated samples were distributed separately from the unstimulated samples for both time points (Figure 3.13 A and B).

Based on the filtered and normalized data, the differential expression analysis was performed between the CD40 stimulated and unstimulated samples for the two time points using DESeq2. Genes with the adjusted p-value less than 0.01 and false discovery rate (FDR) 1% (Benjamini-Hochberg correction) were considered to be significantly differentially expressed. The results of the differential expression analysis showed that, for the 12h time point, there were 2029 significantly up-regulated genes and 1988 significantly down-regulated genes (Appendix 4, 5). For the 24h time point, there were 2046 significantly up-regulated genes and 1986 significantly down-regulated genes (Appendix 6.7). The separations between the CD40 stimulated samples and the unstimulated samples for two time points, respectively, were observed by the PCA analyses of the significantly differentially expressed genes (Figure 3.14 A and B).

The results of the differential expression analysis showed that the CD40 stimulation induced by the soluble CD40 ligand system caused a significant difference in gene expression on primary CLL cells at the transcriptional level.

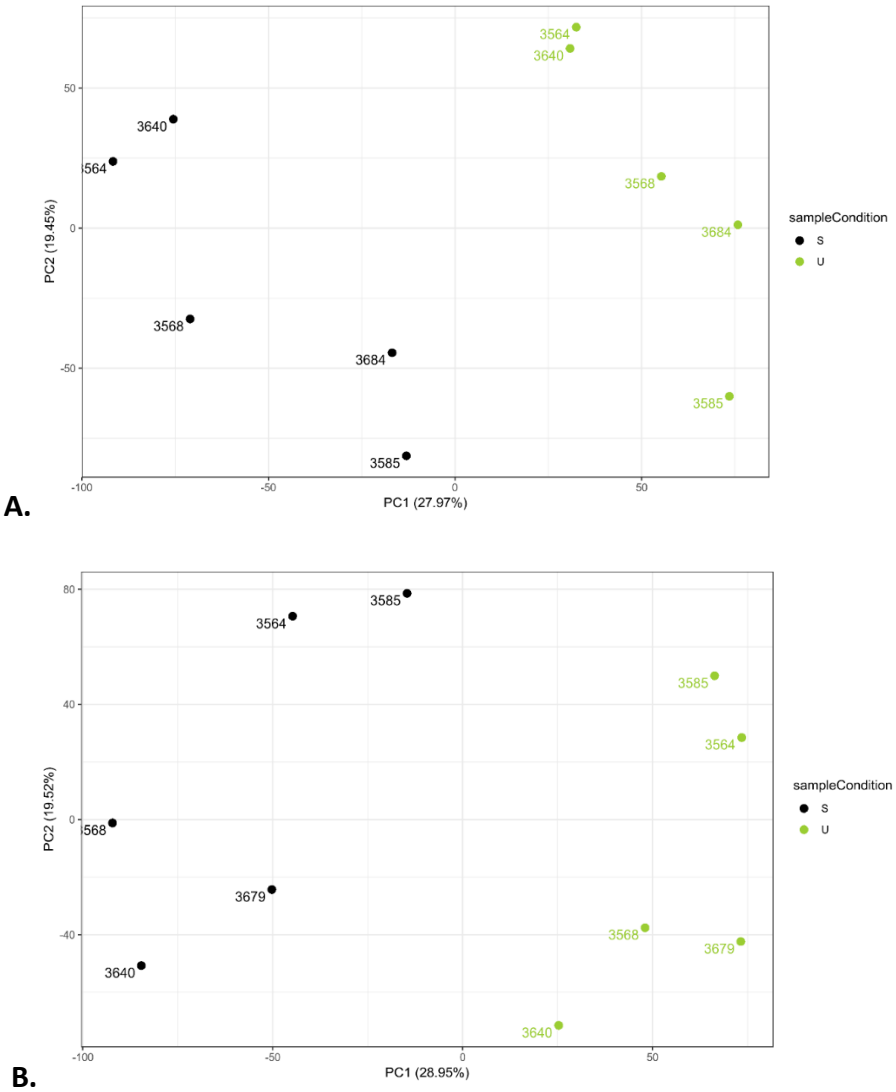

Figure 3.13 PCA for all genes. (A) the results of 12h data. (B) the results of 24h data. Black spots labelled with s represent the CD40 stimulated samples. Green spots labelled with u represent the CD40 unstimulated samples.

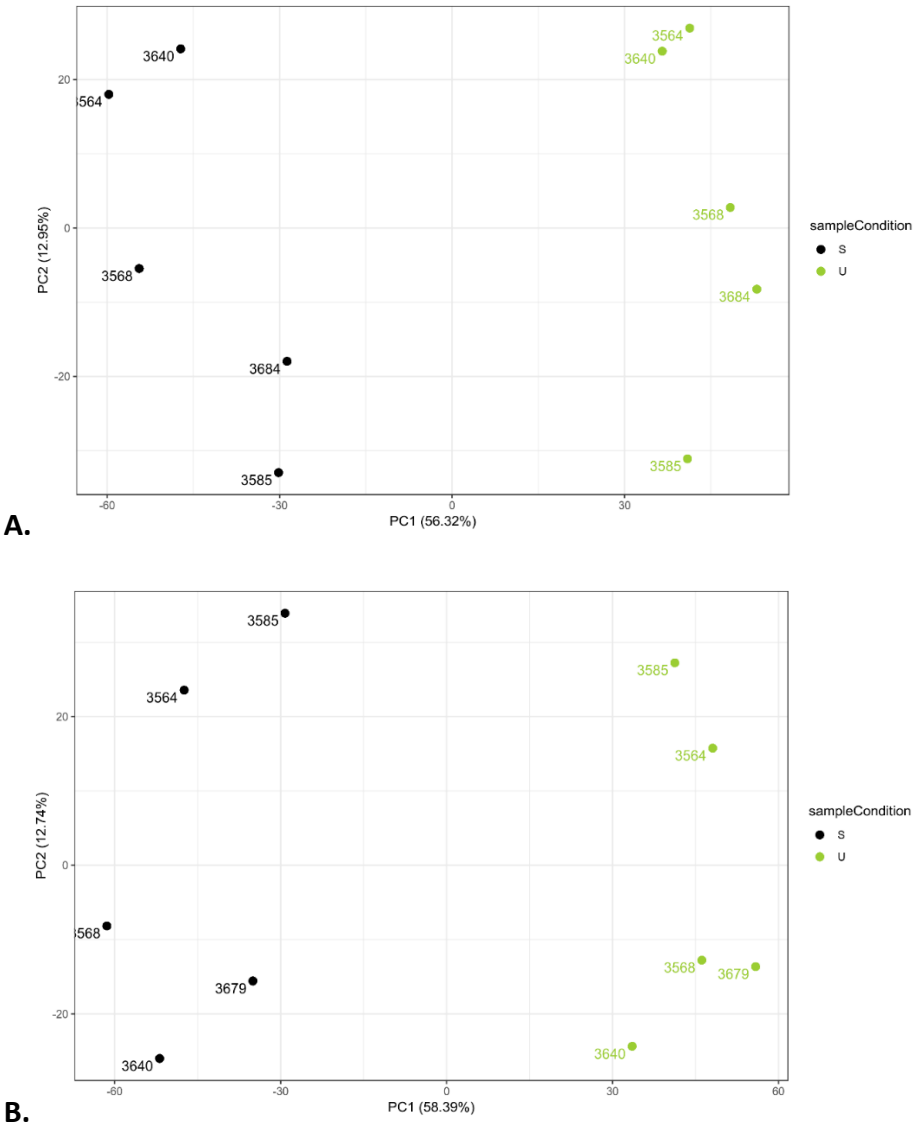

Figure 3.14 PCA for significantly differentially expressed genes ($p_{adjusted}$ value < 0.01, FDR 1%). (A) the results of 12h data. (B) the results of 24h data. Black spots labelled with s represent the CD40 stimulated samples. Green spots labelled with u represent the CD40 unstimulated samples.

3.3.2.2 The changes in gene expression at the transcriptional level induced by the soluble CD40 ligand system do not differ significantly from 12h to 24h

To figure out whether the changes in gene expression induced by the soluble CD40 ligand differ significantly with time, the differentially expressed genes identified at the two time points were compared. For 12h time point, the number of significantly differentially expressed genes was 4017 with 2029 genes up-regulated and 1988 genes down-regulated. For 24h time point, the number of significantly differentially expressed genes was 4032 with

2046 genes up-regulated and 1986 genes down-regulated. The results of the comparison showed that there were 3269 genes consistently presenting at both lists and the percentages of consistency were 81% for both (Figure 3.15 A). The numbers of the consistent gene targets for significantly up-regulated and significantly down-regulated were 1671 and 1598 and they made up over 80% of all the significantly differentially expressed gene targets (Figure 3.15 B and C).

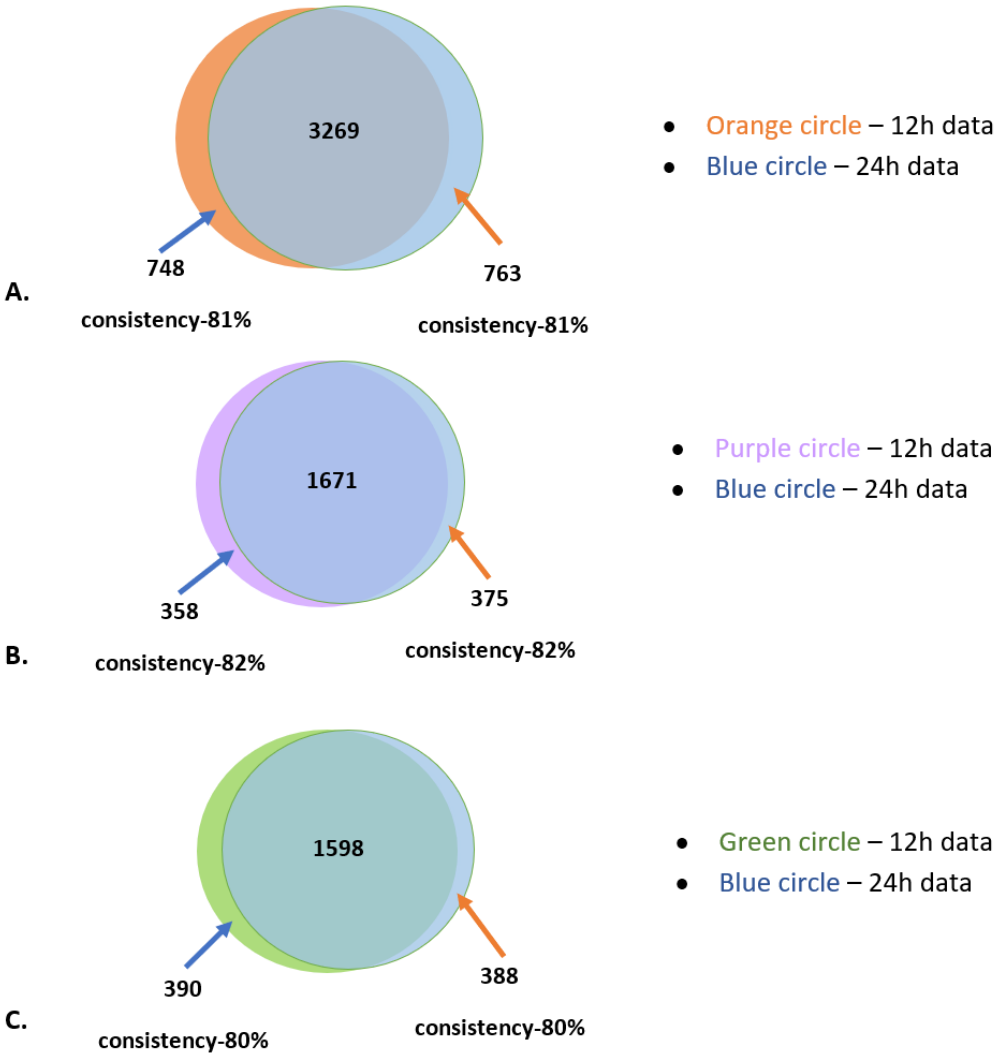

Figure 3.15 Comparing the significantly differentially expressed genes detected between 12h and 24h time points. (A) Comparison of all the significantly differentially expressed genes detected; (B) Comparison of the significantly up-regulated genes detected; (C) Comparison of the significantly down-regulated genes.

Based on the results of the comparison (summarized in Table 3.3), it was clear that the majority constituents of the 12h data and the 24h data were similar, which suggested that

the changes in gene expression induced by the soluble CD40 ligand on primary CLL cells at the transcriptional level have not altered much from 12h to 24h. Because of the similarity, further analysis will be focused on the differentially expressed genes obtained at the 24h time point for simplicity.

Table 3.3 Summary of the data comparison between 12h and 24h

	12h data	24h data	Consistency *	%**
All the genes detected	17231	17487	16856	98%/96%
All significant (Padj<0.01)	4017	4032	3269	81%/81%
Significantly up-regulated (Padj<0.01)	2029	2046	1671	82%/82%
Significantly down-regulated (Padj<0.01)	1988	1986	1598	80%/80%

*: Consistency means the genes consistently present on both lists;
**%: the percentage of consistent genes in 12h data/ the percentage of consistent genes in 24h data.

3.3.2.3 The changes in gene expression of CLL cells activated by the soluble CD40 ligand method are similar to that of the CLL cells activated by the co-culture method

The gene expression profile obtained from this study was compared with the published dataset of differentially expressed genes induced by the co-culture system (Pascutti et al., 2013). The data obtained with 24h stimulation from both studies were compared. Using the adjusted p-value less than 0.05 as a cut-off, 6306 genes were found to be significantly differentially expressed with 2804 up-regulated and 3502 down-regulated in the published study. In this study with the adjusted p-value less than 0.01 and the False discovery rate (FDR) of 1%, 4032 genes were found to be differentially expressed in CLL cells induced by the soluble CD40 ligand, with 2046 up-regulated and 1986 down-regulated.

The comparison between the soluble CD40 ligand and the co-culture system was analysed using GSEA 4.0.3. The results showed that the up-regulated gene targets induced by the soluble CD40 ligand were very similar to those up-regulated by the co-culture CD40 system. The enrichment score (Figure 3.16 A) of the up-regulated gene targets was strongly positive, which indicated a strong overlap of the up-regulated gene targets between the two sets of data. A similar conclusion was drawn with the analysis of the down-regulated gene targets (Figure 3.16 B). The false discovery rate q-values (shorten as FDR q-val in Table 3.4) of the up-regulated and down-regulated (Table 3.4) were both less than 0.0005, indicating they

were highly significant. Based on the results, the high level of similarity in gene expression induced by the soluble CD40 ligand and co-culture system was unlikely caused by random chance. The results of GSEA therefore show that the changes in gene expression induced by the soluble CD40 ligand on primary CLL cells were very similar to that induced by the co-culture system.

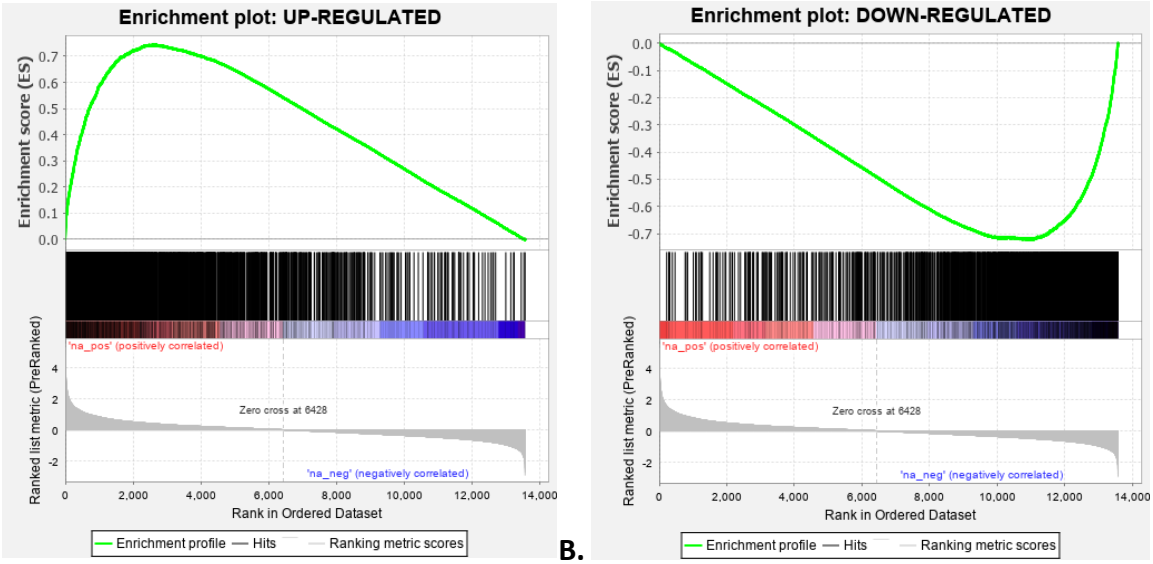

Figure 3.16 Enrichment plots of the comparison for the up-regulated targets and down-regulated targets between the two sets of data.

Table 3.4 The FDR q-value of the comparison of the up/down regulated gene targets.

	GS follow link to MSigDB	GS DETAILS	SIZE	ES	NES	NOM p-val	FDR q-val	FWER p-val	RANK AT MAX	LEADING EDGE
1	UP-REGULATED	Details ...	1818	0.74	3.82	0.000	0.000	0.000	2585	tags=60%, list=19%, signal=64%

	GS follow link to MSigDB	GS DETAILS	SIZE	ES	NES	NOM p-val	FDR q-val	FWER p-val	RANK AT MAX	LEADING EDGE
1	DOWN-REGULATED	Details ...	1747	-0.72	-4.00	0.000	0.000	0.000	2520	tags=63%, list=19%, signal=67%

Note: The GSEA software only uses 3 decimal places. The FDR q-value here for the up-regulated and down-regulated are both reported as 0, which means the values are less than 0.0005 indicating they are highly significant. p-val: p-value; q-val: q-value.

3.3.2.4 Gene expression profile of CLL cells treated with the soluble CD40 ligand is similar to that of CLL cells localised in the lymph node

The paper published by Herishanu and colleagues in 2011 reported the differential gene expression profiles of the CLL cells in lymph nodes, bone marrow, and peripheral blood as well (Herishanu et al., 2011). To determine whether the gene expression profile of CLL cells induced by the soluble CD40 ligand resembles that of CLL cells localised from any of the tissue sites, assisted by bioinformaticians from Prof. Falciani's group, the gene expression data from this study was compared to the data from the published study. The gene expression data induced by the soluble CD40 ligand were divided into four groups, '12h up', '12h down', '24h up', and '24h down'. The four sets of data were further compared separately with the three ranked lists of the differentially expressed genes in CLL cells located between the different tissues (lymph node versus bone marrow, lymph node versus peripheral blood, bone marrow versus peripheral blood). The GSEA results have been shown in Table 3.5, Table 3.6, and Table 3.7.

Table 3.5 The positive retrieved enrichment in the comparison between the gene expression data induced by the soluble CD40 ligand and the ranked list of lymph node vs bone marrow

	GS follow link to MSigDB	GS DETAILS	SIZE	ES	NES	NOM p-val	FDR q-val	FWER p-val	RANK AT MAX	LEADING EDGE
Pos1	12_UP	Details ...	98	0.6	2.4	0	0	0	3358	tags=48%, list=20%, signal=60%
Pos2	24_UP	Details ...	83	0.5	2	0	0	0	3502	tags=46%, list=21%, signal=58%

Note: The GSEA software only uses 3 decimal places. The FDR q-val here for the up-regulated and down-regulated are both reported as 0, which means the values are less than 0.0005 indicating they are highly significant. p-val: p-value; q-val: q-value.

Table 3.6 The positive and negative retrieved enrichment in the comparison between the gene expression data induced by the soluble CD40 ligand and the ranked list of lymph node vs peripheral blood

	GS follow link to MSigDB	GS DETAILS	SIZE	ES	NES	NOM p-val	FDR q-val	FWER p-val	RANK AT MAX	LEADING EDGE
Pos1	12_UP	Details ...	98	0.52	2.12	0	0	0	4128	tags=52%, list=25%, signal=69%
Pos2	24_UP	Details ...	83	0.36	1.42	0.02	0.036	0.046	3318	tags=30%, list=20%, signal=37%
Neg1	24_DOWN	Details ...	52	-0.46	-1.69	0.002	0.001	0.003	4208	tags=50%, list=25%, signal=67%

Note: The GSEA software only uses 3 decimal places. The FDR q-val here for the up-regulated and down-regulated are both reported as 0, which means the values are less than 0.0005 indicating they are highly significant. p-val: p-value; q-val: q-value.

Table 3.7 The negative retrieved enrichment in the comparison between the gene expression data induced by the soluble CD40 ligand and the ranked list of bone marrow vs peripheral blood

	GS follow link to MSigDB	GS DETAILS	SIZE	ES	NES	NOM p-val	FDR q-val	FWER p-val	RANK AT MAX	LEADING EDGE
Neg1	24_DOWN	Details ...	52	-0.4	-1.7	0.009	0.012	0.007	3190	tags=40%, list=19%, signal=50%

Note: The GSEA software only uses 3 decimal places. The FDR q-val here for the up-regulated and down-regulated are both reported as 0, which means the values are less than 0.0005 indicating they are highly significant. p-val: p-value; q-val: q-value.

The results of the comparison showed that gene targets up-regulated at 12h and 24h by the soluble CD40 ligand were also up-regulated in the ranked list of lymph nodes versus bone marrow. This indicated that the genes up-regulated by the soluble CD40 ligand can also be found in CLL cells located in the lymph node.

Results also showed that gene targets up-regulated at 12h and 24h by the soluble CD40 ligand were up-regulated in the ranked list of lymph nodes versus peripheral blood. At the same time, gene targets down-regulated by the soluble CD40 ligand at 24h were down-regulated in the ranked list of lymph nodes versus peripheral blood as well. It further suggests that CD40 stimulation by the soluble CD40 ligand simulated the interaction of CLL cells with the lymph node microenvironment.

The results of the comparison analysis showed that gene targets down-regulated by the soluble CD40 ligand at 24h were also down-regulated in the ranked list of bone marrow versus peripheral blood. This indicated that genes down-regulated by the soluble CD40 ligand can also be found in CLL cells located in the bone marrow. It suggested that the soluble CD40 ligand simulated the negative influences in gene expression of CLL cells by the bone marrow.

In summary, the main results from the RNA sequencing study showed that: (1) changes to gene expression induced by the soluble CD40 ligand were similar to the changes induced by the co-culture system; (2) gene expression profile of CLL cells treated with the soluble CD40 ligand were similar to that of CLL cells localised in the lymph nodes, indicating that CD40

stimulation induced by the soluble CD40 ligand imitated the interaction of CLL cells with T cells within lymph nodes.

3.4 Discussion

The experiments of cell death induction in primary CLL cells showed that CD40 stimulation protected primary CLL cells from both spontaneous and drug-induced cell death, indicating that CD40 stimulation induced pro-survival signals on CLL cells. Ideally, it was preferable to repeat the treatment of each case three times separately for technical replicates, but the limited supply of primary CLL samples restricted the repeat of experiments for each case for the research project. To obtain a reliable result, at least three primary CLL cases were applied for each drug treatment except for fludarabine treatment. The primary CLL cases were taken randomly from the biobank to avoid selection bias. Those considerations above help to make the results more persuasive. The variation from case to case in response to each drug largely reflects the heterogeneity of CLL.

The results of fludarabine treatment were consistent with previously published data showing that CD40 stimulated CLL cells resist to the induction of cell death by fludarabine (Romano et al., 1998b, Kitada et al., 1999, Kater et al., 2004). One paper reported that CD40 stimulation sensitized CLL cells to fludarabine treatment in 2003 (De Totero et al., 2003), which seems contradictory to the data present here in this study. However, there were several issues mainly related to different methodologies. Firstly, in their study, the cells used as controls to the CD40 stimulated CLL cells were CLL cells cultured under standard conditions, the so-called 'resting cells'. In contrast, in this study, the primary CLL cells co-cultured with the parental fibroblasts were used as the controls. It is known that the co-culture condition can influence CLL cells through, in addition to CD40 stimulation, 'cell-to-cell' contacts and exposing CLL cells to secreted chemokines and cytokines by the fibroblasts (Ghia et al., 2002, Pascutti et al., 2013), which may affect their response to drug treatment. Therefore, it is more rigorous to use the same culture condition consistently throughout the experiments to accurately determine the response of CD40-stimulated CLL cells to

fludarabine. This was also the reason that the drug treatment following the CD40 stimulation was conducted on the primary CLL cells that collected from the co-culture system. From this point of view, the soluble CD40 ligand stimulation method is a better choice to study the specific influence of CD40 stimulation. Therefore, soluble CD40 ligand stimulation method was chosen for the proteomics study in this project. Secondly, the ratio of the CD40-expressing fibroblasts and primary CLL cells in the co-culture system was 1:100 in the study reported by De Totero and colleagues, which was different from this study where the ratio at 1:10 applied here. Besides, the duration of CD40 stimulation, the concentration of fludarabine and the duration of fludarabine treatment used in their study were all different from this study. Therefore, it is likely that the discrepancy of the results is caused by the different methods used in the studies.

Regarding the responses of CD40-stimulated CLL cells to the treatment with ABT-199 and bendamustine, the results were consistent among the cases comparing with the results of fludarabine, even though variations in response was still observed across CLL cases. CD40 stimulation protects CLL cells from cell death induced by these two cytotoxic drugs. Given the heterogeneous nature of CLL, these variations are not unexpected. These results from this study thus are consistent with the previously published data (Thijssen et al., 2015, Bojarczuk et al., 2016, Chapman et al., 2017, Jayappa et al., 2017, Brocco et al., 2017, Thijssen et al., 2013). For bendamustine, the results of two cases showed that the unstimulated primary CLL cells from #3259 and #3436 were not as sensitive to bendamustine, as previously reported in other studies (Purroy et al., 2015). In the published paper, the LC_{50} of bendamustine in primary CLL cells maintained in standard culture condition was 27.48μM (Purroy et al., 2015). The decreased sensitivity to bendamustine may partly be attributed to the co-culture system, in which parental fibroblasts may have lower the cell responsiveness due to changes in cell adhesion status.

The investigation of the effect of CD40 stimulation on the drug-induced cell death indicates that CD40 stimulation induces pro-survival signals on primary CLL cells. The drugs applied in this study, namely fludarabine, ABT-199, and bendamustine, have different cytotoxic mechanisms. This suggests that the pro-survival signals induced by CD40 stimulation can

lead to chemo-resistance for CLL cells. The theory that the chemo-resistance phenomenon induced by CD40 stimulation may be mediated through common pro-survival signals/pathways can be supported by evidence. Many studies have shown that the ligation of CD40 on CLL cells results in increased expression of several anti-apoptotic proteins, such as BCL-XL (Granziero et al., 2001, Kitada et al., 1999, Pedersen et al., 2002, Kater et al., 2004), MCL-1 (Scielzo et al., 2011, MCCaig et al., 2011, Smit et al., 2007), Bfl-1 (Kater et al., 2004, Tromp et al., 2010) and BCL-2 (Scielzo et al., 2011) and decreased expression of pro-apoptotic proteins such as BH3-only proteins Noxa (Smit et al., 2007) and Harakiri (Hrk) (Kater et al., 2004). In addition, CD40 stimulation activates the NF-κB signalling pathways, which promotes the survival and proliferation of CLL cells (Furman et al., 2000, Lee et al., 1999, Romano et al., 1998b).

The analysis of mRNA sequencing data showed that stimulating primary CLL cells using the soluble CD40 ligand system can induce similar changes at the gene expression level to that induced by the co-culture system. The gene expression profile of CLL cells treated with the soluble CD40 ligand can resemble that of the CLL cells residing in the lymph nodes. Thus, the results of the gene expression study provided the reassurance that the soluble CD40 ligand can be used in the proposed proteomics study.

The gene expression profile obtained from CLL cells stimulated by the soluble CD40 stimulation was not exactly the same as that from the CLL cells stimulated by the co-culture system. The differences are not unexcepted. First of all, the methods of the two CD40 stimulation are different. During the experiment, it has been noticed that compared with CD40 stimulation induced by the soluble CD40 ligand, the co-culture system was better in sustaining the high viability of primary CLL cells, which indicates that there are some additional factors providing support to primary CLL cell besides CD40 stimulation. As mentioned above, it is obvious that the co-culture system causes not only the direct activation of the CD40 receptor on CLL cells by CD154 ligand expressed on the fibroblasts but also the cell-to-cell contacts which could activate other signalling pathways (Samuel et al., 2016, Nikitaki et al., 2016). The different forms of stimulation will thus inevitably cause differences in results, which makes reasonable to use the soluble CD40 ligand stimulation

method to study the specific influence induced by CD40 stimulation. Secondly, the gene profiles induced by the two CD40 stimulation systems were generated using the primary CLL samples from different patients, which could explain, at least in part, the differences in the gene expression. CLL is a heterogeneous disease so the variation in response to CD40 stimulation across samples from different patients is unsurprising. It is, however, clear that the more biological replicates were used, the more accuracy of results could be achieved. With the limitation in the supply of the primary CLL cases, 6 cases were considered to be the minimum number for the study of gene expression profiling. Due to the low quantity of RNA in 2 out of the 24 RNA samples, RNA sequencing data was generated from only 22 samples. Moreover, the final bioinformatics analysis for comparison of gene expression between CD40-stimulated and unstimulated cells had to rely on sequencing data from 20 paired samples from 5 primary CLL cases. The reduction in the number of cases from 6 to 5 affects the results as well.

In summary, in this part of study, the cytoprotective effect of CD40 stimulation against spontaneous and drug-induced cell death in CLL cells was independently confirmed. Comparing the gene expression profiles of CLL cells stimulated by the soluble CD40 ligand to that induced by the co-culture system, it was demonstrated that stimulation induced by the soluble CD40 ligand produced similar changes in gene expression in primary CLL cells that were stimulated by the co-culture system. Furthermore, the results revealed that the gene expression profile of CLL cells treated with the soluble CD40 ligand shared a high degree of similarity to that of CLL cells localised in the lymph nodes of patients with CLL. This novel finding thus indicates that CD40 stimulation induced by the soluble CD40 ligand can mimic the interaction of CLL cells with T cells in the lymph node microenvironment. Therefore, altogether, the above results provided reassurance that the soluble CD40 ligand can be used in the proposed proteomics study to study global changes in protein expression induced by CD40 stimulation on primary CLL cells.

Chapter 4. CD40 stimulation changes the protein expression in primary CLL cells at a global level, affecting a variety of biological processes

4.1 Background

Analysing the differentially expressed proteins induced by CD40 stimulation on primary CLL cells at a global level is the key part of this project. Mass spectrometry techniques have been applied to the study of CLL for several years (Thurgood et al., 2017, Eagle et al., 2015, Johnston et al., 2018), but they have not been used to study the effect of CD40 stimulation on CLL cells. Proteins perform the functions of individual genes. However, the imperfect correlation between the level of transcription (mRNA) and the level of protein translation makes it necessary to study the gene expression at the level of protein expression (de Sousa Abreu et al., 2009, Chen et al., 2002). The biological effects of CD40 stimulation at the cellular level presented in the previous chapter indicate that CD40 stimulation induces pro-survival signals that protect primary CLL cells from spontaneous and drug-induced apoptosis. It is thus possible that the levels of expression of many proteins are altered by CD40 stimulation, leading to the manifestation of the anti-apoptotic phenotype in CLL cells. The latest technique of mass spectrometry allows us to measure the change in the expression of proteins induced by CD40 stimulation comprehensively. Analysing those differentially expressed proteins can provide us with a better view of the influence of CD40 stimulation in primary CLL cells at the protein translational level, which in turn helps to identify the molecules/pathways mediating the pro-survival signals.

To achieve a good signal-to-noise ratio in protein samples used for the mass spectrometry analysis, I used the soluble CD40 ligand stimulation method to induce the CD40 stimulation on primary CLL cells. As described in the previous chapter, the co-culture method of CD40 stimulation requires primary CLL cells to be co-cultured with CD154-expressing fibroblasts, which could result in the contamination of the protein extracts from the co-cultured primary CLL cells with variable amounts of proteins from the fibroblast, thus obscuring the accuracy of the proteomic analysis. The analysis of the mRNA sequencing data described in the

previous chapter confirms that CLL cells stimulated by the soluble CD40 ligand have a similar gene expression profile to that of CLL cells stimulated by the co-culture CD40 stimulation system. The technique of mass spectrometry (MS) applied here was the isobaric tags for relative and absolute quantitation (iTRAQ). The principle of this technique has been provided in the Methodology Chapter.

4.2 Aims

This part of the study aims at identifying differentially expressed proteins induced by CD40 stimulation in primary CLL cells using iTRAQ-MS and investigating the biological significance of the differentially expressed proteins through bioinformatic analysis.

4.3 Methods

The workflow of iTRAQ-MS is shown in Figure 4.1. with each step described in the following sections.

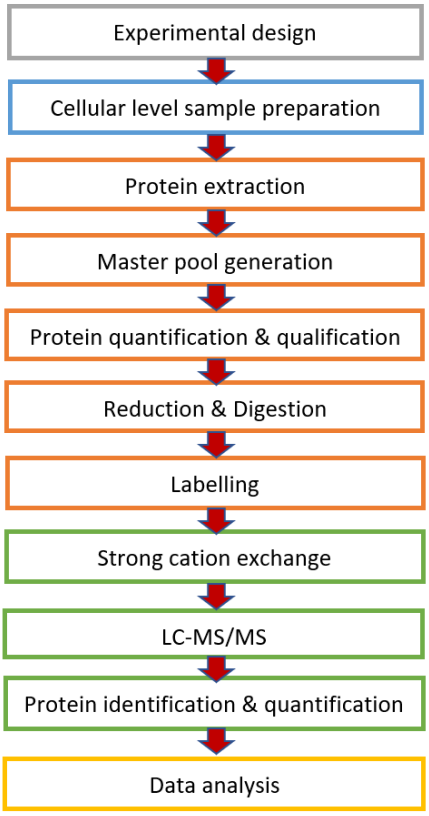

Figure 4.1 The workflow of the iTRAQ-MS process

4.3.1 The design of the iTRAQ experiment

As recommended by the collaborators at the Bioinformatics Team at the University of Liverpool, a minimum number of six primary CLL cases is required to produce sufficient statistical power for the meaningful analysis of the proteomics data. The cellular proteins extracted from the primary CLL cells incubated with or without the soluble CD40 ligand for 12h and 24h were generated for the iTRAQ-MS analysis. Besides, the cellular proteins extracted from the primary CLL cells at 0h time point were also prepared. Thus, five protein samples were generated from each primary CLL case. In total, there were thirty protein samples generated from six primary CLL cases.

The kit applied to this part was the iTRAQ® Reagents - 8plex (AB SCIEX, USA), which provides eight channels to analyse eight protein samples for each iTRAQ assay. Therefore, it needs at least four iTRAQ assays to complete the analysis of all thirty protein samples. To compare the results generated from all the iTRAQ assays, it is necessary to generate a common comparator. Accordingly, the design for analysing all thirty protein samples by iTRAQ-MS was described as follows:

1) To produce the common comparators, master pools were generated by collecting 50µg of proteins from each protein sample with the concentration of 100µg/20µl;
2) To have technical replicates, each iTRAQ assay had two channels for the master pools leaving the other six channels for protein samples to be analysed in each assay (as a result, five iTRAQ assays were performed to complete the analysis of all thirty samples);
3) To avoid operational bias, thirty protein samples from six primary CLL cases were allocated randomly across the five iTRAQ assays.

According to the above design, the detailed information of the sample allocation for each iTRAQ assay was generated randomly, as shown in Table 4.1.

Table 4.1. Grouping information of five iTRAQ experiments

iTRAQ No.1	iTRAQ No.2	iTRAQ No.3	iTRAQ No.4	iTRAQ No.5
Pool 1	Pool 1	Pool 1	Pool 1	Pool 1
Pool 2	Pool 2	Pool 2	Pool 2	Pool 2
3650-24t	3587-0	3607-12t	3640-12t	3606-24c
3587-24c	3605-12c	3650-24c	3607-0	3607-24c
3640-24t	3650-12t	3640-12c	3587-24t	3607-12c
3640-0	3587-12t	3605-0	3607-24t	3606-12c
3606-12t	3587-12c	3606-24t	3605-24t	3650-12c
3605-24c	3640-24c	3606-0	3605-12t	3650-0

Note: The four-digit number is the case number of the primary CLL samples used in this study. '-0' represents the samples collected at 0h time point; '-12c' represents the 12h CD40 unstimulated samples; '-12t' represents the 12h CD40 stimulated samples; '-24c' represents the 24h CD40 unstimulated samples; '-24t' represents the 24h CD40 stimulated samples.

4.3.2 Cellular protein sample preparation

The criteria for primary CLL case selection were:

1) the percentage of the CLL cells expressing both CD5 and CD19 should be at least 80%;

2) the initial viability of the primary CLL cells at 0h should be over 70% and the viability at 24h should be over 30%;

3) the minimum number of primary CLL cells used in each sample should be 40 million (to generate a minimum of 100μg of proteins needed for iTRAQ analysis).

The schematic of the sample preparation for each primary CLL case is shown in Figure 4.2. For each CLL case, the cell sample at 0h time point was harvested immediately after the thawing and recovery of the cryopreserved primary sample. The rest of the cells were cultured in the 6-well plate with a density of 5×10^6/ml. For CD40 stimulation, the primary CLL cells were treated with 0.1μg/ml HA-tagged CD40 ligand and 0.5μg/ml anti-HA antibody for 12h or 24h, respectively. For the unstimulated controls, CLL cells were treated with 0.5μg/ml anti-HA antibody for 12h or 24h, respectively.

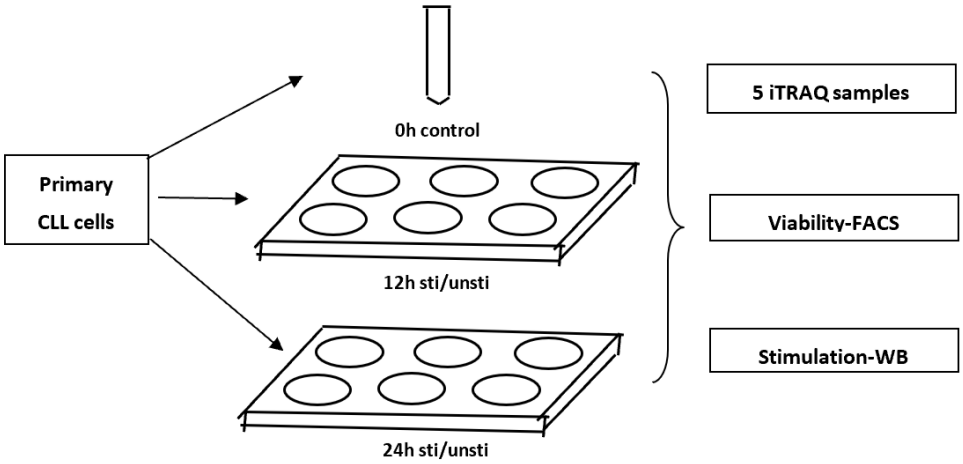

Figure 4.2 Schematic diagram of the preparation of each CLL sample for iTRAQ assay. 0h control: CLL cells harvested immediately after recovery without any manipulations; 12h/24h sti: CD40 stimulated CLL cells with 0.1µg/ml HA-tagged CD40 ligand + 0.5µg/ml anti-HA antibody for 12h/24h; 12h/24h unsti: CLL cells cultured with 0.5µg/ml anti-HA antibody for 12h/24h as unstimulated controls.

The viability of each sample was monitored by flow cytometry to meet the criteria of sample selection and the stimulation status was checked by Western blotting for BCL-XL with a specific BCL-XL antibody. The results of the six cases that passed all the tests are shown in Table 4.2, Figure 4.3, and Figure 4.4, respectively.

Table 4.2 The percentage of CD5 and CD19 double-positive CLL cells of the primary CLL samples used for iTRAQ assays

Case No.	Purity (%)
#3587	99.16
#3605	98.64
#3607	93.64
#3606	98.34
#3640	98.44
#3650	82.63

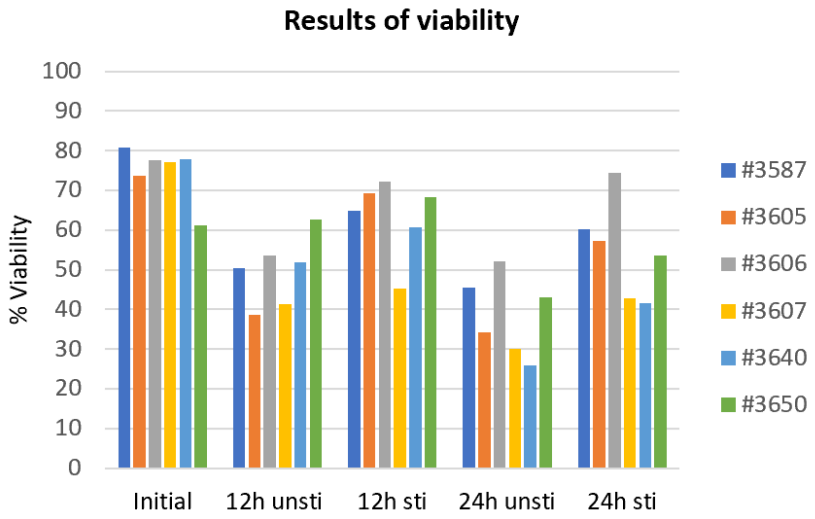

Figure 4.3 Viability of the samples used for iTRAQ assays. Initial: the viability of primary CLL cells after recovery. 12h/24h unsti: the viability of primary CLL cells incubated with 0.5µg/ml anti-HA antibody for 12h/24h. 12h/24h sti: the viability of primary CLL cells incubated with 0.1µg/ml HA-tagged CD40 ligand and 0. 5µg/ml anti-HA antibody for 12h/24h.

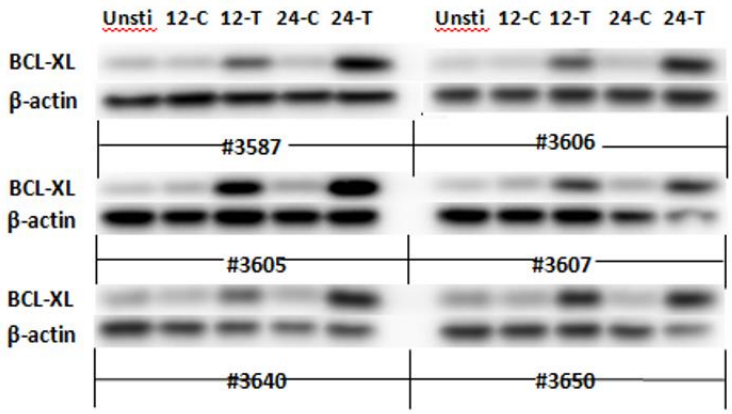

Figure 4.4 Confirmation of the CD40 activation status of primary CLL cells incubated with or without the soluble CD40 ligand. Western blotting was used to monitor the induction of the expression of BCL-XL as a marker for CD40 activation status. Unsti: 0h un-stimulated control, proteins extracted from the primary CLL cells were harvested after recovery; 12-/24-C: proteins extracted from the un-stimulated primary CLL cells that incubated with 0.5µg/ml anti-HA antibody for 12h/24h; 12-/24-T: proteins extracted from the stimulated primary CLL cells incubated with 0.1µg/ml HA-tagged CD40 ligand and 0. 5µg/ml anti-HA antibody for 12h/24h.

4.3.3 Protein extraction, quantification, and qualification

The entire procedure of the protein extraction was performed on ice. The primary CLL cells used for protein samples were washed three times using PBS, pH7.4 (0.89g KH_2PO_4 and

4.42g Na_2HPO_4 dissolved in 500ml ddH_2O) with centrifugation and removal of the supernatant between each wash. After washing, 50µl of 0.5M TEAB with 0.1% SDS was added to each sample and each sample was gently vortexed to mix well. The samples were sonicated three times using a probe sonicator and centrifuged at 20,000g, 4℃, for 15 minutes. After the centrifugation, the supernatant was transferred to the corresponding new labelled tubes. For each sample, 30µl was taken out for protein quantification using Bradford assay and the rest of the protein samples were stored at -80℃.

The 30µl of each sample taken out for the protein quantification was further diluted in 1:1, 1:5, 1:10, and 1:20 with phosphate buffer. The dilutions were plated on the 96-well plate with replicates. A standard curve of bovine serum albumin (BSA) in PBS was prepared from 0.1-2mg/ml and this was also plated in duplicate. Into each well was then added 250µl Bradford Reagent (Sigma Aldrich, Gillingham, UK), and the absorbance at 540nm was read on a spectrophotometer (Molecular Devices). The quantity of each sample was calculated according to the formula generated from the standard curve.

The quality of the samples was checked by running SDS-PAGE. For each sample, the volume of extract containing 10µg proteins was calculated and this volume was placed into a new 0.5ml Eppendorf tube. LC-MS-grade H_2O was added to make the volume up to 9µl. Then 3µl of 4× Laemmli sample buffer (8% SDS, 40% glycerol, 0.008% bromophenol blue, 0.25M Tris-HCl pH6.8, 5% β-mercaptoethanol) was added to the samples and they were heated for 10 minutes at 100℃. The samples were loaded onto a freshly-made 12% SDS-PAGE gel together with the SEEBLUE2 marker (the process of gel making has been described in chapter 2). After electrophoresis, the stacking gel was removed and the resolving gel was transferred into a plastic box with freshly made fix-solution (40% Methanol with 7% Acetic Acid). The gels were fixed for 30 minutes and then stained with 80% Coomassie Brilliant Blue solution (0.1% Coomassie Blue, 2% phosphoric acid, 10% ammonium sulphate) containing 20% HPLC grade methanol overnight at room temperature. Before being scanned, the gels were de-stained in 10% Acetic Acid with 25% Methanol for 60 seconds, rinsed with 25% methanol once, and then agitated overnight in 25% methanol to complete destaining. The

gels were scanned using a GS800 calibrated imaging densitometer (Bio-Rad). The results are shown in Figure 4.5.

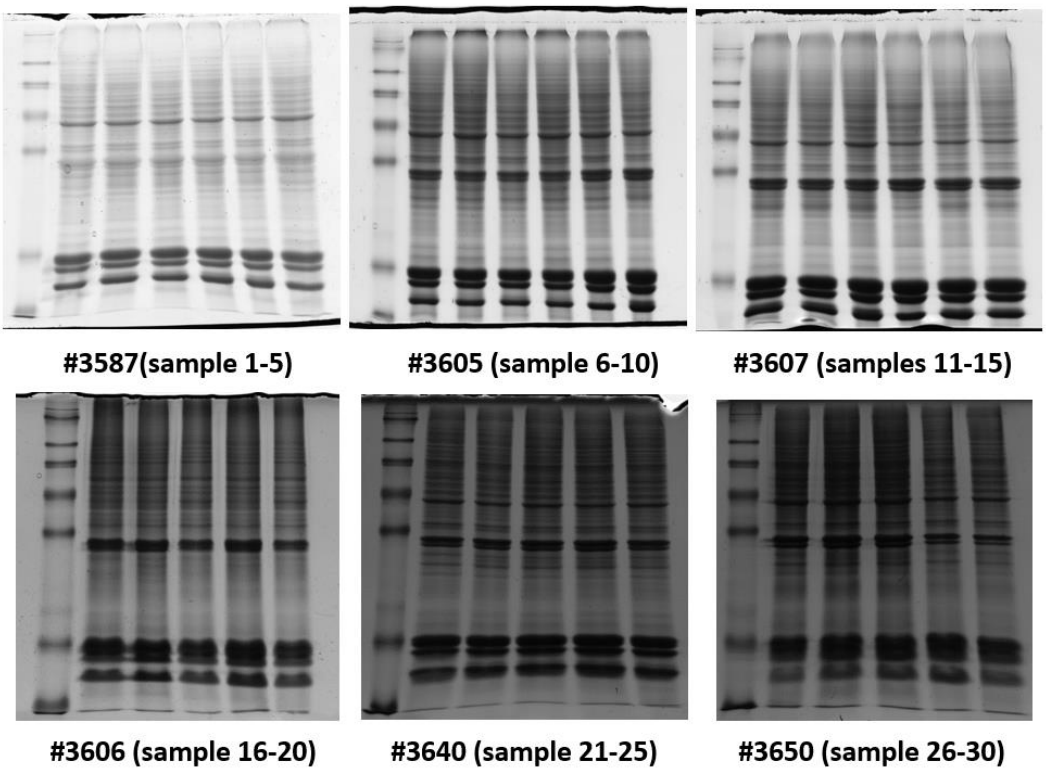

Figure 4.5 Protein quality determination by SDS-PAGE for all 30 protein samples used for iTRAQ-MS assays. For each gel, the first column of protein bands on the left was generated by SEEBLUE2 markers and the rest columns of protein bands were generated by the protein samples to be studied. The last sample on gel #3587, the first sample on gel #3605, and the last sample on gel #3607 were the samples from other cases that failed. The graph of #3587(sample 1-5) shows a lighter view comparing with the other five graphs because the staining duration was only 2h for that gel and the duration of the other 5 was overnight.

4.3.4 Generation of the master pool from thirty samples

According to the design and the number of iTRAQ assays, there should be 10 pools for five iTRAQ assays. Depending on the observed quantification of each sample, the volume required for 50µg was calculated and aliquots from all samples were pooled together. The final concentration was adjusted to 100µg/20µl using 0.5M TEAB with 0.1% SDS and aliquoted to 20µl each vial.

4.3.5 Reduction, digestion, and labelling

Aliquots of 100µg of protein from each sample were reduced with tris(2-carboxyethyl) phosphine (TCEP), the cysteine residues were capped with methyl methanethiosulfate (MMTS) and the proteins were digested with sequencing grade modified trypsin (catalogue number 0000276726, Promega, USA). After the overnight digestion, peptides were labelled with individual isobaric tags using 8plex reagents. The samples were then pooled and diluted to 4ml with 10mM KH2PO4 + 25% ACN. The pH value of the pool was adjusted to less than 3 with 500mM phosphoric acid.

4.3.6 Sample fractionation

Sample fractionation was achieved via the strong cation exchange chromatography using a Polysulfoethyl A column (200×4.6mm, 5µm, 300A, Poly LC, Columbia, MD) at a flow rate of 1ml/min. The gradient was from 10mM potassium dihydrogen phosphate and 25% (w/v) ACN to 0.5M potassium chloride, 10mM potassium dihydrogen phosphate, and 25% (w/w/v) ACN for 90 minutes. After the fractionation, 17 fractions were collected for each iTRAQ assay and the fractions were dried overnight by centrifugation under the vacuum condition. Then, the fractions were reconstituted with 1ml of 0.1% trifluoroacetic acid (TFA) and desalted by using the high-recovery protein column (4.6×50mm, Agilent, Berkshire, UK) on an Agilent 1260 HPLC system. The operations of this step were performed with the help of my secondary supervisor Dr. Rosalind Jenkins.

4.3.7 LC-MS analysis of iTRAQ samples

The desalted fractions were reconstituted in 40µl of 0.1% formic acid and aliquots of 5µl were delivered into a TripleTOF 6600 system (SCIEX) via an Eksigent NanoLC 400 system (SCIEX) mounted with a NanoAcquity 5µm, 180µm × 20mm C_{18} trap and 1.7µm, 75µm × 250mm analytical column (Water). A NanoSpray III source was fitted with a 10 µm inner diameter PicoTip emitter (New Objective, Woburn, MA). The trap column was washed with 2% ACN/0.1% formic acid for 10 minutes at 2.5 µl/min before switching in-line with the analytic column. A gradient of 2-50% ACN/0.1% (v/v) formic acid over 90 minutes was

applied to the column at a flow rate of 300nl/min. Spectra were acquired automatically in positive ion mode using information-dependent acquisition powered by Analyst TF 1.7 software (SCIEX), with survey scans of 250ms, MS/MS accumulation time of 100ms, and with monitoring of 25 most intense ions (total cycle time 2.75s). MS/MS spectra were acquired using a threshold of 100 counts/s and with the dynamic exclusion for 12s. The rolling collision energy was increased automatically by selecting the iTRAQ check box in Analyst and manually by increasing the collision energy intercepts by 5. This helps to ensure that the peptide precursor ions are efficiently fragmented leading to more consistent quantitative signals from the iTRAQ reporter ions. The operations of this step were performed with the help of my secondary supervisor Dr. Rosalind Jenkins.

4.3.8 iTRAQ data readout and data analysis

The data searching was performed using ProteinPilot 5.0 and the Paragon Algorithm (SCIEX) against the Swiss-Prot database (2017-4, 20201 human entries), with MMTS as a fixed modification of cysteine residues and biological modifications allowed. Mass tolerance for precursor and fragment ions was 10ppm. In addition, the data searching was also performed against a reversed decoy database and only proteins lying with a 1% global false discovery rate were taken forward for analysis (Shilov, I.V et al., 2007; Tang W.H. et al., 2008). This helps to exclude false-positive protein identifications. The protein identification was by several constituent peptides with at least 90% confidence in the correct sequence assignment.

Ratios for each iTRAQ label were obtained, using the master pools as the denominator. Data from the five iTRAQ experiments were merged using RStudio (v 1.0.143, RStudio Inc). Ratios were converted to their natural log and data analysis was performed using Partek Genomic Suite software (v.7.18.0518, Partek Inc.St.Louis, MO, USA). Hierarchical cluster analysis and principal component analysis (PCA) were performed on data batch corrected for the iTRAQ experiment. Proteins that were differentially expressed between the unstimulated and stimulated samples for 12h and 24h were revealed using a 2-way ANOVA on the non-corrected data, with both the stimulation status and the cases of primary CLL samples as

factors. Relevant volcano plots were derived from these data. The functional data analysis was performed by using the Protein Analysis Through Evolutionary Relationships (PANTHER) and Database for Annotation, Visualization, and Integrated Discovery (DAVID) online.

4.4 Results

The results will be divided into three parts (Figure 4.6): an overview of the proteomics data using hierarchical cluster analysis and principal component analysis (PCA), the differential expression analysis using the analysis of variance (ANOVA), and the functional enrichment analysis performed using the PANTHER and DAVID.

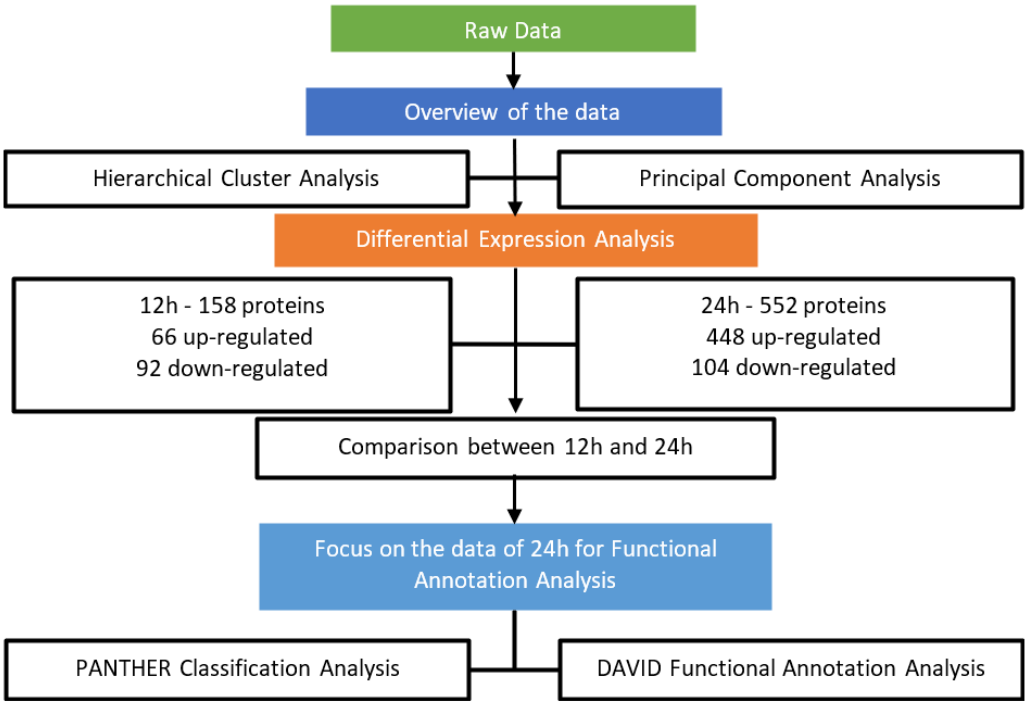

Figure 4.6 The workflow of iTRAQ-MS data analysis.

The raw data from the iTRAQ-MS assay was generated from 27 samples. Three samples (#3650-12h stimulated, #3650-24h unstimulated, and #3650-24h stimulated) failed to be labelled and processed well for analysis due to the quality of the iTRAQ 8plex kit.

There were 5583 proteins identified in five iTRAQ assays with a 1% false discovery rate (FDR) and 5303 proteins had been identified in all 27 iTRAQ samples. Among the 5303 proteins, 4093 proteins were quantified in all samples and these proteins were analysed further.

The master pool in each iTRAQ assay was used as a common comparator so that the five iTRAQ experiments could be merged. As described, there were two master pools in each iTRAQ experiment, and they were used as technical replicates. The raw data based on the master pool labelled with the iTRAQ reagent of 113-mass reporter group was called the 113-dataset and the raw data based on the master pool labelled with the iTRAQ reagent of 114-mass reporter group was called the 114-dataset. Theoretically, the protein data based on the 113-master pool and that based on the 114-master pool should be the same. However, in reality, there were some differences between 113 and 114 datasets. Based on whether the mean ratio of all the proteins to the pool is close to 1 as the criteria of the quality for the datasets, the 113-dataset was considered to be better than the 114-dataset. That is the reason why the 113-dataset was taken for further analysis.

4.4.1 The heterogeneity of CLL cases predominates the difference in the overall protein expression across CLL samples

Hierarchical cluster analysis and PCA were performed to get a visualized overview of the extent of the dispersion of the data. Initially, the hierarchical cluster analysis and the PCA were performed on the iTRAQ data minus the pools with no correction applied (Figure 4.7). The hierarchical clustering showed that samples from the same primary CLL case were assembled together (Figure 4.7 A). When performing the PCA, the variables were changed by using the incubation time (Figure 4.7 B), the incubation time together with the stimulation status (Figure 4.7 C), the iTRAQ experiment number (Figure 4.7 D), and the number of primary CLL cases (Figure 4.7 E), respectively. Comparing the PCA labelled with different variables, the results showed that samples separated based on the number of primary CLL cases and there was no clear separation when taking the other three variables.

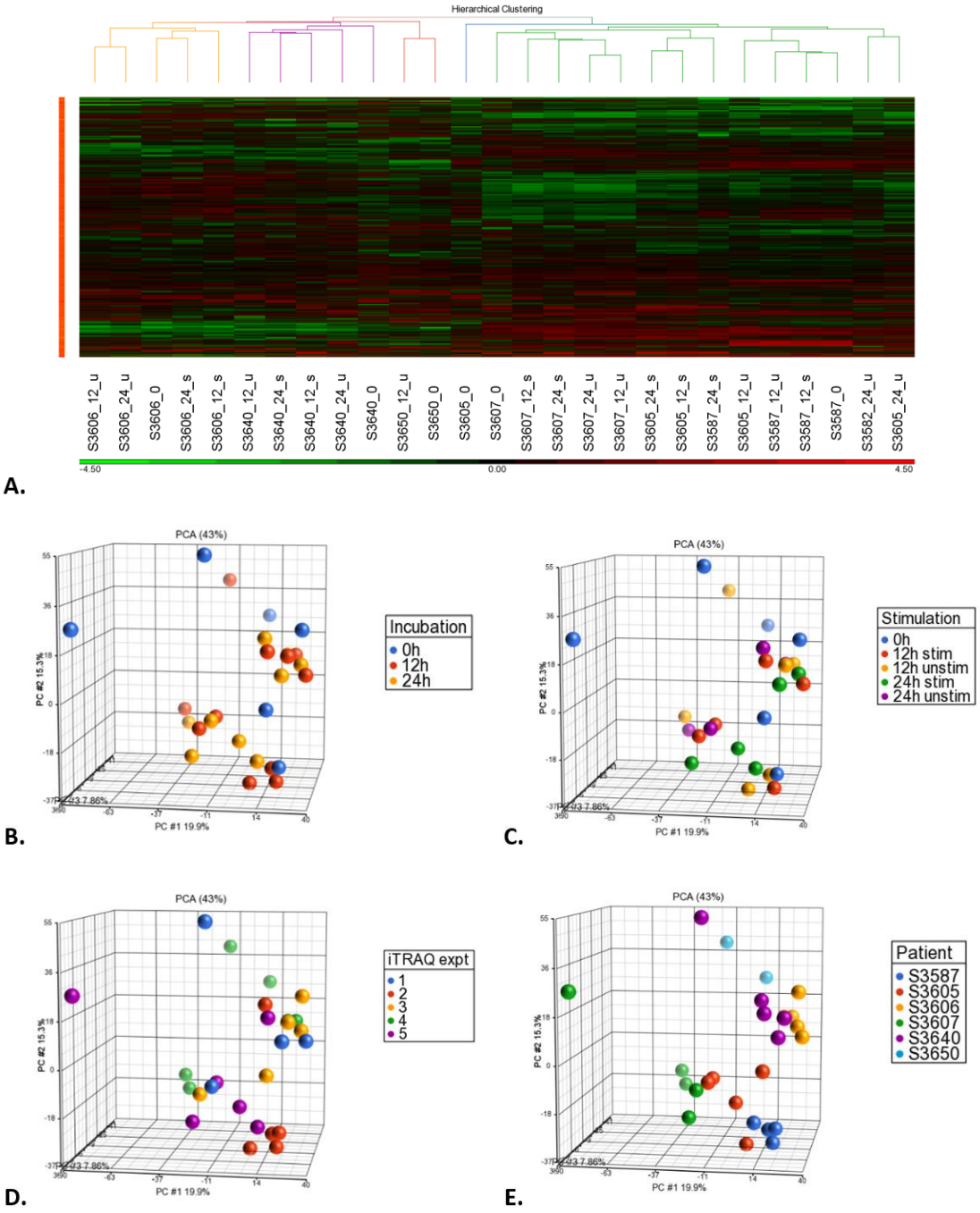

Figure 4.7 Hierarchical cluster analysis and PCA of the proteomics data generated by iTRAQ-MS assay without any correction. (A) the results of the hierarchical cluster show that samples from the same primary CLL case are assembled. (B) the PCA taking the incubation time as the variable shows no separation of the samples. (C) the PCA taking the incubation time together with the stimulation status as the variable shows no separation. (D) the PCA taking the iTRAQ experiment number as the variable shows no separation. (E) the PCA taking the number of primary CLL cases as the variable shows the separation of the samples.

The initial analysis indicated that it was necessary to perform a batch correction to remove the effect of the source of the samples, the number of primary CLL cases. Based on the data minus the pools with batch correction for the cases of the primary CLL samples, the hierarchical clustering showed that the CD40 stimulated and unstimulated samples were partially assembled (Figure 4.8 A), which indicated some separation between the CD40 stimulated and the unstimulated samples. However, the results of PCA showed that the separation based on the number of primary CLL cases, which observed previously, became blurry (Figure 4.8 B). Instead, samples were separated to a certain degree based on the iTRAQ experiment number (Figure 4.8 C).

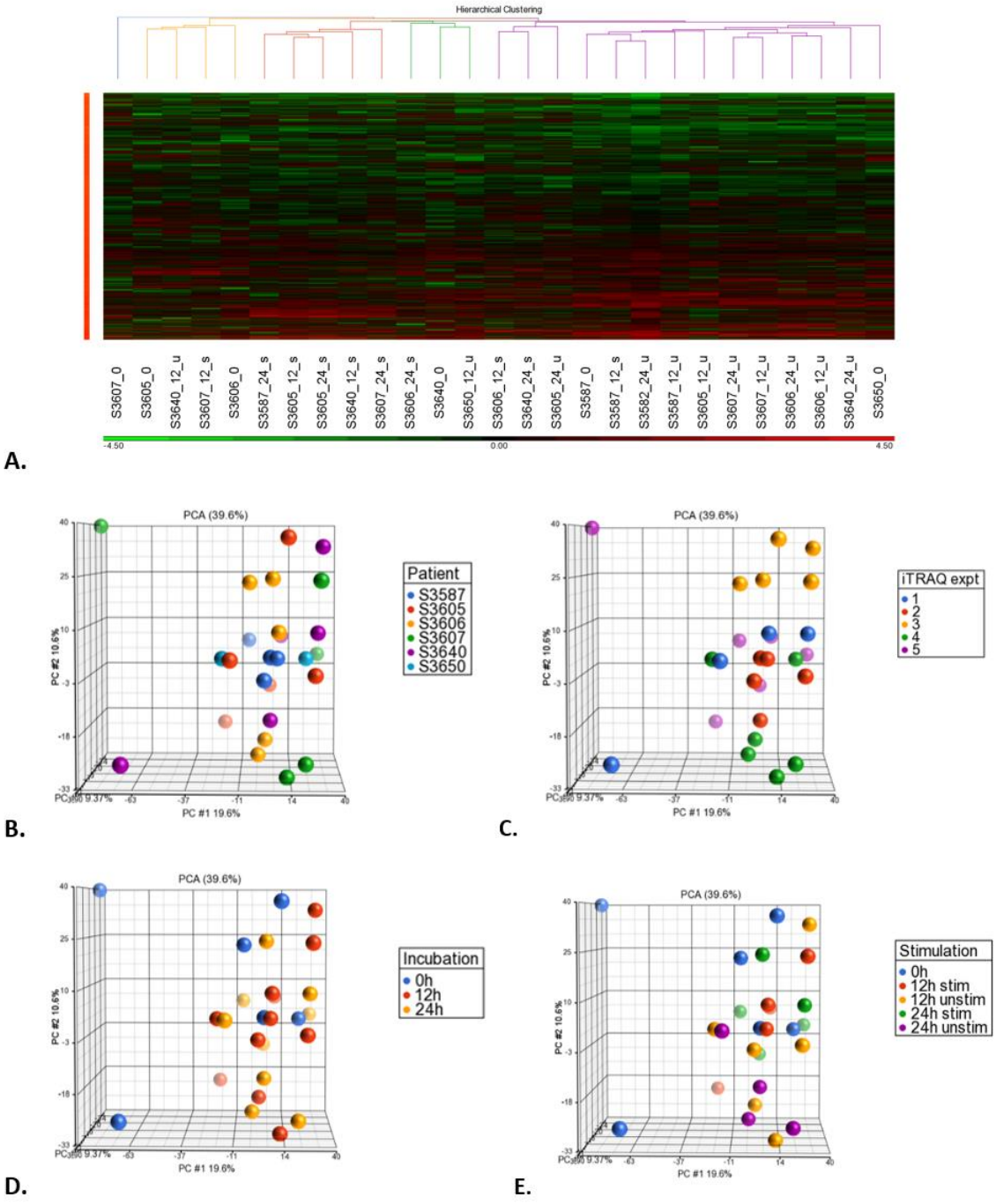

Figure 4.8 Hierarchical cluster analysis and PCA of the proteomics data with the correction for the cases of primary CLL samples. (A) the result of hierarchical cluster analysis shows that the CD40 stimulated and unstimulated samples are partially assembled. (B) the PCA taking the number of primary CLL cases as the variable shows no clear separation. (C) the PCA taking the iTRAQ experiment number as the variable shows a separation to a certain degree. (D) the PCA taking the incubation time as the variable shows no separation. (E) the PCA taking the incubation time together with the stimulation status as the variable shows no separation.

Based on the above results, it was reasonable to perform batch correction for both the cases of primary CLL samples and the iTRAQ experiment number. The results showed that the correction for both variables mixed the samples up and removed any obvious clusters (Figure 4.9). Under this circumstance, reviewing the distribution of all samples across five iTRAQ experiments, quite by chance, the iTRAQ experiment 4 was dominated by CD40 unstimulated samples and iTRAQ experiment 5 was dominated by CD40 stimulated samples (Table 4.1). Therefore, correcting for the iTRAQ experiment would remove much of the true differences between CD40 unstimulated samples and CD40 stimulated samples. It was thus reasonable to take the cases of primary CLL samples as a variable alongside the stimulation status: only the batch correction for the cases should be performed for the analysis.

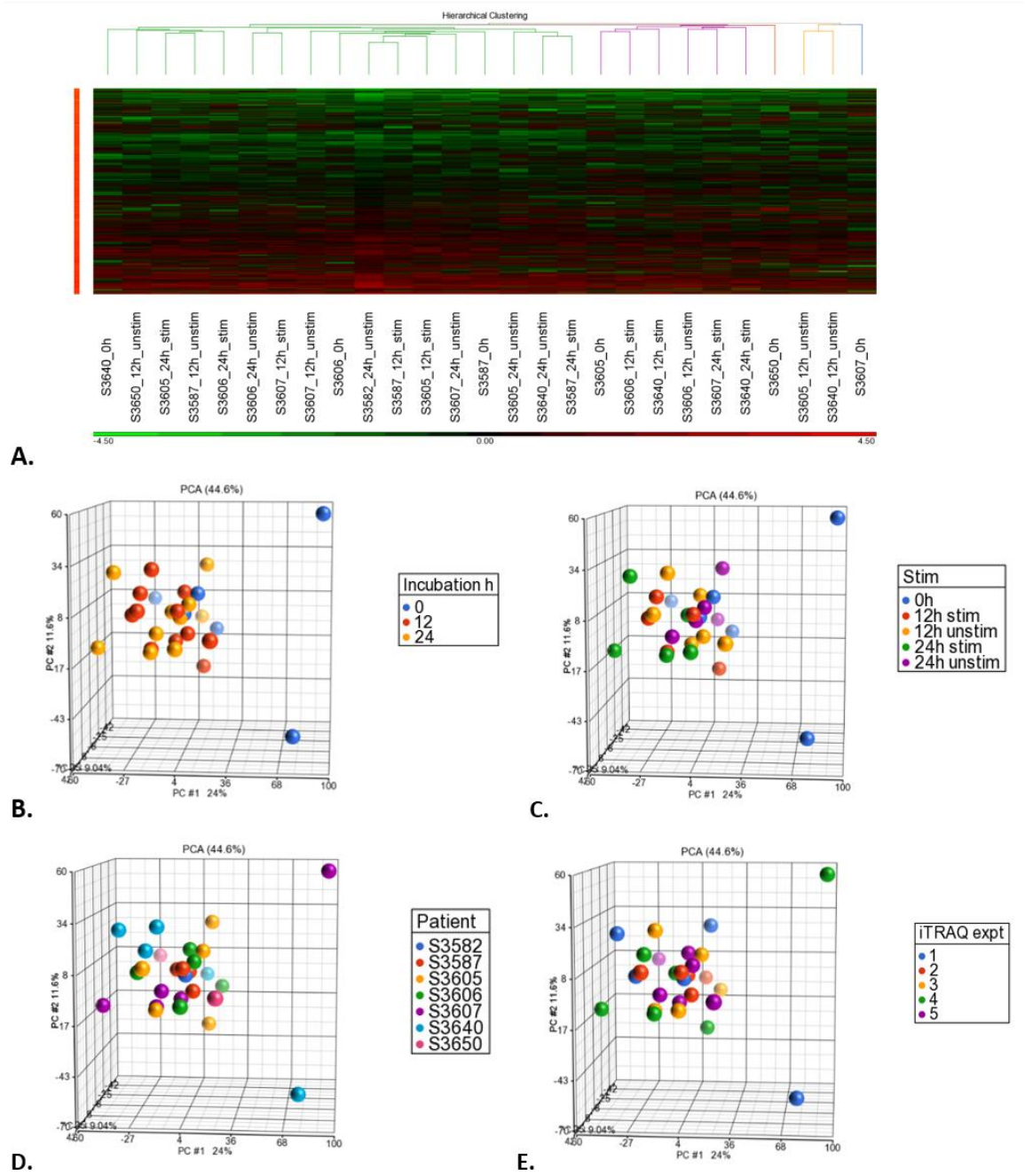

Figure 4.9 Hierarchical cluster analysis and PCA of the proteomics data with the correction for both the number of primary CLL cases and the number of the iTRAQ experiments. The results of the hierarchical cluster analysis (A) and the PCA (B, C, D, E) show no clear separation of the samples.

To get a further view, the data with batch correction for the cases of primary CLL samples were replotted with the two time points respectively taking the CD40 stimulation status as the variable (Figure 4.10). Results displayed the separation between the CD40 stimulated and the unstimulated samples, among which the separation was more obvious at the 24h time point (Figure 4.10 B) compared with that of the 12h time point (Figure 4.10 A).

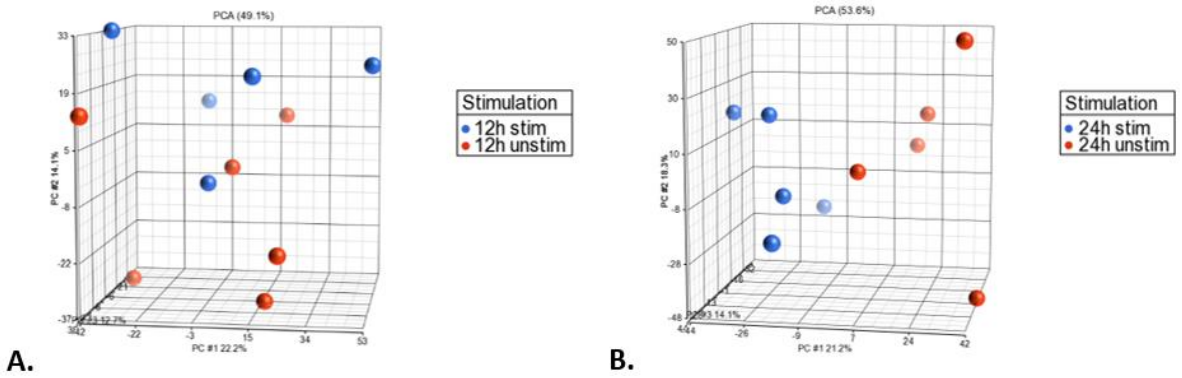

Figure 4.10 PCA of the proteomics data generated from two separate time points (data with batch correction for the number of primary CLL cases). (A) the PCA of the data generated from the 12h time point shows a separation between the CD40 stimulated and the unstimulated samples. (B) the PCA of the data generated from the 24h time point shows an obvious separation between the CD40 stimulation and the unstimulated samples.

The results of hierarchical cluster analysis and PCA showed that:

1) within 24h stimulation, the influence of heterogeneity, which is a comprehensively accepted trait of CLL, was predominant for the differences across different primary CLL cases. The changes caused by soluble CD40 stimulation did not conquer the influence of heterogeneity.

2) After removing the effect of the source of primary CLL cells (the cases of primary CLL cells), the results showed that the soluble CD40 stimulation induced differential expression of proteins on primary CLL cells and the difference became more obvious with 24h incubation.

4.4.2 CD40 stimulation causes significant changes in the protein expression of primary CLL cells at a global level, and the number of the differentially expressed proteins induced by the soluble CD40 stimulation increases with the time of stimulation

The statistical method used to identify the differentially expressed proteins was the analysis of variance (ANOVA) with the 2-way ANOVA on the non-corrected data, with both the stimulation status and the cases of primary CLL samples as factors due to the results of the hierarchical cluster analysis and PCA. The statistically significant expressed proteins were determined by a p-value of less than 0.05 with 1% FDR. With ANOVA analysis, 158 proteins were differentially expressed with 12h CD40 stimulation (Appendix 8). 552 proteins were differentially expressed with 24h CD40 stimulation (Appendix 9). Volcano plots were used to get a visualized view of the difference induced by the soluble CD40 stimulation method in primary CLL cells at the protein expression level (Figure 4.11).

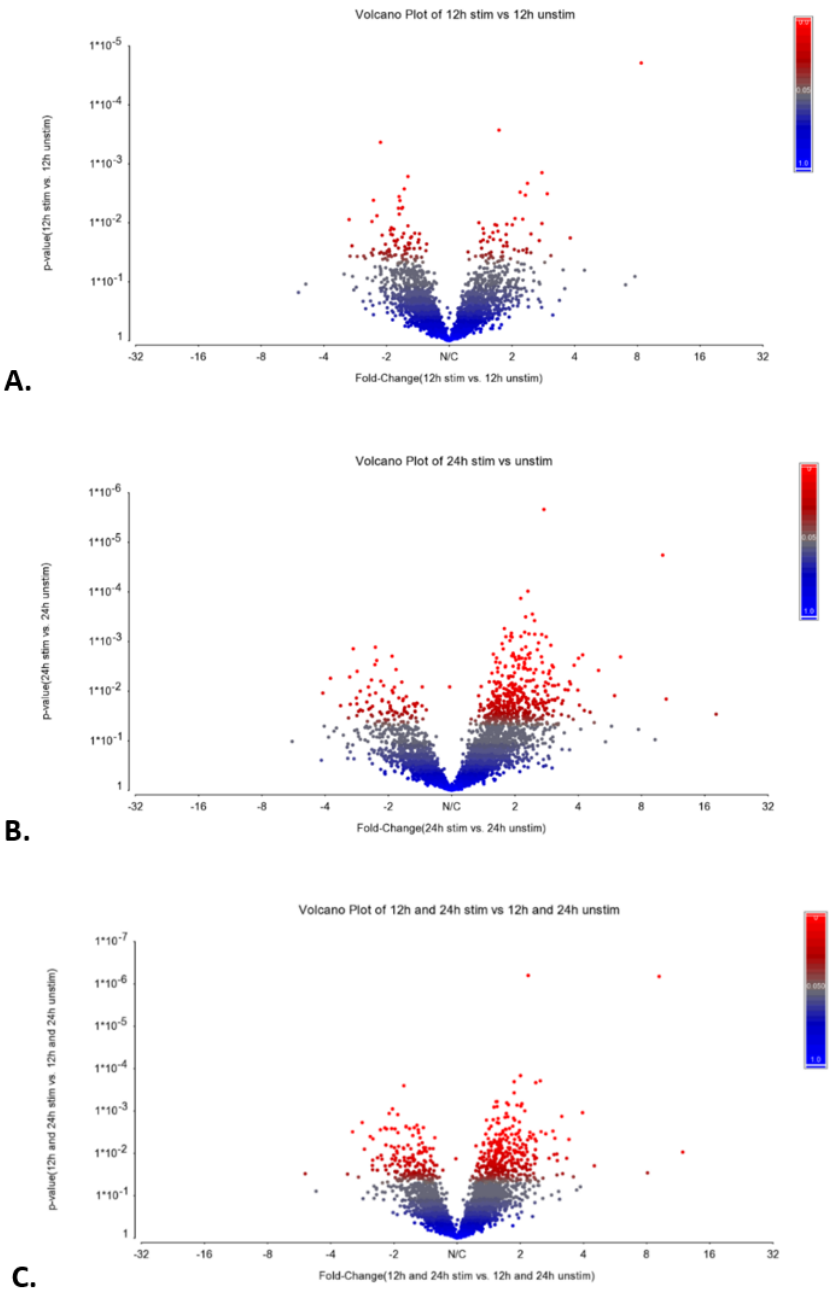

Figure 4.11 Visualizing the differentially expressed proteins induced by the soluble CD40 ligand in primary CLL cells. Red dots: differential expression with p-value < 0.05; Blue dots: differential expression with p-value > 0.05. (A) the volcano plot based on the 12h proteomics data generated by iTRAQ-MS assay with the batch correction for the number of primary CLL cases; (B) the volcano plot based on the 24h proteomics data generated by iTRAQ-MS assay with the batch correction for the number of primary CLL cases; (C) the volcano plot based on the 12h and 24h data generated by iTRAQ-MS assay with the batch correction for the number of primary CLL cases.

Comparing the differential expression lists of the two time points, 57 proteins were present on both lists (Figure 4.12).

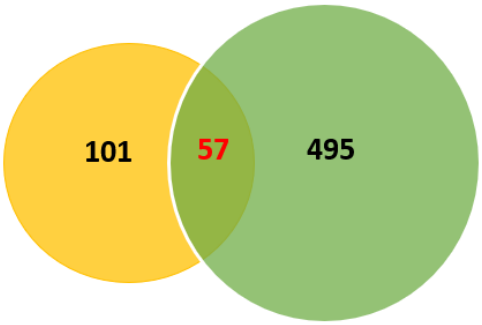

Figure 4.12 Comparison of the differentially expressed proteins in CD40 stimulated CLL cells between 12h and 24h. The yellow circle represents the 158 differentially expressed proteins at 12h; the green circle represents the 552 differentially expressed proteins at 24h. The 57 proteins include 35 proteins present on both of the significantly up-regulated lists, 19 proteins present on both of the significantly down-regulated lists, and 3 proteins present on both lists but the directions of regulation induced by CD40 stimulation were different at two time points.

When it comes to the up-regulated and down-regulated proteins, the 12h differential expression list showed that there were 158 proteins significantly differentially expressed with 66 proteins up-regulated and 92 proteins down-regulated. The 24h differential expression list showed that there were 552 proteins significantly differentially expressed with 448 proteins up-regulated and 104 proteins down-regulated. Comparing the up and down regulated proteins between 12h and 24h, there were 35 proteins present on both of the significantly up-regulated lists (Table 4.3) and there were 19 proteins present on both of the significantly down-regulated lists (Table 4.4). There were 3 proteins present on both lists but the directions of regulation induced by CD40 stimulation were different at two time points (O43707, Q9NRL2, P41212). For the 35 proteins consistently present on both up-regulated lists, the fold-change of 32 individual proteins stayed at a similar level from 12h to 24h with that of several proteins increases. For the 19 proteins consistently present on both down-regulated lists, the fold-change of the individual proteins stayed at a similar level from 12h to 24h.

Table 4.3 Thirty-five concurrently up-regulated proteins at 12h and 24h (ranking by the first alphabet of the accession of proteins in the order of A-Z)

Accession	Name of the proteins	12h Fold-change	24h Fold-change
O00471	Exocyst complex component 5	2.07	2.14
O00764	Pyridoxal kinase	2.37	2.37
O14579	Coatomer subunit epsilon	1.63	1.87
O43172	U4/U6 small nuclear ribonucleoprotein Prp4	1.45	1.66
O43847	Nardilysin	1.97	2.09
O60499	Lymphocyte antigen 75	1.42	1.70
O60508	Pre-mRNA-processing factor 17	1.76	2.01
O75694	Nuclear pore complex protein Nup155	1.43	1.66
O95163	Elongator complex protein 1	1.59	1.83
O95298	NADH dehydrogenase [ubiquinone] 1 subunit C2	1.89	2.15
P16070	CD44 antigen	2.15	2.36
P19838	Nuclear factor NF-kappa-B p105 subunit	1.73	2.75
P30050	60S ribosomal protein L12	1.23	1.23
P31153	S-adenosylmethionine synthase isoform type-2	1.53	1.54
P40763	Signal transducer and activator of transcription 3	1.44	1.47
P48960	CD97 antigen	1.62	2.48
P49588	Alanine—tRNA ligase, cytoplasmic	1.45	2.42
P52292	Importin subunit alpha-1	2.32	2.67
P52294	Importin subunit alpha-5	2.36	2.40
Q13077	TNF receptor-associated factor 1	8.35	10.10
Q13501	Sequestosome-1	1.74	2.20
Q14137	Ribosome biogenesis protein BOP1	1.50	2.33
Q14699	Raftlin	2.87	4.05
Q3LXA3	Triokinase/FMN cyclase	1.55	1.69
Q6BCY4	NADH-cytochrome b5 reductase 2	1.62	2.56
Q86X10	Ral GTPase-activating protein subunit beta	1.52	1.63
Q8IVM0	Coiled-coil domain-containing protein 50	2.01	1.95
Q8IWA4	Mitofusin-1	1.81	1.93
Q92900	Regulator of nonsense transcripts 1	1.39	1.37
Q92918	Mitogen-activated protein kinase kinase 1	1.87	1.77
Q96RU3	Formin-binding protein 1	1.66	1.86
Q9H334	Forkhead box protein P1	1.41	1.49
Q9H444	Charged multivesicular body protein 4b	2.70	3.67
Q9NX20	39S ribosomal protein L16, mitochondrial	1.58	2.36
Q9UJX3	Anaphase-promoting complex subunit 7	2.78	2.27

Note: Fold-change 12h: The ratio of protein expression level between CD40 stimulated/unstimulated at 12h time point; Fold-change 24h: The ratio of protein expression level between CD40 stimulated/unstimulated at 24h time point.

Table 4.4 Nineteen concurrently down-regulated proteins at 12h and 24h (ranking by the first alphabet of the accession of proteins in the order of A-Z)

Accession	Name of the proteins	12h Fold-change	24h Fold-change
O75475	PC4 and SFRS1-interacting protein	-2.16	-2.21
P02768	Serum albumin	-2.93	-3.38
P20674	Cytochrome c oxidase subunit 5A, mitochondrial	-2.05	-2.07
P23443	Ribosomal protein S6 kinase beta-1	-2.00	-1.98
P49321	Nuclear autoantigenic sperm protein	-1.53	-1.47
P61803	Dolichyl-diphosphooligasaccharide—protein glycosyltransferase subunit DAD1	-1.62	-1.82
P62341	Selenoprotein T	-1.90	-2.76
Q13033	Striatin-3	-1.59	-1.78
Q13610	Periodic tryptophan protein 1 homolog	-3.03	-2.66
Q15031	Probable leucine--tRNA ligase, mitochondrial	-2.35	-2.00
Q15075	Early endosome antigen 1	-1.43	-1.46
Q5VZK9	F-actin-uncapping protein LRRC16A	-2.31	-1.92
Q86SX6	Glutaredoxin-related protein 5, mitochondrial	-1.58	-2.32
Q8N442	Translation factor GUF1, mitochondrial	-1.67	-1.92
Q969F9	Hermansky-Pudlak syndrome 3 protein	-1.98	-2.72
Q96P31	Fc receptor-like protein 3	-2.33	-2.72
Q9HAV7	GrpE protein homolog 1, mitochondrial	-1.60	-1.92
Q9NUP1	Biogenesis of lysosome-related orgenelles complex 1 subunit 4	-1.99	-2.46
Q9UK58	Cyclin-L1	-1.83	-2.30

Note: Fold-change 12h: The negative ratio of protein expression level between CD40 stimulated/unstimulated at 12h time point; Fold-change 24h: The negative ratio of protein expression level between CD40 stimulated/unstimulated at 24h time point.

The results of the comparison showed that CD40 stimulation changed the protein expression in primary CLL cells at a global level and that the changes induced by the CD40 stimulation increased with time. As a result, further functional analysis was focused on the differential expression data of the 24h time point. The reasons were explained as follows. Firstly, the hierarchical cluster analysis and the PCA results showed that the influence of CD40 stimulation became more obvious with 24h stimulation, which suggested that the influence of CD40 stimulation increased with time. Secondly, the data showed that the number of the differentially expressed proteins at 24h (552) was much more than that at 12h (158), which, once again, indicated that the influence of CD40 stimulation on the protein expression was greater at 24h than 12h. The data obtained at 24h can provide more

information compared with that at 12h. In addition, the effect of CD40 stimulation-induced protection on primary CLL cells was observed at 24h following CD40 stimulation, as described previously. Based on the above reasons, further analysis will focus on the differentially expressed proteins at the 24h time point.

4.4.3 Functional analysis of the differentially expressed proteins induced by CD40 stimulation

4.4.3.1 The classification of the differentially expressed proteins by PANTHER classification system

The protein classification analysis by PANTHER version 14.1 gave a brief view of the 552 statistically differentially expressed proteins induced by the soluble CD40 stimulation system in primary CLL cells. Among the 552 significantly differentially expressed proteins, there were 550 proteins which can be mapped by Panther version14.1 with 2 unmapped proteins (I3L1I5 and Q9NUQ7). Meanwhile, the classification analysis was performed by PANTHER on all the proteins quantified (4093 proteins) as well. Among the 4093 identified proteins, there were 4080 proteins were identified and applied in the PANTHER analysis with 13 proteins unable to map (I3L1I5, Q9NUQ7, P04229, P58557, P30042, P09669, Q96HY6, P62861, P04439, P42167, Q9BT23, L0R6Q1, Q9NRK6).

Classified by cellular component, the 550 identified proteins were grouped into fourteen categories (Table 4.5). Comparing with that of all proteins quantified (Table 4.6), the constituents and the rank were similar with a slight difference. Situations were similar in the classification by molecular function (Table 4.7 and 4.8) and biological process (Table 4.9 and 4.10). The constituents of the classification for all the proteins quantified were a little more than that of the classification for the differentially expressed proteins. The ranks were slightly different in several constituents.

Table 4.5 Classification by the cellular component of the differentially expressed proteins at 24h time point (550 of 552 proteins were mapped by PANTHER 14.1)

	Category names	Number	% in 550
1	Cell	316	57.50%
2	Cell part	316	57.50%
3	Organelle	215	39.10%
4	Protein-containing complex	139	25.30%
5	Organelle part	118	21.50%
6	Membrane	69	12.5%
7	Membrane-enclosed lumen	41	7.5%
8	Membrane part	35	6.4%
9	Extracellular region part	9	1.60%
10	Extracellular region	9	1.60%
11	Synapse part	7	1.30%
12	Synapse	7	1.30%
13	Supramolecular complex	7	1.30%
14	Cell junction	3	0.50%

Note: Number: the number of proteins in the correlated term;

% in 550: the percentage of (the number of proteins in each term/550).

Table 4.6 Classification by the cellular component of all the proteins quantified in 27 samples (4080 of 4093 proteins were mapped by PANTHER 14.1)

	Category names	Number	% in 4080
1	Cell	2264	55.50%
2	Cell part	2264	55.50%
3	Organelle	1732	42.50%
4	Protein-containing complex	1051	25.80%
5	Organelle part	1041	25.50%
6	Membrane	614	15.00%
7	Membrane-enclosed lumen	392	9.60%
8	Membrane part	320	7.80%
9	Extracellular region part	52	1.30%
10	Extracellular region	52	1.30%
11	Supramolecular complex	48	1.20%
12	Synapse	38	0.90%
13	Synapse part	36	0.90%
14	Cell junction	22	0.50%

Note: Number: the number of proteins in the correlated term;

% in 4080: the percentage of the number of proteins in each term in 4080.

Table 4.7 Classification by the protein class of the differentially expressed proteins at 24h time point (550 of 552 proteins were mapped by PANTHER 14.1)

	Category names	Number	% in 550
1	Metabolite interconversion enzyme	63	11.50%
2	Translational protein	43	7.80%
3	Nucleic acid binding protein	42	7.60%
4	Protein modifying enzyme	29	5.30%
5	Cytoskeletal protein	20	3.60%
6	Protein-binding activity modulator	19	3.50%
7	Membrane traffic protein	19	3.50%
8	Gene-specific transcriptional regulator	17	3.10%
9	Scaffold/adaptor protein	15	2.70%
10	Transporter	12	2.20%
11	Chromatin/chromatin-binding, or -regulatory protein	9	1.60%
12	Chaperone	9	1.60%
13	Defense/immunity protein	4	0.70%
14	Extracellular matrix protein	2	0.40%
15	Transfer/carrier protein	2	0.40%
16	Transmembrane signal receptor	2	0.40%
17	Intercellular signal molecule	1	0.20%
18	Calcium-binding protein	1	0.20%
19	Storage protein	1	0.20%

Note: Number: the number of proteins in the correlated term;

% in 550: the percentage of (the number of proteins in each term/550).

Table 4.8 Classification by the protein class of all the proteins quantified in 27 samples
(4080 of 4093 proteins were mapped by PANTHER 14.1)

	Category names	Number	% in 4080
1	Metabolite interconversion enzyme	472	11.60%
2	Nucleic acid binding protein	404	9.90%
3	Protein modifying enzyme	260	6.40%
4	Translational protein	209	5.10%
5	Membrane traffic protein	147	3.60%
6	Protein-binding activity modulator	125	3.10%
7	Cytoskeletal protein	121	3.00%
8	Transporter	119	2.90%
9	Gene-specific transcriptional regulator	113	2.80%
10	Scaffold/adaptor protein	85	2.10%
11	Chromatin/chromatin-binding, or -regulatory protein	80	2.00%
12	Chaperone	46	1.10%
13	Defense/immunity protein	29	0.70%
14	Calcium-binding protein	22	0.50%
15	Transfer/carrier protein	14	0.30%
16	Intercellular signal molecule	12	0.30%
17	Transmembrane signal receptor	9	0.20%
18	Extracellular matrix protein	6	0.10%
19	Cell adhesion molecule	3	0.10%
20	Storage protein	2	0.00%
21	Cell junction protein	1	0.00%
22	Structural protein	1	0.00%

Note: Number: the number of proteins in the correlated term;

% in 4080: the percentage of the number of proteins in each term in 4080.

Table 4.9 Classification by the biological process of the differentially expressed proteins at 24h time point (550 of 552 proteins were mapped by PANTHER 14.1)

	Category names	Number	% in 550
1	Cellular process	268	48.70%
2	Metabolic process	193	35.10%
3	Biological regulation	108	19.60%
4	Cellular component organization or biogenesis	106	19.30%
5	Localization	68	12.40%
6	Response to stimulus	47	8.50%
7	Signaling	32	5.80%
8	Developmental process	16	2.90%
9	Multicellular organismal process	9	1.60%
10	Immune system process	8	1.50%
11	Multi-organism process	7	1.30%
12	Locomotion	6	1.10%
13	Biological adhesion	6	1.10%
14	Cell population proliferation	4	0.70%
15	Reproductive process	2	0.40%
16	Reproduction	2	0.40%

Note: Number: the number of proteins in the correlated term;

% in 550: the percentage of the number of proteins in each term in 550.

Table 4.10 Classification by the molecular function of all the proteins identified in 27 samples (4080 of 4093 proteins were mapped by PANTHER 14.1)

	Category names	Number	% in 4080
1	Cellular process	1929	47.30%
2	Metabolic process	1448	35.50%
3	Biological regulation	846	20.70%
4	Cellular component organization or biogenesis	724	17.70%
5	Localization	478	11.70%
6	Response to stimulus	408	10.00%
7	Signaling	231	5.70%
8	Developmental process	115	2.80%
9	Multicellular organismal process	92	2.30%
10	Immune system process	67	1.60%
11	Locomotion	42	1.00%
12	Multi-organism process	39	1.00%
13	Reproduction	26	0.60%
14	Reproductive process	26	0.60%
15	Biological adhesion	26	0.60%
16	Cell population proliferation	21	0.50%
17	Biological phase	6	0.10%
18	Growth	5	0.10%
19	Pigmentation	3	0.10%

Note: Number: the number of proteins in the correlated term;
% in 4080: the percentage of the number of proteins in each term in 4080.

These results showed that the differentially expressed proteins induced by CD40 stimulation were involved in a variety of biological activities in primary CLL cells, which suggested that CD40 stimulation changed the features of primary CLL cells in broad aspects. Based on the results of the comparison, the influences induced by CD40 stimulation did not aggregate on any particular class of proteins at the protein translational level.

4.4.3.2 CD40 stimulation regulates a variety of biological processes of primary CLL cells

The functional annotation analysis of the significantly differentially expressed proteins was analyzed by DAVID version 6.8. The 448 proteins that were significantly upregulated following 24h CD40 stimulation were submitted to DAVID 6.8 with all the proteins quantified in the iTRAQ experiment (4093) used as the background proteome. The functional annotation analysis gave out a list of 82 annotation clusters ranking by the

highest to lowest enrichment scores with the EASA threshold set to 1.0. A summary of the categories with FDR less than 0.5 is shown in Table 4.11. For the 104 down-regulated proteins (with one of the proteins, I3L1I5 cannot be mapped), the results of the functional annotation gave out 16 functional annotation clusters with the EASE threshold of 1.0 but none of these revealed a significant enrichment (the categories with FDR less than 1.0 is shown in Table 4.12).

To catch an overall view of the functional overrepresentation of biological processes for the differentially expressed proteins induced by CD40 stimulation, the statistically significantly up and down regulated differentially expressed proteins were inputted respectively to the Reactome Pathway Database version 73 released on June 17, 2020. The biological processes overrepresented with a p-value less than 0.05 are highlighted in yellow in the Figure 4.13 and 4.14.

The results of the functional annotation analysis were not particularly conclusive as the enrichment scores were not high. However, they do suggest that cell-cell adhesion may be altered by CD40 stimulation. Previously in Chapter 3, the differentially expressed genes induced by the soluble CD40 ligand method in primary CLL cells had been obtained by the RNA sequencing analysis. To make a comparison of the effect induced by the CD40 stimulation between the protein expression level and the transcriptional level, the functional annotation analysis of the significantly differentially expressed genes of the RNA-seq data at 24h time point was performed using DAVID. The results of the functional annotation analysis of the 2046 significantly up-regulated genes gave out 271 clusters ranking by the highest to lowest enrichment scores with the EASA threshold set to 1.0 and the top one cluster on the list was the cell-cell adhesion (Appendix 10). It indicated that CD40 stimulation regulated cell-cell adhesion in primary CLL cells at the transcriptional level as well. Among the 82 clusters obtained by the statistically significantly up-regulated proteins induced by CD40 stimulation in primary CLL cells, 73 clusters can be found on the list of the 271 clusters obtained by the significantly up-regulated genes. The results of the functional annotation analysis of the 1986 significantly down-regulated genes showed 227 clusters ranking by the enrichment scores with the EASA threshold set to 1.0 (Appendix 11).

For the 16 clusters obtained by the statistically significantly down-regulated proteins induced by CD40 stimulation in primary CLL cells, 15 clusters were present on the list of the 227 clusters obtained by the significantly down-regulated genes.

The comparison of the functional annotation clusters between the iTRAQ data and the RNA-seq data showed similar biological alterations induced by CD40 stimulation, which increased the confidence of the iTRAQ data. In addition, it was encouraging that the cell-cell adhesion ranks on the top of both up-regulated functional annotation cluster lists. The results at both transcriptional level and protein expression level synergistically suggested that the biological process of the cell-cell adhesion in primary CLL cells was changed by the CD40 stimulation. Based on this finding, further investigation was focused on the proteins in the cell-cell adhesion cluster.

38 proteins of the differentially up-regulated proteins induced by CD40 stimulation were allocated in the cluster of cell-cell adhesion (Table 4.13). Classifying the 38 proteins according to the molecular function by PANTHER, 15 proteins perform as binding molecules (Table 4.14), 7 proteins are involved in catalytic activity, and the other 4 proteins are classified in the categories of translation regulator activity, transcription regulator activity, and molecular function regulator. Classifying the 38 proteins according to the protein class by PANTHER, 8 proteins are cytoskeletal protein (Table 4.15); 5 proteins are metabolite interconversion enzyme; others are classified into the categories of the membrane traffic protein, the scaffold/adaptor protein, chaperone, the calcium-binding protein, the protein-binding activity modulator, the gene-specific transcriptional regulator and the translation protein. 8 proteins can be mapped into pathways by PANTHER and the detailed information is shown in Table 4.16.

Table 4.11 The DAVID functional annotation categories (with the FDR<0.5) of the 448 statistically up-regulated proteins induced by CD40 stimulation in primary CLL cells at 24h time point

Annotation Cluster 1	**Enrichment Score: 3.4362324490527985**					
Category	**Term**	**Count**	**%**	**Genes**	**Benjamini**	**FDR**
GOTERM_BP_DIRECT	**GO:0098609~cell-cell adhesion**	37	8.26	Q9NYL9, Q7KZF4, P06733, P26641, Q92616, P14618, Q9Y266, Q9Y6W5, Q96C19, Q9H444, Q04637, P63244, P42224, Q7L1Q6, P40121, Q9Y6E2, P31939, Q9Y5X1, P22234, P55010, Q9Y5X3, P62258, P42566, P46060, P07737, O75874, P26196, O00571, P37802, Q16181, P00338, Q99497, P49327, Q15691, P08238, P60228, P62424	0.36	0.36
GOTERM_CC_DIRECT	**GO:0005913~cell-cell adherens junction**	38	8.48	Q9NYL9, Q7KZF4, P06733, P26641, Q92616, P14618, Q9Y266, Q9Y6W5, P07948, Q96C19, Q9H444, Q04637, P63244, P42224, Q7L1Q6, P40121, Q9Y6E2, P31939, Q9Y5X1, P22234, P55010, Q9Y5X3, P62258, P42566, P46060, P07737, O75874, P26196, O00571, P37802, Q16181, P00338, Q99497, P49327, Q15691, P08238, P60228, P62424	0.05	0.05
GOTERM_MF_DIRECT	**GO:0098641~cadherin binding involved in cell-cell adhesion**	37	8.26	Q9NYL9, Q7KZF4, P06733, P26641, Q92616, P14618, Q9Y266, Q9Y6W5, Q96C19, Q9H444, Q04637, P63244, P42224, Q7L1Q6, P40121, Q9Y6E2, P31939, Q9Y5X1, P22234, P55010, Q9Y5X3, P62258, P42566, P46060, P07737, O75874, P26196, O00571, P37802, Q16181, P00338, Q99497, P49327, Q15691, P08238, P60228, P62424	0.36	0.36
Annotation Cluster 2	**Enrichment Score: 2.042696846327676**					
Category	**Term**	**Count**	**%**	**Genes**	**Benjamini**	**FDR**
UP_KEYWORDS	**Protein biosynthesis**	28	6.25	P54577, P26641, P26640, O43776, O00267, Q04637, O60841, Q9P2J5, P26639, P41250, P23588, P55010, P15170, O15371, O15372, O43583, P49591, P49411, P23381, P14868, P68104, Q14241, P49589, P20042, P49588, P60228, P56192, P06730	0.00	0.00
GOTERM_BP_DIRECT	**GO:0006418~tRNA aminoacylation for protein translation**	13	2.90	P54577, P26640, P49591, P23381, P14868, O43776, Q9P2J5, P26639, Q15181, P41250, P49589, P49588, P56192	0.44	0.44
UP_KEYWORDS	**Aminoacyl-tRNA synthetase**	12	2.68	P54577, P49591, P26640, Q9P2J5, P26639, P41250, P23381, P14868, P49589, P49588, O43776, P56192	0.07	0.07
KEGG_PATHWAY	**hsa00970:Aminoacyl-tRNA biosynthesis**	12	2.68	P54577, P49591, P26640, Q9P2J5, P26639, P41250, P23381, P14868, P49589, P49588, O43776, P56192	0.41	0.41
Annotation Cluster 3	**Enrichment Score: 1.906322068791872**					
Category	**Term**	**Count**	**%**	**Genes**	**Benjamini**	**FDR**
UP_KEYWORDS	**Nucleotide-binding**	89	19.87	P25098, A3KMH1, P54577, Q08AF3, P07900, Q8IY21, P07948, Q86YS6, Q3LXA3, P51149, O00148, P42025, O60841, Q9P2J5, P62195, P41250, P15170, P55072, Q8IYB8, P05771, Q13043, Q92930, P07437, Q9UL25, P51151, O75414, P49411, Q9GZZ9, P26196, P23919, O00159, Q9UJ70, P68104, Q8WV93, P22102, Q8IWA4, O15523, P00973, Q15477, Q13131, P51003, P00492, P26640, P14618, Q92918, Q9UN37, P31153, Q8N3C0, O00442, Q13418,	0.12	0.12

				O43776, P36404, O00764, O60942, P49915, Q9H4B7, Q6DD88, P26639, O94804, P55010, P78371, P22234, Q92598, P40227, P22314, P49591, Q8WYJ6, P20591, P23381, P31749, P14868, O00571, P17980, Q8TD19, Q9HCC0, P34932, Q7L014, Q16181, Q5T9A4, Q92620, P23458, P49589, P49588, P45985, P49903, Q92900, P08238, Q9NRF8, P56192		
UP_KEYWORDS	**ATP-binding**	69	15.40	P25098, A3KMH1, P54577, Q08AF3, P07900, Q8IY21, P07948, Q3LXA3, O00148, P42025, Q9P2J5, P62195, P41250, P55072, Q8IYB8, P05771, Q13043, O75414, Q9GZZ9, P26196, P23919, O00159, Q9UJ70, Q8WV93, P22102, O15523, P00973, Q15477, Q13131, P51003, P26640, P14618, Q92918, Q9UN37, P31153, Q8N3C0, O00442, Q13418, O43776, O00764, P49915, P26639, O94804, P78371, P22234, Q92598, P40227, P22314, P49591, P23381, P31749, P14868, O00571, P17980, Q8TD19, Q9HCC0, P34932, Q7L014, Q5T9A4, Q92620, P23458, P49589, P49588, P45985, P49903, Q92900, P08238, Q9NRF8, P56192	0.41	0.41
Annotation Cluster 5	**Enrichment Score: 1.5960740052665232**					
Category	**Term**	**Count**	**%**	**Genes**	**Benjamini**	**FDR**
UP_KEYWORDS	**GTPase activation**	14	3.13	P50395, P46060, Q9H2M9, Q86YV0, O43665, Q9BTW9, Q8TC07, Q86TI0, Q86X10, Q68EM7, Q9P107, P31150, Q8N264, P98171	0.42	0.42
Annotation Cluster 8	**Enrichment Score: 1.2506074698725398**					
Category	**Term**	**Count**	**%**	**Genes**	**Benjamini**	**FDR**
UP_KEYWORDS	**TPR repeat**	12	2.68	P49792, P19878, O76094, Q9BXJ9, O15550, Q13042, P50502, Q9H3S7, Q9UJX3, Q08752, Q13451, Q02790	0.47	0.46
Annotation Cluster 10	**Enrichment Score: 1.2029888687808314**					
Category	**Term**	Count	%	Genes	Benjamini	FDR
KEGG_PATHWAY	**hsa03013:RNA transport**	23	5.13	P49792, O15371, P46060, O15372, Q14974, Q86V81, Q96J01, P11940, Q9BTX1, O75694, Q7L576, P51114, Q04637, O60841, P68104, P23588, P55010, P20042, Q92900, P60228, Q8WUM0, Q9UKX7, P06730	0.41	0.41

Table 4.12 The DAVID functional annotation categories (with the FDR<1.0) of the 104 statistically down-regulated proteins induced by CD40 stimulation in primary CLL cells at 24h time point

Annotation Cluster 1	Enrichment Score: 1.7999646816124586					
Category	**Term**	**Count**	**%**	**Genes**	**Benjamini**	**FDR**
UP_SEQ_FEATURE	**site:Not glycated**	3	2.91	P68871, P02768, P69905	0.40	0.40
UP_SEQ_FEATURE	**glycosylation site:N-linked (Glc) (glycation)**	3	2.91	P68871, P02768, P69905	0.40	0.40
GOTERM_MF_DIRECT	**GO:0019825~oxygen binding**	3	2.91	P68871, P02768, P69905	0.74	0.74
UP_KEYWORDS	**Glycation**	3	2.91	P68871, P02768, P69905	0.67	0.67

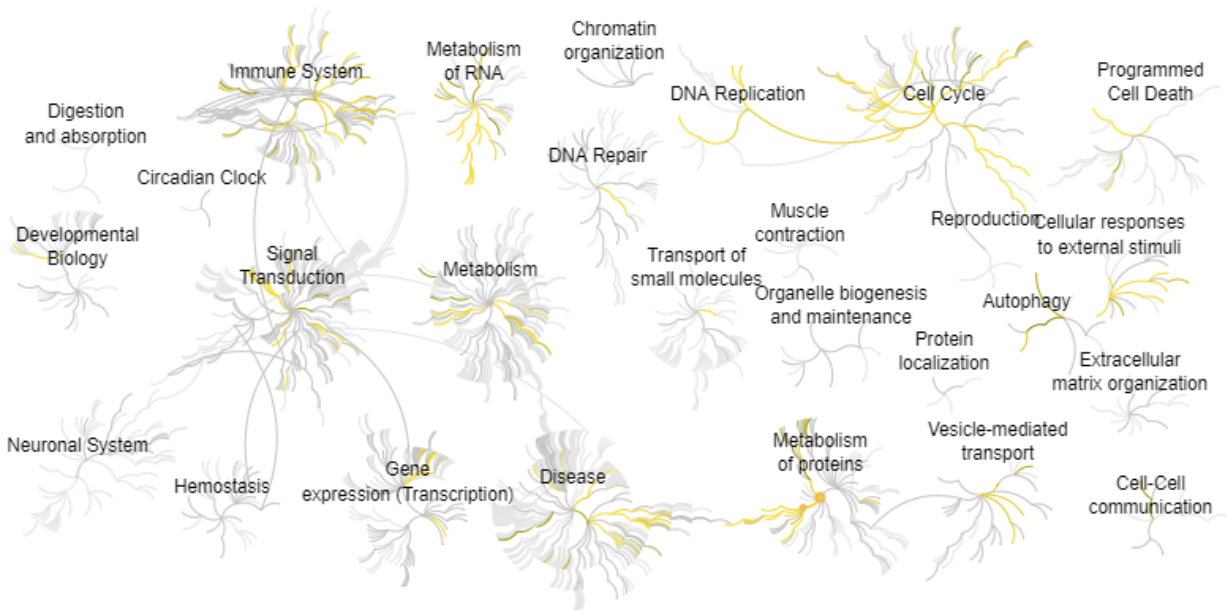

Figure 4.13 Illustrations of the functional overrepresentation analysis of the 448 up-regulated proteins by Reactome version 72. The yellow color represents the degree of overrepresentation with a p-value of less than 0.05.

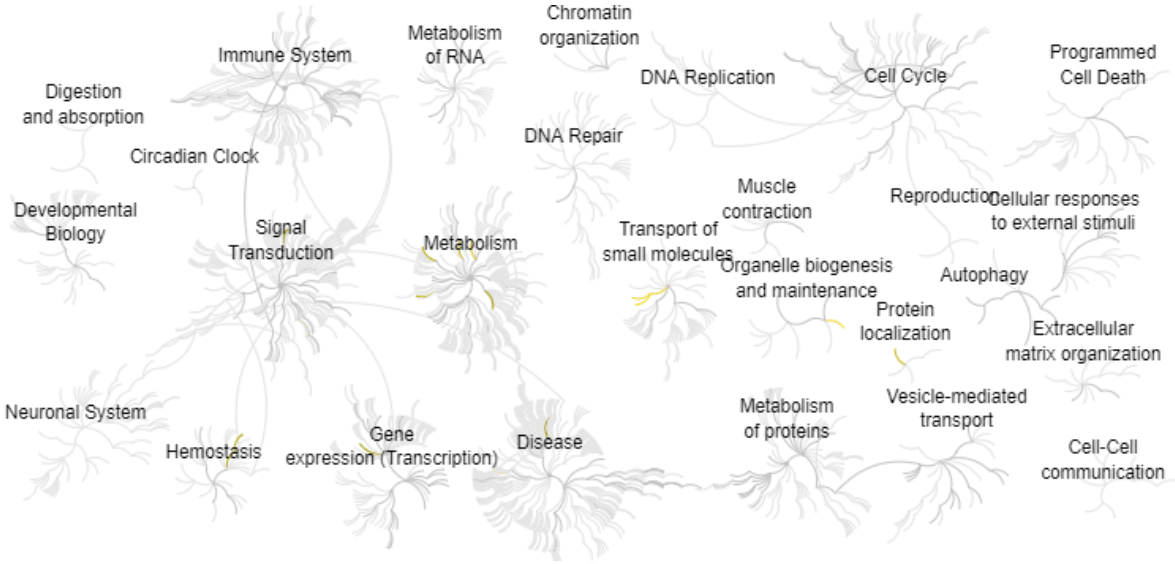

Figure 4.14 Illustrations of the functional overrepresentation analysis of the 104 down-regulated proteins by Reactome version 72. The yellow color represents the degree of overrepresentation with a p-value of less than 0.05.

Table 4.13 The 38 proteins in the cell-cell adhesion cluster identified by DAVID functional annotation analysis (ranking by the fold-change of ANOVA)

Protein	Accession	Fold-change	p-value
Charged multivesicular body protein 4b	Q9H444	3.67	0.01
EF-hand domain-containing protein D2	Q96C19	3.09	0.01
ATP-dependent RNA helicase DDX3X	O00571	2.89	0.00
Protein DJ-1	Q99497	2.48	0.03
Eukaryotic translation initiation factor 4 gamma 1	Q04637	2.45	0.01
60S ribosomal protein L7a	P62424	2.30	0.01
Fatty acid synthase	P49327	2.30	0.00
Basic leucine zipper and W2 domain-containing protein 2	Q9Y6E2	2.30	0.03
Wiskott-Aldrich syndrome protein family member 2	Q9Y6W5	2.25	0.00
Bifunctional purine biosynthesis protein PURH	P31939	2.25	0.00
Ran GTPase-activating protein 1	P46060	2.22	0.00
Septin-7	Q16181	2.22	0.00
Tyrosine-protein kinase Lyn	P07948	2.20	0.00
14-3-3 protein epsilon	P62258	2.20	0.00
Multifunctional protein ADE2	P22234	2.15	0.01
Elongation factor 1-gamma	P26641	2.13	0.00
Heat shock protein HSP 90-beta	P08238	1.92	0.01
Profilin-1	P07737	1.88	0.01
Eukaryotic translation initiation factor 3 subunit E	P60228	1.80	0.00
Macrophage-capping protein	P40121	1.80	0.04
Microtubule-associated protein RP/EB family member 1	Q15691	1.78	0.03
Basic leucine zipper and W2 domain-containing protein 1	Q7L1Q6	1.76	0.02
eIF-2-alpha kinase activator GCN1	Q92616	1.76	0.00
Epidermal growth factor receptor substrate 15	P42566	1.75	0.02
Sorting nexin-9	Q9Y5X1	1.75	0.04
Sorting nexin-5	Q9Y5X3	1.72	0.04
Alpha-enolase	P06733	1.68	0.02
L-lactate dehydrogenase A chain	P00338	1.67	0.03
Isocitrate dehydrogenase [NADP] cytoplasmic	O75874	1.64	0.04
Pyruvate kinase PKM	P14618	1.64	0.01
Staphylococcal nuclease domain-containing protein 1	Q7KZF4	1.64	0.02
Transgelin-2	P37802	1.62	0.00
Receptor of activated protein C kinase 1	P63244	1.57	0.01
Eukaryotic translation initiation factor 5	P55010	1.57	0.03
Probable ATP-dependent RNA helicase DDX6	P26196	1.55	0.02
Signal transducer and activator of transcription 1-alpha/beta	P42224	1.51	0.03
Nuclear migration protein nudC	Q9Y266	1.41	0.02
Tropomodulin-3	Q9NYL9	1.38	0.02

Note: Fold-change: the expression of the protein in CD40 stimulated/the expression of the protein in unstimulated; p-value: the p-value of ANOVA.

Table 4.14 The 15/38 proteins that classified into the binding category according to the molecular function by PANTHER (ranking by the first alphabet of the accession of proteins in the order of A-Z)

Accession	Name of the protein	PANTHER Protein Class
P07737	Profilin-1 (PFN-1 ortholog)	non-motor actin binding_protin
P07948	Tyrosine-protein kinase Lyn	-
P08238	Heat shock protein HSP90-beta	Hsp90 family chaperone
P26196	Probable ATP-dependent RNA helicase DDX6	-
P42224	Signal transducer and activator of transcription-1 alpha/beta	DNA-binding transcription factor
P55010	Eukaryotic translation initiation factor 5	translation initiation factor
P62424	60S ribosomal protein L7a	ribosomal protein
P63244	Receptor of activated protein C kinase 1	-
Q04637	Eukaryotic translation initiation factor 4 gamma 1	translation initiation factor
Q15691	Microtubule-associated protein RP/EB family member 1	non-motor microtubule binding_protein
Q16181	Septin-7	cytoskeletal protein
Q7KZF4	Staphylococcal nuclease domain-containing protein 1	-
Q9NYL9	Tropomodulin-3	actin or actin-binding cytoskeletal protein
Q9Y266	Nuclear migration protein nudC	microtubule or microtubule-binding cytoskeletal protein
Q9Y5X3	Sorting nexin-5	-

Table 4.15 The 8/38 proteins that classified into the cytoskeletal protein category according to the protein class by PANTHER (ranking by the first alphabet of the accession of proteins in the order of A-Z)

Accession	Name of the protein	PANTHER Protein Class
P07737	Profilin-1	non-motor actin binding_protin
P37802	Transgelin-2	non-motor actin binding_protin
P40121	Macrophage-capping protein	non-motor actin binding_protin
Q15691	Microtubule-associated protein RP/EB family member 1	non-motor microtubule binding_protein
Q16181	Septin-7	cytoskeletal protein
Q9NYL9	Tropomodulin-3	actin or actin-binding cytoskeletal protein
Q9Y266	Nuclear migration protein nudC	microtubule or microtubule-binding cytoskeletal protein
Q9Y6W5	Wiskott-Aldrich syndrome protein family member 2	non-motor actin binding_protin

Table 4.16 The 8/38 proteins that mapped into the pathways by PANTHER

Accession	Name of the protein	PATHER protein class	Mapped pathways
P42224	Signal transducer and activator of transcription-1 alpha/beta	DNA-binding transcription factor	EGF receptor signaling pathway
			PDGF signaling pathway
			JAK/STAT signaling pathway
			Ras Pathway
			Angiogenesis
			Interleukin signaling pathway
			Interferon-gamma signaling pathway
			Inflammation mediated by chemokine and cytokine signaling pathway
			p53 pathway feedback loops 2
			Oxidative stress response
P07948	Tyrosine-protein kinase Lyn	-	B cell activation
			Cadherin signaling pathway
			CCKR signaling map
			Parkinson disease
P62258	14-3-3 protein epsilon	scaffold/adaptor protein	EGF receptor signaling pathway
			FGF signaling pathway
			Parkinson disease
P14618	Pyruvate kinase PKM	-	Glycolysis
			Pyruvate metabolism
P07737	Profilin-1	non-motor actin binding protein	Cytoskeletal regulation by Rho GTPase
P06733	Alpha-enolase	lyase	Glycolysis
P31939	Bifunctional purine biosynthesis protein PURH	hydrolase transferase	De novo purine biosynthesis
P40121	Macrophage-capping protein	non-motor actin binding protein	FAS signaling pathway

In summary, the iTRAQ data showed that CD40 stimulation regulated a variety of biological processes in primary CLL cells by changing the protein expression at a global level. The results of the functional analysis of the iTRAQ data suggested that CD40 stimulation up-regulated the expression of proteins involved in the cell adhesion in primary CLL cells, which can be supported by the functional analysis of the RNA-seq data. Therefore, the proteins in the cell-cell adhesion cluster became the candidates of the functional study for this project.

4.5 Discussion

The aim of this part of the study was to investigate the influence of CD40 stimulation induced by the soluble CD40 ligand method on gene expression at the translational level in primary CLL cells. Although the reliability of mass spectrometry is generally good, there are several issues that need to be pointed out when interpreting the data.

Firstly, there were six primary CLL cases applied in this part of the study and this was actually the minimum number of cases required for meaningful analysis of the proteomics data. It was mainly due to the limited access to primary CLL samples available in large quantities for sufficient protein extraction. From the statistics point of view, a higher number of primary CLL cases will make the study more powerful. However, the acquisition of the iTRAQ-MS data including the preliminary tests, sample preparation, mass spectrometry processes, and data analysis already took 10 months of study. The loss of three protein samples resulting from a manufacturing problem with the iTRAQ reagent also reduces the confidence to draw any clear conclusion directly from these data, thus making the validation by independent method necessary for the selected candidates before conducting the further study.

Secondly, the difficulty in maintaining the good viability of primary CLL cells cultured *in vitro* affected the analysis of the proteomics data. Although it was desirable to collect CLL cells in culture at multiple time points over a period of time in order to obtain dynamic information on protein expression influenced by the CD40 stimulation, it was impossible to keep the viability of primary CLL cells at a satisfactory level for longer than 24h *in vitro*. It was shown that the viabilities of the primary CLL cells from the six cases already decreased to an average of 43.1% (ranging from 25.79%-52.0%) after 24h in culture. In order to obtain a

relative better viability for the samples used for iTRAQ assays, the samples generated from primary cases were selected with the criteria that the initial viability should be over 70% and that the viability after incubation should be over 30%. Although the viability of several samples did not meet the criteria, the six cases used for iTRAQ assays were the optimum cases that exhibited acceptable viability compared to the cases excluded. Basing on the data obtained, 24h time point was thus chosen as the end of incubation with the soluble CD40 ligand method.

Finally, some proteins known to be up-regulated by CD40 stimulation were not identified by iTRAQ-MS in the data obtained in this study. The total number of proteins identified here was 5303 with 4093 of them being quantified for analysis. So far, the maximum number of identified proteins for primary CLL cells by mass spectrometry study has been 8694 with nearly 6000 of these proteins being relatively quantitated (Johnston et al., 2018). The proteins that have not been detected by iTRAQ-MS in this study include BCL-XL, MCL-1, BID, and CD95. The expression of BCL-XL (Q07817) has been known to be up-regulated by CD40 stimulation in CLL cells (Vogler et al., 2009a, Kitada et al., 1999, Kater et al., 2004) and it has been used as a marker for the activation of the CD40 signalling pathway in CD40-stimulated CLL cells in this study. MCL-1 (Q07820) is a pro-survival member of the proteins belonging to the BCL-2 family and BID (P55957) is a pro-apoptotic BH3-only protein in the family as well. As described earlier, the expression of these two proteins can be upregulated by CD40 stimulation (Kater et al., 2004, Kitada et al., 1999). The expression of the death receptor CD95 (also known as FAS, P25445), a member of the TNF-R superfamily, was also reported to be up-regulated by CD40 stimulation in CLL cells (Chu et al., 2002, Kater et al., 2004). The method used to detect the four proteins from the above studies was Western blotting. According to the published information, it was noticed that these four proteins were absent from the lists of identified proteins in the data obtained in this study. Several reasons can be possibly responsible for this outcome, which are explained below.

1) Capturing proteins with low molecular weight and with a low abundance of expression is a recognised challenge for mass spectrometry (Penno et al., 2009, Rzagalinski and Volmer, 2017). The smaller the molecular weight of a protein, the lower the number of peptides constituting this protein, which leads to less chance for this protein to be identified by MS-based techniques. This may be one of the reasons for the loss of the protein BCL-XL and BID

in the data. Protein BCL-XL and BID are relatively small proteins according to their molecular weight (26.049kDa for BCL-XL and 21.995kDa for BID, provided by Uniprot). Using the theoretical digestion tools provided online by ExPASy (Swiss Institute of Bioinformatics), 20 peptides can be digested from the protein BCL-XL using Trypsin but only 9 of the 20 peptides fall into the m/z range that can be identified by iTRAQ-MS with the m/z setting used in this study from 400 m/z to 1800 m/z. This further reduces the chance of BCL-XL to be caught by the iTRAQ-MS, which is similar to the situation for BID. Using the online tool, Protein Atlas, to check the abundance of the protein BCL-XL, MCL-1, BID, and CD95 in human tissue, it can be found that no detected expression level of these four proteins in the normal B cells in the blood. Although these proteins have been observed at a higher level in CLL cells, to what extent, the level of their expressions increases under the background of the tremendous number of proteins expressed in CLL cells is uncertain.

2) Membrane proteins and the proteins located in specific organelles are difficult to be extracted depending on the protein extraction methods used for MS-based proteomics analysis. It has been reported that the identification of membrane proteins is a recognised challenge for mass spectrometer analysis due to their intrinsic feature that they consist of both hydrophilic and hydrophobic regions and that they are amphipathic to water (Santoni et al., 2000). Researchers have been trying to improve the methods to identify membrane proteins using mass spectrometers (Prados-Rosales et al., 2019), but, here in this study, there was no specific procedures performed to maintain the cell membrane-bound proteins as the aim was to investigate the effect of CD40 stimulation at a global protein expression level. This may be one reason for the loss of membrane-bound proteins such as the cell surface receptor protein CD95 (Peter et al., 2015, Hjalmar et al., 2002). BCL-XL, MCL-1, and BID are the mitochondrial membrane-associated proteins (Vander Heiden et al., 1997, Bae et al., 2000, Renshaw et al., 2004). Besides the hydrophobic features of the membrane-bound proteins mentioned above, it should be noted that the proteins located in the organelles are relatively difficult to be extracted based on the extraction methods used for MS-based analysis, whereas a more rigorous extraction method was used for the Western blotting. The extraction of proteins used in MS-based analysis is short of the process of heating the samples at 95℃ in Laemmli sample buffer, which may reduce the chance of some organelle proteins to be detected by MS-based techniques.

3) The instability of proteins affects their chance to be caught by MS-based techniques (Goodwin, 2012). Unstable proteins may be lost during the process of the experiment due to their instability. The website ExPASy provides a method to automatically estimate the stability of proteins *in vitro* by calculating the instability index of proteins. ExPASy uses an instability index formula published by Kunchur Guruprasad and colleagues in 1990 (Guruprasad et al., 1990). The authors compared the stable and unstable proteins and found that the dipeptides of the unstable proteins were significantly different from those of the stable proteins. Depending on the instability, they gave out weight values for each dipeptide, and the instability index is determined according to the dipeptides and their weight values of the protein to be studied. Using this method, the protein MCL-1 and BID are classified as unstable proteins, which may be another reason for their absence in the data present in this study.

4) The intrinsic chemistry of the proteins affects the possibility of them being identified by MS-based techniques. The iTRAQ-MS analysis was performed in a positive ion mode and the peptides positively charged are easier to be detected. Taking the four proteins as an example, analysing the amino acid composition of these proteins using ExPASy, the information of the four proteins showed that the ratio of the positively charged residues to the negatively charged residues of BCL-XL, MCL-1, BID, and CD95 are 20:30, 41:47, 22:29, and 48:43, respectively. It can be found that the positively charged residues in the protein BCL-XL, MCL-1, and BID are less than the negatively charged residues, which indicates that the peptides of these proteins may not ionise as readily. The chemistry of the peptides will also affect how they behave during the two different chromatography separations. This may further reduce the possibility of these proteins to be detected based on the accumulating factors discussed above.

These are some possible reasons for the missing proteins in the data present here. It is notable that some Western blotting detectable proteins, such as BCL-XL, are missing to be identified by MS-based techniques. Excepted for the different strengths of the protein extraction methods as mentioned above, the principles of these two methods should be responsible for the conflict phenomenon as well. Western blotting is used to detected individual protein targets. As long as using a good antibody, Western blotting can sensitively probe the target protein and disregard the others, improving the potential dynamic range of

detection. However, the aim of using the discovery MS-base technique is to capture all the protein expressed in samples by analysing the peptides generated from the hundreds and thousands of proteins. Under the background of the huge signals, the sensitivity to detect one protein is decreased.

For this part of the study, all these issues were considered, and considerable effort was made to avoid bias affecting the data analysis. The iTRAQ-MS data reported here provide preliminary and interesting information about the influence on protein expression induced by CD40 stimulation in primary CLL cells. Although the functional analysis of the RNA-seq data provides support to the iTRAQ data, further study is needed to validate and confirm the findings reported in this study.

Using mass spectrometry-based techniques, 158 and 552 differentially expressed proteins induced by CD40 stimulation were identified at 12h and 24h time points, respectively. The increase in the number of significantly differentially expressed proteins in this period suggests that the effect of CD40 stimulation on protein expression becomes greater as time passes by. Studies have reported that the influences on the expression of some known target proteins induced by CD40 stimulation changes over time (Scielzo et al., 2011, Girbl et al., 2013). The PANTHER classification analysis shows that the 552 differentially expressed proteins induced by CD40 stimulation exhibit a range of molecular functions that are involved in a variety of biological processes. Results obtained in this study are thus in line with the published reports, which increases the confidence for the further functional studies of those differentially expressed proteins.

The NF-κB signalling pathway is involved in many essential biological processes of cells including cell survival, proliferation, and apoptosis. It is known that CD40 stimulation can induce strong activation of the NF-κB signalling pathway in primary CLL cells, through both canonical and non-canonical activation pathways (Gasparini et al., 2014, Mansouri et al., 2016, Vallabhapurapu et al., 2008). The canonical pathway is mediated by the formation of RelA with p50 complex which translocates into the nucleus to activate the gene transcription of the downstream targets (Gasparini et al., 2014). p50 and its precursor p105 are also called NF-κB1. The non-canonical pathway is mediated by the formation of RelB with p50 and p52, with both complexes of RelB with p50 and RelB with p52 then translocating into the nucleus for the activation (Gasparini et al., 2014). p52 and its

precursor p100 are also known as NF-κB2. In proteomics data, it has been shown that the NF-κB p105 subunit and the NF-κB p100 subunit are significantly up-regulated by CD40 stimulation by over 2-fold for both proteins (2.47 and 2.11, respectively). Meanwhile, TRAF1, one of the members of TRAF family proteins mediating the activation of the canonical NF-κB signaling pathway (Xie et al., 2006, Bishop et al., 2007), is also on the list of the differentially expressed proteins and is up-regulated by CD40 stimulation with over 10-fold increase as detected by iTRAQ-MS in this study. Also, a negative regulator of NF-κB signalling, TRAF family member-associated NF-κB activator (TANK) (Bonif et al., 2006), is significantly down-regulated by CD40 stimulation with a 1.5-fold decrease in expression. These data are consistent with the published results that CD40 stimulation activates the canonical and non-canonical activation of NF-κB signalling pathways.

The tyrosine protein kinase LYN is up-regulated by CD40 stimulation in CLL cells after 24h incubation with a 2.2-fold increase in expression, as detected in this study. It is known that the BCR signalling pathway is chronically activated in CLL B cells (Packham and Stevenson, 2010, Quiroga et al., 2009). The expression of LYN, a critical component of the BCR signalling network, is also abnormally overexpressed when compared with normal B cells (Contri et al., 2005). The expression level of LYN is inversely correlated with the treatment-free survival of CLL patients (Wang et al., 2013). It has also been reported that CD40 signalling and BCR signalling can crosstalk with each other. It has thus been shown that CD40 stimulation up-regulates the expression of CD79b (one of the proximal components mediating BCR signalling pathways) and BCR on primary CLL cells (Minuzzo et al., 2005). Some pathways can be regulated by both CD40 signalling and BCR activation including phosphatidylinositol 3-kinase (PI3K) pathway, phospholipase Cγ2 (PLCγ2), and NF-κB pathways (Ren et al., 1994, Amrein, 2011, Ten Hacken and Burger, 2014). Some targets modulated by BCR signaling can also be regulated by CD40 stimulation on primary CLL cells such as the B cell activating factor (BAFF), the proliferation-inducing ligand (APRIL), and their receptors (Ferrer et al., 2014). The data obtained in this study thus add further evidence that the crosstalk between CD40 signalling and BCR signalling pathways occurs in CD40-stimulated CLL cells.

The expression of CD5 has been known as one of the characteristics of CLL cells (Friedman et al., 2018). Comparing with the CLL cells from the peripheral blood of patients, the CLL

cells from the lymph nodes express a higher level of CD5 (Pasikowska et al., 2016). This suggests that the expression of CD5 is induced by the microenvironment factors *in vivo*. The data obtained here that CD40 stimulation increases the expression of CD5 by 2.46-fold suggests that the increase in CD5 expression in CLL cells from lymph nodes may be mediated by CD40 stimulation. Meanwhile, the expression of CD44 is also up-regulated by CD40 stimulation at the 24h time point with a 2.36-fold in this study. The function of CD44 in CLL is still under investigation. It has two forms in CLL, the soluble form and the cell membrane-bound form. Several studies have reported that the soluble form is upregulated by CD40 stimulation from the microenvironment, which in turn helps the proliferation of CLL cells, and that the expression level of the protein is associated with the disease progression (Eisterer et al., 2004, Gutjahr et al., 2018). It has also been shown that the expression of the cell membrane-bound form of CD44 increased during the disease progression in a murine model of CLL and that its expression can be up-regulated by the signals from the CLL microenvironment including the CD40 plus IL-4 stimulation on primary CLL cells (Fedorchenko et al., 2013). In 2017, Yandong Shen and colleagues reported that CD40 stimulation changed the expression of surface proteins depicting the immunophenotypes of CLL cells and that one of the proteins was CD97 that was found to be upregulated by CD40 stimulation in the CLL cells from the patients with progressive disease (Shen et al., 2018b). Consistent with that, the data present here show that the expression of CD97 is upregulated by the CD40 ligand stimulation method with a 2.48-fold increase. Therefore, the proteomics data in this study have confirmed many previously published results.

Furthermore, the proteomics data in this study also provide some interesting insight into the role of some proteins in the survival of CLL cells, which could be potentially promising targets for therapeutic intervention. Several heat shock proteins (HSP) (HSP90-beta, HSO90-alpha, HSP105, and HSP70 protein 4) were at higher expression level CD40 stimulated primary CLL cells comparing with unstimulated cells. HSP inhibition has been introduced into the research of CLL ever since the beginning of the 21st century (Jones et al., 2004) but the mechanisms of how the inhibitors of the heat shock proteins work are still unclear.

The role of HSP90 in CLL has been studied by many research groups. It has been reported that HSP90 functions as a part of the support network for the correct folding of proteins involved in the essential signal transduction including the signalling for cell survival and

proliferation (Neckers, 2002, Bruserud et al., 2006). A high-affinity conformation of Hsp90 that is commonly found in cancerous but not in normal cells is a chaperone protein that interacts with client proteins to inhibit the degradation (Goetz et al., 2003, Kamal et al., 2003). In CLL, it has been reported that the inhibition of Hsp90 abolished the NF-κB signalling and that Hsp90 inhibitors can inhibit the pro-survival signalling provided by the CLL microenvironment and induce apoptosis of CLL cells (Hertlein et al., 2010, Walsby et al., 2012). Previous work from our laboratory has shown that Hsp90 inhibitors have promising therapeutic potential as they are effective in inducing apoptosis of CLL cells with dysfunctional p53 (Lin et al., 2008). It was found that geldanamycin, an HSP90 inhibitor, exhibited different effects on the wild-type p53 and mutated p53 and killed CLL cells through promoting the degradation of mutant p53 whilst upregulating the expression of wild-type p53 (Lin et al., 2008). Besides, it has been demonstrated that HSP90 inhibitors are cytotoxic to primary CLL cells regardless of the functional status of p53 in these cells (Lin et al., 2008, Best et al., 2010) and that HSP90 inhibitors can work synergistically with fludarabine by interfering with the DNA damage repair (Best et al., 2012, Kaufman et al., 2015). In 2016, Timothy Chen and colleagues reported that the HSP90 inhibitor can activate p38 signalling and inhibit the phosphorylation of AKT/STAT3, which further interferes with the migration and survival of CLL cells (Chen et al., 2016). In addition, it was reported that inhibiting HSP90 led to the destabilization of several BCR kinases including LYN, spleen tyrosine kinase, Bruton tyrosine kinase, and AKT, and induced apoptosis in CLL cells with and without survival support from co-culture with stromal cells or soluble CD40 ligand plus IL-4 (Guo et al., 2017). These data indicate that HSP90 may be involved in a variety of biological signalling processes. The proteomics data obtained in this study show that the expression of both HSP90-alpha and HSP90-beta is up-regulated by CD40 stimulation, linking the expression of HSP90 to CD40 activation, which provides a rationale for further investigation into the role of HSP90 in CD40 stimulation-mediated survival in CLL.

The proteomics data present here also show that HSP70 is upregulated by CD40 stimulation in CLL cells. It has been reported that HSP70 was overexpressed in CLL cells and critical in the survival of CLL cells, and its expression was correlated to poor prognosis of the patients with CLL (Frezzato et al., 2019, Rosati et al., 2012). Altogether, the data obtained in this

study and that of others implicate an important role of HSPs in the survival of CLL cells mediated by the microenvironmental factors, which merits further investigation.

According to the functional enrichment analysis by DAVID, the cluster with the highest enrichment score is the cell-cell adhesion, which is supported by the functional analysis of the RNA-seq data obtained previously in Chapter 3. Cell adhesion molecules are involved in the interaction between malignant cells and the surrounding cells/tissues (the microenvironment) and play an important role in cell differentiation, survival, proliferation, and migration (Makrilia et al., 2009, Farahani et al., 2014). Owing to the characteristics of CLL cells, CLL has been regarded as a good model for the investigation of the functional role of cell adhesion molecules in the disease progression (Burger, 2013, Burger and Gribben, 2014). In 2015, by analyzing the differentially expressed proteins between UM-CLL and U-CLL, we reported that the cell migration pathways in UM-CLL cells were defective compared to M-CLL cells and that UM-CLL cells expressed an increased level of adhesion molecules (Eagle et al., 2015). This suggests that UM-CLL cells are being preferentially retained in the lymph node microenvironment. The clinical correlation analysis confirms that patients with UM-CLL were twice likely to develop lymphadenopathy (Eagle et al., 2015), which explains, at least in part, why patients with UM-CLL have a poor clinical outcome. It is likely that many other molecules involved in cell migration and trafficking are also dysregulated in CLL cells. The improved understanding of the tumor microenvironment and the biological processes that cell adhesion molecules are involved in is starting to inform the strategy for developing novel cancer therapies (Klonisch et al., 2008, Floor et al., 2011). It has been demonstrated that the novel small molecular inhibitors, ibrutinib, and idelalisib, can disrupt the cell migration into lymph nodes and/or mobilize CLL cells from the microenvironment to re-enter the circulation so to make leukemic cells susceptible to the cytotoxic agents (Tissino et al., 2018, Herman et al., 2015, Burger, 2012a). The antagonists of CXCR4 have been under intense investigation and some of them are currently undergoing clinical evaluation (Burger et al., 2005, Andritsos et al., 2010, Andritsos et al., 2019). These data indicate that agents targeting cell-cell adhesion and cell migration are promising strategies for the treatment of CLL patients.

In vivo, CLL cells migrate between the peripheral blood, lymph nodes, bone marrow, and secondary lymphoid tissues. The trafficking and homing of CLL cells depend on the

interaction with different adhesion molecules and chemokines such as CXCR4/CXCL12, CXCR5/CXCL13, CCL3, CCL4, and CD49d (Nadkarni et al., 1998, Ramsay and Rodriguez-Justo, 2013, Burger and Gribben, 2014). It has been known that the cell adhesion molecules are differentially expressed on CLL cells localized in different tissue components *in vivo* (Han et al., 2014, Dürig et al., 2001). CLL cells from the peripheral blood of patients exhibit a higher level CXCR4 comparing with those from lymph nodes (Möhle et al., 1999, Barretina et al., 2003, Pasikowska et al., 2016), which is consistent with the finding that the cell-cycle arrested, quiescent CLL cells express a higher level of CXCR4 and CXCR5 comparing with the proliferating CLL cells (Bennett et al., 2007). These early findings indicate a significant role of the microenvironment in regulating the expression of the cell adhesion molecules in CLL. CD40-CD154 interaction represents important crosstalk between CLL cells and T cells in the lymph nodes and evidence shows that it regulates the expression of molecules involved in cell migration and trafficking exists. It has been reported that together with IL-4, CD40 stimulation up-regulates the expression of adhesion-related molecule CD38 as well as ZAP-70 in CLL cells (Willimott et al., 2007).

The proteomics data obtained here in this study provides evidence for the notion that the CD40-CD154 crosstalk between CLL cells and T cells within the microenvironment regulates the cell adhesion in CLL cells. Alpha-enolase is one of the 38 proteins in the cell-cell adhesion cluster. It is a tumor-derived antigen and its expression has been reported to be up-regulated in proliferating CLL cells in the lymph nodes and also associated with a shorter time to first treatment (Griggio et al., 2017). The iTRAQ-MS data showed that the expression of alpha-enolase was regulated by CD40 stimulation.

The results of the classification of the 38 proteins in the cell-cell adhesion cluster show that 15 of them have been classified into the binding category according to their molecular function (Table 4.15) and 8 proteins have been classified into cytoskeletal proteins (Table 4.16), which indicates that CD40 stimulation may regulate the cell adhesion of CLL cells via changing the cytoskeletal proteins and binding capability. In the 38 proteins, 8 proteins can be mapped into pathways by PANTHER (Table 4.17). Tyrosine kinase LYN was classified into this cell-cell adhesion cluster and it was mapped into the pathways of B cell activation and cadherin signalling pathway. The role of BCR signalling in the cell migration of CLL cells has been studied by many researchers with conflicting findings (Packham and Stevenson, 2010).

The iTRAQ-MS data indicate that the crosstalk between CD40 stimulation and the BCR signalling pathway may also regulate cell adhesion collectively. For instance, signal transducer and activator of transcription-1 (STAT-1) alpha/beta and 14-3-3 protein epsilon were mapped into the EGF receptor signalling pathway that is involved in the growth, survival, proliferation, and differentiation of cells (Oda et al., 2005). STAT-1 alpha/beta was also mapped in the JAK/STAT signalling pathway in this study. One paper has demonstrated that targeting JAKs inhibited the CD40L/IL-21 induced proliferation in CLL cells (Slinger et al., 2017).

Based on its important role in CLL and the results of the iTRAQ-MS data, the proteins in the cell-cell adhesion cluster were taken as the candidates for further study. The protein, ATP-dependent RNA helicase DDX3X (O00571), was mapped into the JAK/STAT signalling pathway and up-regulated by CD40 stimulation with a 2.89-fold increase (Table 4.14). However, the biological function of DDX3X in CLL has not been investigated, which will form the topic of the next chapter.

In summary, the iTRAQ-MS analysis identified the differentially expressed proteins that were involved in a variety of biological activities in CD40-stimulated CLL cells. Further studies are required to uncover the specific mechanisms of the regulation of these differentially expressed proteins induced by CD40 stimulation and their functional significance in CLL.

Chapter 5. DDX3X potentially plays a role in the CD40 stimulation induced pro-survival signals in CLL cells

5.1 Background

As described in the previous chapter, according to the functional analysis of the 448 significantly up-regulated proteins induced by CD40 stimulation on CLL cells, the top-scored category (with the highest enrichment score) on the DAVID functional annotation clusters list is the 'cell-cell adhesion' (Table 4.12 in Chapter 4). This category includes 38 proteins and the expression of sixteen out of the 38 proteins was upregulated by CD40 stimulation by over two folds compared to that in the unstimulated cells. The ATP-dependent RNA helicase DDX3X (O00571) is one of them with its expression up-regulated by CD40 stimulation by 2.89 folds.

DDX3X is a member of the DEAD (Asp-Glu-Ala-Asp)-box RNA helicases superfamily that present in almost all organisms and plays a crucial role in many biological processes (Li et al., 2014). In humans, DDX3X has a homolog, DDX3Y, which shares a 92% protein sequence identity with DDX3X (Kim et al., 2001). However, DDX3X and DDX3Y show different functions in various organs (Kim et al., 2001). DDX3X is located on the X-chromosome and it is ubiquitously transcribed in all human tissues (Park et al., 1998).

The biological functions of the protein DDX3X have so far not been extensively studied. In recent years, it has been shown that DDX3X may play a role in the biology of cancer. It was initially reported that the mRNA level of DDX3X increases by 64% of hepatocellular carcinoma (Huang et al., 2004). However, other research groups reported that levels of DDX3X expression decrease in most patients with liver cancer (50-73%), as detected by qPCR and immunohistochemistry, and that its expression has a positive association with the expression of p21 (Chao et al., 2006, Chang et al., 2006). The contradictory findings indicate a complex role DDX3X plays in different types of cancer. Later, DDX3X has been studied in breast cancer, lung cancer, gall bladder cancer, colorectal cancer. It has been shown that the increased expression level of DDX3X in breast cancer is correlated to poor survival (Bol et al., 2013). Besides, several studies reported that the inhibitors of DDX3X induced apoptosis in breast cancer cell lines (Xie et al., 2015, van Voss et al., 2017, Van Voss et al., 2018).

Similarly, it has been reported that the overexpression of DDX3X correlates to aggressive lung cancer (Bol et al., 2015). The expression level of DDX3X is a promising biomarker that positively correlates with the WHO pathologic grading and poor survival outcome in human gliomas (Hueng et al., 2015). In a study of colon cancer, however, DDX3X shows a different role, as the level of its expression indicates a good prognosis for the survival of the patients (Su et al., 2015).

In CLL, the gene DDX3X was reported to be one of the most mutated genes, with the mutations detected in 3% of the patients with the disease (Wang et al., 2011a). Similar results were also reported by another study that DDX3X is mutated in 2.4% of the patients with CLL (Puente et al., 2011). In 2015, DDX3X mutations were reported to be a recurrent event during the convergent evolution of CLL (Ojha et al., 2015a). The incidence of DDX3X mutation in IGHV-UM CLL was reported to be significantly higher than that of IGHV-M CLL (24% versus 3%, respectively); moreover, DDX3X mutation was found to be more common in the patients with the relapsed disease (17%) than those with stable disease (4%) (Ojha et al., 2015b). Importantly, CLL cells with DDX3X mutations have lost the expression of DDX3X protein (Ojha et al., 2015b), indicating that mutations can lead to the inactivation of the function of DDX3X. Taken together, the above results suggest that DDX3X functions as a tumour suppressor in CLL. DDX3X mutations have also been founded in the natural killer/T cell lymphoma (NK/T cell lymphoma) and were linked to poor prognosis (Jiang et al., 2015).

Functional studies have shown that DDX3X is involved in the biological processes of cell survival, apoptosis, cell cycle, and proliferation (Chao et al., 2006, Lai et al., 2010, Sun et al., 2013, Bol et al., 2015). In a study of breast cancer, DDX3X was reported to be localised in the mitochondria and an inhibitor of DDX3X can reduce the mitochondrial translocation which consequently leads to the decrease in the oxygen consumption rates and the intracellular ATP concentrations and the increase in reactive oxygen species (ROS) and finally induces apoptosis (Van Voss et al., 2018). It was also reported that, together with GSK3 and cIAP, DDX3X was involved in the formation of an anti-apoptotic protein complex that counterbalances the extrinsic apoptotic signalling cascade initiated by the activation of death receptors (Sun et al., 2008). Furthermore, it was reported that DDX3X can increase the expression level of the transcription factor SNAIL, leading to increased migration and metastasis of breast cancer cells and that knocking down DDX3X using shRNA decreased

proliferation and migration of breast cancer cells (Sun et al., 2011). In addition, DDX3X has been reported to regulate the DNA-damage-induced apoptosis by directly interacting with p53, resulting in the accumulation of p53 inside the cells (Sun et al., 2013). It was also reported that p53 was a direct transcriptional activator of DDX3X and that the inactivation of p53 down-regulated DDX3X, resulting in the increased cell proliferation of lung cancer cells (Wu et al., 2011). Inhibiting DDX3X also caused cell cycle arrest and apoptosis of lung cancer cells (Bol et al., 2015). However, in hepatocellular carcinoma, it was reported that increased expression of DDX3X led to the down-regulation in the expression of Cyclin D1 and up-regulation in the level of p21, causing cell death and G1 phase cell cycle arrest of the hepatocellular carcinoma cells (Wang et al., 2018).

Therefore, studies have indicated a complicated, yet not fully characterized, the role of DDX3X in many biological processes, which requires further study to clarify its functions in different types of cancer cells. The results generated from the proteomics study in this project, together with the background information described above, make DDX3X a suitable candidate for the functional study of its role in mediating CD40 stimulation induced pro-survival signals in CLL cells.

5.2 Hypothesis

Protein DDX3X plays a role in the pro-survival effect induced by CD40 stimulation in CLL cells.

5.3 Methods

5.3.1 Cells and cell culture

Thawed primary CLL cells were cultured in RPMI 1640 medium with 10% heat-inactivated FBS, 1%L-Glutamine, and 1% Penicillin/Streptomycin at a cell density of 4×10^6/ml.

Human HG-3 and MEC1 cell lines were cultured in T-75 culture flasks with RPMI 1640 medium with 10% FBS, 1%L-Glutamine, and 1% Penicillin/Streptomycin. The cells were passaged every 4-5 days. Before the experiment, HG-3 and MEC1 cells were cultured at a cell density of 0.5×10^6/ml.

5.3.2 Materials

RK-33 (an inhibitor of DDX3X) was purchased from the Selleckchem (catalogue number S8246, Houston, USA) and, once received, dissolved at a stock concentration of 100mM in DMSO and kept at -20℃ in the aliquot size of 10µl. On the day of the experiment, RK-33 stock was further diluted to the required concentrations in DMSO.

FITC Annexin V was purchased from the BD Pharmingen (catalogue number 556420, BD Biosciences, Oxford, UK). Fluorescent viability dye 7-AAD was purchased from Invitrogen (catalogue number 2032240, Life Technologies, UK). The information about the antibodies used for Western blot within this chapter has been listed in Table 5.1.

Table 5.1 Antibodies used for Western blot in Chapter 5

Antibodies	Company	Catalogue No.	Isotype
DDX3X (D19B4) Rabbit mAb	Cell Signalling	#8192	Rabbit IgG
BCL-XL	Cell Signalling	#2762	Rabbit
TRAF2 (C192) Antibody	Cell Signalling	#4724	Rabbit
Anti-rabbit IgG, HRP-linked Antibody	Cell Signalling	#7074	Anti-rabbit IgG
Anti-mouse IgG, HRP-linked Antibody	Cell Signalling	#7076	Anti-mouse IgG

The siRNA reagents were purchased from the Dhmarmacon (Horizon, Cambridge, UK) including the ON-TARGETplus Human DDX3X (1654) siRNA-SMARTpool (catalogue number L-006874-02-0005), the ON-TARGETplus Non-targeting Pool (catalogue number D-001810-10-05), the DhmarmaFECT 1 Transfection Reagent (catalogue number T-2001-02) and the 5× siRNA Buffer (catalogue number B-002000-UB-100). The ON-TARGETplus Human DDX3X (1654) siRNA-SMARTpool consists of 4 siRNA targets of DDX3X. The detailed information of the ON-TARGETplus Human DDX3X (1654) siRNA-SMARTpool and the ON-TARGETplus Non-targeting Pool has been shown in Table 5.2. After being delivered, the ON-TARGETplus Human DDX3X (1654) siRNA-SMARTpool was resuspended in 1× siRNA Buffer (diluted from the 5× siRNA Buffer) according to the recommended protocol from the Dharmocaon Horizon. The resuspended siRNA-SMARTpool was aliquoted into smaller volumes and kept in the -20℃ freezer. The DharmaFECT Transfection Reagent was kept in the fridge at 4℃.

Table 5.2 Detailed information on the ON-TARGETplus Human DDX3X (1654) siRNA-SMARTpool

Name	Target sequence
ON-TARGETplus SMARTpool siRNA J-006874-06	CAGAUUUAGUGGAGGGUUU
ON-TARGETplus SMARTpool siRNA J-006874-07	GCAACACUGGGAUUAAUUU
ON-TARGETplus SMARTpool siRNA J-006874-08	GAUGCUGGCUCGUGAUUC
ON-TARGETplus SMARTpool siRNA J-006874-18	GGUAUUAGCACCAACGAGA
ON-TARGETplus Non-targeting Pool	UGGUUUACAUGUCGACUAA
	UGGUUUACAUGUUGUGUGA
	UGGUUUACAUGUUUUCUGA
	UGGUUUACAUGUUUUCCUA

5.3.3 RK-33 treatment

For experiments on primary CLL cells, thawed primary CLL cells were cultured at a cell density of 4×10^6/ml in the 24 or 6-well plates with 1ml per well and treated with RK-33 at a range of concentrations. After 24h, primary CLL cells were harvested for cell death assay by flow cytometry or cell number count using the trypan blue exclusion method.

For the experiment on HG-3 and MEC1 cell lines, cells were cultured at a cell density of 0.5×10^6/ml in the 24 or 6-well plates with 1ml per well and treated with RK-33 at a range of concentrations. After incubation for 24h, 48h, or 72h, cells were harvested separately at each time point for cell death assay by flow cytometry or cell number count using the trypan blue exclusion method.

5.3.4 CD40 stimulation on HG-3 and MEC1 cell lines

HG-3 or MEC1 cells were cultured at a cell density of 0.5×10^6/ml in the 6-well plates with 5ml cell suspension in each well. For CD40 stimulation, cells were treated with 0.1µg/ml soluble HA-tagged CD40 ligand and 0.5µg/ml anti-HA antibody. As the unstimulated control, cells were treated with 0.5µg/ml anti-HA antibody. Cells were harvested after 12h or 24h separately for further downstream assays.

5.3.5 Cell death assay

For monitoring cell death in primary CLL cells or cell lines, the cell death assay by flow cytometry was used throughout the study. The detailed procedures of cell death assay have been described in section 2.3.2 of the Methodology Chapter.

To monitor the number of viable cells, cell count was performed using the Cellometer following staining the cells with Trypan blue dye. In brief, at the end of incubation, 20µl of cells were collected from each sample and mixed with 20µl of 0.1% Trypan Blue solution (catalogue number T8154, Sigma-Aldrich, UK). Cells excluding Trypan blue dye from each sample were counted on the Cellometer.

5.3.6 Western blot

The processes of Western blot have been described in section 2.3.3 of the Methodology Chapter. Recommended by the manufacture, the HeLa cell line and K256 cell line were used as the positive control for the antibody of DDX3X.

5.3.7 siRNA knockdown

siRNA knockdown experiment was performed using HG-3 and MEC1 cell lines. Briefly, 2×10^5 cells per well were plated in the 48-well plates. The siRNA and the siControl were diluted using the serum-free RPMI medium, respectively. The DharmaFECT transfection reagent was also diluted using the serum-free RPMI medium. The diluted reagents were incubated for 5 minutes. Then, the diluted siRNA or the siControl were added into the diluted DharmaFECT transfection reagent with gently pipetting to mix well. The mixed reagents were incubated for another 20 minutes. The knocking down and control reagents were then loaded into the suspending cells in corresponding wells. The volume of each well was then topped with RPMI culture medium (with 10% heat-inactivated FBS, 1%L-Glutamine, and 1%, Penicillin/Streptomycin) to reach 1ml per well. The cells with knocking down reagents were kept in an incubator with the atmosphere containing 5% CO_2 at 37℃. The workflow of the processes has been shown in Figure 5.1.

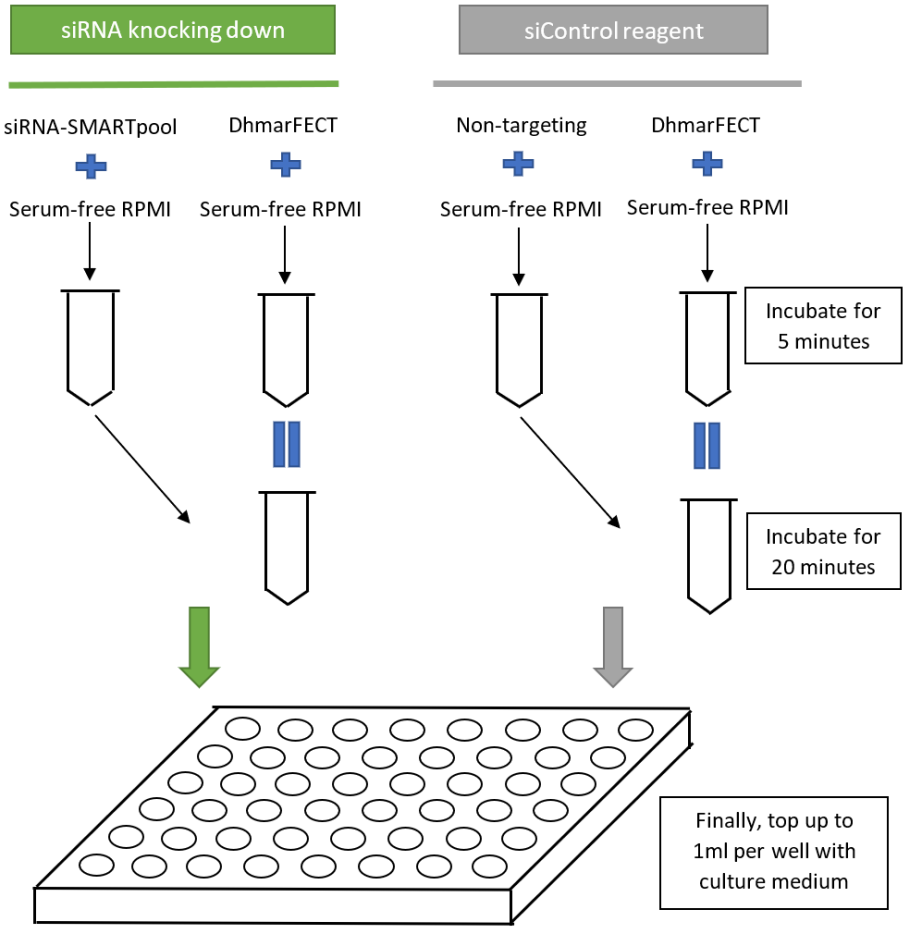

Figure 5.1 The workflow of siRNA knockdown experiment using the ON-TARGETplus SMARTpool siRNAs specific to DDX3X

5.4 Results

5.4.1 CD40 stimulation up-regulates the expression of DDX3X in primary CLL cells

To validate data from the iTRAQ-MS analysis, the Western blotting method was used to examine the expression of DDX3X using the same CLL cases that were applied in the proteomics study. Due to the unavailability of one case, the other five primary CLL cases were used for validation. Primary CLL cells were incubated with and without the soluble CD40 ligand for 24h and the CD40 stimulated and unstimulated cells were then harvested for Western blotting analysis.

Results of Western blotting showed that CD40 stimulation upregulated the expression of DDX3X in the primary CLL cells from five cases, individually (Figure 5.2). The pooled results showed that the up-regulated expression of DDX3X induced by CD40 stimulation was

statistically significant (p-value < 0.01) (Figure 5.2 B). Results of validation were consistent with the iTRAQ-MS data that CD40 stimulation increases the expression of DDX3X with the incubation for 24h.

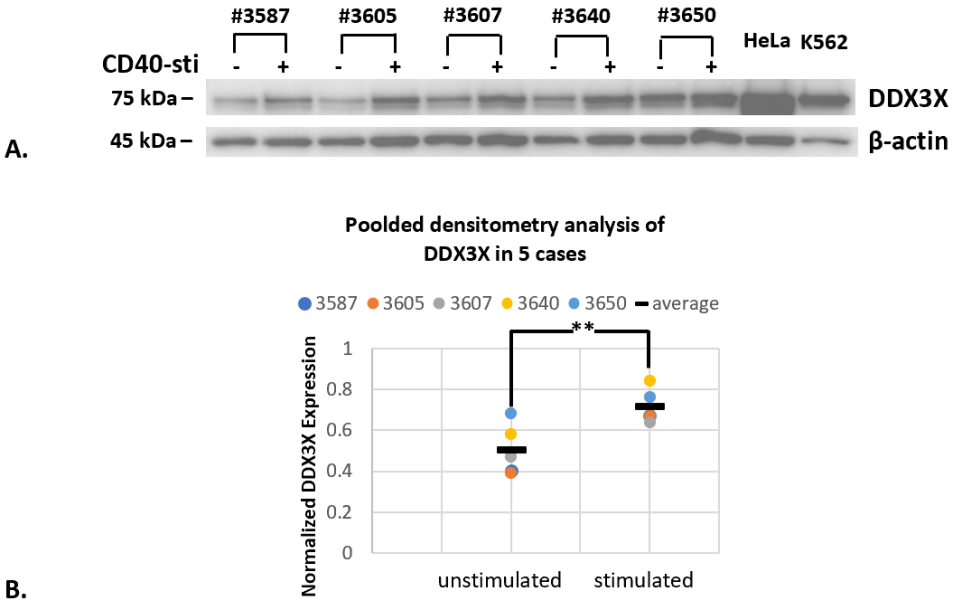

Figure 5.2 Validation of the iTRAQ data for the up-regulated expression of DDX3X induced by CD40 stimulation. For CD40 stimulation, cells were incubated with 0.1µg/ml HA-tagged CD40 ligand and 0.5µg/ml anti-HA antibody. For the unstimulated control, cells were incubated with 0.5µg/ml anti-HA antibody. After 24h, cells were collected for Western blotting. (A) Western blotting of DDX3X expression in primary CLL cells from 5 cases. Hela and K562 cells were used as positive controls for the antibody. (B) pooled densitometry analysis of DDX3X expression in 5 cases. The difference of the averaged DDX3X expression between the CD40 stimulated and unstimulated primary CLL cells is statistically significant with p-value < 0.01 (using the two-tailed, paired Student's t-test).

5.4.2 Inhibitor of DDX3X, RK-33, induces cell death in primary CLL cells

After the validation, the investigation moved on to the role of DDX3X in the survival of CLL cells. For this purpose, a novel inhibitor of DDX3X, RK-33, was introduced in this part of the study. It has been reported that RK-33 can inhibit the expression of DDX3X and induce cell death in different types of cancer cells (Bol et al., 2015, van Voss et al., 2015, Xie et al., 2016). By incubating CLL cells with RK-33 at a range of concentrations for 24h, the results showed that RK-33 induced cell death in the primary CLL cells from 4 primary cases individually in a concentration-dependent manner (Figure 5.3). Pooled data showed that RK-33 induced cell death in primary CLL cells with the LC_{50} of 3.89µM (Figure 5.4).

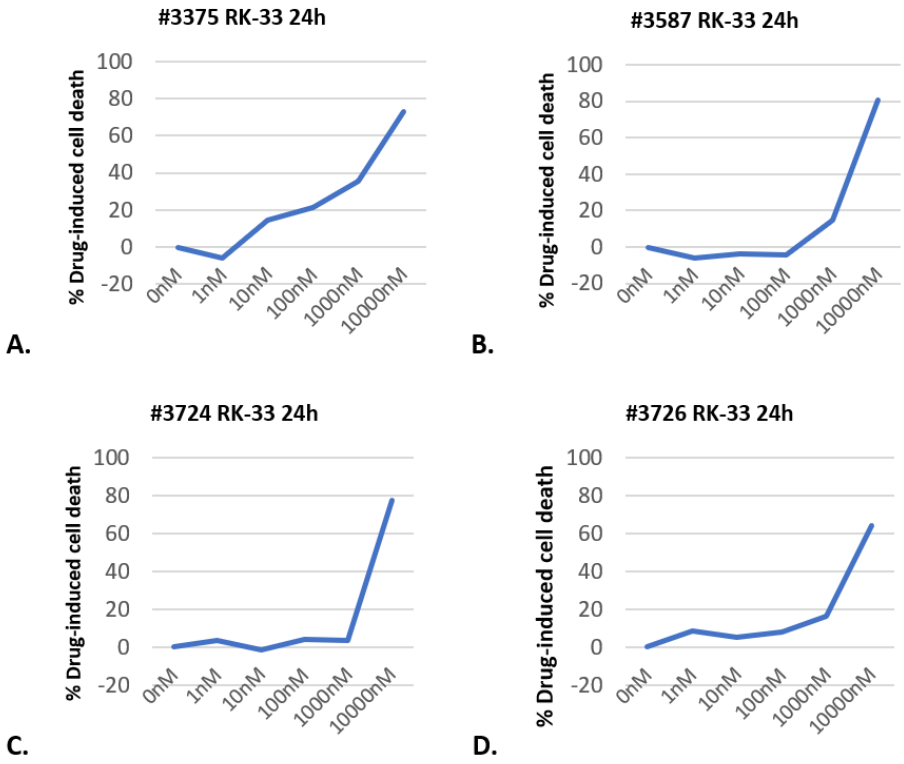

Figure 5.3 Results of the cell death induced by RK-33 in individual primary CLL cases. Thawed primary CLL cells were cultured at a density of 4×10^6/ml and treated with RK-33 for 24h. Then, cells were harvested for cell death assay using flow cytometry. Drug-induced cell death = [(% cell death of drug-treated cells - % cell death of untreated cells)/(100 - % cell death of untreated cells)] × 100. (A)-(D) results of RK-33 induced cell death for four individual CLL samples.

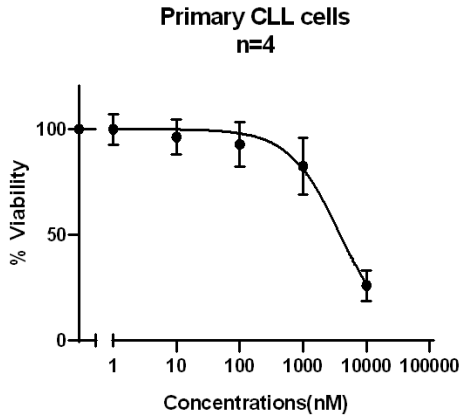

Figure 5.4 Pooled results of the cell death induced by RK-33 in primary CLL cells. Results of analysing the data of RK-33 induced cell death generated by four primary CLL cases using GraphPad Prism 8 and the LC_{50} is calculated from this nonlinear statistical analysis.

Meanwhile, to see whether RK-33 inhibited the expression of DDX3X, the expression of DDX3X in primary cells treated with RK-33 was monitored using Western blotting. No results for primary case #3375 because of the insufficient number of primary cells obtained. As

shown in Figure 5.5, the expression of DDX3X remained largely unaffected by the treatment of RK-33 till at the concentration of 10000nM (Figure 5.5 A and B). However, the corresponding expression of β actin decreased concurrently with the expression of DDX3X, which indicated that the decrease of DDX3X expression may be caused by the degradation of all the proteins in dead cells induced by RK-33.

These results of RK-33 on primary CLL cells suggest that DDX3X protein may play a role in the survival of primary CLL cells. However, whether or not RK-33 induces cell death by interfering with the DDX3X expression in CLL cells is not clear. Due to the difficulty in maintaining the good viability of primary CLL cells *in vitro*, further functional studies were performed using two CLL cell lines, the HG-3 and MEC1 cells.

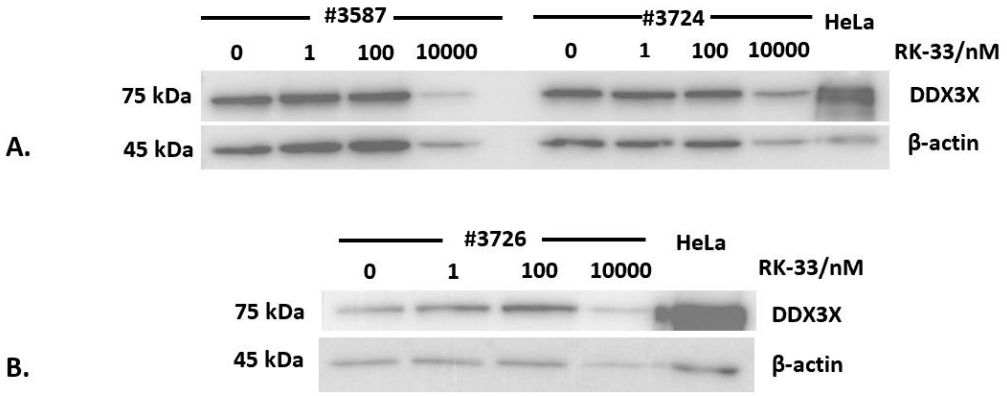

Figure 5.5 Level of DDX3X expression in primary CLL cells treated with RK-33. Thawed primary CLL cells were cultured at a cell density of 4×10^6/ml and treated with RK-33. CLL cells were harvested after 24h for Western blotting. (A) and (B) shows the expression of DDX3X in primary CLL cells from three primary CLL cases treated with indicated concentrations of RK-33.

5.4.3 HG-3 cells and MEC1 cells express DDX3X

To use the HG-3 cells and MEC1 cells for the functional study of DDX3X, it is necessary to investigate whether these two types of CLL cell lines express the protein DDX3X at a similar level to that of primary CLL cells, whether the soluble CD40 ligand can activate the CD40 signalling pathway in these cells, and whether the DDX3X expression can be up-regulated by CD40 stimulation using the soluble CD40 ligand. Therefore, the expression of DDX3X and BCL-XL in HG-3 cells and MEC1 cells with and without CD40 stimulation for 12h and 24h, respectively, were investigated using western blot. Meanwhile, the expression of DDX3X in

the primary CLL cells from three cases was tested to make a comparison with that in HG-3 cells and MEC1 cells.

Results of Western blotting showed that the basal level of expression of DDX3X in HG-3 cells was similar to that in primary CLL cells (Figure 5.6). Under the same concentration of soluble CD40 ligand stimulation method, the expression of DDX3X in HG-3 cells was not visually up-regulated by CD40 stimulation. Meanwhile, the expression of BCL-XL was mildly up-regulated by CD40 stimulation in HG-3 cells.

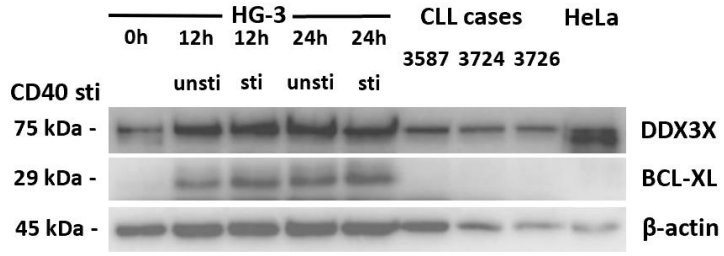

Figure 5.6 The expression of DDX3X in HG-3 cells with or without CD40 stimulation. 12h/24h sti: HG-3 cells were incubated with 0.1μg/ml HA-tagged CD40 ligand and 0.5μg/ml anti-HA antibody for 12h/24h. 12h/24h unsti: HG-3 cells were incubated with 0.5μg/ml anti-HA antibody for 12h/24h. In the end of the incubation, cells were collected for Western blotting.

Similar results were also seen in MEC1 cells. MEC1 cells expressed DDX3X as well and its basal expression level was similar to that in primary CLL cells (Figure 5.7). The expression of DDX3X in MEC1 cells were not visually up-regulated by CD40 stimulation. The expression of BCL-XL in MEC1 cells was obviously up-regulated by CD40 stimulation.

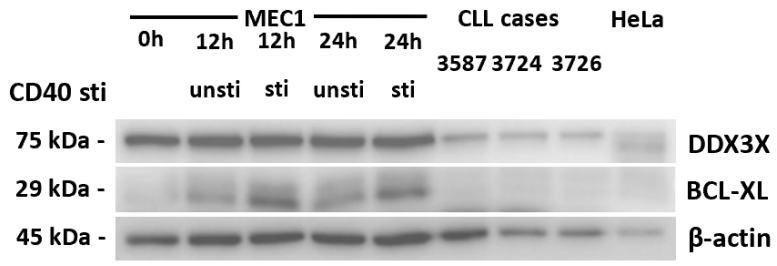

Figure 5.7 The expression of DDX3X in MEC1 cells with or without CD40 stimulation. 12h/24h sti: MEC1 cells were incubated with 0.1μg/ml HA-tagged CD40 ligand and 0.5μg/ml anti-HA antibody for 12h/24h. 12h/24h unsti: MEC1 cells were incubated with 0.5μg/ml anti-HA antibody for 12h/24h. In the end of the incubation, cells were collected for Western blotting.

These results showed that both HG-3 and MEC1 cells expressed DDX3X similarly to that in primary CLL cells. The mildly up-regulated expression of BCL-XL indicated that HG-3 and MEC1 cells responded to CD40 stimulation using the soluble CD40 ligand method. However, the expression of DDX3X was not upregulated by soluble CD40 ligand with the same dosage used in primary CLL cells. This suggested that the dosage of soluble CD40 ligand method should be further optimized to obtain a more obvious effect of CD40 stimulation.

5.4.4 RK-33 induces cell death in HG-3 and MEC1 cells

To investigate the effect of RK-33 on HG-3 cells and MEC1 cells, cells were treated with RK-33 at a range of concentrations (0μM, 0.1μM, 1μM, 10μM, 100μM). The cell death after RK-33 treatment was monitored at three time points, 24h, 48h, and 72h.

The results of three independent experiments have been shown in Figure 5.8. RK-33 induced cell death in both HG-3 cells and MEC1 cells in a concentration-dependent manner, which is similar to that observed in primary CLL cells. There was no obvious difference in cell death across three time points (24h, 48h, and 72h). The LC_{50} was calculated using GraphPad prism 8.0. The LC_{50} remained largely unchanged across 24h, 48h, and 72h time points (Table 5.3). Since HG-3 cells express wild type p53 whereas MEC1 cells do not (Ravikrishnan et al., 2019, Carrà et al., 2017), the similar response pattern in both cell lines indicates that RK-33 may induce cell death independently of the status of p53.

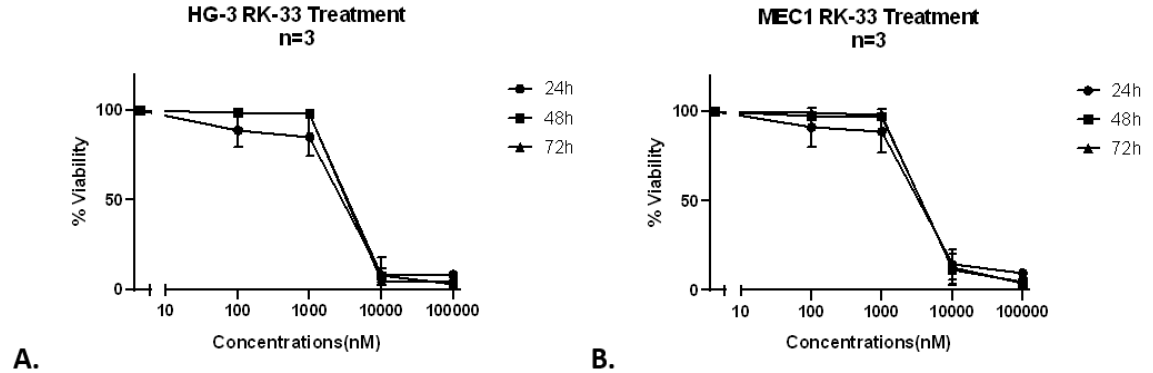

Figure 5.8 Induction of cell death by RK-33 in HG-3 and MEC1 cells. (A) results of analysing the data of RK-33 induced cell death in HG-3 cells generated by three independent experiments using GraphPad Prism 8. (B) results of analysing the data of RK-33 induced cell death in MEC1 cells generated by three independent experiments using GraphPad Prism 8. The LC_{50} of RK-33 in HG-3 cells and MEC1 cells at each time is calculated from this nonlinear statistical analysis.

Table 5.3 LC_{50} of RK-33 in HG-3 and MEC1 cells at three time points

	24h	48h	72h
LC_{50} of HG-3	2.64μM	4.10μM	3.85μM
LC_{50} of MEC1	3.44μM	4.44μM	4.69μM

5.4.5 RK-33 inhibits the expression of DDX3X in HG-3 and MEC1 cells

To figure out whether RK-33 affects the expression of DDX3X in HG-3 cells and MEC1 cells, the two types of cells were treated with 0μM, 1μM, 3μM, 10μM for 24h and harvested for the detection of DDX3X expression by Western blotting. As shown in Figure 5.9, the expression of DDX3X was inhibited by RK-33 at concentrations between 3μM and 10μM.

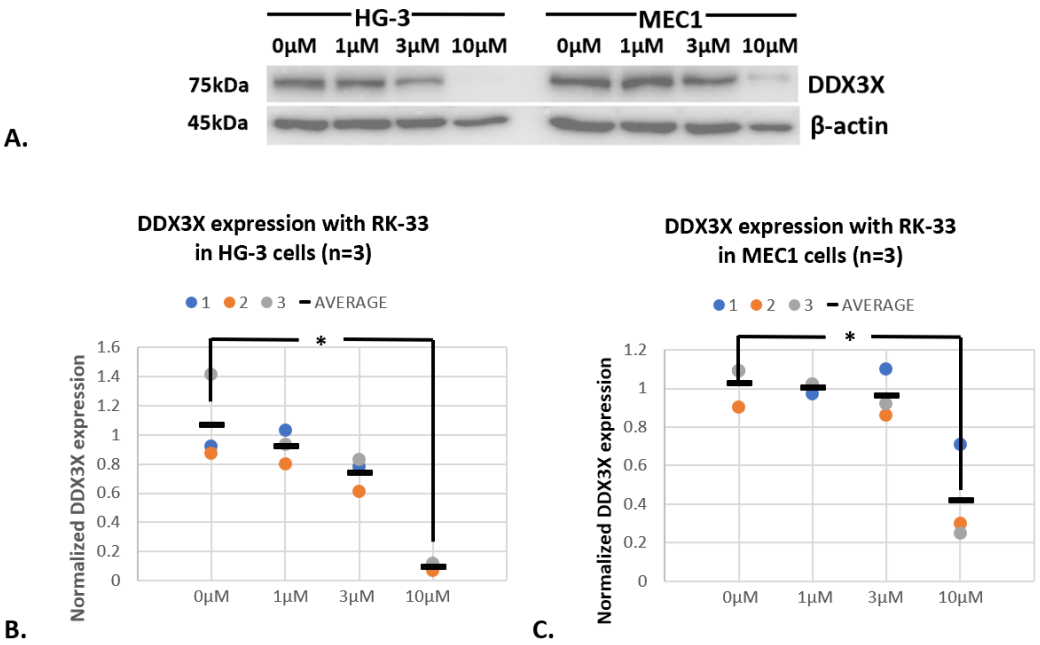

Figure 5.9 DDX3X expression after RK-33 treatment in HG-3 and MEC1 cells. (A) Western blotting of DDX3X expression in HG-3 and MEC1 cells after 24h RK-33 treatment. (B) densitometry analysis of DDX3X expression from three independent experiments after RK-33 treatment in HG-3 cells. The difference of the averaged DDX3X expression between the control cells and the cells treated with 10μM of RK-33 is statistically significant with the p-value < 0.05. (C) densitometry analysis of DDX3X expression from three independent experiments after RK-33 treatment in MEC1 cells. The difference of the averaged DDX3X expression between the control cells and the cells treated with 10μM of RK-33 is statistically significant with the p-value < 0.05. Statistical significance was determined by the two-tailed, paired Student's t-test.

5.4.6 RK-33 has no effect on the proliferation of HG-3 and MEC1 cells

To investigate whether RK-33 affects the proliferation of HG-3 or MEC1 cells, HG-3 cells and MEC1 cells were incubated with RK-33 under the cytotoxicity concentration and counted the absolute number of viable cells using Trypan blue dye at the end of incubation.

The results showed that RK-33 did not affect the number of viable cells in both HG-3 cells and MEC1 cells with the concentrations of 0.1μM and 1μM which are all below the LC_{50} of RK-33 for both types of cells (Figure 5.10 and Figure 5.11). There seemed a decrease in the number of viable cells at 48h in results from HG-3 cells but the decrease was not statistically significant.

Based on these results, RK-33 at the concentrations that do not induce a significant level of cell death does not affect the proliferation of HG-3 and MEC1 cells.

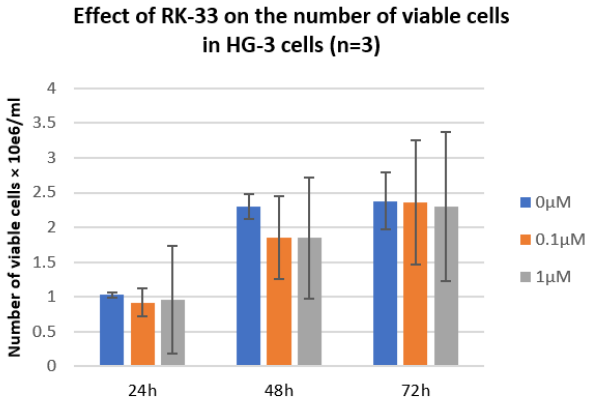

Figure 5.10 Effect of RK-33 under the cytotoxic concentration on the proliferation of HG-3 cells. HG-3 cells were cultured at a cell density of 0.5×10^6/ml and treated with RK-33 at the indicated concentrations. After incubation for 24h, 48h, or 72h, cells were harvested separately at each time point and the absolute number of viable cells that exclude Trypan blue dye of each sample was counted using the Cellometer. These results were generated by three independent experiments (mean ± SD). No statistical significance was achieved using a two-tailed, paired Student's t-test.

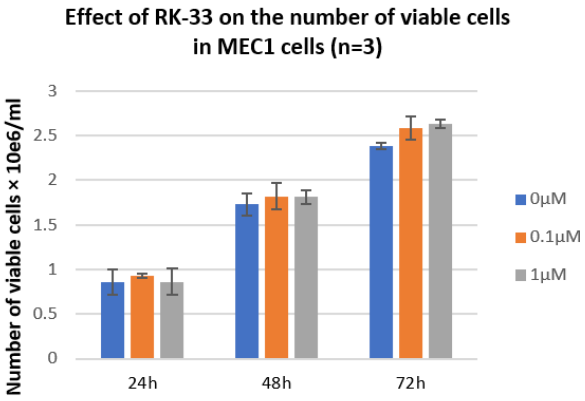

Figure 5.11 Effects of RK-33 under the cytotoxic concentration on the proliferation of MEC1 cells. MEC1 cells were cultured at a cell density of 0.5×10^6/ml and treated with RK-33 at the indicated concentrations. After incubation for 24h, 48h, or 72h, cells were harvested separately at each time point and the absolute number of viable cells that exclude Trypan blue dye of each correlated sample was counting using the Cellometer. These results were generated by three independent experiments (mean ± SD). No statistical significance was achieved using a two-tailed, paired Student's t-test.

5.4.7 RK-33 partially abrogates CD40 stimulation mediated protection against fludarabine-induced cell death in CLL cells

The data in Chapter 3 showed that CD40 stimulation protected primary CLL cells from drug-induced cell death. To investigate whether DDX3X inhibitor can affect the CD40 stimulation induced cytoprotection, firstly, it was necessary to figure out whether CD40 stimulation can protect CLL cell lines from drug-induced cell death. The drug used in this part was fludarabine. Since fludarabine induces cell death in a p53-dependent manner (Pettitt, 2003), MEC1 cells that do not express wild type p53 are not appropriate for the fludarabine-involved experiments (Stacchini et al., 1999). Therefore, fludarabine-involved experiments were only performed on HG-3 cells.

To know the response-pattern of HG-3 cells to fludarabine, HG-3 cells were treated with fludarabine at the concentrations of 0.3μM, 1μM, 3μM, 10μM, 30μM and incubated for 24h, 48h, and 72h. As shown in Figure 5.12, fludarabine induced cell death in HG-3 cells in a time- and concentration-dependent manner.

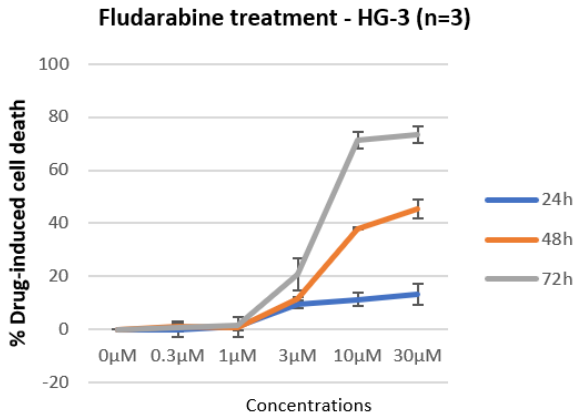

Figure 5.12 Fludarabine treatment on HG-3 cells. Cells were cultured at a cell density of 0.5×10^6/ml and incubated with fludarabine at concentrations of 0.3μM, 1μM, 3μM, 10μM, 30μM for 24h, 48h, and 72h. Cells were harvested separately at each time point for cell death assay using flow cytometry. Drug-induced cell death = [(% cell death of drug-treated cells - % cell death of untreated cells)/(100 - % cell death of untreated cells)] × 100. (A) pooled results of fludarabine induced cell death in HG-3 cells by three independent experiments (mean ± SD).

Previously data in section 5.4.3 has shown that the expression of BCL-XL in HG-3 cells can be up-regulated by the soluble CD40 ligand and the up-regulation of the expression of BCL-XL was more obvious with the incubation of 24h comparing to that of 12h (Figure 5.6 A), which proved that HG-3 cells respond to CD40 stimulation. To determine whether CD40 stimulation can protect HG-3 cells from fludarabine-induced cell death, HG-3 cells were incubated with and without the soluble CD40 ligand for 24h, respectively, and then the CD40 stimulated and the unstimulated HG-3 cells were treated with fludarabine with a range of concentrations for a further 48h. Cells were harvested at the end of incubation for cell death assay using flow cytometry.

Results showed that CD40 stimulation protected HG-3 cells from fludarabine-induced cell death (Figure 5.13), a result consistent with what we have observed on primary CLL cells. The difference in cell death between the CD40 stimulated and unstimulated cells was statistically significant at the concentration of 3μM, 10μM, and 30μM (p-value < 0.05, respectively).

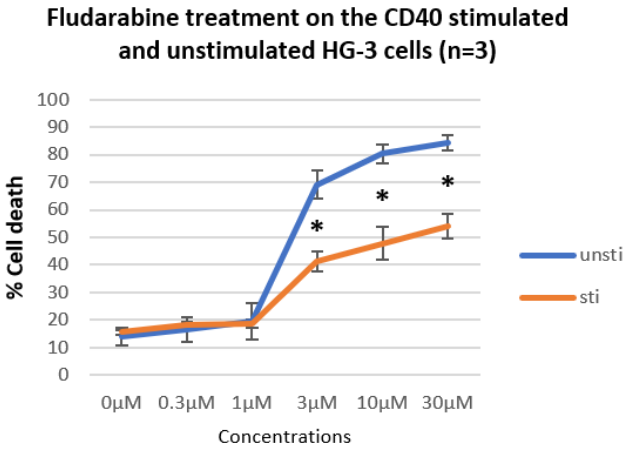

Figure 5.13 Effect of CD40 stimulation on fludarabine-induced cell death in HG-3 cells. For CD40 stimulation, HG-3 cells were incubated with 0.1μg/ml HA-tagged CD40 ligand and 0.5μg/ml anti-HA antibody for 24h. As unstimulated controls, HG-3 cells were treated with 0.5μg/ml anti-HA antibody alone for 24h. Both the CD40 stimulated and unstimulated cells were treated with fludarabine for another 48h. *: p-value < 0.05 (using the two-tailed, paired Students' t-test).

In order to investigate whether RK-33 affects the cytoprotective effect of CD40 stimulation against fludarabine-induced cell death in HG-3 cells, HG-3 cells were treated in four ways as the following: HG-3 cells incubated with 0.1μg/ml HA-tagged CD40 ligand, 0.5μg/ml anti-HA antibody and 3μM of RK-33 (CD40 sti+ RK-33+); HG-3 cells incubated with 0.5μg/ml anti-HA antibody and 3μM of RK-33 (CD40 sti- RK-33+); HG-3 cells incubated with 0.1μg/ml HA-tagged CD40 ligand and 0.5μg/ml anti-HA antibody (CD40 sti+ RK-33-); HG-3 cells incubated with 0.5μg/ml anti-HA antibody (CD40 sti- RK-33-). The HG-3 cells in the former two types of treatments (with the treatment of RK-33) are taken as the observation group and the HG-3 cells in the latter two types of treatments (without RK-33 treatment) are taken as the control group. After the incubation of 24h, cells from each group with different treatments were harvested for Western blotting and further fludarabine treatment, respectively. Western blotting was used to check the expression of BCL-XL to confirm the CD40 stimulation in cells treated with the soluble CD40 ligand, and to check the expression level of DDX3X in CD40-stimulated cells. Cells harvested from each type of treatment for further fludarabine treatment were treated with 3μM of fludarabine for another 48h and finally collected for cell death assay in the end. The concentration of fludarabine at 3μM was used as the previous results showed that CD40 stimulation has exhibited a significantly cytoprotective effect in HG-3 cells treated with 3μM of fludarabine (Figure 5.13).

The first concentration of RK-33 used in this experiment was 3μM, which was based on the LC_{50} of RK-33 in HG-3 cells. After 24h incubation, CD40 stimulation was successfully established in the HG-3 cells both in the observation and control groups with the expression of BCL-XL up-regulated in the CD40 stimulated HG-3 in each group (Figure 5.14 A and B). The increased expression of BCL-XL induced by CD40 stimulation in the control group is statistically significant (p-value < 0.01) but that in the observation group is not.

For the expression of DDX3X, comparing to that of the cells without RK-33 treatment, the expression of DDX3X in the cells treated with 3μM of RK-33 was inhibited (Figure 5.14 A and C). However, the corresponding expression of β actin in those cells declines at the same time. The results of DDX3X expression with 3μM of RK-33 presented here were different from that of the previous results on HG-3 cells (Figure 5.9). This can be explained by the poor viability after 24h incubation in the observation groups (Figure 5.14 D), in which 3μM of RK-33 induced fierce cell death in almost all of the cells and led to all proteins degraded in the dead cells.

The results of cell death after 24h incubation showed that, for the cells incubated without RK-33, the viability of the CD40 stimulated HG-3 cells (76.92% ± 3.82) was higher than that of the unstimulated cells (71.97% ± 2.52), and the difference was statistically significant (p-value < 0.05) (Figure 5.14 D, columns labelled with '-RK33 (3μM)' on the left side). Similar results were seen for the cells incubated with RK-33. The viability of the CD40 stimulated HG-3 cells treated with 3μM of RK-33 (8.02% ± 0.78) was higher than that of the unstimulated cells treated with 3μM of RK-33 (3.76% ± 0.09), and the difference was statistically significant (p-value < 0.01) (Figure 5.14 D, columns labelled with '+RK33 (3μM)' on the right side).

However, due to the low viability in the HG-3 cells treated with 3μM of RK-33 as a result of its cytotoxic effect, cells treated with 3μM of RK-33 cannot be used for further treatment with fludarabine.

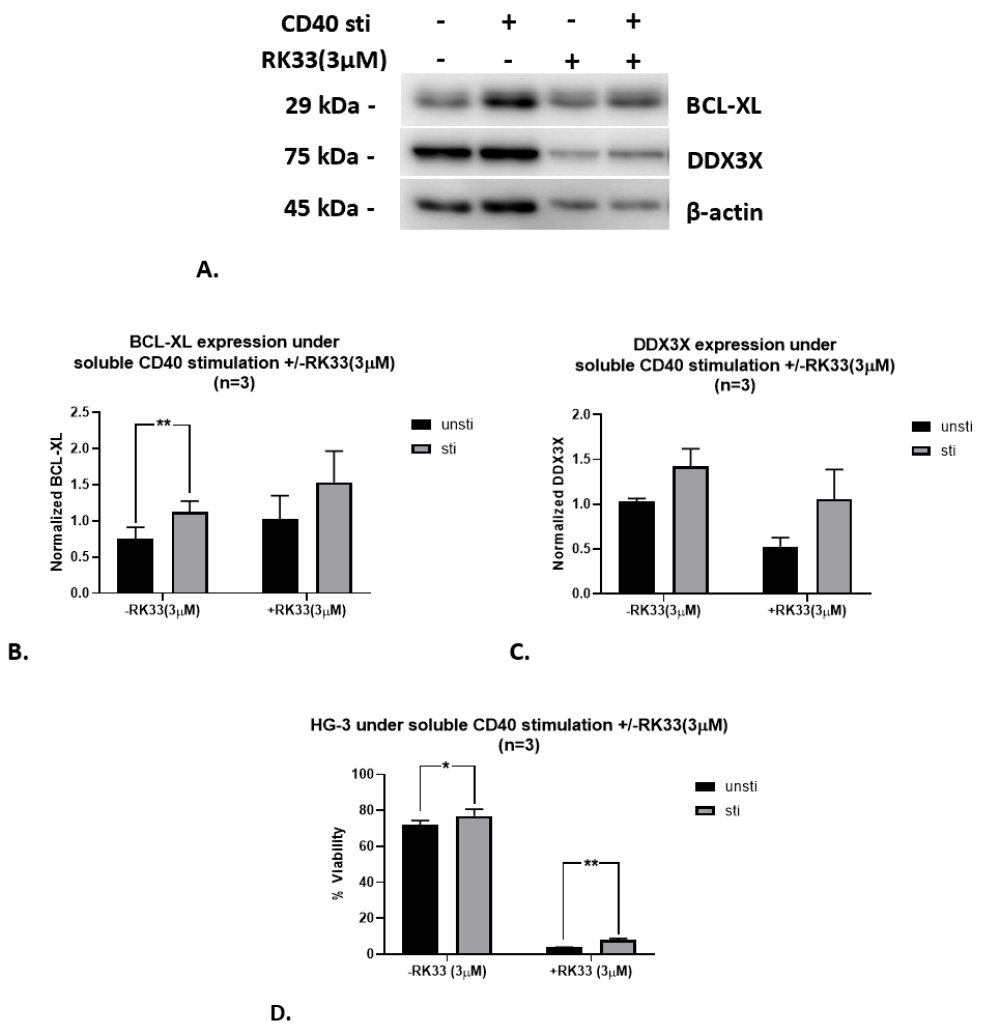

Figure 5.14 Results of the CD40 stimulated and unstimulated HG-3 cells treated with or without 3μM of RK-33. HG-3 cells were incubated with four different types of interferences: incubated with 0.1μg/ml HA-tagged CD40 ligand and 0.5μg/ml anti-HA antibody (CD40 sti+ RK-33-), incubated with 0.5μg/ml anti-HA antibody (CD40 sti- RK-33-), incubated with 0.1μg/ml HA-tagged CD40 ligand, 0.5μg/ml anti-HA antibody and 3μM of RK-33 (CD40 sti+ RK-33+), incubated with 0.5μg/ml anti-HA antibody and 3μM of RK-33 (CD40 sti+ RK-33+). Cells from each type were harvested after 24h for Western blotting and cell death assay. (A) Western blotting of the expression of BCL-XL and DDX3X in HG-3 cells. (B) densitometry analysis of the BCL-XL expression. (C) densitometry analysis of the DDX3X expression. (D) the viability of the cells incubated with four types of interferences after 24h incubation. Results were generated from the data of three independent experiments (mean ± SD). Statistical significance was determined using the two-tailed, paired Students' t-test. *: p-value < 0.05; **: p-value < 0.01.

To reduce the cell death induced by RK-33 for HG-3 cells in the observation group before further treatment of fludarabine, the concentration of RK-33 was reduced to 1μM with other conditions kept unchanged in the experiment.

Under this condition, the results of Western blotting after 24h incubation showed that the expression of BCL-XL in the CD40 stimulated HG-3 cells in both the control and the observation group was higher than that in the corresponding unstimulated HG-3 cells (Figure 5.15 A and B). The up-regulated expression of BCL-XL induced by CD40 stimulation in the cells incubated without 1μM of RK-33 was statistically significant (p-value < 0.05) but that in the cells incubated with 1μM of RK-33 was not (Figure 5.15 B). The decrease caused by 1μM of RK-33 in the up-regulated expression of BCL-XL induced by CD40 stimulation indicated that the effect of CD40 stimulation may be affected by 1μM of RK-33.

However, no inhibition of the DDX3X expression in cells treated with 1μM of RK-33 was observed (Figure 5.15 A). In addition, although CD40 stimulation increased the expression of DDX3X in the cells incubated with and without 1μM of RK-33, no statistical significance was observed between the CD40 stimulated and unstimulated cells (Figure 5.15 C).

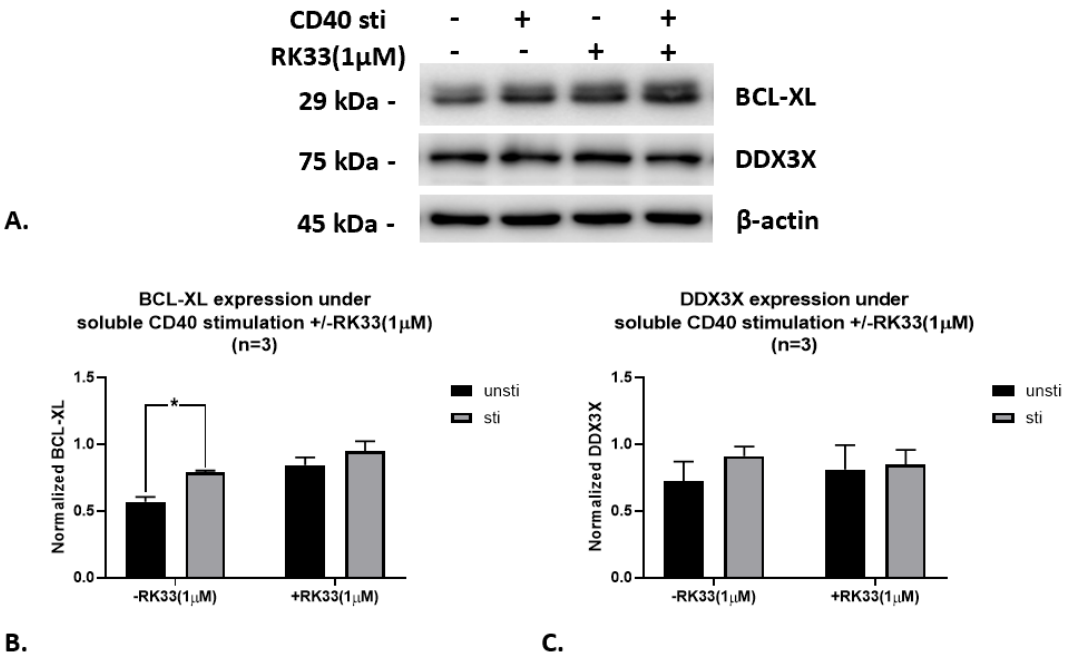

Figure 5.15 Results of the expression of BCL-XL and DDX3X in the CD40 stimulated and unstimulated HG-3 cells treated with or without 1μM of RK-33. The expression of BCL-XL and DDX3X were investigated in HG-3 cells with four different types of interferences: cells incubated with 0.1μg/ml HA-tagged CD40 ligand and 0.5μg/ml anti-HA antibody, cells incubated with 0.5μg/ml anti-HA antibody, cells incubated with 0.1μg/ml HA-tagged CD40 ligand, 0.5μg/ml anti-HA antibody and 1μM of RK-33, cells incubated with 0.5μg/ml anti-HA antibody and 1μM of RK-33. (A) western blotting results of the BCL-XL and DDX3X expression in HG-3 cells. (B) densitometry analysis results of the expression of BCL-XL. (C) densitometry analysis results of the expression of DDX3X. Results were generated from the data of three independent experiments (mean ± SD). Statistical significance was determined using the two-tailed, paired Students' t-test. *: p-value < 0.05; **: p-value < 0.01.

The results of viability after 24h incubation showed that the cytoprotective effect of CD40 stimulation was reduced by the treatment of 1μM of RK-33 (Figure 5.16 A). In the absence of 1μM of RK-33, the viability of the CD40 stimulated HG-3 cells (69.96% ± 2.80) was significantly higher than that of the unstimulated HG-3 cells (66.23% ± 2.20) (p-value < 0.01). In the presence of 1μM of RK-33, the difference in viability between the CD40 stimulated and unstimulated HG-3 cells was not statistically significant (66.66% ± 2.15 for CD40 stimulated cells and 63.98% ± 0.56 for unstimulated cells).

Based on the above observations, the CD40 stimulated and unstimulated HG-3 cells in the presence or absence of 1μM of RK-33 were further treated with fludarabine for another 48h.

After further fludarabine treatment, the results showed that the protection induced by CD40 stimulation against fludarabine-induced cell death was partially abolished by 1μM of RK-33 (Figure 5.16 B). Without the treatment of 1μM of RK-33, the cell death of the CD40 stimulated HG-3 cells treated with fludarabine was significantly lower (45.27% ± 0.73) than that of the unstimulated cells (55.80% ± 2.08) (p-value < 0.05). However, with the treatment of 1μM of RK-33, fludarabine-induced cell death of CD40 stimulated HG-3 cells (47.98% ± 1.74) was similar to that in the unstimulated HG-3 cells (49.19% ± 0.83).

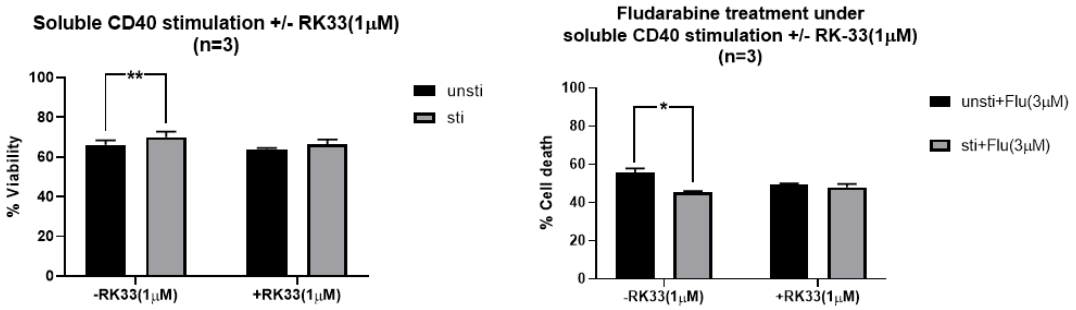

A. **B.**

Figure 5.16 RK-33 (1μM) affects the survival protection induced by CD40 stimulation in HG-3 cells. (A) 24h results of viabilities of the cells incubated with 0.5μg/ml anti-HA antibody, the cells incubated with 0.1μg/ml HA-tagged CD40 ligand and 0.5μg/ml anti-HA antibody, the cells incubated with 0.5μg/ml anti-HA antibody and 1μM of RK-33, the cells incubated with 0.1μg/ml HA-tagged CD40 ligand, 0.5μg/ml anti-HA antibody and 1μM of RK-33. (B) cell death of the above cells treated with fludarabine for a further 48h. Results were generated from the data of three independent experiments (mean ± SD). Statistical significance was analysing using the two-tailed, paired Student's t-test. *: p-value < 0.05; **: p-value < 0.01.

The above experiment was then performed on primary CLL cells. The concentration of RK-33 applied was 1μM and the concentration of fludarabine applied was 3μM. The procedure was the same as that performed on HG-3 cells.

After 24h, the status of CD40 stimulation was confirmed by the up-regulation of the expression of BCL-XL in the primary CLL cells from three CLL cases (Figure 5.17 A and B). The treatment of 1μM of RK-33 made no difference in the increased expression of BCL-XL induced by CD40 stimulation in primary CLL cells (Figure 5.17 A, B, C). Similar to the results of HG-3 cells, 1μM of RK-33 did not inhibit the expression of DDX3X in these primary CLL cells and had no effect on the up-regulated expression of DDX3X (Figure 5.17 A, B, D, E;

Figure E was further normalized from Figure D with the up-regulation of DDX3X being normalized to be visualized more clearly).

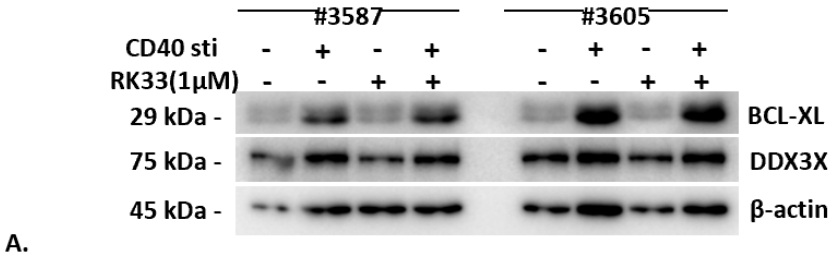

A.

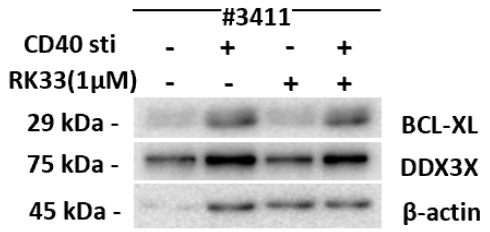

B.

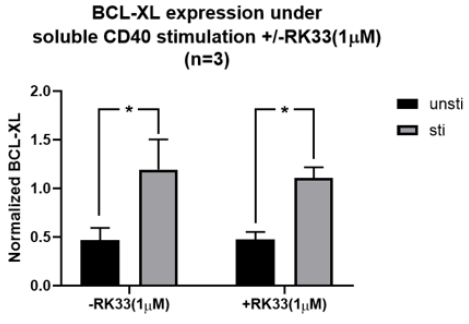

C.

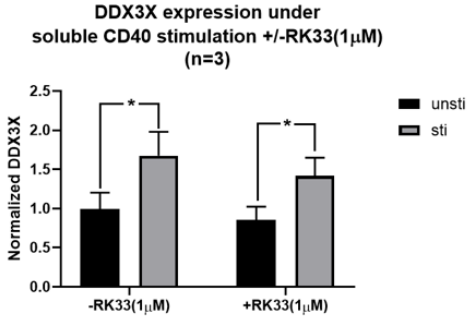

D.

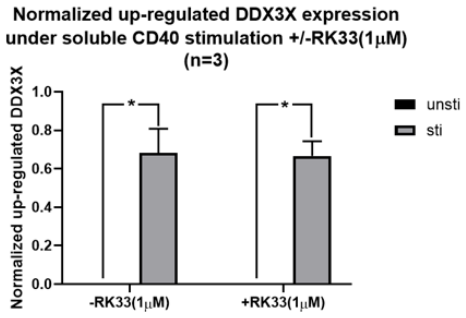

E.

Figure 5.17 Results of the expression of BCL-XL and DDX3X in the CD40 stimulated and unstimulated primary CLL cells treated with or without 1μM of RK-33. The expression of BCL-XL and DDX3X were investigated in the primary CLL cells of each case with four different types of interferences: cells incubated with 0.1μg/ml HA-tagged CD40 ligand and 0.5μg/ml anti-HA antibody (CD40 sti+ RK-33-), cells incubated with 0.5μg/ml anti-HA antibody (CD40 sti- RK-33-), cells incubated with 0.1μg/ml HA-tagged CD40 ligand, 0.5μg/ml anti-HA antibody and 1μM of RK-33 (CD40 sti+ RK-33+), cells incubated with 0.5μg/ml anti-HA antibody and 1μM of RK-33 (CD40 sti+ RK-33+). Cells from each type were harvested after the incubation of 24h for Western blotting. (A) and (B) Western blotting of the BCL-XL and DDX3X expression in primary CLL cells from three cases. (C) and (D) densitometry analysis of BCL-XL and DDX3X expression. (E) normalized up-regulated DDX3X expression. Statistical significance was analysing using the two-tailed, paired Student's t-test. *: p-value < 0.05.

The results of viability after 24h incubation showed that the treatment with 1μM of RK-33 made no difference in the cytoprotective effect induced by CD40 stimulation in primary CLL cells based on the results of cells from individual cases and the pooled results (Figure 5.18).

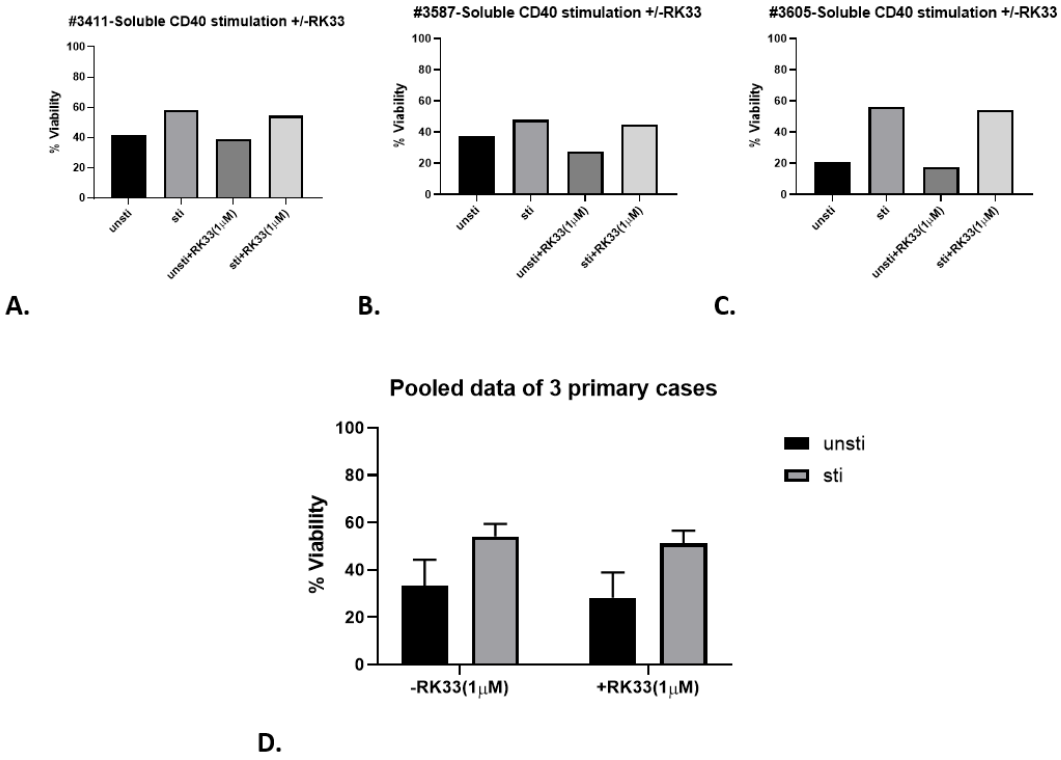

Figure 5.18 Viability of the CD40 stimulated and unstimulated CLL cells with or without incubation with RK-33(1μM) for 24h. Viabilities were detected in cells incubated with 0.5μg/ml anti-HA antibody for 24h, cells incubated with 0.1μg/ml HA-tagged CD40 ligand and 0.5μg/ml anti-HA antibody for 24h, cells incubated with 0.5μg/ml anti-HA antibody and 1μM of RK-33 for 24h, cells incubated with 0.1μg/ml HA-tagged CD40 ligand, 0.5μg/ml anti-HA antibody and 1μM of RK-33 for 24h. (A), (B), (C) are results of individual cases. (D) pooled results of three cases (mean ± SD). No statistically significant difference was observed between the CD40 stimulated and the unstimulated primary CLL cells neither with nor without the treatment of 1μM of RK-33.

Then, the CD40 stimulated and unstimulated primary CLL cells treated with or without 1μM of RK-33 were further treated with 3μM of fludarabine for another 48h. Results of the primary CLL cells from case #3411 and #3587 showed that the cytoprotective effect induced by CD40 stimulation against the fludarabine-induced cell death was partially reduced by 1μM of RK-33 (Figure 5.19 A and B). However, the results of case #3605 showed that 1μM of RK-33 made no influence on the cytoprotective effect (Figure 5.19 C). Despite the variation, the pooled results showed that the statistically significant decrease of fludarabine-induced cell death caused by CD40 stimulation was negated by 1μM of RK-33 (Figure 5.19 D).

These results suggest that RK-33 partially abrogated the cytoprotective effect induced by CD40 stimulation against fludarabine-induced cell death in primary CLL cells, but there may be a variation in primary CLL cells from different cases.

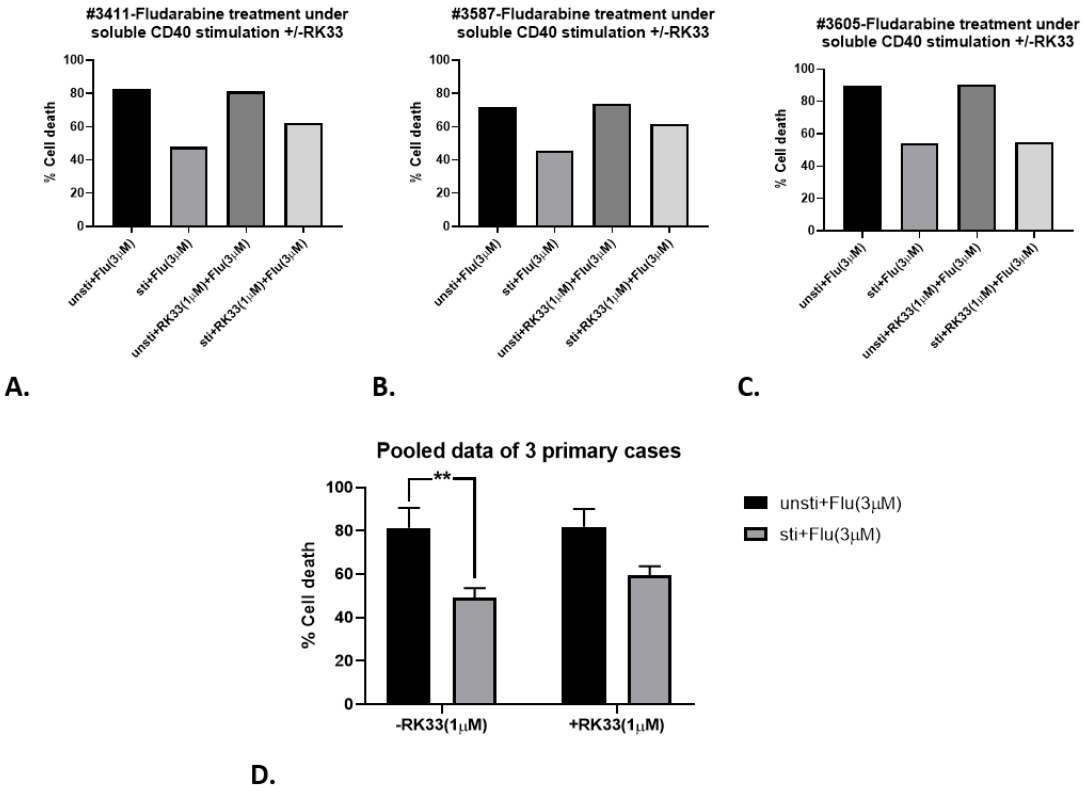

Figure 5.19 Effect of RK-33 on fludarabine-induced cell death in the CD40 stimulated and unstimulated CLL cells. Cell death was detected in: cells incubated with 0.5μg/ml anti-HA antibody for 24h and incubated with 3μM of fludarabine for another 48h, cells incubated with 0.1μg/ml HA-tagged CD40 ligand and 0.5μg/ml anti-HA antibody for 24h and incubated with 3μM of fludarabine for another 48h, cells incubated with 0.5μg/ml anti-HA antibody and 1μM of RK-33 for 24h and incubated with 3μM of fludarabine for another 48h, cells incubated with 0.1μg/ml HA-tagged CD40 ligand, 0.5μg/ml anti-HA antibody and 1μM of RK-33 for 24h and incubated with 3μM of fludarabine for another 48h. (A), (B), (C) are results of individual cases. (D) pooled results of three cases (mean ± SD). The difference between the CD40 stimulated and the unstimulated primary CLL cells without the treatment of 1μM of RK-33 is statistically significant (p-value < 0.01, using the two-tailed, paired Student's test).

Collectively, the data on both primary CLL cells and CLL cell lines showed that the DDX3X inhibitor, RK-33, induced cell death on CLL cells and partially abrogated the survival protection induced by CD40 stimulation against fludarabine-induced cell death, which indicates that DDX3X may potentially play a role in the survival of CLL cells and may be involved in mediating the CD40 stimulation induced pro-survival signals. Based on these

Western blot results, the expression of DDX3X was not inhibited obviously by RK-33 of 1μM in both primary CLL cells and HG-3 cells, which led to the question whether RK-33 induced cell death in CLL cells by inhibiting the expression of DDX3X protein. To answer this question, the siRNAs knockdown experiments were performed using CLL cell lines to investigate whether inhibiting the expression of DDX3X affected the survival of CLL cells.

5.4.8 The effect of DDX3X knockdown by siRNAs on HG-3 and MEC1 cells

The knockdown experiments were performed using siRNAs specific to DDX3X on HG-3 cells and MEC1 cells. Non-specific targeting siRNA was used as a control. Non-transfected cells (referred to as the 'wild type' cells) were also included in each knockdown experiment. Cell death was monitored at the end of treatment by flow cytometry.

Results from HG-3 cells showed that, comparing with that in the siControl cells, knocking down DDX3X in HG-3 cells led to no statistically significant increase in cell death (Figure 5.20).

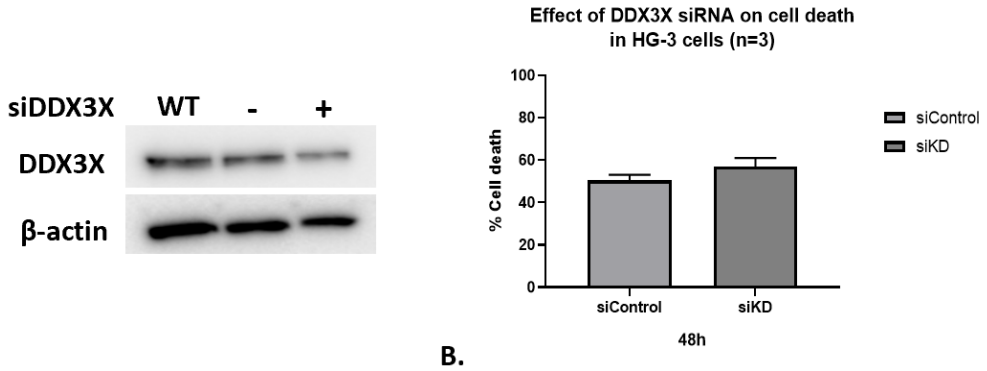

Figure 5.20 Effect of knocking down DDX3X in HG-3 cells. HG-3 cells were transfected with the SMARTpool siRNAs of DDX3X at 100nM and incubated for 48h. As a control, HG-3 cells were transfected with the SMARTpool control siRNA at 100nM for 48h. Untransfected cells were used for comparison. (A) Western blotting of the DDX3X expression in HG-3 cells. (B) effect of knocking down DDX3X on cell death as measured by flow cytometry using Annexin V and 7-AAD. The difference in cell death between the DDX3X knocking down cells and the siControl cells was not statistical significance.

Similar results were found in MEC1 cells that knocking down DDX3X using siRNAs in MEC1 cells caused no statistically significant increase in cell death (Figure 5.21).

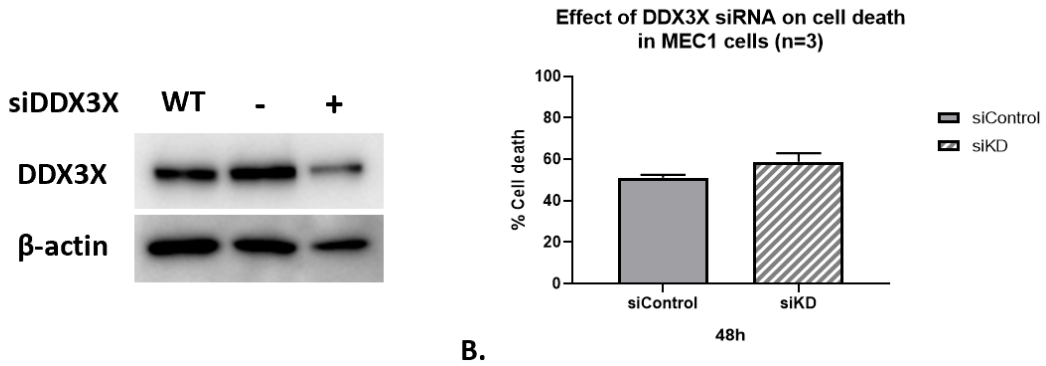

A. B.

Figure 5.21 Effect of knocking down DDX3X in MEC1 cells. MEC1 cells were transfected with the SMARTpool siRNAs of DDX3X at 100nM and incubated for 48h. As a control, cells were also transfected with the SMARTpool control siRNA at 100nM for 48h. Untransfected cells were also used in the experiments for comparison. (A) Western blotting results of DDX3X expression in MEC1 cells. (B) Effect of DDX3X siRNAs on cell death as measured by flow cytometry using Annexin V and 7-AAD. The difference in cell death between the DDX3X knocking down cells and the siControl cells was not statistical significance.

Based on the above results that the increases in cell death caused by knocking down DDX3X in HG-3 and MEC1 cells were not statistically significant, no definitive conclusion can be drawn that inhibiting the expression of DDX3X affects the survival of CLL cells. The optimization of DDX3X knockdown has continued till the sudden outbreak of the COVID-19 pandemic that caused the cessation of the knockdown experiments.

In summary, DDX3X appears to play a role in the pro-survival effects mediated by CD40 stimulation on CLL cells. The function of DDX3X may vary across different primary CLL cases. DDX3X inhibitor RK-33 induced apoptosis on both HG-3 cells and MEC1 cells, indicating that RK-33-induced cell death does not involve p53.

5.5 Discussion

The functional results from the preliminary study suggest that DDX3X is an interesting molecule to study in the context of CD40 stimulation-mediated survival in CLL cells.

The results showed that the inhibitor of DDX3X, RK-33, induces cell death of both primary CLL cells (LC_{50}=3.89μM at 24h) and two types of CLL cell lines (HG-3 cells: LC_{50}=2.64μM at 24h, 4.1μM at 48h, 3.85μM at 72h, respectively; MEC1 cells: LC_{50}=3.44μM at 24h, 4.44μM at

48h, 4.69μM at 72h, respectively) with similar LC_{50}s for each type of cells. These results are in line with published reports of RK-33 on other types of cancer cells. As a specific inhibitor of DDX3X, RK-33 inhibits the viability of several lung cancer cell lines highly expressing DDX3X with LC_{50} between 4.4 and 8.4μM (Bol et al., 2015). RK-33 shows cytotoxicity on colorectal cancer cell lines with LC_{50} ranging from 3μM to 7μM, and at the same time, it also inhibits the survival of patient-derived colorectal cancer spheroid cell lines with LC_{50} ranging from 3μM to 9μM (van Voss et al., 2015). For breast cancer, RK-33 induces cell death of breast cancer cell lines with LC_{50} between 2.8 and 4.5μM (Van Voss et al., 2018). The LC_{50} of RK-33 on medulloblastoma cell lines ranges from 2.5μM to 3.5μM (Tantravedi et al., 2019).

Results also showed that RK-33 partially abrogated the cytoprotective effect induced by CD40 stimulation against fludarabine-induced cell death in both HG-3 cells and primary CLL cells from two cases but RK-33 made no difference on the primary CLL cells from case #3605. It may suggest a variation of RK-33 on primary CLL cells from different cases, which is in line with other reports. It has been reported that the expression level of DDX3X on different types of cells affects their sensitivity to RK-33 (Van Voss et al., 2018, Xie et al., 2016, Bol et al., 2015). Due to the fact that CLL is a highly heterogeneous disease, it is possible that the expression level of DDX3X protein is different in individual patients. In addition to the heterogeneous expression status of DDX3X, the mutation status may also influence the sensitivity of RK-33 in primary CLL cell and the occurrence of DDX3X mutation has been reported in various type of diseases (Kellaris et al., 2018, Jiang et al., 2015, Pugh et al., 2012) including CLL. It was reported that nine genes were mutated at significant frequencies including five genes with unestablished roles in CLL and that one of them was DDX3X (Wang et al., 2011a). Later in 2015, DDX3X mutation was identified by analysing peripheral blood samples from 136 patients with CLL (Vollbrecht et al., 2015). Furthermore, it has been reported by Juhi Ojha and colleagues that DDX3X mutations were associated with the progression of CLL and play a role in the convergent evolution of CLL (Ojha et al., 2015a, Ojha et al., 2015b). These findings indicate DDX3X expression varies across different patients and even in the same patient in different stages of CLL, which may be the reason for the variation of the sensitivity to RK-33 among the primary CLL cells from different cases.

Although some interesting results with RK-33 were obtained in this part of study, it is clear that these results are not enough to generate strong conclusions for the role of DDX3X in

the pro-survival effect induced by CD40 stimulation due to undefined mechanism of RK-33 and unsatisfied DDX3X knocking results based on the results present here in this part. For the function of RK-33 on inhibiting DDX3X protein, it has been reported that RK-33 induces cell death and decreases the expression of DDX3X protein on lung cancer cells (Bol et al., 2015) and medulloblastoma cells (Tantravedi et al., 2019). Guus M Bol and colleagues reported that 50nM of RK-33 can specifically inhibit the expression of DDX3X by reducing the unwinding activity of the homolog of DDX3X in yeast (Bol et al., 2015). However, results in this study did not show a clear inhibition of DDX3X expression by RK-33 in primary CLL cells when it induced cell death in these cells. In primary CLL cells, the expression of DDX3X in cells treated with 10μM of RK-33 decreased but the correlated expression of β-actin decreased at the same time, which suggested that this decrease was likely caused by the cell death induced by RK-33 with all the proteins degraded. Results on the effect of RK-33 from HG-3 and MEC1 cells showed that RK-33 inhibited the expression of DDX3X in these cells gradually with the increasing concentrations and there were clear declines in the DDX3X expression in the cells treated by 3μM and 10 μM of RK-33 with the correlated β-actin expression unaffected. However, in the later experiments in HG-3 cells, the expression of DDX3X was inhibited by 3μM of RK-33 with the decreased expression of β-actin simultaneously. Based on these contradictory results, it is inconclusive to say that RK-33 induces cell death by inhibiting the expression of DDX3X in HG-3 cells. Together with the results obtained from primary CLL cells, although RK-33 induced cell death in CLL cells, the data in this part of study did not clarify the mechanism underlying RK-33-induced cell death. Furthermore, results from the siRNAs knockdown experiments did not provide clear evidence for the role of DDX3X in the survival of CLL cells as well.

In conclusion, the results obtained from this preliminary study indicate that DDX3X protein may be potentially involved in the CD40 stimulation-induced cytoprotective effect against fludarabine-induced cell death. However, further study is required to underpin the specific mechanisms of DDX3X in mediating CD40 stimulation-induced pro-survival signalling in CLL cells.

Chapter 6. General discussion

This study aimed to investigate the molecular mechanisms of the pro-survival effect induced by CD40 stimulation in primary CLL cells using the proteomic approach. The hypothesis of the study was that CD40 stimulation altered the protein expression at a global level, resulting in the survival and drug resistance of CLL cells. The first part of this study confirmed that CD40 stimulation induced by co-culture method exhibited cytoprotective effect in primary CLL cells. The comparison between the gene expression profile of CLL cells stimulated by the soluble CD40 ligand and that induced by the co-culture method showed that the soluble CD40 ligand method produced similar changes in the gene expression in primary CLL cells to that induced by the co-culture method. This finding validated the use of the soluble CD40 ligand in proteomics study to investigate the global changes in protein expression induced by CD40 stimulation in primary CLL cells. Using the iTRAQ-MS technique, the differentially expressed proteins induced by CD40 stimulation in primary CLL cells were identified. Based on the iTRAQ data obtained, the functional annotation analysis and the further functional study was aimed at figuring out the key molecules/pathways that mediated the cytoprotective effect of CD40 stimulation based on the iTRAQ data. Here in this part, the discussion will be focused on the main findings from this research project.

6.1 Independent confirmation of the pro-survival effect induced by the CD40 stimulation in primary CLL cells

Using the co-culture system for CD40 stimulation, the results confirmed that CD40 stimulation protected primary CLL cells from spontaneous and drug-induced cell death. The drugs used in this part of the study include fludarabine, ABT-199, and bendamustine, which are currently used in the CLL clinic. The results of the treatment experiment with each drug were generated from at least 3 primary CLL samples.

With the variation across different samples, the pooled results of fludarabine, ABT-199, and bendamustine showed that CD40 stimulated primary CLL cells exhibited a decreased sensitivity to those drugs comparing with the unstimulated primary CLL cells. These results are consistent with most published papers (Kater et al., 2004, Thijssen et al., 2013) including

those reported by our research group (Chapman et al., 2017, Zhuang et al., 2014). These results support the notion that the signals from the CLL microenvironment promote the survival and drug resistance of CLL cells (Burger, 2013). Although there are instances where these results contradict the reported finding, the discrepancy of the results was possibly caused by the different methods used in the studies. Taking the paper published by De Totero and colleagues in 2003 as an example, they reported that CD40 stimulation sensitized CLL cells to fludarabine treatment by using the CLL cells cultured under standard conditions as the control cells and using the ratio of 1:100 for the CD40-expressing fibroblasts and primary CLL cells in the co-culture system (De Totero et al., 2003), which are different from the experiments conducted in this study. Here in this study, the cells taken as the control were the primary CLL cells co-cultured with the parental fibroblasts that were not expressing CD154, which was more comparable as both sets of primary CLL cells were kept at the same co-culture condition. Besides, the ratio used for the CD40-expressing fibroblasts and primary CLL cells in the co-culture system in this study was 1:10.

The independent confirmation of the predominantly pro-survival effects caused by the CD40 stimulation in primary CLL cells is the foundation of this study.

6.2 The soluble CD40 ligand method can mimic the CD40-CD154 crosstalk within the lymph nodes as the co-culture method

The co-culture method was not appropriate for the proteomics study in this project due to the inevitable mixture of fibroblasts when harvesting the primary CLL cells from the co-culture system. It was thus replaced by the soluble CD40 ligand method to be used for the proteomics study. Although using the soluble CD40 ligand method to activate the CD40 signalling pathways in CLL cells has been well documented (Smallwood et al., 2016, Lezina et al., 2018), whether the effect induced by CD40 activation in primary CLL cells via the co-culture system versus the soluble CD40 ligand is comparable has not been examined previously. To obtain a degree of certainty in the comparability of the two stimulation methods before using the soluble CD40 ligand method for the proteomics study was necessary. The mRNA expression data of the CD40-stimulated primary CLL cells using the co-culture method (Pascutti et al., 2013) provided the reference to compare the effect induced

by the two methods at the transcriptional level. Therefore, the gene expression study in CLL cells stimulated with the soluble CD40 ligand was performed using the RNA sequencing technology.

The results of the comparison analysis showed that the changes in gene expression at the transcriptional level induced by the soluble CD40 ligand in primary CLL cells were similar to that induced by the co-culture system. Furthermore, using the published gene expression profile of CLL cells isolated from the microenvironment of CLL as a comparator (Herishanu et al., 2011), the data analysis showed that the gene expression profile of primary CLL cells treated with the soluble CD40 ligand resembled that of CLL cells residing in the lymph nodes. These results suggested that the soluble CD40 ligand was effective in activating the CD40 signalling pathway in CLL cells in a similar fashion to the co-culture system, which provided the confidence to use it in the proteomics study. In addition, the functional analysis of these RNA-seq data provided support for the results of iTRAQ-MS data. The consistent finding at both the protein expression level and the transcriptional level for the CD40 stimulation-induced effect on primary CLL cells increased the stringency of this study.

6.3 CD40 stimulation up-regulates the expression of proteins involved in the cell adhesion of primary CLL cells

The results of the iTRAQ-MS analysis showed that CD40 stimulation induced a significant change in the levels of protein expression in primary CLL cells. There were 552 significantly differentially expressed proteins detected between the CD40 stimulated and unstimulated primary CLL cells at the 24h time point with 448 of them up-regulated and 104 down-regulated. Based on the results of the PANTHER classification analysis, these differentially expressed proteins were involved in various biological processes with different functions. The DAVID functional annotation analysis of the iTRAQ-MS data was supported by that of the RNA-seq data with most of the categories mapped by the differentially expressed proteins presenting of the lists of categories mapped by the differentially expressed genes of the RNA-seq data. According to the DAVID functional annotation analysis of the 448 significantly up-regulated proteins, the category with the highest enrichment score on the DAVID functional annotation clusters list was the cell-cell adhesion that ranked on the top of

the list of the up-regulated RNA-seq data. These results suggest that CD40 stimulation up-regulates the expression of the proteins involved in the cell adhesion in CLL cells.

Based on the results of the functional annotation analysis of the iTRAQ-MS data and the important role of cell adhesion in CLL, the cell-cell adhesion was taken as the focus of the functional study. The aim was to find a novel target mediating the pro-survival effect of CD40 stimulation in the cell-cell adhesion categories. Looking into the proteins in this category, DDX3X was chosen for further validation and functional study.

6.4 DDX3X may play a role in the pro-survival signals induced by CD40 stimulation in CLL cells

The protein ATP-dependent RNA helicase DDX3X is one of the 38 proteins in the category of cell-cell adhesion and it was up-regulated by CD40 stimulation by over two folds compared to that in the unstimulated cells. The result of Western blotting validated the iTRAQ-MS results that CD40 stimulation induced by the soluble CD40 ligand up-regulated the expression of DDX3X in primary CLL cells from the same five primary CLL samples used in the proteomic study.

To study its role in the survival of primary CLL cells, a selective inhibitor of DDX3X, RK-33, was used in the experiments and found that RK-33 induced cell death in primary CLL cells in a concentration-dependent manner. Due to the difficulty in maintaining the good viability of primary CLL cells *in vitro*, two CLL cell lines, HG-3 and MEC1, was used in the subsequent experiments. CD40 stimulation induced by the soluble CD40 ligand can up-regulate the expression of DDX3X and BCL-XL in both cell lines, a result that was observed in primary CLL cells. Results from the CLL cell lines showed that RK-33 induced cell death in HG-3 and MEC1 cells in a dose-dependent manner, similar to that in primary CLL cells. Furthermore, it was found that RK-33 can partially abrogate the CD40 stimulation mediated protection against fludarabine-induced cell death in HG-3 cells. Similar results can be observed in the primary CLL cells from two primary CLL samples, but the results of the primary CLL cells from the other primary sample showed that RK-33 made no change in the CD40 stimulation mediated protection against fludarabine-induced cell death. Although the pooled results of the primary CLL cells from three primary samples showed that RK-33 partially abrogates the

CD40 stimulation mediated protection against fludarabine-induced cell death, the results from individual cases showed a variation across primary CLL samples.

These results suggest that DDX3X may play a role in the survival of CLL cells and that DDX3X could be potentially involved in the pro-survival signals induced by CD40 stimulation in CLL cells. However, with the inconclusive results from experiments to knockdown DDX3X in HG-3 and MEC1 cells, definitive conclusions cannot be generated based on these preliminary results.

6.5 Future work

Cell adhesion is a hot topic in cancer research as molecules in this category are involved in the differentiation, proliferation, migration, metastasis, and chemo-resistance of malignant cells (Farahani et al., 2014, Makrilia et al., 2009, Damiano et al., 1999). Cell adhesion is important in the pathogenesis and disease progression of CLL (Burger, 2013). In 2015, by analysing the profiles of differentially expressed proteins between the UM-IGHV and U-IGHV CLL cells, our research group demonstrated that the cell adhesion and migration pathways in the UM-IGHV CLL cells were defective compared to those in M-IGHV CLL cells, rendering UM-IGHV CLL cells being retained in the lymph nodes (Eagle et al., 2015), which indicates that the aberration of the cell trafficking may participate in the pathogenesis of CLL. The CLL microenvironment especially the lymph nodes support the survival and proliferation of CLL cells and the cell trafficking of CLL cells between the peripheral blood and the microenvironment is crucial for the disease progression, which is the reason that therapeutic investigation has been trying to interrupt the cell homing and the crosstalk between the CLL cells and the accessory cells in the past decades (Delgado et al., 2020). The clinical observations that the small molecular inhibitors targeting BCR signalling exhibit impressive clinical efficacy by disrupting the cell adhesion and redistributing CLL cells from the tissue microenvironment to peripheral blood (Tissino et al., 2018, Herman et al., 2015) highlighted the importance of targeting the cell-cell adhesion in CLL.

The cell adhesion of CLL cells is directed by the interaction of CLL cells with the accessory cells via regulating the chemokines such as CXCR4/CXCL12, CXCR5/CXCL13, CCL3, CCL4, CCL22, and CD49d (Burger and Gribben, 2014, Han et al., 2014). Among these chemokines, it

has been reported that the secretion of CCL22 by CLL cells can be promoted by the CD40 stimulation (Ghia et al., 2002). CLL cells localized in the lymph nodes express a higher level of CD38 comparing with the CLL cells circulating in the peripheral blood and CD38 is considered involved in the cell adhesion due to its ligand, the platelet endothelial cell adhesion molecule-1 (PECAM1) (Jaksic et al., 2004, Suricoc et al., 2000). It has been reported that CD40 stimulation promoted the cell adhesion of CLL cells by up-regulating the expression of CD38 (Willimott et al., 2007). So far, the cell adhesion of CLL cells has not been fully understood. Considering its important role in CLL, further studies are needed to address the details of the cell adhesion molecules and characterize their role in the disease progression and drug resistance in CLL.

The results of the functional analysis of the iTRAQ-MS data obtained here in this study showed that CD40 stimulation up-regulated the expression of proteins involved in the biological process of the cell adhesion in primary CLL cells, which provides evidence for the notion that CD40-CD154 ligation between CLL cells and T cells within the microenvironment may regulate the cell adhesion status of CLL cells and enable CLL cells to persist in the tissue microenvironment. The proteomics data not only provides a comprehensive view of the effect of CD40 stimulation in primary CLL cells at the global protein expression level but also indicates that targeting the cell-cell adhesion could be an effective therapeutic strategy in CLL. Although the results of the functional study of the protein DDX3X obtained so far are short of stringency to make it a promising target, this study does broaden the mind in the pro-survival signals induced by CD40 stimulation in CLL cells.

Based on the results obtained in this study, further work would be suggested to carry out on the following points.

Firstly, continuing the functional study of the protein DDX3X in CLL cells would be necessary in order to clarify the role of DDX3X in the survival of CLL cells. It would be crucial to optimize the knockdown experiments and to observe the effect of knocking down DDX3X in HG-3 and MEC1 cells, which would provide clear evidence for the role of DDX3X in CLL cells. Obtaining the DDX3X-knockdown HG-3 and MEC1 cells would pave the way to perform the drug treatments on the CD40 stimulated and unstimulated, DDX3X-knockdown, cells to investigate whether knocking DDX3X affect the CD40 stimulation mediated pro-survival signalling.

As the inhibitor of DDX3X, RK-33, can partially abrogate the cytoprotective effect induced by CD40 stimulation against the fludarabine-induced cell death in CLL cells, it would be interesting to figure out whether RK-33 can abrogate the CD40 stimulation-mediated cytoprotection against the cell death induced by other drugs such as ABT-199 and bendamustine (the drugs used in the investigation of the cytoprotective effect of CD40 stimulation in CLL cells at the beginning of this study). In addition, it would be necessary to confirm the mechanism by which RK-33 inhibits the function of DDX3X. Since DDX3X is a RNA helicase protein, RNA duplex formation and unwinding can be studied following increasing concentration of RK-33 (Bol et al., 2015, Sengoku et al., 2006). Besides, introducing at least one more DDX3X inhibitor to see whether similar observation could be obtained would strengthen the finding with RK-33.

Secondly, it would be meaningful to carry on the proteomics study for the CD40 stimulation in CLL cells. On one hand, the proteomic data obtained in this study did provide tremendous information. It is accountable to dig out more message from the data obtained. Besides DAVID, PANTHER, and Reactome, there have been other bioinformatics analysis tools such as Ingenuity Pathway Analysis (IPA) can be used for the data analysis, which may provide more specific information of the pathways changed by CD40 stimulation in primary CLL cells and may exhibit more potential targets to overcome the pro-survival signals and drug resistance caused by CD40 stimulation. On the other hand, to further validate the findings from the obtained data by increasing the number of the primary CLL cases in the study and using different techniques such as SWATH would give more stringency to the findings generated from the omics data.

Thirdly, it would be interesting to compare the RNA-seq data and the proteomics data. Comparing the effect of CD40 stimulation in primary CLL cells between the mRNA level and protein expression level could help to reveal more information on the effect of CD40 stimulation at both transcriptional and translational levels, which potentially advance the understanding of its role in the pathogenesis and disease progression of CLL.

6.6 Conclusions

In summary, this study shows that CD40 stimulation induces predominantly pro-survival signalling in primary CLL cells, which protects CLL from spontaneous and drug-induced cell death. By using the MS-based techniques, this study has shown that CD40 stimulation not only changes the expression of proteins in primary CLL cells at a global level but also regulates specifically the expression of proteins that are involved in the biological process of cell adhesion. Based on the data provided here, it is reasonable to suggest that CD40 stimulation produces a pro-survival effect by enhancing the cell adhesion properties of CLL cells and that DDX3X is likely one of the molecules involved in mediating the pro-survival effect of CD40 stimulation in CLL cells.

Bibliography

ABEDIN, M., WANG, D., MCDONNELL, M., LEHMANN, U. & KELEKAR, A. 2007. Autophagy delays apoptotic death in breast cancer cells following DNA damage. Cell Death & Differentiation, 14, 500-510.

ACIKARA, Ö. B. 2013. Ion exchange chromatography and its applications. Column chromatography, 10, 55744.

ADMONI-ELISHA, L., NAKDIMON, I., SHTEINFER, A., PREZMA, T., ARIF, T., ARBEL, N., MELKOV, A., ZELICHOV, O., LEVI, I. & SHOSHAN-BARMATZ, V. 2016. Novel biomarker proteins in chronic lymphocytic leukemia: impact on diagnosis, prognosis and treatment. PLoS One, 11, e0148500.

AEBERSOLD, R. & MANN, M. 2003. Mass spectrometry-based proteomics. Nature, 422, 198-207.

AFJEHI-SADAT, L. & GARCIA, B. A. 2013. Comprehending dynamic protein methylation with mass spectrometry. Current opinion in chemical biology, 17, 12-19.

AGATHANGELIDIS, A., DARZENTAS, N., HADZIDIMITRIOU, A., BROCHET, X., MURRAY, F., YAN, X.-J., DAVIS, Z., VAN GASTEL-MOL, E. J., TRESOLDI, C. & CHU, C. C. 2012. Stereotyped B-cell receptors in one-third of chronic lymphocytic leukemia: a molecular classification with implications for targeted therapies. Blood, The Journal of the American Society of Hematology, 119, 4467-4475.

AGNOLETTO, C., BRUNELLI, L., MELLONI, E., PASTORELLI, R., CASCIANO, F., RIMONDI, E., RIGOLIN, G. M., CUNEO, A., SECCHIERO, P. & ZAULI, G. 2015. The anti-leukemic activity of sodium dichloroacetate in p53mutated/null cells is mediated by a p53-independent ILF3/p21 pathway. Oncotarget, 6, 2385.

AGUILERA-MONTILLA, N., BAILÓN, E., UCEDA-CASTRO, R., UGARTE-BERZAL, E., SANTOS, A., GUTIERREZ-GONZALEZ, A., PEREZ-SANCHEZ, C., VAN DEN STEEN, P. E., OPDENAKKER, G. & GARCÍA-MARCO, J. A. 2019. MMP-9 affects gene expression in chronic lymphocytic leukemia revealing CD99 as an MMP-9 target and a novel partner in malignant cell migration/arrest. Oncogene, 38, 4605-4619.

AGUILERA-MONTILLA, N., BAILÓN, E., UGARTE-BERZAL, E., UCEDA-CASTRO, R., PRIETO-SOLANO, M., GARCÍA-MARTÍNEZ, E., SAMANIEGO, R., VAN DEN STEEN, P. E., OPDENAKKER, G. & GARCÍA-MARCO, J. A. 2019. Matrix metalloproteinase-9 induces a pro-angiogenic profile in chronic lymphocytic leukemia cells. Biochemical and biophysical research communications, 520, 198-204.

AHEARNE, M. J., WILLIMOTT, S., PIÑON, L., KENNEDY, D. B., MIALL, F., DYER, M. J. & WAGNER, S. D. 2013. Enhancement of CD 154/IL 4 proliferation by the T follicular helper (T fh) cytokine, IL 21 and increased numbers of circulating cells resembling T fh cells in chronic lymphocytic leukaemia. British journal of haematology, 162, 360-370.

AHN, I. E., FAROOQUI, M. Z., TIAN, X., VALDEZ, J., SUN, C., SOTO, S., LOTTER, J., HOUSEL, S., STETLER-STEVENSON, M. & YUAN, C. M. 2018. Depth and durability of response to ibrutinib in CLL: 5-year follow-up of a phase 2 study. Blood, 131, 2357-2366.

ALLEN, C. E. & PARSONS, D. W. 2015. Biological and clinical significance of somatic mutations in Langerhans cell histiocytosis and related histiocytic neoplastic disorders. Hematology 2014, the American Society of Hematology Education Program Book, 2015, 559-564.

AL-MUDALLAL, S. S., AL-DUBAISI, S. S. & HADI, F. A. 2019. The prognostic significance of XL DLEU/LAMP (13q14 deletion) in CCL patients: a cross section study. Al-Qadisiyah Medical Journal, 15, 67-77.

ALVES, B. N., TSUI, R., ALMADEN, J., SHOKHIREV, M. N., DAVIS-TURAK, J., FUJIMOTO, J., BIRNBAUM, H., PONOMARENKO, J. & HOFFMANN, A. 2014. IκBε is a key regulator of B cell expansion by providing negative feedback on cRel and RelA in a stimulus-specific manner. The Journal of Immunology, 192, 3121-3132.

AMREIN, P. C. 2011. The potential for dasatinib in treating chronic lymphocytic leukemia, acute myeloid leukemia, and myeloproliferative neoplasms. Leukemia & lymphoma, 52, 754-763.

ANDERS, S. & HUBER, W. 2010. Differential expression analysis for sequence count data. Nature Precedings, 1-1.

ANDRITSOS, L., BYRD, J. C., JONES, J. A., HEWES, B., KIPPS, T. J., HSU, F. J. & BURGER, J. A. 2010. Preliminary results from a phase I dose escalation study to determine the maximum tolerated dose of plerixafor in combination with rituximab in patients with relapsed chronic lymphocytic leukemia. American Society of Hematology.

ANDRITSOS, L. A., BYRD, J. C., CHEVERTON, P., WU, J., SIVINA, M., KIPPS, T. J. & BURGER, J. A. 2019. A multicenter phase 1 study of plerixafor and rituximab in patients with chronic lymphocytic leukemia. Leukemia & Lymphoma, 60, 3461-3469.

ARPIN, C., DECHANET, J., VAN KOOTEN, C., MERVILLE, P., GROUARD, G., BRIERE, F., BANCHEREAU, J. & LIU, Y.-J. 1995. Generation of memory B cells and plasma cells in vitro. Science, 268, 720-722.

ARRON, J. R., PEWZNER-JUNG, Y., WALSH, M. C., KOBAYASHI, T. & CHOI, Y. 2002. Regulation of the subcellular localization of tumor necrosis factor receptor–associated factor (TRAF) 2 by TRAF1 reveals mechanisms of TRAF2 signaling. The Journal of experimental medicine, 196, 923-934.

ARRON, J. R., VOLOGODSKAIA, M., WONG, B. R., NARAMURA, M., KIM, N., GU, H. & CHOI, Y. 2001. A positive regulatory role for Cbl family proteins in tumor necrosis factor-related activation-induced cytokine (trance) and CD40L-mediated Akt activation. Journal of Biological Chemistry, 276, 30011-30017.

ARRUGA, F. & DEAGLIO, S. 2017. Mechanisms of resistance to targeted therapies in chronic lymphocytic leukemia. Mechanisms of Drug Resistance in Cancer Therapy. Springer.

AWAD, H., KHAMIS, M. M. & EL-ANEED, A. 2015. Mass spectrometry, review of the basics: ionization. Applied Spectroscopy Reviews, 50, 158-175.

BAE, J., LEO, C. P., HSU, S. Y. & HSUEH, A. J. 2000. MCL-1S, a splicing variant of the antiapoptotic BCL-2 family member MCL-1, encodes a proapoptotic protein possessing only the BH3 domain. Journal of Biological Chemistry, 275, 25255-25261.

BAGNARA, D., KAUFMAN, M. S., CALISSANO, C., MARSILIO, S., PATTEN, P. E., SIMONE, R., CHUM, P., YAN, X.-J., ALLEN, S. L. & KOLITZ, J. E. 2011. A novel adoptive transfer model of chronic lymphocytic leukemia suggests a key role for T lymphocytes in the disease. Blood, The Journal of the American Society of Hematology, 117, 5463-5472.

BALAKRISHNAN, K. & GANDHI, V. 2013. Bcl-2 antagonists: a proof of concept for CLL therapy. Investigational new drugs, 31, 1384-1394.

BANCHEREAU, J., BAZAN, F., BLANCHARD, D., BRIÈ, F., GALIZZI, J. P., VAN KOOTEN, C., LIU, Y., ROUSSET, F. & SAELAND, S. 1994. The CD40 antigen and its ligand. Annual review of immunology, 12, 881-926.

BARNIDGE, D. R., JELINEK, D. F., MUDDIMAN, D. C. & KAY, N. E. 2005. Quantitative protein expression analysis of CLL B cells from mutated and unmutated IgVH subgroups using acid-cleavable isotope-coded affinity tag reagents. Journal of proteome research, 4, 1310-1317.

BARR, P. M., SAYLORS, G. B., SPURGEON, S. E., CHESON, B. D., GREENWALD, D. R., O'BRIEN, S. M., LIEM, A. K., MCLNTYRE, R. E., JOSHI, A. & ABELLA-DOMINICIS, E. 2016. Phase 2 study of idelalisib and entospletinib: pneumonitis limits combination therapy in relapsed refractory CLL and NHL. Blood, The Journal of the American Society of Hematology, 127, 2411-2415.

BARRANGOU, R. 2015. The roles of CRISPR–Cas systems in adaptive immunity and beyond. Current opinion in immunology, 32, 36-41.

BARRETINA, J., JUNCA, J., LLANO, A., GUTIERREZ, A., FLORES, A., BLANCO, J., CLOTET, B. & ESTE, J. 2003. CXCR4 and SDF-1 expression in B-cell chronic lymphocytic leukemia and stage of the disease. Annals of hematology, 82, 500-505.

BARRIO, S., SHANAFELT, T., OJHA, J., CHAFFEE, K., SECRETO, C., KORTÜM, K., PATHANGEY, S., VAN-DYKE, D., SLAGER, S. L. & FONSECA, R. 2017. Genomic characterization of high-count MBL cases indicates that early detection of driver mutations and subclonal expansion are predictors of adverse clinical outcome. Leukemia, 31, 170-176.

BENNETT, F., RAWSTRON, A., PLUMMER, M., TUTE, R. D., MORETON, P., JACK, A. & HILLMEN, P. 2007. B-cell chronic lymphocytic leukaemia cells show specific changes in membrane protein expression during different stages of cell cycle. British journal of haematology, 139, 600-604.

BEST, O. G., CHE, Y., SINGH, N., FORSYTH, C., CHRISTOPHERSON, R. I. & MULLIGAN, S. P. 2012. The Hsp90 inhibitor SNX-7081 synergizes with and restores sensitivity to fludarabine in chronic lymphocytic leukemia cells with lesions in the TP53 pathway: a potential treatment strategy for fludarabine refractory disease. Leukemia & lymphoma, 53, 1367-1375.

BEST, O. G. & MULLIGAN, S. P. 2012. Heat shock protein-90 inhibitor, NVP-AUY922, is effective in combination with fludarabine against chronic lymphocytic leukemia cells cultured on CD40L-stromal layer and inhibits their activated/proliferative phenotype. Leukemia & lymphoma, 53, 2314-2320.

BEST, O. G., SINGH, N., FORSYTH, C. & MULLIGAN, S. P. 2010. The novel Hsp-90 inhibitor SNX7081 is significantly more potent than 17-AAG against primary CLL cells and a range of haematological cell lines, irrespective of lesions in the TP53 pathway. British journal of haematology, 151, 185-188.

BINET, J., AUQUIER, A., DIGHIERO, G., CHASTANG, C., PIGUET, H., GOASGUEN, J., VAUGIER, G., POTRON, G., COLONA, P. & OBERLING, F. 1981. A new prognostic classification of chronic lymphocytic leukemia derived from a multivariate survival analysis. Cancer, 48, 198-206.

BIOSCIENCES, B. D. 2000. Introduction to Flow Cytometry: A learning guide. Manual Part, 1.

BIRMINGHAM, A., ANDERSON, E., SULLIVAN, K., REYNOLDS, A., BOESE, Q., LEAKE, D., KARPILOW, J. & KHVOROVA, A. 2007. A protocol for designing siRNAs with high functionality and specificity. Nature protocols, 2, 2068.

BISHOP, G. A. & HOSTAGER, B. S. 2003. The CD40–CD154 interaction in B cell–T cell liaisons. Cytokine & growth factor reviews, 14, 297-309.

BISHOP, G. A., MOORE, C. R., XIE, P., STUNZ, L. L. & KRAUS, Z. J. 2007. TRAF proteins in CD40 signaling. TNF Receptor Associated Factors (TRAFs). Springer.

BOETTCHER, M. & MCMANUS, M. T. 2015. Choosing the right tool for the job: RNAi, TALEN, or CRISPR. Molecular cell, 58, 575-585.

BOISSARD, F., TOSOLINI, M., LIGAT, L., QUILLET-MARY, A., LOPEZ, F., FOURNIÉ, J.-J., YSEBAERT, L. & POUPOT, M. 2017. Nurse-like cells promote CLL survival through LFA-3/CD2 interactions. Oncotarget, 8, 52225.

BOJARCZUK, K., SASI, B. K., GOBESSI, S., INNOCENTI, I., POZZATO, G., LAURENTI, L. & EFREMOV, D. G. 2016. BCR signaling inhibitors differ in their ability to overcome Mcl-1–mediated resistance of CLL B cells to ABT-199. Blood, The Journal of the American Society of Hematology, 127, 3192-3201.

BOL, G. M., RAMAN, V., VAN DER GROEP, P., VERMEULEN, J. F., PATEL, A. H., VAN DER WALL, E. & VAN DIEST, P. J. 2013. Expression of the RNA helicase DDX3 and the hypoxia response in breast cancer. PloS one, 8, e63548.

BOL, G. M., VESUNA, F., XIE, M., ZENG, J., AZIZ, K., GANDHI, N., LEVINE, A., IRVING, A., KORZ, D. & TANTRAVEDI, S. 2015. Targeting DDX 3 with a small molecule inhibitor for lung cancer therapy. EMBO molecular medicine, 7, 648-669.

BONIF, M., MEUWIS, M.-A., CLOSE, P., BENOIT, V., HEYNINCK, K., CHAPELLE, J.-P., BOURS, V., MERVILLE, M.-P., PIETTE, J. & BEYAERT, R. 2006. TNFα-and IKKβ-mediated TANK/I-TRAF phosphorylation: implications for interaction with NEMO/IKKγ and NF-κB activation. Biochemical Journal, 394, 593-603.

BOSCH, F. & DALLA-FAVERA, R. 2019. Chronic lymphocytic leukaemia: from genetics to treatment. Nature Reviews Clinical Oncology, 16, 684-701.

BOYD, R., ADAM, P., PATEL, S., LOADER, J., BERRY, J., REDPATH, N., POYSER, H., FLETCHER, G., BURGESS, N. & STAMPS, A. 2003. Proteomic analysis of the cell-surface membrane in chronic lymphocytic leukemia: identification of two novel proteins, BCNP1 and MIG2B. Leukemia, 17, 1605-1612.

BRETONES, G., ÁLVAREZ, M. G., ARANGO, J. R., RODRÍGUEZ, D., NADEU, F., PRADO, M. A., VALDÉS-MAS, R., PUENTE, D. A., PAULO, J. A. & DELGADO, J. 2018. Altered patterns of global protein synthesis and translational fidelity in RPS15-mutated chronic lymphocytic leukemia. Blood, The Journal of the American Society of Hematology, 132, 2375-2388.

BROCCO, F., TER BURG, H., FERNANDES, S., TAM, C. S., FORCONI, F., GUERRA, R. M., BIRD, G., WALENSKY, L. D., BROWN, J. R. & KATER, A. P. 2017. Dissecting the role of individual Bcl-2 members in response and resistance to ibrutinib or venetoclax in CLL. Blood, 130, 262-262.

BRUMMELKAMP, T. R., BERNARDS, R. & AGAMI, R. 2002. A system for stable expression of short interfering RNAs in mammalian cells. science, 296, 550-553.

BRUSERUD, Ø., TRONSTAD, K. J., MCCORMACK, E. & GJERTSEN, B. T. 2006. Is targeted chemotherapy an alternative to immunotherapy in chronic lymphocytic leukemia? Cancer Immunology, Immunotherapy, 55, 221-228.

BUGGINS, A. G., PEPPER, C., PATTEN, P. E., HEWAMANA, S., GOHIL, S., MOORHEAD, J., YALLOP, D., THOMAS, N. S. B., MUFTI, G. J. & FEGAN, C. 2010. Interaction with vascular endothelium enhances survival in primary chronic lymphocytic leukemia cells via NF-κB activation and de novo gene transcription. Cancer research, 70, 7523-7533.

BURGER, J. A. 2012. Inhibiting B-cell receptor signaling pathways in chronic lymphocytic leukemia. Current hematologic malignancy reports, 7, 26-33.

BURGER, J. A. 2012. Targeting the microenvironment in chronic lymphocytic leukemia is changing the therapeutic landscape. Current opinion in oncology, 24, 643-649.

BURGER, J. A. 2013. The CLL cell microenvironment. Advances in Chronic Lymphocytic Leukemia. Springer.

BURGER, J. A., BARR, P. M., ROBAK, T., OWEN, C., GHIA, P., TEDESCHI, A., BAIREY, O., HILLMEN, P., COUTRE, S. E. & DEVEREUX, S. 2020. Long-term efficacy and safety of first-line ibrutinib treatment for patients with CLL/SLL: 5 years of follow-up from the phase 3 RESONATE-2 study. Leukemia, 34, 787-798.

BURGER, J. A., BURGER, M. & KIPPS, T. J. 1999. Chronic lymphocytic leukemia B cells express functional CXCR4 chemokine receptors that mediate spontaneous migration beneath bone marrow stromal cells. Blood, The Journal of the American Society of Hematology, 94, 3658-3667.

BURGER, J. A. & BÜRKLE, A. 2007. The CXCR4 chemokine receptor in acute and chronic leukaemia: a marrow homing receptor and potential therapeutic target. British journal of haematology, 137, 288-296.

BURGER, J. A. & GRIBBEN, J. G. The microenvironment in chronic lymphocytic leukemia (CLL) and other B cell malignancies: insight into disease biology and new targeted therapies. Seminars in cancer biology, 2014. Elsevier, 71-81.

BURGER, J. A. & KIPPS, T. J. 2002. Chemokine receptors and stromal cells in the homing and homeostasis of chronic lymphocytic leukemia B cells. Leukemia & lymphoma, 43, 461-466.

BURGER, J. A., LI, K. W., KEATING, M. J., SIVINA, M., AMER, A. M., GARG, N., FERRAJOLI, A., HUANG, X., KANTARJIAN, H. & WIERDA, W. G. 2017. Leukemia cell proliferation and death in chronic lymphocytic leukemia patients on therapy with the BTK inhibitor ibrutinib. JCI insight, 2.

BURGER, J. A., O'BRIEN, S., FOWLER, N., ADVANI, R., SHARMAN, J. P., FURMAN, R. R., IZUMI, R., BUGGY, J., LOURY, D. & HAMDY, A. 2010. The Bruton's tyrosine kinase inhibitor, PCI-32765, is well tolerated and demonstrates promising clinical activity in chronic lymphocytic leukemia (CLL) and small lymphocytic lymphoma (SLL): an update on ongoing phase 1 studies. American Society of Hematology.

BURGER, J. A., QUIROGA, M. P., HARTMANN, E., BÜRKLE, A., WIERDA, W. G., KEATING, M. J. & ROSENWALD, A. 2009. High-level expression of the T-cell chemokines CCL3 and CCL4 by chronic lymphocytic leukemia B cells in nurselike cell cocultures and after BCR stimulation. Blood, The Journal of the American Society of Hematology, 113, 3050-3058.

BURGER, J. A., TEDESCHI, A., BARR, P. M., ROBAK, T., OWEN, C., GHIA, P., BAIREY, O., HILLMEN, P., BARTLETT, N. L. & LI, J. 2015. Ibrutinib as initial therapy for patients with chronic lymphocytic leukemia. New England Journal of Medicine, 373, 2425-2437.

BURGER, J. A., TSUKADA, N., BURGER, M., ZVAIFLER, N. J., DELL'AQUILA, M. & KIPPS, T. J. 2000. Blood-derived nurse-like cells protect chronic lymphocytic leukemia B cells from spontaneous apoptosis through stromal cell–derived factor-1. Blood, The Journal of the American Society of Hematology, 96, 2655-2663.

BURGER, M., HARTMANN, T., KROME, M., RAWLUK, J., TAMAMURA, H., FUJII, N., KIPPS, T. J. & BURGER, J. A. 2005. Small peptide inhibitors of the CXCR4 chemokine receptor (CD184) antagonize the activation, migration, and antiapoptotic responses of CXCL12 in chronic lymphocytic leukemia B cells. Blood, 106, 1824-1830.

BÜRKLE, A., NIEDERMEIER, M., SCHMITT-GRÄFF, A., WIERDA, W. G., KEATING, M. J. & BURGER, J. A. 2007. Overexpression of the CXCR5 chemokine receptor, and its ligand, CXCL13 in B-cell chronic lymphocytic leukemia. Blood, The Journal of the American Society of Hematology, 110, 3316-3325.

CALIGARIS‐CAPPIO, F. 2003. Role of the microenvironment in chronic lymphocytic leukaemia. British journal of haematology, 123, 380-388.

CALIGARIS-CAPPIO, F., GOBBI, M., BOFILL, M. & JANOSSY, G. 1982. Infrequent normal B lymphocytes express features of B-chronic lymphocytic leukemia. The Journal of experimental medicine, 155, 623-628.

CALIN, G. A., DUMITRU, C. D., SHIMIZU, M., BICHI, R., ZUPO, S., NOCH, E., ALDLER, H., RATTAN, S., KEATING, M. & RAI, K. 2002. Frequent deletions and down-regulation of micro-RNA genes miR15 and miR16 at 13q14 in chronic lymphocytic leukemia. Proceedings of the national academy of sciences, 99, 15524-15529.

CALISSANO, C., DAMLE, R. N., MARSILIO, S., YAN, X.-J., YANCOPOULOS, S., HAYES, G., EMSON, C., MURPHY, E. J., HELLERSTEIN, M. K. & SISON, C. 2011. Intraclonal complexity in chronic lymphocytic leukemia: fractions enriched in recently born/divided and older/quiescent cells. Molecular Medicine, 17, 1374-1382.

CAMPO, E., CYMBALISTA, F., GHIA, P., JÄGER, U., POSPISILOVA, S., ROSENQUIST, R., SCHUH, A. & STILGENBAUER, S. 2018. TP53 aberrations in chronic lymphocytic leukemia: an overview of the clinical implications of improved diagnostics. haematologica, 103, 1956-1968.

CARRÀ, G., PANUZZO, C., TORTI, D., PARVIS, G., CRIVELLARO, S., FAMILIARI, U., VOLANTE, M., MORENA, D., LINGUA, M. F. & BRANCACCIO, M. 2017. Therapeutic inhibition of USP7-PTEN network in chronic lymphocytic leukemia: a strategy to overcome TP53 mutated/deleted clones. Oncotarget, 8, 35508.

CARTHEW, R. W. & SONTHEIMER, E. J. 2009. Origins and mechanisms of miRNAs and siRNAs. Cell, 136, 642-655.

CATOVSKY, D., RICHARDS, S., MATUTES, E., OSCIER, D., DYER, M., BEZARES, R., PETTITT, A., HAMBLIN, T., MILLIGAN, D. & CHILD, J. 2007. Assessment of fludarabine plus cyclophosphamide for patients with chronic lymphocytic leukaemia (the LRF CLL4 Trial): a randomised controlled trial. The Lancet, 370, 230-239.

CERHAN, J. R. & SLAGER, S. L. 2015. Familial predisposition and genetic risk factors for lymphoma. Blood, 126, 2265-2273.

CERVANTES-GOMEZ, F., LAMOTHE, B., WOYACH, J. A., WIERDA, W. G., KEATING, M. J., BALAKRISHNAN, K. & GANDHI, V. 2015. Pharmacological and protein profiling suggests venetoclax

(ABT-199) as optimal partner with ibrutinib in chronic lymphocytic leukemia. Clinical cancer research, 21, 3705-3715.

CHAIT, B. T. 2006. Mass spectrometry: bottom-up or top-down? Science, 314, 65-66.

CHALERMSKULRAT, W., MCKINNON, K. P., BRICKEY, W. J., NEURINGER, I. P., PARK, R. C., STERKA, D. G., LONG, B. R., MCNEILLIE, P., NOELLE, R. J. & TING, J. P. 2006. Combined donor specific transfusion and anti-CD154 therapy achieves airway allograft tolerance. Thorax, 61, 61-67.

CHANG, P., CHI, C., CHAU, G., LI, F., TSAI, Y., WU, J. & LEE, Y. W. 2006. DDX3, a DEAD box RNA helicase, is deregulated in hepatitis virus-associated hepatocellular carcinoma and is involved in cell growth control. Oncogene, 25, 1991-2003.

CHAO, C.-H., CHEN, C.-M., CHENG, P.-L., SHIH, J.-W., TSOU, A.-P. & LEE, Y.-H. W. 2006. DDX3, a DEAD box RNA helicase with tumor growth–suppressive property and transcriptional regulation activity of the p21waf1/cip1 promoter, is a candidate tumor suppressor. Cancer research, 66, 6579-6588.

CHAPMAN, E. A., OATES, M., MOHAMMAD, I. S., DAVIES, B. R., STOCKMAN, P. K., ZHUANG, J. & PETTITT, A. R. 2017. Delineating the distinct role of AKT in mediating cell survival and proliferation induced by CD154 and IL-4/IL-21 in chronic lymphocytic leukemia. Oncotarget, 8, 102948.

CHE, Y., BEST, O. G., ZHONG, L., KAUFMAN, K. L., MACTIER, S., RAFTERY, M., GRAVES, L. M., MULLIGAN, S. P. & CHRISTOPHERSON, R. I. 2013. Hsp90 inhibitor SNX-7081 dysregulates proteins involved with DNA repair and replication and the cell cycle in human chronic lymphocytic leukemia (CLL) cells. Journal of Proteome Research, 12, 1710-1722.

CHEN, G., GHARIB, T. G., HUANG, C.-C., TAYLOR, J. M., MISEK, D. E., KARDIA, S. L., GIORDANO, T. J., IANNETTONI, M. D., ORRINGER, M. B. & HANASH, S. M. 2002. Discordant protein and mRNA expression in lung adenocarcinomas. Molecular & cellular proteomics, 1, 304-313.

CHEN, J. 2016. The cell-cycle arrest and apoptotic functions of p53 in tumor initiation and progression. Cold Spring Harbor perspectives in medicine, 6, a026104.

CHEN, T. L., GUPTA, N., LEHMAN, A., RUPPERT, A. S., YU, L., OAKES, C. C., CLAUS, R., PLASS, C., MADDOCKS, K. J. & ANDRITSOS, L. 2016. Hsp90 inhibition increases SOCS3 transcript and regulates migration and cell death in chronic lymphocytic leukemia. Oncotarget, 7, 28684.

CHEN, X., XIONG, L., CHEN, B., LIU, L., LI, R., RAMAGIRI, S., SAHANA, M., PLISE, E., CHEONG, J. & LE, H. Quantitative Analysis of Transporter Protein using TripleTOF® 6600 System.

CHERNUSHEVICH, I. & THOMSON, B. 2003. MS/MS scan methods for a quadrupole/time of flight tandem mass spectrometer. Google Patents.

CHERNUSHEVICH, I. V., LOBODA, A. V. & THOMSON, B. A. 2001. An introduction to quadrupole–time-of-flight mass spectrometry. Journal of mass spectrometry, 36, 849-865.

CHESON, B. D. & LEONI, L. 2011. Bendamustine: Mechanism of action and clinical data. Clinical advances in hematology & oncology: H&O, 9, 1.

CHOE, L., D'ASCENZO, M., RELKIN, N. R., PAPPIN, D., ROSS, P., WILLIAMSON, B., GUERTIN, S., PRIBIL, P. & LEE, K. H. 2007. 8-plex quantitation of changes in cerebrospinal fluid protein expression in subjects undergoing intravenous immunoglobulin treatment for Alzheimer's disease. Proteomics, 7, 3651-3660.

CHOI, M. S., BOISE, L. H., GOTTSCHALK, A. R., QUINTANS, J., THOMPSON, C. B. & KLAUS, G. G. 1995. The role of bcl-xL in CD40-mediated rescue from anti-μ-induced apoptosis in WEHI-231 B lymphoma cells. European journal of immunology, 25, 1352-1357.

CHU, P., DEFORCE, D., PEDERSEN, I. M., KIM, Y., KITADA, S., REED, J. C. & KIPPS, T. J. 2002. Latent sensitivity to Fas-mediated apoptosis after CD40 ligation may explain activity of CD154 gene therapy in chronic lymphocytic leukemia. Proceedings of the National Academy of Sciences, 99, 3854-3859.

CLARK, E. A. & LEDBETTER, J. A. 1994. How B and T cells talk to each other. Nature, 367, 425-428.

COCHRAN, D. A., EVANS, C. A., BLINCO, D., BURTHEM, J., STEVENSON, F. K., GASKELL, S. J. & WHETTON, A. D. 2003. Proteomic analysis of chronic lymphocytic leukemia subtypes with mutated or unmutated Ig VH genes. Molecular & Cellular Proteomics, 2, 1331-1341.

CONESA, A., MADRIGAL, P., TARAZONA, S., GOMEZ-CABRERO, D., CERVERA, A., MCPHERSON, A., SZCZEŚNIAK, M. W., GAFFNEY, D. J., ELO, L. L. & ZHANG, X. 2016. A survey of best practices for RNA-seq data analysis. Genome biology, 17, 13.

CONTRI, A., BRUNATI, A. M., TRENTIN, L., CABRELLE, A., MIORIN, M., CESARO, L., PINNA, L. A., ZAMBELLO, R., SEMENZATO, G. & DONELLA-DEANA, A. 2005. Chronic lymphocytic leukemia B cells contain anomalous Lyn tyrosine kinase, a putative contribution to defective apoptosis. The Journal of clinical investigation, 115, 369-378.

COTTER, R. J. 1999. Peer Reviewed: The New Time-of-Flight Mass Spectrometry. Analytical chemistry, 71, 445A-451A.

CRASSINI, K., MULLIGAN, S. P. & BEST, O. G. 2015. Targeting chronic lymphocytic leukemia cells in the tumor microenviroment: A review of the in vitro and clinical trials to date. World Journal of Clinical Cases: WJCC, 3, 694.

CRASSINI, K., SHEN, Y., MULLIGAN, S. & GILES BEST, O. 2017. Modeling the chronic lymphocytic leukemia microenvironment in vitro. Leukemia & lymphoma, 58, 266-279.

CROMPOT, E., VAN DAMME, M., PIETERS, K., VERMEERSCH, M., PEREZ-MORGA, D., MINEUR, P., MAEREVOET, M., MEULEMAN, N., BRON, D. & LAGNEAUX, L. 2017. Extracellular vesicles of bone marrow stromal cells rescue chronic lymphocytic leukemia B cells from apoptosis, enhance their migration and induce gene expression modifications. Haematologica, 102, 1594-1604.

CUMMINS, P. M., ROCHFORT, K. D. & O'CONNOR, B. F. 2017. Ion-exchange chromatography: basic principles and application. Protein Chromatography. Springer.

DAC, B. 2000. Introduction to Flow Cytometry: A Learning Guide, Manual Part Number: 11-11032-01. BD Biosciences.

DAMESHEK, W. 1967. Chronic lymphocytic leukemia—an accumulative disease of immunologically incompetent lymphocytes. Blood, 29, 566-584.

DAMIANO, J. S., CRESS, A. E., HAZLEHURST, L. A., SHTIL, A. A. & DALTON, W. S. 1999. Cell adhesion mediated drug resistance (CAM-DR): role of integrins and resistance to apoptosis in human myeloma cell lines. Blood, The Journal of the American Society of Hematology, 93, 1658-1667.

DAMLE, R. N., WASIL, T., FAIS, F., GHIOTTO, F., VALETTO, A., ALLEN, S. L., BUCHBINDER, A., BUDMAN, D., DITTMAR, K. & KOLITZ, J. 1999. Ig V Gene Mutation Status and CD38 Expression As Novel Prognostic Indicators in Chronic Lymphocytic Leukemia: Presented in part at the 40th Annual

Meeting of The American Society of Hematology, held in Miami Beach, FL, December 4-8, 1998. Blood, The Journal of the American Society of Hematology, 94, 1840-1847.

DAMM, F., MYLONAS, E., COSSON, A., YOSHIDA, K., DELLA VALLE, V., MOULY, E., SCOURZIC, L., SHIRAISHI, Y., CHIBA, K. & TANAKA, H. 2014. Acquired initiating mutations in early hematopoietic cells of CLL patients. Cancer discovery, 4, 1088-1101.

DAVIES, C. C., MAK, T. W., YOUNG, L. S. & ELIOPOULOS, A. G. 2005. TRAF6 is required for TRAF2-dependent CD40 signal transduction in nonhemopoietic cells. Molecular and cellular biology, 25, 9806-9819.

DAVIES, C. C., MASON, J., WAKELAM, M. J., YOUNG, L. S. & ELIOPOULOS, A. G. 2004. Inhibition of phosphatidylinositol 3-kinase-and ERK MAPK-regulated protein synthesis reveals the pro-apoptotic properties of CD40 ligation in carcinoma cells. Journal of Biological Chemistry, 279, 1010-1019.

DE ROOIJ, M. F., KUIL, A., GEEST, C. R., ELDERING, E., CHANG, B. Y., BUGGY, J. J., PALS, S. T. & SPAARGAREN, M. 2012. The clinically active BTK inhibitor PCI-32765 targets B-cell receptor–and chemokine-controlled adhesion and migration in chronic lymphocytic leukemia. Blood, The Journal of the American Society of Hematology, 119, 2590-2594.

DE SOUSA ABREU, R., PENALVA, L. O., MARCOTTE, E. M. & VOGEL, C. 2009. Global signatures of protein and mRNA expression levels. Molecular BioSystems, 5, 1512-1526.

DE TOTERO, D., TAZZARI, P. L., CAPAIA, M., MONTERA, M. P., CLAVIO, M., BALLEARI, E., FOA, R. & GOBBI, M. 2003. CD40 triggering enhances fludarabine-induced apoptosis of chronic lymphocytic leukemia B-cells through autocrine release of tumor necrosis factor-alpha and interferon-gama and tumor necrosis factor receptor-I-II upregulation. Haematologica, 88, 148-158.

DEL GIUDICE, I., ROSSI, D., CHIARETTI, S., MARINELLI, M., TAVOLARO, S., GABRIELLI, S., LAURENTI, L., MARASCA, R., RASI, S. & FANGAZIO, M. 2012. NOTCH1 mutations in+ 12 chronic lymphocytic leukemia (CLL) confer an unfavorable prognosis, induce a distinctive transcriptional profiling and refine the intermediate prognosis of+ 12 CLL. haematologica, 97, 437-441.

DELGADO, J., NADEU, F., COLOMER, D. & CAMPO, E. 2020. Chronic lymphocytic leukemia: from molecular pathogenesis to novel therapeutic strategies. haematologica, 105.

DÖHNER, H., STILGENBAUER, S., BENNER, A., LEUPOLT, E., KRÖBER, A., BULLINGER, L., DÖHNER, K., BENTZ, M. & LICHTER, P. 2000. Genomic aberrations and survival in chronic lymphocytic leukemia. New England Journal of Medicine, 343, 1910-1916.

DÖHNER, H., STILGENBAUER, S., JAMES, M. R., BENNER, A., WEILGUNI, T., BENTZ, M., FISCHER, K., HUNSTEIN, W. & LICHTER, P. 1997. 11q deletions identify a new subset of B-cell chronic lymphocytic leukemia characterized by extensive nodal involvement and inferior prognosis. Blood, The Journal of the American Society of Hematology, 89, 2516-2522.

DÜHREN-VON MINDEN, M., ÜBELHART, R., SCHNEIDER, D., WOSSNING, T., BACH, M. P., BUCHNER, M., HOFMANN, D., SUROVA, E., FOLLO, M. & KÖHLER, F. 2012. Chronic lymphocytic leukaemia is driven by antigen-independent cell-autonomous signalling. Nature, 489, 309-312.

DÜRIG, J., SCHMÜCKER, U. & DÜHRSEN, U. 2001. Differential expression of chemokine receptors in B cell malignancies. Leukemia, 15, 752-756.

EAGLE, G. L., ZHUANG, J., JENKINS, R. E., TILL, K. J., JITHESH, P. V., LIN, K., JOHNSON, G. G., OATES, M., PARK, K. & KITTERINGHAM, N. R. 2015. Total proteome analysis identifies migration defects as a

major pathogenetic factor in immunoglobulin heavy chain variable region (IGHV)-unmutated chronic lymphocytic leukemia. Molecular & Cellular Proteomics, 14, 933-945.

EICHHORST, B., ROBAK, T., MONTSERRAT, E., GHIA, P., HILLMEN, P., HALLEK, M. & BUSKE, C. 2015. Chronic lymphocytic leukaemia: ESMO Clinical Practice Guidelines for diagnosis, treatment and follow-up. Annals of Oncology, 26, v78-v84.

EICHHORST, B. F., BUSCH, R., HOPFINGER, G., PASOLD, R., HENSEL, M., STEINBRECHER, C., SIEHL, S., JÄGER, U., BERGMANN, M. & STILGENBAUER, S. 2006. Fludarabine plus cyclophosphamide versus fludarabine alone in first-line therapy of younger patients with chronic lymphocytic leukemia. Blood, 107, 885-891.

EISTERER, W., BECHTER, O., SÖDERBERG, O., NILSSON, K., TEROL, M., GREIL, R., THALER, J., HEROLD, M., FINKE, L. & GÜNTHERT, U. 2004. Elevated levels of soluble CD44 are associated with advanced disease and in vitro proliferation of neoplastic lymphocytes in B-cell chronic lymphocytic leukaemia. Leukemia research, 28, 1043-1051.

ELGUETA, R., BENSON, M. J., DE VRIES, V. C., WASIUK, A., GUO, Y. & NOELLE, R. J. 2009. Molecular mechanism and function of CD40/CD40L engagement in the immune system. Immunological reviews, 229, 152-172.

ELGUOSHY, A., HIRAO, Y., XU, B., SAITO, S., QUADERY, A. F., YAMAMOTO, K., MITSUI, T., YAMAMOTO, T. & JPROS, C. X. P. T. O. 2017. Identification and validation of human missing proteins and peptides in public proteome databases: Data mining strategy. Journal of Proteome Research, 16, 4403-4414.

ENGVALL, E., JONSSON, K. & PERLMANN, P. 1971. Enzyme-linked immunosorbent assay. II. Quantitative assay of protein antigen, immunoglobulin G, by means of enzyme-labelled antigen and antibody-coated tubes. Biochimica et Biophysica Acta (BBA)-Protein Structure, 251, 427-434.

ERMINI, L., OLIVIERI, C., RIZZI, E., CORTI, G., BONNAL, R., SOARES, P., LUCIANI, S., MAROTA, I., DE BELLIS, G. & RICHARDS, M. B. 2008. Complete mitochondrial genome sequence of the Tyrolean Iceman. Current Biology, 18, 1687-1693.

FABBRI, G. & DALLA-FAVERA, R. 2016. The molecular pathogenesis of chronic lymphocytic leukaemia. Nature Reviews Cancer, 16, 145-162.

FABBRI, G., RASI, S., ROSSI, D., TRIFONOV, V., KHIABANIAN, H., MA, J., GRUNN, A., FANGAZIO, M., CAPELLO, D. & MONTI, S. 2011. Analysis of the chronic lymphocytic leukemia coding genome: role of NOTCH1 mutational activation. Journal of Experimental Medicine, 208, 1389-1401.

FALKMER, U. G. 1992. Methodologic sources of errors in image and flow cytometric DNA assessments of the malignancy potential of prostatic carcinoma. Human pathology, 23, 360-367.

FARAHANI, E., PATRA, H. K., JANGAMREDDY, J. R., RASHEDI, I., KAWALEC, M., RAO PARITI, R. K., BATAKIS, P. & WIECHEC, E. 2014. Cell adhesion molecules and their relation to (cancer) cell stemness. Carcinogenesis, 35, 747-759.

FEDORCHENKO, O., STIEFELHAGEN, M., PEER-ZADA, A. A., BARTHEL, R., MAYER, P., ECKEI, L., BREUER, A., CRISPATZU, G., ROSEN, N. & LANDWEHR, T. 2013. CD44 regulates the apoptotic response and promotes disease development in chronic lymphocytic leukemia. Blood, The Journal of the American Society of Hematology, 121, 4126-4136.

FERRER, G., BOSCH, R., HODGSON, K., TEJERO, R., ROUÉ, G., COLOMER, D., MONTSERRAT, E. & MORENO, C. 2014. B cell activation through CD 40 and IL 4R ligation modulates the response of chronic lymphocytic leukaemia cells to BAFF and APRIL. British journal of haematology, 164, 570-578.

FLOOR, S., VAN STAVEREN, W., LARSIMONT, D., DUMONT, J. E. & MAENHAUT, C. 2011. Cancer cells in epithelial-to-mesenchymal transition and tumor-propagating–cancer stem cells: distinct, overlapping or same populations. Oncogene, 30, 4609-4621.

FOY, T. M., LAMAN, J. D., LEDBETTER, J. A., ARUFFO, A., CLAASSEN, E. & NOELLE, R. J. 1994. gp39-CD40 interactions are essential for germinal center formation and the development of B cell memory. Journal of Experimental Medicine, 180, 157-163.

FREZZATO, F., RAGGI, F., MARTINI, V., SEVERIN, F., TRIMARCO, V., VISENTIN, A., SCOMAZZON, E., ACCORDI, B., BRESOLIN, S. & PIAZZA, F. 2019. HSP70/HSF1 axis, regulated via a PI3K/AKT pathway, is a druggable target in chronic lymphocytic leukemia. International journal of cancer, 145, 3089-3100.

FRIEDMAN, D. R., GUADALUPE, E., VOLKHEIMER, A., MOORE, J. O. & WEINBERG, J. B. 2018. Clinical outcomes in chronic lymphocytic leukaemia associated with expression of CD5, a negative regulator of B‐cell receptor signalling. British journal of haematology, 183, 747-754.

FU, J., LIU, Y. & ZHANG, X. 2002. CD40 ligandization promotes IL-6 and Flt3 ligand production of bone marrow stromal cells. Zhonghua xue ye xue za zhi= Zhonghua Xueyexue Zazhi, 23, 585-587.

FURMAN, R. R., ASGARY, Z., MASCARENHAS, J. O., LIOU, H.-C. & SCHATTNER, E. J. 2000. Modulation of NF-κB activity and apoptosis in chronic lymphocytic leukemia B cells. The Journal of Immunology, 164, 2200-2206.

FURMAN, R. R., BYRD, J. C., BROWN, J. R., COUTRE, S. E., BENSON JR, D. M., WAGNER-JOHNSTON, N. D., FLINN, I. W., KAHL, B. S., SPURGEON, S. E. & LANNUTTI, B. 2010. CAL-101, an isoform-selective inhibitor of phosphatidylinositol 3-kinase P110δ, demonstrates clinical activity and pharmacodynamic effects in patients with relapsed or refractory chronic lymphocytic leukemia. American Society of Hematology.

GAIDANO, G., BALLERINI, P., GONG, J. Z., INGHIRAMI, G., NERI, A., NEWCOMB, E. W., MAGRATH, I. T., KNOWLES, D. M. & DALLA-FAVERA, R. 1991. p53 mutations in human lymphoid malignancies: association with Burkitt lymphoma and chronic lymphocytic leukemia. Proceedings of the National Academy of Sciences, 88, 5413-5417.

GANDHI, V. & BURGER, J. A. 2009. Bendamustine in B-cell malignancies: the new 46-year-old kid on the block. Clinical cancer research, 15, 7456-7461.

GANNETT, L. 2008. The human genome project.

GARDAM, S., SIERRO, F., BASTEN, A., MACKAY, F. & BRINK, R. 2008. TRAF2 and TRAF3 signal adapters act cooperatively to control the maturation and survival signals delivered to B cells by the BAFF receptor. Immunity, 28, 391-401.

GASPARINI, C., CELEGHINI, C., MONASTA, L. & ZAULI, G. 2014. NF-κB pathways in hematological malignancies. Cellular and molecular life sciences, 71, 2083-2102.

GHIA, P., PLUTA, A., WACH, M., LYSAK, D., KOZAK, T., SIMKOVIC, M., KAPLAN, P., KRAYCHOK, I., ILLES, A. & DE LA SERNA, J. 2020. ASCEND: Phase III, Randomized Trial of Acalabrutinib Versus Idelalisib

Plus Rituximab or Bendamustine Plus Rituximab in Relapsed or Refractory Chronic Lymphocytic Leukemia. Journal of Clinical Oncology, JCO. 19.03355.

GHIA, P., STROLA, G., GRANZIERO, L., GEUNA, M., GUIDA, G., SALLUSTO, F., RUFFING, N., MONTAGNA, L., PICCOLI, P. & CHILOSI, M. 2002. Chronic lymphocytic leukemia B cells are endowed with the capacity to attract CD4+, CD40L+ T cells by producing CCL22. European journal of immunology, 32, 1403-1413.

GILAR, M., OLIVOVA, P., DALY, A. E. & GEBLER, J. C. 2005. Two-dimensional separation of peptides using RP-RP-HPLC system with different pH in first and second separation dimensions. Journal of separation science, 28, 1694-1703.

GIRBL, T., HINTERSEER, E., GRÖSSINGER, E. M., ASSLABER, D., OBERASCHER, K., WEISS, L., HAUSER-KRONBERGER, C., NEUREITER, D., KERSCHBAUM, H. & NAOR, D. 2013. CD40-mediated activation of chronic lymphocytic leukemia cells promotes their CD44-dependent adhesion to hyaluronan and restricts CCL21-induced motility. Cancer research, 73, 561-570.

GIVAN, A. L. 2001. Principles of flow cytometry: an overview. Methods in cell biology, 63, 19-50.

GIVAN, A. L. 2011. Flow cytometry: an introduction. Flow cytometry protocols. Springer.

GOETZ, M., TOFT, D., AMES, M. & ERLICHMAN, C. 2003. The Hsp90 chaperone complex as a novel target for cancer therapy. Annals of oncology, 14, 1169-1176.

GOODWIN, R. J. 2012. Sample preparation for mass spectrometry imaging: small mistakes can lead to big consequences. Journal of proteomics, 75, 4893-4911.

GOODWIN, R. J. 2012. Sample preparation for mass spectrometry imaging: small mistakes can lead to big consequences. Journal of proteomics, 75, 4893-4911.

GORR, T. A. & VOGEL, J. 2015. Western blotting revisited: critical perusal of underappreciated technical issues. PROTEOMICS–Clinical Applications, 9, 396-405.

GRANZIERO, L., GHIA, P., CIRCOSTA, P., GOTTARDI, D., STROLA, G., GEUNA, M., MONTAGNA, L., PICCOLI, P., CHILOSI, M. & CALIGARIS-CAPPIO, F. 2001. Survivin is expressed on CD40 stimulation and interfaces proliferation and apoptosis in B-cell chronic lymphocytic leukemia. Blood, The Journal of the American Society of Hematology, 97, 2777-2783.

GRDISA, M. 2003. Influence of CD40 ligation on survival and apoptosis of B-CLL cells in vitro. Leukemia research, 27, 951-956.

GREINER, A., KNÖRR, C., QIN, Y., SEBALD, W., SCHIMPL, A., BANCHEREAU, J. & MÜLLER-HERMELINK, H. 1997. Low-grade B cell lymphomas of mucosa-associated lymphoid tissue (MALT-type) require CD40-mediated signaling and Th2-type cytokines for in vitro growth and differentiation. The American journal of pathology, 150, 1583.

GRIFFITHS, J. A., SCIALDONE, A. & MARIONI, J. C. 2018. Using single-cell genomics to understand developmental processes and cell fate decisions. Molecular systems biology, 14, e8046.

GRIGGIO, V., MANDILI, G., VITALE, C., CAPELLO, M., MACOR, P., SERRA, S., CASTELLA, B., PEOLA, S., FOGLIETTA, M. & DRANDI, D. 2017. Humoral immune responses toward tumor-derived antigens in previously untreated patients with chronic lymphocytic leukemia. Oncotarget, 8, 3274.

GRIGGIO, V., VITALE, C., TODARO, M., RIGANTI, C., KOPECKA, J., SALVETTI, C., BOMBEN, R., DAL BO, M., MAGLIULO, D. & ROSSI, D. 2020. HIF-1α is over-expressed in leukemic cells from TP53-disrupted patients and is a promising therapeutic target in chronic lymphocytic leukemia. haematologica, 105, 1042-1054.

GROSS, J. H. 2006. Mass spectrometry: a textbook, Springer Science & Business Media.

GUIDUCCI, C., VALZASINA, B., DISLICH, H. & COLOMBO, M. P. 2005. CD40/CD40L interaction regulates CD4+ CD25+ T reg homeostasis through dendritic cell-produced IL-2. European journal of immunology, 35, 557-567.

GUO, A., LU, P., LEE, J., ZHEN, C., CHIOSIS, G. & WANG, Y. 2017. HSP90 stabilizes B-cell receptor kinases in a multi-client interactome: PU-H71 induces CLL apoptosis in a cytoprotective microenvironment. Oncogene, 36, 3441-3449.

GUPTA, S., MANUBHAI, K., KULKARNI, V. & SRIVASTAVA, S. 2016. An overview of innovations and industrial solutions in Protein Microarray Technology. Proteomics, 16, 1297-1308.

GUPTA, S. K., VISWANATHA, D. & PATEL, K. P. 2020. Evaluation of Somatic Hypermutation Status in Chronic Lymphocytic Leukemia in the Era of Next Generation Sequencing. Frontiers in Cell and Developmental Biology, 8, 357.

GURUPRASAD, K., REDDY, B. B. & PANDIT, M. W. 1990. Correlation between stability of a protein and its dipeptide composition: a novel approach for predicting in vivo stability of a protein from its primary sequence. Protein Engineering, Design and Selection, 4, 155-161.

GUTJAHR, J. C., SZENES, E., TSCHECH, L., ASSLABER, D., SCHLEDERER, M., ROOS, S., YU, X., GIRBL, T., STERNBERG, C. & EGLE, A. 2018. Microenvironment-induced CD44v6 promotes early disease progression in chronic lymphocytic leukemia. Blood, The Journal of the American Society of Hematology, 131, 1337-1349.

HAGEMANN, C., MEYER, C., STOJIC, J., EICKER, S., GERNGRAS, S., KÜHNEL, S., ROOSEN, K. & VINCE, G. H. 2006. High efficiency transfection of glioma cell lines and primary cells for overexpression and RNAi experiments. Journal of neuroscience methods, 156, 194-202.

HALLAERT, D. Y., JASPERS, A., VAN NOESEL, C. J., VAN OERS, M. H., KATER, A. P. & ELDERING, E. 2008. c-Abl kinase inhibitors overcome CD40-mediated drug resistance in CLL: implications for therapeutic targeting of chemoresistant niches. Blood, The Journal of the American Society of Hematology, 112, 5141-5149.

HALLEK, M. 2019. Chronic lymphocytic leukemia: 2020 update on diagnosis, risk stratification and treatment. American journal of hematology, 94, 1266-1287.

HALLEK, M., FISCHER, K., FINGERLE-ROWSON, G., FINK, A. M., BUSCH, R., MAYER, J., HENSEL, M., HOPFINGER, G., HESS, G. & VON GRÜNHAGEN, U. 2010. Addition of rituximab to fludarabine and cyclophosphamide in patients with chronic lymphocytic leukaemia: a randomised, open-label, phase 3 trial. The Lancet, 376, 1164-1174.

HALLEK, M., SHANAFELT, T. D. & EICHHORST, B. 2018. Chronic lymphocytic leukaemia. The Lancet, 391, 1524-1537.

HAMBLIN, T. J., DAVIS, Z., GARDINER, A., OSCIER, D. G. & STEVENSON, F. K. 1999. Unmutated Ig VH genes are associated with a more aggressive form of chronic lymphocytic leukemia. Blood, The Journal of the American Society of Hematology, 94, 1848-1854.

HAMES, B. D. 1998. Gel electrophoresis of proteins: a practical approach, OUP Oxford.

HAMILTON, E., PEARCE, L., MORGAN, L., ROBINSON, S., WARE, V., BRENNAN, P., THOMAS, N. S. B., YALLOP, D., DEVEREUX, S. & FEGAN, C. 2012. Mimicking the tumour microenvironment: three different co-culture systems induce a similar phenotype but distinct proliferative signals in primary chronic lymphocytic leukaemia cells. British journal of haematology, 158, 589-599.

HAN, T., EZDINLI, E. Z., SHIMAOKA, K. & DESAI, D. V. 1973. Chlorambucil vs. combined chlorambucil-corticosteroid therapy in chronic lymphocytic leukemia. Cancer, 31, 502-508.

HAN, T.-T., FAN, L., LI, J.-Y. & XU, W. 2014. Role of chemokines and their receptors in chronic lymphocytic leukemia: function in microenvironment and targeted therapy. Cancer biology & therapy, 15, 3-9.

HAN, X. 2010. Multi-dimensional mass spectrometry-based shotgun lipidomics and the altered lipids at the mild cognitive impairment stage of Alzheimer's disease. Biochimica et Biophysica Acta (BBA)-Molecular and Cell Biology of Lipids, 1801, 774-783.

HANAHAN, D. & WEINBERG, R. A. 2011. Hallmarks of cancer: the next generation. cell, 144, 646-674.

HAUER, J., PÜSCHNER, S., RAMAKRISHNAN, P., SIMON, U., BONGERS, M., FEDERLE, C. & ENGELMANN, H. 2005. TNF receptor (TNFR)-associated factor (TRAF) 3 serves as an inhibitor of TRAF2/5-mediated activation of the noncanonical NF-κB pathway by TRAF-binding TNFRs. Proceedings of the National Academy of Sciences, 102, 2874-2879.

HAYDEN, R. E., PRATT, G., DAVIES, N., KHANIM, F., BIRTWISTLE, J., DELGADO, J., PEARCE, C., SANT, T., DRAYSON, M. & BUNCE, C. 2009. Treatment of primary CLL cells with bezafibrate and medroxyprogesterone acetate induces apoptosis and represses the pro-proliferative signal of CD40-ligand, in part through increased 15dΔ 12, 14, PGJ 2. Leukemia, 23, 292-304.

HE, J. Q., OGANESYAN, G., SAHA, S. K., ZARNEGAR, B. & CHENG, G. 2007. TRAF3 and its biological function. TNF Receptor Associated Factors (TRAFs). Springer.

HERISHANU, Y., PÉREZ-GALÁN, P., LIU, D., BIANCOTTO, A., PITTALUGA, S., VIRE, B., GIBELLINI, F., NJUGUNA, N., LEE, E. & STENNETT, L. 2011. The lymph node microenvironment promotes B-cell receptor signaling, NF-κB activation, and tumor proliferation in chronic lymphocytic leukemia. Blood, The Journal of the American Society of Hematology, 117, 563-574.

HERMAN, S. E., GORDON, A. L., HERTLEIN, E., RAMANUNNI, A., ZHANG, X., JAGLOWSKI, S., FLYNN, J., JONES, J., BLUM, K. A. & BUGGY, J. J. 2011. Bruton tyrosine kinase represents a promising therapeutic target for treatment of chronic lymphocytic leukemia and is effectively targeted by PCI-32765. Blood, 117, 6287-6296.

HERMAN, S. E., MUSTAFA, R. Z., JONES, J., WONG, D. H., FAROOQUI, M. & WIESTNER, A. 2015. Treatment with Ibrutinib Inhibits BTK-and VLA-4–Dependent Adhesion of Chronic Lymphocytic Leukemia Cells In Vivo. Clinical Cancer Research, 21, 4642-4651.

HERNDON, T. M., CHEN, S.-S., SABA, N. S., VALDEZ, J., EMSON, C., GATMAITAN, M., TIAN, X., HUGHES, T. E., SUN, C. & ARTHUR, D. C. 2017. Direct in vivo evidence for increased proliferation of CLL cells in lymph nodes compared to bone marrow and peripheral blood. Leukemia, 31, 1340-1347.

HERTLEIN, E., WAGNER, A. J., JONES, J., LIN, T. S., MADDOCKS, K. J., TOWNS III, W. H., GOETTL, V. M., ZHANG, X., JARJOURA, D. & RAYMOND, C. A. 2010. 17-DMAG targets the nuclear factor-κB family of proteins to induce apoptosis in chronic lymphocytic leukemia: clinical implications of HSP90 inhibition. Blood, The Journal of the American Society of Hematology, 116, 45-53.

HJALMAR, V., HAST, R. & KIMBY, E. 2002. Cell surface expression of CD25, CD54, and CD95 on B‐and T‐cells in chronic lymphocytic leukaemia in relation to trisomy 12, atypical morphology and clinical course. European journal of haematology, 68, 127-134.

HONEY, K., COBBOLD, S. P. & WALDMANN, H. 1999. CD40 ligand blockade induces CD4+ T cell tolerance and linked suppression. The Journal of Immunology, 163, 4805-4810.

HOPFGARTNER, G., VARESIO, E., TSCHÄPPÄT, V., GRIVET, C., BOURGOGNE, E. & LEUTHOLD, L. A. 2004. Triple quadrupole linear ion trap mass spectrometer for the analysis of small molecules and macromolecules. Journal of Mass Spectrometry, 39, 845-855.

HOSTAGER, B. S., HAXHINASTO, S. A., ROWLAND, S. L. & BISHOP, G. A. 2003. Tumor necrosis factor receptor-associated factor 2 (TRAF2)-deficient B lymphocytes reveal novel roles for TRAF2 in CD40 signaling. Journal of Biological Chemistry, 278, 45382-45390.

HSU, P. D., LANDER, E. S. & ZHANG, F. 2014. Development and applications of CRISPR-Cas9 for genome engineering. Cell, 157, 1262-1278.

HUANG, J.-S., CHAO, C.-C., SU, T.-L., YEH, S.-H., CHEN, D.-S., CHEN, C.-T., CHEN, P.-J. & JOU, Y.-S. 2004. Diverse cellular transformation capability of overexpressed genes in human hepatocellular carcinoma. Biochemical and biophysical research communications, 315, 950-958.

HUENG, D.-Y., TSAI, W.-C., CHIOU, H.-Y. C., FENG, S.-W., LIN, C., LI, Y.-F., HUANG, L.-C. & LIN, M.-H. 2015. DDX3X biomarker correlates with poor survival in human gliomas. International journal of molecular sciences, 16, 15578-15591.

HUNTER, C. & SEYMOUR, S. 2015. Improved data quality using variable Q1 window widths in SWATH™ acquisition-Data independent acquisition on the TripleTOF® 6600 and 5600+ systems. AB SCIEX Technical Note, 10090114-01.

HUSBY, S. & GRØNBÆK, K. 2017. Mature lymphoid malignancies: origin, stem cells, and chronicity. Blood advances, 1, 2444-2455.

HÜTTMANN, A., KLEIN-HITPASS, L., THOMALE, J., DEENEN, R., CARPINTEIRO, A., NÜCKEL, H., EBELING, P., FÜHRER, A., EDELMANN, J. & SELLMANN, L. 2006. Gene expression signatures separate B-cell chronic lymphocytic leukaemia prognostic subgroups defined by ZAP-70 and CD38 expression status. Leukemia, 20, 1774-1782.

IEZZI, G., SONDEREGGER, I., AMPENBERGER, F., SCHMITZ, N., MARSLAND, B. J. & KOPF, M. 2009. CD40–CD40L cross-talk integrates strong antigenic signals and microbial stimuli to induce development of IL-17-producing CD4+ T cells. Proceedings of the National Academy of Sciences, 106, 876-881.

INDOVINA, P., MARCELLI, E., PENTIMALLI, F., TANGANELLI, P., TARRO, G. & GIORDANO, A. 2013. Mass spectrometry-based proteomics: The road to lung cancer biomarker discovery. Mass spectrometry reviews, 32, 129-142.

ITCHAKI, G. & BROWN, J. R. 2016. The potential of venetoclax (ABT-199) in chronic lymphocytic leukemia. Therapeutic advances in hematology, 7, 270-287.

JACOB, A., POUND, J. D., CHALLA, A. & GORDON, J. 1998. Release of clonal block in B cell chronic lymphocytic leukaemia by engagement of co-operative epitopes on CD40. Leukemia research, 22, 379-382.

JAGLA, B., AULNER, N., KELLY, P. D., SONG, D., VOLCHUK, A., ZATORSKI, A., SHUM, D., MAYER, T., DE ANGELIS, D. A. & OUERFELLI, O. 2005. Sequence characteristics of functional siRNAs. Rna, 11, 864-872.

JAGLOWSKI, S. M., JONES, J. A., NAGAR, V., FLYNN, J. M., ANDRITSOS, L. A., MADDOCKS, K. J., WOYACH, J. A., BLUM, K. A., GREVER, M. R. & SMUCKER, K. 2015. Safety and activity of BTK inhibitor ibrutinib combined with ofatumumab in chronic lymphocytic leukemia: a phase 1b/2 study. Blood, The Journal of the American Society of Hematology, 126, 842-850.

JAKSIC, O., KARDUM PARO, M. M., KARDUM SKELIN, I., KUSEC, R., PEJSA, V. & JAKSIC, B. 2004. CD38 on B-cell chronic lymphocytic leukemia cells has higher expression in lymph nodes than in peripheral blood or bone marrow. Blood, 103, 1968-1969.

JARVINEN, L. Z., BLAZAR, B. R., ADEYI, O. A., STROM, T. B. & NOELLE, R. J. 2003. CD154 on the surface of CD4+ CD25+ regulatory T cells contributes to skin transplant tolerance. Transplantation, 76, 1375-1379.

JAYAPPA, K. D., PORTELL, C. A., GORDON, V. L., CAPALDO, B. J., BEKIRANOV, S., AXELROD, M. J., BRETT, L. K., WULFKUHLE, J. D., GALLAGHER, R. I. & PETRICOIN, E. F. 2017. Microenvironmental agonists generate de novo phenotypic resistance to combined ibrutinib plus venetoclax in CLL and MCL. Blood advances, 1, 933-946.

JENKINS, S. J., PERONA-WRIGHT, G. & MACDONALD, A. S. 2008. Full development of Th2 immunity requires both innate and adaptive sources of CD154. The Journal of Immunology, 180, 8083-8092.

JIANG, L., GU, Z.-H., YAN, Z.-X., ZHAO, X., XIE, Y.-Y., ZHANG, Z.-G., PAN, C.-M., HU, Y., CAI, C.-P. & DONG, Y. 2015. Exome sequencing identifies somatic mutations of DDX3X in natural killer/T-cell lymphoma. Nature genetics, 47, 1061-1066.

JOHNSTON, H. E., CARTER, M. J., LARRAYOZ, M., CLARKE, J., GARBIS, S. D., OSCIER, D., STREFFORD, J. C., STEELE, A. J., WALEWSKA, R. & CRAGG, M. S. 2018. Proteomics profiling of CLL versus healthy B-cells identifies putative therapeutic targets and a subtype-independent signature of spliceosome dysregulation. Molecular & Cellular Proteomics, 17, 776-791.

JONES, D. T., ADDISON, E., NORTH, J. M., LOWDELL, M. W., HOFFBRAND, A. V., MEHTA, A. B., GANESHAGURU, K., FOLARIN, N. I. & WICKREMASINGHE, R. G. 2004. Geldanamycin and herbimycin A induce apoptotic killing of B chronic lymphocytic leukemia cells and augment the cells' sensitivity to cytotoxic drugs. Blood, 103, 1855-1861.

JONES, N. D., VAN MAURIK, A., HARA, M., SPRIEWALD, B. M., WITZKE, O., MORRIS, P. J. & WOOD, K. J. 2000. CD40-CD40 ligand-independent activation of CD8+ T cells can trigger allograft rejection. The Journal of Immunology, 165, 1111-1118.

KALE, J., OSTERLUND, E. J. & ANDREWS, D. W. 2018. BCL-2 family proteins: changing partners in the dance towards death. Cell Death & Differentiation, 25, 65-80.

KAMAL, A., THAO, L., SENSINTAFFAR, J., ZHANG, L., BOEHM, M. F., FRITZ, L. C. & BURROWS, F. J. 2003. A high-affinity conformation of Hsp90 confers tumour selectivity on Hsp90 inhibitors. Nature, 425, 407-410.

KANG, M. H. & REYNOLDS, C. P. 2009. Bcl-2 inhibitors: targeting mitochondrial apoptotic pathways in cancer therapy. Clinical cancer research, 15, 1126-1132.

KASHUBA, E., EAGLE, G. L., BAILEY, J., EVANS, P., WELHAM, K. J., ALLSUP, D. & CAWKWELL, L. 2013. Proteomic analysis of B-cell receptor signaling in chronic lymphocytic leukaemia reveals a possible role for kininogen. Journal of proteomics, 91, 478-485.

KATER, A. P., EVERS, L. M., REMMERSWAAL, E. B., JASPERS, A., OOSTERWIJK, M. F., VAN LIER, R. A., VAN OERS, M. H. & ELDERING, E. 2004. CD40 stimulation of B‐cell chronic lymphocytic leukaemia cells enhances the anti‐apoptotic profile, but also Bid expression and cells remain susceptible to autologous cytotoxic T‐lymphocyte attack. British journal of haematology, 127, 404-415.

KAUFMAN, K. L., JENKINS, Y., ALOMARI, M., MIRZAEI, M., BEST, O. G., PASCOVICI, D., MACTIER, S., MULLIGAN, S. P., HAYNES, P. A. & CHRISTOPHERSON, R. I. 2015. The Hsp90 inhibitor SNX-7081 is synergistic with fludarabine nucleoside via DNA damage and repair mechanisms in human, p53-negative chronic lymphocytic leukemia. Oncotarget, 6, 40981.

KAUR, V. & SWAMI, A. 2017. Ibrutinib in CLL: a focus on adverse events, resistance, and novel approaches beyond ibrutinib. Annals of Hematology, 96, 1175-1184.

KEATS, J. J., FONSECA, R., CHESI, M., SCHOP, R., BAKER, A., CHNG, W.-J., VAN WIER, S., TIEDEMANN, R., SHI, C.-X. & SEBAG, M. 2007. Promiscuous mutations activate the noncanonical NF-κB pathway in multiple myeloma. Cancer cell, 12, 131-144.

KEHRY, M. R. 1996. CD40-mediated signaling in B cells. Balancing cell survival, growth, and death. The Journal of Immunology, 156, 2345-2348.

KELLARIS, G., KHAN, K., BAIG, S. M., TSAI, I.-C., ZAMORA, F. M., RUGGIERI, P., NATOWICZ, M. R. & KATSANIS, N. 2018. A hypomorphic inherited pathogenic variant in DDX3X causes male intellectual disability with additional neurodevelopmental and neurodegenerative features. Human genomics, 12, 11.

KELLEHER, N. L. 2004. Peer reviewed: Top-down proteomics. ACS Publications.

KIKUSHIGE, Y., ISHIKAWA, F., MIYAMOTO, T., SHIMA, T., URATA, S., YOSHIMOTO, G., MORI, Y., IINO, T., YAMAUCHI, T. & ETO, T. 2011. Self-renewing hematopoietic stem cell is the primary target in pathogenesis of human chronic lymphocytic leukemia. Cancer cell, 20, 246-259.

KIM, Y.-S., LEE, S.-G., PARK, S. H. & SONG, K. 2001. Gene structure of the human DDX3 and chromosome mapping of its related sequences. Molecules and cells, 12, 209-214.

KIRKPATRICK, D. S., DENISON, C. & GYGI, S. P. 2005. Weighing in on ubiquitin: the expanding role of mass-spectrometry-based proteomics. Nature cell biology, 7, 750-757.

KITADA, S., ZAPATA, J. M., ANDREEFF, M. & REED, J. C. 1999. Bryostatin and CD40-ligand enhance apoptosis resistance and induce expression of cell survival genes in B-cell chronic lymphocytic leukaemia. British journal of haematology, 106, 995-1004.

KITTAI, A. S. & WOYACH, J. A. 2019. Resistance Mechanisms to Targeted Agents in Chronic Lymphocytic Leukemia. The Cancer Journal, 25, 428-435.

KLANOVA, M. & KLENER, P. 2020. BCL-2 proteins in pathogenesis and therapy of B-cell non-Hodgkin lymphomas. Cancers, 12, 938.

KLEIN, A., DIAZ, S., FERREIRA, I., LAMBLIN, G., ROUSSEL, P. & MANZI, A. E. 1997. New sialic acids from biological sources identified by a comprehensive and sensitive approach: liquid chromatography-electrospray ionization-mass spectrometry (LC-ESI-MS) of SIA quinoxalinones. Glycobiology, 7, 421-432.

KLEIN, U., LIA, M., CRESPO, M., SIEGEL, R., SHEN, Q., MO, T., AMBESI-IMPIOMBATO, A., CALIFANO, A., MIGLIAZZA, A. & BHAGAT, G. 2010. The DLEU2/miR-15a/16-1 cluster controls B cell proliferation and its deletion leads to chronic lymphocytic leukemia. Cancer cell, 17, 28-40.

KLEIN, U., RAJEWSKY, K. & KÜPPERS, R. 1998. Human immunoglobulin (Ig) M+ IgD+ peripheral blood B cells expressing the CD27 cell surface antigen carry somatically mutated variable region genes: CD27 as a general marker for somatically mutated (memory) B cells. The Journal of experimental medicine, 188, 1679-1689.

KLEIN, U., TU, Y., STOLOVITZKY, G. A., MATTIOLI, M., CATTORETTI, G., HUSSON, H., FREEDMAN, A., INGHIRAMI, G., CRO, L. & BALDINI, L. 2001. Gene expression profiling of B cell chronic lymphocytic leukemia reveals a homogeneous phenotype related to memory B cells. The Journal of experimental medicine, 194, 1625-1638.

KLONISCH, T., WIECHEC, E., HOMBACH-KLONISCH, S., ANDE, S. R., WESSELBORG, S., SCHULZE-OSTHOFF, K. & LOS, M. 2008. Cancer stem cell markers in common cancers–therapeutic implications. Trends in molecular medicine, 14, 450-460.

KNOSPE, W. H., LOEB JR, V. & GROUP, W. C. F. T. S. C. S. 1980. Biweekly chlorambucil treatment of lymphocytic lymphoma. American Journal of Clinical Oncology, 3, 329-336.

KNUDSEN, B. S. & MIRANTI, C. K. 2006. The impact of cell adhesion changes on proliferation and survival during prostate cancer development and progression. Journal of cellular biochemistry, 99, 345-361.

KOBAYASHI, T., WALSH, P. T., WALSH, M. C., SPEIRS, K. M., CHIFFOLEAU, E., KING, C. G., HANCOCK, W. W., CAAMANO, J. H., HUNTER, C. A. & SCOTT, P. 2003. TRAF6 is a critical factor for dendritic cell maturation and development. Immunity, 19, 353-363.

KOOMEN, J., HAWKE, D. & KOBAYASHI, R. 2005. Developing an understanding of proteomics: an introduction to biological mass spectrometry. Cancer investigation, 23, 47-59.

KRUEGER, U., BERGAUER, T., KAUFMANN, B., WOLTER, I., PILK, S., HEIDER-FABIAN, M., KIRCH, S., ARTZ-OPPITZ, C., ISSELHORST, M. & KONRAD, J. 2007. Insights into effective RNAi gained from large-scale siRNA validation screening. Oligonucleotides, 17, 237-250.

KURIEN, B. T. & SCOFIELD, R. H. 2006. Western blotting. Methods, 38, 283-293.

KUROSAKI, T. 2000. Functional dissection of BCR signaling pathways. Current opinion in immunology, 12, 276-281.

KURTOVA, A. V., BALAKRISHNAN, K., CHEN, R., DING, W., SCHNABL, S., QUIROGA, M. P., SIVINA, M., WIERDA, W. G., ESTROV, Z. & KEATING, M. J. 2009. Diverse marrow stromal cells protect CLL cells from spontaneous and drug-induced apoptosis: development of a reliable and reproducible system to assess stromal cell adhesion-mediated drug resistance. Blood, The Journal of the American Society of Hematology, 114, 4441-4450.

LAFOURESSE, F., BELLARD, E., LAURENT, C., MOUSSION, C., FOURNIÉ, J.-J., YSEBAERT, L. & GIRARD, J.-P. 2015. L-selectin controls trafficking of chronic lymphocytic leukemia cells in lymph node high endothelial venules in vivo. Blood, The Journal of the American Society of Hematology, 126, 1336-1345.

LAGNEAUX, L., DELFORGE, A., BRON, D., DE BRUYN, C. & STRYCKMANS, P. 1998. Chronic lymphocytic leukemic B cells but not normal B cells are rescued from apoptosis by contact with normal bone marrow stromal cells. Blood, The Journal of the American Society of Hematology, 91, 2387-2396.

LAI, M.-C., CHANG, W.-C., SHIEH, S.-Y. & TARN, W.-Y. 2010. DDX3 regulates cell growth through translational control of cyclin E1. Molecular and cellular biology, 30, 5444-5453.

LAMPSON, B. L. & DAVIDS, M. S. 2017. The development and current use of BCL-2 inhibitors for the treatment of chronic lymphocytic leukemia. Current hematologic malignancy reports, 12, 11-19.

LANDAU, D. A., TAUSCH, E., TAYLOR-WEINER, A. N., STEWART, C., REITER, J. G., BAHLO, J., KLUTH, S., BOZIC, I., LAWRENCE, M. & BÖTTCHER, S. 2015. Mutations driving CLL and their evolution in progression and relapse. Nature, 526, 525-530.

LANDGREN, O., RAPKIN, J. S., CAPORASO, N. E., MELLEMKJAER, L., GRIDLEY, G., GOLDIN, L. R. & ENGELS, E. A. 2007. Respiratory tract infections and subsequent risk of chronic lymphocytic leukemia. Blood, 109, 2198-2201.

LARSEN, C. P., ALEXANDER, D. Z., HOLLENBAUGH, D., ELWOOD, E. T., RITCHIE, S. C., ARUFFO, A., HENDRIX, R. & PEARSON, T. C. 1996. CD40-gp39 INTERACTIONS PLAY A CRITICAL ROLE DURING ALLOGRAFT REJECTION: Suppression of Allograft Rejection by Blockade of the CD40-gp39 Pathway1. Transplantation, 61, 4-9.

LEE, H. H., DADGOSTAR, H., CHENG, Q., SHU, J. & CHENG, G. 1999. NF-κB-mediated up-regulation of Bcl-x and Bfl-1/A1 is required for CD40 survival signaling in B lymphocytes. Proceedings of the National Academy of Sciences, 96, 9136-9141.

LEE, S. Y., REICHLIN, A., SANTANA, A., SOKOL, K. A., NUSSENZWEIG, M. C. & CHOI, Y. 1997. TRAF2 is essential for JNK but not NF-κB activation and regulates lymphocyte proliferation and survival. Immunity, 7, 703-713.

LEHNERT, A. M., MOTTRAM, P. L., HAN, W., WALTERS, S. N., PATEL, A. T., HAWTHORNE, W. J., COWAN, P. J., D'APICE, A. J. & O'CONNELL, P. J. 2001. Blockade of the CD28 and CD40 pathways result in the acceptance of pig and rat islet xenografts but not rat cardiac grafts in mice. Transplant immunology, 9, 51-56.

LEQUIN, R. M. 2005. Enzyme immunoassay (EIA)/enzyme-linked immunosorbent assay (ELISA). Clinical chemistry, 51, 2415-2418.

LEZINA, L., SPRIGGS, R. V., BECK, D., JONES, C., DUDEK, K. M., BZURA, A., JONES, G. D., PACKHAM, G., WILLIS, A. E. & WAGNER, S. D. 2018. CD40L/IL-4–stimulated CLL demonstrates variation in translational regulation of DNA damage response genes including ATM. Blood advances, 2, 1869-1881.

LI, P.-P., FENG, L.-L., CHEN, N., GE, X.-L., LV, X., LU, K., DING, M., YUAN, D. & WANG, X. 2015. Metadherin contributes to the pathogenesis of chronic lymphocytic leukemia partially through Wnt/β-catenin pathway. Medical Oncology, 32, 21.

LI, Q., ZHANG, P., ZHANG, C., WANG, Y., WAN, R., YANG, Y., GUO, X., HUO, R., LIN, M. & ZHOU, Z. 2014. DDX3X regulates cell survival and cell cycle during mouse early embryonic development. Journal of biomedical research, 28, 282.

LIN, K., ROCKLIFFE, N., JOHNSON, G., SHERRINGTON, P. D. & PETTITT, A. R. 2008. Hsp90 inhibition has opposing effects on wild-type and mutant p53 and induces p21 expression and cytotoxicity irrespective of p53/ATM status in chronic lymphocytic leukaemia cells. Oncogene, 27, 2445-2455.

LIU, Z., LIU, J., ZHANG, T., SHI, M., CHEN, X., CHEN, Y. & YU, J. 2020. Destabilization of ROR1 enhances activity of Ibrutinib against chronic lymphocytic leukemia in vivo. Pharmacological Research, 151, 104512.

LOONEY, T., QUEST, G., FEILOTTER, H. & DAVIS, Z. 2020. Clonal lineage analysis of CLL research samples by IGH chain sequencing to reveal novel CLL subgroups defined by ongoing class-switch recombination and somatic hypermutation. American Society of Clinical Oncology.

LÓPEZ-GUERRA, M., XARGAY-TORRENT, S., FUENTES, P., ROLDÁN, J., GONZÁLEZ-FARRÉ, B., ROSICH, L., SILKENSTEDT, E., GARCÍA-LEÓN, M. J., LEE-VERGÉS, E. & GIMÉNEZ, N. 2019. Specific NOTCH1 antibody targets DLL4-induced proliferation, migration, and angiogenesis in NOTCH1-mutated CLL cells. Oncogene, 1-13.

LUNDBERG, E. & BORNER, G. H. 2019. Spatial proteomics: a powerful discovery tool for cell biology. Nature Reviews Molecular Cell Biology, 20, 285-302.

LUQMAN, M., KLABUNDE, S., LIN, K., GEORGAKIS, G. V., CHERUKURI, A., HOLASH, J., GOLDBECK, C., XU, X., KADEL III, E. E. & LEE, S. H. 2008. The antileukemia activity of a human anti-CD40 antagonist antibody, HCD122, on human chronic lymphocytic leukemia cells. Blood, The Journal of the American Society of Hematology, 112, 711-720.

LUTZNY, G., KOCHER, T., SCHMIDT-SUPPRIAN, M., RUDELIUS, M., KLEIN-HITPASS, L., FINCH, A. J., DÜRIG, J., WAGNER, M., HAFERLACH, C. & KOHLMANN, A. 2013. Protein kinase c-β-dependent activation of NF-κB in stromal cells is indispensable for the survival of chronic lymphocytic leukemia B cells in vivo. Cancer cell, 23, 77-92.

MACBEATH, G. 2002. Protein microarrays and proteomics. Nature genetics, 32, 526-532.

MACBEATH, G., KOEHLER, A. N. & SCHREIBER, S. L. 1999. Printing small molecules as microarrays and detecting protein− ligand interactions en masse. Journal of the American Chemical Society, 121, 7967-7968.

MADDOCKS, K. J., RUPPERT, A. S., LOZANSKI, G., HEEREMA, N. A., ZHAO, W., ABRUZZO, L., LOZANSKI, A., DAVIS, M., GORDON, A. & SMITH, L. L. 2015. Etiology of ibrutinib therapy discontinuation and outcomes in patients with chronic lymphocytic leukemia. JAMA oncology, 1, 80-87.

MAGLIULO, D. & BERNARDI, R. 2018. HIF-α factors as potential therapeutic targets in leukemia. Expert Opinion on Therapeutic Targets, 22, 917-928.

MAHMOOD, T. & YANG, P.-C. 2012. Western blot: technique, theory, and trouble shooting. North American journal of medical sciences, 4, 429.

MAJIDINIA, M., MIRZA-AGHAZADEH-ATTARI, M., RAHIMI, M., MIHANFAR, A., KARIMIAN, A., SAFA, A. & YOUSEFI, B. 2020. Overcoming multidrug resistance in cancer: Recent progress in nanotechnology and new horizons. IUBMB life, 72, 855-871.

MAKRILIA, N., KOLLIAS, A., MANOLOPOULOS, L. & SYRIGOS, K. 2009. Cell adhesion molecules: role and clinical significance in cancer. Cancer investigation, 27, 1023-1037.

MALEKI, Y., ALAHBAKHSHI, Z., HEIDARI, Z., MORADI, M. T., RAHIMI, Z., YARI, K., RAHIMI, Z., AZNAB, M., AHMADI-KHAJEVAND, M. & BAHREMAND, F. 2019. NOTCH1, SF3B1, MDM2 and MYD88 mutations in patients with chronic lymphocytic leukemia. Oncology letters, 17, 4016-4023.

MANSOURI, L., PAPAKONSTANTINOU, N., NTOUFA, S., STAMATOPOULOS, K. & ROSENQUIST, R. NF-κB activation in chronic lymphocytic leukemia: a point of convergence of external triggers and intrinsic lesions. Seminars in cancer biology, 2016. Elsevier, 40-48.

MANSOURI, L., SUTTON, L.-A., LJUNGSTRÖM, V., BONDZA, S., ARNGÅRDEN, L., BHOI, S., LARSSON, J., CORTESE, D., KALUSHKOVA, A. & PLEVOVA, K. 2015. Functional loss of IκBε leads to NF-κB deregulation in aggressive chronic lymphocytic leukemia. Journal of Experimental Medicine, 212, 833-843.

MARSHALL, L. S., ARUFFO, A., LEDBETTER, J. A. & NOELLE, R. J. 1993. The molecular basis for T cell help in humoral immunity: CD40 and its ligand, gp39. Journal of clinical immunology, 13, 165-174.

MARTINEZ-MORENO, M., LEIVA, M., AGUILERA-MONTILLA, N., SEVILLA-MOVILLA, S., DE VAL, S. I., ARELLANO-SANCHEZ, N., GUTIÉRREZ, N., MALDONADO, R., MARTÍNEZ-LÓPEZ, J. & BUÑO, I. 2016. In vivo adhesion of malignant B cells to bone marrow microvasculature is regulated by α4β1 cytoplasmic-binding proteins. Leukemia, 30, 861-872.

MAYER, R. L., SCHWARZMEIER, J. D., GERNER, M. C., BILECK, A., MADER, J. C., MEIER-MENCHES, S. M., GERNER, S. M., SCHMETTERER, K. G., PUKROP, T. & REICHLE, A. 2018. Proteomics and metabolomics identify molecular mechanisms of aging potentially predisposing for chronic lymphocytic leukemia. Molecular & Cellular Proteomics, 17, 290-303.

MCCAIG, A. M., COSIMO, E., LEACH, M. T. & MICHIE, A. M. 2011. Dasatinib inhibits B cell receptor signalling in chronic lymphocytic leukaemia but novel combination approaches are required to overcome additional pro-survival microenvironmental signals. British journal of haematology, 153, 199-211.

MERINO, R., GRILLOT, D., SIMONIAN, P. L., MUTHUKKUMAR, S., FANSLOW, W. C., BONDADA, S. & NUNEZ, G. 1995. Modulation of anti-IgM-induced B cell apoptosis by Bcl-xL and CD40 in WEHI-231 cells. Dissociation from cell cycle arrest and dependence on the avidity of the antibody-IgM receptor interaction. The Journal of Immunology, 155, 3830-3838.

MESSMER, B. T., MESSMER, D., ALLEN, S. L., KOLITZ, J. E., KUDALKAR, P., CESAR, D., MURPHY, E. J., KODURU, P., FERRARINI, M. & ZUPO, S. 2005. In vivo measurements document the dynamic cellular kinetics of chronic lymphocytic leukemia B cells. The Journal of clinical investigation, 115, 755-764.

MILNE, K., STURROCK, B. & CHEVASSUT, T. 2020. Chronic Lymphocytic Leukaemia in 2020: the Future Has Arrived. Current Oncology Reports, 22, 1-9.

MINUZZO, S., INDRACCOLO, S., TOSELLO, V., PIOVAN, E., CABRELLE, A., TRENTIN, L., SEMENZATO, G. & AMADORI, A. 2005. CD40 activation of B-CLL cells is associated with augmented intracellular levels of CD79b and increased BCR expression in a subset of patients. Leukemia, 19, 1099-1101.

MISCHERIKOW, N. & HECK, A. J. 2011. Targeted large‐scale analysis of protein acetylation. Proteomics, 11, 571-589.

MITCHISON, N. 2004. T-cell–B-cell cooperation. Nature Reviews Immunology, 4, 308-312.

MÖHLE, R., FAILENSCHMID, C., BAUTZ, F. & KANZ, L. 1999. Overexpression of the chemokine receptor CXCR4 in B cell chronic lymphocytic leukemia is associated with increased functional response to stromal cell-derived factor-1 (SDF-1). Leukemia, 13, 1954-1959.

MONTRESOR, A., TOFFALI, L., MIRENDA, M., RIGO, A., VINANTE, F. & LAUDANNA, C. 2015. JAK2 tyrosine kinase mediates integrin activation induced by CXCL12 in B-cell chronic lymphocytic leukemia. Oncotarget, 6, 34245.

MORAES, F. & GÓES, A. 2016. A decade of human genome project conclusion: Scientific diffusion about our genome knowledge. Biochemistry and Molecular Biology Education, 44, 215-223.

MORITZ, C. P. 2020. 40 years Western blotting: A scientific birthday toast. Journal of proteomics, 212, 103575.

MUSENGA, A. & COWAN, D. A. 2013. Use of ultra-high pressure liquid chromatography coupled to high resolution mass spectrometry for fast screening in high throughput doping control. Journal of Chromatography A, 1288, 82-95.

NADKARNI, J. J., PERAMBAKAM, S. M., RATHORE, V. B., AMIN, K. M., PARIKH, P. M., NARESH, K. & ADVANI, S. H. 1998. Expression of adhesion molecules in B-cell chronic lymphocytic leukaemia: an analysis in lymphoid compartments-peripheral blood, bone marrow and lymph node. Cancer biotherapy & radiopharmaceuticals, 13, 269-274.

NAGATA, S. & GOLSTEIN, P. 1995. The Fas death factor. Science, 267, 1449-1456.

NAKANO, H., SAKON, S., KOSEKI, H., TAKEMORI, T., TADA, K., MATSUMOTO, M., MUNECHIKA, E., SAKAI, T., SHIRASAWA, T. & AKIBA, H. 1999. Targeted disruption of Traf5 gene causes defects in CD40-and CD27-mediated lymphocyte activation. Proceedings of the National Academy of Sciences, 96, 9803-9808.

NECKERS, L. 2002. Hsp90 inhibitors as novel cancer chemotherapeutic agents. Trends in molecular medicine, 8, S55-S61.

NIALL, H. D. 1973. [36] Automated edman degradation: The protein sequenator. Methods in enzymology. Elsevier.

NIKITAKI, Z., MAVRAGANI, I. V., LASKARATOU, D. A., GIKA, V., MOSKVIN, V. P., THEOFILATOS, K., VOUGAS, K., STEWART, R. D. & GEORGAKILAS, A. G. Systemic mechanisms and effects of ionizing radiation: A new old paradigm of how the bystanders and distant can become the players. Seminars in cancer biology, 2016. Elsevier, 77-95.

NING, S., FUESSEL, S., KOTZSCH, M., KRAEMER, K., KAPPLER, M., SCHMIDT, U., TAUBERT, H., WIRTH, M. P. & MEYE, A. 2004. siRNA-mediated down-regulation of survivin inhibits bladder cancer cell growth. International journal of oncology, 25, 1065-1136.

NITA-LAZAR, A., SAITO-BENZ, H. & WHITE, F. M. 2008. Quantitative phosphoproteomics by mass spectrometry: past, present, and future. Proteomics, 8, 4433-4443.

NOVÁKOVÁ, L. 2013. Challenges in the development of bioanalytical liquid chromatography–mass spectrometry method with emphasis on fast analysis. Journal of Chromatography A, 1292, 25-37.

NÜSSE, M. & MARX, K. 1997. Flow cytometric analysis of micronuclei in cell cultures and human lymphocytes: advantages and disadvantages. Mutation Research/Genetic Toxicology and Environmental Mutagenesis, 392, 109-115.

O'BRIEN, S., JONES, J. A., COUTRE, S. E., MATO, A. R., HILLMEN, P., TAM, C., ÖSTERBORG, A., SIDDIQI, T., THIRMAN, M. J. & FURMAN, R. R. 2016. Ibrutinib for patients with relapsed or refractory chronic lymphocytic leukaemia with 17p deletion (RESONATE-17): a phase 2, open-label, multicentre study. The Lancet Oncology, 17, 1409-1418.

ODA, K., MATSUOKA, Y., FUNAHASHI, A. & KITANO, H. 2005. A comprehensive pathway map of epidermal growth factor receptor signaling. Molecular systems biology, 1, 2005.0010.

ODELL, I. D. & COOK, D. 2013. Immunofluorescence techniques. The Journal of investigative dermatology, 133, e4.

O'FARRELL, P. H. 1975. High resolution two-dimensional electrophoresis of proteins. Journal of biological chemistry, 250, 4007-4021.

O'HAYRE, M., SALANGA, C. L., KIPPS, T. J., MESSMER, D., DORRESTEIN, P. C. & HANDEL, T. M. 2010. Elucidating the CXCL12/CXCR4 signaling network in chronic lymphocytic leukemia through phosphoproteomics analysis. PloS one, 5, e11716.

OJHA, J., AYRES, J., SECRETO, C., TSCHUMPER, R., RABE, K., VAN DYKE, D., SLAGER, S., SHANAFELT, T., FONSECA, R. & KAY, N. E. 2015. Deep sequencing identifies genetic heterogeneity and recurrent convergent evolution in chronic lymphocytic leukemia. Blood, The Journal of the American Society of Hematology, 125, 492-498.

OJHA, J., SECRETO, C. R., RABE, K. G., VAN DYKE, D. L., KORTUM, K. M., SLAGER, S. L., SHANAFELT, T. D., FONSECA, R., KAY, N. E. & BRAGGIO, E. 2015. Identification of recurrent truncated DDX3X mutations in chronic lymphocytic leukaemia. British journal of haematology, 169, 445.

O'LEARY, M. H. 1988. Carbon isotopes in photosynthesis. Bioscience, 38, 328-336.

OLSEN, J. V., ONG, S.-E. & MANN, M. 2004. Trypsin cleaves exclusively C-terminal to arginine and lysine residues. Molecular & Cellular Proteomics, 3, 608-614.

OLSON, R. J., ZETTLER, E. R. & DURAND, M. D. 1993. Phytoplankton analysis using flow cytometry. Handbook of methods in aquatic microbial ecology, 175-186.

ORMEROD, M. 1998. The study of apoptotic cells by flow cytometry. Leukemia, 12, 1013-1025.

OS, A., BÜRGLER, S., RIBES, A. P., FUNDERUD, A., WANG, D., THOMPSON, K. M., TJØNNFJORD, G. E., BOGEN, B. & MUNTHE, L. A. 2013. Chronic lymphocytic leukemia cells are activated and proliferate in response to specific T helper cells. Cell reports, 4, 566-577.

OUAAZ, F., ARRON, J., ZHENG, Y., CHOI, Y. & BEG, A. A. 2002. Dendritic cell development and survival require distinct NF-κB subunits. Immunity, 16, 257-270.

PACKHAM, G. & STEVENSON, F. The role of the B-cell receptor in the pathogenesis of chronic lymphocytic leukaemia. Seminars in cancer biology, 2010. Elsevier, 391-399.

PADDISON, P. J., CAUDY, A. A., BERNSTEIN, E., HANNON, G. J. & CONKLIN, D. S. 2002. Short hairpin RNAs (shRNAs) induce sequence-specific silencing in mammalian cells. Genes & development, 16, 948-958.

PAN, S., CHEN, R., AEBERSOLD, R. & BRENTNALL, T. A. 2011. Mass spectrometry based glycoproteomics—from a proteomics perspective. Molecular & Cellular Proteomics, 10.

PANAYIOTIDIS, P., JONES, D., GANESHAGURU, K., FORONI, L. & HOFFBRAND, A. 1996. Human bone marrow stromal cells prevent apoptosis and support the survival of chronic lymphocytic leukaemia cells in vitro. British journal of haematology, 92, 97-103.

PARK, S.-H., LEE, S., KIM, Y. & SONG, K. 1998. Assignment of a human putative RNA helicase gene, DDX3, to human X chromosome bands p11. 3--> p11. 23. Cytogenetic and Genome Research, 81, 178.

PARKER, D. C., GREINER, D. L., PHILLIPS, N. E., APPEL, M. C., STEELE, A. W., DURIE, F. H., NOELLE, R. J., MORDES, J. P. & ROSSINI, A. A. 1995. Survival of mouse pancreatic islet allografts in recipients treated with allogeneic small lymphocytes and antibody to CD40 ligand. Proceedings of the National Academy of Sciences, 92, 9560-9564.

PASCUTTI, M. F., JAK, M., TROMP, J. M., DERKS, I. A., REMMERSWAAL, E. B., THIJSSEN, R., VAN ATTEKUM, M. H., VAN BOCHOVE, G. G., LUIJKS, D. M. & PALS, S. T. 2013. IL-21 and CD40L signals from autologous T cells can induce antigen-independent proliferation of CLL cells. Blood, The Journal of the American Society of Hematology, 122, 3010-3019.

PASIKOWSKA, M., WALSBY, E., APOLLONIO, B., CUTHILL, K., PHILLIPS, E., COULTER, E., LONGHI, M. S., MA, Y., YALLOP, D. & BARBER, L. D. 2016. Phenotype and immune function of lymph node and peripheral blood CLL cells are linked to transendothelial migration. Blood, The Journal of the American Society of Hematology, 128, 563-573.

PATEL, V. J., THALASSINOS, K., SLADE, S. E., CONNOLLY, J. B., CROMBIE, A., MURRELL, J. C. & SCRIVENS, J. H. 2009. A comparison of labeling and label-free mass spectrometry-based proteomics approaches. Journal of proteome research, 8, 3752-3759.

PATIL, M. P. N. 2017. HPLC Method Development–A Review. Journal of Pharmaceutical Research and Education, 1, 243-260.

PATTEN, P. E., BUGGINS, A. G., RICHARDS, J., WOTHERSPOON, A., SALISBURY, J., MUFTI, G. J., HAMBLIN, T. J. & DEVEREUX, S. 2008. CD38 expression in chronic lymphocytic leukemia is regulated by the tumor microenvironment. Blood, The Journal of the American Society of Hematology, 111, 5173-5181.

PEDERSEN, I. M., KITADA, S., LEONI, L. M., ZAPATA, J. M., KARRAS, J. G., TSUKADA, N., KIPPS, T. J., CHOI, Y. S., BENNETT, F. & REED, J. C. 2002. Protection of CLL B cells by a follicular dendritic cell line is dependent on induction of Mcl-1. Blood, The Journal of the American Society of Hematology, 100, 1795-1801.

PENNO, M. A., ERNST, M. & HOFFMANN, P. 2009. Optimal preparation methods for automated matrix-assisted laser desorption/ionization time-of-flight mass spectrometry profiling of low molecular weight proteins and peptides. Rapid Communications in Mass Spectrometry: An International Journal Devoted to the Rapid Dissemination of Up-to-the-Minute Research in Mass Spectrometry, 23, 2656-2662.

PEPPER, C., MAHDI, J., BUGGINS, A., HEWAMANA, S., WALSBY, E., MAHDI, E., AL-HAZA'A, A., MAHDI, A. J., LIN, T. T. & PEARCE, L. 2011. Two novel aspirin analogues show selective cytotoxicity in primary chronic lymphocytic leukaemia cells that is associated with dual inhibition of Rel A and COX-2. Cell proliferation, 44, 380-390.

PETER, M., HADJI, A., MURMANN, A., BROCKWAY, S., PUTZBACH, W., PATTANAYAK, A. & CEPPI, P. 2015. The role of CD95 and CD95 ligand in cancer. Cell death & differentiation, 22, 549-559.

PETTITT, A. R. 2003. Mechanism of action of purine analogues in chronic lymphocytic leukaemia. British journal of haematology, 121, 692-702.

PHAM, T. V., PIERSMA, S. R., OUDGENOEG, G. & JIMENEZ, C. R. 2012. Label-free mass spectrometry-based proteomics for biomarker discovery and validation. Expert review of molecular diagnostics, 12, 343-359.

PHARMINGEN, B. Annexin V-FITC. Europe, 32, 720.211.

PILON, C., LEVAST, B., MEURENS, F., LE VERN, Y., KERBOEUF, D., SALMON, H., VELGE-ROUSSEL, F., LEBRANCHU, Y. & BARON, C. 2009. CD40 engagement strongly induces CD25 expression on porcine dendritic cells and polarizes the T cell immune response toward Th1. Molecular immunology, 46, 437-447.

PLANDER, M., SEEGERS, S., UGOCSAI, P., DIERMEIER-DAUCHER, S., IVANYI, J., SCHMITZ, G., HOFSTÄDTER, F., SCHWARZ, S., ORSO, E. & KNÜCHEL, R. 2009. Different proliferative and survival capacity of CLL-cells in a newly established in vitro model for pseudofollicles. Leukemia, 23, 2118-2128.

POON, T. C. & JOHNSON, P. J. 2001. Proteome analysis and its impact on the discovery of serological tumor markers. Clinica chimica acta, 313, 231-239.

POZZO, F., BITTOLO, T., ARRUGA, F., BULIAN, P., MACOR, P., TISSINO, E., GIZDIC, B., ROSSI, F. M., BOMBEN, R. & ZUCCHETTO, A. 2016. NOTCH1 mutations associate with low CD20 level in chronic lymphocytic leukemia: evidence for a NOTCH1 mutation-driven epigenetic dysregulation. Leukemia, 30, 182-189.

PRADOS-ROSALES, R. C., ARAGONESES-CAZORLA, G., ESTEVEZ, H., GARCIA-CALVO, E., MACHUCA, A. & LUQUE-GARCIA, J. L. 2019. Strategies for Membrane Protein Analysis by Mass Spectrometry. Advancements of Mass Spectrometry in Biomedical Research. Springer.

PRAY, L. 2008. Eukaryotic genome complexity. Nature Education, 1, 96.

PRIETO, D., SOTELO, N., SEIJA, N., SERNBO, S., ABREU, C., DURÁN, R., GIL, M., SICCO, E., IRIGOIN, V. & OLIVER, C. 2017. S100-A9 protein in exosomes from chronic lymphocytic leukemia cells promotes NF-κB activity during disease progression. Blood, The Journal of the American Society of Hematology, 130, 777-788.

PROPST, S. M., ESTELL, K. & SCHWIEBERT, L. M. 2002. CD40-mediated activation of NF-κB in airway epithelial cells. Journal of Biological Chemistry, 277, 37054-37063.

PUENTE, X. S., BEÀ, S., VALDÉS-MAS, R., VILLAMOR, N., GUTIÉRREZ-ABRIL, J., MARTÍN-SUBERO, J. I., MUNAR, M., RUBIO-PÉREZ, C., JARES, P. & AYMERICH, M. 2015. Non-coding recurrent mutations in chronic lymphocytic leukaemia. Nature, 526, 519-524.

PUENTE, X. S., PINYOL, M., QUESADA, V., CONDE, L., ORDÓÑEZ, G. R., VILLAMOR, N., ESCARAMIS, G., JARES, P., BEÀ, S. & GONZÁLEZ-DÍAZ, M. 2011. Whole-genome sequencing identifies recurrent mutations in chronic lymphocytic leukaemia. Nature, 475, 101-105.

PUGH, T. J., WEERARATNE, S. D., ARCHER, T. C., KRUMMEL, D. A. P., AUCLAIR, D., BOCHICCHIO, J., CARNEIRO, M. O., CARTER, S. L., CIBULSKIS, K. & ERLICH, R. L. 2012. Medulloblastoma exome sequencing uncovers subtype-specific somatic mutations. Nature, 488, 106-110.

PULLMAN, B. & PULLMAN, A. 1959. The electronic structure of the purine-pyrimidine pairs of DNA. Biochimica et biophysica acta, 36, 343-350.

PURROY, N., ABRISQUETA, P., CARABIA, J., CARPIO, C., PALACIO, C., BOSCH, F. & CRESPO, M. 2015. Co-culture of primary CLL cells with bone marrow mesenchymal cells, CD40 ligand and CpG ODN promotes proliferation of chemoresistant CLL cells phenotypically comparable to those proliferating in vivo. Oncotarget, 6, 7632.

QU, X. 2009. Targeting TRAF proteins to manipulate CD40 signaling pathways in inflammatory disease and cancer, University of Louisville.

QUESADA, V., CONDE, L., VILLAMOR, N., ORDÓÑEZ, G. R., JARES, P., BASSAGANYAS, L., RAMSAY, A. J., BEÀ, S., PINYOL, M. & MARTÍNEZ-TRILLOS, A. 2012. Exome sequencing identifies recurrent mutations of the splicing factor SF3B1 gene in chronic lymphocytic leukemia. Nature genetics, 44, 47.

QUEZADA, S. A., FULLER, B., JARVINEN, L. Z., GONZALEZ, M., BLAZAR, B. R., RUDENSKY, A. Y., STROM, T. B. & NOELLE, R. J. 2003. Mechanisms of donor-specific transfusion tolerance: preemptive induction of clonal T-cell exhaustion via indirect presentation. Blood, 102, 1920-1926.

QUIROGA, M. P., BALAKRISHNAN, K., KURTOVA, A. V., SIVINA, M., KEATING, M. J., WIERDA, W. G., GANDHI, V. & BURGER, J. A. 2009. B-cell antigen receptor signaling enhances chronic lymphocytic leukemia cell migration and survival: specific targeting with a novel spleen tyrosine kinase inhibitor, R406. Blood, 114, 1029-1037.

RAI, K. R., SAWITSKY, A., CRONKITE, E. P., CHANANA, A. D., LEVY, R. N. & PASTERNACK, B. 1975. Clinical staging of chronic lymphocytic leukemia.

RAMOS-VARA, J. & MILLER, M. 2014. When tissue antigens and antibodies get along: revisiting the technical aspects of immunohistochemistry—the red, brown, and blue technique. Veterinary pathology, 51, 42-87.

RAMSAY, A. D. & RODRIGUEZ‐JUSTO, M. 2013. Chronic lymphocytic leukaemia–the role of the microenvironment pathogenesis and therapy. British journal of haematology, 162, 15-24.

RAMSAY, A. G., JOHNSON, A. J., LEE, A. M., GORGÜN, G., LE DIEU, R., BLUM, W., BYRD, J. C. & GRIBBEN, J. G. 2008. Chronic lymphocytic leukemia T cells show impaired immunological synapse

formation that can be reversed with an immunomodulating drug. The Journal of clinical investigation, 118, 2427-2437.

RAVIKRISHNAN, J., LAI, T.-H., MUHOWSKI, E., BRINTON, L., WILLIAMS, K., THOMPSON, A., BLACHLY, J. S., OZER, H. G., BYRD, J. C. & LAPALOMBELLA, R. 2019. Role of Mutant p53 in the Progression of Chronic Lymphocytic Leukemia. American Society of Hematology Washington, DC.

RAWLINGS, D. J., SCHWARTZ, M. A., JACKSON, S. W. & MEYER-BAHLBURG, A. 2012. Integration of B cell responses through Toll-like receptors and antigen receptors. Nature reviews Immunology, 12, 282-294.

REES-UNWIN, K. S., FARAGHER, R., UNWIN, R. D., ADAMS, J., BROWN, P. J., BUCKLE, A. M., PETTITT, A., HUTCHINSON, C. V., JOHNSON, S. M. & PULFORD, K. 2010. Ribosome-associated nucleophosmin 1: increased expression and shuttling activity distinguishes prognostic subtypes in chronic lymphocytic leukaemia. British journal of haematology, 148, 534-543.

REN, C. L., MORIO, T., FU, S. M. & GEHA, R. S. 1994. Signal transduction via CD40 involves activation of lyn kinase and phosphatidylinositol-3-kinase, and phosphorylation of phospholipase C gamma 2. The Journal of experimental medicine, 179, 673-680.

RENARD, N., DUVERT, V., BLANCHARD, D., BANCHEREAU, J. & SAELAND, S. 1994. Activated CD4+ T cells induce CD40-dependent proliferation of human B cell precursors. The Journal of Immunology, 152, 1693-1701.

RENSHAW, S. A., DEMPSEY, C. E., BARNES, F. A., BAGSTAFF, S. M., DOWER, S. K., BINGLE, C. D. & WHYTE, M. K. 2004. Three novel Bid proteins generated by alternative splicing of the human Bid gene. Journal of Biological Chemistry, 279, 2846-2855.

RICCIARDI, M. R., PETRUCCI, M. T., GREGORJ, C., ARIOLA, C., LEMOLI, R. M., FOGLI, M., MAURO, F. R., CERRETTI, R., FOÀ, R. & MANDELLI, F. 2001. Reduced susceptibility to apoptosis correlates with kinetic quiescence in disease progression of chronic lymphocytic leukaemia. British journal of haematology, 113, 391-399.

RICHES, J. C., DAVIES, J. K., MCCLANAHAN, F., FATAH, R., IQBAL, S., AGRAWAL, S., RAMSAY, A. G. & GRIBBEN, J. G. 2013. T cells from CLL patients exhibit features of T-cell exhaustion but retain capacity for cytokine production. Blood, 121, 1612-1621.

RICHES, J. C., O'DONOVAN, C. J., KINGDON, S. J., MCCLANAHAN, F., CLEAR, A. J., NEUBERG, D. S., WERNER, L., CROCE, C. M., RAMSAY, A. G. & RASSENTI, L. Z. 2014. Trisomy 12 chronic lymphocytic leukemia cells exhibit upregulation of integrin signaling that is modulated by NOTCH1 mutations. Blood, 123, 4101-4110.

ROBERTSON, L., PLUNKETT, W., MCCONNELL, K., KEATING, M. & MCDONNELL, T. J. 1996. Bcl-2 expression in chronic lymphocytic leukemia and its correlation with the induction of apoptosis and clinical outcome. Leukemia, 10, 456-459.

ROJO, M. G., BUENO, G. & SLODKOWSKA, J. 2009. Review of imaging solutions for integrated quantitative immunohistochemistry in the Pathology daily practice. Folia histochemica et cytobiologica, 47, 349-354.

ROMANO, M. F., LAMBERTI, A., TASSONE, P., ALFINITO, F., COSTANTINI, S., CHIURAZZI, F., DEFRANCE, T., BONELLI, P., TUCCILLO, F. & TURCO, M. C. 1998. Triggering of CD40 antigen inhibits

fludarabine-induced apoptosis in B chronic lymphocytic leukemia cells. Blood, The Journal of the American Society of Hematology, 92, 990-995.

ROSATI, A., BASILE, A., FALCO, A., D'AVENIA, M., FESTA, M., GRAZIANO, V., DE LAURENZI, V., ARRA, C., PASCALE, M. & TURCO, M. C. 2012. Role of BAG3 protein in leukemia cell survival and response to therapy. Biochimica et Biophysica Acta (BBA)-Reviews on Cancer, 1826, 365-369.

ROSATI, E., SABATINI, R., RAMPINO, G., TABILIO, A., DI IANNI, M., FETTUCCIARI, K., BARTOLI, A., COACCIOLI, S., SCREPANTI, I. & MARCONI, P. 2009. Constitutively activated Notch signaling is involved in survival and apoptosis resistance of B-CLL cells. Blood, The Journal of the American Society of Hematology, 113, 856-865.

ROSS, P. L., HUANG, Y. N., MARCHESE, J. N., WILLIAMSON, B., PARKER, K., HATTAN, S., KHAINOVSKI, N., PILLAI, S., DEY, S. & DANIELS, S. 2004. Multiplexed protein quantitation in Saccharomyces cerevisiae using amine-reactive isobaric tagging reagents. Molecular & cellular proteomics, 3, 1154-1169.

ROSSI, D., FANGAZIO, M., RASI, S., VAISITTI, T., MONTI, S., CRESTA, S., CHIARETTI, S., DEL GIUDICE, I., FABBRI, G. & BRUSCAGGIN, A. 2012. Disruption of BIRC3 associates with fludarabine chemorefractoriness in TP53 wild-type chronic lymphocytic leukemia. Blood, 119, 2854-2862.

ROSSI, D. & GAIDANO, G. 2013. Richter syndrome. Advances in Chronic Lymphocytic Leukemia. Springer.

ROSSI, D., KHIABANIAN, H., SPINA, V., CIARDULLO, C., BRUSCAGGIN, A., FAMÀ, R., RASI, S., MONTI, S., DEAMBROGI, C. & DE PAOLI, L. 2014. Clinical impact of small TP53 mutated subclones in chronic lymphocytic leukemia. Blood, The Journal of the American Society of Hematology, 123, 2139-2147.

ROWLAND, S. L., TREMBLAY, M. M., ELLISON, J. M., STUNZ, L. L., BISHOP, G. A. & HOSTAGER, B. S. 2007. A novel mechanism for TNFR-associated factor 6-dependent CD40 signaling. The Journal of Immunology, 179, 4645-4653.

RZAGALINSKI, I. & VOLMER, D. A. 2017. Quantification of low molecular weight compounds by MALDI imaging mass spectrometry–A tutorial review. Biochimica et Biophysica Acta (BBA)-Proteins and Proteomics, 1865, 726-739.

SÄEMANN, M., KELEMEN, P., ZEYDA, M., BÖHMIG, G. & STAFFLER, G. CD40 triggered human monocyte-derived dendritic cells convert to tolerogenic dendritic cells when JAK3 activity is inhibited. Transplantation proceedings, 2002. 1407-1408.

SÄEMANN, M. D., DIAKOS, C., KELEMEN, P., KRIEHUBER, E., ZEYDA, M., BÖHMIG, G. A., HÖRL, W. H., BAUMRUKER, T. & ZLABINGER, G. J. 2003. Prevention of CD40‐triggered dendritic cell maturation and induction of T‐cell hyporeactivity by targeting of Janus kinase 3. American Journal of Transplantation, 3, 1341-1349.

SAMUEL, J., JAYNE, S., CHEN, Y., MAJID, A., WIGNALL, A., WORMULL, T., NAJEEB, H., LUO, J.-L., JONES, G. D. & MACIP, S. 2016. Posttranscriptional upregulation of p53 by reactive oxygen species in chronic lymphocytic leukemia. Cancer research, 76, 6311-6319.

SANTONI, V., MOLLOY, M. & RABILLOUD, T. 2000. Membrane proteins and proteomics: un amour impossible? ELECTROPHORESIS: An International Journal, 21, 1054-1070.

SARTORIUS, R., D'APICE, L., BARBA, P., GUARDIOLA, J., SANTONI, A., VELOTTI, F. & DE BERARDINIS, P. 2003. Induction of human NK cell-mediated cytotoxicity by CD40 triggering on antigen presenting cells. Cellular immunology, 221, 81-88.

SATPATHY, S., WAGNER, S. A., BELI, P., GUPTA, R., KRISTIANSEN, T. A., MALINOVA, D., FRANCAVILLA, C., TOLAR, P., BISHOP, G. A. & HOSTAGER, B. S. 2015. Systems-wide analysis of BCR signalosomes and downstream phosphorylation and ubiquitylation. Molecular systems biology, 11, 810.

SCARFÒ, L., FERRERI, A. J. & GHIA, P. 2016. Chronic lymphocytic leukaemia. Critical reviews in oncology/hematology, 104, 169-182.

SCHIMMER, A. D., MUNK-PEDERSEN, I., MINDEN, M. D. & REED, J. C. 2003. Bcl-2 and apoptosis in chronic lymphocytic leukemia. Current treatment options in oncology, 4, 211-218.

SCHOENMAKERS, P. J. 1986. Optimization of chromatographic selectivity: a guide to method development, Elsevier.

SCHÖNBECK, U. & LIBBY, P. 2001. The CD40/CD154 receptor/ligand dyadRID="†" ID="†" Review. Cellular and Molecular Life Sciences CMLS, 58, 4-43.

SCHROERS, R., GRIESINGER, F., TRÜMPER, L., HAASE, D., KULLE, B., KLEIN-HITPASS, L., SELLMANN, L., DÜHRSEN, U. & DÜRIG, J. 2005. Combined analysis of ZAP-70 and CD38 expression as a predictor of disease progression in B-cell chronic lymphocytic leukemia. Leukemia, 19, 750-758.

SCHULZE, W. X. & USADEL, B. 2010. Quantitation in mass-spectrometry-based proteomics. Annual review of plant biology, 61, 491-516.

SCIELZO, C., APOLLONIO, B., SCARFO, L., JANUS, A., MUZIO, M., TEN HACKEN, E., GHIA, P. & CALIGARIS-CAPPIO, F. 2011. The functional in vitro response to CD40 ligation reflects a different clinical outcome in patients with chronic lymphocytic leukemia. Leukemia, 25, 1760-1767.

SEIFERT, M., SELLMANN, L., BLOEHDORN, J., WEIN, F., STILGENBAUER, S., DÜRIG, J. & KÜPPERS, R. 2012. Cellular origin and pathophysiology of chronic lymphocytic leukemia. Journal of Experimental Medicine, 209, 2183-2198.

SEIFFERT, M. 2020. HIF-1α: a potential treatment target in chronic lymphocytic leukemia. haematologica, 105, 856.

SEIJKENS, T., ENGEL, D., TJWA, M. & LUTGENS, E. 2010. The role of CD154 in haematopoietic development. Thrombosis and haemostasis, 104, 639-701.

SENGOKU, T., NUREKI, O., NAKAMURA, A., KOBAYASHI, S. & YOKOYAMA, S. 2006. Structural basis for RNA unwinding by the DEAD-box protein Drosophila Vasa. Cell, 125, 287-300.

SHAPIRO, H. M. 2005. Practical flow cytometry, John Wiley & Sons.

SHARMAN, J. P., BANERJI, V., FOGLIATTO, L. M., HERISHANU, Y., MUNIR, T., WALEWSKA, R., FOLLOWS, G., KARLSSON, K., GHIA, P. & CORBETT, G. 2019. ELEVATE TN: Phase 3 study of acalabrutinib combined with obinutuzumab (O) or alone vs o plus chlorambucil (Clb) in patients (Pts) with treatment-naive chronic lymphocytic leukemia (CLL). American Society of Hematology Washington, DC.

SHEN, Y., BEST, O. G., MULLIGAN, S. P. & CHRISTOPHERSON, R. I. 2018. Ibrutinib and idelalisib block immunophenotypic changes associated with the adhesion and activation of CLL cells in the tumor microenvironment. Leukemia & lymphoma, 59, 1927-1937.

SHILOH, Y. & ZIV, Y. 2013. The ATM protein kinase: regulating the cellular response to genotoxic stress, and more. Nature reviews Molecular cell biology, 14, 197-210.

SINGH, R., HARSHMAN, S. W., RUPPERT, A. S., MORTAZAVI, A., LUCAS, D. M., THOMAS-AHNER, J. M., CLINTON, S. K., BYRD, J. C., FREITAS, M. A. & PARTHUN, M. R. 2015. Proteomic profiling identifies specific histone species associated with leukemic and cancer cells. Clinical proteomics, 12, 1-14.

SLAGER, S. L., BENAVENTE, Y., BLAIR, A., VERMEULEN, R., CERHAN, J. R., COSTANTINI, A. S., MONNEREAU, A., NIETERS, A., CLAVEL, J. & CALL, T. G. 2014. Medical history, lifestyle, family history, and occupational risk factors for chronic lymphocytic leukemia/small lymphocytic lymphoma: the InterLymph Non-Hodgkin Lymphoma Subtypes Project. Journal of the National Cancer Institute Monographs, 2014, 41-51.

SLINGER, E., THIJSSEN, R., KATER, A. & ELDERING, E. 2017. Targeting antigen-independent proliferation in chronic lymphocytic leukemia through differential kinase inhibition. Leukemia, 31, 2601-2607.

SMALLWOOD, D. T., APOLLONIO, B., WILLIMOTT, S., LEZINA, L., ALHARTHI, A., AMBROSE, A. R., DE ROSSI, G., RAMSAY, A. G. & WAGNER, S. D. 2016. Extracellular vesicles released by CD40/IL-4–stimulated CLL cells confer altered functional properties to CD4+ T cells. Blood, 128, 542-552.

SMIT, L. A., HALLAERT, D. Y., SPIJKER, R., DE GOEIJ, B., JASPERS, A., KATER, A. P., VAN OERS, M. H., VAN NOESEL, C. J. & ELDERING, E. 2007. Differential Noxa/Mcl-1 balance in peripheral versus lymph node chronic lymphocytic leukemia cells correlates with survival capacity. Blood, 109, 1660-1668.

SMITH, C. A., FARRAH, T. & GOODWIN, R. G. 1994. The TNF receptor superfamily of cellular and viral proteins: activation, costimulation, and death. Cell, 76, 959-962.

SMOOK, M., HEERINGA, P., DAMOISEAUX, J., DAEMEN, M., DE WINTHER, M., GIJBELS, M., BECKERS, L., LUTGENS, E. & TERVAERT, J. C. 2005. Leukocyte CD40L deficiency affects the CD25+ CD4 T cell population but does not affect atherosclerosis. Atherosclerosis, 183, 275-282.

SNYDER, L. R., KIRKLAND, J. J. & GLAJCH, J. L. 2012. Practical HPLC method development, John Wiley & Sons.

SÖDERBERG, O., CHRISTIANSEN, I., CARLSSON, M. & NILSSON, K. 1997. CD40 ligation inhibits IL‐2 and SAC+ IL‐2 induced proliferation in chronic lymphocytic leukaemia cells. Scandinavian journal of immunology, 45, 706-714.

SOUERS, A. J., LEVERSON, J. D., BOGHAERT, E. R., ACKLER, S. L., CATRON, N. D., CHEN, J., DAYTON, B. D., DING, H., ENSCHEDE, S. H. & FAIRBROTHER, W. J. 2013. ABT-199, a potent and selective BCL-2 inhibitor, achieves antitumor activity while sparing platelets. Nature medicine, 19, 202-208.

SPERLING, J., AZUBEL, M. & SPERLING, R. 2008. Structure and function of the Pre-mRNA splicing machine. Structure, 16, 1605-1615.

STACCHINI, A., ARAGNO, M., VALLARIO, A., ALFARANO, A., CIRCOSTA, P., GOTTARDI, D., FALDELLA, A., REGE-CAMBRIN, G., THUNBERG, U. & NILSSON, K. 1999. MEC1 and MEC2: two new cell lines

derived from B-chronic lymphocytic leukaemia in prolymphocytoid transformation. Leukemia research, 23, 127-136.

STACCHINI, A., ARAGNO, M., VALLARIO, A., ALFARANO, A., CIRCOSTA, P., GOTTARDI, D., FALDELLA, A., REGE-CAMBRIN, G., THUNBERG, U. & NILSSON, K. 1999. MEC1 and MEC2: two new cell lines derived from B-chronic lymphocytic leukaemia in prolymphocytoid transformation. Leukemia research, 23, 127-136.

STALL, A. M., FARINAS, M. C., TARLINTON, D. M., LALOR, P. A., HERZENBERG, L. A. & STROBER, S. 1988. Ly-1 B-cell clones similar to human chronic lymphocytic leukemias routinely develop in older normal mice and young autoimmune (New Zealand Black-related) animals. Proceedings of the National Academy of Sciences, 85, 7312-7316.

STAMATOPOULOS, K., AGATHANGELIDIS, A., ROSENQUIST, R. & GHIA, P. 2017. Antigen receptor stereotypy in chronic lymphocytic leukemia. Leukemia, 31, 282-291.

STANKOVIC, T. & SKOWRONSKA, A. 2014. The role of ATM mutations and 11q deletions in disease progression in chronic lymphocytic leukemia. Leukemia & lymphoma, 55, 1227-1239.

STEVENSON, F. K., KRYSOV, S., DAVIES, A. J., STEELE, A. J. & PACKHAM, G. 2011. B-cell receptor signaling in chronic lymphocytic leukemia. Blood, The Journal of the American Society of Hematology, 118, 4313-4320.

STEWART, A. J., O'REILLY, E. J., MORIARTY, R. D., BERTONCELLO, P., KEYES, T. E., FORSTER, R. J. & DENNANY, L. 2015. A cholesterol biosensor based on the NIR electrogenerated-chemiluminescence (ECL) of water-soluble CdSeTe/ZnS quantum dots. Electrochimica Acta, 157, 8-14.

STILGENBAUER, S., EICHHORST, B. F., SCHETELIG, J., COUTRE, S., SEYMOUR, J. F., MUNIR, T., PUVVADA, S. D., WENDTNER, C.-M., ROBERTS, A. W. & JURCZAK, W. 2015. Venetoclax (ABT-199/GDC-0199) monotherapy induces deep remissions, including complete remission and undetectable MRD, in ultra-high risk relapsed/refractory chronic lymphocytic leukemia with 17p deletion: results of the pivotal international phase 2 study. American Society of Hematology Washington, DC.

STILGENBAUER, S., SCHNAITER, A., PASCHKA, P., ZENZ, T., ROSSI, M., DÖHNER, K., BÜHLER, A., BÖTTCHER, S., RITGEN, M. & KNEBA, M. 2014. Gene mutations and treatment outcome in chronic lymphocytic leukemia: results from the CLL8 trial. Blood, 123, 3247-3254.

STRATI, P., ABRUZZO, L. V., WIERDA, W. G., O'BRIEN, S., FERRAJOLI, A. & KEATING, M. J. 2015. Second cancers and Richter transformation are the leading causes of death in patients with trisomy 12 chronic lymphocytic leukemia. Clinical Lymphoma Myeloma and Leukemia, 15, 420-427.

STRAW, A. D., MACDONALD, A. S., DENKERS, E. Y. & PEARCE, E. J. 2003. CD154 plays a central role in regulating dendritic cell activation during infections that induce Th1 or Th2 responses. The Journal of Immunology, 170, 727-734.

SU, C.-Y., LIN, T.-C., LIN, Y.-F., CHEN, M.-H., LEE, C.-H., WANG, H.-Y., LEE, Y.-C., LIU, Y.-P., CHEN, C.-L. & HSIAO, M. 2015. DDX3 as a strongest prognosis marker and its downregulation promotes metastasis in colorectal cancer. Oncotarget, 6, 18602.

SU, X., LUCAS, D. M., ZHANG, L., XU, H., ZABROUSKOV, V., DAVIS, M. E., KNAPP, A. R., YOUNG, D. C., PAYNE, P. R. & PARTHUN, M. R. 2009. Validation of an LC–MS based approach for profiling histones in chronic lymphocytic leukemia. Proteomics, 9, 1197-1206.

SULLIVAN, C. A. & CHUNG, G. G. 2008. Biomarker validation: in situ analysis of protein expression using semiquantitative immunohistochemistry-based techniques. Clinical Colorectal Cancer, 7, 172-177.

SUN, M., SONG, L., LI, Y., ZHOU, T. & JOPE, R. S. 2008. Identification of an antiapoptotic protein complex at death receptors. Cell Death & Differentiation, 15, 1887-1900.

SUN, M., SONG, L., ZHOU, T., GILLESPIE, G. Y. & JOPE, R. S. 2011. The role of DDX3 in regulating Snail. Biochimica et Biophysica Acta (BBA)-Molecular Cell Research, 1813, 438-447.

SUN, M., ZHOU, T., JONASCH, E. & JOPE, R. S. 2013. DDX3 regulates DNA damage-induced apoptosis and p53 stabilization. Biochimica et Biophysica Acta (BBA)-Molecular Cell Research, 1833, 1489-1497.

SURICOC, N., DIANZANI, U., MEHTAD, K. & MALAVASI, F. 2000. CD38/CD31, a receptor/ligand system ruling adhesion and signaling in human leukocytes. Human CD38 and Related Molecules, 75, 99-120.

SUTANDY, F. R., QIAN, J., CHEN, C. S. & ZHU, H. 2013. Overview of protein microarrays. Current protocols in protein science, 72, 27.1. 1-27.1. 16.

SWERDLOW, S., CAMPO, E., HARRIS, N. L., JAFFE, E., PILERI, S., STEIN, H., THIELE, J., ARBER, D., HASSERJIAN, R. & LE BEAU, M. 2017. WHO classification of tumours of haematopoietic and lymphoid tissues (Revised 4th edition). IARC: Lyon, 421.

SZE, S. K., GE, Y., OH, H. & MCLAFFERTY, F. W. 2002. Top-down mass spectrometry of a 29-kDa protein for characterization of any posttranslational modification to within one residue. Proceedings of the National Academy of Sciences, 99, 1774-1779.

TANTRAVEDI, S., VESUNA, F., WINNARD JR, P. T., MARTIN, A., LIM, M., EBERHART, C. G., BERLINICKE, C., RAABE, E., VAN DIEST, P. J. & RAMAN, V. 2019. Targeting DDX3 in medulloblastoma using the small molecule inhibitor RK-33. Translational oncology, 12, 96-105.

TE RAA, G., DERKS, I., NAVRKALOVA, V., SKOWRONSKA, A., MOERLAND, P., VAN LAAR, J., OLDREIVE, C., MONSUUR, H., TRBUSEK, M. & MALCIKOVA, J. 2015. The impact of SF3B1 mutations in CLL on the DNA-damage response. Leukemia, 29, 1133-1142.

TEMPLIN, M. F., STOLL, D., SCHWENK, J. M., PÖTZ, O., KRAMER, S. & JOOS, T. O. 2003. Protein microarrays: promising tools for proteomic research. Proteomics, 3, 2155-2166.

TEN HACKEN, E. & BURGER, J. A. 2014. Molecular pathways: targeting the microenvironment in chronic lymphocytic leukemia—focus on the B-cell receptor. Clinical cancer research, 20, 548-556.

THIJSSEN, R., GEEST, C. R., DE ROOIJ, M. F., LIU, N., FLOREA, B. I., WELLER, K., OVERKLEEFT, H. S., VAN OERS, M. H., SPAARGAREN, M. & KATER, A. P. 2013. Possible mechanisms of resistance to the novel BH3-mimetic ABT-199 in in vitro lymph node models of CLL–the role of Abl and Btk. American Society of Hematology Washington, DC.

THIJSSEN, R., SLINGER, E., WELLER, K., GEEST, C. R., BEAUMONT, T., VAN OERS, M. H., KATER, A. P. & ELDERING, E. 2015. Resistance to ABT-199 induced by microenvironmental signals in chronic lymphocytic leukemia can be counteracted by CD20 antibodies or kinase inhibitors. Haematologica, 100, e302.

THOMPSON, A., SCHÄFER, J., KUHN, K., KIENLE, S., SCHWARZ, J., SCHMIDT, G., NEUMANN, T. & HAMON, C. 2003. Tandem mass tags: a novel quantification strategy for comparative analysis of complex protein mixtures by MS/MS. Analytical chemistry, 75, 1895-1904.

THURGOOD, L. A., CHATAWAY, T. K., LOWER, K. M. & KUSS, B. J. 2017. From genome to proteome: Looking beyond DNA and RNA in chronic lymphocytic leukemia. Journal of proteomics, 155, 73-84.

THURGOOD, L. A., DWYER, E. S., LOWER, K. M., CHATAWAY, T. K. & KUSS, B. J. 2019. Altered expression of metabolic pathways in CLL detected by unlabelled quantitative mass spectrometry analysis. British journal of haematology, 185, 65-78.

TISSINO, E., BENEDETTI, D., HERMAN, S. E., TEN HACKEN, E., AHN, I. E., CHAFFEE, K. G., ROSSI, F. M., DAL BO, M., BULIAN, P. & BOMBEN, R. 2018. Functional and clinical relevance of VLA-4 (CD49d/CD29) in ibrutinib-treated chronic lymphocytic leukemia. The Journal of experimental medicine, 215, 681-697.

TOBIAS, E. S., CONNOR, M. & FERGUSON-SMITH, M. 2011. Essential medical genetics, John Wiley & Sons.

TOMIHARA, K., KATO, K., MASUTA, Y., NAKAMURA, K., TANAKA, T., HIRATSUKA, H. & HAMADA, H. 2007. Gene transfer of the CD40-ligand to human dendritic cells induces NK-mediated antitumor effects against human carcinoma cells. International journal of cancer, 120, 1491-1498.

TRETTER, T., SCHULER, M., SCHNELLER, F., BRASS, U., ESSWEIN, M., AMAN, M. J., HUBER, C. & PESCHEL, C. 1998. Direct Cellular Interaction with Activated CD4+ T Cells Overcomes Hyporesponsiveness of B-Cell Chronic Lymphocytic Leukemiain Vitro. Cellular immunology, 189, 41-50.

TROMP, J. M., TONINO, S. H., ELIAS, J. A., JASPERS, A., LUIJKS, D. M., KATER, A. P., VAN LIER, R. A., VAN OERS, M. H. & ELDERING, E. 2010. Dichotomy in NF-κB signaling and chemoresistance in immunoglobulin variable heavy-chain-mutated versus unmutated CLL cells upon CD40/TLR9 triggering. Oncogene, 29, 5071-5082.

TSUKADA, N., BURGER, J. A., ZVAIFLER, N. J. & KIPPS, T. J. 2002. Distinctive features of “nurselike” cells that differentiate in the context of chronic lymphocytic leukemia. Blood, The Journal of the American Society of Hematology, 99, 1030-1037.

TURCOTTE, F., LAGASSÉ, P., PRUD'HOMME, D. & GENDRON, R. 1994. Regulated pre-employment medical examinations and their effect on the utilization of health services: the experience of 1,498 police cadets, Quebec, 1988. Canadian journal of public health= Revue canadienne de sante publique, 85, 348-350.

URBICH, C., MALLAT, Z., TEDGUI, A., CLAUSS, M., ZEIHER, A. M. & DIMMELER, S. 2001. Upregulation of TRAF-3 by shear stress blocks CD40-mediated endothelial activation. The Journal of clinical investigation, 108, 1451-1458.

VALLABHAPURAPU, S., MATSUZAWA, A., ZHANG, W., TSENG, P.-H., KEATS, J. J., WANG, H., VIGNALI, D. A., BERGSAGEL, P. L. & KARIN, M. 2008. Nonredundant and complementary functions of TRAF2 and TRAF3 in a ubiquitination cascade that activates NIK-dependent alternative NF-κB signaling. Nature immunology, 9, 1364.

VALSECCHI, R., COLTELLA, N., BELLONI, D., PONENTE, M., TEN HACKEN, E., SCIELZO, C., SCARFÒ, L., BERTILACCIO, M. T. S., BRAMBILLA, P. & LENTI, E. 2016. HIF-1α regulates the interaction of chronic lymphocytic leukemia cells with the tumor microenvironment. Blood, 127, 1987-1997.

VAN ATTEKUM, M. H., VAN BRUGGEN, J. A., SLINGER, E., LEBRE, M. C., REINEN, E., KERSTING, S., ELDERING, E. & KATER, A. P. 2017. CD40 signaling instructs chronic lymphocytic leukemia cells to attract monocytes via the CCR2 axis. haematologica, 102, 2069-2076.

VAN GENT, R., KATER, A. P., OTTO, S. A., JASPERS, A., BORGHANS, J. A., VRISEKOOP, N., ACKERMANS, M. A., RUITER, A. F., WITTEBOL, S. & ELDERING, E. 2008. In vivo dynamics of stable chronic lymphocytic leukemia inversely correlate with somatic hypermutation levels and suggest no major leukemic turnover in bone marrow. Cancer research, 68, 10137-10144.

VAN KOOTEN, C. & BANCHEREAU, J. 1997. Functions of CD40 on B cells, dendritic cells and other cells. Current opinion in immunology, 9, 330-337.

VAN KOOTEN, C. & BANCHEREAU, J. 2000. CD40-CD40 ligand. Journal of leukocyte biology, 67, 2-17.

VAN VOSS, M. H., VESUNA, F., BOL, G. M., AFZAL, J., TANTRAVEDI, S., BERGMAN, Y., KAMMERS, K., LEHAR, M., MALEK, R. & BALLEW, M. 2018. Targeting mitochondrial translation by inhibiting DDX3: a novel radiosensitization strategy for cancer treatment. Oncogene, 37, 63-74.

VAN VOSS, M. R. H., VAN DIEST, P. J. & RAMAN, V. 2017. Targeting RNA helicases in cancer: The translation trap. Biochimica et Biophysica Acta (BBA)-Reviews on Cancer, 1868, 510-520.

VAN VOSS, M. R. H., VESUNA, F., TRUMPI, K., BRILLIANT, J., BERLINICKE, C., DE LENG, W., KRANENBURG, O., OFFERHAUS, J. G., BÜRGER, H. & VAN DER WALL, E. 2015. Identification of the DEAD box RNA helicase DDX3 as a therapeutic target in colorectal cancer. Oncotarget, 6, 28312.

VANDER HEIDEN, M. G., CHANDEL, N. S., WILLIAMSON, E. K., SCHUMACKER, P. T. & THOMPSON, C. B. 1997. Bcl-xL regulates the membrane potential and volume homeostasis of mitochondria. Cell, 91, 627-637.

VARDI, A., AGATHANGELIDIS, A., SUTTON, L.-A., GHIA, P., ROSENQUIST, R. & STAMATOPOULOS, K. 2014. Immunogenetic studies of chronic lymphocytic leukemia: revelations and speculations about ontogeny and clinical evolution. Cancer research, 74, 4211-4216.

VOGLER, M., BUTTERWORTH, M., MAJID, A., WALEWSKA, R. J., SUN, X.-M., DYER, M. J. & COHEN, G. M. 2009. Concurrent up-regulation of BCL-XL and BCL2A1 induces approximately 1000-fold resistance to ABT-737 in chronic lymphocytic leukemia. Blood, The Journal of the American Society of Hematology, 113, 4403-4413.

VOLLBRECHT, C., MAIRINGER, F. D., KOITZSCH, U., PEIFER, M., KOENIG, K., HEUKAMP, L. C., CRISPATZU, G., WILDEN, L., KREUZER, K.-A. & HALLEK, M. 2015. Comprehensive analysis of disease-related genes in chronic lymphocytic leukemia by multiplex PCR-based next generation sequencing. PloS one, 10, e0129544.

VON TRESCKOW, J., EICHHORST, B., BAHLO, J. & HALLEK, M. 2019. The treatment of chronic lymphatic leukemia. Deutsches Ärzteblatt International, 116, 41.

WALKER, J. M. 2005. The proteomics protocols handbook, Springer.

WALSBY, E., PEARCE, L., BURNETT, A. K., FEGAN, C. & PEPPER, C. 2012. The Hsp90 inhibitor NVP-AUY922-AG inhibits NF-κB signaling, overcomes microenvironmental cytoprotection and is highly synergistic with fludarabine in primary CLL cells. Oncotarget, 3, 525.

WALSH, C. 2006. Posttranslational modification of proteins: expanding nature's inventory, Roberts and Company Publishers.

WALSH, G. 2002. Biochemistry and Biotechnology. John Willey & Sons.

WANG, D., FREEMAN, G. J., LEVINE, H., RITZ, J. & ROBERTSON, M. J. 1997. Role of the CD40 and CD95 (APO-1/Fas) antigens in the apoptosis of human B-cell malignancies. British journal of haematology, 97, 409-417.

WANG, L., LAWRENCE, M. S., WAN, Y., STOJANOV, P., SOUGNEZ, C., STEVENSON, K., WERNER, L., SIVACHENKO, A., DELUCA, D. S. & ZHANG, L. 2011. SF3B1 and other novel cancer genes in chronic lymphocytic leukemia. New England Journal of Medicine, 365, 2497-2506.

WANG, Y.-H., FAN, L., WANG, L., ZHANG, R., ZOU, Z.-J., FANG, C., ZHANG, L.-N., LI, J.-Y. & XU, W. 2013. Expression levels of Lyn, Syk, PLCγ2 and ERK in patients with chronic lymphocytic leukemia, and higher levels of Lyn are associated with a shorter treatment-free survival. Leukemia & lymphoma, 54, 1165-1170.

WANG, Z., KARRAS, J. G., HOWARD, R. G. & ROTHSTEIN, T. L. 1995. Induction of bcl-x by CD40 engagement rescues sIg-induced apoptosis in murine B cells. The Journal of Immunology, 155, 3722-3725.

WANG, Z., RAO, D. D., SENZER, N. & NEMUNAITIS, J. 2011. RNA interference and cancer therapy. Pharmaceutical research, 28, 2983-2995.

WANG, Z., SHEN, G.-H., XIE, J.-M., LI, B. & GAO, Q.-G. 2018. Rottlerin upregulates DDX3 expression in hepatocellular carcinoma. Biochemical and biophysical research communications, 495, 1503-1509.

WASINGER, V. C., CORDWELL, S. J., CERPA-POLJAK, A., YAN, J. X., GOOLEY, A. A., WILKINS, M. R., DUNCAN, M. W., HARRIS, R., WILLIAMS, K. L. & HUMPHERY-SMITH, I. 1995. Progress with gene-product mapping of the Mollicutes: Mycoplasma genitalium. Electrophoresis, 16, 1090-1094.

WILLIMOTT, S., BAOU, M., HUF, S. & WAGNER, S. D. 2007. Regulation of CD38 in proliferating chronic lymphocytic leukaemia cells stimulated with CD154 and IL-4.

WILLIMOTT, S., MERRIAM, T. & WAGNER, S. D. 2011. Apoptosis induces Bcl-XS and cleaved Bcl-XL in chronic lymphocytic leukaemia. Biochemical and biophysical research communications, 405, 480-485.

WITKOWSKA, M., NOWAK, W., CEBULA-OBRZUT, B., MAJCHRZAK, A., MEDRA, A., ROBAK, T. & SMOLEWSKI, P. 2014. Spontaneous in vitro apoptosis of de novo chronic lymphocytic leukemia cells correlates with risk of the disease progression. Cytometry Part B: Clinical Cytometry, 86, 410-417.

WOODLOCK, T. J., BETHLENDY, G. & SEGEL, G. B. 2001. Prohibitin expression is increased in phorbol ester-treated chronic leukemic B-lymphocytes. Blood Cells, Molecules, and Diseases, 27, 27-34.

WRIGHT, E. P., PARTRIDGE, M. A., PADULA, M. P., GAUCI, V. J., MALLADI, C. S. & COORSSEN, J. R. 2014. Top-down proteomics: Enhancing 2D gel electrophoresis from tissue processing to high-sensitivity protein detection. Proteomics, 14, 872-889.

WU, C. 2007. Focal adhesion: a focal point in current cell biology and molecular medicine. Cell adhesion & migration, 1, 13-18.

WU, D.-W., LIU, W.-S., WANG, J., CHEN, C.-Y., CHENG, Y.-W. & LEE, H. 2011. Reduced p21WAF1/CIP1 via Alteration of p53-DDX3 pathway is associated with poor relapse-free survival in early-stage human papillomavirus–associated lung cancer. Clinical Cancer Research, 17, 1895-1905.

WU, S.-J., CHIANG, C.-J., LIN, C.-T., TIEN, H.-F. & LAI, M.-S. 2016. A nationwide population-based cross-sectional comparison of hematological malignancies incidences between Taiwan and the United States of America. Annals of hematology, 95, 165-167.

WU, S.-J., HUANG, S.-Y., LIN, C.-T., LIN, Y.-J., CHANG, C.-J. & TIEN, H.-F. 2010. The incidence of chronic lymphocytic leukemia in Taiwan, 1986-2005: a distinct increasing trend with birth-cohort effect. Blood, The Journal of the American Society of Hematology, 116, 4430-4435.

XIE, M., VESUNA, F., BOTLAGUNTA, M., BOL, G. M., IRVING, A., BERGMAN, Y., HOSMANE, R. S., KATO, Y., WINNARD JR, P. T. & RAMAN, V. 2015. NZ51, a ring-expanded nucleoside analog, inhibits motility and viability of breast cancer cells by targeting the RNA helicase DDX3. Oncotarget, 6, 29901.

XIE, M., VESUNA, F., TANTRAVEDI, S., BOL, G. M., VAN VOSS, M. R. H., NUGENT, K., MALEK, R., GABRIELSON, K., VAN DIEST, P. J. & TRAN, P. T. 2016. RK-33 radiosensitizes prostate cancer cells by blocking the RNA helicase DDX3. Cancer research, 76, 6340-6350.

XIE, P., HOSTAGER, B. S. & BISHOP, G. A. 2004. Requirement for TRAF3 in signaling by LMP1 but not CD40 in B lymphocytes. The Journal of experimental medicine, 199, 661-671.

XIE, P., HOSTAGER, B. S., MUNROE, M. E., MOORE, C. R. & BISHOP, G. A. 2006. Cooperation between TNF receptor-associated factors 1 and 2 in CD40 signaling. The Journal of Immunology, 176, 5388-5400.

YAMAMOTO, S., NAKANISHI, K. & MATSUNO, R. 1988. Ion-exchange chromatography of proteins, CRC Press.

YEH, W.-C., SHAHINIAN, A., SPEISER, D., KRAUNUS, J., BILLIA, F., WAKEHAM, A., DE LA POMPA, J. L., FERRICK, D., HUM, B. & ISCOVE, N. 1997. Early lethality, functional NF-κB activation, and increased sensitivity to TNF-induced cell death in TRAF2-deficient mice. Immunity, 7, 715-725.

YOLKEN, R. H. 1980. Enzyme-linked immunosorbent assay (ELISA): a practical tool for rapid diagnosis of viruses and other infectious agents. The Yale journal of biology and medicine, 53, 85.

YOUNES, A., SNELL, V., CONSOLI, U., CLODI, K., ZHAO, S., PALMER, J. L., THOMAS, E. K., ARMITAGE, R. J. & ANDREEFF, M. 1998. Elevated levels of biologically active soluble CD40 ligand in the serum of patients with chronic lymphocytic leukaemia. British journal of haematology, 100, 135-141.

ZARNEGAR, B. J., WANG, Y., MAHONEY, D. J., DEMPSEY, P. W., CHEUNG, H. H., HE, J., SHIBA, T., YANG, X., YEH, W.-C. & MAK, T. W. 2008. Noncanonical NF-κB activation requires coordinated assembly of a regulatory complex of the adaptors cIAP1, cIAP2, TRAF2 and TRAF3 and the kinase NIK. Nature immunology, 9, 1371-1378.

ZENZ, T., KRÖBER, A., SCHERER, K., HÄBE, S., BÜHLER, A., BENNER, A., DENZEL, T., WINKLER, D., EDELMANN, J. & SCHWÄNEN, C. 2008. Monoallelic TP53 inactivation is associated with poor prognosis in chronic lymphocytic leukemia: results from a detailed genetic characterization with long-term follow-up. Blood, The Journal of the American Society of Hematology, 112, 3322-3329.

ZHANG, B., WHITEAKER, J. R., HOOFNAGLE, A. N., BAIRD, G. S., RODLAND, K. D. & PAULOVICH, A. G. 2019. Clinical potential of mass spectrometry-based proteogenomics. Nature Reviews Clinical Oncology, 16, 256-268.

ZHANG, F., WEN, Y. & GUO, X. 2014. CRISPR/Cas9 for genome editing: progress, implications and challenges. Human molecular genetics, 23, R40-R46.

ZHENG, X., LI, Y., LI, X. C., ROY-CHAUDHURY, P., NICKERSON, P., TIAN, Y., SAYEGH, M. & STROM, T. Blockade of CD40L/CD40 costimulatory pathway in a DST presensitization model of islet allograft leads to a state of Allo-Ag specific tolerance and permits subsequent engraftment of donor strain islet or heart allografts. Transplantation proceedings, 1999. Elsevier, 627-628.

ZHUANG, J., LAING, N., OATES, M., LIN, K., JOHNSON, G. & PETTITT, A. R. 2014. Selective IAP inhibition results in sensitization of unstimulated but not CD 40‐stimulated chronic lymphocytic leukaemia cells to TRAIL‐induced apoptosis. Pharmacology research & perspectives, 2, e00081.

ZIMMERMANN, M. & MEYER, N. 2011. Annexin V/7-AAD staining in keratinocytes. Mammalian Cell Viability. Springer.

Appendix

Appendix 1. The information about the materials and the component of reagents used to complete Western blotting

RIPA buffer for lysis (100ml)

Components	Quantum	Company	Catalogue NO.
50mM Tris pH7.6	5ml of 1M stock	SIGMA	77861
1% (w/v) Triton-X100	1ml of 100%	SIGMA	9002931
150mM NaCl	3ml of 5M stock	SIGMA	7647145
0.1% (w/v) SDS	0.5ml of 20% stock	SIGMA	151213
0.5%(w/v) Na Deoxycholate	5ml of 10% stock	SIGMA	302954
dH2O	85.5ml	Laboratory scope	-
Protease inhibitors (before use)	10µl/ml	SIGMA	P8430
Phosphatase inhibitor	10µl/ml	Millipore	524625

4×Sample buffer (50ml)

Components	Quantum	Company	Catalogue NO.
250mM Tris-HCl (pH6.8)	12.5ml of 500mM Tris-HCl	SIGMA	1185531
SDS	20ml 20%SDS	SIGMA	151213
Glycerol	17.5ml for 20%SDS	Fisher Chemical	56815
Bromophenol blue	0.07g	Fisher BioReagents	115399

Note: Add 25µl/ml β-mercaptoethanol (catalogue number 60242, SIGMA) before use.

2×Sample buffer (100ml)

Components	Quantum	Company	Catalogue NO.
125mM Tris-HCl (pH6.8)	6.25ml of 1M Tris-HCl	SIGMA	1185531
SDS	10ml 20%SDS	SIGMA	151213
Glycerol	15ml	Fisher Chemical	56815
Bromophenol blue	50mg	Fisher BioReagents	115399
20mM EDTA	2ml of 500mM EDTA stock	SIGMA	6004
dH2O	16.75ml	Laboratory scope	-

Note: Add 50µl/ml β-mercaptoethanol (catalogue number 60242, SIGMA) before use.
1×Sample buffer consists of 1:1 2×Sample buffer and dH_2O adding 100µl/ml β-mercaptoethanol (catalogue number 60242, SIGMA) before use.

Resolving gel (12%)

Components	10ml	20ml	Company	Catalogue NO.
30% Acrylamide	4ml	8ml	National Diagnostics	EC890
4×ProtoGel®Resolving Buffer	2.5ml	5ml	National Diagnostics	EC892
dH2O	3.4ml	6.8ml	Laboratory scope	-
10% APS	100µl	200µl	SIGMA	7727540
TEMED	4µl	8µl	SIGMA	T7024

Stacking gel (5%)

Components	5ml	10ml	Company	Catalogue NO.
30% Acrylamide	830µl	1.7ml	National Diagnostics	EC890
ProtoGel®Stacking Buffer	1.25ml	2.5ml	National Diagnostics	EC892
dH2O	2.9ml	5.7ml	Laboratory scope	-
10% APS	50µl	100µl	SIGMA	7727540
TEMED	5µl	10µl	SIGMA	T7024

Running buffer (0.1%SDS)

Components	Quantum	Company	Catalogue NO.
dH2O	900ml	Laboratory scope	-
10×Tris 0.25M Glycine (1.92M) solution	100ml	National Diagnostics	EC880
20%SDS	5ml	SIGMA	151213

Transfer buffer

Components	Quantum	Company	Catalogue NO.
dH2O	900ml	Laboratory scope	-
10×Tris 0.25M Glycine (1.92M) solution	100ml	National Diagnostics	EC880

1M Tris-HCl (pH7.5)

Components	Quantum	Company	Catalogue NO.
Tris-base	121.14g in 900ml dH2O	Fisher BioReagents	77861
Concentrated HCl to pH7.5	-	SIGMA	7647010
dH2O	Add up to 1000ml	Laboratory scope	-

10×TBST

Components	Quantum	Company	Catalogue NO.
1M Tris-HCl (pH7.5)	200ml	Fisher BioReagents	EC890
5M NaCl (292.2g in 1000ml dH2O)	300ml	SIGMA	7647145
dH2O	490ml	Laboratory scope	-
Tween-20	10ml	Fisher BioReagents	153087

1×TBST

Components	Quantum	Company	Catalogue NO.
10×TBST	100ml	Laboratory scope	-
dH2O	900ml	Laboratory scope	-

5% milk/1×TBST – Blocking solution

Components	Quantum	Company	Catalogue NO.
Dried milk powder	5g	-	-
1×TBST	100ml	Laboratory scope	-

Appendix 2. The percentage of the CD5 and CD19 double-positive cells and the initial viability of the CLL samples used in this project

Case No.	Purity (%)	Iso-type control (%)	Initial Viability (%)
#3369	97.74	0.05	85.7
#3381	97.05	0.09	89.4
#3396	97.25	0.13	75.9
#3637	84.15	0.05	87.4
#3640	98.44	0.58	89.9
#3642	94.97	2.99	83
#3274	98.17	0.18	74.3
#3368	98.24	0.43	77.1
#3436	96.56	3.11	89.7
#3259	91.82	0.04	63.6
#3684	97.38	0.13	48.05
#3679	97.12	0.09	60.1
#3564	97.88	0.18	74.4
#3568	99.54	0.26	78.45
#3585	97.39	0.49	71.8
#3587	99.16	0.15	74.8
#3605	98.64	0.06	88.2
#3607	93.64	0.22	76.1
#3606	98.34	0.05	92.4
#3650	82.63	0.33	76.3
#3375	99.10	0.06	86.1
#3724	92.57	0.14	75.9
#3726	95.54	0.43	89.3
#3411	91.49	0.35	81.8

Appendix 3. The clinical information of the CLL samples used in this project

Case No.	Gender	Age at Diagnosis	Age at sample collection	IGVH status	Chromosomal status	TP53 mutation	Staging (Rai-Binnet Score)	WBC	Absolute Lymphocyte Count	Date of sample collection	Treated or not when collected the sample
#3369	male	37	39	NA	13q-	NA	NA	163.5	157	01.10.2013	untreated
#3381	female	67	74	NA	normal	NA	NA	157.4	149.7	13.01.2014	treated
#3396	female	53	67	NA	17p-	NA	C	80.2	76.1	02.04.2014	treated
#3637	male	66	69	unmutated	11q-, 13q-	no	A	144.6	134.9	24.01.2018	untreated
#3640	male	78	82	unmutated	13q- equivocal	no	A	177.5	163.4	31.01.2018	untreated
#3642	male	67	73	unmutated	normal	no	C	129.4	122.8	31.01.2018	treated
#3259	male	NA	70	NA	NA	NA	NA	209	123.1	20.07.2011	treated
#3411	male	NA	72	unmutated	11q-, 13q-	NA	C	167.3	155.6	15.05.2014	treated
#3274	female	NA	54	NA	normal	NA	NA	167.6	157	12.12.2011	untreated
#3368	male	NA	78	NA	NA	NA	NA	163.3	156.8	26.09.2013	NA
#3436	male	NA	72	NA	13q-	NA	B	144.3	137	27.11.2014	untreated
#3684	male	75	84	mutated	13q-	no	A	230.1	220.8	28.06.2018	untreated
#3679	male	53	54	NA	13q-	no	C	171.4	164.7	06.06.2018	untreated
#3564	male	52	84	NA	11q-, 13q-	NA	C	63	58.7	28.06.2017	treated
#3568	male	72	76	unmutated	normal	no	C	155.8	148.9	20.06.2017	treated
#3585	male	66	68	unmutated	11q-, 13q-	no	A	109	101.4	16.08.2017	untreated
#3587	male	54	55	mutated	13q-	no	NA	257.2	>200	16.08.2017	untreated
#3605	male	60	63	mutated	13q-	no	B	252.8	244	27.09.2017	untreated
#3607	male	66	69	mutated	normal	no	B	254.2	247.7	02.10.2017	untreated
#3606	male	58	67	unmutated	13q-	no	B	109.2	103.6	28.09.2017	treated
#3650	female	63	70	mutated	normal	no	B	119.6	110	17.03.2018	untreated
#3375	male	NA	54	NA	17p-	NA	C	227.4	222.9	04.11.2013	untreated
#3724	female	51	55	mutated	normal	no	NA	112.8	104.5	12.02.2019	untreated
#3726	male	68	76	unmutated	normal	no	C	178.8	173.5	04.03.2019	untreated

Appendix 4. Significantly up-regulated genes induced by the soluble CD40 ligand in primary CLL cells at 12h time point

12h up-regulated	Expression LevelS12	Expression LevelU12	12h up-regulated	Expression LevelS12	Expression LevelU12	12h up-regulated	Expression LevelS12	Expression LevelU12
AAGAB	9.256011	9.003318	GRHPR	9.263214	8.051995	PSIMCT-1	5.663009	5.191410
AAR2	9.346214	9.043955	GRIK4	4.191847	2.609938	PSMA1	9.173545	8.666355
AARS	10.189509	9.466772	GRINA	10.725953	9.835385	PSMA2	8.088428	7.656642
ABCC4	7.577703	6.366143	GRN	11.603842	11.054979	PSMA4	9.321643	8.750837
ABCD2	6.118235	5.544507	GRSF1	9.977703	9.312355	PSMA7	9.199402	8.917967
ABCE1	9.538806	8.855400	GRWD1	9.628595	9.145817	PSMB2	9.203474	8.699490
ABCF1	9.648649	9.232733	GSPT1	10.112179	9.852286	PSMB3	6.115053	5.685184
ABCF2	9.019185	8.551853	GSTP1	11.064527	10.677623	PSMB5	9.151188	8.483791
ABHD17C	6.495063	5.805425	GTDC1	6.793932	6.161983	PSMC4	8.483435	8.116819
ABTB2	10.337517	7.844249	GTF2A1	10.411366	10.130684	PSMD1	7.306777	6.737840
AC003665.1	3.863562	3.282114	GTF2E1	8.760415	8.530163	PSMD11	9.784806	9.450524
AC147651.4	8.334240	7.436902	GTF2F2	7.653450	7.297758	PSMD14	7.390923	6.938708
ACADVL	11.497702	11.178647	GTF2H5	7.710751	7.369063	PSMD3	10.259729	9.908698
ACBD6	8.238478	7.806272	GTF3C4	8.928162	8.528596	PSMD7	9.957423	9.617296
ACHE	5.969000	4.618249	GTF3C6	7.343403	6.659632	PSMD8	9.781932	9.529896
ACKR3	6.145289	5.514225	GTPBP4	8.651006	8.069171	PSME3	11.131769	10.562255
ACOT2	8.391101	8.064345	GTPBP6	10.100292	9.819894	PSMG3	9.665421	9.190929
ACOT4	6.680733	5.664072	GYS1	8.930057	8.652322	PTEN	10.552010	10.303792
ACSL1	9.308463	8.628872	H6PD	10.279945	9.982420	PTENP1	9.654346	9.440832
ACSL4	9.858334	8.975369	HAPLN3	6.956224	4.845370	PTGER4	10.307080	9.694277
ACTB	15.611714	14.544635	HBS1L	8.458305	8.160482	PTGES2	9.749565	9.078002
ACTG1	13.781399	13.105393	HCG18	9.258225	8.985932	PTGES3	11.574262	11.244639
ACTN4	9.903357	9.553102	HCG26	7.979811	7.382561	PTGIR	9.471067	6.483238
ACTR1B	10.333735	9.905625	HCG4B	7.620615	7.255750	PTGS1	6.158393	5.604180
ACTR2	12.645088	12.368916	HCLS1	10.231580	9.949346	PTK2B	10.358451	9.838244
ACTR3	11.783228	11.116749	HCP5	11.245443	10.386545	PTMS	9.088485	8.380509
ACTR3B	6.620526	5.803147	HDAC9	9.212388	8.619653	PTP4A2	11.968089	11.790436
ADA	7.510680	6.880008	HDGF	11.181015	10.970992	PTP4A3	6.091216	5.120392
ADAM8	10.023564	9.518922	HEATR1	7.315771	6.918060	PTPN1	12.384293	11.933975
ADAMDEC1	7.139362	5.494089	HEATR2	8.174699	7.661946	PTPN11	10.495493	10.165320
ADAMTS7	8.372208	7.057737	HEG1	8.154099	7.793908	PTRH1	5.771048	5.102195
ADAT2	7.506210	7.022905	HERPUD1	11.852293	10.925377	PTRH2	8.369742	7.835384
ADCY3	7.367668	6.614701	HIAT1	9.147558	8.890987	PUF60	9.613488	9.203292
ADIRF	5.459807	4.518399	HIGD1A	8.853699	8.319363	PUS7	6.807199	5.913644
ADM2	6.670071	4.766879	HIGD2A	8.967330	8.698724	PVR	6.680267	6.066827
ADO	10.428206	9.974932	HILPDA	7.315397	6.554359	PVRL1	9.909654	8.370234
ADPRH	10.892489	9.994082	HIRA	9.409655	9.051076	PVT1	7.064409	6.352451
ADRBK2	10.557090	10.352690	HIVEP1	11.485925	11.126778	PYCR1	8.638816	6.002589
ADSL	7.307228	6.733004	HIVEP3	7.975547	7.613628	PYCRL	8.085164	7.635504
AEN	10.299696	9.916067	HK2	8.531849	7.539227	QTRT1	9.320957	8.823283
AFG3L2	9.051034	8.689496	HLA-A	13.677543	13.340863	QTRTD1	9.511574	9.207938
AGFG1	10.009360	9.659038	HLA-B	14.117028	13.747961	RAB10	11.057099	10.704691
AGMAT	7.326662	6.461741	HLA-C	13.145320	12.789693	RAB11A	10.027781	9.487014
AGPAT3	11.094415	10.518510	HLA-DQA1	9.679669	8.821028	RAB12	8.461320	8.164088
AGPAT6	10.819073	10.601589	HLA-DQA2	7.565875	6.877922	RAB13	9.178755	7.820693
AGRN	7.658349	6.870882	HLA-E	14.520928	14.114734	RAB1B	11.118396	10.908575
AGTRAP	7.559562	6.952701	HLA-F	12.100771	11.262980	RAB21	10.936219	10.175567
AHCY	9.067913	8.563794	HLA-L	7.627063	6.676007	RAB27A	8.808915	8.542725
AIFM2	8.010675	7.703569	HMGA1	11.177178	10.310230	RAB39A	6.862118	6.327111
AIMP1	8.654396	8.369632	HMGCR	8.646798	8.294940	RAB39B	9.035531	8.767330
AIMP2	7.421053	6.589969	HMGCS1	9.778085	9.124515	RAB3GAP2	9.918136	9.432611
AK2	10.338549	9.931328	HMGN1	10.352153	10.142080	RAB3IP	8.467985	8.105754
AKAP1	8.527040	8.204112	HN1L	10.357663	9.736927	RAB7L1	11.870498	10.686606
AKR1A1	8.924394	8.286027	HNF1B	4.627412	3.670208	RAB8B	11.235435	10.795309
ALCAM	9.038592	8.403593	HNRNPAB	10.413653	10.101189	RAB9A	9.916596	8.491283
ALDH18A1	8.759973	8.432149	HNRNPC	11.462771	11.222112	RABEPK	6.766994	6.382401

ALDH1B1	9.099338	7.815578	HNRNPF	12.396139	12.105977	RABL3	8.484302	7.895676
ALDH2	6.961776	5.831180	HNRNPK	11.623456	11.322897	RAC1	10.275315	9.999725
ALDH4A1	6.654372	6.231954	HNRNPLL	7.591413	7.250920	RAD21	11.033243	10.813024
ALKBH2	7.718734	7.127971	HNRNPM	11.406021	11.009740	RAD23A	10.131143	9.916437
ALPK1	7.502941	7.119979	HNRNPR	10.850992	10.423518	RAD23B	10.682054	10.396216
ALYREF	8.775687	8.407182	HNRNPU	12.194361	11.892015	RAD50	8.573766	8.162928
AMMECR1L	9.493709	9.223611	HOMEZ	9.007058	8.332257	RAD51B	6.044670	5.321608
ANAPC11	7.895185	7.549517	HOXB9	4.551969	3.080923	RAD51D	7.913949	7.301516
ANAPC16	11.135178	10.762998	HPRT1	7.360438	6.971148	RAET1K	4.338818	3.715513
ANAPC7	9.127265	8.755856	HSD17B10	8.216727	7.845982	RALA	9.870172	9.231925
ANKLE2	12.083160	10.907245	HSD17B12	8.641750	8.266814	RAN	10.377104	9.969764
ANKRD10	11.778189	10.869217	HSF5	7.213046	6.802449	RANBP1	8.168864	7.876727
ANKRD33B	11.104928	8.242676	HSP90AA1	12.917488	12.640526	RANGAP1	11.138740	10.729797
ANKRD40	9.615788	9.282026	HSP90AB1	12.604690	11.961245	RAP1A	9.332633	9.091226
ANO9	10.394148	9.739824	HSP90B1	9.788531	9.102982	RAP1B	8.631704	8.280213
ANP32A	10.473727	9.857048	HSP90B2P	10.339330	9.604162	RAP2A	10.020897	9.219124
ANP32AP1	9.102031	8.555915	HSPA5	12.301816	11.354424	RAPGEF1	13.301506	12.868224
ANP32B	10.169018	9.875351	HSPA8	12.762689	12.236699	RARA	10.845141	10.328107
ANP32C	6.587065	5.946851	HSPA9	10.062931	9.789998	RASGRP1	8.091857	7.474283
ANP32E	11.299989	10.875229	HSPBP1	8.313820	7.547349	RASGRP3	9.913317	9.497151
ANXA2	8.797058	8.205150	HTATIP2	8.818797	8.502679	RASSF2	12.255757	11.682624
ANXA2P2	11.836475	11.233888	HTRA2	10.016193	9.249324	RASSF4	8.931454	7.446972
ANXA5	9.631339	9.051796	HUS1	7.610643	7.206752	RAVER1	10.353988	9.923348
ANXA6	7.482076	6.572545	HUWE1	10.671940	10.202379	RBBP9	9.774705	9.058142
ANXA7	9.959067	8.971183	HYAL2	7.959797	7.585948	RBM12	10.648325	10.110669
AP1AR	9.312161	8.877617	HYLS1	7.736969	7.160555	RBM19	9.577846	9.113838
AP1S2	8.850973	8.568426	HYOU1	11.616451	10.406065	RBM3	11.180729	10.528096
AP1S3	10.968400	10.257385	IARS	8.423948	7.618998	RBMXL1	9.528496	9.204034
AP2B1	10.936047	10.748371	IBTK	8.826112	8.541871	RBPJ	10.978764	10.374523
APEX1	11.024108	10.685236	ICAM1	11.377633	9.065293	RCC1	8.652468	8.175380
API5	10.435192	10.148789	ICAM5	6.102511	5.132353	RCC2	11.205569	10.812909
APLF	5.985820	5.389928	IDI2	6.209045	5.770746	RCCD1	8.032754	7.586998
APMAP	10.202233	9.932862	IER2	12.421553	12.071578	RCL1	7.190208	6.729486
APOA1BP	7.912845	7.582394	IER3	10.689677	9.128214	RCN1	6.725084	5.087660
APOBEC3C	10.846960	10.343415	IER5	13.697152	13.211522	RELB	11.598600	10.944967
APOBEC3G	11.322227	10.632457	IFFO2	9.133017	8.815325	RELT	10.642824	10.077155
APOL1	8.169604	7.603972	IFIH1	9.329084	8.589873	REXO4	9.533940	9.244496
APPL1	10.483406	10.127446	IFNGR1	9.698731	9.245856	RFC2	7.262540	6.848776
APRT	8.941912	8.376543	IFNGR2	10.815312	10.107537	RFFL	7.529424	6.785458
AREL1	9.629572	9.358834	IFNLR1	11.041222	10.581757	RFK	8.569090	8.244520
ARF3	11.519796	11.034853	IFRD2	7.584502	7.202052	RFTN1	12.584965	10.744772
ARFRP1	9.072079	8.778852	IGF2BP3	5.211991	4.525232	RFX5	11.238357	10.548310
ARHGAP17	9.706396	9.202335	IGSF3	11.560030	9.803718	RGS1	9.324597	8.801499
ARHGAP23	4.808932	4.095887	IKBKE	7.360930	6.830859	RHBDF1	5.966780	5.436807
ARHGAP24	10.694199	10.195834	IKZF1	12.063314	11.511552	RHBDF2	9.482415	9.124876
ARHGAP31	10.764561	9.336045	IL10	7.423423	6.552633	RHOA	12.784304	12.584038
ARHGDIA	12.299706	11.937890	IL13RA1	10.317806	8.445946	RHOF	6.291897	4.477722
ARHGEF12	9.398122	8.931677	IL17REL	6.892092	5.005894	RHOG	11.426735	10.489954
ARHGEF2	11.415668	10.830021	IL21R	11.914741	10.152103	RIMS3	7.841725	6.773615
ARID5A	10.768647	10.160957	IL21R-AS1	5.121855	4.215186	RIOK1	7.981105	7.484223
ARL1	8.869260	8.554881	IL23A	7.345607	6.931515	RIPK2	7.752799	7.330298
ARL13B	7.506652	7.206905	IL2RA	11.510583	10.888850	RND1	7.749141	7.372651
ARL14EP	8.799172	8.536348	IL2RG	12.174424	11.625127	RNF115	8.311515	7.933530
ARL2	8.169176	7.592133	IL4I1	9.182611	6.512612	RNF121	8.841872	8.359273
ARL8B	10.578694	10.207872	IL6R	9.633417	8.808908	RNF145	10.609933	9.442461
ARMC5	9.337959	9.046180	IL7	7.890480	6.909876	RNF19B	10.113722	9.451164
ARMC6	8.355739	7.663511	ILDR1	3.839730	3.153503	RNF207	6.488288	4.867717
ARNTL2	7.814163	4.868201	ILF2	9.924035	9.605054	RNF208	4.823199	3.920208
ARPC1B	9.608316	9.340805	IMP4	8.086554	7.755140	RNGTT	8.651627	8.377867
ARPC2	10.455337	9.994432	IMPACT	5.946046	5.484599	RNU105A	3.887342	3.094583
ARPC4	11.537078	11.051833	INADL	8.196151	7.877720	ROMO1	8.724796	8.349268

ARPC5	11.400014	10.879719	INTS3	9.108029	8.603054	RP1-	3.569691	2.675058
ARPP19	12.155098	11.793856	INTS6	9.751409	9.009740	RP11-	3.323552	2.796464
ARRDC3-	5.177772	4.507539	INTS9	7.471791	7.102505	RP11-	5.782077	4.850655
ARSB	7.943820	7.618619	IPO4	6.667753	6.164576	RP11-	4.348011	3.287398
ASCC3	8.136109	7.742027	IPO5	9.795220	9.227020	RP11-	5.267217	4.611505
ASNA1	8.430965	8.118900	IPO7	9.893182	9.630484	RP11-	4.845581	3.865848
ASNS	8.234373	7.811411	IQSEC1	11.201182	9.873240	RP11-	9.578296	9.051459
ASUN	6.774301	6.362086	IRAK1	11.102710	10.533361	RP3-	7.080828	6.211177
ASXL1	11.910294	11.533720	IREB2	9.619440	9.384924	RP5-	6.062545	5.460780
ATAD3A	8.100628	7.808242	IRF4	12.468818	11.240521	RPAP2	7.395297	7.030706
ATF3	8.731129	8.438866	IRF5	12.104352	11.180653	RPAP3	7.432205	7.061975
ATF4	12.608717	12.376152	IRGQ	9.538916	9.227743	RPEL1	7.128120	6.736934
ATF5	11.862233	10.532545	ISCU	11.317681	11.094557	RPF2	6.852316	6.051300
ATF6	9.305916	9.029366	ISOC1	8.315318	8.041550	RPIA	8.697813	8.192367
ATF7IP	10.827350	10.491456	ISOC2	7.597349	6.754931	RPL10	9.827840	9.613037
ATIC	7.485868	7.013968	ITFG3	9.324040	8.718894	RPL10A	9.763781	9.493320
ATOH8	2.984570	2.243190	ITPA	8.527174	8.161340	RPL13	10.508582	10.185761
ATP2A2	10.576713	10.189415	ITPKC	8.929784	8.643198	RPL23P8	9.248619	8.904879
ATP2B1	10.323781	10.020917	ITPR1	8.598943	8.218820	RPL36AL	10.943469	10.657415
ATP2C1	7.998444	7.683370	IZUMO4	9.974277	9.171454	RPL4	10.628963	10.323989
ATP5B	11.220849	10.935564	JADE2	12.297476	11.981609	RPL7L1	10.562698	10.204124
ATP5EP2	11.265551	10.934503	JADE3	9.942357	9.411266	RPLP0	10.134589	9.799597
ATP5F1	7.731070	7.442787	JAGN1	9.546085	9.142441	RPN1	10.593258	10.384773
ATP5G2	8.036150	7.594922	JAK3	10.862289	9.651735	RPP25L	8.342257	7.959012
ATP5S	7.818807	7.478195	JAM2	5.772376	5.110698	RPS19	7.416890	7.078945
ATP6V0E1	10.699416	10.191436	JAZF1	10.033043	9.637496	RPS2	10.731486	10.362487
ATP6V1C2	8.689475	7.891869	JMJD4	6.474725	5.982685	RPS27A	8.887305	8.303740
ATXN10	8.447156	8.194055	JPH4	5.304516	2.997228	RPS6	11.516685	11.198891
AURKAPS1	5.948796	5.424078	JRK	9.753419	9.542198	RPS6KA1	9.900873	9.208866
AVEN	7.758568	6.987216	JUN	13.528094	13.021744	RPS6KC1	8.429745	8.066560
AZIN1	11.533852	11.291753	JUNB	14.493838	13.939454	RPS6KL1	4.265310	3.304986
B2M	15.184164	14.974225	KARS	7.793907	7.456427	RPSA	6.638492	6.252458
B3GALT6	10.077850	9.099776	KATNBL1P6	8.416134	8.117025	RPSAP58	12.120815	11.737755
B3GNT7	8.760188	7.896666	KCNK5	5.414365	4.197407	RPTOR	9.007456	8.411353
B4GALNT1	3.574023	2.706582	KCNN1	8.062119	4.781480	RPUSD4	8.950144	8.701966
B4GALT2	7.858132	7.161741	KCP	4.015421	3.365429	RQCD1	10.016496	9.704151
B4GALT5	10.703519	9.185909	KCTD10	9.775679	9.497121	RRAS2	10.067127	9.770227
B4GALT7	8.030696	7.679279	KCTD17	8.787078	8.508917	RRP1	8.104671	7.711420
BAHD1	10.082192	9.852304	KDM2B	11.950407	10.703619	RRP12	7.845652	7.289168
BAI2	2.977708	2.429234	KEAP1	9.948132	9.712928	RRP15	8.364454	7.672902
BAIAP2L1	4.187723	3.327401	KHDRBS1	11.529163	10.932504	RRS1	9.214384	7.921808
BANF1	9.675965	9.151806	KIAA0020	6.101271	5.305200	RSL1D1	10.928292	10.449668
BASP1	12.503963	10.344033	KIAA0391	8.266833	7.945841	RSL24D1	9.918204	9.572991
BATF	8.968438	7.950558	KIAA1211	3.531650	2.535657	RTCB	9.584050	8.791048
BATF3	6.436584	4.849153	KIAA1430	10.230383	9.771561	RTFDC1	9.459008	9.134388
BAZ1A	10.143439	9.550940	KIAA1524	5.129028	4.525288	RTKN	6.330375	5.424538
BCAR3	8.383231	7.781202	KIF13A	8.132336	7.858804	RUFY3	10.023809	9.069223
BCAT1	8.924151	7.216212	KIF1C	10.890506	9.819573	RUNX3	12.630383	11.857551
BCL2	14.124109	13.136038	KIF21B	9.289600	8.848100	RUVBL1	7.609156	6.748104
BCL2A1	9.708914	8.328437	KIF26B	5.680498	4.040075	S100A10	8.545113	8.053415
BCL2L1	11.536553	9.211531	KIF3B	9.943679	9.165903	S100A11	7.785208	7.394681
BCL2L10	4.667537	4.084619	KLC2	9.148853	8.779259	S100A14	7.092619	4.029068
BCL2L13	9.726058	9.517907	KLF6	12.883064	12.609178	S100A2	4.336601	3.649564
BCL7A	8.881724	8.314884	KNOP1	7.727935	7.135074	S100A6	10.545826	9.993454
BEND3	7.425224	6.912900	KRAS	11.213271	10.992642	S1PR2	8.084482	7.340364
BHLHE40	12.639737	11.252874	KYNU	6.054740	5.360301	SACS	9.432536	9.064015
BHLHE40-	3.463083	2.857035	L1CAM	8.564395	7.585918	SAMD14	7.033048	4.848988
BID	8.543125	7.546188	LACTB	9.830454	8.810380	SAMSN1	10.039179	9.455172
BIRC3	12.989007	12.430355	LAGE3	8.953112	8.587363	SAMSN1-	4.851996	3.098236
BLK	12.252541	11.967060	LAMP1	11.143929	10.773051	SAP30	5.767065	4.961487
BLMH	7.896224	7.501864	LARP1	11.050886	10.787462	SARS	9.868655	9.632624

BLVRA	6.386454	5.499274	LARP4	9.443444	8.998273	SBF2-AS1	8.131558	7.734923
BMP1	5.694350	5.185836	LARS	9.039013	8.439238	SCARF1	5.805059	5.211026
BRI3	9.795800	9.158625	LARS2	7.396622	7.013992	SCD	8.131510	7.459929
BRPF3	10.363012	10.027476	LAS1L	8.574630	8.245452	SCFD2	7.407688	6.330016
BSG	11.701028	11.442830	LAT2	10.107925	9.094717	SCOC	9.143557	8.881550
BSPRY	8.590347	7.979748	LCMT2	8.503889	7.935106	SCP2	10.290194	10.087677
BST2	9.793400	9.487038	LCP1	13.642567	11.918107	SDC4	7.622864	5.850085
BTBD19	7.051170	6.249555	LDHA	10.243880	9.658443	SDF2L1	8.983759	8.001779
BTF3	9.501823	9.088413	LDHB	7.890874	7.344771	SDF4	10.947192	10.535492
BTG3	7.775011	7.230484	LENG9	6.525069	6.059557	SEC11C	6.354326	5.566989
BTLA	10.854749	10.406172	LHFP	5.918685	4.433218	SEC13	8.856370	8.568263
BTN2A2	10.229816	9.130683	LHX2	3.602095	2.672178	SEC14L1P1	6.764362	6.383798
BYSL	8.145960	7.064114	LIG3	7.762688	7.124744	SEC22A	7.699343	7.377751
BZRAP1-AS1	9.591147	8.630263	LILRB2	8.589492	8.155210	SEC23B	8.207426	7.863279
BZW2	6.329339	5.762125	LILRB4	8.981240	7.565176	SEC23IP	8.981885	8.687748
C10orf10	7.225582	5.778357	LINC00158	5.113471	3.208406	SEC61A2	8.255381	7.915788
C10orf2	9.257867	8.509199	LINC00173	4.972585	4.141330	SEC61B	7.859168	7.364735
C10orf32	8.408186	8.021088	LINC00265	7.095712	6.581448	SEH1L	8.789817	8.308204
C10orf55	4.242774	2.624682	LINC00338	8.078596	7.184333	SELT	10.710593	10.442661
C11orf31	8.898228	8.608453	LINC00515	3.375319	2.878384	SEMA4C	7.354501	5.641354
C11orf95	8.566578	8.059569	LINC00665	7.200113	6.855250	SEMA7A	11.446911	9.519861
C12orf43	8.112581	7.649717	LINC00984	8.884088	8.426391	SENP1	8.634645	8.285477
C12orf77	4.291059	3.341051	LINC00998	8.342215	7.839630	SEPT11	9.481165	8.717265
C14orf1	8.386673	7.906342	LINC01104	3.433286	2.552604	SEPT8	8.461260	7.680134
C14orf166	7.572469	7.163110	LINC01160	3.298697	2.617719	SERBP1	11.213197	10.802955
C14orf169	9.414157	9.105280	LINC01181	2.927813	2.075934	SERPINB9	12.138071	11.578691
C14orf80	8.151611	7.559685	LLPH	8.394391	7.995107	SERPINE2	4.371443	3.463739
C15orf57	9.966143	9.403436	LMAN1	9.972987	9.691893	SESN2	8.055081	7.763078
C17orf89	6.738522	6.202972	LMNB2	11.741368	10.294573	SET	12.433178	11.825314
C17orf96	7.998565	6.797124	LOC10012903	9.887750	9.474657	SF3B14	7.786237	7.456918
C17orf99	6.683980	4.825585	LOC10012936	9.184827	8.627339	SF3B3	10.099420	9.761348
C19orf10	8.563781	8.120912	LOC10012969	6.034883	5.531376	SF3B4	8.836720	8.494349
C19orf24	8.952494	8.649309	LOC10013045	8.644012	7.688259	SFPQ	11.915323	11.615860
C19orf70	8.285816	7.698072	LOC10013074	8.412395	7.930207	SFT2D1	8.363270	7.864996
C1QBP	8.522942	7.878788	LOC10013211	5.318803	4.025159	SFXN1	9.264127	8.764176
C1orf200	5.897460	4.867423	LOC10013283	5.575448	4.673991	SFXN2	6.778114	6.088841
C22orf34	6.975432	6.337293	LOC10026816	4.329737	3.679387	SGCB	7.426343	7.063479
C4orf32	8.898191	8.372486	LOC10028817	8.671765	7.646599	SGPP2	11.260688	10.068816
C4orf46	8.480663	7.425944	LOC10050671	11.798962	11.580043	SH2B3	11.193569	10.553447
C5orf30	7.867079	7.423878	LOC10050763	5.452930	4.628455	SH2D3A	8.259788	7.845933
C6orf222	6.172351	5.487354	LOC10050765	6.320200	5.451051	SH3BP2	9.947772	9.667107
C7orf73	8.554600	8.185282	LOC10099657	6.669391	6.014196	SH3KBP1	9.906799	9.508552
C8orf33	9.700158	9.381583	LOC10106026	5.360342	3.680770	SHFM1	6.649517	6.055358
C9orf117	5.244279	4.688096	LOC10192768	4.057834	2.955250	SHMT2	9.618174	9.233861
CA2	5.761211	5.075693	LOC10192769	3.760280	2.735708	SIAH2	10.977517	10.351597
CACNA1G	3.873093	3.095910	LOC10192784	6.084834	5.490044	SIRPA	10.626592	9.389811
CAD	8.257997	7.913038	LOC10192797	3.971225	2.618329	SLAMF7	11.211327	9.256657
CALM3	11.063039	10.790890	LOC10192848	6.114238	5.385114	SLC12A3	4.259711	3.568015
CALR	12.911045	11.921672	LOC10192876	4.065058	3.529402	SLC12A4	9.141707	8.673835
CAMKK2	9.376300	9.051778	LOC10192934	5.054254	4.194839	SLC15A4	9.982382	9.550010
CAMSAP3	5.437607	4.927204	LOC10192940	3.267133	2.797563	SLC16A9	2.991449	2.380868
CAND1	10.423039	10.113435	LOC10192975	6.785038	6.196743	SLC1A4	10.355945	9.651182
CANX	11.787964	11.188812	LOC10192975	2.836179	2.289221	SLC1A5	10.474659	9.660735
CAP1	11.102680	10.826547	LOC10272372	6.687577	4.418400	SLC20A1	10.220572	9.495860
CAPN2	9.714372	9.274573	LOC10272382	4.629105	3.214623	SLC24A1	7.819292	7.185680
CAPNS1	10.435700	10.069202	LOC10272399	6.942992	6.481115	SLC25A11	8.686647	8.197967
CAPRIN1	10.609125	10.377276	LOC10272453	9.109907	8.572991	SLC25A15	6.321422	5.845051
CAPZA1	11.511840	11.225360	LOC115110	6.646704	6.103659	SLC25A24	8.879852	8.593323
CAPZB	9.476251	9.123694	LOC152225	2.587676	1.942877	SLC25A25	9.147710	8.878830
CARM1	9.654080	9.095533	LOC284454	8.590412	8.098747	SLC25A32	9.083862	8.766953
CARS	7.690638	7.267942	LOC339192	13.402807	12.592124	SLC25A33	7.080930	6.572980

CASP7	9.731238	9.034232	LOC341056	8.731934	8.494729	SLC25A39	9.543027	9.261028
CASZ1	9.914726	8.823517	LOC388813	5.108670	3.457616	SLC25A4	8.148023	7.865793
CAV1	8.682713	6.502447	LOC389834	5.586548	5.089561	SLC25A43	8.802400	8.132264
CBX1	10.165120	9.491544	LOC644189	4.496397	3.982172	SLC25A5	10.569954	10.366539
CBX6	11.879689	11.142314	LOC730101	7.047545	6.181732	SLC25A51	7.668999	7.375275
CCDC102A	6.509152	5.407948	LOC80154	6.446572	5.700951	SLC26A2	9.299678	9.081315
CCDC103	4.901644	3.695815	LONRF1	8.948800	8.590309	SLC27A4	7.943434	7.531247
CCDC106	8.847660	8.490678	LOR	3.377930	2.802276	SLC29A1	8.873356	7.895483
CCDC12	8.413108	7.783854	LPCAT1	11.397116	10.509205	SLC2A13	8.544210	7.598399
CCDC124	9.719717	9.089945	LRCH3	8.761516	8.415594	SLC2A6	8.991125	7.905587
CCDC167	6.512192	5.657411	LRP8	7.507688	6.548363	SLC35A4	10.661640	10.272316
CCDC28B	7.722293	6.859425	LRPPRC	8.541675	8.181947	SLC35B2	11.534850	10.706688
CCDC50	12.013091	10.825192	LRRC59	9.885167	9.585542	SLC35F2	9.836964	9.060814
CCDC71	8.668626	7.920502	LRRFIP2	8.268118	7.715765	SLC37A1	9.821182	9.243690
CCDC82	8.801616	8.536577	LSM1	8.481004	8.179143	SLC38A1	12.929844	12.495711
CCDC86	8.677921	7.677374	LSM3	8.008086	7.654207	SLC38A7	7.680050	7.319995
CCL17	5.145427	2.921747	LSP1	11.642754	10.588470	SLC39A1	11.214945	10.520578
CCL22	12.494669	8.329182	LSP1P3	6.114087	5.367595	SLC39A14	9.337536	8.518891
CCL24	5.235802	4.605691	LTA	8.622104	7.118318	SLC39A6	9.487601	9.056463
CCND1	9.477733	8.187206	LTV1	7.724918	7.244915	SLC41A2	8.293492	7.345430
CCND2	10.572196	10.008827	LY75	10.308267	9.447374	SLC43A3	10.261226	8.259404
CCNI2	6.720067	5.914530	LYPLA2	9.439847	9.183354	SLC45A3	7.752959	5.771268
CCR7	14.898123	13.786232	LYPLAL1	6.512243	6.070089	SLC4A5	7.115923	6.701782
CCT3	9.946289	9.332549	LYRM2	9.434610	9.045490	SLC50A1	10.358006	9.796564
CCT4	9.669446	9.269484	LYRM4	8.159721	7.298678	SLC6A6	11.986711	11.073272
CCT5	8.643892	7.969060	MAATS1	4.803499	4.004052	SLC6A9	5.221606	4.489325
CCT6A	9.814161	9.365851	MACF1	10.036319	9.223320	SLC7A1	11.049844	10.089773
CCT7	10.471522	9.864100	MACROD2	5.517062	4.856001	SLC9A7	11.918241	11.133172
CD1C	4.684411	3.504720	MAGI2	5.023555	4.448702	SLC9A7P1	6.148104	5.436999
CD200	11.044718	10.508780	MAGOH2	8.011581	7.655332	SLC9A8	9.936136	9.547615
CD40	11.670835	10.007706	MAK16	7.603438	7.202031	SLCO5A1	5.691275	4.560033
CD58	9.755725	8.310571	MALSU1	7.488097	6.956944	SLMO2	10.060536	9.790847
CD59	10.510348	9.808142	MAML2	9.053602	8.551818	SMARCA4	8.742818	8.476650
CD70	10.389670	9.473074	MANBAL	8.210854	7.831417	SMARCAD1	8.431871	8.170924
CD80	7.828150	5.955129	MANF	8.612142	7.812189	SMARCC1	10.402872	10.124210
CD82	12.849682	11.651063	MAP3K8	9.886350	8.899934	SMARCE1	9.720444	9.481551
CD83	13.652377	12.484969	MAP4	11.184566	10.567141	SMC3	7.714293	7.382313
CD84	11.621804	11.274538	MAP6	6.232511	5.826159	SMC6	8.982377	8.510471
CD86	8.781821	7.720265	MAP7D1	9.887230	9.669886	SMG1	11.696785	11.151671
CD97	11.487555	10.603464	MAP7D3	6.791853	6.413169	SMG7	10.240103	9.956829
CDC42	11.821705	11.069530	MAPK11	8.765926	7.565920	SMG9	8.911703	8.519468
CDC42EP2	6.987545	5.926480	MAPK13	10.131777	9.686028	SMIM12	10.048967	9.637967
CDC42EP3	10.807343	10.447605	MAPKAP1	10.288910	9.815600	SMIM13	8.347857	8.048732
CDC42SE1	12.214796	11.661197	MAPKBP1	9.195404	8.584036	SMIM15	9.043093	8.671185
CDK17	9.777131	9.469233	MAPRE1	10.497813	10.097130	SMKR1	5.675721	5.073154
CDK18	5.822684	4.624855	MARCKS	11.280039	9.350658	SMO	4.705386	4.200066
CDK2AP1	9.113586	8.711323	MARCKSL1	11.982586	10.934436	SMPD2	7.283505	6.875675
CDK4	8.921973	8.334912	MARS2	8.737303	8.448389	SMPD5	4.795881	4.058754
CDKAL1	7.358088	6.997379	MARVELD2	4.849846	4.318869	SMS	7.724484	7.035880
CDKN1A	12.182156	11.307742	MAT2A	10.974501	10.684514	SMYD5	9.067977	8.552394
CDKN2A	7.913435	7.396754	MATR3	11.696912	11.481704	SNAP23	10.656311	10.365396
CDKN2B	7.699946	6.937670	MB21D1	8.369321	7.963686	SND1	9.478363	9.009270
CEBPG	10.851503	10.420744	MBD3	10.616658	10.355241	SNHG10	8.698803	8.376436
CEP135	8.049326	7.339968	MCCC2	9.368760	8.724262	SNHG15	8.053105	7.600824
CEP170B	6.583437	5.965674	MDFIC	12.319648	11.306853	SNHG16	9.377654	8.469271
CEP19	7.902229	7.464534	MDH1	7.784923	7.410557	SNHG3	9.727811	9.075386
CERS4	8.544056	7.254510	MDH2	8.688961	8.385943	SNHG4	6.718329	5.530204
CETN2	7.381665	7.062865	MED1	10.538592	10.251143	SNN	12.625588	11.291943
CETP	5.312108	4.430854	MED22	10.293709	9.716431	SNORA73A	4.455523	3.799926
CFL1	12.485507	12.054871	MEF2C	10.981940	10.520573	SNORD80	6.196790	5.685461
CFLAR	13.311085	12.067622	MESDC1	11.272117	10.756322	SNRPB	8.933357	8.627669

CFLAR-AS1	4.161791	3.487543	MEST	6.262334	5.686833	SNRPD1	7.136582	6.460304
CHAC1	6.910119	5.486986	METAP1D	5.001095	4.404794	SNRPD3	10.774062	10.459643
CHAC2	6.267317	5.587548	METAP2	8.924867	8.612290	SNX11	11.762398	9.753592
CHCHD1	7.471256	7.154834	METTL1	6.824001	5.354088	SNX12	9.736112	9.416188
CHCHD2	7.876265	7.475073	METTL2B	8.065076	7.764473	SNX17	9.730636	9.386740
CHCHD3	8.649964	8.210045	MEX3C	12.395017	12.059848	SNX20	9.946492	9.309721
CHMP4B	11.703399	10.610259	MFN2	10.385053	10.119394	SNX8	11.224229	10.940229
CHMP6	7.986943	7.405995	MFSD1	7.835040	7.470045	SOCS1	9.698435	8.316994
CHRNA6	6.020930	4.077555	MFSD10	9.686419	9.277547	SP2	9.466367	9.199842
CHST10	9.036059	8.528021	MFSD2A	7.189336	6.142415	SPAG7	8.399184	8.090969
CHST7	9.939214	8.009777	MGAT2	11.133809	10.695157	SPATA31D1	3.272763	2.264391
CHTF8	10.704600	10.499848	MGC70870	6.218303	5.127459	SPATC1	4.600958	3.832915
CHTOP	10.915804	10.673459	MGC72080	6.044529	5.586713	SPCS1	8.920904	8.655552
CIAPIN1	8.213618	7.850654	MGLL	9.822260	7.647067	SPCS3	11.198919	10.995147
CIB2	6.543973	5.946269	MICAL3	10.451809	9.943934	SPECC1	7.217105	6.006451
CILP2	4.108292	3.467930	MIIP	9.935980	8.994541	SPHK1	7.851412	6.973475
CINP	7.855419	7.182084	MINA	7.326604	6.725157	SPI1	10.589254	10.213813
CIRH1A	7.081357	6.637570	MIPEP	5.433849	4.882014	SPIB	12.026962	10.874213
CKB	8.665482	7.241171	MIR155HG	12.757305	10.086014	SPIN3	8.815260	8.485990
CLCF1	6.634531	5.763222	MIR17HG	7.293608	6.434861	SPINT2	11.113093	10.642085
CLCN5	7.560657	6.528655	MIR22HG	9.024159	8.551916	SPPL2A	8.183646	7.671443
CLECL1	8.664612	8.216446	MIR4444-2	8.835368	8.585389	SPR	6.606046	5.642969
CLIC1	11.522770	11.207350	MKNK2	13.183453	12.598034	SPRYD3	9.276411	9.009356
CLIC2	5.341926	4.343794	MLH3	8.536051	8.206959	SPRYD4	7.795652	7.407690
CLIP2	9.294735	7.104494	MLLT11	6.880012	6.399215	SQLE	9.745765	8.271877
CLN6	8.913165	8.083001	MLST8	8.347630	7.774104	SQRDL	7.762558	7.449478
CLNS1A	8.671966	8.281588	MMAB	6.668573	6.206132	SRC	10.234945	9.163659
CLPB	7.121259	6.497751	MMD	9.215053	8.135761	SRFBP1	7.839910	7.222369
CLSPN	5.303277	4.781041	MMP9	8.068881	7.614915	SRGN	13.815140	12.455413
CLTA	9.933284	9.615444	MMRN2	6.479455	5.746661	SRM	7.888093	7.170912
CLUH	9.768784	9.529628	MOB3A	11.707178	11.448120	SRP14	10.845261	10.597441
CMTM6	11.906102	11.035585	MOCS3	8.691873	8.408015	SRP54	8.002305	7.602252
CNN3	6.820960	6.206765	MON1A	7.413187	7.071667	SRP72	9.179310	8.894731
CNOT11	9.709498	9.408008	MORC2	7.705041	7.409334	SRP9	9.967364	9.680590
CNP	10.937742	10.466064	MORF4L1	10.596830	10.206773	SRPK1	9.797016	9.274638
COA1	8.012314	7.741720	MOSPD2	7.756927	7.397681	SRSF1	11.964795	11.642513
COA3	8.287246	7.821741	MPDU1	8.430558	7.922400	SRSF3	11.775462	11.517350
COA4	8.991358	8.394548	MREG	7.117557	5.181648	SSNA1	10.592804	10.302425
COA7	7.579890	6.927995	MRP63	9.529458	9.225579	SSRP1	9.809276	9.349716
COBLL1	8.973517	8.495395	MRPL11	8.322521	7.917183	ST3GAL1	10.486214	9.973642
COCH	9.078915	7.588296	MRPL12	8.062596	7.357958	ST3GAL2	10.486006	10.061668
COL1A1	6.857237	5.215448	MRPL14	9.168564	8.284072	ST8SIA4	10.843849	9.545750
COLGALT2	4.685596	4.058487	MRPL15	8.627101	8.153648	STAP2	2.961430	2.451475
COMMD1	8.959038	7.707865	MRPL17	8.207521	7.880207	STARD10	9.096085	8.154828
COMMD5	9.871237	9.548700	MRPL19	8.804502	8.530259	STARD4	8.162209	7.843439
COMT	8.701420	8.316849	MRPL24	7.731779	7.050431	STAT1	9.574033	9.158250
COPG2	6.497973	5.974801	MRPL27	7.580221	7.122976	STAT5A	11.260231	10.026999
COPRS	7.994143	7.443738	MRPL28	8.666877	8.245364	STEAP3	6.180058	4.477834
COPZ1	10.285138	10.034126	MRPL3	8.714764	7.919215	STOML1	6.726405	5.811719
CORO6	11.326468	9.427760	MRPL32	8.764322	8.483957	STPG1	7.281647	6.644455
COX17	5.823426	5.370415	MRPL36	7.846684	7.515602	STRAP	9.597562	9.372553
COX5A	6.973045	6.557911	MRPL37	9.389296	9.049630	STX11	9.973688	9.446696
COX7A2L	9.487810	9.261207	MRPL39	6.557266	6.047090	STX3	7.829944	7.467894
CPEB1	7.223028	6.629153	MRPL40	7.746094	7.440217	SUB1	8.829184	8.215384
CPNE2	6.813111	5.054804	MRPL42	8.386018	8.079644	SUMO2	10.377199	10.051161
CPNE5	9.438786	8.176859	MRPL45	7.265070	6.915338	SUMO3	10.027051	9.665123
CPNE7	5.106484	4.110497	MRPL47	5.847583	5.295347	SUPT16H	10.124193	9.755732
CPSF2	9.391464	9.009151	MRPL51	8.165865	7.801180	SUPT3H	6.186837	5.488567
CR2	6.738845	6.267896	MRPL54	7.966280	7.678616	SURF4	11.443944	11.243865
CRIP1	9.296509	8.634115	MRPS10	9.432713	9.037823	SVIP	8.340869	8.051238
CRIP2	8.525555	7.370123	MRPS12	8.916956	8.502359	SWAP70	12.675376	12.150692

CRLS1	8.638347	8.323464	MRPS16	9.692154	9.287874	SYMPK	9.642911	9.255631
CRSP8P	8.388007	8.076656	MRPS17	7.119269	6.710258	SYNCRIP	10.469994	10.163489
CRTC2	10.589636	10.314304	MRPS23	7.432696	7.047559	SYNE3	8.207979	7.745970
CRYZ	7.827242	7.390413	MRPS28	7.806816	6.994973	SYNGR2	13.464185	12.528527
CSF1	8.588056	6.895638	MRPS33	7.751515	7.189834	SYNJ2	7.782166	7.020278
CSF2	3.451823	2.519772	MRPS35	8.508645	8.079009	SYNPO	10.153722	6.053756
CSF2RB	9.883117	9.054114	MRTO4	9.376004	8.341824	SYT17	9.050578	8.232258
CSF3	2.606239	2.029545	MS4A1	12.410872	11.717764	SZRD1	11.298148	10.933748
CSK	11.623607	11.186092	MSANTD4	8.795737	8.440738	TAB2	11.698378	11.232393
CSNK1G3	9.468515	8.941899	MSMO1	9.264134	8.547382	TAF15	9.916657	9.692615
CSTF2T	10.428796	10.232224	MST1R	6.111841	4.128007	TAF4B	8.064006	7.610541
CTPS1	7.377039	6.450445	MTA1	9.388249	9.103762	TAF5L	9.516795	9.237243
CTSC	9.199341	8.659425	MTAP	8.241751	7.850007	TAF9	9.081695	8.683228
CTSH	11.163654	10.291645	MTFP1	8.452006	7.512362	TAGLN2	13.733980	12.258672
CTTNBP2NL	7.716314	6.905920	MTHFD1L	6.363676	5.366743	TANK	10.302654	9.919676
CX3CL1	2.437301	1.690263	MTHFD2	9.586608	8.622228	TAP1	11.298724	10.679740
CXCR5	12.877559	12.456348	MTMR2	8.146492	7.740246	TAP2	10.642251	10.327914
CYB561	7.340160	5.860772	MTMR4	11.463440	10.080724	TAPBP	12.220394	11.749237
CYB5A	6.638878	5.441235	MTMR9	9.645543	8.858495	TARS	8.906904	8.242432
CYB5B	10.242533	9.825445	MTSS1	10.668071	10.013121	TBC1D22B	8.561056	8.138291
CYB5R2	7.796194	6.022419	MTX2	6.815552	6.325500	TBC1D2B	10.032208	9.049683
CYBRD1	10.000142	8.534640	MVP	10.797627	10.067148	TBCB	9.020743	8.769184
CYC1	9.632930	9.306122	MYB	7.228954	6.209127	TBL1XR1	10.805846	10.543076
CYCS	10.174257	9.733597	MYBBP1A	7.726272	7.146765	TBRG4	9.772698	9.482597
CYFIP1	7.757823	7.233206	MYBL2	8.380864	7.945249	TCF12	9.723818	9.501486
CYLD	11.957030	11.459893	MYC	10.521312	8.832113	TCF20	10.742757	10.514774
CYP27B1	4.688566	4.015042	MYCBP2	10.096442	9.827925	TCF7	10.890489	9.567722
CYP51A1	9.487350	9.021214	MYH11	7.425173	6.732373	TCFL5	10.794507	10.201306
CYTH1	13.210518	12.945769	MYH9	12.357891	11.893985	TCTN1	7.198530	6.707298
DAD1	10.362795	9.889217	MYL12B	10.701749	10.474596	TDRD7	8.141130	7.637010
DAP	10.800324	10.443981	MYL9	8.638088	8.191431	TDRKH	6.205373	5.778333
DARS	9.018839	8.580734	MYO1C	10.545967	9.401048	TELO2	8.992727	8.566623
DARS2	8.004923	7.481526	MYO1D	7.995384	7.436831	TET3	10.009276	9.606236
DAZAP1	10.447024	10.004127	MYOCD	3.657431	2.533665	TFAM	9.661708	9.330951
DBI	10.096713	9.038786	NAA15	9.488540	9.182523	TFB2M	8.398647	8.089942
DBNL	9.770108	9.464781	NAA20	8.178708	7.849925	TFEB	11.050039	10.468347
DCAF13	5.692635	5.084592	NAA25	8.398306	8.090280	TFG	8.981978	8.521861
DCAF13P3	6.161997	5.648552	NAA50	11.571565	11.348541	TFRC	10.875171	10.233623
DCAF7	11.113488	10.896294	NABP1	9.322625	8.761503	THEM4	6.952775	6.442299
DCTD	10.147021	9.838452	NAF1	7.874467	7.579441	THEM5	7.933563	6.165744
DCTN5	10.351948	10.115690	NAGLU	8.847153	8.407871	THG1L	8.080807	7.399275
DCTN6	6.581235	6.112838	NAMPT	9.799490	9.291278	THOP1	10.122039	9.236033
DCTPP1	9.675015	9.134683	NAP1L1	11.102057	10.511211	THUMPD3-	8.230218	7.867865
DCUN1D1	8.303378	8.003244	NARS2	7.495338	7.082037	TICAM1	10.124846	9.717919
DDB1	9.601359	9.378747	NAT10	8.685440	8.303054	TIFA	10.326543	9.891646
DDHD2	8.081965	7.778292	NAT9	9.488378	9.222720	TIGIT	10.130076	9.547364
DDOST	8.633030	8.317007	NBEAL2	10.685164	9.337119	TIMM10	7.241020	6.844844
DDR1	9.958871	9.027884	NBN	9.422974	8.639423	TIMM13	8.198853	7.844592
DDX10	7.309083	6.929355	NCBP2	10.543839	10.243878	TIMM17A	8.482745	8.088809
DDX18	9.840314	9.497607	NCF2	10.544384	8.471848	TIMM23	7.829759	7.283416
DDX21	11.354940	10.516788	NCK2	10.857647	10.043718	TIMM8A	7.164370	6.811764
DDX47	8.749479	8.405781	NCL	11.857741	11.436288	TIMM9	6.431036	5.881282
DEGS1	10.233627	9.841084	NCOA4	10.550600	10.346336	TIMMDC1	9.760773	9.382093
DENND4A	10.185760	9.134229	NCOA5	10.103580	9.816639	TINF2	10.837482	10.442720
DENND5A	9.334771	8.511276	NCOA7	9.079821	8.786396	TIPRL	9.533614	9.004596
DENR	9.495007	9.261046	NDE1	10.433147	8.952034	TJP2	6.968203	6.295178
DESI1	9.162396	8.748994	NDFIP1	10.218709	9.801049	TLCD1	6.183977	5.369223
DFFA	8.578228	8.229136	NDFIP2	7.916157	7.351055	TLE1	9.250661	8.652293
DFNB31	12.965166	12.582890	NDUFA4	7.849776	7.466117	TLR1	7.695650	7.363802
DGAT2	8.420599	7.389074	NDUFA8	7.055210	6.704298	TLR10	8.833414	7.895474
DHCR24	7.689489	6.633202	NDUFAF1	8.254683	7.990096	TLR6	9.700161	9.213184

DHCR7	7.657594	7.147511	NDUFAF3	8.050014	7.717489	TMA16	8.416628	7.794665
DHRS12	7.029881	6.604067	NDUFAF4	7.651546	7.346801	TMCC1-AS1	5.051503	4.224050
DHRS7	9.016918	8.721945	NDUFB3	7.048868	6.634061	TMCC3	8.939670	8.105878
DHRS7B	6.798910	6.345372	NDUFB7	8.515000	8.078525	TMED3	9.304947	8.902384
DHX33	8.625903	8.232490	NDUFB9	7.974564	7.627240	TMED9	10.200919	9.959840
DHX34	8.613748	8.309339	NDUFS6	6.611317	6.201486	TMEM102	8.747298	8.423509
DHX37	8.631942	8.050883	NECAP2	10.720064	10.045006	TMEM106A	8.104373	7.752912
DIMT1	7.908405	7.598020	NEDD4L	7.856244	7.346799	TMEM120A	8.223630	6.802074
DIS3L2	7.451744	7.104865	NEDD9	8.872628	8.002982	TMEM120B	8.766664	8.008669
DKC1	9.030074	8.693965	NEIL2	8.164141	7.794952	TMEM14A	6.556240	5.909211
DLD	8.198101	7.707401	NEK6	8.522214	7.881888	TMEM14B	8.346705	7.950855
DLGAP3	7.776070	6.578548	NEK9	10.641730	10.426091	TMEM164	8.397424	7.731006
DLGAP4	11.236919	10.845215	NETO2	8.717319	8.291630	TMEM168	8.593803	8.129816
DNAJA1	9.689130	9.205302	NFAT5	11.029340	10.612006	TMEM170B	9.024246	7.910410
DNAJB11	8.367030	7.820572	NFE2L1	12.212051	11.444550	TMEM177	6.759224	5.987786
DNAJB5	7.687672	6.629075	NFIX	5.820519	5.088990	TMEM185B	10.036960	9.460988
DNAJC14	9.930186	9.698660	NFKB1	11.887017	10.673714	TMEM192	8.626213	8.184823
DNAJC30	8.179926	7.565202	NFKB2	11.847562	10.689427	TMEM205	9.535070	9.033125
DNLZ	8.142304	7.767429	NFKBIA	13.378991	11.513359	TMEM230	10.439878	9.974428
DNMT3A	9.282571	8.547111	NFKBID	10.603088	10.218152	TMEM241	6.025012	5.339959
DNPH1	7.860551	7.261405	NFKBIE	11.680319	10.479515	TMEM254	7.613192	7.184004
DOCK10	9.786693	8.975882	NFKBIZ	11.660519	10.729128	TMEM261	8.443876	7.971988
DOHH	8.596377	8.292136	NHP2	9.171962	8.453737	TMEM5	7.576723	7.102482
DOK4	5.091302	4.290893	NIFK	7.896608	7.378999	TMEM54	5.223252	3.972289
DOT1L	10.395443	10.009420	NINJ1	9.387193	8.372370	TMEM63B	8.501244	7.546992
DPF3	3.827762	3.278327	NIP7	8.965383	8.337970	TMEM69	8.385371	7.863926
DPH2	9.731684	9.148639	NIPA2	10.501131	10.189379	TMEM97	6.977199	6.424672
DPH3	9.000870	8.755716	NIPAL2	9.465169	9.153351	TMOD3	10.140120	9.905852
DPH3P1	7.145036	6.629473	NIPAL4	7.144390	6.044852	TMSB4X	13.337793	12.755582
DPH6	5.474051	4.809115	NKAP	8.576469	8.306636	TMTC2	7.454597	7.016989
DPP3	8.044724	7.468552	NKIRAS2	9.462384	9.088322	TNF	9.313076	8.862826
DPP4	5.615889	4.437248	NLE1	7.255620	6.826055	TNFAIP2	10.123882	7.738956
DRAM1	8.535357	7.883267	NLN	8.157936	7.562048	TNFAIP3	12.626986	11.050334
DTD2	8.233984	7.657512	NLRC5	11.336702	10.857789	TNFAIP8	12.002535	11.279374
DUS3L	8.094284	7.819374	NMD3	8.468278	8.166291	TNFRSF10B	11.718629	11.153782
DUSP2	11.610133	11.226466	NME1	6.761669	5.270193	TNFRSF14	11.110170	10.422705
DUSP22	11.308190	10.526991	NME3	9.507197	8.954945	TNFRSF18	11.484693	9.588800
DUSP23	8.116866	7.778484	NOB1	8.640507	8.214267	TNFRSF1B	12.974022	12.670121
DUSP5	11.353803	10.364759	NOL10	7.529011	7.168125	TNFRSF4	9.518841	7.287392
DYNLT3	9.098009	8.730422	NOL3	4.347847	3.758208	TNFRSF8	7.803850	5.861107
E2F3	8.954177	8.588114	NOL6	9.050206	8.539976	TNFRSF9	11.446292	8.237760
E2F4	9.943281	9.738082	NOL7	9.426097	9.052982	TNFSF14	6.944501	6.183331
EARS2	8.127183	7.245363	NOLC1	10.483801	9.874967	TNFSF4	9.415078	6.609572
EBI3	9.269462	5.199360	NOM1	9.161347	8.917194	TNIP1	11.138068	10.849795
EBNA1BP2	7.371788	6.830576	NONO	11.351430	11.131721	TNIP2	10.909777	9.939449
ECE1	12.490048	11.491398	NOP10	9.136509	8.700580	TNKS1BP1	9.322958	8.241286
ECE2	6.384320	5.681868	NOP14	8.139814	7.697511	TNPO2	10.021142	9.756997
ECHDC3	6.021558	5.100659	NOP14-AS1	7.353937	6.881610	TOMM22	9.647716	8.906735
EDARADD	11.561143	10.386043	NOP16	7.879438	7.267071	TOMM34	8.587237	8.157183
EED	8.292183	7.855362	NOP2	9.022405	8.726353	TOMM40	8.906000	8.460348
EEF1A1	9.740196	8.878996	NPAT	9.223587	8.738073	TOMM40L	6.324965	5.933175
EEF1B2	7.747933	7.397113	NPEPPS	9.915555	9.691010	TOMM5	8.988147	8.653162
EEF1E1	6.170963	5.640734	NPLOC4	11.049301	10.794901	TOMM6	9.479941	9.042533
EEF2K	10.179386	9.494892	NPM1	8.798452	8.370647	TOMM70A	9.835480	9.575854
EEFSEC	8.009831	7.581077	NPRL3	7.515490	7.011852	TOR4A	9.770530	9.540890
EFHD2	11.458127	10.770600	NR6A1	6.438676	4.427152	TP53	9.936214	9.541956
EFNA1	3.699841	3.097234	NRAS	10.748267	10.003370	TP53BP2	9.720210	9.213191
EFNB1	7.483093	6.948633	NRBF2	9.150481	8.589771	TP53I11	11.218256	10.448119
EFTUD2	8.188129	7.859283	NRIP1	7.584296	7.070123	TP63	3.847818	3.262194
EGOT	4.023727	2.740179	NRP2	7.944364	6.181097	TPI1	10.360010	10.071867
EHD1	13.106831	12.220688	NRXN2	4.326183	3.380007	TPRN	8.811648	8.338478

EHD4	10.141257	9.688717	NSDHL	6.806515	6.336584	TRADD	10.377793	9.619065
EID1	10.358631	10.086009	NSRP1	9.017231	8.740755	TRAF1	14.294991	11.341724
EIF1	12.563976	12.269308	NSUN4	9.346961	8.979846	TRAF2	9.516173	9.124961
EIF2A	8.742341	8.377545	NT5DC1	8.300796	7.820537	TRAF3	11.424986	11.066430
EIF2B1	8.841053	8.600033	NT5DC2	7.116475	6.560155	TRAF4	12.142777	11.327350
EIF2D	7.484642	7.052035	NT5DC3	7.832365	7.522877	TRAF7	8.410695	8.090477
EIF2S1	9.730198	9.233359	NTN1	5.032037	4.376422	TRAPPC1	9.070315	8.796528
EIF2S2	8.864998	8.479561	NTNG1	5.265678	4.719032	TRDMT1	6.346366	5.903685
EIF2S3	10.714865	10.400510	NUCKS1	11.297647	10.977246	TRIM44	11.335897	11.069679
EIF3B	10.155828	9.744755	NUDCD1	7.423995	6.911040	TRIP10	10.328015	8.631040
EIF3J	9.591579	9.283072	NUDT19	8.425106	8.086554	TRIP12	10.483927	10.166014
EIF4E2	9.651182	9.400125	NUDT9P1	4.622940	3.894760	TRIP13	3.809468	3.191958
EIF4G1	10.600627	10.091480	NUP153	10.555562	10.143840	TRIP6	6.714911	6.301206
EIF4H	10.932307	10.715490	NUP35	5.801097	5.359713	TRMT1	9.275649	8.942430
EIF5A	10.928464	10.310727	NUP62	12.430531	11.549157	TRMT10C	8.994675	8.661997
EIF5B	9.245331	8.854386	NUP93	6.984993	6.568522	TRMT2A	8.804333	8.515659
EIF6	8.885419	8.439548	NUPL1	9.101593	8.679578	TRMT5	7.927207	7.415474
ELAC1	6.580964	6.120649	NUS1	7.913726	7.485205	TRMT6	8.254027	7.896044
ELAVL1	10.664109	10.131774	NUTF2	9.234528	8.672746	TRMT61A	9.628466	8.746008
ELK1	9.563684	9.201237	NXPH3	3.903172	2.837690	TRMT61B	7.857321	7.447324
ELK3	9.482506	8.724017	OAS3	8.327328	7.615395	TRPM7	10.135779	9.830924
ELL2	9.172741	8.682189	OGFOD1	8.756864	8.499564	TRUB2	7.778759	7.374902
ELMO2	8.806734	8.553729	OLA1	7.206073	6.796271	TSC22D2	10.582004	10.134665
ELP6	7.239468	6.887568	OPA3	10.086520	9.543271	TSEN15	9.129782	8.495589
EMC3-AS1	6.760477	6.230543	ORAI1	11.274131	10.287912	TSN	10.132302	9.924649
EMG1	7.243880	6.647704	ORMDL2	8.166927	7.615106	TSPAN18	7.017012	5.534969
EMILIN2	10.098620	9.302277	OSBPL9	8.013765	7.529188	TSPAN31	8.068237	7.702755
EMP3	9.613166	8.990700	OSGIN2	9.166562	8.832662	TSPAN33	12.303193	10.283235
ENO1	10.994280	9.882808	OSTC	8.496213	8.177574	TSPAN9	5.325559	4.601334
ENPP4	9.647524	8.756243	OTUD4	10.477484	10.069244	TSR1	8.312162	7.795862
ENPP5	4.598702	3.988937	OTUD6B	7.685564	7.349359	TTC27	6.512870	5.873235
ENSA	10.999292	10.527974	OTUD7B	7.250872	6.303337	TTC7A	10.331215	9.996718
EPHB4	5.191450	4.449017	OXTR	5.635789	3.807741	TTC7B	4.275766	3.605484
EPM2AIP1	10.810939	10.164185	P4HA1	8.528242	8.203408	TTF2	9.356586	8.327812
EPRS	8.982949	8.643499	PA2G4	9.775445	9.552060	TTLL12	8.444566	8.069751
EPS15	11.036546	10.059130	PA2G4P4	10.020433	9.623298	TTPAL	9.322595	8.937734
ERAL1	8.685289	8.213674	PABPC4	10.547606	10.317212	TUBA1B	10.848457	10.210065
ERAP1	9.887675	9.659699	PAICS	9.134846	7.699182	TUBA1C	9.199981	8.133569
ERH	10.043745	9.677365	PAK1	8.545398	8.048614	TUBB	12.707796	11.604997
ERI3	8.424851	8.126820	PAK1IP1	6.522006	5.764698	TUBB2B	2.841586	2.242760
ESAM	6.254439	4.830313	PANDAR	9.177343	8.838755	TUBB4B	11.643196	11.331979
ESF1	8.003242	7.484752	PANK3	8.602533	8.328188	TVP23A	7.276266	6.155615
ESPL1	6.890428	5.672931	PANX1	9.027620	8.586872	TWISTNB	8.683693	8.169561
ESR1	6.083984	5.631277	PAOX	8.214119	7.750512	TXLNA	10.989458	10.664550
ETFA	7.017212	6.201779	PAQR7	8.854436	8.368501	TXLNB	9.126221	8.634355
ETFDH	6.581891	6.143651	PAQR8	9.523847	8.904218	TXN	7.501624	5.910335
ETS1	12.672549	12.313324	PARK7	9.891294	9.018842	TXNDC9	7.556201	7.197992
ETV3	10.436978	10.066657	PARP1	9.838794	9.506090	TXNL4A	10.294624	9.937864
ETV3L	3.139902	2.375260	PARP12	9.786372	9.523261	TYK2	11.027574	10.565079
EXO5	8.017360	7.665233	PARP14	11.659602	11.181127	TYMP	9.613168	9.319997
EXOC4	8.561517	8.246410	PASK	10.532334	10.087788	TYW3	8.768483	8.371809
EXOSC4	8.307846	7.899326	PATL1	9.429255	9.108881	UBAP2	7.856436	7.548913
EZH2	8.067831	7.127078	PAX5	13.281801	12.240065	UBAP2L	9.294265	9.043515
F13A1	4.777664	4.247873	PBRM1	9.651934	9.380841	UBE2A	9.629728	9.370900
FAIM	5.940826	5.505305	PCK2	8.463421	7.692137	UBE2D1	7.966103	7.663846
FAM105B	10.233823	9.556243	PCNX	10.172700	9.847484	UBE2E1	9.390119	9.127862
FAM114A1	6.856539	6.263542	PDAP1	9.882140	9.475328	UBE2E2	6.433376	6.063342
FAM118A	9.454661	9.173249	PDCD11	8.672859	8.281096	UBE2G2	10.688357	10.301486
FAM129A	8.018693	6.484584	PDCD4	11.601370	10.813439	UBE2K	9.785201	9.528023
FAM136A	9.539524	9.285749	PDCD4-AS1	8.760851	8.351390	UBE2N	10.234794	9.844370
FAM168A	10.085239	9.682018	PDE7A	10.853305	10.387463	UBE2NL	4.539745	4.006996

FAM174B	7.258122	6.590849	PDF	7.073132	6.078748	UBE2Z	12.385105	11.696911
FAM195B	9.788144	9.246058	PDIA3	10.376355	9.818654	UBE3A	10.384362	10.093619
FAM208B	10.059183	9.785314	PDIA3P1	12.175497	11.522090	UBE3C	9.670613	9.272981
FAM20B	9.954516	9.691905	PDIA4	10.011790	9.409025	UBFD1	10.022616	9.666346
FAM213B	9.684299	8.760150	PDLIM5	8.511091	8.159868	UBIAD1	9.488096	9.175826
FAM35A	7.508943	7.119892	PDZD11	6.104070	5.663184	UBLCP1	8.896982	8.258346
FAM3C	7.973045	7.621746	PEA15	12.538113	11.685491	UBQLN4	9.046778	8.790737
FAM49A	9.340787	8.167888	PEAK1	10.507036	10.196644	UBR4	10.074611	9.726865
FAM60A	11.823095	10.838077	PEF1	10.190571	9.722666	UBTD2	8.570790	8.221371
FAM83H	6.759413	6.014580	PELP1	9.694943	9.453192	UCK2	9.219775	8.467990
FAM86C1	5.403617	4.853249	PES1	8.910037	8.361037	UEVLD	8.298677	7.907438
FAM86DP	5.772754	5.354781	PET112	6.001971	5.504172	UGDH	8.709954	8.126218
FAM98A	8.616719	8.277720	PEX10	6.814891	6.184313	UHRF1BP1L	8.453281	8.106538
FAM98B	8.492891	7.809622	PEX26	9.951161	9.585986	UMPS	8.915494	8.425477
FARSA	8.165520	7.818446	PFAS	8.629303	7.898671	UNC119	9.356146	8.784654
FARSB	6.418428	5.728445	PFDN1	9.470067	9.173954	UPK3A	4.180361	3.508476
FAS	9.197810	7.359137	PFKM	7.820353	7.215517	UPP1	6.751064	6.293203
FASN	9.207352	8.398556	PFN1	13.246138	12.142713	UQCRFS1	8.515445	8.213243
FASTKD2	8.354698	7.893753	PGAM1	8.294589	7.810328	URB1	7.981934	7.325966
FBRS	11.729537	11.442207	PGAP2	8.055788	7.750183	URB2	8.758657	7.892362
FBRSL1	10.796395	10.385901	PGBD4	6.822748	6.307238	URM1	9.819218	9.592057
FBXL15	10.127009	9.766797	PGD	9.003495	8.531775	USP10	10.126587	9.710156
FBXL19-AS1	7.033082	6.513874	PGK1	9.683183	9.293224	USP12	11.682897	10.871620
FBXO22	7.664799	7.192479	PGLS	8.838932	8.504468	USP14	8.891787	8.585538
FBXO45	8.387721	8.113579	PGM2	7.199569	6.787160	USP5	9.035419	8.741064
FBXW5	10.932340	10.715262	PHAX	9.268312	8.965056	UST	7.062327	6.144689
FBXW7	8.853351	8.559273	PHB	9.962317	9.057233	UTP14A	7.447608	7.028466
FCER2	10.318987	10.035967	PHLDA2	6.007557	4.862256	UTP14C	9.591462	9.330928
FCGBP	7.265702	6.453789	PHLDB1	6.510090	5.512804	UTP15	7.572322	7.072309
FCHSD2	10.723601	10.153547	PHPT1	8.688569	8.163534	UTP20	7.013375	6.528684
FDX1L	6.980084	6.397543	PICALM	9.668145	9.396461	UTP3	10.300720	10.022778
FDXACB1	6.839687	6.361020	PIGV	8.421741	7.868879	UVRAG	10.386338	9.948415
FEN1	8.812823	8.437314	PIGW	7.745143	6.997210	VAMP8	9.857040	9.588616
FERMT3	9.918868	9.611577	PIGX	8.542610	8.144933	VARS	9.265724	8.390139
FGF2	5.633130	4.946195	PIK3CA	8.865319	8.395123	VASP	10.456152	10.105105
FH	6.161355	5.681020	PIK3CD	11.617311	11.079126	VBP1	9.011944	8.637342
FHOD1	9.608529	8.593707	PIKFYVE	10.310258	10.060474	VCP	11.403338	10.968154
FILIP1L	10.024974	9.362351	PIM1	13.276048	12.783845	VDAC1	10.325222	9.408011
FJX1	2.225670	1.653672	PIM2	12.886344	12.433879	VIM	11.406069	10.003573
FKBP11	7.156528	6.796760	PIM3	12.411253	11.934360	VKORC1	9.605630	9.241107
FKBP1A	10.010083	9.582641	PINX1	7.452150	6.960361	VMP1	9.973448	9.603005
FKBP2	8.786262	8.411954	PIP5K1A	9.705481	9.443053	VOPP1	11.044500	10.360267
FKBP5	9.978102	9.121054	PIPSL	11.670281	11.174747	VPS13A	8.039587	7.533280
FKRP	8.841880	8.550253	PISD	9.614068	9.317349	VPS25	7.829250	7.455321
FKTN	8.045750	7.468121	PITPNB	10.088450	9.491887	VPS29	9.388680	9.118605
FLAD1	9.399397	9.161590	PKIG	9.868467	9.327650	VPS37C	8.375623	8.012260
FLJ13224	4.083211	3.421382	PKM	12.908717	11.664732	VTA1	8.785572	8.509943
FLNA	12.291272	11.965005	PKN3	7.932098	7.163627	WARS	11.255112	9.945227
FLNB	9.294826	8.372285	PLA2G4C	6.883091	5.884382	WARS2	7.562730	7.148344
FLOT1	9.355959	8.883141	PLAGL1	9.337374	8.287766	WBP4	7.638530	7.336013
FLVCR2	6.394650	5.805037	PLAGL2	9.527218	9.248221	WBSCR16	9.391856	9.172848
FMNL1	12.574550	12.203994	PLAU	7.726272	4.957648	WDFY1	10.738492	10.317470
FMNL3	10.860717	9.882385	PLCB3	8.134647	7.205018	WDR1	11.139408	10.718894
FMO5	10.027877	9.648700	PLD2	8.173363	7.717127	WDR12	6.550665	5.934566
FMOD	13.178568	12.568257	PLEC	13.370491	12.986661	WDR17	6.600760	6.090990
FNBP1	13.141927	11.889397	PLEK	11.820043	9.573045	WDR3	7.292173	6.680622
FNDC3B	7.093915	6.426965	PLEKHA7	8.607026	7.993442	WDR36	9.053057	8.678816
FOXC1	5.387073	4.907138	PLEKHG1	12.249664	11.854104	WDR4	8.040739	7.295192
FOXN3-AS1	4.972550	3.871487	PLEKHG5	5.008240	4.328656	WDR43	9.119591	8.469512
FOXP1	12.063357	11.716763	PLEKHM2	11.087140	10.782799	WDR5	9.774212	9.451674
FOXP4	11.156509	9.639759	PLEKHO2	10.310016	10.041502	WDR75	7.465193	7.071988

FPGS	9.716776	9.120571	PLGRKT	6.103763	5.401875	WDR77	8.785428	8.158238
FRK	3.869077	3.168217	PLIN3	9.783327	9.188785	WDR89	9.285981	8.951965
FSCN1	8.359925	6.735501	PLLP	4.001018	2.919481	WHAMMP3	6.578473	5.663220
FSD1L	8.281042	7.202633	PLXNA1	10.758591	9.352370	WIZ	9.367094	8.938105
FUNDC2	8.092592	7.666260	PMM2	9.268322	8.672864	WNK1	11.747667	11.503728
FUT4	8.318240	7.819279	PNO1	8.648479	7.953727	WNT10B	4.978477	4.084999
FUT8	8.026474	7.606743	PNP	8.329640	8.005619	WNT4	7.063380	4.618728
FXN	7.258313	6.609287	PNPO	8.004336	7.676939	WSB2	10.060612	9.741505
FXYD2	2.782408	2.256710	PNPT1	7.552026	7.033123	WWP2	9.087196	8.840427
FXYD6	7.205289	5.942479	POFUT1	9.309040	8.884672	XBP1	10.632708	9.965839
FZD6	6.214363	5.388860	POGLUT1	8.568576	8.275839	XPO1	10.469334	10.190956
G3BP1	11.143771	10.642575	POLA2	7.857485	7.172694	XPO4	9.519483	9.236519
G6PC3	7.975146	7.615333	POLD2	9.776221	9.264789	XPO5	8.153275	7.764126
GABPB1	8.885364	8.405799	POLDIP2	9.423997	9.012998	XPOT	8.525360	8.078514
GADD45GIP	10.090108	9.624760	POLR1B	8.694538	8.201542	XRCC5	10.014226	9.708329
GALNT10	9.378978	8.891046	POLR2D	9.295356	8.977444	XRCC6	9.717395	9.299643
GALNT2	12.118198	11.268887	POLR2K	9.033526	8.749009	YARS	9.769455	9.167552
GAR1	7.954412	7.419015	POLR2L	7.320525	6.961812	YARS2	8.390225	8.095343
GARS	8.313743	7.556704	POLR3A	8.150369	7.840235	YBX1	10.934528	10.523804
GART	8.854727	8.234206	POLR3H	8.591184	8.059028	YIF1A	8.449970	8.154144
GBE1	7.387729	6.710232	POP1	6.897258	6.343253	YKT6	11.024983	10.791576
GBGT1	8.448187	7.522117	POR	9.199681	8.743459	YWHAB	11.913422	11.649651
GBP1	5.379221	4.595941	POU2F1	9.637037	9.358057	YWHAE	11.154669	10.601266
GBP4	8.824976	8.277743	POU3F1	7.190971	6.161185	YWHAG	11.709213	11.358525
GCDH	8.321036	7.721776	PPA1	6.537332	5.505475	YWHAQ	11.056517	10.743142
GCFC2	7.693007	7.343095	PPAP2A	6.710423	6.196099	ZBED4	9.464340	9.093862
GCN1L1	9.683952	9.389101	PPARA	10.093210	9.313365	ZBTB10	11.225886	10.497397
GEMIN4	9.101899	8.702469	PPIA	10.499905	10.125560	ZBTB11-	5.648287	5.168952
GEMIN5	7.752069	7.283346	PPID	8.324802	7.786611	ZBTB17	9.735666	9.391653
GEMIN8	8.124135	7.707728	PPIF	10.319382	9.493192	ZBTB32	11.885600	10.650887
GEN1	9.346103	9.056499	PPIL1	9.005520	7.992625	ZBTB46	7.226931	6.371113
GFI1	7.837560	6.999398	PPIP5K1	7.953659	7.645027	ZBTB5	11.128985	10.405202
GFM1	7.864778	7.416451	PPP1R11	10.582639	10.322294	ZC3H15	9.313589	9.043010
GGACT	6.640305	6.026339	PPP1R14B	9.603229	8.188461	ZC3H4	9.870583	9.507618
GGCT	7.874824	7.361200	PPP1R15B	11.939538	11.607335	ZC3H7B	11.396274	10.516069
GHITM	9.933420	9.662755	PPP1R7	7.434149	7.067590	ZCCHC7	10.033184	9.473843
GHRL	4.229131	3.471176	PPP1R9B	12.979889	11.832230	ZCRB1	8.840581	8.547557
GIPC1	8.136982	7.738207	PPP2CA	10.145646	9.941799	ZDHHC16	7.932238	7.625697
GJD3	6.905464	6.134697	PPP2R1A	9.330812	9.096271	ZDHHC18	11.044687	10.241992
GLB1	7.800182	7.449630	PPP2R2D	9.286233	9.011759	ZFAND3	10.798376	10.538253
GLRX3	7.668560	7.301183	PPP3CB	8.820565	8.377265	ZFHX2	7.328407	5.512616
GLUD1	10.372901	10.147006	PPP5C	7.701738	7.230559	ZFHX3	9.143519	8.888074
GLYR1	10.728079	10.467554	PPRC1	10.246130	9.685230	ZFP36L1	14.349030	13.274213
GMEB1	7.801590	7.378809	PPT1	9.488273	9.237922	ZFP41	8.097987	7.788214
GMFB	9.864544	9.579812	PPTC7	10.941491	10.694623	ZFYVE26	9.225504	8.755941
GNAI3	9.648212	9.389955	PRCC	10.425794	10.160781	ZMAT3	9.418587	9.135108
GNB1	11.958349	11.788055	PRDX1	9.207868	8.227622	ZMIZ2	11.906237	11.381084
GNB2L1	12.310337	12.078001	PRDX3	9.362231	8.959195	ZNF202	8.655611	8.328010
GNG2	11.678765	11.280919	PRDX4	6.835312	6.228462	ZNF207	9.812598	9.378150
GNG4	4.739941	4.084788	PRDX6	9.394917	9.109747	ZNF22	10.661479	10.172978
GNG8	8.391163	5.687375	PRELID1	8.506013	7.992342	ZNF239	6.055177	5.323164
GNL3	7.536946	7.196495	PREX1	10.426619	9.729047	ZNF260	9.919221	9.386619
GNL3L	9.754527	9.397114	PRKAG2-AS1	6.090511	5.295968	ZNF267	10.561853	10.013919
GNN	4.698072	4.074675	PRKAR1B	8.334243	7.426230	ZNF281	9.684547	9.186884
GNPDA1	9.336072	8.919020	PRKCD	9.124562	8.249949	ZNF385C	7.040418	5.985955
GNPNAT1	7.572381	7.212993	PRKDC	9.458682	9.076730	ZNF485	6.211379	5.618005
GOLGA4	9.763829	9.549074	PRMT1	9.225952	8.859490	ZNF506	9.621447	9.188562
GOSR1	9.676146	9.366938	PRMT2	10.085140	9.825305	ZNF593	7.719083	7.218397
GOSR2	10.047498	9.622517	PRMT3	7.097821	6.597144	ZNF598	9.885906	9.611324
GOT2	9.627328	8.727060	PRMT6	9.777467	9.460416	ZNF629	7.697979	7.345888
GPATCH2L	10.070567	9.860935	PROB1	7.677366	7.223478	ZNF660	5.848110	5.393682

GPATCH4	9.435879	8.314691	PROSER1	9.590228	9.340378	ZNF706	8.578383	8.005280
GPN1	8.166313	7.853822	PRPF19	9.700425	9.392673	ZNF710	10.424204	9.833169
GPR132	11.048303	9.984089	PRPF40B	7.804841	7.209735	ZNF770	10.899827	10.656945
GPR137	10.098102	9.431562	PRR18	7.312743	6.236891	ZNF780B	8.201468	7.877446
GPR137B	8.429158	7.901980	PRRC2C	11.822686	11.491226	ZNF788	6.545033	5.402474
GPR153	7.107124	6.219872	PRRG4	6.145901	4.992237	ZNFX1	11.231209	10.546836
GPR157	8.054558	7.129877	PRRT2	6.903383	5.736598	ZNHIT6	8.797898	8.385863
GPR55	6.507167	5.394587	PRRT3	8.165058	6.210247	ZRANB2	10.155034	9.850461
GPRIN1	7.621375	7.216902	PRSS2	3.432196	2.727453	ZSCAN2	9.873474	8.701526
GPSM3	11.010178	10.689030	PSAT1	5.512466	4.372260	ZSWIM4	9.725050	8.338401
GRASP	9.295785	8.960126						

Appendix 5. Significantly down-regulated genes induced by the soluble CD40 ligand in primary CLL cells at 12h time point

12h down-regulated	Expression LevelS12	Expression LevelU12	12h down-regulated	Expression LevelS12	Expression LevelU12	12h down-regulated	Expression LevelS12	Expression LevelU12
AATK	6.133189	6.749115	GRAP	7.997716	8.521510	PVRIG	7.588851	8.343843
ABCA1	5.973675	6.767113	GRB7	5.092449	5.661817	PXK	9.158629	9.634712
ABCA2	4.834033	5.429726	GRIK3	4.735380	5.422001	PYCARD	5.784908	6.638890
ABCA7	8.470958	9.591706	GRIN3B	6.251483	6.785992	PYROXD2	6.510701	6.903359
ABCB1	4.608725	5.705022	GRK5	7.025424	7.660943	QPCTL	8.435864	9.080690
ABCB8	7.902289	8.198055	GRK6	8.537255	8.866517	QRICH2	6.436064	6.837585
ABCC2	4.338211	5.000297	GSDMB	7.444153	8.253443	QSOX1	8.800525	9.081656
ABCC5	6.844759	7.369519	GSDMD	10.032947	10.317981	QSOX2	10.224398	11.398356
ABCD1	6.129854	6.797413	GSE1	9.230798	9.764541	RAB11FIP4	8.502227	9.462823
ABCD4	8.529159	8.883973	GSTM4	5.032980	5.655547	RAB31	9.405049	9.663168
ABCG1	7.634479	8.143359	GTPBP1	10.461498	10.877026	RAB33B	8.740516	9.003045
ABHD10	7.903102	8.230830	GTSF1L	4.343880	5.072657	RAB37	7.181481	8.058940
ABHD14A	5.573807	6.242763	GUCY2C	4.608779	5.179024	RAB3D	6.473006	6.985621
ABHD14B	9.481911	9.789333	GUSBP11	7.849724	8.372132	RAB40B	4.759678	5.591309
ABHD15	9.786064	10.645422	GYLTL1B	7.929450	8.834090	RAB40C	8.595411	9.091081
ABHD16A	7.385525	7.768014	H1FX-AS1	5.423147	6.247697	RAB6B	4.842499	5.334095
ABHD17A	8.948996	9.586660	H2AFJ	8.950285	9.317964	RABAC1	8.035641	8.395935
ABHD3	8.060583	8.414214	HAGH	6.460491	6.965559	RABEP2	8.534016	8.861350
ABHD4	9.061040	9.455371	HAS3	5.256872	5.797601	RAD9A	8.202491	8.918814
ABI3	3.778964	4.313899	HAUS8	6.144151	6.599591	RALB	8.817555	9.109791
ABLIM1	9.748820	10.694978	HBP1	8.898411	9.151143	RALGDS	9.134213	9.666851
ABR	11.317246	11.597567	HCG23	4.415453	5.512879	RALGPS2	10.806984	11.195940
ABTB1	9.307446	9.878499	HCG27	5.587147	6.395982	RANBP10	9.452674	9.759268
AC074289.	7.206153	7.675569	HCN2	4.392883	5.149239	RAP1GAP2	5.111532	6.322159
ACACB	5.708070	6.748499	HDAC1	10.078287	10.293154	RAPGEF2	8.634316	9.171403
ACAD8	8.048175	8.480083	HDAC10	8.231103	8.806651	RAPGEF3	8.043623	8.931204
ACAP1	8.476415	9.175375	HDAC5	8.372640	9.020000	RARRES3	4.621867	5.298837
ACAP2	9.802013	10.035609	HDAC7	11.285861	12.005942	RASA2	8.583111	8.897256
ACAP3	6.602093	7.104923	HEATR5B	7.803049	8.126348	RASA3	7.596418	9.158674
ACBD4	7.812576	8.132696	HEATR6	7.687235	8.085990	RASAL1	5.484986	6.417132
ACD	8.113525	8.417379	HECA	10.358230	10.809660	RASAL3	9.404958	9.658980
ACRC	6.074742	6.608365	HELZ2	9.761569	10.258493	RASD1	7.766963	8.503600
ACSF2	6.390143	7.153407	HERC3	7.585876	8.051632	RASGRP2	9.196907	10.227206
ACSM1	4.895042	5.486403	HEXDC	9.157525	9.399863	RASSF1	9.435357	9.904248
ACSM3	4.017295	5.039782	HGSNAT	9.518951	9.873857	RASSF7	8.879235	9.337233
ACSS1	9.222871	9.780176	HHEX	8.942484	9.837704	RB1CC1	9.114157	9.403434
ACSS2	6.380653	6.953800	HIP1R	6.996844	8.418407	RBL2	9.777917	10.054221
ADAM28	9.737601	10.376487	HIRIP3	7.458607	7.816084	RBM33	10.345634	10.727822
ADAM29	5.385311	5.974511	HIST1H1C	8.711670	9.103416	RBM38	11.877033	12.676641
ADAMTS6	6.647804	7.728968	HIST1H2AC	8.236810	8.697503	RBM39	11.110248	11.350753
ADCK2	8.411243	8.872034	HIST1H2BD	7.363954	7.896124	RBM5	10.075314	10.370533
ADCK3	8.548656	9.017088	HIST2H2BE	7.212281	7.621381	RBM5-AS1	5.972606	6.383502
ADCY4	4.317554	4.947945	HLA-DMA	10.080573	10.818787	RBMS2	6.624578	7.343560
ADCY9	5.019681	5.544475	HLA-DMB	9.846079	10.700509	RCN3	5.426221	5.993934
ADD3	9.248780	9.835022	HMCES	8.225735	8.798913	RCOR1	9.009501	9.313104
ADHFE1	4.018967	4.578741	HMGB2	8.689514	9.088870	RCOR3	9.132271	9.364035
ADM	7.206325	7.943240	HMGN3	9.045223	9.501433	RCSD1	11.676576	12.496041
ADPGK	10.376106	10.691632	HMOX1	9.911535	10.712648	REC8	6.538022	6.972879
ADRB2	7.423097	8.212271	HNRNPU-	8.211931	8.534725	REEP2	3.595279	4.407040
ADRBK1	11.384728	11.803205	HOMER2	7.856529	8.502867	REEP5	9.301668	9.595123
AES	12.083341	12.390484	HPCAL1	9.399352	10.476313	RELL1	3.943880	4.530999
AFAP1L2	3.647477	4.286356	HPS3	7.432939	7.930086	REM2	6.095153	6.988161
AFF1	8.847233	9.171482	HRK	5.464400	6.173399	RERE	9.971686	10.480111
AFF3	10.330349	10.843432	HS2ST1	8.661962	9.014164	REST	9.748158	10.005614
AFF4	10.322327	10.617507	HS3ST1	8.449186	8.879847	REV3L	8.634384	9.124888
AGFG2	7.883589	8.290486	HSD17B11	8.652646	9.054799	RFC5	7.507528	7.822487

AGPAT5	10.697817	11.499960	HSDL1	8.751460	9.120977	RFX1	7.784084	8.219485
AHCYL2	7.614685	7.963869	HSH2D	10.660703	11.128966	RFX7	9.086156	9.372220
AHDC1	8.820625	9.295512	HSPA7	5.092305	5.930550	RGCC	7.958183	9.203274
AHI1	7.636596	8.074539	HSPBAP1	7.207226	7.572417	RGL2	8.770918	9.185766
AHNAK	13.658364	14.037162	HSPG2	5.190947	5.794598	RGL4	8.162692	8.618997
AHSA2	10.403873	10.647037	HTATSF1P2	6.840287	7.750692	RGMB	7.489607	7.945997
AK1	7.819495	8.673349	HTRA3	4.371417	5.920171	RGS14	8.029768	8.679525
AKAP8L	9.251761	9.655961	ID3	12.476878	13.181651	RGS2	10.778911	11.784790
AKAP9	9.309062	9.584024	IDS	11.809656	12.195561	RHBDL1	4.885492	5.547147
AKIP1	7.234394	7.754659	IER5L	7.048551	7.416035	RHOB	10.155095	10.476382
AKNA	11.266922	11.579818	IFFO1	8.633431	9.113453	RHOBTB2	9.402958	9.920320
AKR7A2	7.257890	7.606683	IFI16	10.124042	10.362669	RHOH	11.236112	11.873766
AKT2	11.004235	11.270433	IFIT2	6.578272	7.191054	RHPN1	8.879991	9.884127
ALAD	8.242243	9.022849	IFITM1	6.108431	6.778861	RICTOR	9.018117	9.350232
ALDH3A2	7.775564	8.442052	IFNAR2	9.190470	9.661205	RILPL1	4.963055	5.896285
ALDH5A1	9.645917	10.360725	IFT57	8.997732	9.428015	RILPL2	10.178438	10.515205
ALKBH4	7.197659	7.586700	IGIP	7.193167	7.532628	RIN3	10.258510	10.779131
ALKBH5	10.837891	11.272378	IGSF8	8.058436	8.745264	RINL	9.676402	9.922413
ALKBH6	7.683129	8.007853	IKZF3	12.008473	12.331165	RITA1	7.958093	8.398009
ALOX15P1	4.436965	5.060935	IKZF5	8.992221	9.328012	RMI2	4.837376	5.547324
ALOX5	10.358093	10.965044	IL10RB	9.010366	9.278254	RN7SK	8.219503	8.649636
ALOX5AP	7.442012	8.387270	IL11RA	6.856667	7.520060	RNASE4	4.524366	5.149459
ALX3	6.466696	6.913096	IL16	10.695893	11.405375	RNASE6	6.031679	7.370077
AMDHD1	3.580233	4.193436	IL17RA	9.208831	9.597057	RNASEL	8.002411	8.429297
AMFR	10.536876	10.977919	IL1R1	4.356608	4.935972	RNASET2	8.821844	10.586025
AMH	4.670040	5.214378	IL1RAP	6.364588	6.906282	RNF113A	9.231032	9.645644
AMN	5.042376	5.598243	IL24	6.719040	7.596447	RNF122	6.487833	6.928238
AMT	6.262857	6.807356	IL27RA	8.351263	8.727791	RNF125	6.165343	7.037496
AMY2B	5.907363	6.364947	ILF3-AS1	7.986957	8.335352	RNF130	8.178960	8.565446
AMZ2	9.910971	10.318514	INF2	8.627624	9.473770	RNF135	8.199684	8.556753
ANAPC4	7.038698	7.345787	ING1	9.620655	10.025611	RNF149	9.474679	9.936752
ANK1	5.416342	6.521979	ING2	7.447629	7.820764	RNF166	8.269763	9.095731
ANKMY1	7.176582	7.533414	ING4	8.103686	8.487843	RNF19A	9.449944	9.973906
ANKMY2	7.085334	7.443162	INO80E	9.212549	9.568863	RNF213	10.486957	10.791491
ANKRA2	7.974963	8.450435	INPP5A	8.173986	8.845767	RNF24	6.779816	7.421146
ANKRD13A	10.421929	10.815246	INPP5D	10.341620	10.769307	RNF38	9.785074	10.120919
ANKRD13D	7.863416	8.230662	INPPL1	9.920803	10.161482	RNF41	10.657678	11.335469
ANKRD34A	4.391013	5.140965	INSIG2	8.323545	8.752144	RNF44	10.227713	10.776986
ANKRD42	7.374457	7.930625	IP6K2	9.746680	10.207471	RNFT2	4.581723	5.197117
ANKRD44	10.006203	10.561394	IPW	5.035797	5.624413	RNR1	13.322638	13.620757
ANKZF1	9.184297	9.885873	IQCE	8.100087	8.540213	RNR2	16.127030	16.502298
ANO8	5.481329	6.413373	IQGAP2	5.150194	5.789666	ROGDI	5.625195	6.119891
ANTXR2	7.722352	9.011103	IRAK4	9.454629	9.715441	ROR1	9.412609	9.930454
ANTXRLP1	2.827585	3.686061	IRF2BPL	10.990003	11.584495	RP11-	2.838588	4.131693
ANXA2R	5.508866	6.483043	IRF3	10.296607	10.781304	RP11-	4.268582	5.089189
AP001258.	5.599763	6.333566	IRF7	9.297194	9.559710	RP11-	3.694991	4.651188
AP1B1	10.126709	10.538820	IRF8	11.915815	12.200497	RP11-	3.880514	4.606785
AP3S1	7.380994	7.822216	IRS1	8.189886	8.923291	RP6-	4.606457	5.215655
APAF1	8.727843	9.112861	IRS2	9.619933	10.178857	RPAIN	7.745849	8.071039
APBB2	8.529929	10.117987	ISYNA1	6.993392	7.444557	RPL13A	11.723627	11.993568
APBB3	7.955512	8.276893	ITGAL	7.932705	9.101738	RPL32P3	7.111743	7.457084
APCDD1	2.869949	3.541978	ITGAX	9.077260	9.413319	RPRD2	9.355908	10.030800
APOLD1	5.099555	5.731262	ITGB1	9.256280	9.755301	RPS27	8.498282	8.811310
AQP3	4.670698	5.307525	ITGB1BP1	6.974638	7.338069	RPS6KB2	7.998226	8.366763
ARAP1	9.487039	9.981271	ITGB5	5.256636	5.715976	RRBP1	8.702590	9.006995
ARHGAP12	7.697412	8.201041	ITGB7	7.984086	9.077756	RRM2B	10.124019	10.450301
ARHGAP19	8.562408	8.836825	ITIH4	6.579964	7.142359	RSBN1L	8.460275	8.841795
ARHGAP27	9.984989	10.486292	ITM2B	10.258709	10.575394	RUNDC1	9.228970	9.684035
ARHGAP33	6.583244	7.047364	ITPKB	12.283549	12.500566	RUNX1	8.964628	9.293885
ARHGAP4	9.848457	10.203349	ITPR2	9.375663	9.858296	S1PR1	8.015101	9.325855
ARHGAP9	9.102367	10.167333	ITPRIP	9.414289	9.769206	S1PR4	9.502185	10.159136

ARHGDIB	11.394938	11.754543	IVD	9.453667	9.721903	SAFB2	9.275459	9.686396
ARHGEF1	9.557943	10.109026	JAG1	2.847352	3.483278	SAP25	7.771041	8.470685
ARHGEF10L	7.384348	8.111379	JDP2	8.173256	8.777817	SAT1	10.331825	10.927009
ARHGEF3	8.807645	9.582519	JHDM1D-	6.730788	7.498769	SAT2	8.838371	9.206612
ARHGEF6	8.434574	8.885534	JMJD1C	10.468769	10.921338	SATB1	6.972442	7.679454
ARID4A	8.720744	9.108563	JMJD7	5.788096	6.591463	SBDSP1	8.442283	8.711127
ARID5B	10.514759	11.239107	JMY	9.583949	10.093216	SBF1	10.045007	10.386280
ARL15	6.864498	7.295578	JOSD1	11.283854	11.626243	SBK1	6.481650	7.170317
ARL3	6.608880	6.998932	JPH3	4.012257	4.631160	SBNO1	9.893205	10.154252
ARL4C	9.674513	10.242108	JUND	13.335080	13.761307	SC5D	9.097525	9.325229
ARMCX3	9.984088	10.278971	KANK1	7.367444	7.969767	SCAI	7.557084	7.992673
ARNT	8.950500	9.217360	KANK2	5.476894	6.586185	SCAMP1	7.640331	8.258352
ARRB2	8.428264	9.072799	KAT2A	8.746278	9.109484	SCART1	5.128932	5.626940
ARRDC2	11.517205	12.059445	KAT2B	8.268281	8.710569	SCIMP	7.686709	9.311069
ARRDC3	9.743028	10.424728	KAT6B	8.790609	9.546522	SCML4	3.675990	4.568693
ARSK	5.727405	6.191369	KBTBD3	5.889916	6.398685	SCN4A	3.122356	4.133780
ASAP3	3.717792	4.396950	KBTBD6	7.702775	8.155164	SCXB	6.375952	7.587769
ASF1A	8.732559	9.233229	KCNA3	9.610452	10.719469	SDC3	7.401552	8.158357
ASIC3	5.476159	6.052770	KCNAB1	3.975992	4.512120	SDHA	7.098376	7.464381
ASTE1	7.066390	7.439022	KCND1	5.867774	6.465886	SDK2	6.322866	7.019871
ATAD2	7.308077	7.704549	KCNH2	5.187388	6.343969	SDR39U1	8.407852	8.747444
ATG12	9.295285	9.573289	KCNJ11	8.692808	9.450228	SEC11A	9.160091	9.469592
ATG16L2	7.473090	8.205298	KCNQ1	4.462993	5.298380	SEC31B	7.835716	8.169277
ATG2B	8.924266	9.296832	KCTD7	8.847590	9.474136	SEC62	10.755305	10.992582
ATG4B	9.487156	9.738683	KDELC2	6.014585	6.582624	SECISBP2L	10.270943	10.569468
ATG9A	9.229815	9.621286	KDM3A	8.596695	9.075598	SEL1L3	9.733660	10.609882
ATHL1	11.690117	12.409917	KDM6A	8.199089	8.498903	SELO	9.034261	9.655517
ATM	10.043656	10.620575	KDM7A	9.415449	10.235622	SELP	4.927213	5.509226
ATP10D	7.183621	7.575620	KHDRBS2	5.207042	5.748439	SELPLG	8.458654	9.100101
ATP13A1	8.915959	9.183728	KHK	3.424715	3.920893	SEMA4B	8.937823	10.279032
ATP2A3	11.316258	12.449012	KIAA0040	10.731834	11.448674	SEMA4D	9.149556	9.968537
ATP2B4	9.565318	10.610168	KIAA0226	11.057331	11.692215	SENP7	7.538689	7.975237
ATP6V0C	11.026993	11.355344	KIAA0355	9.152098	9.545492	SEPHS2	10.361755	10.708036
ATP6V0E2	7.059980	7.633361	KIAA0430	11.033623	11.281939	SEPN1	8.902561	9.198027
ATP6V1G2	4.124284	4.755513	KIAA0586	6.601041	7.023259	SEPT6	10.577185	11.325044
ATP7A	7.036465	7.453913	KIAA1377	5.423529	6.120764	SEPT7P2	6.412185	6.832383
ATPIF1	8.280458	8.644329	KIAA1407	8.318679	9.035598	SEPT9	12.723690	13.428689
ATXN1L	10.316599	10.580783	KIAA1432	9.175176	9.433182	SEPW1	8.351059	8.720531
ATXN7L1	6.469470	7.078136	KIAA1551	11.820386	12.186443	SERINC1	10.736066	11.000369
AUH	6.407891	6.878557	KIAA1683	6.953866	8.185895	SERINC4	7.519847	8.415393
AVPI1	5.260989	6.277919	KIF22	7.717690	8.147398	SERINC5	8.594518	9.000172
AVPR2	3.846338	4.484104	KIF3C	6.440654	7.166535	SERPINF1	6.837941	7.299864
AXIN1	9.975522	10.288741	KIFC2	9.098552	9.432321	SERPINI1	4.831047	5.367528
AZI1	6.443477	6.863353	KISS1R	5.441094	5.882635	SERTAD3	9.743604	10.003438
B3GNT1	6.521754	7.512429	KLC4	6.832759	7.294964	SESN1	7.680719	8.271992
B4GALT1	11.057331	11.748091	KLF10	10.003246	10.526103	SESN3	11.635677	12.628836
B4GALT3	9.136041	9.428957	KLF2	9.713611	10.789509	SESTD1	8.148186	8.865095
BAG1	9.487159	9.813857	KLF3	7.303258	7.936228	SETBP1	8.739334	9.229075
BAIAP3	6.487222	7.920626	KLF9	9.198526	9.700265	SETD2	10.489253	10.697485
BAK1	6.755606	7.211618	KLHDC3	8.755676	9.102857	SETD7	7.894909	8.409998
BANP	8.275387	8.969904	KLHL14	7.637533	8.470276	SETDB2	8.232586	8.656299
BBS2	7.444461	7.881312	KLHL15	8.553740	8.865414	SF3B1	11.264831	11.480793
BBS4	7.111482	7.443368	KLHL2	8.509271	9.103282	SFI1	7.438433	7.836599
BBX	10.097629	10.348848	KLHL24	9.597484	10.352596	SFMBT1	10.056685	10.569356
BCAS4	8.552594	9.140874	KLHL3	4.874261	5.372509	SFSWAP	9.059363	9.299176
BCL11A	9.884017	10.699775	KLHL32	3.619751	4.454348	SFTPB	5.875039	7.490736
BCR	7.667134	8.115698	KMT2E	10.716049	11.019854	SFXN3	8.093679	9.318320
BDH2	5.117609	5.637664	KMT2E-AS1	8.385366	8.672159	SGK223	9.984047	10.391449
BEND4	9.838418	10.098019	KNTC1	5.647240	6.181924	SGPP1	11.336000	11.716125
BEST4	5.904869	6.353178	KPNA5	8.142312	8.451272	SGSH	7.886866	8.506549
BET1L	10.075610	10.314348	KSR2	6.363684	7.204870	SGSM2	10.047012	10.602482

BICD2	10.053549	10.545566	LAG3	6.610896	7.093939	SGSM3	9.267024	9.517614
BIN1	7.534472	8.123213	LAIR1	5.992883	6.606772	SH2B1	10.222514	10.575469
BLNK	7.906647	8.303382	LAMA5	7.006159	7.898062	SH3BGRL2	8.464632	8.925289
BMPR2	10.140846	10.764546	LAPTM4A	9.718665	10.065440	SH3BP5	8.644918	9.014126
BNIP3L	9.498887	10.032303	LAPTM5	13.510297	14.136980	SH3BP5-AS1	7.644499	8.096543
BRICD5	5.957509	6.629293	LATS2	7.591019	7.955483	SH3TC1	9.749393	10.219963
BRWD1	9.552325	9.914410	LAX1	9.044887	10.114380	SHISA5	9.988748	10.656362
BTBD2	9.709400	10.080100	LBH	11.966835	12.425985	SIAH1	8.678080	8.935949
BTBD6	9.323592	9.800344	LCK	6.953137	7.939691	SIDT1	8.301978	9.105287
BTG2	13.128953	13.773045	LCN10	6.819327	7.256991	SIDT2	8.401091	9.187241
BTK	8.681938	9.067381	LCP2	6.022057	6.662608	SIGIRR	8.051068	8.540322
BTN3A1	9.495923	9.975912	LDB1	10.572748	11.113378	SIGLEC10	7.358068	8.478397
BTN3A2	9.727151	9.988034	LDLRAD4	9.299357	10.172818	SIK2	7.266443	7.655368
BTNL2	2.015475	2.503942	LDLRAP1	7.862125	8.670102	SIK3	9.575045	10.074912
BZRAP1	6.658635	7.499009	LENG8	12.470509	12.810973	SIMC1	7.939700	8.439132
C10orf118	8.816477	9.063290	LEPRE1	8.528151	8.885571	SIPA1L1	10.313261	10.763285
C11orf21	6.779389	7.385376	LEPREL4	5.199962	5.659600	SIPA1L3	9.928247	10.825237
C11orf24	7.929042	8.455084	LEPROTL1	8.420653	8.819288	SIRT2	7.924211	8.524406
C11orf30	8.218725	8.467697	LGALS8	7.261604	7.747817	SIT1	7.946372	8.813856
C11orf35	6.691125	7.824103	LGI4	2.598308	3.232777	SKI	10.375295	10.815154
C11orf68	9.745511	10.011099	LGMN	5.346517	5.856234	SKOR1	3.513173	4.222253
C11orf80	6.129263	6.539421	LGR4	3.658812	4.402862	SLA	9.388119	10.491409
C12orf10	7.210669	7.529462	LHFPL2	9.423371	9.775692	SLAMF6	10.172832	10.536176
C12orf76	7.959098	8.436957	LHPP	7.394007	8.183721	SLBP	8.822573	9.160970
C15orf62	6.828473	7.368949	LIG1	7.068479	7.848847	SLC12A6	10.489424	10.864599
C16orf54	7.855526	8.891885	LIMD1	9.301848	9.763448	SLC12A9	8.924618	9.249591
C16orf74	7.346644	8.496270	LIME1	6.815862	7.801970	SLC13A5	3.741783	4.723963
C16orf86	6.603434	7.281723	LIMK2	8.709889	9.260004	SLC14A1	4.021864	5.467586
C17orf103	7.932512	8.714264	LIN7B	5.808708	6.378225	SLC16A14	3.839525	4.476001
C17orf59	9.444293	9.794674	LINC-PINT	8.667484	9.339054	SLC16A4	4.877353	5.443416
C17orf62	10.959717	11.187681	LINC00202-	2.772861	3.434054	SLC16A7	7.588971	8.554980
C19orf38	4.778811	5.680146	LINC00304	4.280301	4.872751	SLC17A9	7.542427	8.140661
C19orf66	7.895481	8.167819	LINC00324	4.974232	5.715572	SLC18B1	6.650567	7.670849
C19orf68	8.221310	8.511236	LINC00339	6.864287	7.509756	SLC22A17	3.684763	4.635453
C1QTNF6	6.641371	7.581241	LINC00426	4.565268	5.576078	SLC22A18	3.169111	3.733614
C1orf162	6.245772	6.868669	LINC00525	4.145483	5.009445	SLC23A1	4.902925	5.661107
C1orf35	8.187660	8.613026	LINC00593	2.579307	3.120593	SLC23A3	5.945808	6.387129
C1orf95	6.202419	6.682193	LINC00672	5.383523	5.887674	SLC25A28	9.550996	10.128506
C2CD2L	6.828760	7.402397	LINC00674	9.927943	10.367972	SLC25A29	10.069950	10.543024
C2orf15	3.954130	4.475580	LINC00847	8.736562	9.427920	SLC25A36	9.568566	9.833864
C2orf81	7.074453	7.483965	LINC00886	4.217689	4.843109	SLC25A42	7.342311	8.363375
C3orf58	8.203456	8.636678	LINC00926	11.327949	11.874717	SLC26A11	7.300504	7.993456
C5orf45	6.514378	7.265780	LINC00954	4.107383	4.609336	SLC26A6	6.692237	7.251190
C6orf48	10.585965	11.062277	LINC01000	9.586914	9.941722	SLC27A1	6.970370	7.340541
C9orf72	7.991252	8.436468	LINC01004	6.724918	7.570059	SLC27A3	7.213379	7.895621
C9orf89	6.919767	7.374736	LINC01011	3.706255	4.701439	SLC29A3	7.199232	7.509684
CA11	7.414319	8.099430	LINC01023	5.231918	5.874614	SLC2A11	6.873347	7.738123
CA3	2.829509	3.306231	LINC01089	8.504520	8.956302	SLC2A3	8.337502	9.043030
CABIN1	9.110351	9.403168	LINGO3	6.038788	8.115116	SLC2A4RG	7.898382	8.503660
CABLES1	10.536549	11.134210	LLGL1	7.501637	7.851013	SLC30A1	7.583249	8.051347
CABP4	3.465594	4.627525	LMBR1L	8.883465	9.266758	SLC35E2B	9.794951	10.187934
CACNA1C	3.639025	4.162985	LMF2	9.646735	9.891559	SLC37A2	7.557893	8.000031
CACNA2D2	5.298180	5.954232	LMNB1	7.195175	7.870435	SLC39A10	7.832414	8.315005
CACNB2	4.977550	5.699816	LMO4	8.835106	9.340011	SLC44A2	9.713082	10.251933
CALCOCO1	9.442995	10.127637	LMO7	7.753084	8.341336	SLC46A1	4.691173	5.285200
CALHM2	8.630222	9.177471	LMTK2	8.496922	8.945184	SLC46A3	7.365075	7.776110
CALM1	11.695785	12.059396	LNX2	7.877908	8.195083	SLC48A1	8.870225	9.474573
CAMK2G	8.280636	8.660491	LOC100128	5.006548	5.506546	SLC6A16	7.537872	7.906183
CAMKK1	6.669715	8.221036	LOC100129	5.596130	6.431284	SLC7A5P2	6.990005	7.353641
CAPN14	5.387449	5.915812	LOC100129	6.775283	7.833694	SLC7A7	8.611853	9.134587
CAPN3	7.616348	8.168220	LOC100129	8.824679	9.361364	SLC9A1	8.763880	9.459183

CAPRIN2	8.061746	8.497186	LOC100130	4.451583	5.033736	SLCO4A1	9.483179	9.949996
CAPS	7.632302	8.093126	LOC100287	2.006616	2.473012	SLFN11	7.779146	8.210145
CARD11	9.777374	10.257478	LOC100287	3.985828	4.752101	SMAD3	7.534040	7.982787
CARD14	5.447382	6.433126	LOC100289	5.713850	6.248340	SMARCC2	10.272275	10.514635
CARD8	9.749755	10.055272	LOC100294	8.111829	8.386008	SMARCD3	5.558534	6.153761
CARF	6.887429	7.326108	LOC100505	6.469464	7.299439	SMC4	8.117439	8.389797
CARHSP1	8.466389	9.186136	LOC100505	7.937118	9.482197	SMCHD1	10.164578	10.913995
CARNS1	7.247302	8.169913	LOC100506	5.744349	6.228236	SMPD1	7.897605	8.291140
CARS2	7.378284	7.791627	LOC100506	4.570345	5.106827	SMPD3	5.451067	6.070002
CASP10	5.884888	6.625319	LOC100506	7.091323	7.458584	SNAI3	5.111714	6.153653
CASP8	9.333403	9.739087	LOC100507	3.703751	4.685603	SNED1	7.966414	8.934070
CASP9	7.953873	8.354723	LOC100507	8.278475	8.917009	SNPH	6.632093	7.497313
CBFA2T2	9.241511	9.664118	LOC100652	6.185091	7.446827	SNTB2	7.513429	8.540057
CBLB	8.397134	8.832176	LOC100996	5.759581	6.731520	SNX2	7.867927	8.244169
CBX4	9.854180	10.659846	LOC100996	4.473729	5.016734	SNX21	6.067108	6.454709
CBX8	5.140850	6.211451	LOC101409	2.789825	3.285763	SNX25	7.616554	7.929591
CCBL1	5.281380	5.876164	LOC101927	3.310262	4.083246	SNX27	8.947773	9.199316
CCDC109B	6.897476	7.616563	LOC101927	2.937039	3.466685	SNX30	8.045473	9.033860
CCDC134	4.928386	5.500389	LOC101927	6.925476	7.461688	SORBS3	7.455528	8.023162
CCDC163P	5.339163	6.032296	LOC101927	3.609486	4.271104	SOS1	9.200747	9.434358
CCDC28A	7.121752	7.582698	LOC101927	6.428085	7.684114	SOS2	9.155929	9.430400
CCDC42B	3.131041	3.791425	LOC101928	3.793462	4.445993	SOWAHD	8.046558	8.934843
CCDC62	4.706058	5.249698	LOC101928	6.429934	7.442057	SOX12	9.258273	10.091368
CCDC64	10.616587	11.118721	LOC101928	2.366138	2.880159	SP110	7.038412	7.864494
CCDC69	11.178068	11.535165	LOC101928	6.565578	7.446391	SP140	8.056782	8.740792
CCDC88A	10.655747	11.002569	LOC101928	5.735705	6.146271	SP140L	8.179918	8.435573
CCDC88C	9.724954	10.036722	LOC101928	3.202624	3.883143	SPAG4	6.879282	7.674200
CCM2	8.899069	9.291149	LOC101929	4.682490	5.634924	SPAG5	6.344714	6.729074
CCND3	10.009725	10.419694	LOC101929	6.504546	6.975361	SPATA13	7.869211	8.285432
CCNDBP1	9.014298	9.324135	LOC101929	2.653382	3.162111	SPATA2L	8.614765	9.160356
CCNL1	11.080721	11.315489	LOC101929	2.318216	2.932015	SPIN4	7.610884	8.388423
CCNL2	11.703099	12.034827	LOC101930	6.679957	7.105781	SPOCK2	12.798579	13.464626
CCP110	8.050237	8.459314	LOC101930	2.037691	2.486777	SPPL2B	8.481127	8.852237
CCPG1	6.768492	7.270286	LOC102723	3.919802	4.486758	SPSB3	10.008613	10.551214
CCR6	5.784255	8.037080	LOC102723	9.970197	10.214820	SPTAN1	9.253328	9.606988
CCS	7.513089	7.904199	LOC102723	4.001830	4.676058	SPTBN1	10.113406	10.760968
CD163	6.782986	7.296012	LOC102723	4.789183	5.513903	SPTBN5	5.826250	6.873031
CD1D	5.021847	6.012555	LOC102723	3.053626	3.552905	SRGAP3	4.472610	5.343256
CD24	8.580865	9.722592	LOC102723	3.030386	3.522537	SRPK2	8.600918	8.901380
CD244	5.371056	6.401675	LOC102724	3.458455	4.160720	SRRM2	13.492675	13.865527
CD27	7.715420	9.417691	LOC102724	5.680842	6.419666	SRSF5	11.811211	12.038195
CD27-AS1	5.495974	6.097152	LOC102724	6.620752	7.250678	SRSF7	10.826031	11.030349
CD320	7.675861	8.002148	LOC102724	5.803984	6.505117	SRSF8	9.962444	10.240890
CD47	10.735401	10.983711	LOC102724	2.106591	2.486267	SS18L1	8.104325	8.506481
CD48	10.158133	10.590270	LOC102724	6.118230	6.895854	SSBP2	4.143614	4.979442
CD5	10.395187	11.328686	LOC102724	8.500546	9.653967	SSH2	10.607338	11.222635
CD52	9.192961	10.342752	LOC102724	5.169001	5.628024	SSTR3	5.524803	6.578785
CD6	9.120489	10.554378	LOC113230	5.096430	5.660594	ST6GAL1	12.494466	12.781821
CD7	5.118054	5.647975	LOC146880	8.312966	8.844160	ST6GALNAC4	9.922308	10.528563
CD72	6.843653	7.506895	LOC202181	6.476132	7.078305	ST6GALNAC6	11.395415	11.871134
CD79A	11.558193	12.258203	LOC220729	6.160879	6.887635	STAG3L5P-	7.782312	8.150359
CD79B	9.796234	11.281623	LOC284023	6.870374	7.231821	STAMBPL1	8.213026	8.529536
CD99	9.526941	9.824963	LOC390937	4.238015	5.017624	STAP1	7.621300	8.018389
CDC16	8.400122	8.738531	LOC440461	5.292322	6.828100	STARD3	9.042874	9.363182
CDC25B	8.532746	9.551281	LOC645638	6.639956	8.060997	STARD5	7.536206	8.174087
CDC40	8.252916	8.589446	LOC646719	8.044764	8.318814	STARD9	7.139171	7.575869
CDCA7L	7.453058	8.338330	LOC648987	7.029059	7.366113	STAT2	10.298652	10.967331
CDIP1	9.522393	9.773124	LOC652276	7.189965	7.739955	STIM1	9.588252	9.981010
CDIPT	9.811797	10.184619	LOC728392	7.596318	8.803020	STIM2	9.337549	9.772430
CDK11A	7.707044	8.111582	LOC728743	9.203883	9.946768	STK24	9.630272	10.086029
CDK11B	7.078542	7.420295	LOC728752	5.424280	6.076861	STMN3	7.601033	9.316920

CDK13	9.443027	9.681978	LPAR5	9.151384	9.521672	STOX1	4.359868	4.971877
CDK19	8.826838	9.232589	LPCAT4	7.251341	8.287853	STRN	9.180262	9.444148
CDK5RAP3	10.655117	10.853959	LPIN2	9.510103	10.002568	STX10	8.098501	8.505280
CDKN1B	11.032895	11.541821	LPP	8.568942	9.218041	STX16	10.204798	10.478306
CDKN2AIP	9.824935	10.142935	LRCH4	9.425170	9.917768	STX7	10.101785	10.468864
CDKN2D	7.427991	8.441026	LRFN1	5.964269	6.845998	STXBP2	8.354013	8.639924
CDS2	9.941087	10.144235	LRIG1	8.197405	8.898006	SUFU	7.070944	7.499309
CEACAM21	6.461557	7.435726	LRMP	8.313274	8.924887	SUGP2	10.959042	11.221773
CECR1	7.165762	8.761520	LRP10	11.904853	12.115187	SULF2	7.298565	7.809550
CELF6	6.709803	7.182807	LRP5L	6.992365	7.349553	SUMF2	8.380406	8.661081
CELSR2	3.702538	4.270571	LRRC16A	6.130468	6.580105	SUN2	10.733659	11.166879
CEMP1	6.987224	7.703233	LRRC25	6.670252	7.392467	SUSD3	5.661222	7.059454
CENPM	4.698199	5.330770	LRRC37A4P	7.036872	7.667730	SUV420H2	6.989784	7.560831
CENPT	8.706960	9.182883	LRRC37B	5.933111	6.370908	SVILP1	3.342436	4.227689
CEP250	8.758633	9.095521	LRRC45	6.707240	7.158559	SYCP3	4.167367	4.850989
CEP57	9.026915	9.281149	LRRC56	6.201387	7.259129	SYK	11.737752	12.142039
CEP85L	7.893762	8.528326	LRRC6	2.102782	2.789786	SYNE2	10.073920	10.614440
CEP95	7.763478	8.324897	LRRC8A	8.397411	8.720788	SYNGAP1	8.507320	8.944885
CERK	9.866232	10.691475	LRRC8C	7.203113	7.540662	SYNRG	10.006327	10.299365
CHAD	4.183616	5.115969	LRRK2	7.744374	8.281870	SYPL1	9.384946	9.675221
CHAMP1	8.687493	9.016092	LRRN2	5.417733	6.014979	SYTL1	8.848493	10.144967
CHIT1	3.511815	4.153005	LRWD1	7.429239	8.092407	SYVN1	9.476113	9.829963
CHMP1B	11.000911	11.284378	LSM4	9.172430	9.476143	TACC1	11.076986	11.434627
CHPT1	8.021409	9.064773	LSM8	8.788368	9.077686	TACC3	7.507860	8.813970
CHRNB1	7.579562	8.124073	LTBP3	7.959121	8.730428	TAF1	8.759301	9.040141
CHST11	10.229200	10.843283	LUC7L	9.785128	10.183546	TAF1L	9.529254	9.805007
CHST12	7.923714	8.331003	LUC7L3	10.594974	10.911650	TAF5	6.539663	6.944379
CHST15	9.721904	10.770820	LY6G5B	7.171720	7.643920	TAGLN	7.359598	8.371188
CHST2	11.599514	11.948950	LY86	6.368913	6.893939	TAOK2	9.971046	10.233067
CHTF18	8.522656	8.824501	LY9	9.624283	10.852811	TAPSAR1	7.400627	7.770003
CIB1	8.180158	8.938488	LYL1	8.308230	8.948321	TAPT1	8.148924	8.540689
CIC	10.262561	10.483579	LZTS2	9.289296	9.937707	TARSL2	6.568438	7.040820
CIPC	9.367726	9.833531	MAD1L1	7.580812	8.470846	TAZ	8.876652	9.214237
CIRBP	11.811451	12.039045	MADD	9.241084	9.662561	TBC1D1	9.583678	9.939129
CITED2	8.895305	9.234156	MAFK	10.225128	10.625033	TBC1D10C	9.186844	10.176337
CKAP2	7.404835	8.084765	MAGEE1	6.469266	6.904612	TBC1D20	9.720120	9.983161
CKAP4	10.853626	11.230284	MALAT1	12.597430	12.950099	TBC1D22A	9.380862	9.717821
CLASRP	8.986964	9.443646	MAN1A1	9.581318	9.999139	TBC1D27	8.641089	9.906811
CLCN4	7.288841	7.948054	MAN1B1	8.706183	9.202122	TBC1D9	9.781103	10.993644
CLDN15	8.341075	8.698287	MAN1C1	3.144119	3.786059	TBCC	10.100865	10.316301
CLDN23	5.824498	6.608888	MAN2A1	9.792644	10.180878	TBKBP1	7.349353	7.969075
CLEC2B	4.974808	5.464554	MAN2A2	9.636863	10.304973	TBL1X	9.304990	9.734369
CLEC4C	2.921898	3.665699	MAN2B2	9.039963	9.286362	TBX21	8.098130	8.583972
CLK1	10.228920	10.795583	MAP3K1	10.920603	11.873896	TBXA2R	3.826945	4.517668
CLK3	8.543011	8.878349	MAP3K12	6.078473	6.598834	TCAP	5.467370	6.043798
CLK4	8.301336	8.609774	MAP3K2	10.397572	10.750544	TCEA2	7.048910	7.547909
CLMN	7.878465	9.398409	MAP3K3	9.166757	9.533805	TCEAL1	7.881146	8.668981
CLSTN1	10.257762	10.613994	MAP3K9	8.907502	9.506867	TCF25	9.083985	9.422348
CLSTN3	8.562419	9.237768	MAP4K1	6.956381	7.375049	TCF7L1	3.861782	4.416825
CMIP	9.030967	9.576185	MAP4K2	7.579930	8.167321	TCIRG1	9.652365	10.047758
CMTM1	5.057069	5.613990	MAPK8IP3	11.151583	11.904048	TCL1B	2.586932	3.131696
CNNM2	6.654556	7.127135	MAPKAPK5	8.103862	8.382750	TCL6	3.734490	4.250803
CNNM3	9.841291	10.081511	MAPRE2	9.219004	9.943559	TCP11L2	8.351610	9.052751
CNNM4	8.147668	8.627407	Mar-01	8.482444	9.765274	TECR	5.753189	6.449630
CNOT6L	9.601298	9.854605	Mar-08	10.488795	10.808252	TEP1	9.196882	9.475405
CNR2	9.880523	10.386521	Mar-09	9.666042	9.902850	TERF2IP	11.128875	11.460810
CNTD2	3.706981	4.320371	MAST3	8.258654	9.324556	TEX264	8.553483	8.869833
CNTRL	8.726680	8.997214	MAST4	6.038145	6.872776	TFAP4	6.578656	7.108260
COG4	7.534305	7.900384	MAX	10.235421	10.506270	TFDP2	8.191075	8.574637
COL4A3	6.424212	7.529103	MBD4	9.478290	10.101118	TGFBI	7.042415	8.237343
COL4A4	6.411658	7.362059	MBNL3	9.788629	10.196104	THAP11	10.205827	10.639664

COL9A3	9.965914	11.288402	MBOAT1	6.279116	6.984269	THAP9-AS1	9.142882	9.405864
COLCA1	4.754437	5.311942	MBP	11.395323	11.836426	THBS4	2.830321	3.673325
COLGALT1	9.965321	10.280380	MC1R	6.404130	7.015503	THEM6	7.379659	7.831677
COQ10A	7.893404	8.275718	MCEE	6.768637	7.186958	THEMIS2	10.854192	11.207629
CORO1A	10.383930	10.642531	MCF2L	5.792562	6.246495	THRA	6.373520	7.357519
CORO1B	8.742570	9.522160	MCM5	9.221746	9.511306	THYN1	6.111380	6.672098
COTL1	11.783570	12.280302	MCM6	7.217107	7.967143	TIA1	10.312664	10.527240
CPEB2	7.621976	8.180365	MDGA1	5.787426	6.286384	TIGD3	5.299538	6.031056
CPLX1	1.893486	2.545885	MEAF6	9.157799	9.421569	TIMP2	9.058857	9.858665
CPNE1	9.710866	9.989101	MECP2	10.893597	11.156827	TIPARP	8.586136	9.112358
CRAMP1L	9.900517	10.293129	MED25	7.212427	7.587064	TIRAP	7.348063	7.706721
CREB3L2	10.707116	11.213868	MEGF6	8.513138	9.467940	TLR4	5.995922	6.566219
CREBRF	10.044355	10.374172	MEN1	9.713856	9.983476	TLR7	7.006870	7.701982
CREBZF	10.844842	11.150669	METRNL	7.957091	8.537105	TLR9	9.506839	10.084130
CREM	9.349922	10.268201	METTL7A	9.307567	10.800312	TM2D3	8.463589	8.710882
CRIP3	4.455056	5.083313	METTL8	9.901449	10.179192	TM7SF2	6.074833	6.736677
CRIPAK	6.999388	7.353361	MFN1	7.626940	8.086498	TMEM107	6.272864	6.908253
CRLF3	9.637857	10.054475	MFSD8	7.971198	8.338008	TMEM109	10.311470	10.987433
CROCC	7.577609	8.035353	MGAT1	11.642552	12.045841	TMEM110	8.903078	9.239143
CRTAP	8.772007	9.386445	MGAT5	9.751593	10.264343	TMEM123	11.575513	12.097209
CRTC1	8.299473	8.696913	MGEA5	11.338833	11.707436	TMEM129	9.634006	10.091432
CRTC3	8.895620	9.175382	MGME1	8.624541	9.113526	TMEM134	7.953530	8.509004
CRY2	9.390535	9.658577	MIA3	9.550832	9.843140	TMEM140	9.429598	9.869211
CRYM	4.132480	5.741265	MIAT	7.292749	7.664577	TMEM143	6.169497	6.698871
CRYM-AS1	4.569796	5.493053	MIB2	9.137959	9.608089	TMEM154	8.918909	9.221603
CSNK1G2	10.321690	10.613929	MIDN	10.070354	10.824176	TMEM156	5.755893	6.459977
CTBP1	9.970846	10.235085	MIF4GD	8.982288	9.891933	TMEM159	8.066358	8.647090
CTD-	2.638331	3.253087	MINK1	8.885922	9.383830	TMEM175	7.624407	8.190126
CTDSP2	11.448690	11.823138	MIR142	9.569555	9.902930	TMEM184B	8.684164	8.970579
CTLA4	8.319957	9.805099	MIR1914	4.804915	5.592758	TMEM198B	6.726962	7.136176
CTNNBIP1	6.765022	7.431659	MIR378I	7.562457	9.043994	TMEM2	8.232164	9.278559
CTRL	6.087684	6.479509	MIR548AR	4.726354	5.330384	TMEM219	8.435957	8.753446
CTSF	6.366085	7.692041	MIR600HG	9.056971	9.685791	TMEM236	5.434839	5.949172
CTSK	4.636445	5.287705	MIR647	4.048867	4.700342	TMEM245	9.717601	9.934979
CUL4B	8.983257	9.315246	MIR8071-2	7.630362	8.167606	TMEM259	12.327953	12.535098
CUTA	9.491837	9.875794	MIS18BP1	8.133582	8.615109	TMEM38A	4.897349	5.913160
CXCL16	8.563365	9.622004	MKRN1	10.243222	10.567629	TMEM55B	9.842896	10.089152
CXCR4	13.788205	14.674559	MLKL	6.304095	6.874097	TMEM56	5.785460	6.688276
CXXC1	9.382050	9.692023	MMP11	5.191982	5.737165	TMEM59	8.722783	9.098478
CXXC5	11.195582	11.450360	MMP17	6.116928	7.048781	TMEM62	7.209867	7.725042
CYFIP2	10.644416	11.312744	MNT	8.490941	9.190705	TMEM63A	8.057787	9.091134
CYP4V2	7.719299	8.134709	MOAP1	9.234097	9.644762	TMEM66	11.821458	12.472671
CYSLTR1	6.659844	7.415759	MORC3	10.315755	10.552976	TMEM71	4.966275	6.609253
CYTH2	8.730151	9.157865	MOV10	7.678493	7.960820	TMEM79	7.498577	7.869021
CYTIP	10.419754	11.234759	MPHOSPH8	10.130056	10.428958	TMEM80	7.682523	8.354477
D2HGDH	8.009389	8.414620	MPPE1	5.980983	6.504518	TMEM86B	7.186929	7.635965
DAAM1	7.236260	7.569053	MPRIP	9.736632	10.138820	TMF1	9.905193	10.184642
DAB2IP	5.771159	6.602746	MPZ	5.449759	6.101168	TMPRSS6	5.361845	6.064534
DACT1	6.790661	7.799970	MR1	8.893565	9.255973	TMUB2	9.956599	10.249848
DAGLB	7.570560	7.906200	MRI1	9.300904	9.717919	TMX4	8.785616	9.630459
DAPK2	6.148745	7.737531	MRO	1.837065	2.488249	TNFRSF13B	9.317777	10.292392
DBF4	7.212483	7.561965	MROH1	7.861825	8.308971	TNFRSF13C	8.885864	10.327040
DBNDD1	5.372409	6.356626	MROH6	6.809401	7.832574	TNFRSF17	2.574325	3.127818
DBP	6.613576	7.704955	MRPL55	6.929850	7.417020	TNFSF10	5.458443	6.109876
DCAF15	8.971239	9.392781	MSI2	11.521656	12.218268	TNFSF12	7.619045	8.349893
DCLRE1C	8.671880	9.270166	MSL2	10.502427	10.885839	TNFSF9	9.444886	10.022440
DCST2	2.889807	3.461429	MSL3	9.002215	9.435988	TNK2	10.188257	10.968269
DDAH2	8.333439	8.909511	MST4	8.847440	9.188987	TNKS	9.148084	9.365072
DDB2	8.188674	8.521329	MSTO2P	6.429657	6.989132	TNKS2	9.586367	9.984687
DDX26B	8.256819	8.639834	MT1F	4.384969	5.299089	TNNI2	4.984266	5.719524
DDX3Y	10.647068	10.865333	MTHFR	9.255777	9.614545	TNRC6B	9.464978	10.119326

DEAF1	7.151848	7.779319	MTIF3	8.166071	8.489706	TNRC6C	8.441728	8.732735
DEDD2	10.821919	11.118184	MTMR9LP	7.018192	7.854352	TNRC6C-AS1	9.449427	9.776318
DEF6	8.311369	8.962931	MTSS1L	6.385707	7.358071	TNS3	8.508114	9.209193
DEF8	9.734321	10.329729	MTURN	8.159344	8.936546	TNXB	4.549803	5.071711
DEGS2	7.365740	8.476399	MUC20	5.161903	5.722611	TOB1	9.268211	9.635260
DENND1C	9.206569	9.504006	MUSTN1	4.119894	4.630889	TOM1	8.219136	8.871936
DENND5B	8.863595	9.228488	MX2	7.370585	8.310612	TOP1MT	7.811753	8.602167
DENND6A	7.758102	8.219350	MXD1	9.180741	9.553111	TP53I13	10.805405	11.541423
DENND6B	6.022784	6.667104	MXD4	9.201469	9.935834	TP53INP1	8.764568	9.385653
DEPDC5	7.484627	8.100128	MXI1	9.351173	10.045208	TP53INP2	8.179773	8.593881
DFFB	6.969785	7.320959	MYH7B	5.568301	6.069894	TPCN1	9.176353	10.140333
DGCR2	9.945031	10.210919	MYLIP	8.771121	9.166593	TPCN2	8.408690	8.920752
DGKA	8.325350	9.222105	MYO15B	7.670066	8.018349	TPP1	10.609975	11.043185
DGKD	9.684614	10.143825	MYO1F	7.148722	7.641951	TPST2	8.798822	9.152090
DGKE	8.443803	8.837087	MYO5C	6.425863	6.913521	TRABD	9.525969	10.612266
DGKQ	8.726985	9.030795	MYO9B	10.968806	11.351779	TRABD2A	6.195459	6.894272
DHX58	5.935273	6.366604	MYOM1	5.085682	5.985240	TRAF3IP2	7.086646	7.625472
DICER1-AS1	5.457935	6.024229	MZB1	7.816867	8.266659	TRAF3IP3	8.441620	8.994525
DIP2B	8.689159	8.971859	N4BP2	8.570774	8.861567	TRAF5	8.843682	9.614448
DIRAS1	5.635301	6.519214	NAA16	8.001647	8.401587	TRAM2	9.153824	9.878944
DIRC2	5.796123	6.612837	NAA40	9.366986	9.699894	TRAPPC2L	8.068031	9.289385
DLL1	6.066551	6.737970	NAAA	7.573153	8.181447	TRIB1	9.722994	10.486511
DMPK	8.951945	9.265988	NAB2	8.932102	10.033203	TRIM14	8.300252	8.795054
DMXL1	9.133693	9.435769	NADK	9.807504	10.099868	TRIM22	10.082894	10.546520
DNAJB13	5.969942	6.666576	NAGK	9.196412	9.531616	TRIM25	9.132000	9.587603
DNAJB2	11.261603	11.570218	NAGPA	7.824754	8.155919	TRIM38	9.648818	10.188216
DNAJB9	9.023350	9.283826	NAPRT1	8.729793	9.194369	TRIM39	8.643815	8.895877
DNAJC4	8.266069	8.821578	NAPSB	9.475912	9.800597	TRIM52	8.375634	8.793785
DNASE1L2	4.905950	5.567506	NARF	7.774579	8.059265	TRIM65	8.923241	9.332526
DNASE2	8.446791	8.845297	NASP	7.315813	7.670453	TRIM66	7.420658	7.737597
DNHD1	8.532389	8.989070	NBPF11	7.460332	8.033317	TRIM7	4.946070	6.289501
DNMBP	9.322892	10.020548	NBPF15	7.203546	7.531151	TRIM8	10.121835	10.513000
DOK2	8.118200	8.403342	NCAPD2	7.299712	7.704941	TRNAA26	2.372849	3.088980
DOK3	7.252802	8.350839	NCAPH2	8.343024	8.653922	TRNE	10.862485	11.117640
DOPEY1	7.085241	7.536941	NCF4	8.031550	8.842358	TRNK	10.138304	10.360791
DOPEY2	7.414728	7.747716	NCOA2	9.446978	9.715040	TRNL1	8.525660	8.906082
DPAGT1	7.422328	8.036582	NCOA3	12.022518	12.260819	TRNP	9.682068	10.159892
DPEP2	8.158205	9.457162	NDRG1	9.231521	10.389891	TRNS1	10.385581	10.708783
DPH1	6.396205	6.863350	NDRG2	4.961433	5.532992	TRPS1	6.522564	7.095143
DPH7	8.777561	9.052198	NDUFC1	5.557943	6.199728	TRPV1	7.119320	7.664875
DPM3	9.537961	9.884789	NDUFS2	6.712081	7.194987	TSC1	9.436286	9.761052
DSTYK	8.342426	8.695858	NEK7	9.788055	10.317744	TSC22D1	8.083693	8.759188
DUOX2	2.817827	4.347256	NFATC1	10.013658	10.911003	TSC22D3	11.069814	12.573865
DUSP26	3.424331	4.339244	NFATC3	9.993900	10.332279	TSEN54	8.064295	8.542318
DUSP7	6.893286	7.318115	NFX1	9.420908	9.739283	TSHZ1	7.801659	8.377940
DYRK1B	7.694156	8.141150	NHLRC3	7.807673	8.225800	TSHZ2	4.670996	5.876824
DYRK2	9.044329	9.495965	NIPSNAP3B	6.117727	6.811343	TSPAN32	4.879388	5.481705
E2F7	4.334582	5.163247	NISCH	10.730802	11.149138	TSPYL2	12.303171	12.804712
E4F1	8.565077	8.818447	NKD1	4.769105	5.706008	TSSK3	7.070533	7.887918
ECI1	7.734652	8.068989	NKTR	10.837553	11.249229	TSTD1	8.370253	8.787073
EFCAB12	3.759928	4.798152	NLRC3	8.464577	9.086152	TTC13	7.167589	7.554917
EFCAB13	5.918720	6.403375	NLRP1	9.370604	10.429823	TTC21A	5.345863	6.601337
EFCAB4A	6.137706	7.189506	NLRP6	6.644224	7.259681	TTC24	6.151279	6.771111
EFHC1	6.817567	7.223731	NMB	7.818529	8.500635	TTC28-AS1	7.528578	7.878194
EFNA3	5.483622	6.047499	NMT2	6.438364	7.125066	TTC3	9.402826	10.183319
EGLN1	9.259990	9.606053	NNT	7.711213	8.009091	TTC3P1	8.523507	9.278461
EHD3	8.689564	9.732482	NOSIP	7.150039	7.956460	TTC9	8.630043	9.290719
EHMT1	10.491950	10.975356	NPHP3	6.859570	7.376316	TTYH3	9.769446	10.371268
EHMT2	8.401280	8.893189	NPR2	4.842691	5.294674	TUBA4A	9.909297	10.820228
ELF1	11.328869	11.560383	NPRL2	7.096046	7.629903	TUBB4A	4.862251	5.548730
ELFN2	3.576182	4.577458	NQO2	6.391782	7.164977	TUBG2	6.014518	6.483178

ELMSAN1	9.909607	10.492647	NR1D1	6.712072	7.228343	TUFT1	5.044166	5.466953
ELOF1	9.628449	9.917285	NR1D2	9.302866	9.869768	TULP4	8.505039	8.913630
EML4	9.579058	9.923017	NR3C1	11.529748	11.815130	TXNDC15	9.161677	9.436777
EMR4P	6.261451	7.080459	NR3C2	4.661574	5.182179	TXNDC16	5.654069	6.209626
ENC1	8.326696	9.912481	NR4A1	10.457055	10.835300	TXNIP	12.189966	13.126286
ENDOV	6.939221	7.355566	NR4A2	9.924593	10.665573	U2AF1L4	8.174223	8.657763
ENGASE	9.783274	10.148196	NSUN7	4.011925	4.750853	UBA7	7.884058	8.451952
ENPP2	4.727364	5.852979	NT5C2	9.687179	9.993980	UBAC2	8.835503	9.294945
ENTHD2	10.198218	10.666820	NT5E	2.653821	3.366242	UBALD1	8.656408	9.031562
EP400	10.369762	10.813033	NTN5	2.736008	3.205833	UBAP1L	5.203255	5.767372
EPB41	10.767210	10.994680	NUAK2	10.683458	10.956307	UBE2G1	9.562473	9.951837
EPB41L4A-	8.790712	9.147921	NUB1	8.352424	8.757364	UBE2H	10.640243	10.929215
EPHB6	8.195338	8.657045	NUDT17	5.740746	6.270163	UBL4A	8.872394	9.184188
EPHX1	7.017937	8.220787	NUMA1	10.899880	11.432127	UBN2	8.882831	9.250013
EPS15L1	8.364827	8.771379	NUMBL	6.616713	7.267147	UBR2	8.800645	9.080573
EPS8L2	7.662902	8.892119	NUP85	7.549594	7.986614	UBTF	10.872049	11.102501
ERBB2IP	10.073792	10.332255	NXF1	10.571878	11.051442	UBXN11	6.986321	7.399203
ERCC6	7.215803	7.550205	OAS2	8.837370	9.496462	UCKL1	7.923836	8.644657
ERF	10.424454	10.901599	OBSCN	7.176507	7.940133	UCKL1-AS1	5.992437	6.620474
ERMN	5.696187	6.495164	ODF2L	6.870189	7.197889	UCN	4.626888	5.521500
ERMP1	7.339954	7.706900	OGFOD2	7.757489	8.179343	UHRF2	9.233554	9.644783
ERP29	10.083042	10.836218	OGFR	10.621915	10.836956	ULK1	9.225187	9.909288
ESYT1	9.392782	9.969350	OGFR-AS1	4.615748	5.248875	UNC5CL	6.835747	7.425221
EVI5L	7.512667	7.830653	OGT	11.851027	12.165607	UNC93B1	9.392033	9.779728
EVL	8.554424	9.044601	ORAI2	12.312134	13.081224	UNKL	9.084015	9.434910
EYS	4.044213	4.549849	ORAI3	9.214082	9.472470	UPF3A	7.912754	8.330122
EZR	13.060175	13.496880	ORM2	3.749554	4.386349	UQCRB	7.740910	8.106981
FAIM3	10.881011	12.147648	OSBPL11	9.018254	9.357289	USF1	9.431646	9.958842
FAM102A	10.105261	10.707639	OSBPL3	6.648385	7.236814	USP11	8.606994	8.925301
FAM102B	7.734864	8.576748	OSBPL7	7.697280	8.174353	USP13	7.589933	7.938866
FAM111A	9.051653	9.643364	OSBPL8	9.073585	9.388564	USP15	8.698260	8.953256
FAM111B	6.296707	7.990343	OSER1-AS1	6.809008	7.250031	USP20	8.862110	9.254765
FAM117A	9.777709	10.060223	OTUD1	9.796865	10.349405	USP21	8.772061	9.146895
FAM117B	7.966368	8.849904	OVGP1	6.037259	6.538790	USP28	8.026320	8.505633
FAM120C	6.326657	6.995432	OXR1	8.032750	8.372178	USP3	9.178885	9.407013
FAM129C	9.023210	10.333919	P2RX1	6.949101	8.113017	USP48	8.359561	8.651220
FAM134A	10.517393	10.768226	P2RX5	5.633269	6.374442	USP53	7.232655	7.581664
FAM134C	9.907202	10.311827	P4HTM	8.730420	9.418310	USP6NL	8.635418	8.999053
FAM13A-	4.644562	5.242985	PACS2	8.307973	8.672479	USP8	8.818162	9.167869
FAM159A	6.839793	7.330614	PAIP2	10.173342	10.458602	USPL1	9.490136	9.814636
FAM167B	4.084406	4.765177	PAIP2B	7.466622	8.163529	UTRN	7.771586	8.387835
FAM178A	9.105286	9.436315	PAN2	8.709327	9.300514	VAMP1	9.347425	10.212651
FAM193B	10.001108	10.527868	PANK1	5.647662	6.359120	VAMP2	10.494623	10.922091
FAM20A	3.925545	4.468174	PAPD5	8.292226	8.569102	VAMP4	8.504742	8.825564
FAM210B	7.245459	7.793391	PAPD7	9.129675	9.680712	VAMP5	7.372925	7.701464
FAM214A	8.605546	9.676050	PAPOLG	8.271844	8.573335	VASH1	7.634636	8.007980
FAM217B	8.370932	8.703073	PARD6A	7.671486	8.443828	VAT1	10.136745	10.693485
FAM26F	5.500341	6.192759	PARP15	10.407021	10.716140	VAV1	7.193247	7.637508
FAM43A	8.761940	10.090857	PARP16	7.345006	7.733422	VGLL4	8.029868	8.358128
FAM46A	7.106163	7.521119	PARP4	8.718416	9.087352	VIPR1	6.653476	7.175961
FAM46C	10.462108	11.444296	PARVG	8.564574	9.421165	VNN2	6.693436	7.258470
FAM63B	6.923214	7.590654	PATL2	6.654172	7.182981	VPREB3	6.158349	7.371381
FAM65B	9.820740	10.910179	PBXIP1	11.063074	12.348149	VPS11	8.857144	9.153330
FAM73B	9.556967	9.801155	PCBP4	7.876326	8.184956	VPS13C	10.132376	10.352360
FAM76A	7.656214	8.019732	PCDH9	5.037308	5.962840	VPS26B	7.769576	8.606204
FAM76B	8.854390	9.153176	PCF11	10.442840	10.675817	VWA5A	4.986424	5.485415
FAM78A	9.454377	10.136842	PCM1	9.052248	9.282706	WASH2P	5.293496	5.730648
FAM89B	9.566585	9.974526	PCMTD2	9.759498	10.200278	WBP2	10.172821	10.452324
FAM8A1	7.488678	8.425106	PCOLCE	5.012493	5.682989	WDR19	5.716763	6.498161
FARP2	7.459994	7.806834	PCP2	5.007082	5.639200	WDR34	7.945039	8.382785
FAXDC2	4.729495	6.504227	PCSK7	9.483444	9.948045	WDR37	8.435207	8.813055

FBXL16	5.937166	6.450378	PCYOX1	8.295183	8.948464	WDR52	6.825240	7.305678
FBXL20	8.814698	9.424835	PDE4A	8.352960	9.223207	WDR54	6.535852	7.118899
FBXL3	10.365904	10.615842	PDE4B	11.357694	11.777547	WDR74	7.983100	8.291068
FBXO10	9.191486	10.294236	PDE7B	4.754555	6.298709	WDR90	7.433413	7.766255
FBXO15	3.215359	4.048794	PDGFD	6.938982	7.420570	WFIKKN1	4.016317	4.916781
FBXO18	9.386447	9.632113	PDIK1L	7.678689	8.065567	WHSC1	9.552048	9.839877
FBXO21	9.430987	9.819747	PDK3	8.308838	8.758424	WIPF1	11.487602	11.952482
FBXO32	6.666385	7.917332	PDK4	6.294045	7.319272	WNT16	5.836915	6.264780
FBXO33	8.930994	9.382873	PDLIM1	8.562436	9.498229	WNT3	9.327378	9.967734
FBXO44	9.170375	9.537249	PDP1	8.692799	9.370561	WSB1	10.459574	10.743654
FBXO9	8.579870	9.013078	PDPK1	10.100798	10.498426	XAB2	8.513218	8.786079
FCGR2B	8.078852	8.782827	PDPR	9.918845	10.206283	XAF1	7.895972	8.578882
FCGR3A	6.152125	6.665864	PDXDC2P	6.321283	6.896840	XKRX	6.269214	7.241268
FCGRT	8.521760	9.115571	PDXK	8.788124	9.210474	XPC	9.724890	10.061000
FCHO2	6.999559	7.509603	PECAM1	9.511264	10.503156	XXYLT1-AS2	6.758202	7.651515
FCHSD1	8.350814	8.766951	PEG10	8.801794	10.154407	XYLT1	9.465020	10.111011
FCRL1	7.728396	8.160657	PELI2	7.039963	7.467473	XYLT2	7.718274	8.150806
FCRL2	8.068538	8.845014	PER1	9.688571	10.299158	YPEL1	7.942245	8.605516
FCRLA	9.644855	10.678799	PEX1	7.771925	8.188685	YPEL2	9.969722	10.884158
FCRLB	5.667689	6.392084	PEX5L	2.648191	3.156667	YPEL3	10.524072	11.227572
FER1L4	4.010051	4.643179	PEX6	8.770280	9.066273	YPEL4	3.321757	4.276776
FGD3	8.468591	9.448254	PFKFB3	8.843424	9.359292	YPEL5	10.956567	11.507696
FGF22	2.587078	3.245644	PGAM2	7.857143	8.396992	ZBED6	8.347691	8.660097
FGFR1	7.682941	8.202146	PGBD2	8.280659	8.557514	ZBP1	5.677379	7.218432
FGFR1OP	7.398192	7.766971	PGM2L1	8.016898	8.450413	ZBTB1	10.955731	11.270760
FGL2	6.222558	6.601358	PGPEP1	8.172682	9.126190	ZBTB11	9.145998	9.445513
FHDC1	5.501349	6.237076	PHC3	10.339676	10.773814	ZBTB14	8.530060	8.849880
FLI1	9.264164	9.833435	PHF1	10.261433	10.623586	ZBTB18	10.569639	11.135100
FLJ10038	7.424381	7.915273	PHF10	6.874529	7.341400	ZBTB2	9.085511	9.366880
FLJ32255	7.744199	8.489583	PHF12	9.641911	10.042149	ZBTB20	8.604613	9.101418
FLJ42258	5.947016	6.801358	PHF19	8.388283	8.823753	ZBTB38	10.543435	10.851378
FLJ44342	6.376689	7.230382	PHF2	9.236882	9.482758	ZBTB4	11.009518	11.734646
FLT1	5.505945	5.957103	PHF3	10.289628	10.589862	ZBTB40	10.313517	10.572185
FLYWCH1	9.347118	9.702207	PHF7	6.038726	6.992684	ZBTB41	8.193699	8.530404
FMR1	8.897438	9.205902	PHIP	9.552442	9.829743	ZBTB44	10.270798	10.674770
FN3K	3.855339	4.444605	PHKB	8.573794	9.082301	ZC3H11A	10.302267	10.625848
FN3KRP	8.613282	8.887707	PHKG2	8.023116	8.346852	ZC3H3	8.778419	9.185062
FNBP4	10.732871	11.045661	PHTF2	8.637925	8.880933	ZC3H6	7.643649	8.048756
FOLR2	2.511209	3.140909	PI4KA	7.278949	7.653162	ZC4H2	6.366650	6.737372
FOSB	10.218175	10.471421	PIDD	8.226646	8.675113	ZCCHC11	9.685899	10.061754
FOSL2	8.712739	9.314652	PIH1D1	8.766341	9.011632	ZCCHC14	6.998694	7.484478
FOXJ2	9.163383	9.446977	PIK3IP1	9.953773	10.760814	ZCCHC18	7.415280	8.190439
FOXO3	7.710509	8.254120	PIK3R1	9.020786	9.334805	ZCCHC2	8.979175	9.360559
FOXO4	9.321751	9.844210	PIP5KL1	4.954323	5.750413	ZDHHC20	10.819577	11.057106
FRAT1	7.887102	8.763219	PITPNM1	10.144960	10.553227	ZDHHC8	9.674896	9.909633
FRAT2	8.405748	9.047434	PITPNM2	9.613802	10.806899	ZER1	9.079020	9.507271
FRMD8	9.846276	10.065080	PKIA	7.181023	7.774241	ZFAND2B	8.059587	8.537627
FRMD8P1	8.697389	8.988543	PKN2	8.519805	8.771001	ZFP14	7.930833	8.362674
FRY	7.683655	8.451528	PLA2G15	7.108969	7.641015	ZFP30	7.815103	8.141721
FUCA1	9.080911	9.452319	PLA2G4B	4.499828	5.170232	ZFP36L2	11.806513	12.986661
FUZ	6.728539	7.528590	PLA2G6	7.223059	7.568510	ZFP64	7.829307	8.324548
FXYD1	3.112946	3.627917	PLAC9	3.650455	4.208004	ZHX2	10.897864	11.338397
FXYD5	7.782667	8.355873	PLCB2	8.498381	9.015550	ZHX3	6.912212	7.780314
FXYD7	4.086196	5.481156	PLCD1	4.792269	5.417205	ZIK1	8.249636	8.690029
FZD3	7.223813	7.896181	PLCG1	9.064017	9.427354	ZKSCAN8	9.843298	10.054972
GAA	8.243748	8.642256	PLCG2	8.154647	9.115745	ZMYM3	8.342762	8.910024
GAB2	9.696769	10.489925	PLCH2	6.490566	7.170513	ZMYND15	3.547227	4.204713
GAB3	7.096943	7.428629	PLCL2	10.211708	10.549660	ZMYND8	8.030524	8.438943
GABARAPL	8.234491	8.777779	PLCXD1	7.916426	8.181930	ZNF10	7.653888	8.286307
GABARAPL	6.184529	6.616750	PLD3	8.563995	8.887936	ZNF101	8.590284	9.066579
GAK	9.678003	10.044604	PLD4	2.865686	3.456299	ZNF107	11.076054	11.910763

GAL3ST4	3.124887	3.645709	PLEKHA2	11.534749	12.498465	ZNF137P	7.392978	7.726225
GALK1	6.095605	6.491927	PLEKHA3	8.560613	8.915017	ZNF14	8.304603	8.601256
GALM	5.559671	6.233197	PLEKHG7	2.156266	2.756356	ZNF181	8.086832	8.360869
GALNS	8.464871	8.848253	PLEKHM1	8.847815	9.131169	ZNF182	8.077200	8.357461
GALNT3	5.860723	6.323214	PLEKHM1P	6.966586	7.366811	ZNF184	8.082250	8.422018
GALR2	3.730343	4.510656	PLK1S1	6.244892	6.723819	ZNF211	9.060520	9.498993
GAPDH	11.652124	11.888623	PLK2	6.835149	7.241420	ZNF224	7.084624	7.480551
GAS7	6.825376	7.396223	PLP2	10.286080	10.699349	ZNF248	7.950252	8.476661
GATAD1	9.678920	9.898051	PLXND1	8.766234	10.413918	ZNF250	7.575379	7.952059
GATM	6.628605	7.121469	PMM1	6.606709	7.014373	ZNF266	10.979972	11.492441
GATS	8.201142	8.506439	PNMA5	5.787281	6.559524	ZNF273	7.489178	7.809169
GCC2	9.105312	9.420436	PNOC	5.919688	6.572153	ZNF275	9.149077	9.371756
GCHFR	7.601200	8.137797	PNPLA2	10.337295	10.990806	ZNF30	5.500866	5.983478
GCLC	8.866777	9.138254	PNPLA7	6.181029	7.413247	ZNF304	8.708785	8.977223
GCNT2	7.354434	7.791559	PNPLA8	8.972647	9.534749	ZNF318	9.716905	10.032923
GDE1	9.076656	9.349398	PNRC1	11.671833	12.052963	ZNF324	7.577579	7.952447
GDF11	6.821368	7.238410	POFUT2	9.554029	9.856417	ZNF331	9.858796	10.850839
GDF7	7.223427	7.830254	POLI	8.078500	8.375220	ZNF335	8.533672	8.875345
GDPD1	4.836868	5.504822	POLR2A	11.202887	11.523289	ZNF362	7.476166	7.901811
GDPD3	5.701194	6.434117	POLR3GL	8.218894	8.579793	ZNF367	6.292707	6.797933
GFOD1	8.026594	9.059989	PP7080	8.241461	8.579391	ZNF394	9.850628	10.110642
GGA2	11.843252	12.947867	PPARD	9.071386	9.824898	ZNF395	10.522494	11.336246
GGA3	10.281704	10.786848	PPM1D	8.682267	9.048631	ZNF420	7.723749	8.024885
GH1	3.673550	4.324812	PPM1J	4.555932	5.374052	ZNF439	8.084138	8.709601
GHDC	8.517712	8.897716	PPM1K	11.094791	11.705290	ZNF441	7.800679	8.234593
GIGYF1	10.930393	11.141058	PPOX	7.414564	7.892039	ZNF443	4.961438	5.522535
GIPR	3.496856	4.149104	PPP1R12B	7.797324	8.184707	ZNF487	4.480348	5.116777
GIT2	9.378430	9.913214	PPP1R32	4.789603	5.597100	ZNF510	8.462734	8.719863
GKAP1	5.101303	5.674361	PPP1R37	8.863519	9.121753	ZNF540	5.794655	6.656633
GLCCI1	7.612058	8.244544	PPP1R3E	7.908267	8.751273	ZNF548	8.872817	9.205345
GLI1	4.861096	5.476480	PPP2R5A	9.931140	10.205015	ZNF569	7.484048	8.083320
GLIPR1	7.806639	8.800315	PPP2R5C	10.369936	10.898137	ZNF575	4.803644	5.503796
GM2A	10.246113	10.955648	PPP6R2	9.025896	9.322870	ZNF589	8.898818	9.194138
GMCL1	7.419958	7.768913	PRC1	6.504971	7.054445	ZNF592	10.254471	10.512368
GMEB2	9.595595	9.984911	PRDM2	12.422987	12.772597	ZNF595	7.297537	7.939653
GMFG	6.413312	6.814777	PRICKLE1	4.628682	5.720444	ZNF615	7.860302	8.211976
GNA13	11.637537	11.881008	PRICKLE2	2.261932	2.787186	ZNF627	7.970662	8.278136
GNAO1	6.134217	7.114427	PRKAR2A	9.445878	9.711862	ZNF652	8.647479	9.157508
GNAZ	6.826825	7.796849	PRKCB	11.069654	11.474835	ZNF654	8.377947	8.687484
GNB5	9.000790	9.988991	PRKCE	8.534402	9.622876	ZNF667	5.793637	6.189179
GNG7	7.391989	9.699179	PRKCSH	9.109237	9.575673	ZNF671	8.685030	9.018308
GNL1	9.668105	9.970507	PRKD2	8.436242	8.827700	ZNF675	8.270327	8.522476
GNPTAB	10.412407	10.728793	PRKX	8.974264	9.645325	ZNF699	7.357948	7.830270
GNRH1	5.004545	5.546131	PROC	3.268809	3.865955	ZNF700	8.288623	8.705352
GOLGA1	7.331251	7.831958	PRR12	9.502627	9.967238	ZNF75D	7.764135	8.102414
GOLGA2P5	7.591021	8.569150	PRUNE	8.708390	8.938574	ZNF763	6.047648	6.478341
GOLGA8B	9.247623	9.548564	PRX	6.820117	7.500682	ZNF767	8.709459	9.066665
GORASP1	8.806483	9.345344	PTAR1	10.035614	10.366047	ZNF776	9.238460	9.474932
GPATCH11	8.617671	8.910654	PTCH1	4.683725	5.283571	ZNF791	8.069907	8.424502
GPCPD1	9.202075	9.722096	PTP4A1	10.256683	10.476113	ZNF792	6.561854	6.968390
GPLD1	5.685776	6.527283	PTPN12	9.680322	10.005813	ZNF815P	4.129018	5.025899
GPM6A	6.838589	7.639325	PTPN18	10.291396	10.774095	ZNF821	7.153703	7.898698
GPR152	2.272336	2.846027	PTPN22	8.068919	9.076870	ZNF831	7.759459	8.762444
GPR155	7.031886	8.595968	PTPN7	10.791922	11.053745	ZNF862	8.978615	9.380629
GPR18	6.843750	8.444761	PTPRC	10.591800	11.306562	ZNF92	8.913216	9.698205
GPRASP1	7.996842	8.698931	PTPRCAP	10.503651	11.914591	ZSCAN18	9.841149	10.138604
GPRIN3	5.610673	6.023336	PTPRE	8.269751	8.743076	ZSWIM6	8.100975	8.535029
GPT2	9.118758	10.817960	PTPRVP	4.417513	5.199809			

Appendix 6. Significantly up-regulated genes induced by the soluble CD40 ligand in primary CLL cells at 24h time point

24h up-regulated	Expression LevelS24	Expression LevelU24	24h up-regulate	Expression LevelS24	Expression LevelU24	24h up-regulated	Expression LevelS24	Expression LevelU24
A1BG	7.953602	7.591251	GPSM3	11.135677	10.772795	PSD	6.837553	6.255325
AAGAB	9.188062	8.913403	GPX4	9.674541	9.234401	PSIMCT-1	5.673029	5.066073
AAR2	9.379451	9.095487	GRHPR	9.092238	7.690434	PSMA1	9.015821	8.502967
AARS	10.214361	9.682146	GRIK4	4.809248	2.879310	PSMA4	9.211167	8.650856
ABCC4	8.064724	6.619467	GRIN1	3.559553	2.351340	PSMA7	9.060082	8.672845
ABCD2	7.182471	6.394765	GRINA	10.993166	10.123794	PSMB1	7.950799	7.572439
ABCE1	9.516025	8.979339	GRN	11.771573	11.278014	PSMB2	9.177748	8.698735
ABCF1	9.549374	9.109554	GRSF1	10.046311	9.260831	PSMB5	9.051453	8.375940
ABCF2	8.969114	8.487731	GRWD1	9.341053	8.883131	PSMC2	7.624181	7.284260
ABHD17C	6.641581	5.957670	GSTP1	11.256427	10.884975	PSMC4	8.181014	7.814791
ABTB2	10.037128	7.339014	GTDC1	7.203960	6.505307	PSMD1	7.204116	6.586985
AC058791.1	4.574611	3.922992	GTF2H3	8.807539	8.484859	PSMD11	9.897823	9.503473
AC147651.4	8.123056	7.268723	GTF2H5	7.849693	7.484557	PSMD12	7.253541	6.816966
ACACA	7.589446	7.207003	GTF3C4	8.852180	8.545375	PSMD14	7.276049	6.530631
ACAD9	7.207953	6.774966	GTF3C6	7.522765	6.709447	PSMD3	10.230640	9.814660
ACADVL	11.532584	11.149527	GTPBP4	8.542398	8.071243	PSMD7	9.900365	9.502075
ACBD6	8.226261	7.710660	GTPBP6	9.919791	9.671483	PSME3	11.002021	10.496613
ACHE	6.768688	4.742802	GYS1	9.005394	8.694453	PSMG3	9.374916	8.886819
ACKR3	6.692507	5.580341	H6PD	10.655701	10.370266	PTEN	10.667304	10.433113
ACOT2	8.416423	8.005588	HAPLN3	7.242398	4.912322	PTGER4	10.310253	9.410302
ACOT4	6.553445	5.451856	HBS1L	8.417542	7.998345	PTGES2	9.894379	9.079558
ACSL1	9.613888	8.765114	HCG26	8.331340	7.701408	PTGES3	11.490620	11.201296
ACSL4	9.967204	9.063832	HCLS1	10.366310	9.919086	PTGIR	9.973834	7.084023
ACTB	16.011360	14.509096	HCN3	8.408519	7.803331	PTK2B	10.750176	9.969431
ACTG1	13.975809	12.978394	HCP5	11.339949	10.391123	PTMS	9.291615	8.484564
ACTN4	10.010649	9.531149	HDAC9	9.388910	8.592509	PTP4A3	6.623716	5.344837
ACTR1B	10.146929	9.763903	HEATR1	7.392285	6.956633	PTPN1	12.385055	11.838354
ACTR2	12.782099	12.498458	HEATR2	7.961268	7.454270	PTPN11	10.479156	10.181199
ACTR3	11.924207	11.182534	HEG1	8.341664	7.791966	PTPRF	4.666223	4.049622
ACTR3B	6.788065	5.768757	HELLS	4.860758	4.331003	PTPRO	7.416406	6.998408
ADA	7.878489	6.952115	HERPUD1	11.654757	10.669929	PTRH1	5.462714	4.932335
ADAM8	9.882809	9.422415	HIGD1A	8.722714	8.192657	PTRH2	8.187149	7.718312
ADAMDEC1	8.108818	6.232325	HIGD2A	8.918177	8.616641	PUF60	9.388272	9.003443
ADAMTS7	8.326577	6.992316	HILPDA	7.294816	6.412307	PUS7	6.357719	5.509326
ADAT2	7.674849	7.130231	HIRA	9.583283	9.134908	PVR	7.247235	6.661869
ADCY3	7.382646	6.624957	HIVEP1	11.591735	11.140702	PVRL1	10.027763	8.200008
ADIRF	6.080527	4.557205	HIVEP3	8.068183	7.339419	PYCR1	8.260983	6.064941
ADM2	7.381417	5.716318	HK2	8.429150	7.651651	QSER1	8.908262	8.603950
ADNP	11.195404	10.957899	HLA-A	13.401634	13.136565	QTRT1	9.142368	8.651669
ADO	10.396168	10.010414	HLA-B	14.013841	13.672862	QTRTD1	9.471702	9.103348
ADPRH	10.896998	10.045864	HLA-C	12.883030	12.561046	RAB10	11.161529	10.774853
ADSL	7.320443	6.719633	HLA-	12.509490	12.033920	RAB11A	10.275003	9.534631
AEBP2	9.405431	9.124496	HLA-	9.750306	8.769536	RAB13	9.623606	8.262157
AGFG1	10.040350	9.716423	HLA-	7.516829	6.666058	RAB21	10.663142	9.962045
AGL	8.655202	8.365370	HLA-	11.089092	10.437605	RAB39A	6.978702	6.321346
AGMAT	7.469726	6.370287	HLA-	10.204951	9.534120	RAB3GAP2	10.167510	9.616959
AGPAT3	11.333868	10.598322	HLA-E	14.287375	13.991160	RAB3IP	8.595232	8.258827
AGPAT6	10.812414	10.549432	HLA-F	11.900973	10.939797	RAB44	3.997764	2.934756
AGRN	7.645800	6.789048	HLA-L	7.877141	6.794364	RAB7L1	11.767513	10.560577
AGTRAP	7.629613	7.182788	HMGA1	11.214332	10.222061	RAB8B	11.436951	10.855283
AHCY	8.931351	8.477557	HMGCR	8.771814	8.252869	RAB9A	9.989506	8.411926
AIFM2	8.231195	7.827311	HMGCS1	9.903464	9.121187	RABGGTB	8.324886	8.023890
AIMP2	7.462382	6.420642	HMGN1	10.215162	9.949769	RABL3	8.495328	8.060644
AIRE	3.452527	2.193258	HN1L	10.419693	9.768490	RAC1	10.320348	10.009101
AK2	10.438867	10.072937	HNF1B	4.957731	3.753008	RAD23B	10.720336	10.424021
AKAP12	8.203482	7.732816	HNRNPA	10.543968	10.082707	RAD50	8.973068	8.560301

AKR1A1	8.789518	8.184293	HNRNPC	11.312624	11.103650	RAD51B	6.299134	5.327946
ALCAM	9.230131	8.433582	HNRNPF	12.385032	12.145393	RAD51D	7.998153	7.328008
ALDH18A1	8.606723	8.317696	HNRNPK	11.638322	11.404710	RAET1K	4.719089	3.764198
ALDH1B1	9.005862	7.955346	HNRNPM	11.612016	11.013579	RALA	9.832778	9.267196
ALDH2	7.176307	5.949927	HNRNPR	10.861054	10.383544	RAN	10.145716	9.710003
ALDH4A1	7.005663	6.245962	HNRNPU	12.378062	12.014735	RANGAP1	10.975680	10.560294
ALKBH2	7.500857	6.915137	HOMEZ	9.094890	8.321394	RAP1A	9.500058	9.172359
ALPK1	7.904115	7.337242	HOXB9	4.581664	2.984829	RAP1B	8.612859	8.301324
ALYREF	8.330915	7.865124	HPRT1	7.189994	6.755705	RAP1GAP	3.321751	2.691571
AMMECR1L	9.370920	9.106913	HSD17B1	8.035130	7.628584	RAP2A	10.270108	9.331164
AMPD3	9.872936	9.488498	HSF5	7.324718	6.973520	RAPGEF1	13.248279	12.889253
AMZ1	6.294603	5.625254	HSP90AA	12.548079	12.196879	RARA	10.513489	10.011484
ANAPC16	11.296770	10.994903	HSP90AB	12.314392	11.562649	RASGRF1	10.836455	10.442816
ANAPC7	9.327347	8.948659	HSP90B1	9.296806	8.837077	RASGRP3	10.171754	9.541075
ANKLE2	12.021287	10.871417	HSP90B2	10.032137	9.479475	RASSF2	12.456385	11.721278
ANKRD10	11.890276	10.883952	HSPA5	11.804135	11.144612	RASSF4	9.871375	8.032284
ANKRD27	8.184743	7.826271	HSPA8	12.400208	11.864253	RAVER1	10.440696	9.869810
ANKRD33B	11.139125	8.218603	HSPA9	9.932558	9.615700	RBBP9	9.707895	8.885143
ANO9	10.858147	9.867610	HSPB7	2.670670	2.122148	RBM12	10.755761	10.211914
ANP32A	10.748163	10.018870	HSPBP1	8.242288	7.553472	RBM19	9.800825	9.201659
ANP32AP1	9.286902	8.651712	HTRA2	9.973806	9.042910	RBM20	7.249210	6.079333
ANP32C	6.675776	6.060284	HUS1	7.527147	7.134973	RBM3	11.328704	10.511416
ANP32E	11.333460	10.940295	HUWE1	10.950328	10.500300	RBM45	6.188943	5.738012
ANXA2	8.724797	8.195545	HYAL2	8.012983	7.450556	RBMXL1	9.590626	9.307357
ANXA2P2	11.914294	11.317552	HYLS1	7.942028	7.261607	RBPJ	11.353922	10.566045
ANXA5	9.646031	9.102403	HYOU1	11.511247	10.224233	RCC2	11.122618	10.713460
ANXA6	7.985273	6.696232	IARS	8.422468	7.872966	RCCD1	8.300561	7.822372
ANXA7	10.015786	8.976671	IARS2	8.588394	8.284148	RCL1	7.067901	6.611755
AP1AR	9.222218	8.835470	ICAM1	11.410798	9.076789	RCN1	7.093702	5.373989
AP1S1	8.986207	8.645087	ICAM4	5.491791	4.917147	RELB	11.458717	10.545069
AP1S3	10.979358	10.274773	ICAM5	6.848085	5.433557	RELT	10.572859	9.849657
AP2B1	11.018343	10.766864	ICOSLG	5.269345	4.615022	REXO4	9.489454	9.146673
APEX1	11.005438	10.633308	IER2	12.275053	11.771473	RFC2	7.252233	6.696947
API5	10.555976	10.235367	IER3	10.794818	9.285861	RFC3	6.166268	5.657307
APITD1	3.761836	3.132643	IER5	13.514664	12.822380	RFFL	7.536187	6.835488
APLF	5.966964	5.356468	IFFO2	9.347917	8.953580	RFK	8.289172	7.958123
APOBEC3C	11.059527	10.434204	IFIH1	9.393138	8.598635	RFTN1	11.813577	9.827169
APOBEC3G	11.210267	10.593039	IFNGR1	9.763201	9.346301	RFX5	11.475747	10.587760
APOL1	8.846609	8.088551	IFNGR2	10.780364	10.100596	RGS1	8.959302	8.054632
APOOL	7.443268	7.083600	IFNLR1	10.922159	10.417373	RHBDF1	6.025289	5.224910
APPL1	10.673339	10.251585	IFRD2	7.276652	6.905462	RHBDF2	9.590654	9.182923
APRT	8.808586	8.340067	IGF2BP3	5.472191	4.663039	RHEB	6.468299	6.069171
AREL1	9.577296	9.212915	IGSF3	11.656065	10.033678	RHOF	6.047007	4.355731
ARF3	11.611093	11.064610	IKBKE	7.546157	6.847147	RHOG	11.143218	10.286219
ARFRP1	9.054112	8.732964	IKZF1	12.265137	11.757679	RIMS3	8.079275	6.973859
ARHGAP17	10.328129	9.490501	IKZF4	7.243872	6.813610	RIOK1	7.851200	7.360997
ARHGAP23	5.647904	4.441719	IL10	7.086514	6.314350	RIPK2	7.667464	7.224282
ARHGAP24	10.911241	10.522226	IL13RA1	10.566159	8.618030	RND1	7.764950	7.002037
ARHGAP31	10.810990	9.313572	IL15RA	7.014825	6.564333	RNF115	8.304450	7.888037
ARHGDIA	12.182496	11.848816	IL17REL	8.423473	5.468503	RNF145	10.600670	9.445000
ARHGEF12	9.569177	9.205075	IL1B	6.749199	6.130541	RNF182	2.601409	1.992390
ARHGEF2	11.512911	10.896419	IL21R	11.810773	9.905667	RNF19B	10.064001	9.302498
ARID5A	10.731250	9.928932	IL21R-	5.032682	3.902798	RNF207	6.995711	4.745560
ARL1	8.988852	8.627915	IL2RG	12.086532	11.452626	RNF208	5.442153	3.761991
ARL2	8.098157	7.606917	IL4I1	9.527967	7.216275	RNF215	6.601413	6.148230
ARMC6	8.106244	7.461291	IL4R	12.719160	12.470609	RNU105A	3.628224	2.744276
ARNTL2	8.498157	5.300441	IL6R	10.428230	9.308310	ROMO1	8.573124	8.056302
ARPC2	10.498219	9.943726	IL7	8.189277	7.073533	RP1-249H1.4	4.628848	2.829985
ARPC4	11.511566	10.965202	ILDR1	3.973019	3.262706	RP11-290F5.2	6.310941	5.255382
ARPC5	11.473633	10.827694	ILF2	9.663101	9.348415	RP11-356I2.4	6.618250	5.390153
ARPP19	12.148530	11.765525	IMPDH2	8.423418	8.099304	RP11-3P17.4	13.638275	13.429107

ARRDC3-AS1	5.114430	4.371524	INADL	8.317792	8.052028	RP11-	4.679204	3.291198
ARSB	8.261271	7.774163	INSL3	3.643327	3.019264	RP11-536C5.7	5.142525	4.519127
ASAP1	8.340180	7.956147	INSM1	6.583691	5.264408	RP11-	6.353958	5.866697
ASB2	4.288624	3.616974	INSRR	1.782933	1.268095	RP11-87E22.2	4.400496	3.126149
ASCC3	8.433754	8.014500	INTS3	9.404100	8.754706	RP3-	7.157037	6.274172
ASNA1	8.198430	7.783191	INTS6	9.775688	8.928177	RP4-	3.263373	2.700392
ASUN	6.857551	6.382267	INTS9	7.567917	7.136101	RPAP3	7.373702	7.001978
ASXL1	12.098316	11.639824	IPO4	6.455161	6.000686	RPEL1	7.197457	6.690161
ATAD2B	9.212634	8.922296	IPO5	9.812190	9.216624	RPF2	7.115596	6.160861
ATAD3A	8.030086	7.664174	IPO7	9.897482	9.549128	RPIA	8.437565	8.107845
ATF5	11.879009	10.556126	IQSEC1	11.774107	10.255995	RPL10	9.903455	9.581177
ATF7IP	11.243586	10.726702	IRAK1	11.068272	10.468975	RPL10A	9.542559	9.268882
ATG7	6.765557	6.349219	IRF2BP2	12.274639	11.958229	RPL13	10.519326	10.046809
ATIC	7.280811	6.785505	IRF4	12.626079	11.276572	RPL23A	6.979419	6.537247
ATOH8	3.567482	2.704664	IRF5	12.125198	11.048608	RPL23P8	9.263394	8.965291
ATP2B1	10.546738	10.072132	IRGQ	9.334378	9.052990	RPL29	12.721501	12.473222
ATP2C1	8.046513	7.716500	ISOC2	7.392895	6.501594	RPL36AL	10.750207	10.511685
ATP5B	11.093055	10.770413	ITFG3	9.386246	8.832176	RPL4	10.538156	10.180273
ATP5EP2	11.316277	10.961029	ITIH1	3.038724	2.283052	RPL7L1	10.559447	10.211236
ATP5G1	7.258256	6.780906	ITPA	8.456971	7.983761	RPLP0	10.100347	9.681470
ATP5G2	7.983415	7.560760	ITPKC	8.718697	8.416923	RPLP1	10.013713	9.674591
ATP6V0A2	9.269476	8.996934	ITPR1	9.025708	8.669258	RPS14P3	12.074066	11.814551
ATP6V0E1	10.534356	10.039391	IWS1	8.654431	8.371764	RPS2	10.513381	10.021096
ATXN1	11.185682	10.877902	IZUMO4	9.841516	8.867929	RPS27A	8.591690	7.883617
AURKAPS1	6.238717	5.488641	JADE2	12.251599	12.025805	RPS6	11.417879	11.077320
AVEN	7.407921	6.780420	JADE3	10.290708	9.721067	RPS6KA1	10.045625	9.305438
B3GALT6	9.941047	8.992557	JAGN1	9.450964	8.980003	RPS6KC1	8.251239	7.810793
B3GNT7	8.275147	7.548849	JAK3	11.108855	9.586581	RPS6KL1	4.473933	3.368396
B4GALNT1	4.062392	2.883996	JAM2	5.955225	5.138586	RPSA	6.596267	6.114268
B4GALT2	7.615176	7.135456	JAZF1	10.202301	9.751484	RPSAP58	12.148064	11.728933
B4GALT5	10.484103	8.907964	JMJD4	6.455379	5.952648	RPSAP9	3.718654	3.164912
B4GALT7	8.113070	7.690219	JPH4	6.439699	3.243410	RPTOR	9.362913	8.682687
BAHD1	10.168699	9.857148	JRK	9.877125	9.580698	RPUSD2	9.138040	8.561813
BAI2	3.151312	2.184390	JUN	12.996036	12.379234	RQCD1	9.965768	9.497832
BAIAP2L1	4.488149	3.621163	JUNB	14.086714	13.351132	RRP1	8.051443	7.705651
BANF1	9.351906	8.778517	KCNC3	8.150285	7.776745	RRP12	7.397526	6.744615
BASP1	13.272714	10.851975	KCNH3	5.653749	4.707706	RRP15	8.278223	7.818586
BATF	8.917502	7.997360	KCNN1	8.511966	5.248535	RRS1	9.092649	8.022408
BATF3	6.833039	4.885071	KCP	4.280979	3.569228	RSL1D1	10.946226	10.464287
BAZ1A	9.961502	9.386272	KCTD10	9.805545	9.480084	RSL24D1	9.699376	9.447976
BCAR3	8.369939	7.582849	KDM2B	12.268910	10.714558	RSU1	8.942696	8.546183
BCAT1	9.309865	7.757046	KHDRBS1	11.652400	10.967165	RTCB	9.538481	8.726300
BCCIP	7.720163	7.301681	KIAA0020	5.902294	5.224695	RTFDC1	9.577629	9.160482
BCKDHB	6.778784	6.248323	KIAA0391	8.311961	7.824285	RTKN	6.481769	5.501242
BCL2	14.198866	13.221322	KIAA1045	2.664470	2.104108	RUFY3	10.298589	9.186544
BCL2A1	9.392760	7.820882	KIAA1191	10.435796	10.025585	RUNX3	12.596069	11.756227
BCL2L1	11.493424	9.135548	KIAA1211	4.338624	2.991933	RUVBL1	7.573473	6.696404
BCL7A	9.111780	8.329193	KIAA1430	10.298336	9.903549	S100A10	8.714577	8.121591
BEND3	7.257881	6.709128	KIF13A	8.575798	8.253213	S100A14	7.223578	3.868838
BHLHE40	12.544377	11.275516	KIF1C	11.276370	9.933755	S100A2	4.122547	3.530971
BID	8.367325	7.678342	KIF21B	9.413559	9.035801	S100A6	10.467818	9.901778
BIRC3	13.052305	12.315273	KIF26B	5.150088	3.503692	S1PR2	8.149520	7.573102
BLK	12.368407	12.050104	KIF3B	10.090637	9.163625	SAMD14	7.524524	5.007918
BLMH	7.944299	7.425929	KLC2	9.069490	8.619309	SAMSN1	10.431034	9.625640
BLVRA	6.678430	5.619401	KLF6	12.656963	12.362437	SAMSN1-AS1	5.376193	3.741976
BMP1	5.805288	5.262282	KLF7	8.471615	8.017316	SAP30	5.253952	4.570271
BMP2K	9.541088	8.969050	KLHL42	8.370961	8.042674	SCARF1	6.332898	5.568616
BNIP1	6.506248	6.023196	KNOP1	7.788044	7.165746	SCD	8.820482	8.127994
BNIP3	7.176892	6.819566	KPNA6	10.665557	10.371578	SCFD2	7.398097	6.292158
BRI3	9.713801	9.169265	KRAS	11.288874	10.971437	SCLT1	6.250410	5.780682
BRIX1	8.014112	7.654140	KREMEN	5.510570	4.471036	SCOC	9.198322	8.931367

BRPF3	10.412945	9.995979	L1CAM	8.918726	7.857928	SCRN1	11.557863	11.306716
BSG	11.599480	11.294517	L3MBTL4	5.575276	5.036345	SDF2L1	8.507634	7.823733
BSPRY	8.615770	7.981703	LACTB	9.719532	8.703973	SDF4	10.640890	10.345442
BST2	9.680979	9.233069	LAGE3	8.726482	8.391347	SDR42E1	6.251427	5.816878
BTBD19	7.432743	6.569788	LAMP1	11.292403	10.931516	SEC11C	6.228411	5.526326
BTF3	9.331644	8.970954	LARP1	11.218238	10.968893	SEC13	8.670902	8.354378
BTG3	7.778639	7.313267	LARP4	9.410389	8.971292	SEC14L1	10.705399	10.355784
BTLA	10.762009	10.358610	LARS	8.977550	8.384273	SEC22A	7.692742	7.292941
BTN2A2	10.445081	9.024415	LARS2	7.517846	6.981058	SEC23B	8.114213	7.789182
BYSL	7.944979	6.792926	LAS1L	8.628135	8.294985	SEC61A2	8.458106	7.792157
BZRAP1-AS1	9.723518	8.611387	LAT2	10.330119	9.191869	SEC61B	7.444333	6.853811
BZW2	6.200291	5.594327	LCAT	7.045089	6.572970	SEH1L	8.709331	8.333180
C10orf10	7.822418	6.104466	LCMT2	8.346444	7.800231	SEL1L	10.136026	9.883401
C10orf2	9.140223	8.427869	LCP1	14.157744	12.285062	SEMA4C	7.799256	6.027704
C10orf32	8.303047	8.003915	LDHA	10.236663	9.535798	SEMA7A	11.003286	8.985579
C10orf55	4.511275	2.830362	LDHB	8.066238	7.386818	SENP1	8.677877	8.357190
C11orf31	8.884223	8.471332	LHFP	5.925815	4.102411	SEPT11	9.756610	8.750257
C11orf82	5.881863	5.401111	LHX2	3.622940	2.626554	SEPT5-GP1BB	3.034781	2.174196
C11orf95	8.666916	7.973348	LIG3	7.829841	7.019258	SEPT8	8.573040	7.496849
C12orf43	8.059812	7.618953	LILRB4	9.082356	7.743070	SERBP1	11.179379	10.838959
C12orf77	5.049610	3.866476	LINC0015	5.815112	3.647209	SERPINB9	11.594833	11.160468
C14orf1	8.482813	7.938300	LINC0017	5.714353	4.403198	SERPINE2	4.011177	3.295255
C14orf166	7.466282	7.000882	LINC0026	7.416980	6.841520	SET	12.516851	11.895729
C14orf169	9.372301	8.969259	LINC0033	8.124814	7.089845	SF3B3	10.156046	9.802861
C14orf80	8.185197	7.396758	LINC0051	4.114114	3.281087	SF3B4	8.741027	8.419412
C15orf57	10.589128	9.603219	LINC0098	8.974505	8.622160	SFPQ	11.947009	11.534271
C17orf89	6.401457	5.888603	LINC0099	8.336538	7.959765	SFT2D1	8.567571	7.892011
C17orf96	8.203131	6.720264	LINC0110	4.001038	2.763155	SFXN1	9.282866	8.750944
C17orf99	7.287339	4.563586	LINC0116	4.201704	3.048852	SFXN2	6.867724	6.001226
C19orf12	9.319003	9.087586	LITAF	12.434706	11.985278	SGCA	4.061217	3.389853
C19orf24	8.677582	8.363457	LLPH	8.335882	7.939998	SGPP2	11.199077	10.021414
C19orf70	8.048328	7.417836	LMNB2	11.615476	10.076240	SH2B3	11.001734	10.415952
C1QBP	8.338885	7.631167	LOC1001	10.630176	9.951731	SH2D3A	8.366765	7.716548
C1QTNF1	3.465747	2.356049	LOC1001	9.200580	8.709067	SH3BP1	9.068065	8.721831
C1orf186	8.858338	8.324919	LOC1001	6.272497	5.489784	SH3KBP1	10.174902	9.735481
C1orf200	6.325141	5.399718	LOC1001	8.933209	7.787680	SHFM1	6.477378	5.864859
C1orf86	8.806632	8.497204	LOC1001	8.784828	8.134899	SHISA8	5.231134	4.283978
C21orf67	4.249848	3.503518	LOC1001	5.766741	4.242214	SHMT2	9.436222	9.086987
C22orf34	6.865515	6.127635	LOC1001	5.095900	4.415323	SIAH2	10.794560	10.184566
C2orf16	3.819208	3.274989	LOC1001	7.181492	6.689643	SIRPA	10.794584	9.607924
C3orf38	9.141322	8.834557	LOC1002	4.611713	3.901168	SIRT6	7.967322	7.551424
C4orf46	8.148278	7.113655	LOC1002	8.424403	7.481713	SLAMF1	8.327258	6.621369
C5orf30	7.661271	7.179371	LOC1005	9.211494	8.906990	SLAMF7	11.361824	9.122259
C6orf222	6.388092	5.429877	LOC1005	5.764861	5.086807	SLC12A3	5.392142	3.998781
C6orf223	2.106453	1.592190	LOC1005	6.557749	5.846712	SLC12A4	9.303069	8.683257
C7orf73	8.591247	8.216109	LOC1009	7.088988	6.067210	SLC15A4	10.006976	9.632488
C8orf33	9.516507	9.217284	LOC1010	5.674149	3.435746	SLC16A9	3.268723	2.552510
C9orf64	8.604541	8.340379	LOC1019	4.720274	3.273982	SLC1A4	9.966951	9.404181
CA2	5.609804	4.891981	LOC1019	4.600329	2.977562	SLC1A5	10.249016	9.626715
CACNA1G	4.603383	3.390988	LOC1019	4.584538	2.951310	SLC20A1	10.187021	9.374367
CAD	8.444592	8.092975	LOC1019	7.572771	7.093581	SLC24A1	8.106206	7.466238
CALM3	11.158910	10.811147	LOC1019	6.173001	5.356958	SLC25A11	8.639399	8.152269
CALR	12.626098	11.741731	LOC1019	4.618436	4.094097	SLC25A15	6.581229	6.113477
CAMSAP3	5.867303	4.965287	LOC1019	3.071862	2.280516	SLC25A23	8.246838	7.847384
CAND1	10.463160	10.174110	LOC1019	5.302177	4.020667	SLC25A25	9.218836	8.844971
CANX	11.705785	11.222020	LOC1019	6.846600	6.171484	SLC25A39	9.456361	9.077371
CAP1	11.169937	10.815333	LOC1019	2.811435	2.098308	SLC25A43	9.003165	8.390473
CAPG	8.715512	8.240410	LOC1027	4.176273	3.334876	SLC25A6	12.471555	12.153506
CAPN2	9.638868	9.317650	LOC1027	7.507497	4.997806	SLC27A4	7.764237	7.256371
CAPNS1	10.390149	9.975554	LOC1027	3.767447	2.851139	SLC29A1	8.976710	7.904880
CAPRIN1	10.598411	10.379790	LOC1027	5.239223	2.978049	SLC2A13	8.778194	7.769419

CAPZA1	11.481159	11.144503	LOC1027	7.256461	6.418571	SLC2A6	9.175845	7.963926
CAPZB	9.520476	9.148075	LOC1027	3.089498	2.675014	SLC30A9	8.331182	8.020838
CARM1	9.814978	9.105947	LOC1027	9.470493	8.794283	SLC35A4	10.728173	10.346561
CASP7	9.393260	8.744881	LOC1027	3.494412	2.590908	SLC35B2	11.695293	10.636735
CAST	9.959532	9.717281	LOC1151	7.179445	6.361784	SLC35F2	9.790013	8.922853
CASZ1	9.819394	8.648408	LOC1522	3.068965	2.259602	SLC37A1	9.666444	9.010784
CAV1	9.341877	6.987543	LOC3391	13.247178	12.384287	SLC38A1	13.074333	12.654633
CBFA2T3	11.288445	10.977795	LOC3888	5.713336	3.712012	SLC38A7	7.925877	7.527687
CBX1	10.188892	9.532883	LOC3898	6.407863	5.762117	SLC39A1	11.127842	10.461976
CBX6	11.845521	11.078819	LOC6441	4.750638	4.038190	SLC39A14	9.168908	8.449448
CCDC102A	6.240188	5.208173	LOC7301	7.713049	6.433161	SLC39A6	9.456755	9.119328
CCDC103	4.876476	3.393288	LOC8015	6.879704	6.200797	SLC41A2	8.121338	7.165818
CCDC106	9.066360	8.540694	LOC9078	7.865736	7.556029	SLC43A3	10.185178	8.169521
CCDC12	8.279608	7.656416	LONP2	9.242088	8.995059	SLC45A3	8.063136	5.923671
CCDC124	9.596485	8.890022	LONRF1	8.791004	8.344453	SLC50A1	10.001130	9.547619
CCDC141	6.948607	6.533315	LPCAT1	11.355819	10.382481	SLC6A6	12.208553	11.236378
CCDC167	6.478796	5.579804	LPP-AS1	2.683619	1.979767	SLC7A1	10.787451	9.944271
CCDC28B	7.917564	6.789111	LPP-AS2	4.990305	4.481924	SLC9A7	12.240234	11.461486
CCDC50	12.170925	10.965191	LRCH3	8.986462	8.548406	SLC9A7P1	6.503839	5.735416
CCDC71	8.750833	8.062651	LRP4	2.601126	2.005358	SLC9A8	9.947234	9.561050
CCDC82	8.789498	8.511295	LRP8	8.296582	6.847032	SLCO5A1	5.594875	4.282219
CCDC86	8.481129	7.589879	LRPPRC	8.535209	8.116338	SMARCA4	8.812218	8.547144
CCDC94	7.891740	7.578746	LRRC26	3.224873	1.917604	SMARCC1	10.477291	10.188316
CCL17	6.092118	3.230058	LRRC41	9.304003	9.009577	SMC6	8.947372	8.565225
CCL22	12.668254	8.194835	LRRC57	7.929529	7.621628	SMG1	12.020902	11.375825
CCL24	5.827783	4.962395	LRRFIP2	8.637428	7.855030	SMG7	10.401506	10.061761
CCND1	9.814171	8.206277	LSM6	6.845759	6.355912	SMG9	8.926757	8.504020
CCND2	10.879597	10.098483	LSP1	11.941956	10.767040	SMIM12	9.944179	9.497801
CCNI2	6.673379	5.720699	LSP1P3	6.112828	5.408166	SMIM15	9.032649	8.717686
CCR7	14.789242	13.672239	LSS	9.298652	8.890232	SMKR1	5.241108	4.652760
CCT3	9.804482	9.126152	LTA	8.529837	7.204848	SMO	4.921032	4.055190
CCT4	9.391023	9.076716	LTV1	7.544290	7.056399	SMPD2	7.197873	6.712547
CCT5	8.387743	7.834906	LY75	10.386110	9.369329	SMPD5	4.750706	3.844699
CCT6A	9.727002	9.278320	LYPLA2	9.347404	9.039746	SMS	7.750231	7.161475
CCT7	10.296253	9.692355	LYPLAL1	6.642090	6.095040	SMYD5	8.980703	8.451516
CD1C	4.396649	3.490266	LYRM2	9.446194	9.082567	SNAP23	10.706049	10.400538
CD200	11.030507	10.373927	LYRM4	8.077523	7.251943	SNAP47	9.223785	8.854853
CD40	11.534593	9.810700	MAATS1	5.340486	4.395465	SND1	9.537265	9.086820
CD58	9.505495	8.173851	MACF1	10.380762	9.531165	SNF8	7.876747	7.448690
CD59	10.554165	9.822915	MALSU1	7.448230	6.938983	SNHG16	9.007607	8.176152
CD70	9.835922	8.715651	MAML2	9.498283	8.952241	SNHG3	9.538158	8.900614
CD74	14.497895	14.066901	MANBAL	8.040053	7.696889	SNHG4	6.836550	5.717510
CD80	7.667405	5.771856	MANF	7.995998	7.580982	SNN	12.898935	11.363079
CD82	12.637159	11.577043	MAP3K13	7.867132	7.511523	SNORA73A	4.153938	3.379051
CD83	13.308793	12.021020	MAP3K8	9.682477	8.539663	SNORD80	6.031671	5.555513
CD84	11.926531	11.583100	MAP4	11.533107	10.677504	SNRPD1	7.096244	6.394598
CD86	8.799380	7.647640	MAP6	6.935215	6.137012	SNRPD3	10.913850	10.614957
CD97	11.352271	10.348227	MAPK11	8.712058	7.248237	SNX11	11.812194	9.567149
CDC42	11.841224	11.057363	MAPK13	10.280873	9.811360	SNX12	9.687112	9.402701
CDC42EP2	7.080565	5.857928	MAPKAP	10.470859	10.004471	SNX17	9.719376	9.281714
CDC42EP3	10.769459	10.437082	MAPKBP	9.583109	8.718776	SNX20	10.168775	9.341466
CDC42EP5	2.664137	1.928244	MAPRE1	10.408562	9.889636	SNX8	11.394601	11.086672
CDC42SE1	12.105565	11.496130	MARCKS	11.679886	9.817279	SNX9	11.098790	10.672767
CDH22	2.024944	1.479020	MARCKSL	11.908468	10.593525	SOCS1	9.594919	7.781802
CDK17	9.888664	9.485166	MARS2	8.738997	8.439851	SOCS2	4.513999	3.536134
CDK18	6.845537	5.099665	MARVEL	5.407525	4.767621	SP2	9.534290	9.260610
CDK2	8.957970	8.673715	MAT2A	10.723302	10.471975	SPAG7	8.220232	7.898086
CDK2AP1	8.969894	8.498836	MATR3	11.774953	11.560317	SPATA24	6.425116	5.895691
CDK4	8.841566	8.277300	MB21D1	8.189145	7.767485	SPATA31D1	3.539993	2.278301
CDKAL1	7.279457	6.918695	MCCC2	9.436617	8.774579	SPATS2	8.498204	8.051663
CDKN1A	12.031648	10.829380	MCL1	13.500600	13.243667	SPDYE3	6.929736	6.425122

CDKN2A	7.736886	7.031619	MCM3AP	4.988807	4.456693	SPECC1	7.259613	5.864901
CDKN2B	7.301119	6.543264	MCOLN2	10.021575	9.613968	SPHK1	7.275416	6.793675
CDYL2	6.186658	5.615564	MCOLN3	2.907361	2.399498	SPI1	10.523073	10.197785
CEBPG	10.797983	10.427928	MCRS1	8.187665	7.914586	SPIB	11.988670	10.843813
CEP135	8.403790	7.371395	MDFIC	12.276155	11.367507	SPIN3	9.225114	8.871072
CEP19	7.900799	7.438851	MDH2	8.718175	8.368267	SPINT1	8.992087	8.435186
CEP78	7.325591	6.943163	MED1	10.737255	10.497846	SPINT2	11.131217	10.618761
CERS4	8.660782	7.322158	MED14	8.846640	8.473905	SPN	11.418648	10.980221
CETN2	7.289656	6.881196	MED19	7.271978	6.790520	SPPL2A	8.121444	7.551839
CETP	5.719091	4.784837	MED22	10.306701	9.624732	SPR	6.290335	5.424845
CFL1	12.519633	11.994344	MEF2BN	6.731621	6.204200	SPRYD3	9.239665	8.970191
CFLAR	13.608410	12.277976	MEF2C	11.196847	10.584444	SPRYD4	7.885642	7.427227
CFLAR-AS1	5.221013	4.268974	MEGF8	9.031735	8.765617	SQLE	9.954796	8.439803
CFP	5.983891	4.856617	MESDC1	11.112655	10.641382	SQRDL	7.881218	7.518491
CGN	3.717528	3.020615	METAP1	5.027514	4.282596	SRC	10.121322	9.162560
CHAC1	6.583815	5.471676	METAP2	8.916329	8.603783	SREBF2	11.462777	10.989311
CHAC2	6.010173	5.247957	METTL1	6.493107	5.204620	SRFBP1	7.611511	7.055999
CHAF1B	5.015002	4.477831	METTL10	6.681130	6.292443	SRGN	13.682865	12.161971
CHCHD3	8.551335	8.019293	METTL21	8.674809	8.307471	SRM	7.513651	6.879680
CHCHD6	3.831021	3.054542	MEX3C	12.334423	12.052005	SRP14	10.767247	10.482463
CHML	8.823891	8.471805	MFI2	6.536731	5.858704	SRP72	9.165052	8.911784
CHMP4A	8.455797	8.142906	MFN2	10.359174	10.030459	SRP9	10.011892	9.710680
CHMP4B	11.607510	10.447964	MFSD10	9.590740	9.201500	SRPK1	9.878828	9.246642
CHMP6	7.941653	7.485625	MFSD2A	6.815323	5.703461	SRSF1	11.989553	11.603490
CHRNA6	6.773219	4.646282	MGAT2	11.079864	10.584718	SRSF3	11.583964	11.267951
CHST10	8.685332	8.203622	MGAT3	5.605551	4.914558	SSNA1	10.521427	10.075770
CHST7	9.829457	7.928500	MGC708	6.674419	5.411652	SSRP1	9.687863	9.165313
CHTOP	10.870733	10.631817	MGLL	10.663509	8.477564	SSTR2	3.594907	2.429830
CIAPIN1	8.040379	7.679931	MGRN1	10.073213	9.775712	ST13	10.064867	9.800159
CIB2	6.711000	5.999986	MICAL3	10.709531	10.182653	ST3GAL1	10.986346	10.300497
CINP	7.644849	7.160125	MIIP	10.156774	9.058871	ST3GAL2	10.646583	10.107513
CISD3	6.997685	6.623133	MINA	7.222425	6.655518	ST3GAL5	10.530533	10.016114
CKB	8.974726	7.152464	MIR155H	12.907790	10.004295	ST8SIA4	10.537679	9.417279
CLCF1	6.223747	5.436035	MIR17HG	7.055611	5.924536	STAP2	3.668425	2.975640
CLCN5	7.998736	7.001415	MIR21	4.344983	3.734492	STARD10	9.002322	8.010391
CLECL1	8.778888	8.417246	MIR22HG	8.295670	7.890238	STAT1	9.935369	9.443659
CLIC2	6.255091	4.539876	MIR3654	13.337313	13.049240	STAT5A	11.290817	9.977508
CLIP2	9.987514	7.585678	MIR4444-	8.846359	8.426913	STAT6	12.492624	12.239493
CLN6	8.994240	8.257652	MIR497H	4.307308	3.565208	STEAP3	6.386256	5.005016
CLNS1A	8.769329	8.292723	MKL1	9.867952	9.495254	STOML1	6.890216	5.931248
CLPB	6.989751	6.473624	MKNK2	13.304230	12.519412	STOML2	7.256802	6.922063
CLPTM1	10.271562	9.935670	MLH1	7.492326	7.041913	STPG1	7.357077	6.617532
CLSPN	5.231883	4.556089	MLLT11	6.663882	6.031382	STX11	9.663538	9.034849
CLTA	9.909421	9.550972	MLST8	8.227149	7.696026	SUB1	8.759635	8.263845
CLTC	10.180966	9.923349	MMAB	6.953990	6.418230	SUMO2	10.196871	9.872388
CLTCL1	5.107843	4.521598	MMD	9.464756	8.255330	SUMO3	10.086692	9.724191
CMAS	8.289670	8.013097	MMRN2	7.108313	5.954388	SUPT16H	10.192546	9.790139
CMTM6	11.813486	10.972872	MNAT1	6.284586	5.862100	SUPT3H	6.495574	5.862931
CNN3	7.417174	6.856768	MON1A	7.193688	6.754319	SWAP70	12.808022	12.190991
CNOT11	9.770683	9.379909	MORF4L1	10.448895	10.051168	SYBU	5.983792	5.229991
CNP	11.214670	10.513341	MOSPD2	7.824352	7.410548	SYCE2	5.006044	4.497154
CNTNAP1	8.481074	7.895106	MPC1	8.979210	8.446777	SYMPK	9.648007	9.250217
COA3	8.345816	7.900714	MPDU1	8.274138	7.948898	SYNCRIP	10.566291	10.283210
COA4	8.807218	8.305453	MREG	7.971909	5.521629	SYNE3	8.583435	8.228668
COA7	7.657207	7.144646	MRP63	9.437891	9.067680	SYNGR2	13.380578	12.300491
COBLL1	9.540771	8.883899	MRPL11	8.055803	7.716037	SYNJ2	7.715490	6.712407
COCH	9.252136	7.901357	MRPL12	8.011146	7.261570	SYNPO	11.025539	6.323091
COL19A1	7.939462	7.444749	MRPL14	8.832552	7.929503	SYT17	9.407469	8.437999
COL1A1	7.629171	5.117609	MRPL16	8.802281	8.507309	SZRD1	11.198975	10.791518
COL9A2	10.270022	9.866758	MRPL17	8.046787	7.655030	TAB2	11.553687	11.223011
COLGALT2	5.210730	4.390427	MRPL19	8.957190	8.683135	TAF15	10.069282	9.802790

COMMD1	8.993205	7.648802	MRPL24	7.576342	6.928469	TAF4B	8.028766	7.420561
COMMD5	9.775343	9.447461	MRPL27	7.599070	6.980424	TAF5L	9.493696	9.183214
COMT	8.715150	8.296035	MRPL28	8.555566	8.031914	TAF9	9.177985	8.821669
COPRS	7.741211	7.340373	MRPL3	8.584175	7.900647	TAF9B	8.099539	7.786539
CORO6	11.864646	9.593335	MRPL32	8.657064	8.301490	TAGAP	12.071207	11.718208
COX17	5.615030	5.113404	MRPL37	9.422928	8.992084	TAGLN2	13.617466	12.122300
COX5A	6.954684	6.486773	MRPL39	6.624917	5.975292	TANK	10.217328	9.772231
CPEB1	7.427411	6.936547	MRPL40	7.942541	7.486570	TAP1	11.071466	10.425583
CPNE2	7.302622	5.142851	MRPL45	7.637088	7.210470	TAP2	10.828102	10.293474
CPNE5	9.726883	7.964174	MRPS10	9.397562	9.047628	TAPBP	12.207179	11.665484
CPNE7	5.142090	4.360138	MRPS11	6.939326	6.530366	TARS	8.776039	8.238759
CPSF2	9.579927	9.203885	MRPS14	8.565994	8.161508	TBC1D17	8.253803	7.828656
CR2	7.628683	7.038069	MRPS16	9.654813	9.291228	TBC1D22B	8.512978	8.132941
CRIP1	9.455016	8.440499	MRPS17	6.920477	6.440778	TBC1D2B	10.219667	9.234209
CRIP2	9.249701	7.385702	MRPS23	7.386555	7.012722	TBCEL	8.060485	7.701068
CRTC2	10.635525	10.335107	MRPS28	7.595000	6.873471	TBL1XR1	11.150652	10.776738
CSF1	8.885294	7.203217	MRPS33	7.616966	7.039984	TBRG4	9.613552	9.281102
CSF2	2.073407	1.481129	MRTO4	9.081578	8.133592	TCEAL3	8.846994	8.577637
CSF2RB	10.152559	9.256732	MS4A1	12.507295	11.796376	TCEB1	7.141575	6.715236
CSK	11.818491	11.281720	MSANTD	8.782911	8.339895	TCEB3	9.408874	9.058029
CSNK1G3	9.520561	8.949075	MSMO1	9.390022	8.585485	TCF7	10.947356	9.473242
CSNK2A1	9.655232	9.431295	MST1R	7.678711	4.570930	TCFL5	10.975638	10.118637
CSNK2A3	9.948822	9.654310	MTA1	9.677694	9.237356	TCTN1	8.306627	7.059413
CSRP1	8.834306	8.515968	MTAP	8.316077	7.964437	TCTN3	7.623013	7.259493
CSTF2T	10.487570	10.232049	MTCH2	7.613151	7.224868	TDRD7	8.238374	7.638845
CTPS1	7.112944	6.166866	MTERF	7.862287	7.547290	TDRKH	6.478735	5.955987
CTSC	9.547249	8.996951	MTFP1	8.086604	7.106995	TELO2	8.946880	8.541920
CTSH	11.380326	10.420333	MTHFD1L	5.908789	5.210805	TES	8.559992	8.093958
CTTN	6.341524	5.919034	MTHFD2	9.325535	8.512286	TET3	10.310335	9.757883
CTTNBP2NL	7.844100	7.132932	MTMR12	9.330666	9.036675	TFAM	9.718268	9.404374
CX3CL1	2.519949	1.712950	MTMR2	8.272547	7.842252	TFDP1	8.551536	8.040328
CYB561	7.271512	6.081993	MTMR4	11.435499	10.079325	TFEB	11.210961	10.418445
CYB5A	6.675070	5.489653	MTMR9	9.753843	8.789365	TFG	8.865984	8.390251
CYB5B	10.210656	9.712040	MTSS1	10.593960	10.026656	TFRC	10.872786	10.238087
CYB5R2	7.353256	5.369088	MVP	10.916383	9.932245	TGIF2	10.663700	10.320166
CYBRD1	10.859098	9.021554	MYB	7.738301	6.409937	THEM4	7.361773	6.856913
CYC1	9.430389	8.999415	MYBBP1	7.628226	7.111029	THEM5	8.400445	6.380402
CYCS	9.875819	9.553078	MYBL2	8.901945	8.348308	THG1L	8.208517	7.292539
CYFIP1	8.023921	7.453287	MYC	10.282933	8.578441	THOP1	10.278221	9.164835
CYLD	11.966134	11.471752	MYEOV2	7.514197	7.084359	THTPA	7.856317	7.527029
CYP51A1	9.699267	9.037231	MYH11	7.596932	6.812436	THUMPD3-	8.282229	7.913040
CYS1	4.737226	2.423151	MYH9	12.637713	12.021796	TICAM1	10.299337	9.708186
CYTH1	13.297281	13.012785	MYL12B	10.489797	10.236769	TIFA	10.279154	9.890726
DACT3	4.365874	3.749365	MYL9	8.899777	7.768959	TIGD2	6.500526	5.998579
DAD1	10.251737	9.892459	MYO1C	10.590553	9.192320	TIGIT	10.541265	9.948040
DAP	10.801027	10.400093	MYO1D	7.943252	7.340057	TIMM23	7.801453	7.126639
DARS	9.053949	8.581492	MYO1E	9.081245	8.671471	TIMMDC1	9.816092	9.366931
DARS2	8.087212	7.562617	MYO1G	8.264033	7.531546	TINF2	10.668253	10.304810
DAZAP1	10.448031	10.045281	MYOCD	5.429135	3.168388	TIPRL	9.408526	8.977484
DBI	10.118624	8.859756	NAA15	9.446886	9.170263	TJAP1	9.847695	9.509343
DBNL	9.972295	9.561625	NAA20	8.137951	7.801628	TJP2	7.795970	6.414936
DCAF11	10.238501	9.959131	NABP1	9.155892	8.513928	TK1	7.311623	6.611742
DCAF16	9.645327	9.336359	NABP2	8.040419	7.713393	TLCD1	6.116277	5.179699
DCAF7	11.261622	10.944941	NACAD	4.981287	4.245515	TLE1	9.363125	8.455130
DCPS	7.386787	7.016623	NAGLU	9.049834	8.505751	TLR10	9.251322	8.062609
DCTD	10.089044	9.744656	NAMPT	9.577653	9.051504	TLR6	9.627146	9.203461
DCTN1	9.069439	8.812467	NAP1L1	11.225195	10.556249	TMA16	8.318990	7.704358
DCTPP1	9.503838	9.010212	NARS2	7.505315	7.038664	TMCC1-AS1	5.269900	4.766179
DDHD1	10.472514	10.122160	NAT10	8.764464	8.318090	TMCC3	9.608815	8.624612
DDHD2	8.395533	7.921495	NAT9	9.378129	9.132007	TMED3	9.201927	8.909204
DDOST	8.555019	8.246635	NBEAL2	11.189095	9.441445	TMEM102	8.521444	8.225746

DDR1	10.377260	9.289402	NBN	9.689224	8.754780	TMEM106A	8.159463	7.784784
DDR2	5.117448	4.325234	NCBP2	10.451974	10.221198	TMEM120A	8.499654	6.679126
DDX21	11.059120	10.288843	NCF2	11.113571	8.841371	TMEM120B	8.624884	7.826387
DDX47	8.568462	8.237490	NCK2	10.802134	9.982300	TMEM136	5.819658	5.211356
DENND4A	10.280267	9.180465	NCL	11.842902	11.433179	TMEM14A	6.891340	6.181505
DENND5A	9.354418	8.357638	NCLN	10.169707	9.953693	TMEM14B	8.370639	8.047480
DFFA	8.639306	8.194692	NCOA5	10.060597	9.787313	TMEM164	8.754255	7.867608
DGAT2	8.360501	7.278527	NDE1	10.674845	8.970843	TMEM168	8.826621	8.426639
DHCR24	8.269132	6.795008	NDFIP1	10.241461	9.830353	TMEM170B	9.280859	8.261823
DHCR7	7.901455	7.159500	NDFIP2	7.834734	7.442664	TMEM177	6.804431	6.013245
DHTKD1	9.983723	9.632976	NDUFAF1	8.126916	7.806624	TMEM185B	9.885074	9.497928
DHX33	8.633483	8.216421	NDUFB9	7.784829	7.433067	TMEM205	9.326121	8.801284
DHX34	8.663760	8.348095	NDUFS6	6.364928	5.823944	TMEM230	10.404062	10.028212
DHX37	8.636601	7.977375	NEAT1	13.371420	12.825499	TMEM241	5.778585	5.119292
DLD	8.281915	7.695376	NECAP2	10.762162	9.930065	TMEM254	7.706092	7.213030
DLGAP3	8.054068	6.426028	NEDD1	8.534176	8.120368	TMEM261	8.264440	7.862872
DLGAP4	11.369441	10.878491	NEDD8	8.025124	7.660446	TMEM54	5.664094	4.029716
DNAJA1	9.302810	8.762652	NEDD9	9.125081	8.062612	TMEM57	8.988358	8.500850
DNAJB5	7.182959	6.310761	NEIL2	8.188232	7.760702	TMEM63B	8.395882	7.483385
DNAJC14	9.934358	9.710543	NEK6	9.325184	8.278282	TMEM69	8.479523	8.022991
DNAJC30	8.550951	7.912632	NEK9	10.796179	10.574614	TMEM97	7.317336	6.551007
DNM1L	9.080609	8.820099	NENF	7.649064	7.277867	TMOD3	10.149088	9.868521
DNMT3A	9.611954	8.665284	NET1	4.848338	4.244529	TMPO	11.302528	11.016913
DNPH1	7.784866	7.136846	NETO2	8.274082	7.916143	TMSB4X	13.414419	12.676827
DOCK10	10.282608	9.239791	NFAT5	11.213010	10.689407	TNF	8.949074	8.370173
DOCK2	8.681681	8.378734	NFE2L1	12.373860	11.562258	TNFAIP2	10.736036	8.068215
DOK4	5.391410	4.538502	NFIC	9.463345	9.105619	TNFAIP3	12.860713	11.035707
DOT1L	10.429126	10.027518	NFIX	6.217070	5.378633	TNFAIP8	12.050378	11.306214
DPCR1	2.630762	2.018774	NFKB1	11.396952	10.158563	TNFRSF10B	11.681169	11.011731
DPH2	9.544898	8.997128	NFKB2	11.682414	10.198854	TNFRSF14	11.426021	10.478213
DPH3P1	7.486890	6.589820	NFKBIA	13.224680	11.114822	TNFRSF18	10.763610	9.066918
DPH6	5.746192	5.025908	NFKBID	10.354533	9.813712	TNFRSF19	2.515885	1.995011
DPP3	7.784413	7.247810	NFKBIE	11.603261	10.178613	TNFRSF1B	13.188299	12.552761
DRAM1	8.610334	7.898749	NFKBIZ	11.632246	10.479588	TNFRSF4	9.161512	6.680438
DRAM2	9.510078	9.139333	NHP2	8.989614	8.411086	TNFRSF8	8.367201	5.933219
DSE	7.861168	7.360637	NIFK	7.728039	7.243500	TNFRSF9	11.109620	7.540847
DTD1	6.871372	6.475212	NIP7	8.645556	8.114729	TNFSF14	7.404509	6.429335
DTD2	8.286415	7.605375	NIPAL2	9.827578	9.326254	TNFSF4	10.006048	7.109514
DTNB	6.029604	5.469451	NIPAL4	6.464801	5.439813	TNIP1	11.167061	10.707889
DTX2	7.928169	7.444255	NIPSNAP	7.519953	7.112906	TNIP2	10.597779	9.610075
DUSP2	10.835306	10.399224	NKIRAS2	9.348468	8.974161	TNKS1BP1	9.423985	8.200423
DUSP22	11.551397	10.619131	NKX3-1	6.785522	6.368362	TOMM22	9.381762	8.625239
DUSP5	10.511688	9.499164	NLGN4Y	4.057044	2.954845	TOMM34	8.469328	8.133450
DYNC1I2	6.554107	6.177822	NLN	8.473221	8.013981	TOMM40	8.596682	8.143274
DYNLT3	8.969401	8.615046	NLRC5	11.455330	10.921271	TOMM6	9.269566	8.823066
DZIP3	6.581985	5.975435	NME1	6.520077	4.944918	TOR3A	10.182884	9.668716
E2F3	8.844789	8.413429	NME3	9.395136	8.811668	TOR4A	9.837392	9.547233
EARS2	8.153320	7.153925	NOB1	8.599525	8.083376	TP53	9.929461	9.431482
EBI3	9.549301	4.994158	NOC3L	8.563918	8.196723	TP53BP2	9.650856	9.163370
EBNA1BP2	7.093238	6.633015	NOD2	10.852268	10.203598	TP53I11	11.358691	10.502516
ECE1	12.043981	11.065352	NOL3	4.937946	4.221725	TP53I3	6.849350	6.355810
ECE2	6.039201	5.186806	NOL6	8.856735	8.416611	TP63	4.491767	3.691883
ECHDC2	7.907906	7.572098	NOLC1	10.384707	9.825684	TPI1	10.099443	9.789299
ECHDC3	6.080794	5.109297	NONO	11.417875	11.141408	TPRN	8.984444	8.296761
EDARADD	11.426088	10.390748	NOP10	8.854083	8.382442	TPT1-AS1	6.799949	6.194052
EDC3	9.184250	8.859769	NOP14	8.229804	7.604613	TRADD	10.335622	9.521030
EED	8.279121	7.859700	NOP14-	7.227355	6.790656	TRAF1	14.239337	11.126570
EEF1A1	9.729582	8.758479	NOP16	7.448759	6.846314	TRAF2	9.418814	9.008460
EEF1E1	6.053783	5.297491	NPAT	9.481252	8.825183	TRAF3	11.571085	11.080722
EEF2K	10.359934	9.601840	NPB	4.275929	3.670489	TRAF4	11.846510	10.928163
EEFSEC	7.889330	7.567017	NPLOC4	11.187575	10.904465	TRAF7	8.470279	8.011289

EFHD2	11.559802	10.838838	NPM1	8.671944	8.258706	TRANK1	11.398120	11.057652
EFNA1	4.544565	3.769976	NPR1	2.145329	1.522160	TRAPPC12	9.251092	8.985530
EFNB1	7.531296	6.874857	NPRL3	7.697240	7.137706	TRDMT1	6.681462	6.067615
EFTUD2	8.118211	7.765573	NPTX1	7.695826	5.891081	TRIM2	5.990787	5.487060
EGOT	4.881449	2.965081	NR1I2	3.017019	2.520790	TRIM44	11.460265	11.207808
EHD1	13.121143	12.150206	NR5A2	4.167623	3.606298	TRIP10	10.523760	8.607190
EHD4	10.334731	9.712130	NR6A1	6.180024	3.912186	TRIP12	10.589256	10.267871
EHF	3.207745	2.481609	NRAS	10.746205	9.910396	TRIP13	3.670005	3.089365
EIF1	12.235142	11.991569	NRBF2	8.958663	8.510911	TRIP6	6.565267	6.131789
EIF2A	8.680959	8.413282	NRP2	8.573846	6.809732	TRMT10C	8.801477	8.495932
EIF2B1	8.817632	8.550130	NRXN2	5.199100	3.558150	TRMT2A	8.794459	8.466017
EIF2D	7.666707	7.131550	NSDHL	6.840670	6.311140	TRMT5	7.944793	7.479397
EIF2S1	9.636031	9.255287	NSRP1	9.011324	8.706040	TRMT61A	9.478528	8.560524
EIF2S3	10.853582	10.443470	NSUN2	9.907858	9.624865	TRMT61B	7.629207	7.313661
EIF3A	11.685291	11.409324	NSUN4	9.392408	9.047290	TRPM7	10.314735	9.960888
EIF3B	10.042093	9.670602	NT5DC1	8.810870	8.173716	TRUB2	7.717603	7.276478
EIF3I	9.120304	8.811257	NT5DC3	8.237786	7.737772	TSC22D2	10.470967	9.893867
EIF4E2	9.654951	9.383192	NTNG1	4.865111	4.108177	TSEN15	9.329475	8.560993
EIF4G1	10.665817	10.161265	NUCKS1	11.378474	11.096994	TSG101	7.959336	7.596389
EIF5A	10.361440	9.771761	NUDC	8.986567	8.627461	TSPAN18	7.215250	5.561910
EIF5B	9.269656	8.823374	NUDCD1	7.300307	6.917339	TSPAN31	7.959147	7.594450
EIF6	8.610946	8.135765	NUDT18	7.438680	6.967176	TSPAN33	12.153355	10.074833
ELAC1	6.770431	6.256236	NUDT19	8.397237	7.948102	TSR1	8.357539	7.835232
ELAVL1	10.650562	10.117339	NUDT9P1	5.113263	4.408849	TTC1	9.205493	8.877264
ELK1	9.544339	9.079623	NUP153	10.539777	10.113302	TTC27	6.425149	5.832760
ELK3	9.666049	8.852139	NUP35	5.614720	5.114088	TTC39A	2.649169	1.982649
ELL	9.766777	9.497437	NUP62	12.326875	11.441255	TTC7A	10.468069	10.068534
ELL2	9.009600	8.389734	NUP93	7.018251	6.417975	TTF2	9.178933	8.275701
ELMO2	8.831698	8.538192	NUPL1	9.103464	8.752006	TTLL4	7.906704	7.561971
ELOVL1	9.513471	9.231591	NUS1	7.971071	7.593307	TTPAL	9.508952	9.156705
ELP6	7.240933	6.881468	NUTF2	9.119548	8.512166	TUBA1A	10.220039	9.895335
EMC3-AS1	7.136169	6.643308	NXPH3	5.342064	3.099890	TUBA1B	11.053368	10.242069
EMG1	7.055070	6.566244	OAS3	9.311947	8.426734	TUBA1C	9.294054	8.129300
EMILIN2	10.531309	9.703746	ODF3B	8.830132	8.157529	TUBB	13.137887	11.796779
EMP3	9.217676	8.688157	OLA1	7.066930	6.629421	TUBB2A	6.430803	5.899914
EMX1	2.654611	1.847335	OPA3	10.036918	9.516814	TUBB2B	3.264386	2.290128
ENO1	10.870377	9.823198	ORAI1	11.177884	10.168751	TUBB4B	11.355809	10.894341
ENPP4	9.533601	8.815892	ORMDL2	7.987625	7.439559	TVP23A	7.538027	6.081265
ENPP5	4.997864	4.441407	OSBPL9	8.236468	7.657378	TWISTNB	8.732566	8.143546
ENSA	10.919083	10.312115	OSGIN2	9.112446	8.773687	TXLNA	10.948077	10.617696
EPM2AIP1	11.108246	10.351719	OSM	5.716694	5.116151	TXLNB	9.331443	8.735489
EPRS	9.148911	8.799417	OTUD4	10.376022	10.029684	TXN	6.890421	5.584555
EPS15	11.375262	10.190938	OTUD6B	7.676393	7.122848	TXNDC17	6.430715	5.954911
ERAL1	8.700640	8.181161	OTUD7B	7.265234	6.420167	TXNL4A	10.042779	9.735640
ERH	9.811060	9.350398	OXTR	6.089772	4.085986	TYK2	11.239448	10.570181
ERI3	8.417545	8.095982	P2RY8	10.979301	10.553048	TYMP	10.039502	9.388983
ESAM	6.807532	4.952602	PA2G4P4	9.887557	9.528241	TYW3	8.683810	8.336469
ESF1	7.982055	7.450989	PAICS	9.067145	7.752368	UBAP2	7.980203	7.648359
ESPL1	6.809637	5.630699	PAIP1	8.140297	7.829822	UBAP2L	9.408087	9.152711
ESR1	6.533200	6.102701	PAK1	8.859267	8.046870	UBB	12.870243	12.473779
ETFA	6.971312	6.225890	PAK1IP1	6.350293	5.509655	UBE2A	9.549611	9.237902
ETFDH	6.639269	6.139359	PAK4	8.175213	7.800723	UBE2E2	6.441767	5.830951
ETS1	12.867632	12.614606	PANDAR	9.241723	8.932151	UBE2G2	10.619140	10.273282
ETV3	10.534527	10.000196	PANX1	8.939493	8.522510	UBE2N	10.094096	9.719263
ETV3L	4.440082	3.034766	PAOX	8.075254	7.595720	UBE2Z	12.403095	11.604389
EXOC4	8.854383	8.454182	PAQR7	9.041791	8.462287	UBE3A	10.530541	10.152699
EXOSC4	8.117078	7.713219	PAQR8	9.663384	9.007410	UBE3C	9.639318	9.365406
EXOSC5	6.057405	5.459068	PARK7	9.817258	8.970118	UBFD1	10.041359	9.607904
EZH2	8.330396	7.006177	PARP1	10.026364	9.594607	UBLCP1	8.886889	8.268077
F13A1	6.160437	5.084891	PARP12	9.896268	9.523114	UBR4	10.324268	9.974731
FAHD1	8.704235	8.374553	PARP14	11.904127	11.360569	UBTD2	8.502680	8.224583

FAIM	6.011184	5.522033	PASK	10.981400	10.289553	UCK2	9.193717	8.303090
FAM104B	6.386895	5.930823	PATL1	9.468229	9.119959	UEVLD	8.437504	7.952828
FAM105B	10.341602	9.513963	PAX5	13.637816	12.338171	UFC1	9.420276	9.080400
FAM109B	7.380307	6.844794	PCBD1	7.674704	7.313836	UGDH	8.708307	8.173577
FAM114A1	6.765384	6.313198	PCED1B	9.799304	9.366962	ULBP1	4.093235	3.481660
FAM118A	9.269946	8.885551	PCK2	8.614841	7.872326	UMPS	8.968923	8.497001
FAM129A	8.742699	6.823768	PDAP1	9.900779	9.489182	UNC119	9.700245	9.009050
FAM136A	9.668411	9.311970	PDCD11	8.737544	8.302187	UNQ6494	4.048135	2.522928
FAM168A	10.339164	9.915241	PDCD4	11.831086	10.969703	UPF3B	8.564150	8.180017
FAM174B	7.950876	7.520882	PDCD4-	9.021450	8.583927	UPP1	6.619601	5.949520
FAM195B	9.718966	9.085751	PDE7A	10.992366	10.499812	UQCRFS1	8.266017	7.950399
FAM212A	4.027605	3.282434	PDF	6.670219	5.722115	URB1	8.163000	7.500788
FAM213A	4.529831	3.896224	PDGFA	7.565219	6.727757	URB2	8.564399	7.703297
FAM213B	9.872143	8.744736	PDIA3	10.155595	9.725938	URM1	9.809513	9.501099
FAM3C	8.026517	7.659854	PDIA3P1	11.970199	11.462478	USP10	10.082444	9.724278
FAM49A	9.034372	7.532904	PDIA4	9.741226	9.354672	USP12	11.476549	10.738323
FAM60A	11.798208	10.761792	PDLIM4	2.251483	1.633625	USP14	8.954172	8.599662
FAM83H	6.770438	6.109423	PDLIM5	8.624422	8.181209	USP24	10.555240	10.301722
FAM98A	8.630511	8.339721	PEA15	12.475233	11.568256	USP46-AS1	4.406383	3.873363
FAM98B	8.611977	7.905655	PEAK1	10.743976	10.413774	USP5	8.952762	8.581884
FARSB	6.497199	5.989119	PEF1	10.145381	9.557935	UST	6.871780	5.990801
FAS	9.830704	7.626175	PELP1	9.767877	9.457179	UTP15	7.684877	7.175897
FASN	9.420824	8.515989	PEPD	8.258703	7.822845	UTP20	7.008165	6.499428
FASTKD2	8.418093	7.930419	PES1	8.765752	8.127120	UTP3	10.344422	10.058909
FBRS	11.790294	11.373890	PEX10	6.976420	6.315641	UVRAG	10.615780	10.048344
FBRSL1	11.003170	10.482407	PEX26	10.030065	9.628677	VAMP8	9.854073	9.518776
FBXL15	9.878689	9.477920	PFAS	8.731693	7.927263	VANGL2	4.733683	3.819186
FBXL19-AS1	7.258007	6.805217	PFDN1	9.461585	9.161235	VARS	9.101573	8.192714
FBXL8	5.355026	4.563678	PFKM	8.025312	7.171070	VASH2	4.492879	3.577930
FBXO22	7.595360	7.070393	PFN1	13.372133	12.084521	VASP	10.251792	9.937944
FBXO45	8.338523	8.017156	PGAM1	8.112403	7.622913	VBP1	8.969110	8.474776
FBXW4	9.856618	9.547038	PGBD4	6.864357	6.475077	VCP	11.309590	10.864838
FBXW4P1	8.034030	7.675593	PGD	8.978863	8.505778	VDAC1	10.214788	9.315996
FBXW5	10.939534	10.621010	PGK1	9.567916	9.177667	VIM	11.524659	10.094935
FBXW7	9.032337	8.566542	PGLS	8.789199	8.370619	VKORC1	9.372896	9.116591
FCER2	10.562832	10.059279	PGM2	7.262273	6.847716	VMP1	9.729424	9.292584
FCHSD2	10.999991	10.259340	PHAX	9.216365	8.920846	VOPP1	11.026579	10.365345
FDFT1	10.113665	9.713110	PHB	9.900722	8.941577	VPS13A	8.467441	7.900280
FDX1L	6.850569	6.120239	PHLDA2	5.925498	4.951819	VPS25	7.860396	7.418834
FDXACB1	6.909728	6.355560	PHLDA3	5.142452	4.523687	VPS26A	9.148112	8.842783
FEN1	8.594279	8.221496	PHLDB1	6.337751	5.474311	VPS29	9.543081	9.152989
FGF2	5.413179	4.394963	PHPT1	8.601101	8.067807	VPS37C	8.445513	8.072400
FH	6.418058	5.971228	PIGQ	8.949934	8.598714	VPS41	8.605028	8.253017
FHOD1	9.578191	8.588910	PIGR	7.937257	7.384607	VWA7	5.427171	4.825719
FILIP1L	10.356479	9.356375	PIGV	8.385064	7.881258	WAC-AS1	8.658474	8.245668
FJX1	2.977266	2.460644	PIGW	7.755283	6.994328	WARS	11.288968	10.142710
FKBP1A	10.128705	9.707040	PIK3CA	9.010215	8.604648	WARS2	7.389678	6.851963
FKBP2	8.528406	8.183359	PIK3CD	11.917771	11.237567	WDFY1	10.819912	10.382353
FKBP5	10.266723	9.420411	PIM1	13.059208	12.730878	WDR1	11.303678	10.723318
FKRP	8.797542	8.510844	PIM2	12.745028	12.219786	WDR12	6.444299	5.830514
FKTN	8.232403	7.648974	PIM3	11.938148	11.522207	WDR17	7.341882	6.678853
FLJ13224	4.536501	3.719678	PINX1	7.332696	6.846480	WDR3	7.313354	6.722232
FLNA	12.444029	12.078200	PIPSL	11.594161	11.086015	WDR36	9.057770	8.769552
FLNB	9.903276	8.659727	PISD	9.507718	9.160570	WDR4	7.776993	7.095887
FLOT1	9.507440	8.884688	PITPNB	10.016098	9.474371	WDR43	9.008932	8.432003
FLOT2	11.688314	11.382168	PKIG	10.106541	9.407670	WDR44	8.217935	7.923502
FLVCR2	7.144065	6.180121	PKM	12.931438	11.655070	WDR48	9.619798	9.356308
FMNL1	12.437402	12.074592	PKN3	8.408078	7.301871	WDR5	9.621988	9.382540
FMNL3	10.983661	10.020052	PLA2G4C	7.279877	6.208017	WDR77	8.904595	8.211805
FMOD	13.243699	12.700689	PLAGL1	9.372387	8.192631	WDR89	9.284126	8.977215
FNBP1	13.341354	11.893311	PLAGL2	9.634309	9.291964	WHAMMP3	6.697101	5.649219

FNDC3B	7.133154	6.612047	PLAU	7.794186	5.472298	WIZ	9.278124	8.837292
FOXC1	5.756841	4.870722	PLCB3	8.429388	7.291601	WNT10B	5.144813	4.230550
FOXN3-AS1	5.122823	4.151894	PLD2	8.105361	7.684142	WNT4	6.944027	4.843146
FOXP1	12.136943	11.717704	PLEK	12.355095	9.902443	WSB2	10.010132	9.652488
FOXP4	11.613187	9.829255	PLEKHA7	8.316508	7.718625	XBP1	10.160644	9.712154
FPGS	9.602099	9.030815	PLEKHF1	8.329375	7.954924	XPO1	10.599384	10.256652
FRK	4.717449	3.537603	PLEKHF2	11.266619	11.030991	XPO4	9.744651	9.354172
FSCN1	9.600285	7.044685	PLEKHG4	4.385146	3.841998	XPO5	8.211772	7.866963
FSD1L	8.549462	7.187813	PLEKHG5	4.998221	4.181173	XRCC5	10.021571	9.720843
FSTL3	6.905159	5.327823	PLEKHM2	11.214887	10.794330	XRCC6	9.558492	9.140925
FUNDC2	8.145428	7.649637	PLEKHO2	10.395716	10.084185	YARS	9.626249	9.102831
FUOM	5.491880	4.753862	PLGRKT	6.312396	5.436987	YARS2	8.309586	8.019093
FUS	10.423547	10.104296	PLIN3	10.185125	9.168749	YBX1	10.659890	10.276401
FUT10	6.477369	5.468036	PLLP	5.357140	3.326359	YWHAB	11.954201	11.604477
FUT4	9.226678	8.456433	PLXNA1	10.823242	9.136363	YWHAE	11.085052	10.430100
FUT8	7.997890	7.560004	PML	9.846005	9.552496	YWHAG	11.714281	11.372897
FXN	7.265689	6.787700	PMM2	9.198181	8.775496	YWHAQ	11.063740	10.721554
FXYD2	3.506452	2.636457	PNO1	8.293581	7.600141	ZBED4	9.473163	9.158002
FXYD6	8.049348	6.442875	PNPO	8.013158	7.559609	ZBTB10	11.173173	10.155414
FZD6	5.945903	5.398161	PNPT1	7.583083	7.114070	ZBTB11-AS1	5.528837	4.924855
G3BP1	11.391581	10.795282	POFUT1	9.434810	9.014447	ZBTB17	9.641504	9.183090
G6PC3	8.083269	7.678325	POLA2	7.852898	7.040349	ZBTB32	11.686935	10.237519
GABPB1	8.946818	8.430093	POLD2	9.697772	9.176237	ZBTB46	7.638151	6.640016
GADD45GIP	9.884543	9.475281	POLDIP2	9.442185	9.045882	ZBTB5	11.124582	10.282840
GALNT10	9.463449	9.005468	POLDIP3	11.260636	11.014942	ZC3H4	10.044466	9.649573
GALNT11	7.223165	6.742078	POLK	9.241800	8.979511	ZC3H7A	9.889884	9.530099
GALNT16	4.308810	3.719120	POLR1B	8.543267	8.103450	ZC3H7B	11.673579	10.615865
GALNT2	11.905478	11.193128	POLR3H	8.615201	8.109964	ZC3HC1	6.777675	6.317674
GAR1	7.853477	7.328341	POP1	6.806970	6.239227	ZCCHC7	10.279679	9.638488
GAREML	5.883480	5.305227	POP5	7.480235	7.049401	ZDHHC16	7.834317	7.406161
GARS	8.119946	7.443759	POPDC2	6.016003	5.545090	ZDHHC18	10.899137	10.117134
GART	8.923299	8.287375	POR	9.275222	8.530944	ZDHHC23	9.045300	8.717801
GAS5	6.650326	6.254304	POU2F1	10.137552	9.815397	ZFAND3	10.758141	10.453399
GATSL3	6.832459	6.138036	POU3F1	7.915312	6.144523	ZFHX2	7.527393	5.495155
GBE1	7.172272	6.560243	PPA1	6.117443	5.335224	ZFHX3	9.554635	9.172524
GBGT1	8.719648	7.532264	PPAP2A	6.422194	5.948769	ZFP36L1	14.378966	13.264840
GBP1	5.467442	4.773312	PPARA	10.164272	9.376872	ZFYVE26	9.660477	9.022516
GBP4	8.325968	7.748049	PPDPF	9.851421	9.561321	ZMAT3	9.681354	9.277620
GCDH	8.144650	7.418193	PPFIA3	5.443813	4.869245	ZMIZ2	12.061715	11.351671
GCGR	4.483258	2.794604	PPIA	10.470663	10.139280	ZMYM4	8.968046	8.719715
GCN1L1	9.713355	9.428282	PPID	8.390168	7.789071	ZMYM6NB	8.379615	8.083632
GEMIN4	9.154737	8.798989	PPIF	10.076440	9.278107	ZNF135	6.503097	6.034965
GEMIN5	7.754269	7.312029	PPIL1	8.668263	8.012260	ZNF154	9.576726	9.188953
GEMIN8	8.118855	7.596194	PPIP5K1	8.121953	7.726730	ZNF207	9.810543	9.302862
GEN1	9.205402	8.788348	PPP1R14	9.318734	8.083467	ZNF22	10.610312	10.104256
GFI1	8.214589	7.324693	PPP1R15	11.772253	11.493898	ZNF239	6.275331	5.422537
GFM1	7.702974	7.288409	PPP1R7	7.665812	7.178673	ZNF260	9.921369	9.422770
GGACT	7.086148	6.637489	PPP1R9B	13.152565	12.006304	ZNF267	10.451991	9.844640
GGCT	7.843461	7.255475	PPP2R1A	9.309932	9.003669	ZNF281	9.748361	9.262862
GGNBP2	9.161077	8.846246	PPP2R2D	9.343802	9.025824	ZNF282	9.393259	9.036816
GHRL	5.337353	3.846749	PPP3CB	8.977501	8.537384	ZNF292	10.758186	10.509023
GINS4	7.289893	6.794527	PPP5C	7.679915	7.074323	ZNF295-AS1	1.971144	1.497409
GIPC1	8.418452	7.987438	PPRC1	10.219939	9.656591	ZNF296	8.915596	8.649528
GJD3	7.069320	6.200616	PPT1	9.605580	9.352472	ZNF33B	8.599696	8.259510
GLB1	7.907000	7.486299	PRCC	10.346203	10.082666	ZNF385C	6.901386	5.994654
GLRX3	7.482780	7.071085	PRDX1	9.107393	8.367075	ZNF506	9.693350	9.242355
GLYR1	10.758236	10.445629	PRDX3	9.317650	8.998659	ZNF512	8.963276	8.622157
GMEB1	7.785704	7.399022	PRDX4	6.449152	5.753889	ZNF544	8.636854	8.314212
GMFB	9.875280	9.507838	PRELID1	8.166251	7.849291	ZNF563	7.291101	6.821836
GNAI3	9.677917	9.362094	PREX1	10.880736	10.118751	ZNF593	7.360259	6.797689
GNB2L1	12.356545	12.130135	PRKAG2-	6.038361	5.316568	ZNF598	9.830369	9.565500

GNG2	11.761042	11.394173	PRKAR1B	8.013317	7.227849	ZNF629	8.055181	7.598060
GNG8	8.316874	5.585427	PRKCD	9.058549	8.166394	ZNF660	6.438243	5.758802
GNL3L	9.809861	9.495302	PRKDC	9.723252	9.325586	ZNF70	6.166508	5.688498
GNPDA1	9.527696	9.097681	PRMT1	9.070204	8.667742	ZNF706	8.498422	8.014149
GORAB	8.304638	7.994270	PRMT2	10.203759	9.932595	ZNF710	10.701054	10.096776
GOSR1	9.739977	9.468126	PRMT6	9.783213	9.491477	ZNF717	6.392040	5.960938
GOSR2	9.975070	9.624911	PROB1	7.970000	7.408640	ZNF770	11.012646	10.734881
GOT2	9.608301	8.590016	PROSER1	9.752252	9.446514	ZNF780B	8.572998	8.130140
GPATCH4	9.288679	8.203503	PRPF19	9.633366	9.329745	ZNF788	6.458067	5.239809
GPC5	2.006063	1.453279	PRPF40B	8.049812	7.470888	ZNF865	9.928260	9.641350
GPR132	10.860224	9.708898	PRR18	8.060311	6.602980	ZNF878	4.421757	3.666537
GPR137	9.887429	9.088088	PRRC2C	12.014769	11.684178	ZNFX1	11.273591	10.507499
GPR137B	8.551395	7.857030	PRRG4	5.168425	4.207953	ZNHIT6	8.921738	8.540174
GPR153	7.628139	6.106295	PRRT2	7.264727	5.988507	ZRANB2	10.280468	9.942858
GPR157	8.086005	7.216365	PRRT3	8.723047	6.460573	ZSCAN2	9.968385	8.584235
GPR55	6.678010	5.270696	PSAT1	5.278874	4.532170	ZSWIM4	9.940780	8.436791

Appendix 7. Significantly down-regulated genes induced by the soluble CD40 ligand in primary CLL cells at 24h time point

24h down-regulated	Expression LevelS24	Expression LevelU24	24h down-regulated	Expression LevelS24	Expression LevelU24	24h down-regulated	Expression LevelS24	Expression LevelU24
AATK	6.395418	7.030075	GORASP1	9.126231	9.594865	PRKX	8.759110	9.236867
ABCA1	6.256439	6.898599	GPATCH11	8.677886	9.019521	PROC	2.923686	3.781168
ABCA2	5.485456	6.233520	GPCPD1	9.366557	9.795156	PRR12	9.939384	10.344527
ABCA7	8.843768	9.745234	GPLD1	6.155997	6.699796	PRR7-AS1	3.918917	4.726744
ABCA9	8.232258	8.524437	GPM6A	7.247556	8.098215	PRX	6.894216	7.515213
ABCB1	4.882726	6.131992	GPNMB	6.776718	7.488496	PSD3	5.318696	5.860159
ABCB8	7.834352	8.132824	GPR135	5.185373	5.709049	PTAR1	10.112285	10.533664
ABCC2	4.326928	4.950671	GPR152	2.115878	2.799027	PTCH1	4.652244	5.115034
ABCC5	7.255076	7.692944	GPR155	6.854244	8.664547	PTDSS1	9.652372	9.976897
ABCD1	6.157117	6.825752	GPR160	4.813742	5.538552	PTGER2	5.835644	6.274452
ABCG1	7.276963	7.797616	GPR18	6.929675	8.451116	PTP4A1	9.935972	10.213170
ABHD14A	5.562153	6.317231	GPRASP1	8.496170	9.119963	PTPN12	9.784555	10.128484
ABHD15	9.812938	10.717085	GPT2	9.012525	10.669549	PTPN18	10.467096	10.926565
ABHD17A	8.949018	9.414940	GRAP	8.105331	8.664518	PTPN22	8.171906	9.163121
ABHD3	8.030321	8.438978	GRB7	5.337344	5.798560	PTPN4	7.422296	7.854383
ABHD4	9.108055	9.456928	GRIK3	6.276278	7.020193	PTPN7	10.734058	10.984009
ABI3	3.944110	4.635091	GRK5	6.990143	7.891176	PTPRC	10.799966	11.547440
ABLIM1	10.092356	10.970915	GRK6	8.394555	8.949055	PTPRCAP	10.754415	11.955962
ABR	11.654113	11.929546	GSAP	8.478876	8.753476	PTPRE	8.452598	9.084693
AC074289.1	7.192166	7.913105	GSDMB	7.693521	8.536267	PTPRVP	4.977871	5.796248
ACACB	6.045251	7.325650	GSE1	9.607137	10.147011	PURA	9.591146	9.837469
ACAD8	8.010394	8.384588	GSTM4	5.379444	5.874380	PUS7L	7.553271	7.892979
ACAP1	8.388434	9.081230	GTPBP1	10.378433	10.736987	PVRIG	7.724398	8.357316
ACAP2	9.894377	10.135100	GUCA1B	5.461303	5.976747	PXK	9.044449	9.579333
ACAP3	6.378818	7.031814	GUCY2C	4.819611	5.622388	PYCARD	6.178746	7.013052
ACBD4	7.825061	8.188332	GUSBP11	7.979067	8.429769	PYGM	4.887214	5.485969
ACD	7.869561	8.208897	GYLTL1B	8.312880	8.952028	PYHIN1	5.735157	6.281363
ACRBP	4.672360	5.281954	H1FX-AS1	5.547807	6.051611	PYROXD2	6.855000	7.244541
ACRC	5.765498	6.451927	HAS3	5.136938	5.777864	QPCTL	8.027818	8.845425
ACSF2	6.364827	7.046712	HAVCR2	5.146921	5.855253	QRICH2	6.282826	6.715580
ACSM1	5.293030	6.035918	HBP1	8.671168	8.968944	QRSL1	7.941463	8.439541
ACSM3	3.966996	4.796097	HCG23	4.662017	5.643581	QSOX1	8.630469	9.015820
ACSS1	9.179775	9.826222	HCG27	5.670936	6.392131	QSOX2	10.231489	11.456212
ACSS2	6.472960	6.960094	HCN2	4.315146	4.970507	RAB11FIP4	8.513825	9.553294
ADAM10	9.673262	9.898947	HDAC10	8.378730	8.882557	RAB24	7.864374	8.244718
ADAM28	10.109104	10.559521	HDAC5	8.438317	9.034893	RAB30	10.902198	11.346713
ADAM29	5.261535	6.256614	HDAC7	11.360111	12.005918	RAB33B	8.530067	8.945635
ADAMTS6	7.274429	8.023850	HEATR6	7.990930	8.416845	RAB37	7.340829	8.329629
ADARB2	2.484420	2.884187	HECA	10.295887	10.738373	RAB40B	4.919110	5.620674
ADCK2	8.175520	8.719729	HELZ2	9.760824	10.221220	RAB6A	10.160087	10.401060
ADCK3	8.876563	9.246434	HERC3	7.739111	8.341326	RABAC1	7.793428	8.212685
ADCK4	6.806512	7.169606	HEXA	7.989821	8.329329	RABEP2	8.502708	8.920099
ADCY10P1	5.989137	6.540513	HHEX	8.923402	9.932439	RAD9A	8.246969	8.859558
ADCY4	4.452749	5.098705	HIP1R	6.816270	8.244923	RAI1	9.881592	10.213644
ADD3	9.386089	10.024704	HIRIP3	7.249788	7.695591	RALB	8.704546	9.049586
ADHFE1	4.896612	5.609940	HIST1H1C	8.240793	8.618919	RALGDS	9.132162	9.679314
ADM	7.180728	7.842494	HIST1H2AC	7.665345	8.112919	RALGPS2	11.243613	11.551449
ADPGK	10.271180	10.636446	HIST1H2BD	6.959192	7.352832	RAMP1	3.260026	3.984930
ADPRM	7.591603	7.998259	HIST1H2BK	8.563546	8.900916	RANBP10	9.506174	9.795030
ADRB2	7.699567	8.467680	HIST1H2BN	2.758215	3.282642	RAP1GAP2	5.634464	6.959252
ADRBK1	11.461303	11.914380	HIST2H2AC	5.053345	5.526842	RAPGEF2	8.645985	9.162584
AES	12.048377	12.433644	HIST3H2A	4.002524	4.565631	RAPGEF3	8.255901	9.057488
AFAP1L2	3.943945	4.790073	HLA-DMA	10.456342	11.018305	RARRES3	4.619669	5.160308
AFF1	9.127347	9.439158	HMCES	8.052303	8.731648	RASA2	8.614141	8.952377
AFF3	10.948211	11.306171	HMGB1	10.617118	10.899922	RASA3	7.950057	9.200090
AFF4	10.359436	10.679825	HMGB2	8.410322	8.780171	RASAL1	5.864504	6.867719

AGAP7	2.445025	2.968782	HMOX1	9.801652	10.635216	RASGRP2	9.027097	10.183792
AGFG2	7.743343	8.156418	HOMER2	7.909671	8.683635	RASSF1	9.325585	9.839632
AGPAT5	10.696147	11.340269	HOXB2	6.410722	6.853893	RASSF1-AS1	3.438131	4.142104
AHCYL1	9.786836	10.047527	HPCAL1	9.736406	10.590558	RASSF7	8.827168	9.237666
AHCYL2	7.551935	7.914782	HPS3	7.690205	8.110360	RB1CC1	9.270930	9.561196
AHDC1	9.106710	9.553466	HRK	5.150665	6.291363	RBL2	9.942703	10.200393
AHI1	7.520659	8.127525	HS2ST1	8.778920	9.193386	RBM15	9.673159	9.954687
AK1	7.592721	8.710655	HS3ST1	8.803833	9.170148	RBM33	10.548237	10.967140
AKAP8L	9.327288	9.640337	HSD17B11	8.619757	9.156749	RBM38	11.771662	12.594194
AKAP9	9.606988	9.898903	HSD17B13	2.996720	3.559572	RBM43	6.314499	6.873946
AKNA	11.409311	11.745449	HSDL1	8.685066	9.163611	RBM5	10.185001	10.480373
AKT1	9.858591	10.074194	HSH2D	10.957417	11.333713	RBM5-AS1	6.068502	6.504751
AKT2	10.950797	11.200572	HSPA6	11.198634	11.560057	RBMS2	6.528711	7.250683
ALAD	8.357744	9.211547	HSPA7	5.517267	6.364163	RCBTB2	6.605430	7.122831
ALDH3A2	8.269665	8.846314	HSPBAP1	7.215851	7.552616	RCN3	5.832074	6.431481
ALDH3B1	5.429586	6.004102	HSPG2	5.687725	6.437324	RCOR1	8.818772	9.269649
ALDH5A1	10.144505	10.790915	HTATSF1P2	7.308144	8.220164	RCSD1	11.835860	12.728604
ALDH9A1	8.565912	8.838463	HTRA3	4.779088	6.703531	RDH10	5.943171	6.632941
ALKBH4	7.290960	7.854145	HTRA4	2.585942	3.196916	REEP5	9.380685	9.661982
ALKBH5	10.659283	11.176200	ID3	12.043270	12.948612	REM2	6.013330	7.146756
ALKBH6	7.734364	8.063508	IDS	11.814965	12.313892	RERE	10.305561	10.728946
ALOX15P1	4.701698	5.487667	IER5L	6.706005	7.309385	REST	9.796425	10.047206
ALOX5	10.477338	11.119090	IFFO1	8.862875	9.214676	REV3L	8.921205	9.527644
ALOX5AP	7.747270	8.349553	IFI16	10.210428	10.548953	RFX1	7.607511	8.044191
AMDHD2	8.004455	8.473937	IFIT2	6.761660	7.397793	RGCC	7.592945	9.109637
AMFR	10.368222	10.908530	IFITM1	6.560899	7.138391	RGL2	8.690447	9.102764
AMH	4.478103	5.178181	IFNAR2	9.410428	9.825531	RGL4	8.517806	8.826386
AMN	5.776360	6.267648	IFT57	8.897559	9.336568	RGMB	6.970624	7.621245
AMN1	6.943270	7.339767	IGBP1	7.913664	8.228168	RGS14	8.334398	8.871305
AMT	6.541335	7.001831	IGF1R	6.043082	6.515709	RGS2	9.840677	11.173795
AMZ2	9.670973	10.103572	IGIP	7.200791	7.701359	RGS3	5.776434	6.346626
ANK1	5.107590	6.327090	IGSF8	8.051942	8.643015	RHBDD1	9.557100	9.870598
ANKMY1	7.048322	7.602932	IKZF3	12.397704	12.674418	RHBDL1	4.879181	5.911237
ANKRA2	7.965718	8.466941	IKZF5	8.999149	9.318984	RHOB	9.375745	9.788793
ANKRD13A	10.529777	10.856107	IL10RB	8.934115	9.282664	RHOH	11.076360	11.778292
ANKRD13D	8.021832	8.344469	IL11RA	7.228070	7.777637	RHPN1	9.491038	10.398168
ANKRD16	6.621212	7.151929	IL16	10.824063	11.538315	RHPN2	4.841388	5.465901
ANKRD34A	4.551209	5.280431	IL17RA	9.399500	9.768585	RILPL1	5.147351	6.136909
ANKRD42	7.289971	7.860576	IL1R1	4.735437	5.392156	RIN2	5.524847	6.140270
ANKRD44	10.256249	10.755752	IL1RAP	6.224708	6.858959	RIN3	10.440367	10.865066
ANKZF1	9.451734	10.099253	IL24	6.496065	7.673981	RITA1	8.119818	8.596125
ANO8	6.114635	7.139521	IL2RB	9.294908	9.683061	RMRP	5.165192	5.665629
ANPEP	6.082408	6.575388	ILF3-AS1	8.109414	8.509020	RN7SK	8.043687	8.605502
ANTXR2	7.994781	9.246622	IMPA2	5.896393	6.371219	RNASE1	6.788214	7.554883
ANTXRLP1	3.020921	4.140298	INF2	8.616586	9.338698	RNASE4	4.736444	5.345926
ANXA2R	5.704643	6.692838	ING1	9.542173	9.961553	RNASE6	6.591018	8.014642
AP001258.4	5.740823	6.382658	ING2	7.025842	7.469613	RNASEL	8.253550	8.786235
AP1B1	10.175314	10.649775	ING4	8.036174	8.373566	RNASET2	8.936069	10.716693
AP3S1	7.310418	7.754809	INPP5A	7.736778	8.426302	RNF113A	9.113534	9.604264
APAF1	8.828296	9.263119	INPP5D	10.599369	10.901420	RNF125	6.624881	7.108357
APBB2	8.363016	10.153228	INSIG2	8.064825	8.517080	RNF13	8.727299	8.994124
APCDD1	2.998136	3.968540	IP6K2	9.643425	10.055092	RNF130	8.121179	8.711474
APLN	2.452398	2.968170	IPW	5.586360	6.462062	RNF135	7.943318	8.257098
APOE	4.774806	5.387606	IQCD	2.757942	3.388080	RNF149	9.266066	9.792161
APOLD1	5.390534	5.966057	IQCE	8.102048	8.434424	RNF166	8.460120	9.300145
AQP3	4.515602	5.501889	IQGAP2	5.558504	6.564573	RNF19A	9.488776	9.910715
ARAP1	9.647126	10.129645	IQSEC2	4.724852	5.310697	RNF213	10.954108	11.250063
ARHGAP12	8.136183	8.511152	IRAK4	9.429520	9.750539	RNF24	6.923183	7.830520
ARHGAP18	6.322242	6.734140	IRF2BPL	10.627850	11.440333	RNF38	9.844227	10.160676
ARHGAP27	10.048922	10.559210	IRF3	10.287918	10.810910	RNF39	4.848799	5.534243
ARHGAP4	9.875725	10.294411	IRF8	11.726170	12.196400	RNF41	10.443513	11.350604

ARHGAP6	4.712496	5.723432	IRS1	8.455834	9.162577	RNF44	10.508411	10.961987
ARHGAP9	9.086764	10.166427	IRS2	9.495150	10.195661	RNFT2	5.042492	5.565963
ARHGEF1	9.820955	10.316981	ISCA1	8.299877	8.657130	RNR1	13.149383	13.551023
ARHGEF10L	7.676954	8.172796	ISYNA1	7.025898	7.674093	RNR2	15.951059	16.408030
ARHGEF3	8.986087	9.669455	ITGAL	8.014857	9.325902	ROR1	9.701462	10.223515
ARHGEF6	8.683484	9.063994	ITGB1	9.266772	9.904997	RP11-	3.269322	4.582335
ARID4A	8.823706	9.180782	ITGB7	8.336727	9.226981	RP11-	2.321653	2.871465
ARID5B	10.257514	11.022225	ITIH4	6.807900	7.397711	RP11-	4.314264	5.169819
ARL15	7.032487	7.542531	ITK	5.299641	5.846308	RP11-	3.905608	4.961280
ARL3	6.537084	6.988326	ITM2B	10.291375	10.677996	RP11-	2.853107	3.455770
ARL4C	9.999293	10.479715	ITPR2	9.534660	9.942694	RP11-	4.419534	4.950604
ARL6IP6	8.789372	9.074846	ITPRIP	9.218866	9.526143	RP5-	4.177226	4.916115
ARMCX3	9.843858	10.133312	ITPRIPL1	6.926112	7.415771	RPPH1	6.109375	6.641505
ARRB2	8.509338	9.091170	JDP2	8.448662	8.958076	RPRD2	9.507221	10.221384
ARRDC2	11.345343	11.899657	JHDM1D-	7.140427	7.911219	RPS11	9.567449	9.798914
ARRDC3	9.301082	10.035318	JMJD1C	10.641363	11.171572	RPS27	8.247769	8.749132
ARSK	5.553493	6.234027	JMJD7	6.005464	6.732103	RRAD	6.604655	7.063558
AS3MT	3.670703	4.201309	JPH3	3.886623	4.541485	RRM2B	10.038173	10.499535
ASAH1	8.730791	9.211946	JUND	12.794435	13.347067	RSBN1L	8.545347	8.825445
ASF1A	8.965203	9.516688	KANK1	7.140753	7.773340	RTN3	9.205397	9.574898
ASIC3	5.466519	6.343984	KANK2	5.366386	6.578058	RUNDC1	9.079524	9.652979
ASTE1	7.125498	7.565499	KANSL2	8.315496	8.593461	RUNX1	9.310675	9.620814
ATG12	9.246471	9.500526	KAT2A	8.803109	9.226645	S100A8	6.530682	6.956673
ATG16L2	7.691230	8.251515	KAT2B	8.389604	8.769542	S1PR1	8.130991	9.453501
ATG2B	9.232239	9.514951	KAT6B	9.070928	9.738844	S1PR4	9.284737	9.987333
ATG9A	9.251425	9.574716	KBTBD6	7.762504	8.120103	SAFB2	9.358158	9.838844
ATHL1	11.444196	12.159769	KBTBD7	7.330424	7.708051	SAP25	7.922977	8.568321
ATL1	4.837723	5.409893	KCNA3	9.861488	11.136006	SAR1B	8.573465	8.899841
ATM	10.352203	10.949158	KCNAB1	4.476278	4.958251	SAT1	9.963238	10.667609
ATP13A1	8.992689	9.312971	KCND1	6.135476	6.805181	SAT2	8.738391	9.146222
ATP2A1	4.698385	5.209540	KCNH2	5.604407	6.895948	SATB1	7.316871	7.972088
ATP2A3	11.236258	12.463152	KCNJ11	8.498063	9.357947	SBDSP1	8.213995	8.524619
ATP2B4	9.751450	10.854757	KCNQ1	3.700447	4.845017	SBF1	10.092046	10.475467
ATP6V0C	10.973211	11.308956	KCTD12	6.943319	7.421399	SBK1	6.407822	7.129983
ATP6V0E2	7.391622	8.031688	KCTD7	8.868869	9.475538	SBNO1	9.969515	10.222814
ATP6V1G2	3.949697	4.699441	KDM1A	8.507948	8.790771	SCAI	7.820607	8.248796
ATP7A	7.248878	7.616963	KDM3A	8.483040	8.975571	SCAMP1	7.577791	8.303452
ATRN	8.290592	8.625859	KDM7A	9.673821	10.485249	SCARB2	8.276720	8.820977
ATXN1L	10.360744	10.596677	KIAA0040	10.818142	11.614126	SCARF2	4.061969	4.900934
AUP1	9.315461	9.551820	KIAA0226	11.028149	11.617364	SCART1	5.504117	6.205561
AVIL	5.531140	6.082160	KIAA0226L	11.676238	11.908172	SCIMP	7.738148	9.488922
AVP	1.588880	2.216552	KIAA0355	9.235952	9.507379	SCN4A	4.050504	5.147213
AVPI1	5.135086	6.091066	KIAA0430	11.396654	11.680009	SCXB	6.526931	7.801395
AVPR2	3.995314	4.557381	KIAA0513	6.555805	7.177738	SDCCAG3	9.320394	9.632748
AXIN1	9.975606	10.397190	KIAA0586	6.761769	7.220159	SDK2	6.696515	7.647547
B3GNT1	6.817269	7.468649	KIAA0930	8.801875	9.259849	SDR39U1	8.149195	8.542468
B4GALT1	10.967041	11.625391	KIAA1328	6.404417	6.828266	SEC11A	9.037741	9.422083
B4GALT3	8.958051	9.352824	KIAA1377	5.535246	6.440427	SEC31B	7.822762	8.208001
BACE2	8.518601	8.851603	KIAA1407	9.165321	9.891931	SEC62	10.822670	11.110443
BAG1	9.169674	9.536637	KIAA1432	9.239228	9.597828	SECISBP2L	10.444074	10.703673
BAIAP3	6.850395	8.783832	KIAA1551	11.970275	12.430520	SEL1L3	9.724406	10.490161
BANP	8.011047	8.710515	KIAA1683	6.838206	8.010652	SELO	8.929264	9.571980
BBS2	7.565368	7.940960	KIAA1731	8.013333	8.376328	SELPLG	8.709877	9.440677
BBX	10.242521	10.482108	KIAA2018	8.937392	9.251863	SEMA4B	9.061353	10.323491
BCAS4	8.725506	9.125478	KIF20B	7.260239	7.695693	SEMA4D	9.652432	10.247564
BCL11A	10.012169	10.705268	KIF22	7.538899	8.024629	SEMA6B	7.974200	8.301527
BCR	7.659998	8.368065	KIF3C	6.451392	7.083228	SENP7	7.731986	8.224299
BCRP3	1.921886	2.400524	KIFC2	8.926664	9.452492	SEPHS2	10.345781	10.707790
BEST4	5.747724	6.281174	KISS1R	5.388100	6.024426	SEPN1	9.235163	9.631146
BET1L	10.144261	10.417977	KLC4	6.766554	7.382174	SEPT6	10.990917	11.590322
BFSP2	2.088639	2.555296	KLF10	9.770456	10.497591	SEPT9	12.976477	13.584720

BICD2	10.099176	10.756823	KLF16	9.819618	10.050890	SEPW1	8.055486	8.562667
BIN1	7.767954	8.217637	KLF2	9.089364	10.370057	SERINC1	10.841249	11.132702
BLCAP	9.877528	10.149382	KLF3	6.905642	7.461007	SERINC3	9.188736	9.493336
BLNK	8.011656	8.478442	KLF9	9.272505	9.735240	SERINC4	7.473286	8.363514
BMP6	4.076647	5.118873	KLHDC3	8.730100	9.019466	SERINC5	8.963282	9.444904
BMPR2	10.317434	10.995691	KLHL14	7.949151	8.952131	SERPINF1	7.323334	7.887106
BNIP3L	9.792192	10.093615	KLHL15	8.378203	8.742605	SESN1	7.739341	8.370537
BOD1L1	10.927060	11.147994	KLHL2	8.229519	8.864046	SESN3	11.548346	12.590470
BPTF	10.326464	10.617905	KLHL24	9.755932	10.409325	SESTD1	7.892097	8.694297
BREA2	4.482367	5.055226	KLHL3	4.867085	5.517437	SETBP1	9.225334	9.642663
BRICD5	5.889593	6.577696	KLHL32	3.890924	4.769450	SETD7	7.825092	8.446356
BROX	9.346735	9.581885	KLHL8	8.013917	8.313764	SETDB2	8.497578	8.944987
BRWD1	9.633751	10.058149	KMT2E	10.820742	11.085417	SFI1	7.708316	8.039504
BSCL2	4.436340	5.310890	KMT2E-AS1	7.978778	8.357688	SFMBT1	10.092218	10.613237
BTBD2	9.980792	10.283150	KSR2	7.199616	8.006079	SFTPB	5.567586	7.516210
BTBD6	8.980059	9.431602	L3HYPDH	7.767666	8.228133	SFXN3	8.277845	9.333770
BTG2	12.948087	13.709580	LAG3	6.588067	7.173393	SGK223	10.271691	10.647524
BTN1A1	3.078725	3.699601	LAIR1	6.462664	7.172418	SGPP1	11.451474	11.884652
BTN3A1	9.624240	10.045156	LAMA5	6.959960	8.089597	SGSH	8.213197	8.741278
BTN3A2	9.796434	10.051441	LAPTM4A	9.432439	9.871077	SGSM2	9.966520	10.519142
BTNL2	2.649853	3.618768	LAPTM5	13.377488	13.910181	SH3BGRL2	7.139015	7.752409
BZRAP1	6.497954	7.425404	LATS2	7.726183	8.117174	SH3BP5	8.427641	8.926284
C11orf21	7.211460	7.788500	LAX1	9.109487	10.266651	SH3BP5-AS1	7.593665	8.082182
C11orf24	8.075065	8.539547	LBR	9.038036	9.326807	SH3TC1	9.932518	10.442274
C11orf30	8.117839	8.440865	LCK	7.249719	8.138273	SHISA5	10.090849	10.760795
C11orf35	6.819308	7.830480	LCN10	6.614869	7.279522	SIDT1	8.235446	9.134933
C11orf80	6.389284	6.758084	LCN8	4.551383	5.740031	SIDT2	8.610723	9.285658
C12orf23	9.375258	9.649277	LCORL	6.460622	6.853348	SIGIRR	7.983964	8.402222
C12orf42	4.453859	5.056993	LCP2	6.269479	6.858250	SIGLEC10	7.529566	8.767223
C14orf182	4.043320	4.636365	LDB1	10.648618	11.185988	SIK3	9.850357	10.315585
C16orf54	7.848766	8.890279	LDLRAD4	8.751854	9.793863	SIMC1	7.900926	8.260477
C16orf74	7.472204	8.731724	LDLRAP1	8.173324	9.034210	SIPA1L1	10.272902	10.696232
C16orf86	6.869750	7.398254	LEPRE1	8.422284	8.773977	SIPA1L3	10.363168	11.172901
C17orf103	8.146644	8.871803	LEPREL4	5.219057	5.828273	SIRT1	9.606016	9.859534
C17orf59	9.400952	9.811043	LEPROTL1	8.548540	8.940429	SIRT2	8.086991	8.467848
C17orf72	5.017916	5.535219	LGALS8	7.589219	8.084781	SIRT5	7.290979	7.658043
C19orf35	4.940447	5.452136	LGMN	5.988662	6.767947	SIT1	8.415964	9.043230
C19orf38	4.781081	5.708354	LGR4	4.291582	5.135501	SKIL	10.550244	10.867713
C1QTNF6	6.974032	7.975910	LHB	3.123872	3.642334	SKOR1	3.669010	4.616919
C1orf162	7.348386	8.192275	LHFPL2	9.739010	10.163908	SLA	9.663789	10.631162
C1orf228	5.415359	6.065200	LHPP	7.518831	8.714397	SLA2	5.571644	6.189420
C1orf56	7.061631	7.508517	LIG1	7.164222	8.150585	SLAMF6	10.055669	10.545962
C20orf195	6.502128	6.977422	LIMD1	9.495730	9.974733	SLBP	8.512722	8.875367
C2CD2L	6.868470	7.333760	LIME1	6.697297	7.717232	SLC12A6	10.647875	11.121173
C2orf81	7.100308	7.506412	LIMK2	8.798395	9.405065	SLC13A5	3.674848	4.842823
C3AR1	5.840674	6.352879	LIMS1	9.865646	10.253800	SLC14A1	4.157956	5.811666
C3orf58	8.072489	8.581097	LIN7B	5.615402	6.187989	SLC16A4	4.909738	5.570232
C3orf62	6.996719	7.452280	LINC-PINT	8.158372	8.830674	SLC16A7	7.882846	8.732587
C5	3.699492	4.446087	LINC00202-1	3.324573	4.025811	SLC17A5	6.814294	7.210060
C5orf45	6.647343	7.423865	LINC00304	3.829501	4.729280	SLC17A9	7.483152	8.053159
C5orf56	5.262823	5.800600	LINC00339	6.924797	7.717363	SLC18B1	6.451783	7.623174
C6orf48	10.436577	11.133273	LINC00426	4.796303	5.763221	SLC22A17	3.736625	4.518560
C9orf72	7.844689	8.356547	LINC00525	3.823289	4.737353	SLC22A18	3.890213	4.546393
C9orf89	6.858108	7.497833	LINC00565	2.341869	3.117499	SLC23A1	5.287884	6.235518
CA11	7.103690	7.953880	LINC00674	9.976394	10.406303	SLC25A28	9.367031	9.878048
CA14	4.489231	5.342208	LINC00847	8.814578	9.553966	SLC25A29	10.053197	10.479911
CABIN1	9.375611	9.678846	LINC00886	4.672159	5.607497	SLC25A30	8.055032	8.395470
CABLES1	10.744323	11.240470	LINC00888	6.590012	6.959993	SLC25A36	9.813671	10.096948
CABP4	3.685375	4.980961	LINC00921	6.465957	7.031824	SLC25A42	7.387258	8.509341
CACNA2D2	5.458325	6.232223	LINC00926	11.736551	12.138081	SLC25A53	6.050293	6.791997
CACNB2	5.407468	6.036902	LINC01004	6.654596	7.592882	SLC26A11	7.489250	8.089992

CALCOCO1	9.545607	10.131400	LINC01011	4.071474	4.957334	SLC26A6	6.593648	7.123861
CALHM2	8.860245	9.321787	LINC01023	5.086736	5.622674	SLC27A1	7.118829	7.553313
CALM1	11.647266	12.017028	LINC01089	8.633949	8.977588	SLC27A3	7.470585	7.932882
CAMKK1	6.498301	8.087640	LINGO3	6.393066	8.515320	SLC2A11	7.206182	8.004108
CAPN3	8.106952	8.533877	LMNB1	7.069209	7.777846	SLC2A3	7.896609	8.572017
CAPN7	8.892653	9.218785	LMO4	8.707082	9.300859	SLC2A4RG	7.575036	8.368327
CAPRIN2	8.198220	8.655374	LMO7	7.939159	8.500931	SLC30A1	7.790274	8.218337
CAPS	7.849466	8.281951	LMTK2	8.483564	8.990212	SLC35A1	7.818015	8.186576
CARD11	9.916779	10.348547	LOC1001284	5.184460	5.800793	SLC35D1	8.101107	8.404925
CARD14	6.152607	7.143547	LOC1001286	6.479857	6.984796	SLC35E2B	10.026203	10.404924
CARD8	9.926632	10.315717	LOC1001292	5.569287	6.364707	SLC37A2	7.513993	8.100582
CARF	7.285783	7.696965	LOC1001295	6.887545	7.906764	SLC39A10	7.957452	8.500259
CARHSP1	8.565632	9.283102	LOC1001296	8.849328	9.312752	SLC39A3	9.065786	9.348713
CARNS1	7.747301	8.400880	LOC1001309	4.934597	5.498275	SLC39A8	7.112510	7.496610
CARS2	7.555786	8.100717	LOC1002407	4.553488	5.105124	SLC44A2	9.732831	10.380943
CASP10	5.741245	6.405615	LOC1002870	2.175200	2.982703	SLC46A1	5.314071	6.003086
CASP8	9.351259	9.831208	LOC1002871	3.928075	4.630470	SLC48A1	8.905297	9.441941
CASP9	7.844387	8.305281	LOC1002886	5.212647	5.796024	SLC6A16	7.823547	8.145527
CBFA2T2	9.297450	9.715371	LOC1005055	6.397300	7.383986	SLC7A7	8.844911	9.293844
CBFB	10.312700	10.550459	LOC1005055	3.464460	4.233627	SLC7A8	5.320661	5.866936
CBLB	8.651811	9.160367	LOC1005057	8.130389	9.493771	SLC8A1	3.885695	4.404265
CBX3P2	5.128894	5.669815	LOC1005061	3.996271	4.503506	SLC8B1	7.634956	8.014071
CBX4	9.918741	10.737451	LOC1005065	8.933317	9.227142	SLC9A1	8.849334	9.446378
CBX8	4.830437	5.863510	LOC1005066	7.328824	7.751721	SLC9A3R1	9.096664	9.357511
CCBL1	5.446968	6.056830	LOC1005069	6.553869	7.017022	SLFN11	7.795332	8.404536
CCDC109B	6.936096	7.688928	LOC1005072	9.694506	10.052320	SMAD3	7.345431	7.845603
CCDC114	4.661389	5.399291	LOC1005075	3.494890	4.726740	SMARCD3	5.681771	6.354845
CCDC126	6.314832	6.775560	LOC1005076	8.611708	9.151815	SMC4	7.992769	8.333281
CCDC134	4.801231	5.474765	LOC1005077	2.671181	3.418856	SMCHD1	10.237605	10.939665
CCDC163P	5.551014	6.083174	LOC1006527	6.509437	7.565468	SMPD1	7.872393	8.290513
CCDC42B	3.398519	4.418573	LOC1009962	6.375557	7.231112	SNAI3	5.262436	6.572043
CCDC64	10.165428	10.642306	LOC1009965	6.433918	6.923757	SNED1	8.178133	8.935983
CCDC68	5.239630	6.254075	LOC1009967	3.839186	4.493553	SNPH	6.743273	7.380021
CCDC88C	10.128250	10.362788	LOC1014092	2.936901	3.597665	SNTB2	7.533622	8.592835
CCL5	8.852615	9.215583	LOC1019271	1.679845	2.254230	SNX2	8.051428	8.400359
CCM2	8.980456	9.395871	LOC1019272	3.488531	4.409296	SNX25	7.640059	7.980199
CCND3	10.087483	10.425960	LOC1019273	6.026821	6.430672	SNX27	8.974628	9.258913
CCNDBP1	8.894049	9.255255	LOC1019274	7.246861	7.721586	SNX30	8.253005	9.370797
CCNL1	10.903555	11.155307	LOC1019277	3.338261	4.393703	SOBP	5.307162	5.933279
CCNL2	11.769129	12.173898	LOC1019277	4.210670	5.046960	SORBS3	7.857946	8.485777
CCP110	7.998261	8.423346	LOC1019279	6.648306	8.008487	SOS1	9.341176	9.622321
CCPG1	6.617615	7.090001	LOC1019280	3.759232	4.449543	SOS2	9.228843	9.545079
CCR6	5.680125	7.932199	LOC1019284	6.730628	7.905249	SOWAHC	7.211835	7.549064
CD14	7.622521	8.344490	LOC1019285	2.703403	3.420304	SOWAHD	8.472437	9.278972
CD163	7.410952	8.183209	LOC1019287	6.578304	7.266313	SOX12	9.350224	10.208641
CD1D	4.696880	6.076630	LOC1019289	2.443281	3.003616	SP100	10.253388	10.476736
CD24	8.805358	10.120671	LOC1019289	3.070620	3.837968	SP110	7.254929	8.119601
CD244	5.263982	6.087438	LOC1019290	4.633524	5.720038	SP140	8.216088	8.781481
CD248	2.044783	2.797795	LOC1019290	5.374444	5.993478	SP4	9.641103	9.979752
CD27	7.727936	9.651220	LOC1019296	2.411557	3.309496	SPAG4	6.367972	7.158355
CD27-AS1	5.619597	6.393238	LOC1019296	3.115029	4.356992	SPATA13	8.006288	8.416709
CD300A	5.562232	6.103284	LOC1024671	1.745146	2.171493	SPATA2L	8.255877	8.833536
CD300E	6.231633	6.710014	LOC1027233	3.912671	4.522760	SPIN4	7.781651	8.586318
CD320	7.549064	8.043831	LOC1027235	10.234895	10.550649	SPPL2B	8.563640	8.973433
CD36	5.295502	5.888762	LOC1027235	4.117698	4.805532	SPSB3	10.057121	10.405510
CD3E	5.620751	6.100139	LOC1027237	5.182775	5.789020	SPTAN1	9.343236	9.665072
CD47	10.875664	11.193560	LOC1027238	4.785755	5.518208	SPTBN1	10.309498	10.904814
CD48	10.014178	10.490740	LOC1027238	3.026343	3.576099	SPTBN5	6.432046	7.373992
CD5	9.895290	11.082186	LOC1027238	3.063160	3.623777	SRGAP3	4.958419	5.874607
CD52	9.589450	10.505004	LOC1027240	3.490203	4.267983	SRMS	6.771200	7.326973
CD53	10.865756	11.127069	LOC1027242	4.665818	5.329898	SRP14-AS1	6.617434	7.105288

CD6	9.138656	10.453531	LOC1027242	5.557133	6.383908	SRPK2	8.713984	8.984036
CD7	4.751448	5.433895	LOC1027242	3.000819	3.549051	SRRM2	13.765376	14.092242
CD79A	11.898030	12.324810	LOC1027243	6.591723	7.176717	SRSF8	10.015421	10.300127
CD79B	10.293798	11.541910	LOC1027243	2.487621	3.089650	SS18L1	8.105452	8.456299
CD8A	7.280422	7.830405	LOC1027244	6.205074	7.095411	SSBP2	4.094892	4.831876
CD96	5.162466	5.670434	LOC1027245	8.225311	9.678249	SSH2	10.567843	11.288230
CDC25B	8.743952	9.905667	LOC1027246	3.711550	4.318736	SSR1	10.377257	10.579904
CDC40	8.571545	8.911820	LOC113230	4.974542	5.558770	SSTR3	5.875134	7.039146
CDC42BPG	5.426698	6.070811	LOC146880	8.425923	8.928384	ST6GAL1	12.569707	12.891632
CDCA7L	7.743647	8.531603	LOC202181	6.710886	7.278177	ST6GALNAC	9.822347	10.533524
CDHR1	3.718610	4.560075	LOC220729	6.140974	6.841530	ST6GALNAC	11.384609	11.839570
CDIP1	9.575410	9.947260	LOC284023	6.839952	7.215027	STAB1	6.035959	6.478919
CDIPT	9.768760	10.142412	LOC390937	4.345044	5.289497	STAMBPL1	8.399246	8.793938
CDK11A	7.720670	8.083503	LOC400685	2.790152	3.284459	STAP1	7.593264	7.973286
CDK19	9.069831	9.448115	LOC440461	4.758730	6.336821	STARD5	7.568176	8.109065
CDKL1	7.252225	7.698201	LOC441204	3.159428	3.947673	STARD9	7.824442	8.391399
CDKN1B	10.928588	11.462065	LOC645638	6.660390	7.991341	STAT2	10.336414	10.921601
CDKN1C	5.945054	6.393034	LOC648987	7.097404	7.519748	STIM1	9.581612	10.019388
CDKN2AIP	9.728091	10.105811	LOC652276	6.876208	7.393582	STIM2	9.446419	9.851619
CDKN2D	7.379842	8.407598	LOC728392	7.623809	8.916263	STK24	9.654438	10.085111
CDS2	9.912146	10.167939	LOC728743	8.892246	9.782442	STMN1	8.235535	8.589955
CEACAM21	6.618246	7.430917	LOC728752	5.658964	6.283539	STMN3	7.656546	9.194236
CEBPD	4.882320	5.665798	LOC93622	7.595694	7.927770	STOX1	4.281798	4.901982
CEBPE	2.228886	2.811497	LPAR5	9.363437	9.707253	STRN	9.224838	9.554081
CECR1	7.951117	9.605400	LPCAT4	7.250888	8.145532	STX10	8.135257	8.489784
CELF6	6.561885	7.308043	LPIN2	9.600280	10.025828	STX16	10.377212	10.646278
CEMP1	7.042352	7.572072	LPP	9.039088	9.714461	STX7	10.373253	10.725319
CENPM	4.520792	5.063276	LRCH4	9.619687	10.069984	SUFU	7.163531	7.588962
CENPT	8.617404	9.052086	LRFN1	6.211094	7.149607	SUMF2	8.433772	8.739778
CEP85L	8.150218	8.955542	LRIG1	8.632913	9.229752	SUN2	10.794412	11.226315
CEP95	7.829186	8.229762	LRMP	8.748860	9.190499	SUSD3	5.898272	7.437791
CEP97	7.372359	7.780572	LRP1	6.399326	7.075435	SUV420H2	6.932752	7.522321
CERK	9.795266	10.774838	LRP10	11.830262	12.052420	SVILP1	4.026000	5.137475
CERS2	10.080509	10.341164	LRRC25	7.103794	7.984280	SYCE1L	5.348601	5.983671
CES3	2.923329	3.517070	LRRC34	4.964471	5.573814	SYCP3	4.154866	4.878362
CHAD	4.399739	5.222210	LRRC37A3	4.236966	4.817541	SYK	12.024369	12.463342
CHD9	9.253044	9.603312	LRRC37A4P	7.291323	7.868732	SYNE2	10.613964	11.212752
CHIT1	3.641550	4.539599	LRRC37B	6.088435	6.518142	SYNGAP1	8.673794	9.034056
CHMP1B	10.907701	11.207218	LRRC45	6.636263	7.124655	SYNRG	10.142777	10.438959
CHPT1	7.818354	8.907990	LRRC56	6.121375	7.293685	SYPL1	9.346570	9.744487
CHST11	10.238116	10.985108	LRRC58	9.433841	9.689760	SYTL1	8.930233	10.217913
CHST12	7.882563	8.276353	LRRC6	2.793388	3.504919	SYTL3	4.415617	5.015246
CHST15	9.697758	10.774881	LRRC8A	8.337331	8.675525	SYVN1	9.645725	10.023337
CIB1	7.908354	8.610106	LRRC8C	7.032033	7.420391	TACC3	7.309471	8.801061
CIPC	9.424793	9.945081	LRRK2	7.941073	8.567653	TAF1	8.839251	9.154716
CITED2	8.597511	9.037107	LRRN2	5.831552	6.635127	TAF1L	9.714126	10.067300
CKAP2	7.551719	8.041626	LRWD1	7.449766	8.224466	TAF5	6.352175	6.855815
CKAP4	10.696489	11.077660	LSM4	9.087894	9.389547	TAGLN	7.248603	8.393940
CLASRP	9.039680	9.413856	LTBP3	8.300550	9.120787	TAOK2	9.981022	10.251660
CLDN15	8.343006	8.745523	LUC7L	9.550481	9.921450	TAPSAR1	7.351725	7.823782
CLDN23	6.224232	7.202645	LUC7L3	10.758309	11.082746	TAPT1	7.979985	8.473822
CLDND2	4.561052	5.069234	LY9	9.374260	10.563596	TARSL2	6.657129	7.120445
CLEC2B	5.137201	5.692642	LYL1	8.442916	9.024322	TAS1R3	3.784685	4.349204
CLEC4C	3.531764	4.350432	LYPD3	4.996770	5.559790	TAZ	8.835198	9.162874
CLK1	10.097726	10.655823	LZTS2	9.546963	10.086621	TBC1D1	9.828270	10.172878
CLMN	8.427053	10.040462	MAD1L1	7.687900	8.617529	TBC1D10C	9.319610	10.168267
CLSTN1	10.390421	10.712002	MADD	9.239668	9.697150	TBC1D2	6.336769	6.829140
CLSTN3	8.561800	9.209258	MAF	5.624019	6.316036	TBC1D20	9.602517	9.945509
CMIP	9.361247	9.910637	MAFB	8.545007	9.178205	TBC1D22A	9.370203	9.680473
CMKLR1	6.145227	6.615621	MAFK	10.132249	10.622015	TBC1D27	8.428611	9.966118
CMTM1	5.318873	5.927105	MAGEE1	6.790568	7.232653	TBC1D9	9.675472	11.080486

CNNM3	9.835701	10.190451	MAML3	3.034209	3.707938	TBKBP1	7.631753	8.113300
CNNM4	8.028763	8.464320	MAN1A1	9.762530	10.318670	TBL1X	9.285456	9.711830
CNOT6L	9.639092	10.002059	MAN1B1	8.784305	9.258356	TBX19	6.409449	6.860982
CNOT8	9.640700	9.913192	MAN1C1	3.628016	4.364870	TBX21	8.134936	8.542361
CNR2	10.169803	10.616198	MAN2A1	9.854490	10.270385	TBXA2R	4.320663	5.033753
CNTD2	3.597377	4.408369	MAN2A2	9.704721	10.377377	TCAP	5.090281	5.759582
CNTRL	9.016369	9.293026	MAP1LC3B	9.923358	10.172486	TCEA2	6.889174	7.552375
COG4	7.611337	7.972585	MAP2K3	8.981426	9.275695	TCEAL1	7.828529	8.547109
COL18A1	4.714264	6.185639	MAP2K6	2.752027	3.575704	TCF25	8.933071	9.362641
COL4A3	6.734507	7.944816	MAP3K1	10.979571	11.942678	TCF3	11.007463	11.277524
COL4A4	6.657558	7.693414	MAP3K12	6.217259	6.757018	TCF4	12.724598	12.972933
COL6A4P2	2.901860	3.681030	MAP3K14-	6.276886	6.751689	TCL1A	11.304128	11.586886
COL9A3	9.743529	11.133198	MAP3K2	10.401757	10.788376	TCL1B	3.192431	3.831049
COLCA1	4.683561	5.311332	MAP3K3	9.253931	9.589936	TCL6	4.058425	4.833158
COLGALT1	9.979780	10.379175	MAP3K7CL	6.543587	7.075592	TCP11L2	8.031323	8.814209
COQ10A	7.715125	8.099016	MAP3K9	8.900146	9.625101	TDRD6	5.797336	6.277943
CORO1B	9.165370	9.729567	MAP4K1	7.234958	7.680668	TECR	5.724376	6.396180
COTL1	11.994459	12.326597	MAP4K2	7.823454	8.309981	TERF2IP	10.944661	11.289378
CPEB2	7.599910	8.168982	MAPK1	11.314028	11.551544	TEX264	8.483978	8.784776
CPLX1	2.056607	2.623418	MAPK8IP3	11.288326	12.066466	TFAP4	6.880585	7.364877
CPNE1	9.530608	9.839229	MAPKAPK5-	7.994919	8.345862	TGFBI	7.700485	8.989465
CRAMP1L	10.131504	10.537242	MAPRE2	9.403390	10.090307	THAP11	10.132285	10.666443
CRAT	6.903379	7.258645	Mar-01	8.373827	9.855849	THAP9-AS1	9.021103	9.354337
CREB3L2	11.009259	11.558102	MAST3	8.365227	9.323571	THBS1	10.841095	11.343066
CREBRF	10.135709	10.428355	MAST4	7.233216	7.975496	THBS4	3.545118	4.476264
CREBZF	10.957731	11.297122	MAX	10.128969	10.375736	THEM6	7.113098	7.575312
CREM	8.448056	9.443216	MAZ	11.102672	11.319787	THEMIS2	10.628006	11.120084
CRKL	11.174666	11.377139	MBD4	9.442027	10.101687	THRA	6.722015	7.757711
CRLF3	9.512989	9.986451	MBLAC2	7.221683	7.608518	TIA1	10.390164	10.700016
CRTAP	8.976252	9.580253	MBNL3	10.000443	10.505757	TIAL1	9.726499	9.992786
CRTC1	8.627252	9.084244	MBOAT1	7.187643	7.680679	TIGD3	5.400945	5.953023
CRYM	3.985289	5.631930	MBOAT7	8.988812	9.304397	TIMP2	9.522702	10.103726
CRYM-AS1	4.687099	5.655133	MBP	11.364118	11.882163	TINCR	3.311175	3.853448
CSNK1G2	10.367142	10.614454	MBTPS1	9.303948	9.605106	TIPARP	8.178529	8.903067
CTBP1	10.022548	10.353466	MC1R	5.977481	6.897504	TIRAP	7.653649	8.050578
CTD-	3.159939	3.791243	MCM6	7.227696	7.800285	TK2	6.849481	7.358460
CTDSP2	11.585286	11.964716	MECP2	10.925197	11.230799	TLR4	6.670294	7.318699
CTLA4	8.029285	9.429742	MEGF6	8.855803	9.697757	TLR7	7.442059	8.192947
CTNNBIP1	7.021525	7.693168	MEN1	9.790537	10.023803	TLR9	9.592265	10.232564
CTSB	11.687008	12.013009	MERTK	5.554860	6.168423	TM7SF2	6.024067	6.505109
CTSF	7.350237	8.486117	METRNL	7.233310	8.074132	TMED5	10.381161	10.696294
CTSK	4.782733	5.678871	METTL7A	9.777490	11.148077	TMED8	10.131261	10.402745
CTSS	11.513208	11.828049	MFHAS1	10.836023	11.127359	TMEM107	6.189454	6.841385
CUL4B	9.278644	9.615705	MFN1	7.708640	8.143230	TMEM109	10.218445	10.983652
CUTA	9.339315	9.700984	MFSD8	8.071802	8.401284	TMEM110	8.901565	9.250655
CXCL16	8.493280	9.587144	MGAT1	11.555503	12.086707	TMEM123	11.672215	12.162647
CXCR4	13.284547	14.384836	MGAT5	10.040352	10.518437	TMEM127	10.645660	10.912657
CXXC1	9.357277	9.662271	MGEA5	11.655112	11.892324	TMEM129	9.604929	10.005718
CXXC11	2.636247	3.237587	MGME1	8.996103	9.489921	TMEM134	7.792584	8.572692
CXXC5	11.353295	11.622855	MIA3	9.615370	9.943856	TMEM140	9.418989	9.894215
CYBA	9.184877	9.555047	MIAT	7.813520	8.300539	TMEM143	5.996477	6.769607
CYFIP2	10.867847	11.505499	MIB2	8.988336	9.510109	TMEM154	9.001641	9.268518
CYP27A1	7.079387	7.432517	MIDN	9.829455	10.729734	TMEM156	5.757804	6.313412
CYP4V2	7.973522	8.332763	MIF4GD	8.841012	9.737938	TMEM159	7.925526	8.447837
CYSLTR1	6.934135	7.770708	MINK1	9.031135	9.491465	TMEM175	7.682755	8.340551
CYTH2	8.545192	8.961677	MIR1914	4.967396	5.728424	TMEM187	6.599544	6.990598
CYTIP	10.049779	11.060102	MIR223	2.862711	3.444218	TMEM191A	3.822607	4.435065
D2HGDH	8.051592	8.582566	MIR378I	7.685665	9.035887	TMEM2	8.074942	9.224763
DAAM1	7.188216	7.637586	MIR600HG	9.414306	9.968163	TMEM219	8.319117	8.674634
DAB2IP	6.182002	7.056810	MIR8071-2	7.692078	8.161457	TMEM229B	4.442508	5.064983
DACT1	6.394281	7.568404	MIS18BP1	8.231951	8.774139	TMEM236	5.095447	5.738664

DAGLB	7.567608	7.896387	MKRN1	10.261089	10.566869	TMEM259	12.264799	12.541342
DAPK2	6.392188	7.992411	MLKL	6.363046	7.000753	TMEM38A	5.068577	6.118614
DBNDD1	5.739029	6.663768	MLXIP	8.524282	8.875463	TMEM56	5.531333	6.766886
DBP	6.989077	7.898600	MMP17	6.143143	7.109871	TMEM59	8.560756	9.036256
DCAF15	9.028888	9.291330	MN1	3.013219	3.723968	TMEM62	7.279155	7.801419
DCLRE1C	8.781290	9.307969	MNT	8.654979	9.270621	TMEM63A	8.477263	9.447280
DCST2	3.331548	4.011227	MOAP1	9.210208	9.627890	TMEM65	7.364358	7.799601
DCUN1D4	7.451922	7.758355	MORC3	10.356114	10.699920	TMEM66	11.540077	12.336078
DDAH2	8.126293	8.764535	MPEG1	10.248675	10.778626	TMEM71	5.604772	7.457221
DDX12P	4.931712	5.528053	MPHOSPH8	10.178394	10.561849	TMEM79	7.440534	7.950850
DDX26B	8.168815	8.574381	MPP1	5.765175	6.288386	TMEM80	7.926562	8.571958
DEAF1	7.116614	7.564987	MPP7	5.255350	5.934594	TMEM81	5.448664	6.007544
DEDD2	10.328413	10.629182	MPPE1	6.102498	6.521396	TMEM86B	7.387979	7.934024
DEF6	8.580418	9.088795	MPRIP	9.901067	10.348345	TMF1	9.860863	10.144283
DEF8	9.792752	10.463040	MPZ	5.434542	6.243002	TMX4	8.788761	9.775367
DEGS2	7.304103	8.506103	MR1	9.106677	9.505630	TNFRSF13B	8.973391	10.147623
DENND5B	9.146946	9.586050	MRI1	9.523043	9.833661	TNFRSF13C	8.945277	10.245787
DENND6A	7.939243	8.377578	MRO	2.321199	3.138831	TNFSF10	5.673886	6.497303
DENND6B	6.052940	6.921239	MROH1	8.037656	8.391944	TNFSF12	7.878202	8.635935
DEPDC5	7.638060	8.311261	MROH6	6.842118	8.055834	TNFSF8	4.254971	5.094799
DERL3	7.238436	7.820135	MRPL55	6.881970	7.391285	TNFSF9	8.930702	9.496531
DFFB	7.007984	7.425403	MS4A7	6.763860	7.335748	TNK1	5.826921	6.292120
DGCR2	9.945576	10.234010	MSI2	11.871465	12.577444	TNK2	10.346642	11.128173
DGCR9	2.856033	3.769550	MSL2	10.453777	10.809672	TNKS2	9.785942	10.094983
DGKA	8.463061	9.458801	MSL3	8.989121	9.398132	TNNI2	4.744582	5.348879
DGKD	9.892872	10.274904	MST4	8.873736	9.239526	TNNT3	3.522569	4.320684
DGKE	8.343834	8.770977	MSTO2P	6.479902	7.054533	TNRC6B	9.707594	10.391339
DICER1-AS1	5.941747	6.434062	MTERFD3	7.232620	7.602865	TNRC6C	8.733517	9.001551
DIP2C	5.568864	6.874664	MTHFR	9.461566	9.747288	TNS3	8.936322	9.445506
DIRAS1	5.473606	6.287349	MTIF3	8.236158	8.614518	TNXB	4.840840	5.534729
DIRC2	5.692154	6.472345	MTMR3	10.043727	10.267911	TOB1	8.783893	9.212989
DISP1	6.092208	6.740849	MTMR9LP	7.311212	8.095549	TOM1	8.245750	8.829681
DLG2	3.573237	4.559998	MTSS1L	6.584055	8.029707	TOP1MT	8.140624	8.810838
DLL1	6.187223	6.680314	MTURN	8.372052	9.025540	TP53I13	10.722344	11.532560
DMPK	8.987053	9.345187	MUC20	4.939339	5.754773	TPCN1	9.666835	10.655153
DMXL1	9.307493	9.648442	MX2	7.863202	8.563851	TPK1	6.427669	7.023828
DNAH10	5.333076	5.809189	MXD1	8.966126	9.284227	TPP1	10.862474	11.226210
DNAJB13	6.080440	6.930441	MXD3	6.467638	6.902545	TRABD	9.313293	10.602861
DNAJB14	9.563721	9.803935	MXD4	9.443670	10.028944	TRABD2A	6.680121	7.099083
DNAJB9	8.754212	9.146872	MXI1	9.418147	9.977367	TRAF3IP2	7.739271	8.300707
DNAJC1	6.785346	7.290289	MYBL1	4.593968	5.201493	TRAF3IP3	8.738340	9.270622
DNAJC4	8.463367	8.993828	MYH7B	5.869798	6.330438	TRAF5	9.218242	9.961192
DNASE2	8.424411	8.849104	MYO15B	8.509126	8.893083	TRAM2	9.500472	10.187215
DNHD1	9.079607	9.556107	MYO1F	7.624625	7.957989	TRAPPC2L	8.126663	9.404619
DNMBP	9.510519	10.128206	MYO9B	11.160162	11.478778	TRIB1	9.997695	10.791891
DOK2	7.963769	8.374373	MYOM1	5.645049	6.430859	TRIM14	8.623463	8.990823
DOK3	7.843948	9.051374	MZB1	8.248792	8.797089	TRIM22	10.330237	10.749775
DOPEY1	7.316055	7.787419	N4BP2	8.792009	9.083815	TRIM23	7.227246	7.590308
DPAGT1	7.471688	8.092263	NAA16	7.975625	8.340480	TRIM38	9.701218	10.199097
DPEP2	8.610359	9.801387	NAA40	9.442017	9.744612	TRIM39	8.471847	8.765032
DPH1	6.165365	6.669119	NAAA	7.474532	8.098652	TRIM52	8.444723	8.851701
DPH7	8.716168	9.107704	NAALADL1	7.193896	7.532949	TRIM65	8.964412	9.389587
DPM3	9.355394	9.765414	NAB2	8.587100	9.747255	TRIM7	5.284978	6.661681
DSTYK	8.415409	8.838957	NADK	9.771897	10.138840	TRIM8	10.173709	10.567343
DUSP26	3.651864	4.650479	NAGPA	7.749139	8.105223	TRNAA26	2.644382	3.489077
DYNLL2	10.045351	10.351739	NAPRT1	8.877364	9.339383	TRNP	9.637186	10.172156
DYRK1B	7.638027	8.029286	NBPF11	7.532379	8.073686	TRNS1	10.500912	10.818819
DYRK2	9.351066	9.869504	NCAPD2	7.357574	7.731127	TRPS1	6.928769	7.529539
E2F5	7.007129	7.397827	NCEH1	7.292422	7.769000	TRPV1	7.303117	7.870477
EFCAB12	3.660744	4.582015	NCF4	7.862387	8.709950	TSC1	9.527696	9.838653
EFCAB13	6.043420	6.742029	NCOA3	12.288167	12.543751	TSC22D1	8.209094	8.975399

EFCAB4A	6.241756	7.685981	NDRG1	9.108193	10.236159	TSC22D1-	3.759527	4.282536
EFNA3	5.366420	5.937036	NDRG2	5.181540	5.844291	TSC22D3	10.406757	12.138526
EGLN1	9.266610	9.625277	NDST1	8.168375	8.550029	TSEN54	7.860275	8.375223
EHD3	9.477890	10.102200	NDUFC1	5.437137	6.137905	TSHZ1	7.931629	8.406368
EHMT1	10.499702	11.048358	NEK7	9.694979	10.250481	TSHZ2	4.877615	6.153797
EHMT2	8.619016	9.039174	NFATC1	10.199776	10.825943	TSPYL2	11.934315	12.529008
EID2	8.883358	9.156341	NFATC3	10.123845	10.440490	TSSK3	7.089877	7.958089
ELF1	11.296970	11.558821	NFX1	9.588715	9.910684	TSSK6	6.349239	6.760412
ELF2	8.874453	9.179513	NGLY1	8.299492	8.583822	TTC13	7.091905	7.539082
ELFN2	3.414589	4.733303	NHLRC3	8.063355	8.432093	TTC21A	5.962863	7.259952
ELMSAN1	10.183042	10.599192	NIPSNAP3B	6.286516	6.743305	TTC24	5.871724	6.576931
ELOF1	9.550026	9.857473	NISCH	10.905388	11.283938	TTC28-AS1	7.506025	7.941323
EMB	9.731617	10.015394	NKD1	5.217355	5.902183	TTC3	9.584619	10.349392
EML4	9.748099	10.043944	NKG7	5.698522	6.223601	TTC3P1	8.728531	9.474671
ENC1	8.338260	9.846181	NKTR	11.096560	11.549911	TTC9	8.535120	9.192509
ENGASE	9.879921	10.260262	NLRC3	8.867943	9.436065	TTYH3	10.188284	10.679737
ENKD1	6.680041	7.042754	NLRP1	9.572145	10.693312	TUBA4A	9.945519	10.809196
ENPP2	5.488165	6.417453	NLRP6	6.299750	7.152057	TUBG2	6.364057	6.769225
ENTHD2	10.149090	10.580741	NMRK1	5.954146	6.475361	TULP4	8.831309	9.225127
EOMES	5.827830	6.364241	NMT2	6.725901	7.545298	TXNDC12	9.302051	9.609866
EP300	10.955658	11.193741	NOSIP	7.566908	8.408514	TXNDC15	9.061187	9.370379
EP400	10.608443	11.108309	NPHP3	7.094849	7.545313	TXNIP	12.228137	13.293390
EPB41	10.900554	11.292405	NPIPB11	3.365294	3.886833	U2AF1L4	8.067362	8.592130
EPB41L3	5.732439	6.185456	NPRL2	6.983450	7.610359	UBA7	8.112605	8.451289
EPB41L4A-	8.666009	9.123639	NQO2	6.629807	7.406055	UBAC2	8.825228	9.345526
EPHB6	8.062361	8.656597	NR1D1	7.112680	7.626657	UBAP1L	5.211278	5.718925
EPHX1	7.395412	8.641725	NR1D2	9.550598	10.123178	UBE2G1	9.577204	10.032559
EPS15L1	8.362089	8.800623	NR3C1	11.332695	11.642809	UBE2H	10.715925	10.981374
EPS8L2	7.524945	8.495698	NR3C2	4.836796	5.512551	UBN1	9.965082	10.191962
ERBB2IP	10.246764	10.500673	NR4A2	9.065984	9.824129	UBN2	9.023235	9.336591
ERCC6	7.316886	7.688584	NSUN6	7.148256	7.618561	UBR2	8.924589	9.233922
ERF	10.112764	10.624854	NSUN7	4.605438	5.278193	UBXN11	6.907211	7.557599
ERMN	5.878481	6.803392	NT5C2	9.888270	10.260654	UCKL1	7.900662	8.704584
ERP29	10.282332	10.995020	NT5C3A	6.978778	7.332968	UCKL1-AS1	6.179417	6.780808
ESYT1	9.524273	10.079573	NUAK2	10.650583	10.933336	UCN	4.827511	5.434219
ETV5	4.639207	5.388185	NUMA1	11.311746	11.735133	UCP3	5.346556	5.842702
EVL	8.640385	9.181450	NUMBL	6.521791	7.177986	UHRF2	9.028370	9.390215
EZR	12.781126	13.202409	NUP85	7.590405	8.009195	ULK1	9.292309	9.991702
F2R	6.127746	6.685938	NXF1	10.293368	10.753920	UNC5CL	6.719168	7.638509
FAIM3	11.119867	12.355144	OAS2	9.211423	9.858793	UNC93B1	9.466687	9.902647
FAM102A	10.341497	10.937852	OBSCN	8.116449	8.936374	UNKL	9.356099	9.623296
FAM102B	7.718320	8.397291	OGFOD2	7.811898	8.156005	UPF3A	8.017272	8.415733
FAM111A	9.372875	9.910182	OGT	12.103622	12.439197	UQCRB	7.583610	8.111980
FAM111B	6.111105	8.102586	OR13A1	4.147824	4.846070	USF1	9.373610	9.930341
FAM117B	7.966549	8.844644	OR52N4	2.957009	3.774176	USP11	8.324955	8.703336
FAM120C	6.475219	7.049753	ORAI2	12.260660	13.188449	USP20	8.921391	9.237514
FAM129C	9.433547	10.807706	ORM2	3.639565	4.549160	USP21	8.754581	9.195226
FAM134A	10.482331	10.751867	ORMDL1	9.933611	10.277057	USP28	8.082237	8.615363
FAM134C	9.978079	10.281434	OSBP2	6.228814	6.667281	USP53	7.311125	7.685499
FAM13B	9.112022	9.344954	OSBPL11	8.903670	9.405955	USP6NL	8.499918	8.830184
FAM159A	6.310339	7.127835	OSBPL3	7.043130	7.672355	USP8	8.932668	9.240681
FAM167B	4.467881	5.256468	OSBPL5	4.167870	4.719014	USPL1	9.485585	9.775383
FAM178A	9.220089	9.546463	OSBPL7	7.872578	8.280606	UTRN	8.392128	8.993422
FAM193B	10.058542	10.618791	OSBPL8	9.303331	9.575750	VAMP1	9.667474	10.329868
FAM198B	5.941870	6.544739	OSER1-AS1	7.069771	7.489522	VAMP2	10.651979	11.074938
FAM210B	7.820457	8.269177	OTUD1	9.598571	10.198729	VAMP4	8.576634	9.016879
FAM214A	8.902602	9.833293	OVGP1	6.176328	6.978294	VASH1	7.738165	8.369080
FAM217B	8.422453	8.822935	OVOL1	5.371710	5.932278	VAT1	10.202331	10.750358
FAM220A	8.348472	8.680600	OXR1	8.242246	8.542509	VAV1	7.315939	7.760534
FAM222A	5.159251	5.674080	P2RX1	7.718576	9.098444	VGLL4	7.933878	8.244934
FAM26F	5.764647	6.700957	P2RX5	5.406615	6.064706	VIPR1	6.980081	7.525785

FAM43A	9.198136	10.414334	P2RY6	4.613647	5.184825	VMO1	4.596811	5.186683
FAM46A	7.128823	7.634702	P4HTM	8.581332	9.220505	VNN2	7.164540	7.726892
FAM46C	10.285919	11.306376	PACSIN1	2.364067	2.967517	VPREB3	6.303873	7.724564
FAM63B	7.191132	7.874161	PAIP2B	7.816772	8.583296	VPS26B	7.857605	8.802069
FAM65B	9.999721	11.138137	PAN2	8.907627	9.431786	VWA3A	4.046714	4.746794
FAM73B	9.493783	9.744204	PANK1	5.427118	6.259314	WBP2	10.177474	10.530766
FAM76B	8.843599	9.235256	PAPD7	8.990527	9.516953	WDFY4	10.761716	11.022791
FAM78A	9.684060	10.336331	PAPSS2	4.554894	5.333824	WDR19	5.746516	6.427240
FAM89B	9.448111	9.937195	PAQR6	4.846727	5.387192	WDR37	8.703911	8.989303
FAM8A1	7.665836	8.658751	PARD6A	7.732405	8.373995	WDR47	7.206921	7.600586
FAXDC2	5.610566	7.514959	PARP16	7.371225	7.778387	WDR52	6.937653	7.408268
FBXL14	9.645589	9.932894	PARP4	9.031390	9.424764	WDR54	6.639192	7.149698
FBXL16	5.666518	6.369652	PARVG	8.693674	9.608204	WDR74	7.711435	8.047635
FBXL20	9.090698	9.529145	PATL2	7.072288	7.765082	WFIKKN1	3.592566	4.167677
FBXL3	10.214564	10.494303	PBXIP1	11.216156	12.440093	WHSC1	9.692928	9.908316
FBXO10	9.227814	10.018003	PCDH9	4.937854	6.243122	WHSC1L1	10.847592	11.103146
FBXO15	3.197147	4.102268	PCF11	10.359286	10.695989	WIPF1	11.587507	12.176966
FBXO18	9.418454	9.805117	PCMTD2	10.099492	10.473703	WNT3	9.021342	9.920469
FBXO21	9.390026	9.752127	PCOLCE	4.925128	5.632224	WSB1	10.346040	10.647629
FBXO32	7.096601	8.225684	PCP2	4.980941	5.737681	XAF1	8.468052	8.920375
FBXO44	9.311084	9.585862	PCSK7	9.410816	9.927430	XKRX	6.401226	7.337313
FBXO9	8.657897	9.150880	PCYOX1	8.519777	9.150720	XPC	9.708936	10.201474
FCGR2B	8.136848	8.893917	PDE1B	5.801025	6.497324	XXYLT1-AS2	7.004557	7.915926
FCGR2C	2.779775	3.526659	PDE4A	8.044267	8.756800	XYLT1	9.567547	10.267923
FCGR3A	6.388435	7.241791	PDE4B	11.150356	11.588118	XYLT2	7.988640	8.339547
FCGRT	8.935369	9.524448	PDE7B	5.110307	6.752688	YPEL1	8.227148	8.804941
FCHO2	7.181985	7.690181	PDGFD	7.555172	7.954650	YPEL2	9.995632	10.983065
FCHSD1	8.397352	8.779830	PDK3	8.697286	9.108292	YPEL3	10.551439	11.298464
FCRL1	8.071989	8.536621	PDK4	7.068839	8.328900	YPEL4	3.518267	4.397661
FCRL2	7.922816	8.701414	PDLIM1	8.921107	9.653152	YPEL5	10.958313	11.309596
FCRLA	9.842865	10.939973	PDP1	8.597513	9.270187	ZBED6	8.415356	8.879194
FCRLB	5.775447	6.405606	PDPR	10.143027	10.355644	ZBP1	5.415750	7.239335
FGD1	7.885756	8.281740	PDXDC2P	6.140324	6.697397	ZBTB1	10.887841	11.229709
FGD3	8.555568	9.584428	PDXK	8.701011	9.232471	ZBTB11	9.030798	9.448235
FGFBP2	5.363135	6.013487	PECAM1	9.903126	10.698074	ZBTB14	8.725897	8.996061
FGFR1	7.205856	7.595832	PEG10	8.509555	10.152779	ZBTB18	10.531926	11.135647
FGFR1OP	7.373117	7.761230	PELI2	6.942838	7.570142	ZBTB2	9.034452	9.343934
FHDC1	5.254053	6.167901	PER1	9.458995	10.071561	ZBTB20	8.785204	9.443875
FLI1	9.487765	10.033405	PEX1	7.858219	8.380608	ZBTB38	10.543266	10.889219
FLJ10038	7.231803	7.830100	PEX6	8.776091	9.090305	ZBTB4	11.242166	11.939125
FLJ20021	5.008668	5.566601	PFKFB3	8.793985	9.348616	ZBTB40	10.515879	10.821621
FLJ32255	7.972495	8.741436	PGAM2	8.091290	8.717409	ZBTB41	8.192995	8.578554
FLJ38379	3.280222	3.857871	PGM2L1	7.692699	8.395057	ZBTB44	10.232701	10.768645
FLJ42258	6.315870	7.211709	PGPEP1	8.598089	9.468764	ZC3H11A	10.389790	10.725385
FLJ44342	6.673149	7.493969	PHC3	10.528370	11.000181	ZC3H3	8.877373	9.340307
FLT1	5.996407	6.609605	PHF1	9.970966	10.467423	ZC3H6	8.075339	8.503513
FLYWCH1	9.528906	9.849177	PHF10	6.843299	7.321238	ZCCHC11	9.722018	10.197974
FMR1	9.004822	9.277543	PHF12	9.700796	10.038594	ZCCHC14	7.313456	7.881238
FN3K	3.769217	4.409465	PHF13	9.242392	9.505813	ZCCHC18	7.353233	8.447805
FNBP4	10.787241	11.126503	PHF19	8.376921	8.785115	ZCCHC2	8.949510	9.413396
FOLR2	2.367216	3.370751	PHF2	9.223254	9.495065	ZCCHC24	6.194732	6.609896
FOPNL	8.604013	8.897461	PHF3	10.471190	10.740470	ZDHHC20	10.780803	11.067276
FOS	9.056495	9.446771	PHF7	6.128468	6.984191	ZER1	9.277133	9.624907
FOSB	9.314267	9.713014	PHIP	9.709664	9.991177	ZFAND2B	7.929458	8.355842
FOSL2	7.985485	8.570636	PHKB	8.615470	9.002847	ZFP14	8.218628	8.561345
FOXJ2	9.310313	9.649870	PHKG2	8.032771	8.332195	ZFP36L2	11.875325	13.127658
FOXN2	9.093369	9.350617	PHLDA1	7.895883	8.251404	ZFP64	8.045202	8.510551
FOXO3	7.961128	8.462227	PI4K2A	10.140662	10.402749	ZFYVE28	6.326622	6.704644
FOXO4	9.317650	9.881645	PI4KA	7.548581	7.869357	ZHX2	10.945892	11.447311
FPR3	7.392129	7.925276	PID1	5.593082	6.178429	ZHX3	6.949804	7.877903
FRAT1	7.734172	8.599465	PIK3IP1	10.065277	10.871641	ZIK1	8.497347	8.864694

FRAT2	8.320765	8.950476	PIK3R1	9.228085	9.561986	ZKSCAN8	9.987509	10.265291
FRY	8.254513	9.010353	PIP4K2B	9.853952	10.115641	ZMYM3	8.657682	9.104494
FTL	12.515462	12.865330	PIP5KL1	5.213565	6.045408	ZMYM6	8.279882	8.573234
FUCA1	9.676688	10.221398	PITPNC1	7.294052	7.861024	ZMYND10	3.247814	3.951346
FUZ	6.774066	7.572011	PITPNM1	10.087828	10.458500	ZMYND15	3.862105	4.569945
FXYD1	2.864990	3.474882	PITPNM2	10.063453	11.038609	ZMYND8	8.182959	8.627261
FXYD5	7.688616	8.354854	PKD1	9.736438	10.020999	ZNF10	7.486255	8.029936
FXYD7	4.366889	6.010721	PKIA	7.171588	7.793120	ZNF101	8.682461	9.204554
FYB	6.013826	6.656049	PKN2	8.449712	8.779303	ZNF107	10.966446	11.904860
FZD3	7.490647	8.064051	PLA2G15	7.407978	7.850018	ZNF14	8.066692	8.480796
GAA	8.516936	8.970294	PLA2G4B	4.560664	5.138546	ZNF211	9.064781	9.517581
GAB2	9.695725	10.502598	PLAC9	4.095594	4.878264	ZNF219	8.894310	9.189978
GABARAPL1	8.325228	8.941389	PLCB2	9.071073	9.421348	ZNF224	7.252344	7.674999
GABARAPL3	6.171091	6.805819	PLCD1	4.618811	5.544858	ZNF248	8.195289	8.566882
GABRB2	2.530571	3.109537	PLCG2	8.409509	9.214869	ZNF250	7.211458	7.829392
GAK	9.685898	10.125891	PLCH2	7.261830	8.016683	ZNF266	10.794692	11.385694
GALM	6.175972	6.816030	PLCL2	10.284755	10.582316	ZNF273	7.433128	7.792494
GALNS	8.402671	8.843310	PLD3	8.691768	9.144492	ZNF30	5.336340	5.956362
GALNT3	5.519971	6.092381	PLD4	2.984497	3.571469	ZNF304	8.658793	8.990512
GAPT	7.309832	7.755506	PLEKHA2	11.768944	12.585679	ZNF318	9.881901	10.245270
GATAD1	9.794561	10.151914	PLEKHA3	8.442948	8.814856	ZNF331	9.307067	10.276127
GATM	7.042889	7.489733	PLEKHB1	6.316772	6.874143	ZNF335	8.347985	8.795930
GCC2	9.299545	9.555372	PLEKHM1	8.892714	9.178884	ZNF34	6.890517	7.287990
GCHFR	7.805465	8.189154	PLEKHM1P	7.007212	7.418798	ZNF367	6.073740	6.674884
GCLC	9.021459	9.393953	PLK1S1	6.560459	6.974730	ZNF395	10.782825	11.558307
GCNT2	7.374358	7.867151	PLP2	9.896804	10.471979	ZNF439	8.018791	8.786358
GDE1	8.969255	9.305518	PLXND1	9.726213	11.128400	ZNF441	7.924118	8.317246
GDF11	6.921180	7.436380	PMEL	4.034936	4.680156	ZNF487	4.310473	5.170751
GDF7	7.718463	8.612699	PNMA5	5.390997	6.321755	ZNF490	7.131681	7.501887
GDPD1	4.688770	5.221307	PNPLA2	10.216288	10.956675	ZNF516	7.200737	7.788919
GDPD3	5.949021	6.830994	PNPLA7	6.535310	8.074559	ZNF540	5.845400	6.845934
GFOD1	8.037557	8.984444	PNPLA8	9.026886	9.532733	ZNF548	8.811509	9.154550
GGA2	12.043555	12.959809	PNRC1	11.491310	11.887465	ZNF566	7.393226	7.923050
GGA3	10.382535	10.795589	POFUT2	9.369069	9.648037	ZNF569	7.511167	8.131843
GH1	3.525882	4.411478	POLM	9.117723	9.373317	ZNF575	5.003248	5.510336
GHDC	8.558782	9.043320	POLR3GL	8.220264	8.596098	ZNF595	8.133504	8.981992
GIPR	3.679387	4.404236	PPAP2B	5.480715	6.047320	ZNF615	7.931536	8.255725
GIT2	9.558193	10.025268	PPARD	9.059911	9.779642	ZNF627	7.942776	8.263055
GKAP1	4.682013	5.381104	PPM1D	8.400431	8.765148	ZNF652	8.934573	9.411741
GLCCI1	7.719510	8.344246	PPM1J	4.371531	5.476421	ZNF654	8.257681	8.639784
GLI1	4.939790	5.794795	PPM1K	11.293611	11.930100	ZNF667	5.747674	6.088915
GLIPR1	7.695390	8.837542	PPP1R12B	7.937717	8.393019	ZNF671	8.742671	8.988737
GLTSCR2	10.216956	10.433053	PPP1R32	4.643154	5.405927	ZNF699	7.243557	7.885497
GM2A	10.760522	11.321828	PPP1R3E	8.183909	9.041793	ZNF700	8.507417	8.863217
GMCL1	7.473887	7.889810	PPP2R5C	10.544418	11.077917	ZNF703	5.135007	5.793945
GMEB2	9.534705	9.878198	PPP3CA	9.295837	9.630359	ZNF704	3.017126	3.634068
GMFG	6.486907	6.954804	PRC1	6.435888	6.913528	ZNF721	9.712045	9.973855
GNA13	11.534620	11.817368	PRDM2	12.518563	12.833009	ZNF791	7.927168	8.325819
GNAO1	5.164637	6.382627	PRICKLE1	5.182319	6.241397	ZNF815P	4.263324	5.072533
GNAZ	7.084189	8.085829	PRKAR2A	9.389050	9.654574	ZNF821	7.094282	7.739871
GNB5	8.942027	9.790116	PRKCA	5.165391	5.780434	ZNF823	5.555208	5.980860
GNG7	7.413585	9.873069	PRKCB	11.348785	11.908393	ZNF831	7.889246	9.018884
GNL1	9.440126	9.820509	PRKCE	8.913912	9.968235	ZNF853	7.585817	7.991584
GNPTAB	10.597070	10.864116	PRKCH	5.801053	6.242240	ZNF862	9.257505	9.731329
GNPTG	6.099040	6.540563	PRKCSH	9.315728	9.684751	ZNF92	9.126394	10.095460
GOLGA1	7.489169	7.945890	PRKD2	8.457707	8.861025	ZSCAN18	10.012435	10.275554
GOLGA2P5	8.012281	8.878062	PRKD3	9.742707	10.028493	ZSWIM6	7.743843	8.301334

Appendix 8. 158 differentially expressed proteins induced by the soluble CD40 ligand in primary CLL cells at 12h time point

Protein	Accession	p-value(12h stim vs. 12h unstim)	Fold-Change(12h stim vs. 12h unstim)
TNF receptor-associated factor 1	Q13077	1.95E-05	8.34834
Beta-galactosidase	P16278	0.0180556	3.8089
Serine/threonine-protein phosphatase 4 regulatory subunit 1	Q8TF05	0.0359863	3.0761
Putative ribosome-binding factor A, mitochondrial	Q8N0V3	0.00321725	2.95393
Raftlin	Q14699	0.0468653	2.87343
ATP-dependent RNA helicase DDX50	Q9BQ39	0.00141214	2.78484
Anaphase-promoting complex subunit 7	Q9UJX3	0.010285	2.78484
Charged multivesicular body protein 4b	Q9H444	0.0200121	2.70396
Isopentenyl-diphosphate Delta-isomerase 1	Q13907	0.0154446	2.46604
Protein fosB	P53539	0.0321401	2.4615
Pyridoxal kinase	O00764	0.00214469	2.37247
Importin subunit alpha-5	P52294	0.0277964	2.35505
UPF0668 protein C10orf76	Q5T2E6	0.0318233	2.35072
Importin subunit alpha-1	P52292	0.00340447	2.3206
Interferon regulatory factor 5	Q13568	0.029128	2.25736
Thiamine-triphosphatase	Q9BU02	0.0086693	2.2532
RalBP1-associated Eps domain-containing protein 1	Q96D71	0.00302813	2.18776
CD44 antigen	P16070	0.0302177	2.15179
HLA class I histocompatibility antigen, alpha chain E	P13747	0.0466695	2.13206
Exocyst complex component 5	O00471	0.00844907	2.07014
rRNA-processing protein FCF1 homolog	Q9Y324	0.0283591	2.05116
Coiled-coil domain-containing protein 50	Q8IVM0	0.010825	2.00632
Nardilysin	O43847	0.040561	1.96607
Vacuolar protein sorting-associated protein 41 homolog	P49754	0.0247649	1.89496
NADH dehydrogenase [ubiquinone] 1 subunit C2	O95298	0.0105793	1.88799
Ferredoxin-2, mitochondrial	Q6P4F2	0.0215064	1.88452
Mitogen-activated protein kinase kinase kinase kinase 1	Q92918	0.0157866	1.87413

BAG family molecular chaperone regulator 1	Q99933	0.0246946	1.8197
Mitofusin-1	Q8IWA4	0.0369386	1.80634
28S ribosomal protein S5, mitochondrial	P82675	0.0425243	1.7997
PH and SEC7 domain-containing protein 4	Q8NDX1	0.0313628	1.79639
Eukaryotic translation initiation factor 3 subunit K	Q9UBQ5	0.0379199	1.77337
Pre-mRNA-processing factor 17	O60508	0.01962	1.76035
Sequestosome-1	Q13501	0.0444721	1.7378
Nuclear factor NF-kappa-B p105 subunit	P19838	0.000268062	1.73141
Fibronectin	P02751	0.0138861	1.71238
Nucleolar RNA helicase 2	Q9NR30	0.0456201	1.70608
Pre-mRNA-splicing factor 38A	Q8NAV1	0.0110474	1.69044
Formin-binding protein 1	Q96RU3	0.0107497	1.65653
DNA replication licensing factor MCM7	P33993	0.0487353	1.64437
Coatomer subunit epsilon	O14579	0.0191017	1.6293
CD97 antigen	P48960	0.0146525	1.62032
NADH-cytochrome b5 reductase 2	Q6BCY4	0.0393652	1.62032
Elongator complex protein 1	O95163	0.0314496	1.58782
N6-adenosine-methyltransferase 70 kDa subunit	Q86U44	0.0361988	1.58782
39S ribosomal protein L16, mitochondrial	Q9NX20	0.0374456	1.57906
Axin interactor, dorsalization-associated protein	Q96BJ3	0.0174278	1.56459
40S ribosomal protein S20	P60866	0.0329154	1.55597
Triokinase/FMN cyclase	Q3LXA3	0.0402704	1.54739
Telomeric repeat-binding factor 2-interacting protein 1	Q9NYB0	0.04825	1.5332
S-adenosylmethionine synthase isoform type-2	P31153	0.0208195	1.52757
Ral GTPase-activating protein subunit beta	Q86X10	0.0485136	1.52475
Ras-related GTP-binding protein A	Q7L523	0.0444937	1.50245
Ribosome biogenesis protein BOP1	Q14137	0.0348412	1.49968
Centrosome-associated protein CEP250	Q9BV73	0.0150552	1.4642
GPN-loop GTPase 1	Q9HCN4	0.0195359	1.45613

U4/U6 small nuclear ribonucleoprotein Prp4	O43172	0.012533	1.45345
Alanine--tRNA ligase, cytoplasmic	P49588	0.0380601	1.44544
Signal transducer and activator of transcription 3	P40763	0.0357639	1.44278
Nuclear pore complex protein Nup155	O75694	0.0269057	1.42955
Lymphocyte antigen 75	O60449	0.0362861	1.41906
Forkhead box protein P1	Q9H334	0.0207763	1.41384
Regulator of nonsense transcripts 1	Q92900	0.00995453	1.38803
Transcription factor ETV6	P41212	0.0368435	1.33783
E3 ubiquitin-protein ligase CHIP	Q9UNE7	0.0417096	1.24509
60S ribosomal protein L12	P30050	0.031156	1.2314
Centromere/kinetochore protein zw10 homolog	O43264	0.022832	-1.28469
Alpha-actinin-4	O43707	0.0297568	-1.2942
Ribonuclease P protein subunit p40	O75818	0.0465094	-1.34029
Peptidyl-prolyl cis-trans isomerase-like 1	Q9Y3C6	0.0383708	-1.35769
Eukaryotic translation initiation factor 4 gamma 2	P78344	0.0269089	-1.38293
U5 small nuclear ribonucleoprotein 200 kDa helicase	O75643	0.0152873	-1.39059
Nuclear pore complex protein Nup98-Nup96	P52948	0.0193335	-1.40088
Coiled-coil domain-containing protein 58	Q4VC31	0.0214045	-1.41124
Early endosome antigen 1	Q15075	0.0391155	-1.42692
N6-adenosine-methyltransferase subunit METTL14	Q9HCE5	0.0368163	-1.43747
LDLR chaperone MESD	Q14696	0.0439465	-1.45613
Neutral alpha-glucosidase AB	Q14697	0.0150213	-1.4642
Peroxisomal membrane protein 11B	O96011	0.041299	-1.4642
LIM and senescent cell antigen-like-containing domain protein 1	P48059	0.0273038	-1.47503
Diphosphomevalonate decarboxylase	P53602	0.0497517	-1.49968
Mitochondrial antiviral-signaling protein	Q7Z434	0.0172114	-1.51635
Nucleoporin NUP188 homolog	Q5SRE5	0.0375278	-1.52475
Nuclear autoantigenic sperm protein	P49321	0.0179607	-1.5332
Regulation of nuclear pre-mRNA domain-containing protein 1B	Q9NQG5	0.0223404	-1.54454

Zinc finger protein 22	P17026	0.0270537	-1.5531
Presequence protease, mitochondrial	Q5JRX3	0.0233727	-1.56747
NAD-dependent malic enzyme, mitochondrial	P23368	0.0220016	-1.57036
Apoptosis-inducing factor 1, mitochondrial	O95831	0.00163427	-1.57906
Nucleoprotein TPR	P12270	0.0112538	-1.57907
Glutaredoxin-related protein 5, mitochondrial	Q86SX6	0.0460222	-1.58489
Striatin-3	Q13033	0.0276508	-1.59074
GrpE protein homolog 1, mitochondrial	Q9HAV7	0.0332458	-1.59956
Protein disulfide-isomerase A3	P30101	0.046373	-1.60251
Calcium-independent phospholipase A2-gamma	Q9NP80	0.0420105	-1.60842
Regulator of microtubule dynamics protein 1	Q96DB5	0.049153	-1.61139
Dolichyl-diphosphooligosaccharide--protein glycosyltransferase subunit DAD1	P61803	0.0499472	-1.61734
Cytochrome b-245 heavy chain	P04839	0.0253985	-1.63531
Dual adapter for phosphotyrosine and 3-phosphotyrosine and 3-phosphoinositide	Q9UN19	0.0293618	-1.63531
Bromodomain adjacent to zinc finger domain protein 1A	Q9NRL2	0.0337885	-1.63531
Death-inducer obliterator 1	Q9BTC0	0.00266131	-1.64437
Cytochrome b-c1 complex subunit 2, mitochondrial	P22695	0.0151215	-1.65348
Metalloendopeptidase OMA1, mitochondrial	Q96E52	0.041772	-1.65959
Translation factor GUF1, mitochondrial	Q8N442	0.00550369	-1.67494
GDP-D-glucose phosphorylase 1	Q6ZNW5	0.0396605	-1.67803
m-AAA protease-interacting protein 1, mitochondrial	Q8WWC4	0.0356438	-1.68112
Zinc finger protein 800	Q2TB10	0.0175112	-1.68422
Ribosome biogenesis protein BMS1 homolog	Q14692	0.0359627	-1.68422
RNA-binding protein 45	Q8IUH3	0.00569016	-1.69044
NADH dehydrogenase [ubiquinone] 1 alpha subcomplex subunit 9, mitochondrial	Q16795	0.0462323	-1.69356
CD2-associated protein	Q9Y5K6	0.0481226	-1.7187
Tyrosine-protein phosphatase non-receptor type 2	P17706	0.00419286	-1.72504
Transmembrane emp24 domain-containing protein 1	Q13445	0.0071266	-1.7378
Mitochondrial fission factor	Q9GZY8	0.00360017	-1.741

Mitogen-activated protein kinase 1	P28482	0.0477138	-1.74421
Required for meiotic nuclear division protein 1 homolog	Q9NWS8	0.00564363	-1.75388
TBC1 domain family member 5	Q92609	0.0268271	-1.75388
Transmembrane protein 126A	Q9H061	0.0486999	-1.7636
Ubiquitin carboxyl-terminal hydrolase 47	Q96K76	0.0194067	-1.77337
SRSF protein kinase 2	P78362	0.0208254	-1.7997
Ubiquitin carboxyl-terminal hydrolase 8	P40818	0.0349134	-1.80967
Nucleoporin p58/p45	Q9BVL2	0.024014	-1.81301
Cyclin-L1	Q9UK58	0.0354552	-1.82978
CD2 antigen cytoplasmic tail-binding protein 2	O95400	0.020144	-1.83992
Transcription initiation factor TFIID subunit 7	Q15545	0.0127683	-1.84672
Chromobox protein homolog 5	P45973	0.0159766	-1.87413
Lysine-specific demethylase PHF2	O75151	0.0373017	-1.89496
Selenoprotein T	P62341	0.0121287	-1.89845
NADH dehydrogenase [ubiquinone] iron-sulfur protein 8, mitochondrial	O00217	0.01561	-1.90546
Abl interactor 1	Q8IZP0	0.0133336	-1.91955
Ras GTPase-activating protein 2	Q15283	0.0352427	-1.92309
39S ribosomal protein L27, mitochondrial	Q9P0M9	0.0306971	-1.93731
Inactive phospholipase C-like protein 2	Q9UPR0	0.0283558	-1.94446
E3 ubiquitin-protein ligase ARIH1	Q9Y4X5	0.0366734	-1.96246
Hermansky-Pudlak syndrome 3 protein	Q969F9	0.0428015	-1.98061
Biogenesis of lysosome-related organelles complex 1 subunit 4	Q9NUP1	0.0303338	-1.98793
Ribosomal protein S6 kinase beta-1	P23443	0.0330079	-2.00263
ADP-ribosylation factor-binding protein GGA3	Q9NZ52	0.0230564	-2.02488
NADH dehydrogenase [ubiquinone] 1 beta subcomplex subunit 10	O96000	0.0400584	-2.02862
Cytochrome c oxidase subunit 5A, mitochondrial	P20674	0.0331083	-2.05494
Small glutamine-rich tetratricopeptide repeat-containing protein alpha	O43765	0.0336517	-2.06253
HLA class II histocompatibility antigen, DO alpha chain	P06340	0.0413405	-2.08545
Zinc finger and BTB domain-containing protein 20	Q9HC78	0.0162387	-2.10087

52 kDa repressor of the inhibitor of the protein kinase	O43422	0.0316094	-2.12422
Lysine-specific demethylase 4B	O94953	0.000432156	-2.13993
PC4 and SFRS1-interacting protein	O75475	0.0328843	-2.15973
E3 ubiquitin/ISG15 ligase TRIM25	Q14258	0.00757154	-2.22433
F-actin-uncapping protein LRRC16A	Q5VZK9	0.00414821	-2.31206
Histone-lysine N-methyltransferase EZH1	Q92800	0.028239	-2.31633
Fc receptor-like protein 3	Q96P31	0.0353818	-2.33346
Probable leucine--tRNA ligase, mitochondrial	Q15031	0.00950692	-2.35072
RAD50-interacting protein 1	Q6NUQ1	0.0322799	-2.36374
Malectin	Q14165	0.0401762	-2.53046
Nicotinate phosphoribosyltransferase	Q6XQN6	0.0365203	-2.57276
F-box only protein 4	Q9UKT5	0.0371546	-2.76439
Serum albumin	P02768	0.0245536	-2.93224
Stromal interaction molecule 2	Q9P246	0.0366994	-2.99226
Periodic tryptophan protein 1 homolog	Q13610	0.00880606	-3.02552

Appendix 9. 552 differentially expressed proteins induced by the soluble CD40 ligand in primary CLL cells at 24h time point

Protein	Accession	p-value(24h stim vs. 24h unstim)	Fold-Change(24h stim vs. 24h unstim)
Biotinidase	P43251	0.0290927	18.1301
Probable RNA polymerase II nuclear localization protein SLC7A6OS	Q96CW6	0.0144067	10.4906
TNF receptor-associated factor 1	Q13077	1.80E-05	10.0956
PHD finger protein 14	O94880	0.00204098	6.35916
Uncharacterized protein C15orf57	Q9BV29	0.0122798	5.95662
Glutamine-rich protein 1	Q2TAL8	0.00380146	4.99728
Glutathione S-transferase theta-1	P30711	0.0430604	4.7665
Leukosialin	P16150	0.0265614	4.55477
Maspardin	Q9NZD8	0.0245251	4.28023
MKI67 FHA domain-interacting nucleolar phosphoprotein	Q9BYG3	0.00184687	4.20017
Raftlin	Q14699	0.0190648	4.04824
Cleavage sulation factor subunit 2	P33240	0.00216336	4.01667
Nucleoside diphosphate kinase 6	O75414	0.00954956	3.98229
28S ribosomal protein S26, mitochondrial	Q9BYN8	0.00300268	3.8259
OTU domain-containing protein 6B	Q8N6M0	0.0369902	3.78617
Charged multivesicular body protein 4b	Q9H444	0.00717986	3.67451
Poly [ADP-ribose] polymerase 4	Q9UKK3	0.00643273	3.63971
Coiled-coil domain-containing protein 124	Q96CT7	0.0321343	3.5986
Interferon regulatory factor 2-binding protein 2	Q7Z5L9	0.00948054	3.57987
Nucleoporin NDC1	Q9BTX1	0.00928962	3.46364
Myristoylated alanine-rich C-kinase substrate	P29966	0.0155395	3.38272
Cytoplasmic FMR1-interacting protein 1	Q7L576	0.0178261	3.34298
Transmembrane protein 256	Q8N2U0	0.0297293	3.32762
Calcium-binding mitochondrial carrier protein Aralar2	Q9UJS0	0.0074247	3.21909
Ubiquitin-conjugating enzyme E2 variant 2	Q15819	0.0449567	3.21613
SCY1-like protein 2	Q6P3W7	0.0476614	3.20529
Prefoldin subunit 3	P61758	0.0136794	3.19644

Kynurenine--oxoglutarate transaminase 1	Q16773	0.0459935	3.15017
Ras-related protein Rab-9A	P51151	0.0152817	3.09504
EF-hand domain-containing protein D2	Q96C19	0.00773858	3.09077
Glucose-induced degradation protein 8 homolog	Q9NWU2	0.0147596	3.08935
Armadillo repeat-containing X-linked protein 3	Q9UH62	0.0248214	3.05398
U3 small nucleolar RNA-associated protein 6 homolog	Q9NYH9	0.0480777	3.05117
Phosphoglucomutase-1	P36871	0.00327416	3.04322
Histone-arginine methyltransferase CARM1	Q86X55	0.00771575	3.01949
Protein PBDC1	Q9BVG4	0.0313902	3.01902
WASH complex subunit 4	Q2M389	0.00301707	3.00423
Epimerase family protein SDR39U1	Q9NRG7	0.0149061	3.00193
60S acidic ribosomal protein P0	P05388	0.00118466	2.96438
MOB kinase activator 3A	Q96BX8	0.0055357	2.95393
TBC1 domain family member 15	Q8TC07	0.00390331	2.92236
Procollagen galactosyltransferase 1	Q8NBJ5	0.0162711	2.89423
ATP-dependent RNA helicase DDX3X	O00571	0.00446091	2.89379
Ubiquitin-associated and SH3 domain-containing protein B	Q8TF42	0.0153909	2.89024
Ras-related protein Rab-8B	Q92930	0.0291229	2.88669
Galectin-3	P17931	0.0071113	2.88315
Sorting nexin-29	Q8TEQ0	0.0121247	2.8655
Ufm1-specific protease 2	Q9NUQ7	0.0455952	2.85102
60S ribosomal protein L27a	P46776	0.028205	2.84796
ATP-dependent RNA helicase DDX3Y	O15523	0.0427885	2.83835
Rho GTPase-activating protein 24	Q8N264	0.0220466	2.82748
Mini-chromosome maintenance complex-binding protein	Q9BTE3	0.000800414	2.81536
RNA-binding protein 3	P98179	0.0173307	2.80027
Protein transport protein Sec24B	O95487	0.00659407	2.79812
Interferon regulatory factor 4	Q15306	0.0102352	2.79726
RNA-binding protein NOB1	Q9ULX3	0.00977215	2.79383

Repressor of yield of DENV protein	Q9NUL5	0.0243593	2.77843
RNA-binding protein 5	P52756	0.0224248	2.76143
Peflin	Q9UBV8	0.00786793	2.75761
Nuclear factor NF-kappa-B p105 subunit	P19838	2.16E-06	2.74832
Integrator complex subunit 6	Q9UL03	0.0165096	2.73863
Proteasome activator complex subunit 3	P61289	0.00418539	2.72228
Protein Dr1	Q01658	0.0170937	2.72228
Protein preY, mitochondrial	Q96I23	0.0198159	2.71727
Phosphatidate cytidylyltransferase, mitochondrial	Q96BW9	0.0308224	2.71477
Telomere-associated protein RIF1	Q5UIP0	0.0365176	2.70188
Neutrophil cytosol factor 2	P19878	0.00264348	2.6965
UDP-glucose 4-epimerase	Q14376	0.0463269	2.68658
Regulator of G-protein signaling 10	O43665	0.000722122	2.68246
Importin subunit alpha-1	P52292	0.00202849	2.67178
Heterogeneous nuclear ribonucleoproteins A2/B1	P22626	0.014714	2.67055
Target of Myb protein 1	O60784	0.034193	2.64931
Ribosomal RNA-processing protein 7 homolog A	Q9Y3A4	0.0173862	2.64566
mRNA-capping enzyme	O60942	0.0464419	2.62382
Monoacylglycerol lipase ABHD12	Q8N2K0	0.0367521	2.60976
Proto-oncogene c-Rel	Q04864	0.0232571	2.59458
RAS protein activator like-3	Q86YV0	0.0462434	2.59338
Poly [ADP-ribose] polymerase 9	Q8IXQ6	0.00106029	2.5898
28S ribosomal protein S16, mitochondrial	Q9Y3D3	0.0217867	2.58107
Eukaryotic translation initiation factor 4E	P06730	0.0365969	2.57316
COP9 signalosome complex subunit 5	Q92905	0.0183384	2.57079
Elongator complex protein 2	Q6IA86	0.011456	2.56882
Mitochondrial fission process protein 1	Q9UDX5	0.0443249	2.56724
NADH-cytochrome b5 reductase 2	Q6BCY4	0.00146079	2.55741
Unconventional myosin-Ic	O00159	0.00791558	2.54957

NADH dehydrogenase [ubiquinone] 1 beta subcomplex subunit 5, mitochondrial	O43674	0.00827452	2.52038
Serine/threonine-protein kinase 10	O94804	0.00365659	2.51497
Cytohesin-1	Q15438	0.0382285	2.5142
Interferon-induced GTP-binding protein Mx1	P20591	0.0161072	2.51382
Ferritin heavy chain	P02794	0.0211614	2.51073
Tumor protein D54	O43399	0.0477613	2.50496
2',5'-phosphodiesterase 12	Q6L8Q7	0.0190605	2.49766
ADP-ribosylation factor-like protein 2	P36404	0.000712222	2.48618
Nicotinamide phosphoribosyltransferase	P43490	0.0101366	2.4858
CD97 antigen	P48960	0.00037752	2.48085
Protein DJ-1	Q99497	0.0307982	2.47704
Ankyrin repeat and MYND domain-containing protein 2	Q8IV38	0.0144246	2.47514
T-cell surface glycoprotein CD5	P06127	0.00429851	2.4615
Splicing factor U2AF 35 kDa subunit	Q01081	0.0306915	2.45057
Eukaryotic translation initiation factor 4 gamma 1	Q04637	0.00589011	2.44906
THO complex subunit 3	Q96J01	0.0182285	2.44381
Phospholysine phosphohistidine inorganic pyrophosphate phosphatase	Q9H008	0.0159543	2.44118
von Willebrand factor A domain-containing protein 8	A3KMH1	0.017688	2.43781
Probable ATP-dependent RNA helicase DDX60	Q8IY21	0.0334052	2.43781
Electron transfer flavoprotein subunit alpha, mitochondrial	P13804	0.0100192	2.42959
Alanine--tRNA ligase, cytoplasmic	P49588	0.000279067	2.42066
Biliverdin reductase A	P53004	0.0474096	2.40991
Importin subunit alpha-5	P52294	0.0352416	2.40215
Gasdermin-D	P57764	0.0390553	2.37648
Pyridoxal kinase	O00764	0.00362713	2.36774
Asparagine--tRNA ligase, cytoplasmic	O43776	0.00620722	2.36701
39S ribosomal protein L16, mitochondrial	Q9NX20	0.00170604	2.36084
CD44 antigen	P16070	0.0258337	2.35613
Calcineurin subunit B type 1	P63098	0.0380566	2.34387

Tryptophan--tRNA ligase, cytoplasmic	P23381	0.00214031	2.34315
Nuclear factor NF-kappa-B p100 subunit	Q00653	0.0191842	2.33382
Solute carrier family 15 member 4	Q8N697	0.0281797	2.33238
Ribosome biogenesis protein BOP1	Q14137	0.00069963	2.33203
Fragile X mental retardation syndrome-related protein 1	P51114	0.0332517	2.32238
Tricarboxylate transport protein, mitochondrial	P53007	0.0213412	2.31846
2'-5'-oligoadenylate synthase 1	P00973	0.0340321	2.31597
DNA-directed RNA polymerase II subunit RPB7	P62487	0.0281001	2.3142
40S ribosomal protein S25	P62851	0.0141602	2.31171
Carnitine O-palmitoyltransferase 2, mitochondrial	P23786	0.00182727	2.30958
Acidic leucine-rich nuclear phosphoprotein 32 family member B	Q92688	0.0178166	2.30569
Tubulin-specific chaperone D	Q9BTW9	9.65E-05	2.30427
60S ribosomal protein L7a	P62424	0.00624446	2.30215
Fatty acid synthase	P49327	0.00369533	2.30109
Basic leucine zipper and W2 domain-containing protein 2	Q9Y6E2	0.0320287	2.29968
Adaptin ear-binding coat-associated protein 2	Q9NVZ3	0.0262408	2.2751
Lactation elevated protein 1	Q8WV93	0.0272305	2.27405
Dedicator of cytokinesis protein 2	Q92608	0.00626283	2.26917
Eukaryotic translation initiation factor 4B	P23588	0.0371005	2.26882
Anaphase-promoting complex subunit 7	Q9UJX3	0.0431568	2.26604
ATP-dependent RNA helicase DDX39A	O00148	0.0335678	2.26499
Trifunctional purine biosynthetic protein adenosine-3	P22102	0.0165164	2.2643
Proteasome activator complex subunit 1	Q06323	0.0142096	2.26325
Protein FAM160B1	Q5W0V3	0.04093	2.26325
26S proteasome non-ATPase regulatory subunit 8	P48556	0.0168302	2.26256
Beta-2-microglobulin	P61769	0.0477731	2.2577
Wiskott-Aldrich syndrome protein family member 2	Q9Y6W5	0.00128296	2.25251
Anamorsin	Q6FI81	0.0133017	2.25182
Bifunctional purine biosynthesis protein PURH	P31939	0.000317104	2.2494

Eukaryotic peptide chain release factor GTP-binding subunit ERF3A	P15170	0.00220808	2.2494
Heat shock protein 105 kDa	Q92598	0.00343374	2.24182
Mitochondrial import inner membrane translocase subunit Tim23	O14925	0.0241978	2.24078
FYVE, RhoGEF and PH domain-containing protein 2	Q7Z6J4	0.0280965	2.23872
mRNA turnover protein 4 homolog	Q9UKD2	0.00795814	2.23563
Ran GTPase-activating protein 1	P46060	0.000646979	2.22468
60S ribosomal protein L13a	P40429	0.0312392	2.22468
Heterogeneous nuclear ribonucleoprotein L-like	Q8WVV9	0.0292327	2.22399
2',3'-cyclic-nucleotide 3'-phosphodiesterase	P09543	0.0028444	2.22058
Septin-7	Q16181	0.00261056	2.21752
ATP-dependent RNA helicase SUPV3L1, mitochondrial	Q8IYB8	0.0113837	2.20326
HLA class II histocompatibility antigen, DP alpha 1 chain	P20036	0.0272825	2.20056
Glucose-6-phosphate 1-dehydrogenase	P11413	0.0033012	2.19853
Tyrosine-protein kinase Lyn	P07948	0.00349719	2.19786
Sequestosome-1	Q13501	0.0123562	2.19516
Polypeptide N-acetylgalactosaminyltransferase 2	Q10471	0.0360772	2.19213
Elongation factor 1-alpha 1	P68104	0.0314047	2.18911
Cytochrome b5 type B	O43169	0.0109012	2.18776
Adenosine deaminase	P00813	0.0452616	2.18608
14-3-3 protein epsilon	P62258	0.0132332	2.16504
Nuclear pore complex protein Nup50	Q9UKX7	0.0138637	2.16504
B-cell receptor-associated protein 31	P51572	0.0222612	2.16405
Major vault protein	Q14764	0.00215666	2.1594
Astrocytic phosphoprotein PEA-15	Q15121	0.00144226	2.15443
Multifunctional protein ADE2	P22234	0.0138977	2.15146
Chloride intracellular channel protein 4	Q9Y696	0.00887074	2.1475
NADH dehydrogenase [ubiquinone] 1 subunit C2	O95298	0.00570676	2.14684
Peptidyl-prolyl cis-trans isomerase FKBP5	Q13451	0.0151974	2.14223
Rho GTPase-activating protein 4	P98171	0.0217678	2.13862

Exocyst complex component 5	O00471	0.0102886	2.13567
Calcium-binding mitochondrial carrier protein Aralar1	O75746	0.000786399	2.1337
Elongation factor 1-gamma	P26641	0.000134342	2.13075
RNA demethylase ALKBH5	Q6P6C2	0.0497164	2.12292
Probable tRNA N6-adenosine threonylcarbamoyltransferase	Q9NPF4	0.00939343	2.11836
Tubulin beta chain	P07437	0.0236466	2.10766
Peptidyl-prolyl cis-trans isomerase CWC27 homolog	Q6UX04	0.0149023	2.10539
Glutaredoxin-3	O76003	0.0158272	2.10249
Methionine--tRNA ligase, cytoplasmic	P56192	0.00822424	2.09894
Dehydrogenase/reductase SDR family member 4	Q9BTZ2	0.016434	2.09443
Low affinity immunoglobulin gamma Fc region receptor II-b	P31994	0.0212317	2.09443
[Protein ADP-ribosylarginine] hydrolase	P54922	0.0158958	2.09283
Mitochondrial import inner membrane translocase subunit TIM50	Q3ZCQ8	0.00221948	2.0909
Maleylacetoacetate isomerase	O43708	0.0446711	2.09058
Thymidine phosphorylase	P19971	0.00198262	2.08673
Myelin expression factor 2	Q9P2K5	0.00295331	2.08577
Nardilysin	O43847	0.0394559	2.08577
Beta-adrenergic receptor kinase 1	P25098	0.0153114	2.08065
Aspartate aminotransferase, cytoplasmic	P17174	0.00983462	2.08002
Heterogeneous nuclear ribonucleoprotein A0	Q13151	0.00343533	2.07714
Transcription factor BTF3 homolog 4	Q96K17	0.014218	2.07173
Core-binding factor subunit beta	Q13951	0.0174339	2.07109
Lysine-specific demethylase 6A	O15550	0.0327617	2.07078
40S ribosomal protein S19	P39019	0.0259886	2.0676
Telomerase Cajal body protein 1	Q9BUR4	0.0496106	2.06601
Chromatin complexes subunit BAP18	Q8IXM2	0.0147403	2.06475
Peptidyl-prolyl cis-trans isomerase D	Q08752	0.0166786	2.05715
5'-AMP-activated protein kinase catalytic subunit alpha-1	Q13131	0.0287486	2.05715
Vacuolar protein sorting-associated protein 18 homolog	Q9P253	0.0125296	2.05368

Tyrosine-protein kinase JAK1	P23458	0.0451761	2.04676
Platelet-activating factor acetylhydrolase IB subunit beta	P68402	0.00920454	2.03986
Proteasomal ubiquitin receptor ADRM1	Q16186	0.0412679	2.03955
Hepatoma-derived growth factor-related protein 2	Q7Z4V5	0.0251773	2.03767
Suppressor of SWI4 1 homolog	Q9NQ55	0.0355644	2.03236
DNA-directed RNA polymerase III subunit RPC1	O14802	0.0280364	2.02862
39S ribosomal protein L19, mitochondrial	P49406	0.0323636	2.02147
Nuclear pore complex protein Nup133	Q8WUM0	0.00236503	2.02054
FACT complex subunit SSRP1	Q08945	0.00893353	2.01837
F-box only protein 7	Q9Y3I1	0.00723759	2.00909
Pre-mRNA-processing factor 17	O60508	0.0098051	2.00909
E3 SUMO-protein ligase RanBP2	P49792	0.00746106	1.99741
Alpha-ketoglutarate-dependent dioxygenase FTO	Q9C0B1	0.00206533	1.99557
Activating signal cointegrator 1 complex subunit 3	Q8N3C0	0.0113618	1.9922
2'-deoxynucleoside 5'-phosphate N-hydrolase 1	O43598	0.0224039	1.99128
Lysophospholipase-like protein 1	Q5VWZ2	0.00424669	1.99006
Conserved oligomeric Golgi complex subunit 8	Q96MW5	0.00898122	1.98945
Protein MEMO1	Q9Y316	0.0195282	1.98854
Thymidylate kinase	P23919	0.0175527	1.98001
Adenine phosphoribosyltransferase	P07741	0.0105071	1.97818
Heterogeneous nuclear ribonucleoprotein A3	P51991	0.0341586	1.97515
Tubulin beta-1 chain	Q9H4B7	0.0276088	1.9697
Cell division cycle protein 123 homolog	O75794	0.00180055	1.96698
Galectin-1	P09382	0.0462744	1.96607
Polyadenylate-binding protein 1	P11940	0.00172285	1.96065
Proteasome assembly chaperone 1	O95456	0.00314153	1.96065
BRISC complex subunit Abro1	Q15018	0.0120702	1.96005
Peptidyl-prolyl cis-trans isomerase FKBP4	Q02790	0.00505917	1.95854
E3 SUMO-protein ligase ZNF451	Q9Y4E5	0.0194907	1.95434

Coiled-coil domain-containing protein 50	Q8IVM0	0.0197118	1.95374
Metastasis suppressor protein 1	O43312	0.0205979	1.95044
Sorting nexin-11	Q9Y5W9	0.00795026	1.94865
L-lactate dehydrogenase B chain	P07195	0.00855459	1.94835
Serpin B6	P35237	0.0336292	1.94655
THO complex subunit 4	Q86V81	0.0148275	1.94059
Threonine--tRNA ligase, cytoplasmic	P26639	0.0240553	1.93761
Integrator complex subunit 2	Q9H0H0	0.000811417	1.93672
Ubiquitin-like modifier-activating enzyme 1	P22314	0.00685712	1.93523
Pleckstrin	P08567	0.0341085	1.93434
Putative RNA-binding protein 15B	Q8NDT2	0.0019431	1.93315
Mitofusin-1	Q8IWA4	0.0324807	1.93138
Rab GDP dissociation inhibitor alpha	P31150	0.0108754	1.92989
39S ribosomal protein L45, mitochondrial	Q9BRJ2	0.0300575	1.92634
Beta-centractin	P42025	0.0168534	1.92398
ATPase family AAA domain-containing protein 3B	Q5T9A4	0.0456528	1.92339
Rab GDP dissociation inhibitor beta	P50395	0.0006762	1.92309
Heat shock protein HSP 90-beta	P08238	0.0070492	1.91543
Protein kinase C beta type	P05771	0.0368698	1.91396
Eukaryotic translation initiation factor 3 subunit H	O15372	0.000777776	1.91191
Transcription factor BTF3	P20290	0.0104558	1.91103
Schlafen family member 5	Q08AF3	0.00717867	1.91073
Ubiquitin-like modifier-activating enzyme 5	Q9GZZ9	0.0427907	1.91015
Cleft lip and palate transmembrane protein 1-like protein	Q96KA5	0.047828	1.91015
Tyrosine-protein phosphatase non-receptor type 23	Q9H3S7	0.0415599	1.90956
Proteasome subunit beta type-3	P49720	0.00494703	1.90927
Pre-mRNA-splicing factor ATP-dependent RNA helicase PRP16	Q92620	0.0152423	1.90108
Alpha-mannosidase 2C1	Q9NTJ4	0.02874	1.89904
Protein MAK16 homolog	Q9BXY0	0.0132827	1.89496

Integrin-linked protein kinase	Q13418	0.000957061	1.89467
Protein phosphatase 1B	O75688	0.0252751	1.8906
Phosphoglucomutase-2	Q96G03	0.0125834	1.88886
Ras-related protein Rab-21	Q9UL25	0.0478096	1.88365
CDGSH iron-sulfur domain-containing protein 2	Q8N5K1	0.0176341	1.88105
Rab3 GTPase-activating protein non-catalytic subunit	Q9H2M9	0.0367308	1.87932
SNW domain-containing protein 1	Q13573	0.025919	1.87874
Profilin-1	P07737	0.0122101	1.87528
Acylamino-acid-releasing enzyme	P13798	0.0199854	1.87241
RNA-binding protein 39	Q14498	0.045919	1.8704
E3 ubiquitin-protein ligase Itchy homolog	Q96J02	0.0292376	1.86839
Coatomer subunit epsilon	O14579	0.00770775	1.8681
SUMO-activating enzyme subunit 1	Q9UBE0	0.00544303	1.86781
Proteasome-associated protein ECM29 homolog	Q5VYK3	0.00985895	1.86638
Formin-binding protein 1	Q96RU3	0.00503173	1.86123
Protein TASOR	Q9UK61	0.0227575	1.85866
N-acetyl-D-glucosamine kinase	Q9UJ70	0.0468806	1.85467
N-alpha-acetyltransferase 15, NatA auxiliary subunit	Q9BXJ9	0.0180138	1.85353
Formin-like protein 1	O95466	0.0109605	1.84927
60S ribosomal protein L7	P18124	0.0184711	1.84927
Eukaryotic translation initiation factor 3 subunit D	O15371	0.0234629	1.84927
Serine/threonine-protein phosphatase 6 catalytic subunit	O00743	0.0245194	1.84842
Elongation factor Tu, mitochondrial	P49411	0.0163921	1.84728
Sorting nexin-8	Q9Y5X2	0.0119933	1.84473
TBC1 domain family member 1	Q86TI0	0.0328476	1.8436
Heterogeneous nuclear ribonucleoprotein A1	P09651	0.0318222	1.83964
Vacuolar protein sorting-associated protein 29	Q9UBQ0	0.0283354	1.83597
Elongator complex protein 1	O95163	0.0126985	1.82642
Hydroxymethylglutaryl-CoA lyase, mitochondrial	P35914	0.0212215	1.82642

Ras-related protein Rab-43	Q86YS6	0.00915302	1.81858
Ras-related protein Rab-7a	P51149	0.0125488	1.81496
Cysteine--tRNA ligase, cytoplasmic	P49589	0.0424746	1.81273
DnaJ homolog subfamily A member 1	P31689	0.000795578	1.81162
Echinoderm microtubule-associated protein-like 4	Q9HC35	0.0343062	1.81106
Tripeptidyl-peptidase 1	O14773	0.0203784	1.81051
Density-regulated protein	O43583	0.0432634	1.80662
E3 ubiquitin-protein ligase UHRF2	Q96PU4	0.0376525	1.80302
Signal transducer and activator of transcription 6	P42226	0.0431805	1.80274
Ras suppressor protein 1	Q15404	0.0123313	1.80246
Eukaryotic translation initiation factor 2 subunit 2	P20042	0.00310808	1.80136
Eukaryotic translation initiation factor 3 subunit E	P60228	0.00324461	1.79694
Glutaminase kidney isoform, mitochondrial	O94925	0.0115175	1.79418
Macrophage-capping protein	P40121	0.0362662	1.79006
Glycine--tRNA ligase	P41250	0.0387423	1.78402
Charged multivesicular body protein 7	Q8WUX9	0.000547605	1.78101
TAR DNA-binding protein 43	Q13148	0.0322718	1.78101
Glia maturation factor gamma	O60234	0.0186017	1.77855
Vacuolar protein sorting-associated protein 4A	Q9UN37	0.0370589	1.77746
Microtubule-associated protein RP/EB family member 1	Q15691	0.0263022	1.77637
BAG family molecular chaperone regulator 5	Q9UL15	0.0159067	1.77364
Heterogeneous nuclear ribonucleoprotein Q	O60506	0.0112182	1.77256
Elongin-A	Q14241	0.0421967	1.77201
Ena/VASP-like protein	Q9UI08	0.00879917	1.77147
Protein-glutamate O-methyltransferase	Q9H993	0.0282543	1.77147
Mitogen-activated protein kinase kinase kinase kinase 1	Q92918	0.0359439	1.76577
WASH complex subunit 2A	Q641Q2	0.0434773	1.7636
Basic leucine zipper and W2 domain-containing protein 1	Q7L1Q6	0.0222605	1.76035
Protein MIS12 homolog	Q9H081	0.045057	1.76008

Hypoxanthine-guanine phosphoribosyltransferase	P00492	0.0441949	1.75954
Atlastin-3	Q6DD88	0.0370933	1.75873
eIF-2-alpha kinase activator GCN1	Q92616	0.00140335	1.75846
Epidermal growth factor receptor substrate 15	P42566	0.0201482	1.75388
Sorting nexin-9	Q9Y5X1	0.0390693	1.75119
Trifunctional enzyme subunit alpha, mitochondrial	P40939	0.0048547	1.73807
Methylcrotonoyl-CoA carboxylase beta chain, mitochondrial	Q9HCC0	0.00110568	1.7354
Proteasome activator complex subunit 2	Q9UL46	0.0289715	1.72849
Thioredoxin domain-containing protein 17	Q9BRA2	0.0499216	1.7269
HEAT repeat-containing protein 5B	Q9P2D3	0.0274267	1.72372
Sorting nexin-5	Q9Y5X3	0.0356887	1.72134
Nucleosome assembly protein 1-like 4	Q99733	0.0465261	1.72081
CTP synthase 2	Q9NRF8	0.0439451	1.71817
Dipeptidyl peptidase 3	Q9NY33	0.00752285	1.71238
Dedicator of cytokinesis protein 11	Q5JSL3	0.0353968	1.7087
Actin-related protein 2/3 complex subunit 5-like protein	Q9BPX5	0.0329746	1.70818
Non-structural maintenance of chromosomes element 3 homolog	Q96MG7	0.0192634	1.70634
Protein FAM49B	Q9NUQ9	0.0268192	1.70608
Cohesin subunit SA-1	Q8WVM7	0.0124597	1.70504
Heterogeneous nuclear ribonucleoprotein F	P52597	0.0358193	1.70347
Bromodomain adjacent to zinc finger domain protein 1A	Q9NRL2	0.0338605	1.70059
Selenide, water dikinase 1	P49903	0.0291028	1.70007
Serine--tRNA ligase, cytoplasmic	P49591	0.0148983	1.69877
Serpin B9	P50453	0.00267377	1.6972
Lymphocyte antigen 75	O60449	0.00667511	1.69668
Proteasome subunit beta type-2	P49721	0.0082958	1.69564
Carbonyl reductase [NADPH] 1	P16152	0.015069	1.69122
Triokinase/FMN cyclase	Q3LXA3	0.0254454	1.68888
COP9 signalosome complex subunit 1	Q13098	0.0492772	1.68863

Puromycin-sensitive aminopeptidase	P55786	0.0166645	1.68526
Brefeldin A-inhibited guanine nucleotide-exchange protein 2	Q9Y6D5	0.0215852	1.685
Phosducin-like protein 3	Q9H2J4	0.0305924	1.685
Palmitoyl-protein thioesterase 1	P50897	0.0175423	1.67984
Vesicle-associated membrane protein 7	P51809	0.00667651	1.6788
Leupaxin	O60711	0.0230223	1.67597
Alpha-enolase	P06733	0.0166598	1.6752
5'-nucleotidase domain-containing protein 3	Q86UY8	0.0336886	1.67186
L-lactate dehydrogenase A chain	P00338	0.0333437	1.6693
BSD domain-containing protein 1	Q9NW68	0.0285431	1.66392
Inositol monophosphatase 1	P29218	0.0124463	1.66341
MIF4G domain-containing protein	A9UHW6	0.0165722	1.66316
Protein diaphanous homolog 1	O60610	0.00653377	1.66188
Apoptosis inhibitor 5	Q9BZZ5	0.0339207	1.65755
Gamma-enolase	P09104	0.0138555	1.65679
26S protease regulatory subunit 6A	P17980	0.0041091	1.65628
U4/U6 small nuclear ribonucleoprotein Prp4	O43172	0.00340333	1.65501
Vesicle-trafficking protein SEC22b	O75396	0.0485943	1.65196
6-phosphogluconolactonase	O95336	0.0488833	1.64715
Isocitrate dehydrogenase [NADP] cytoplasmic	O75874	0.0402149	1.64462
Pyruvate kinase PKM	P14618	0.0135798	1.64286
Enoyl-CoA delta isomerase 2, mitochondrial	O75521	0.0169667	1.64059
Nucleosome assembly protein 1-like 1	P55209	0.00911904	1.63858
Staphylococcal nuclease domain-containing protein 1	Q7KZF4	0.0171574	1.63807
Programmed cell death protein 4	Q53EL6	0.00213305	1.63631
Aminopeptidase B	Q9H4A4	0.0245548	1.63531
GEM-interacting protein	Q9P107	0.0389433	1.63506
Ral GTPase-activating protein subunit beta	Q86X10	0.0358136	1.63406
8-oxo-dGDP phosphatase NUDT18	Q6ZVK8	0.0207259	1.6318

Serine/threonine-protein kinase 4	Q13043	0.0356113	1.63155
Septin-1	Q8WYJ6	0.0479714	1.6308
Inorganic pyrophosphatase	Q15181	0.00983852	1.63055
Heat shock protein HSP 90-alpha	P07900	0.0213684	1.63055
Transcription elongation factor SPT5	O00267	0.00711501	1.62805
Hsc70-interacting protein	P50502	0.0155641	1.6243
Phosphofurin acidic cluster sorting protein 1	Q6VY07	0.0310635	1.62306
Intron-binding protein aquarius	O60306	0.0277945	1.62281
RAC-alpha serine/threonine-protein kinase	P31749	0.0344816	1.62231
Transgelin-2	P37802	0.00258991	1.62131
Amino-terminal enhancer of split	Q08117	0.0458774	1.61907
Eukaryotic translation initiation factor 5B	O60841	0.0276076	1.61659
Ubiquitin-conjugating enzyme E2 variant 1	Q13404	0.0403794	1.61535
Heat shock 70 kDa protein 4	P34932	0.0342404	1.60966
40S ribosomal protein SA	P08865	0.0125821	1.60892
Dual specificity mitogen-activated protein kinase kinase 4	P45985	0.0381785	1.60645
Translin	Q15631	0.0228205	1.60472
Leucine--tRNA ligase, cytoplasmic	Q9P2J5	0.0463193	1.59612
Trafficking protein particle complex subunit 4	Q9Y296	0.00643442	1.5949
U3 small nucleolar RNA-associated protein 18 homolog	Q9Y5J1	0.0196483	1.59465
Polyadenylate-binding protein 2	Q86U42	0.0345797	1.59417
Helicase SKI2W	Q15477	0.012688	1.59294
Valine--tRNA ligase	P26640	0.0119959	1.58757
Purine nucleoside phosphorylase	P00491	0.017869	1.58125
Alpha-actinin-4	O43707	0.00179521	1.57834
N-alpha-acetyltransferase 50	Q9GZZ1	0.0298238	1.57398
Enhancer of mRNA-decapping protein 4	Q6P2E9	0.010955	1.56723
Receptor of activated protein C kinase 1	P63244	0.0102207	1.56699
Eukaryotic translation initiation factor 5	P55010	0.0341293	1.56579

26S proteasome non-ATPase regulatory subunit 5	Q16401	0.024703	1.56387
Aspartate--tRNA ligase, cytoplasmic	P14868	0.0368339	1.56123
26S protease regulatory subunit 8	P62195	0.0352535	1.55501
Rho GTPase-activating protein 17	Q68EM7	0.00433029	1.55406
U6 snRNA-associated Sm-like protein LSm1	O15116	0.0203529	1.55024
Probable ATP-dependent RNA helicase DDX6	P26196	0.0167281	1.55001
S-adenosylmethionine synthase isoform type-2	P31153	0.0278382	1.53721
Cytochrome c oxidase assembly protein COX15 homolog	Q7KZN9	0.0475679	1.53532
GMP synthase [glutamine-hydrolyzing]	P49915	0.0179324	1.53203
Non-POU domain-containing octamer-binding protein	Q15233	0.028354	1.52031
Protein ABHD16A	O95870	0.0401581	1.52031
Protein NipSnap homolog 2	O75323	0.0355826	1.51891
Transitional endoplasmic reticulum ATPase	P55072	0.0064814	1.50962
Gamma-parvin	Q9HBI0	0.0365916	1.50823
Serine/threonine-protein kinase Nek9	Q8TD19	0.0446036	1.508
Poly(A) polymerase alpha	P51003	0.0215819	1.50776
14-3-3 protein gamma	P61981	0.0371538	1.50753
Signal transducer and activator of transcription 1-alpha/beta	P42224	0.0338373	1.50638
Forkhead box protein P1	Q9H334	0.0149217	1.49142
WW domain-binding protein 11	Q9Y2W2	0.0195123	1.48982
Angio-associated migratory cell protein	Q13685	0.0299831	1.48343
Rho guanine nucleotide exchange factor 6	Q15052	0.0464864	1.48161
Signal transducer and activator of transcription 3	P40763	0.0410562	1.46667
Glycogen phosphorylase, brain form	P11216	0.0346353	1.45479
Tyrosine--tRNA ligase, cytoplasmic	P54577	0.0485097	1.45457
Mediator of RNA polymerase II transcription subunit 19	A0JLT2	0.0444333	1.45367
Tyrosine-protein phosphatase non-receptor type 6	P29350	0.0457777	1.44566
Ribonucleoprotein PTB-binding 1	Q8IY67	0.0311609	1.44455
Probable ATP-dependent RNA helicase DDX46	Q7L014	0.0333495	1.43263

Syntaxin-7	O15400	0.0226319	1.42867
Nuclear pore complex protein Nup155	O75694	0.0431222	1.41297
Nuclear migration protein nudC	Q9Y266	0.024221	1.4108
T-complex protein 1 subunit zeta	P40227	0.0457964	1.38123
RNA 3'-terminal phosphate cyclase	O00442	0.00804896	1.38102
Tropomodulin-3	Q9NYL9	0.0207673	1.37446
Regulator of nonsense transcripts 1	Q92900	0.0183592	1.37046
28S ribosomal protein S31, mitochondrial	Q92665	0.0498167	1.3692
Protein transport protein Sec31A	O94979	0.0246082	1.35477
Cell division cycle protein 16 homolog	Q13042	0.0319791	1.3471
Importin subunit beta-1	Q14974	0.0123401	1.34359
Alcohol dehydrogenase [NADP(+)]	P14550	0.0467433	1.30898
T-complex protein 1 subunit beta	P78371	0.0395673	1.29837
Signal recognition particle subunit SRP72	O76094	0.0366254	1.23804
60S ribosomal protein L12	P30050	0.0451538	1.22838
ATP synthase subunit beta, mitochondrial	P06576	0.00819788	-1.02266
NIF3-like protein 1	Q9GZT8	0.0238727	-1.32069
Transcription factor ETV6	P41212	0.0363868	-1.37067
NFATC2-interacting protein	Q8NCF5	0.00820104	-1.38038
U3 small nucleolar ribonucleoprotein protein MPP10	O00566	0.019745	-1.38463
Protein PAT1 homolog 1	Q86TB9	0.0176136	-1.45904
Early endosome antigen 1	Q15075	0.0416146	-1.45971
Histidine triad nucleotide-binding protein 2, mitochondrial	Q9BX68	0.0174388	-1.46442
Nuclear autoantigenic sperm protein	P49321	0.0409821	-1.46893
E3 ubiquitin-protein ligase BRE1A	Q5VTR2	0.0345769	-1.48206
Treacle protein	Q13428	0.0200764	-1.49211
Microtubule-associated proteins 1A/1B light chain 3B	Q9GZQ8	0.0259131	-1.49257
Putative RNA-binding protein Luc7-like 2	Q9Y383	0.0251501	-1.49394
Chromodomain-helicase-DNA-binding protein 2	O14647	0.0181627	-1.49738

General transcription factor 3C polypeptide 4	Q9UKN8	0.0181051	-1.51985
DNA-directed DNA/RNA polymerase mu	Q9NP87	0.0313207	-1.54739
Putative ATP-dependent RNA helicase DHX57	Q6P158	0.0346027	-1.55907
Endoplasmic reticulum-Golgi intermediate compartment protein 1	Q969X5	0.0345031	-1.57471
NADH dehydrogenase [ubiquinone] 1 alpha subcomplex subunit 5	Q16718	0.0200973	-1.5998
Protein RUBCNL-like	Q9H714	0.0427755	-1.61585
Thioredoxin domain-containing protein 5	Q8NBS9	0.0280112	-1.62306
TRAF family member-associated NF-kappa-B activator	Q92844	0.0497264	-1.62955
NFU1 iron-sulfur cluster scaffold homolog, mitochondrial	Q9UMS0	0.0128814	-1.64462
Ras-related protein R-Ras2	P62070	0.0265708	-1.64665
MICOS complex subunit MIC27	Q6UXV4	0.0213123	-1.67186
PHD finger protein 10	Q8WUB8	0.047776	-1.67803
Mitochondrial import inner membrane translocase subunit Tim29	Q9BSF4	0.023455	-1.68061
Non-receptor tyrosine-protein kinase TYK2	P29597	0.0253325	-1.68138
Sec1 family domain-containing protein 2	Q8WU76	0.0143412	-1.70033
Proline-, glutamic acid- and leucine-rich protein 1	Q8IZL8	0.0412083	-1.70085
Hemoglobin subunit beta	P68871	0.0155362	-1.70713
Stromal interaction molecule 1	Q13586	0.0295351	-1.71501
MICOS complex subunit MIC60	Q16891	0.006552	-1.72743
Microsomal glutathione S-transferase 2	Q99735	0.028978	-1.73061
HAUS augmin-like complex subunit 5	O94927	0.0414767	-1.7346
KH domain-containing, RNA-binding, signal transduction-associated protein 1	Q07666	0.0322671	-1.77883
Striatin-3	Q13033	0.0136901	-1.78457
Mitochondrial import inner membrane translocase subunit Tim10	P62072	0.047086	-1.79171
Dolichyl-diphosphooligosaccharide--protein glycosyltransferase subunit DAD1	P61803	0.0276378	-1.81914
General transcription factor IIE subunit 1	P29083	0.00365695	-1.84049
Diphosphoinositol polyphosphate phosphohydrolase 1	O95989	0.0263519	-1.8578
RNA-binding protein 33	Q96EV2	0.00835339	-1.87384
Factor VIII intron 22 protein	P23610	0.0372488	-1.87384

Epididymis-specific alpha-mannosidase	Q9Y2E5	0.0481366	-1.8851
Histone-lysine N-methyltransferase EHMT1	Q9H9B1	0.0304833	-1.89205
Putative uncharacterized protein LOC100996504	I3L1I5	0.0305771	-1.90049
RNA binding motif protein, X-linked-like-1	Q96E39	0.0107249	-1.90341
GrpE protein homolog 1, mitochondrial	Q9HAV7	0.00968424	-1.91837
Translation factor GUF1, mitochondrial	Q8N442	0.00196922	-1.92103
F-actin-uncapping protein LRRC16A	Q5VZK9	0.0245803	-1.92309
Ras-related protein Rab-22A	Q9UL26	0.0221436	-1.96065
HMG box transcription factor BBX	Q8WY36	0.0197771	-1.96185
Ribosomal protein S6 kinase beta-1	P23443	0.0490742	-1.97545
PAX-interacting protein 1	Q6ZW49	0.0466401	-1.97727
Beta-soluble NSF attachment protein	Q9H115	0.0474986	-1.99434
Zinc finger protein 592	Q92610	0.0265116	-1.99465
Aminoacylase-1	Q03154	0.0167017	-1.99587
Probable leucine--tRNA ligase, mitochondrial	Q15031	0.0378347	-2.00386
Mitotic checkpoint protein BUB3	O43684	0.0272537	-2.02488
H/ACA ribonucleoprotein complex subunit 4	O60832	0.0377822	-2.05305
Coiled-coil domain-containing protein 47	Q96A33	0.040189	-2.05589
Cytochrome c oxidase subunit 5A, mitochondrial	P20674	0.0441697	-2.06633
BLOC-1-related complex subunit 7	Q96B45	0.0371582	-2.07874
RNA-binding protein Raly	Q9UKM9	0.00770624	-2.1096
DIS3-like exonuclease 2	Q8IYB7	0.044843	-2.1252
Syntaxin-8	Q9UNK0	0.0495931	-2.13468
Zinc fingers and homeoboxes protein 2	Q9Y6X8	0.0148283	-2.14289
Stromal cell-derived factor 2-like protein 1	Q9HCN8	0.0157369	-2.14454
Polycomb protein SUZ12	Q15022	0.028815	-2.15642
Selenoprotein T	P62341	0.00630183	-2.1757
Serine/threonine-protein phosphatase PP1-gamma catalytic subunit	P36873	0.0263746	-2.19483
PC4 and SFRS1-interacting protein	O75475	0.0402789	-2.20902

Hydroxyacyl-thioester dehydratase type 2, mitochondrial	P86397	0.0406166	-2.25286
Dual specificity tyrosine-phosphorylation-regulated kinase 1A	Q13627	0.00240256	-2.2737
Cyclin-L1	Q9UK58	0.0108579	-2.30074
Ribosome biogenesis regulatory protein homolog	Q15050	0.0498251	-2.30144
Negative elongation factor A	Q9H3P2	0.00129793	-2.30781
28S ribosomal protein S18b, mitochondrial	Q9Y676	0.0451601	-2.31882
Glutaredoxin-related protein 5, mitochondrial	Q86SX6	0.00292082	-2.32024
Ankyrin repeat domain-containing protein 12	Q6UB98	0.0201826	-2.38086
Ribonuclease K6	Q93091	0.0319991	-2.38525
E3 ubiquitin-protein ligase CBL-B	Q13191	0.00594154	-2.40917
Sideroflexin-3	Q9BWM7	0.0302124	-2.41324
Protein PRRC1	Q96M27	0.0219153	-2.43968
Biogenesis of lysosome-related organelles complex 1 subunit 4	Q9NUP1	0.0119026	-2.45622
Thrombospondin-1	P07996	0.0231613	-2.48161
HAUS augmin-like complex subunit 8	Q9BT25	0.00824208	-2.49153
Coiled-coil domain-containing protein 6	Q16204	0.0406977	-2.51884
Pyridoxine-5'-phosphate oxidase	Q9NVS9	0.0165005	-2.53357
Periodic tryptophan protein 1 homolog	Q13610	0.0248347	-2.65746
Fc receptor-like protein 3	Q96P31	0.0238681	-2.71769
Hermansky-Pudlak syndrome 3 protein	Q969F9	0.00999746	-2.72187
Guanosine-3',5'-bis(diphosphate) 3'-pyrophosphohydrolase MESH1	Q8N4P3	0.0255024	-2.77332
60S ribosomal protein L21	P46778	0.00397915	-2.81882
Sphingosine-1-phosphate phosphatase 1	Q9BX95	0.031117	-2.82705
Histone H1.5	P16401	0.0180346	-2.82835
Sphingomyelin phosphodiesterase 2	O60906	0.013748	-2.84228
Hemoglobin subunit alpha	P69905	0.00139377	-2.94171
NADH dehydrogenase [ubiquinone] 1 alpha subcomplex subunit 12	Q9UI09	0.0183695	-3.03762
PHD and RING finger domain-containing protein 1	Q9P1Y6	0.0051797	-3.05633
Dihydroorotate dehydrogenase (quinone), mitochondrial	Q02127	0.0346953	-3.09409

Serum albumin	P02768	0.0196412	-3.37961
Coagulation factor V	P12259	0.00551603	-3.77514
Serine/threonine-protein kinase 38-like	Q9Y2H1	0.0109114	-4.10204

Appendix 10. The DAVID functional annotation categories (with FDR<0.5) of the 2046 statistically significantly up-regulated genes induced by CD40 stimulation in primary CLL cells at 24h time point

Annotation Cluster 1	Enrichment Score: 15.267468610048383					
Category	**Term**	**Count**	**%**	**Genes**	**Benjamini**	**FDR**
GOTERM_CC_DIRECT	GO:0005913~cell-cell adherens junction	84	4.24	YWHAE, OXTR, TES, HSP90AB1, YWHAB, OLA1, PARK7, ENO1, BZW2, PVR, BAIAP2L1, ATIC, CAPZB, RUVBL1, BSG, EFHD2, FLOT1, FLOT2, TNKS1BP1, TMPO, EIF2A, CAST, LYPLA2, NUDC, DBNL, ANXA2, SWAP70, TMOD3, RANGAP1, SND1, PLCB3, PKM, CTTN, FSCN1, MYH9, CHMP4B, PLIN3, TAGLN2, MAPRE1, RPL29, PFN1, MACF1, SRC, CAPG, ASAP1, UBFD1, CNN3, LDHA, KLC2, LARP1, PUF60, COBLL1, PRDX1, FLNA, FLNB, SNX9, RPS2, TIGIT, PDLIM5, EPS15, PAK4, VASP, PTPN1, HSPA8, HSPA5, STAT1, RPL23A, CGN, PAICS, RAB10, EHD1, RSL1D1, EIF2S3, HNRNPK, EHD4, GIPC1, FASN, CAPZA1, SERBP1, UBAP2, RAN, CD200, EIF4G1, TJP2	0.00	0.00
GOTERM_BP_DIRECT	GO:0098609~cell-cell adhesion	76	3.83	YWHAE, TES, HSP90AB1, YWHAB, OLA1, PARK7, ENO1, BZW2, BAIAP2L1, ATIC, CAPZB, RUVBL1, BSG, EFHD2, TNKS1BP1, TMPO, EIF2A, CAST, LYPLA2, NUDC, DBNL, ANXA2, SWAP70, TMOD3, RANGAP1, SND1, PLCB3, PKM, CTTN, FSCN1, ELMO2, CHMP4B, PLIN3, TAGLN2, MAPRE1, RPL29, PFN1, MACF1, CAPG, ASAP1, UBFD1, CNN3, LDHA, KLC2, LARP1, PUF60, COBLL1, PRDX1, FLNB, SNX9, RPS2, PDLIM5, EPS15, PAK4, VASP, PTPN1, HSPA8, HSPA5, STAT1, RPL23A, CGN, PAICS, RAB10, EHD1, RSL1D1, EIF2S3, HNRNPK, EHD4, GIPC1, FASN, CAPZA1, SERBP1, UBAP2, RAN, EIF4G1, TJP2	0.00	0.00
GOTERM_MF_DIRECT	GO:0098641~cadherin binding involved in cell-cell adhesion	78	3.94	YWHAE, TES, HSP90AB1, YWHAB, OLA1, PARK7, ENO1, BZW2, BAIAP2L1, ATIC, CAPZB, RUVBL1, BSG, EFHD2, TNKS1BP1, TMPO, EIF2A, CAST, LYPLA2, NUDC, DBNL, ANXA2, SWAP70, TMOD3, RANGAP1, SND1, PLCB3, PKM, CTTN, FSCN1, MYH9, CHMP4B, PLIN3, TAGLN2, MAPRE1, RPL29, PFN1, MACF1, SRC, CAPG, ASAP1, UBFD1, CNN3, LDHA, KLC2, LARP1, PUF60, COBLL1, PRDX1, FLNA, FLNB, SNX9, RPS2, PDLIM5, EPS15, PAK4, VASP, PTPN1, HSPA8, HSPA5, STAT1, RPL23A, CGN, PAICS, RAB10, EHD1, RSL1D1, EIF2S3, HNRNPK, EHD4, GIPC1, FASN, CAPZA1, SERBP1, UBAP2, RAN, EIF4G1, TJP2	0.00	0.00
Annotation Cluster 2	**Enrichment Score: 8.30297335731003**					
Category	**Term**	**Count**	**%**	**Genes**	**Benjamini**	**FDR**
UP_KEYWORDS	Mitochondrion	178	8.98	TDRKH, MTCH2, CLPB, PARK7, YARS2, CISD3, TOMM22, LACTB, CHCHD3, MPC1, CHCHD6, FPGS, NARS2, SLC25A43, EARS2, MCCC2, ACSL1, TOMM34, ACSL4, LIG3, ATAD3A, PISD, LARS2, MTHFD2, PPIF, ACOT2, TFAM, VDAC1, TP53, GCDH, SHMT2, MRPL19, COX17, MRPL16, AK2, HTRA2, MRPL17, ARL2, MRPL14, PHB, MRPL12, HIGD1A, MRPL11, PRDX3, NLN, ATP5B, MAATS1, SNN, THEM5, THEM4, CYC1, MCL1, PCK2, COA4, HSPA9, COA3, PRELID1, PNPT1, APOOL, GOT2, MRPL27, MRPL28, PYCR1, ERAL1, KIAA0391, MRPL24, HIGD2A, BCL2, CYCS, ECHDC2, SFXN1, ECHDC3, NDUFAF1, SFXN2, ALDH18A1, GRSF1, BCL2L1, MRPS17, ACADVL, FEN1, GFM1, MRPS16, FASTKD2, MRPS14, MRPS11, MRPL39, MRPS10, ETFA, MRPL37, SQRDL, ATP5G2, ATP5G1, HK2, MRPL32, DHTKD1, C7ORF73, MRPL3, MRPL40, ALDH2, AIFM2, OPA3, C1QBP, UQCRFS1, C19ORF12, DNM1L, COA7, MRPS28, NSUN4, GPX4, MARS2, ACAD9, BCKDHB, MRPS23, TIMM23, DARS2, MRPL45, QTRT1, SLC25A15, TRAF3, NDUFS6, PTRH2, HCLS1, GARS, FXN, DLD, SLC25A11, SLC25A6, NDUFB9, FH, STOML2, TOMM40, ATP5EP2, MTFP1, SRC, GSTP1, MRPS33, ETFDH, MALSU1, NOL3, COX5A, HSD17B10, TBRG4, C19ORF70, PDF, MTHFD1L, ALDH1B1, BNIP1, C10ORF2, MFN2, ROMO1, IARS2, BID, SLC25A23, SLC25A25, GADD45GIP1, CYB5B, METAP1D, TIMMDC1, TRMT10C, FAHD1, CDKN2A,	0.00	0.00

				MDH2, MMAB, BNIP3, LRPPRC, WARS2, FDX1L, AGMAT, ALDH4A1, DNAJA1, SLC25A39, LYRM4, APEX1, TRMT5, CIAPIN1, ABCE1, TRMT61B, TOMM6		
UP_KEYWORDS	**Transit peptide**	93	4.69	MRPS17, ACADVL, GFM1, MRPS16, CLPB, FASTKD2, MRPS11, ETFA, MRPL37, SQRDL, ATP5G2, ATP5G1, YARS2, CISD3, MRPL32, DHTKD1, LACTB, MRPL40, ALDH2, C1QBP, FPGS, NARS2, UQCRFS1, EARS2, MRPS28, MCCC2, NSUN4, GPX4, MARS2, ACAD9, BCKDHB, DARS2, LIG3, MRPL45, PISD, LARS2, MTHFD2, NDUFS6, PTRH2, ACOT2, PPIF, TFAM, DLD, FXN, GCDH, FH, STOML2, SHMT2, MRPL19, MRPL16, ETFDH, MRPL17, HTRA2, MRPL14, MRPL12, COX5A, TBRG4, MRPL11, PRDX3, NLN, ATP5B, PDF, MTHFD1L, ALDH1B1, THEM4, C10ORF2, IARS2, CYC1, PCK2, HSPA9, PRELID1, METAP1D, PNPT1, TRMT10C, FAHD1, APOOL, MDH2, MMAB, GOT2, MRPL28, ERAL1, KIAA0391, MRPL24, LRPPRC, FDX1L, AGMAT, WARS2, ALDH4A1, ECHDC2, ECHDC3, NDUFAF1, GRSF1, TRMT61B	0.00	0.00
UP_SEQ_FEATURE	**transit peptide:Mitochondrion**	84	4.24	MRPS17, ACADVL, GFM1, MRPS16, MRPS11, ETFA, MRPL37, SQRDL, ATP5G2, ATP5G1, YARS2, CISD3, MRPL32, DHTKD1, LACTB, CHCHD3, MRPL40, ALDH2, C1QBP, FPGS, NARS2, NUDT19, UQCRFS1, EARS2, MRPS28, MCCC2, GPX4, MARS2, ACAD9, BCKDHB, DARS2, MRPL45, LARS2, MTHFD2, NDUFS6, PTRH2, ACOT2, PPIF, TFAM, DLD, FXN, GCDH, FH, SHMT2, MRPL19, MRPL16, ETFDH, MRPL17, HTRA2, MRPL14, MRPL12, COX5A, MRPL11, PRDX3, NLN, ATP5B, PDF, MTHFD1L, ALDH1B1, C10ORF2, IARS2, CYC1, DTD1, ISOC2, PCK2, HSPA9, PRELID1, METAP1D, PNPT1, TRMT10C, MDH2, MMAB, GOT2, MRPL28, KIAA0391, MRPL24, LRPPRC, FDX1L, AGMAT, WARS2, ALDH4A1, ECHDC2, ECHDC3, NDUFAF1	0.00	0.00
GOTERM_CC_DIRECT	**GO:0005759~mitochondrial matrix**	58	2.93	ACADVL, GFM1, ETFA, PARK7, YARS2, DHTKD1, ALDH2, C1QBP, FPGS, NARS2, EARS2, MCCC2, MARS2, BCKDHB, DARS2, LARS2, MTHFD2, ACOT2, PPIF, TFAM, GARS, DLD, FXN, TP53, GCDH, FH, SHMT2, ETFDH, ARL2, MALSU1, HSD17B10, PRDX3, ATP5B, MTHFD1L, ALDH1B1, THEM5, THEM4, C10ORF2, IARS2, MCL1, PCK2, GADD45GIP1, TRMT10C, MDH2, MMAB, GOT2, PYCR1, TDRD7, ERAL1, KIAA0391, FDX1L, WARS2, ALDH4A1, LYRM4, TRMT5, ABCE1, TRMT61B, BCL2L1	0.00	0.00
Annotation Cluster 3	**Enrichment Score: 5.321509662085839**					
Category	**Term**	**Count**	**%**	**Genes**	**Benjamini**	**FDR**
UP_KEYWORDS	**Ribonucleoprotein**	63	3.18	MRPS17, RPL4, MRPS16, MRPS14, RPLP1, MRPS11, RPLP0, MRPL39, MRPS10, HNRNPU, HNRNPR, MRPL37, RPL10A, SRP14, MRPL32, EFTUD2, MRPL3, SYNCRIP, MRPL40, RPL36AL, SNRPD1, SNRPD3, MRPS28, RPS6KL1, RPS6, MRPS23, RPSA, MRPL45, SRP9, RBMXL1, RPL7L1, NHP2, RPL29, RPL10, MRPS33, MVP, MRPL19, HEATR1, MRPL16, MRPL17, MRPL14, MRPL12, ZFP36L1, MRPL11, PUF60, SRP72, RPS6KC1, GAR1, RPL13, RPS2, RPS27A, HNRNPA1, MRPL27, MRPL28, RPL23A, MRPL24, HNRNPM, CPEB1, LSM6, HNRNPK, HNRNPF, HNRNPC, NOP10	0.00	0.00
GOTERM_BP_DIRECT	**GO:0006412~translation**	55	2.77	MRPS17, RPL4, HBS1L, MRPS16, MRPS14, RPLP1, MRPS11, RPLP0, MRPL37, RPL10A, YARS2, MRPL32, EFTUD2, MRPL3, RPL36AL, SLC25A43, WARS, RPS6, MRPS23, RPSA, SLC25A15, NHP2, RPL29, SLC25A11, SLC25A6, RPL10, MRPS33, MRPL19, MRPL16, MRPL17, TARS, MRPL14, MRPL11, PDF, RPL13, IGF2BP3, RPS2, RPS27A, SLC25A23, SLC25A25, ABCF1, EEFSEC, DARS, MRPL27, MRPL28, RPL23A, GTF2H3, MRPL24, RSL1D1, CPEB1, SLC25A39, TNIP1, RSL24D1, EIF4G1, FARSB	0.00	0.00
GOTERM_CC_DIRECT	**GO:0005840~ribosome**	39	1.97	RPL4, MRPS17, MRPS16, RPL10, MRPS14, MRPS33, MRPS11, RPLP1, MRPL19, RPLP0, MRPL16, MRPL17, MRPS10, MRPL14, MRPL37, RPL10A, TMA16, MRPL32, MRPL11, MRPL3, RPS6KC1, RPL13, RPS2, RPS27A, ABCF1, MRPS28, RPS6KL1, MRPS23, RPS6, MRPL27, RPL23A, MRPL45, MRPL24, EIF2S1, APEX1, RPL7L1, CANX, RPL29, RSL24D1	0.00	0.00

UP_KEYWORDS	**Ribosomal protein**	39	1.97	RPL4, MRPS17, MRPS16, RPL10, MRPS14, MRPS33, MRPS11, RPLP1, MRPL19, RPLP0, MRPL16, MRPL17, MRPL39, MRPS10, MRPL14, MRPL37, RPL10A, MRPL12, MRPL32, MRPL11, MRPL3, MRPL40, RPL36AL, RPS6KC1, RPL13, RPS2, RPS27A, MRPS28, RPS6KL1, MRPS23, RPS6, MRPL27, MRPL28, RPL23A, RPSA, MRPL45, MRPL24, RPL7L1, RPL29	0.00	0.00
GOTERM_BP_DIRECT	**GO:0070125~mitochondrial translational elongation**	25	1.26	MRPS17, GFM1, MRPS16, MRPS14, MRPS33, MRPS11, MRPL19, MRPL16, MRPL17, MRPL39, MRPS10, MRPL14, MRPL37, MRPL12, MRPL32, MRPL11, MRPL3, MRPL40, MRPS28, GADD45GIP1, MRPS23, MRPL27, MRPL28, MRPL45, MRPL24	0.00	0.00
GOTERM_BP_DIRECT	**GO:0070126~mitochondrial translational termination**	24	1.21	MRPS17, GADD45GIP1, MRPS28, MRPS16, MRPS14, MRPS33, MRPS11, MRPS23, MRPL19, MRPL27, MRPL16, MRPL17, MRPL39, MRPS10, MRPL28, MRPL14, MRPL37, MRPL12, MRPL45, MRPL24, MRPL32, MRPL11, MRPL3, MRPL40	0.00	0.00
GOTERM_MF_DIRECT	**GO:0003735~structural constituent of ribosome**	41	2.07	RPL4, MRPS17, MRPS16, RPL10, MRPS14, MRPS33, MRPS11, RPLP1, MRPL19, RPLP0, MRPL16, MRPL17, MRPL14, MRPL37, RPL10A, MRPL12, MRPL32, MRPL11, MRPL3, RPL36AL, RPL13, SLC25A43, RPS2, RPS27A, SLC25A23, SLC25A25, MRPS23, RPS6, MRPL27, MRPL28, RPL23A, RPSA, MRPL24, SLC25A15, SLC25A39, RPL7L1, MRTO4, RPL29, SLC25A11, RSL24D1, SLC25A6	0.03	0.03
GOTERM_CC_DIRECT	**GO:0005762~mitochondrial large ribosomal subunit**	14	0.71	NSUN4, MRPL19, MRPL27, MRPL16, MRPL17, MRPL39, MRPL28, MRPL14, MRPL37, MRPL12, MRPL24, MRPL32, MRPL11, MRPL3	0.02	0.02
KEGG_PATHWAY	**hsa03010:Ribosome**	30	1.51	RPL4, MRPS17, MRPS16, RPL10, MRPS14, MRPS11, RPLP1, MRPL19, RPLP0, MRPL16, MRPL17, MRPS10, MRPL14, RPL10A, MRPL12, MRPL32, MRPL11, MRPL3, RPL36AL, RPL13, RPS2, RPS27A, RPS6, MRPL27, MRPL28, RPL23A, RPSA, MRPL24, RPL29, RSL24D1	0.01	0.01
Annotation Cluster 4	**Enrichment Score: 5.107139783669251**					
Category	**Term**	**Count**	**%**	**Genes**	**Benjamini**	**FDR**
UP_KEYWORDS	**Protein biosynthesis**	45	2.27	HBS1L, GFM1, VARS, TARS, EPRS, YARS2, LARP1, PDF, LARS, NARS2, TCEB3, TCEB1, EIF2D, IARS2, EIF2B1, EARS2, EIF2A, EIF5A, EEFSEC, YARS, EIF5B, DARS, WARS, MARS2, DARS2, ELL2, EIF2S1, EIF1, WARS2, EEF1A1, AIMP2, LARS2, EIF2S3, EIF6, EIF3I, TAF4B, GARS, IARS, EEF1E1, EIF4E2, EIF3A, FARSB, AARS, EIF3B, EIF4G1	0.00	0.00
GOTERM_BP_DIRECT	**GO:0006418~tRNA aminoacylation for protein translation**	22	1.11	YARS, DARS, WARS, VARS, MARS2, MRPL39, TARS, DARS2, EPRS, YARS2, WARS2, LARS2, AIMP2, LARS, PPA1, NARS2, IARS2, GARS, IARS, EEF1E1, FARSB, AARS	0.00	0.00
UP_KEYWORDS	**Aminoacyl-tRNA synthetase**	19	0.96	YARS, DARS, WARS, VARS, MARS2, TARS, DARS2, EPRS, YARS2, WARS2, LARS2, LARS, NARS2, IARS2, GARS, IARS, EARS2, FARSB, AARS	0.00	0.00
UP_SEQ_FEATURE	**short sequence motif:"KMSKS" region**	11	0.55	YARS, LARS2, WARS, VARS, LARS, MARS2, IARS2, IARS, EPRS, YARS2, EARS2	0.00	0.00
UP_SEQ_FEATURE	**short sequence motif:"HIGH" region**	11	0.55	YARS, LARS2, WARS, VARS, LARS, MARS2, IARS2, IARS, EPRS, YARS2, EARS2	0.00	0.00
INTERPRO	**IPR001412:Aminoacyl-tRNA synthetase, class I, conserved site**	10	0.50	LARS2, WARS, VARS, LARS, IARS2, IARS, EPRS, YARS2, EARS2, WARS2	0.01	0.01

GOTERM_MF_DIRECT	**GO:0002161~aminoacyl-tRNA editing activity**	8	0.40	LARS2, VARS, LARS, IARS2, IARS, DTD1, DTD2, AARS	0.00	0.00
INTERPRO	**IPR014729:Rossmann-like alpha/beta/alpha sandwich fold**	15	0.76	YARS, WARS, VARS, FNBP1, MARS2, ETFA, EPRS, YARS2, WARS2, LARS2, LARS, IARS2, DPH6, IARS, EARS2	0.03	0.03
GOTERM_BP_DIRECT	**GO:0006450~regulation of translational fidelity**	8	0.40	LARS2, VARS, LARS, IARS2, IARS, DTD1, DTD2, AARS	0.06	0.06
KEGG_PATHWAY	**hsa00970:Aminoacyl-tRNA biosynthesis**	19	0.96	YARS, DARS, WARS, VARS, MARS2, TARS, DARS2, EPRS, YARS2, WARS2, LARS2, LARS, NARS2, IARS2, GARS, IARS, EARS2, FARSB, AARS	0.01	0.01
UP_KEYWORDS	**Ligase**	51	2.57	VARS, RTCB, TNFAIP3, UBE3A, EPRS, PRPF19, PFAS, YARS2, RNF115, TRIM2, FPGS, NARS2, EARS2, MCCC2, WARS, ACSL1, MARS2, CAD, DARS2, ACSL4, LIG3, TRAF2, CTPS1, TRAF7, LARS2, TRAF3, GARS, GART, SLC27A4, MGRN1, UBR4, TARS, DTX2, ACACA, MTHFD1L, LARS, IARS2, DPH6, RFFL, YARS, DARS, SIAH2, PAICS, MEX3C, WARS2, TTLL4, RNF182, IARS, DZIP3, AARS, FARSB	0.01	0.01
INTERPRO	**IPR009008:Valyl/Leucyl/Isoleucyl-tRNA synthetase, class Ia, editing domain**	5	0.25	LARS2, VARS, LARS, IARS2, IARS	0.26	0.26
INTERPRO	**IPR013155:Valyl/Leucyl/Isoleucyl-tRNA synthetase, class I, anticodon-binding**	5	0.25	LARS2, VARS, LARS, IARS2, IARS	0.26	0.26
INTERPRO	**IPR002300:Aminoacyl-tRNA synthetase, class Ia**	5	0.25	LARS2, VARS, LARS, IARS2, IARS	0.26	0.26
GOTERM_MF_DIRECT	**GO:0004812~aminoacyl-tRNA ligase activity**	7	0.35	YARS, WARS, VARS, LARS, NARS2, DARS2, IARS	0.23	0.23
Annotation Cluster 5	**Enrichment Score: 4.726262143460878**					
Category	**Term**	**Count**	**%**	**Genes**	**Benjamini**	**FDR**
GOTERM_MF_DIRECT	**GO:0051082~unfolded protein binding**	28	1.41	HSP90AB1, HTRA2, HSP90B1, CHAF1B, HSP90B2P, DNAJB5, CCT7, CCT5, CCT4, CCT3, HSPA9, HSPA8, NPM1, NUDC, HSP90AA1, HSPA5, ST13, PTGES3, TTC1, TUBB4B, TAPBP, CCT6A, DNAJA1, CANX, PFDN1, NDUFAF1, CALR, PPIA	0.00	0.00
UP_KEYWORDS	**Chaperone**	39	1.97	SET, HSP90AB1, COX17, HSPB7, PARK7, HSP90B1, HSP90B2P, DNAJB5, CCT7, CCT5, CCT4, CCT3, BTF3, HSPA9, CD74, HSPA8, NPM1, HSP90AA1, TIMMDC1, ST13, VBP1, ALYREF, PTGES3, TOMM34, DNAJC14, CCT6A, DNAJA1, NPLOC4, DNAJC30, CANX, ANP32E, PSMG3, PFDN1, HYOU1, NDUFAF1, CALR, ABCE1, PPID, FKBP5	0.00	0.00
GOTERM_BP_DIRECT	**GO:0006457~protein folding**	38	1.92	FKBP2, HSP90AB1, FUT10, GNAI3, TXN, HSPBP1, HSP90B1, HSP90B2P, GNG2, DNAJB5, CCT7, CCT5, CCT4, MPDU1, CCT3, PDIA3, HSPA9, HSPA8, NUDC, HSP90AA1, PPIL1, CSNK2A1, ST13, VBP1, SPHK1, TTC1, PDIA4, CCT6A, DNAJA1, FKBP1A, CANX, PPIF, PFDN1, CALR, PPIA, PPID, AARS, FKBP5	0.01	0.01

Annotation Cluster 6	Enrichment Score: 4.5208881415653375					
Category	**Term**	**Count**	**%**	**Genes**	**Benjamini**	**FDR**
GOTERM_BP_DIRECT	**GO:0033209~tumor necrosis factor-mediated signaling pathway**	41	2.07	PSMD12, CD40, PSMD11, PSMD14, TRADD, TNF, PSMA7, TXNDC17, PSMD7, PSMB5, UBB, PSMB2, PSMD3, PSMB1, PTK2B, PSMD1, TNFRSF8, TNFRSF14, RPS27A, RELT, TNFRSF4, EDARADD, TNFSF14, CD70, STAT1, TNFRSF18, TNFRSF9, TNFRSF19, TNFRSF10B, TRAF2, TNFRSF1B, PSMA4, PSMA1, PSMC4, TRAF3, PSME3, TNFSF4, PSMC2, LTA, FAS, BIRC3	0.00	0.00
UP_KEYWORDS	**Proteasome**	20	1.01	USP14, PSMD12, PSMD11, PSMD14, UBE3C, SHFM1, UBE3A, RAD23B, PSMA7, PSMD7, PSMA4, PSMB5, PSMA1, PSMB2, PSMC4, PSME3, PSMC2, PSMD3, PSMB1, PSMD1	0.00	0.00
GOTERM_CC_DIRECT	**GO:0000502~proteasome complex**	22	1.11	USP14, PSMD12, VCP, PSMD11, PSMD14, UBE3C, SHFM1, UBE3A, RAD23B, PSMA7, PSMD7, PSMA4, PSMB5, PSMA1, PSMB2, PSMC4, PSME3, PSMC2, PSMD3, PSMB1, PSMG3, PSMD1	0.00	0.00
GOTERM_BP_DIRECT	**GO:0043488~regulation of mRNA stability**	30	1.51	PSMD12, SET, PSMD11, PSMD14, ANP32A, YWHAB, ELAVL1, PSMA7, ZFP36L1, EXOSC5, PSMD7, XPO1, EXOSC4, PSMB5, UBB, PSMB2, PSMD3, PSMB1, PSMD1, RPS27A, HSPA8, PRKCD, PSMA4, PSMA1, PSMC4, APEX1, PSME3, PSMC2, SERBP1, EIF4G1	0.00	0.00
GOTERM_BP_DIRECT	**GO:0038061~NIK/NF-kappaB signaling**	22	1.11	PSMD12, PSMD11, PSMD14, NFKB1, PSMA7, RELB, NFKB2, PSMD7, PSMA4, PSMB5, PSMA1, UBB, PSMB2, PSMC4, PSME3, PSMC2, PSMD3, PSMB1, PSMD1, RPS27A, IKBKE, BIRC3	0.00	0.00
GOTERM_BP_DIRECT	**GO:0002479~antigen processing and presentation of exogenous peptide antigen via MHC class I, TAP-dependent**	21	1.06	PSMD12, PSMD11, PSMD14, NCF2, HLA-B, HLA-C, HLA-A, HLA-F, PSMA7, HLA-E, PSMD7, PSMA4, PSMB5, PSMA1, PSMB2, PSMC4, PSME3, PSMC2, PSMD3, PSMB1, PSMD1	0.00	0.00
GOTERM_BP_DIRECT	**GO:0050852~T cell receptor signaling pathway**	34	1.72	PSMD12, STOML2, PSMD11, PSMD14, PTEN, PIK3CD, PSMA7, PAK1, PSMD7, PSMB5, UBB, PSMB2, PSMD3, PSMB1, PSMD1, CSK, RPS27A, HLA-DQA2, HLA-DQA1, HLA-DPA1, RIPK2, RFTN1, NFKB1, NFKBIA, PSMA4, PIK3CA, PSMA1, PSMC4, PSME3, PSMC2, UBE2N, TAB2, HLA-DRB1, HLA-DQB1	0.00	0.00
GOTERM_BP_DIRECT	**GO:0002223~stimulatory C-type lectin receptor signaling pathway**	27	1.36	PSMD12, PSMD11, PSMD14, SRC, PSMA7, RELB, PAK1, NRAS, PSMD7, PSMB5, UBB, PSMB2, PSMD3, PSMB1, PSMD1, RPS27A, PRKCD, NFKB1, NFKBIA, PSMA4, PSMA1, PSMC4, PSME3, PSMC2, UBE2N, KRAS, TAB2	0.00	0.00
GOTERM_BP_DIRECT	**GO:0051436~negative regulation of ubiquitin-protein ligase activity involved in mitotic cell cycle**	20	1.01	PSMD12, PSMD11, PSMD14, ANAPC7, ANAPC16, PSMA7, PSMD7, PSMA4, PSMB5, PSMA1, UBB, PSMB2, PSMC4, PSME3, PSMC2, PSMD3, CDK2, PSMB1, PSMD1, RPS27A	0.02	0.02
KEGG_PATHWAY	**hsa03050:Proteasome**	16	0.81	PSMD12, PSMD11, PSMD14, SHFM1, PSMA7, PSMD7, PSMA4, PSMB5, PSMA1, PSMB2, PSMC4, PSME3, PSMC2, PSMD3, PSMB1, PSMD1	0.00	0.00
GOTERM_BP_DIRECT	**GO:0000209~protein polyubiquitination**	37	1.87	PSMD12, PSMD11, UBE3C, PSMD14, MGRN1, RNF19B, PRPF19, FBXO22, PSMA7, RNF115, PSMD7, PSMB5, UBB, PSMB2, PSMD3, PSMB1, PSMD1, RPS27A, LONRF1, CDKN2A, FBXW7, SIAH2, HUWE1,	0.02	0.02

				UBE2A, KLHL42, RNF145, FBXL8, PSMA4, PSMA1, PSMC4, PSME3, PSMC2, BCL2, BLMH, TRIP12, ASB2, DZIP3		
GOTERM_BP_DIRECT	**GO:0060071~Wnt signaling pathway, planar cell polarity pathway**	23	1.16	PSMD12, PSMD11, PSMD14, FZD6, CLTC, AP2B1, PSMA7, CDC42, PSMD7, PSMA4, PSMB5, PSMA1, UBB, PSMB2, PSMC4, PSME3, PSMC2, PSMD3, PSMB1, PSMD1, RAC1, PFN1, RPS27A	0.02	0.02
GOTERM_BP_DIRECT	**GO:0006521~regulation of cellular amino acid metabolic process**	15	0.76	PSMD12, PSMD11, PSMD14, PSMA7, PSMD7, PSMA4, PSMB5, PSMA1, PSMB2, PSMC4, PSME3, PSMC2, PSMD3, PSMB1, PSMD1	0.07	0.07
GOTERM_BP_DIRECT	**GO:0051437~positive regulation of ubiquitin-protein ligase activity involved in regulation of mitotic cell cycle transition**	19	0.96	PSMD12, PSMD11, PSMD14, ANAPC7, ANAPC16, PSMA7, PSMD7, PSMA4, PSMB5, PSMA1, UBB, PSMB2, PSMC4, PSME3, PSMC2, PSMD3, PSMB1, PSMD1, RPS27A	0.08	0.08
GOTERM_BP_DIRECT	**GO:0000165~MAPK cascade**	45	2.27	PSMD12, PSMD11, CSF2, PSMD14, YWHAB, RASGRF1, PDGFA, CSF2RB, IL2RG, FGF2, TNF, PSMA7, ZFP36L1, RASGRP3, PAK1, NRAS, PSMD7, PSMB5, UBB, PSMB2, MYC, PSMD3, PEA15, PSMB1, PTK2B, PSMD1, RPS27A, JAK3, DUSP5, MEF2C, CAV1, GRIN1, MAPK13, EFNA1, MAPK11, PPP5C, PSMA4, DOK4, PSMA1, PSMC4, PSME3, IL1B, PSMC2, KRAS, CALM3	0.10	0.10
GOTERM_BP_DIRECT	**GO:0031145~anaphase-promoting complex-dependent catabolic process**	19	0.96	PSMD12, PSMD11, PSMD14, ANAPC7, ANAPC16, PSMA7, PSMD7, PSMA4, PSMB5, PSMA1, UBB, PSMB2, PSMC4, PSME3, PSMC2, PSMD3, PSMB1, PSMD1, RPS27A	0.11	0.11
GOTERM_BP_DIRECT	**GO:0043161~proteasome-mediated ubiquitin-dependent protein catabolic process**	36	1.82	PSMD12, VCP, PSMD11, ANAPC16, PSMD14, FBXO45, PSMA7, RNF115, PSMD7, MTA1, PSMB5, UBB, PSMB2, PSMD3, PSMB1, PSMD1, RFFL, RPS27A, FBXW5, ANAPC7, SIAH2, UBE2A, RAD23B, PML, KLHL42, ABTB2, RNF145, PSMA4, PSMA1, PSMC4, TBL1XR1, KCTD10, PSME3, PSMC2, TP53, DZIP3	0.16	0.16
GOTERM_BP_DIRECT	**GO:0090263~positive regulation of canonical Wnt signaling pathway**	24	1.21	WNT10B, PSMD12, PSMD11, PSMD14, SRC, CAV1, FGF2, NFKB1, PSMA7, COL1A1, PSMD7, PSMA4, PSMB5, PSMA1, UBB, PSMB2, PSMC4, PSME3, PSMC2, PSMD3, PSMB1, PSMD1, RPS27A, WNT4	0.19	0.19
GOTERM_BP_DIRECT	**GO:0038095~Fc-epsilon receptor signaling pathway**	30	1.51	PSMD12, PSMD11, PSMD14, PSMA7, PAK1, PPP3CB, NRAS, PSMD7, PSMB5, UBB, PSMB2, PSMD3, PSMB1, PSMD1, RAC1, RPS27A, JUN, NFKB1, LAT2, NFKBIA, PSMA4, PIK3CA, PSMA1, PSMC4, PSME3, PSMC2, UBE2N, KRAS, TAB2, CALM3	0.43	0.43
GOTERM_BP_DIRECT	**GO:0090090~negative regulation of canonical Wnt signaling pathway**	28	1.41	PSMD12, PSMD11, PSMD14, PTPRO, LRP4, PSMA7, PSMD7, PSMB5, UBB, PSMB2, PSMD3, G3BP1, PSMB1, DACT3, PSMD1, RPS27A, WNT4, SIAH2, CAV1, FZD6, KREMEN2, CYLD, PSMA4, PSMA1, PSMC4, PSME3, PSMC2, RAPGEF1	0.43	0.43

Annotation Cluster 7	Enrichment Score: 3.57299414474471					
Category	**Term**	**Count**	**%**	**Genes**	**Benjamini**	**FDR**
UP_KEYWORDS	**DNA repair**	51	2.57	SMG1, FEN1, CETN2, BCCIP, SMC6, PRPF19, ALKBH2, CHAF1B, ZFYVE26, RUVBL1, NBN, POLK, PRMT6, GEN1, SUPT16H, PARP1, LIG3, RAD23B, RAD51B, MORF4L1, RAD51D, SFPQ, NEIL2, CINP, VCP, PSMD14, USP10, PRKDC, ASCC3, CLSPN, UVRAG, XRCC6, XRCC5, MCRS1, INTS3, NONO, HUWE1, UBE2A, SSRP1, GTF2H3, MLH1, GTF2H5, PPP5C, RAD50, APEX1, APLF, CDK2, UBE2N, NABP2, NABP1, TRIP12	0.00	0.00
UP_KEYWORDS	**DNA damage**	56	2.83	SMG1, FEN1, CETN2, BCCIP, SMC6, PRPF19, ALKBH2, CHAF1B, ZFYVE26, CCND1, RUVBL1, NBN, POLK, IKBKE, PRMT6, GEN1, SUPT16H, PARP1, HUS1, LIG3, RAD23B, RAD51B, MORF4L1, RAD51D, SFPQ, NEIL2, CINP, VCP, PSMD14, USP10, PRKDC, TANK, ZMAT3, ASCC3, CLSPN, UVRAG, XRCC6, XRCC5, MCRS1, INTS3, NONO, HUWE1, UBE2A, SSRP1, GTF2H3, MLH1, GTF2H5, PPP5C, RAD50, APEX1, APLF, CDK2, UBE2N, NABP2, NABP1, TRIP12	0.00	0.00
Annotation Cluster 8	**Enrichment Score: 3.101539111123744**					
Category	**Term**	**Count**	**%**	**Genes**	**Benjamini**	**FDR**
UP_SEQ_FEATURE	**repeat:WD 3**	45	2.27	MAPKBP1, DYNC1I2, SEH1L, WDR48, WDR1, WDR3, PAK1IP1, WDR4, WDR89, PRPF19, TAF5L, WDR43, DCAF7, WDR44, RPTOR, HIRA, CHAF1B, WDR5, MLST8, KIF21B, DCAF11, EIF2A, FBXW4, UTP15, WDR17, WDR36, SEC13, TLE1, FBXW5, WSB2, EED, FBXW7, NBEAL2, WDR12, WDR77, TRAF7, NEDD1, TBL1XR1, EIF3I, GRWD1, PPP2R2D, CORO6, WDFY1, GEMIN5, EIF3B	0.12	0.12
UP_SEQ_FEATURE	**repeat:WD 4**	43	2.17	MAPKBP1, DYNC1I2, SEH1L, WDR48, WDR1, WDR3, PAK1IP1, WDR4, WDR89, PRPF19, TAF5L, WDR43, DCAF7, WDR44, RPTOR, HIRA, CHAF1B, WDR5, MLST8, KIF21B, DCAF11, FBXW4, UTP15, WDR17, WDR36, SEC13, TLE1, WSB2, EED, FBXW7, NBEAL2, WDR12, WDR77, TRAF7, NEDD1, TBL1XR1, EIF3I, GRWD1, PPP2R2D, CORO6, WDFY1, GEMIN5, EIF3B	0.12	0.12
UP_KEYWORDS	**WD repeat**	45	2.27	MAPKBP1, DYNC1I2, SEH1L, WDR48, WDR1, WDR3, PAK1IP1, WDR4, WDR89, PRPF19, TAF5L, WDR43, DCAF7, WDR44, RPTOR, HIRA, CHAF1B, WDR5, MLST8, KIF21B, DCAF11, EIF2A, FBXW4, UTP15, WDR17, WDR36, SEC13, TLE1, FBXW5, WSB2, EED, FBXW7, NBEAL2, WDR12, WDR77, TRAF7, NEDD1, TBL1XR1, EIF3I, GRWD1, PPP2R2D, CORO6, WDFY1, GEMIN5, EIF3B	0.01	0.00
UP_SEQ_FEATURE	**repeat:WD 5**	40	2.02	MAPKBP1, DYNC1I2, SEH1L, WDR48, WDR1, WDR3, PAK1IP1, WDR89, PRPF19, TAF5L, WDR43, WDR44, RPTOR, HIRA, CHAF1B, WDR5, MLST8, KIF21B, DCAF11, UTP15, WDR17, WDR36, SEC13, TLE1, WSB2, EED, FBXW7, NBEAL2, WDR12, WDR77, TRAF7, NEDD1, TBL1XR1, EIF3I, GRWD1, PPP2R2D, CORO6, WDFY1, GEMIN5, EIF3B	0.12	0.12
UP_SEQ_FEATURE	**repeat:WD 1**	45	2.27	MAPKBP1, DYNC1I2, SEH1L, WDR48, WDR1, WDR3, PAK1IP1, WDR4, WDR89, PRPF19, TAF5L, WDR43, DCAF7, WDR44, RPTOR, HIRA, CHAF1B, WDR5, MLST8, KIF21B, DCAF11, EIF2A, FBXW4, UTP15, WDR17, WDR36, SEC13, TLE1, FBXW5, WSB2, EED, FBXW7, NBEAL2, WDR12, WDR77, TRAF7, NEDD1, TBL1XR1, EIF3I, GRWD1, PPP2R2D, CORO6, WDFY1, GEMIN5, EIF3B	0.12	0.12
UP_SEQ_FEATURE	**repeat:WD 2**	45	2.27	MAPKBP1, DYNC1I2, SEH1L, WDR48, WDR1, WDR3, PAK1IP1, WDR4, WDR89, PRPF19, TAF5L, WDR43, DCAF7, WDR44, RPTOR, HIRA, CHAF1B, WDR5, MLST8, KIF21B, DCAF11, EIF2A, FBXW4, UTP15, WDR17, WDR36, SEC13, TLE1, FBXW5, WSB2, EED, FBXW7, NBEAL2, WDR12, WDR77, TRAF7, NEDD1, TBL1XR1, EIF3I, GRWD1, PPP2R2D, CORO6, WDFY1, GEMIN5, EIF3B	0.12	0.12

SMART	**SM00320:WD40**	43	2.17	MAPKBP1, DYNC1I2, SEH1L, WDR48, WDR1, WDR3, PAK1IP1, WDR4, WDR89, PRPF19, TAF5L, WDR43, DCAF7, WDR44, RPTOR, HIRA, CHAF1B, WDR5, MLST8, KIF21B, DCAF11, FBXW4, UTP15, WDR17, WDR36, SEC13, TLE1, FBXW5, WSB2, EED, FBXW7, NBEAL2, WDR12, WDR77, TRAF7, NEDD1, TBL1XR1, EIF3I, GRWD1, PPP2R2D, CORO6, WDFY1, GEMIN5	0.14	0.14
INTERPRO	**IPR017986:WD40-repeat-containing domain**	49	2.47	MAPKBP1, WDR48, WDR1, WDR3, PAK1IP1, WDR4, WDR89, PRPF19, WDR43, DCAF7, WDR44, RPTOR, CHAF1B, WDR5, MLST8, KIF21B, EIF2A, UTP15, FBXW4, WDR36, SEC13, TLE1, FBXW5, WSB2, EED, FBXW7, WDR77, TRAF7, TBL1XR1, GRWD1, WDFY1, GEMIN5, DYNC1I2, SEH1L, SF3B3, GTF3C4, UBR4, TAF5L, HIRA, DCAF11, WDR17, NBEAL2, WDR12, NEDD1, EIF3I, PPP2R2D, VPS41, CORO6, EIF3B	0.24	0.24
INTERPRO	**IPR001680:WD40 repeat**	43	2.17	MAPKBP1, DYNC1I2, SEH1L, WDR48, WDR1, WDR3, PAK1IP1, WDR4, WDR89, PRPF19, TAF5L, WDR43, DCAF7, WDR44, RPTOR, HIRA, CHAF1B, WDR5, MLST8, KIF21B, DCAF11, FBXW4, UTP15, WDR17, WDR36, SEC13, TLE1, FBXW5, WSB2, EED, FBXW7, NBEAL2, WDR12, WDR77, TRAF7, NEDD1, TBL1XR1, EIF3I, GRWD1, PPP2R2D, CORO6, WDFY1, GEMIN5	0.27	0.27
INTERPRO	**IPR020472:G-protein beta WD-40 repeat**	20	1.01	WDR17, SEH1L, WDR48, WSB2, WDR1, FBXW7, WDR3, PAK1IP1, PRPF19, WDR12, TAF5L, WDR44, TRAF7, TBL1XR1, GRWD1, WDR5, WDFY1, MLST8, GEMIN5, DCAF11	0.27	0.27
INTERPRO	**IPR015943:WD40/YVTN repeat-like-containing domain**	50	2.52	MAPKBP1, WDR48, WDR1, WDR3, PAK1IP1, WDR4, WDR89, PRPF19, WDR43, DCAF7, WDR44, RPTOR, CHAF1B, WDR5, MLST8, KIF21B, EIF2A, UTP15, FBXW4, WDR36, SEC13, TLE1, FBXW5, WSB2, EED, FBXW7, WDR77, TRAF7, TBL1XR1, GRWD1, WDFY1, GEMIN5, DYNC1I2, SEMA7A, SEH1L, MST1R, TAF5L, HIRA, PLXNA1, DCAF11, WDR17, SEMA4C, NBEAL2, WDR12, NEDD1, EIF3I, PPP2R2D, VPS41, CORO6, EIF3B	0.33	0.33
INTERPRO	**IPR019775:WD40 repeat, conserved site**	29	1.46	WDR48, WDR1, WDR3, PAK1IP1, PRPF19, TAF5L, DCAF7, HIRA, CHAF1B, WDR5, MLST8, KIF21B, UTP15, WDR17, WDR36, TLE1, WSB2, EED, FBXW7, WDR12, WDR77, TRAF7, NEDD1, TBL1XR1, EIF3I, GRWD1, CORO6, WDFY1, GEMIN5	0.41	0.41
Annotation Cluster 9	**Enrichment Score: 3.029660564199106**					
Category	**Term**	**Count**	**%**	**Genes**	**Benjamini**	**FDR**
GOTERM_MF_DIRECT	**GO:0005031~tumor necrosis factor-activated receptor activity**	11	0.55	CD40, TNFRSF18, TNFRSF9, TNFRSF19, FAS, TNFRSF10B, TNFRSF8, TNFRSF14, TNFRSF1B, RELT, TNFRSF4	0.01	0.01
SMART	**SM00208:TNFR**	10	0.50	CD40, TNFRSF18, TNFRSF9, TNFRSF19, FAS, TNFRSF10B, TNFRSF8, TNFRSF14, TNFRSF1B, TNFRSF4	0.06	0.06
INTERPRO	**IPR001368:TNFR/NGFR cysteine-rich region**	10	0.50	CD40, TNFRSF18, TNFRSF9, TNFRSF19, FAS, TNFRSF10B, TNFRSF8, TNFRSF14, TNFRSF1B, TNFRSF4	0.24	0.24
UP_SEQ_FEATURE	**repeat:TNFR-Cys 1**	10	0.50	CD40, TNFRSF18, TNFRSF9, TNFRSF19, FAS, TNFRSF10B, TNFRSF8, TNFRSF14, TNFRSF1B, TNFRSF4	0.12	0.12
UP_SEQ_FEATURE	**repeat:TNFR-Cys 2**	10	0.50	CD40, TNFRSF18, TNFRSF9, TNFRSF19, FAS, TNFRSF10B, TNFRSF8, TNFRSF14, TNFRSF1B, TNFRSF4	0.12	0.12
UP_SEQ_FEATURE	**repeat:TNFR-Cys 3**	9	0.45	CD40, TNFRSF18, TNFRSF9, TNFRSF19, FAS, TNFRSF10B, TNFRSF8, TNFRSF14, TNFRSF1B	0.28	0.28

Annotation Cluster 10	Enrichment Score: 2.9714541171122675					
Category	**Term**	**Count**	**%**	**Genes**	**Benjamini**	**FDR**
GOTERM_MF_DIRECT	GO:0003924~GTPase activity	48	2.42	ARF3, HBS1L, RALA, GFM1, ARL1, GNAI3, ARL2, RAP1GAP, RND1, RAP1B, RAB21, CDC42, EFTUD2, ARFRP1, TUBA1C, TUBA1B, RAP1A, TUBA1A, NKIRAS2, MFN2, GNG8, RAC1, DNM1L, GBP1, GBP4, RAB8B, EEFSEC, EIF5B, TUBB, RHOG, ERAL1, RHOF, TUBB4B, GTPBP4, RAB11A, RAB10, EEF1A1, TUBB2B, RAP2A, GNL3L, EIF2S3, TUBB2A, RHEB, RAB13, RAB9A, TSR1, KRAS, RAN	0.00	0.00
UP_KEYWORDS	GTP-binding	56	2.83	ARF3, HBS1L, GFM1, RTKN, RND1, THG1L, EFTUD2, TUBA1C, RAB44, TUBA1B, TUBA1A, NKIRAS2, RAC1, DNM1L, RAB8B, MB21D1, EIF5B, TUBB, RHOG, GTPBP6, RHOF, GTPBP4, EEF1A1, RAP2A, TUBB2B, TUBB2A, RABL3, RALA, NPR1, ARL1, GNAI3, NOLC1, ARL2, RAP1B, RAB21, CDC42, ARFRP1, NRAS, RAP1A, MFN2, GBP1, GBP4, PCK2, EEFSEC, RAB39A, ERAL1, TUBB4B, RAB11A, RAB10, GNL3L, EIF2S3, RHEB, RAB13, RAB9A, KRAS, RAN	0.00	0.00
GOTERM_MF_DIRECT	GO:0005525~GTP binding	65	3.28	ARF3, HBS1L, GFM1, RTKN, HSP90AB1, OLA1, RND1, THG1L, EFTUD2, TUBA1C, RAB44, TUBA1B, TUBA1A, NKIRAS2, ANXA6, RAC1, DNM1L, RAB8B, MB21D1, EIF5B, HSP90AA1, TUBB, RHOG, GTPBP6, RHOF, GTPBP4, NME1, EEF1A1, RAP2A, TUBB2B, TUBB2A, RABL3, RALA, NPR1, ARL1, GNAI3, NOLC1, ARL2, RAP1B, RAB21, CDC42, ARFRP1, NRAS, RAP1A, MFN2, GBP1, GBP4, PCK2, EEFSEC, RAB39A, ERAL1, TUBB4B, RAB11A, RAB10, EHD1, IRGQ, GNL3L, EIF2S3, EHD4, RHEB, RAB13, RAB9A, TSR1, KRAS, RAN	0.01	0.01
UP_SEQ_FEATURE	nucleotide phosphate-binding region:GTP	51	2.57	ARF3, HBS1L, GFM1, RND1, EFTUD2, TUBA1C, RAB44, TUBA1B, TUBA1A, NKIRAS2, RAC1, DNM1L, RAB8B, EIF5B, TUBB, RHOG, GTPBP6, RHOF, GTPBP4, EEF1A1, RAP2A, TUBB2B, TUBB2A, RABL3, RALA, ARL1, GNAI3, ARL2, RAP1B, RAB21, CDC42, ARFRP1, NRAS, RAP1A, MFN2, GBP1, GBP4, PCK2, EEFSEC, RAB39A, ERAL1, TUBB4B, RAB11A, RAB10, GNL3L, EIF2S3, RHEB, RAB13, RAB9A, KRAS, RAN	0.09	0.09
UP_KEYWORDS	Prenylation	30	1.51	RALA, CNP, LMNB2, RND1, RAP1B, RAB21, CDC42, RAB44, NRAS, RAP1A, GNG2, GNG8, RAC1, GBP1, RAB8B, PTGIR, PLA2G4C, RHOG, RAB39A, NAP1L1, RHOF, RAB11A, RAB10, DNAJA1, PTP4A3, RAP2A, RHEB, RAB13, RAB9A, KRAS	0.01	0.01
INTERPRO	IPR005225:Small GTP-binding protein domain	31	1.56	ARF3, RALA, GFM1, ARL1, ARL2, RND1, RAP1B, RAB21, CDC42, EFTUD2, ARFRP1, RAB44, NRAS, RAP1A, NKIRAS2, RAC1, RAB8B, EIF5B, RHOG, RAB39A, ERAL1, RHOF, GTPBP4, RAB11A, RAB10, RAP2A, RHEB, RAB13, RAB9A, KRAS, RAN	0.24	0.24
Annotation Cluster 11	Enrichment Score: 2.89003539041738					
Category	**Term**	**Count**	**%**	**Genes**	**Benjamini**	**FDR**
UP_KEYWORDS	RNA-binding	110	5.55	TDRKH, SPI1, HNRNPU, PHAX, HNRNPR, PARK7, EPRS, SRP14, C14ORF166, EDC3, RAVER1, SNRPD3, EARS2, KDM2B, METTL1, RBMXL1, NCL, NHP2, SRSF3, GEMIN5, MATR3, KHDRBS1, CNP, TRMT2A, ZFP36L1, EMG1, LARP1, ATXN1, ZMAT3, DHX34, G3BP1, GAR1, RBM12, YARS, CHTOP, PNPT1, ZRANB2, PNO1, FUS, ALYREF, NONO, CPSF2, UPF3B, TDRD7, SYNJ2, ERAL1, LARP4, MEX3C, EIF2S1, HNRNPM, CPEB1, HNRNPK, LSM6, HNRNPF, CAPRIN1, HNRNPC, GRSF1, DZIP3, AARS, EIF4G1, MRPS17, DAZAP1, DDX47, FASTKD2, YBX1, ELAVL1, RBM3, IFIH1, SYNCRIP, XPO1, XPO5, EIF5A, NSUN4, ANXA2, NCBP2, NSUN2, RBM19, PPRC1, SRP9, PATL1, SFPQ, OAS3, RBM20, NSRP1, EIF4E2, SF3B4, POLDIP3, NIP7, SRSF1, DDX21, CSTF2T, NOL6, EXOSC5, EXOSC4, PUF60, IGF2BP3, HNRNPA1, TRDMT1, NPM1, TAF15, NIFK, RPL23A, LRPPRC, IMPDH2, APEX1, SERBP1, PDCD4, RBM45, EIF3A, EIF3B	0.00	0.00

INTERPRO	**IPR012677:Nucleotide-binding, alpha-beta plait**	44	2.22	SF3B4, DAZAP1, TMEM63B, POLDIP3, SRSF1, DDX21, CSTF2T, TRMT2A, HNRNPR, ELAVL1, RBM3, SYNCRIP, PUF60, RAVER1, G3BP1, IGF2BP3, RBM12, HNRNPA1, TAF15, NIFK, NCBP2, FUS, ALYREF, NONO, RBM19, UPF3B, RPL23A, SYNJ2, LARP4, PPRC1, HNRNPM, SFPQ, CPEB1, RBMXL1, NCL, HNRNPF, SRSF3, RBM20, NUP35, MATR3, HNRNPC, RBM45, GRSF1, EIF3B	0.24	0.24
INTERPRO	**IPR000504:RNA recognition motif domain**	38	1.92	SF3B4, DAZAP1, POLDIP3, SRSF1, CSTF2T, TRMT2A, HNRNPR, ELAVL1, RBM3, SYNCRIP, PUF60, RAVER1, G3BP1, IGF2BP3, RBM12, HNRNPA1, TAF15, NIFK, NCBP2, FUS, ALYREF, NONO, RBM19, SYNJ2, PPRC1, HNRNPM, SFPQ, CPEB1, RBMXL1, NCL, HNRNPF, SRSF3, RBM20, MATR3, HNRNPC, RBM45, GRSF1, EIF3B	0.26	0.26
SMART	**SM00360:RRM**	35	1.77	SF3B4, DAZAP1, POLDIP3, SRSF1, CSTF2T, HNRNPR, ELAVL1, RBM3, SYNCRIP, PUF60, RAVER1, G3BP1, IGF2BP3, RBM12, HNRNPA1, TAF15, NIFK, NCBP2, FUS, ALYREF, NONO, RBM19, PPRC1, HNRNPM, SFPQ, RBMXL1, NCL, HNRNPF, SRSF3, RBM20, MATR3, HNRNPC, RBM45, GRSF1, EIF3B	0.21	0.21
GOTERM_MF_DIRECT	**GO:0000166~nucleotide binding**	53	2.67	DAZAP1, MRPL39, HNRNPR, ELAVL1, RBM3, SYNCRIP, RAVER1, HSP90AA1, NCBP2, RBM19, PPRC1, SFPQ, RBMXL1, NCL, SRSF3, RBM20, MATR3, HPRT1, SLC27A4, SF3B4, TMEM63B, NPR1, POLDIP3, SRSF1, ADCY3, CSTF2T, TRMT2A, PUF60, G3BP1, IGF2BP3, RBM12, HNRNPA1, TAF15, NIFK, FUS, ALYREF, NONO, UPF3B, RPL23A, SYNJ2, ATP2B1, LARP4, HNRNPM, CPEB1, IMPDH2, HNRNPF, APLF, NUP35, HNRNPC, RBM45, GRSF1, ITPA, EIF3B	0.18	0.18
Annotation Cluster 12	**Enrichment Score: 2.839334091576117**					
Category	**Term**	**Count**	**%**	**Genes**	**Benjamini**	**FDR**
KEGG_PATHWAY	**hsa05140:Leishmaniasis**	21	1.06	IL10, JUN, MARCKSL1, IFNGR1, NCF2, STAT1, IFNGR2, ELK1, TNF, NFKB1, MAPK13, NFKBIA, MAPK11, IRAK1, IL1B, TAB2, HLA-DQA2, HLA-DQA1, HLA-DRB1, HLA-DPA1, HLA-DQB1	0.00	0.00
KEGG_PATHWAY	**hsa05145:Toxoplasmosis**	26	1.31	CD40, GNAI3, TNF, SOCS1, IRAK1, HLA-DQA2, HLA-DQA1, HLA-DPA1, IL10, HSPA8, IFNGR1, STAT1, IFNGR2, TYK2, NFKB1, MAPK13, NFKBIA, MAPK11, BCL2, PPIF, CYCS, TAB2, HLA-DRB1, BIRC3, BCL2L1, HLA-DQB1	0.01	0.01
KEGG_PATHWAY	**hsa05164:Influenza A**	34	1.72	PIK3CD, TNF, ACTB, ACTG1, ICAM1, IFIH1, XPO1, IKBKE, HLA-DQA2, HLA-DQA1, AGFG1, HLA-DPA1, HSPA8, JUN, IFNGR1, STAT1, IFNGR2, TNFRSF10B, TYK2, TICAM1, EIF2S1, NFKB1, PML, MAPK13, NFKBIA, MAPK11, PIK3CA, OAS3, IL1B, FAS, CYCS, VDAC1, HLA-DRB1, HLA-DQB1	0.04	0.04
KEGG_PATHWAY	**hsa05152:Tuberculosis**	34	1.72	SRC, TRADD, CEBPG, LSP1, NOD2, TNF, PPP3CB, IRAK1, LAMP1, ATP6V0A2, BID, HLA-DQA2, HLA-DQA1, HLA-DPA1, IL10, HSPA9, CD74, ARHGEF12, IFNGR1, STAT1, RIPK2, IFNGR2, SPHK1, NFKB1, MAPK13, MAPK11, IL1B, RFX5, BCL2, CYCS, CALM3, TLR6, HLA-DRB1, HLA-DQB1	0.05	0.04
Annotation Cluster 13	**Enrichment Score: 2.429622684629567**					
Category	**Term**	**Count**	**%**	**Genes**	**Benjamini**	**FDR**
KEGG_PATHWAY	**hsa04210:Apoptosis**	20	1.01	DFFA, TRADD, PIK3CD, TNFRSF10B, TRAF2, CSF2RB, CFLAR, TNF, NFKB1, NFKBIA, CASP7, PIK3CA, BCL2, CAPN2, FAS, CYCS, BID, TP53, BIRC3, BCL2L1	0.00	0.00
BIOCARTA	**h_hivnefPathway:HIV-I Nef: negative effector of Fas and TNF**	20	1.01	DFFA, PARP1, PRKDC, TRADD, PRKCD, TRAF2, CFLAR, TRAF1, TNFRSF1B, TNF, NFKB1, LMNB2, ACTG1, NFKBIA, CASP7, BCL2, FAS, CYCS, BID, BIRC3	0.27	0.27

BIOCARTA	**h_deathPathway:Induction of apoptosis through DR3 and DR4/5 Death Receptors**	12	0.61	NFKBIA, CASP7, DFFA, TRADD, BCL2, TNFRSF10B, CYCS, TRAF2, CFLAR, BID, NFKB1, BIRC3	0.47	0.47
Annotation Cluster 14	**Enrichment Score: 2.4213842451549588**					
Category	**Term**	**Count**	**%**	**Genes**	**Benjamini**	**FDR**
GOTERM_BP_DIRECT	**GO:0009168~purine ribonucleoside monophosphate biosynthetic process**	7	0.35	ADSL, ATIC, IMPDH2, GART, PFAS, PAICS, ADA	0.11	0.11
GOTERM_BP_DIRECT	**GO:0006189~'de novo' IMP biosynthetic process**	5	0.25	ADSL, ATIC, GART, PFAS, PAICS	0.13	0.13
UP_KEYWORDS	**Purine biosynthesis**	6	0.30	ADSL, ATIC, IMPDH2, GART, PFAS, PAICS	0.04	0.03
Annotation Cluster 15	**Enrichment Score: 2.3351930481215417**					
Category	**Term**	**Count**	**%**	**Genes**	**Benjamini**	**FDR**
GOTERM_CC_DIRECT	**GO:0071556~integral component of lumenal side of endoplasmic reticulum membrane**	15	0.76	CD74, SPPL2A, HLA-B, HLA-C, HLA-A, HLA-F, TAPBP, HLA-E, CANX, CALR, HLA-DQA2, HLA-DQA1, HLA-DRB1, HLA-DPA1, HLA-DQB1	0.00	0.00
KEGG_PATHWAY	**hsa05416:Viral myocarditis**	23	1.16	CD86, CD40, CD80, CAV1, HLA-B, HLA-C, HLA-A, HLA-F, ACTB, ACTG1, ICAM1, HLA-E, SGCA, CCND1, CYCS, RAC1, BID, HLA-DQA2, HLA-DQA1, HLA-DRB1, HLA-DPA1, HLA-DQB1, EIF4G1	0.00	0.00
KEGG_PATHWAY	**hsa05330:Allograft rejection**	16	0.81	IL10, CD86, CD40, CD80, HLA-B, HLA-C, HLA-A, HLA-F, TNF, HLA-E, FAS, HLA-DQA2, HLA-DQA1, HLA-DRB1, HLA-DPA1, HLA-DQB1	0.00	0.00
KEGG_PATHWAY	**hsa05332:Graft-versus-host disease**	15	0.76	CD86, CD80, HLA-B, HLA-C, HLA-A, HLA-F, TNF, HLA-E, IL1B, FAS, HLA-DQA2, HLA-DQA1, HLA-DRB1, HLA-DPA1, HLA-DQB1	0.00	0.00
GOTERM_BP_DIRECT	**GO:0002474~antigen processing and presentation of peptide antigen via MHC class I**	13	0.66	PDIA3, SEC13, HLA-B, TAP2, HLA-C, TAP1, HLA-A, HLA-F, TAPBP, HLA-E, CANX, CALR, HLA-DQB1	0.01	0.01

KEGG_PATHWAY	**hsa04612:Antigen processing and presentation**	23	1.16	PDIA3, CD74, HSPA8, HSP90AA1, HSP90AB1, HLA-B, TAP2, HLA-C, TAP1, HLA-A, HLA-F, TNF, TAPBP, HLA-E, PSME3, RFX5, CANX, CALR, HLA-DQA2, HLA-DQA1, HLA-DRB1, HLA-DPA1, HLA-DQB1	0.00	0.00
GOTERM_MF_DIRECT	**GO:0042605~peptide antigen binding**	12	0.61	HLA-B, HLA-C, TAP1, DHCR24, HLA-A, HLA-F, HLA-DRB1, HLA-DQA1, HLA-DPA1, TAPBP, HLA-E, HLA-DQB1	0.01	0.01
KEGG_PATHWAY	**hsa04940:Type I diabetes mellitus**	16	0.81	CD86, CD80, HLA-B, HLA-C, HLA-A, HLA-F, TNF, HLA-E, IL1B, LTA, FAS, HLA-DQA2, HLA-DQA1, HLA-DRB1, HLA-DPA1, HLA-DQB1	0.00	0.00
GOTERM_BP_DIRECT	**GO:0060333~interferon-gamma-mediated signaling pathway**	20	1.01	IFNGR1, STAT1, IFNGR2, PRKCD, HLA-B, HLA-C, HLA-A, HLA-F, PML, ICAM1, HLA-E, IRF4, OAS3, IRF5, GBP1, HLA-DQA2, HLA-DQA1, HLA-DRB1, HLA-DPA1, HLA-DQB1	0.02	0.02
INTERPRO	**IPR010579:MHC class I, alpha chain, C-terminal**	6	0.30	HLA-B, HLA-C, HLA-A, HLA-F, HLA-E, HLA-DQB1	0.14	0.14
UP_SEQ_FEATURE	**region of interest:Alpha-1**	8	0.40	HLA-B, HLA-C, HLA-A, HLA-F, HLA-DQA2, HLA-DQA1, HLA-DPA1, HLA-E	0.12	0.12
UP_SEQ_FEATURE	**region of interest:Alpha-2**	8	0.40	HLA-B, HLA-C, HLA-A, HLA-F, HLA-DQA2, HLA-DQA1, HLA-DPA1, HLA-E	0.12	0.12
GOTERM_CC_DIRECT	**GO:0012507~ER to Golgi transport vesicle membrane**	15	0.76	CD74, SEC13, GOSR2, HLA-B, HLA-C, HLA-A, HLA-F, SREBF2, HLA-E, CD59, HLA-DQA2, HLA-DQA1, HLA-DRB1, HLA-DPA1, HLA-DQB1	0.01	0.01
INTERPRO	**IPR001039:MHC class I, alpha chain, alpha1/alpha2**	7	0.35	HLA-B, HLA-C, HLA-A, HLA-F, HLA-DRB1, HLA-E, HLA-DQB1	0.24	0.24
UP_SEQ_FEATURE	**domain:Ig-like C1-type**	11	0.55	HLA-B, HLA-C, HLA-A, HLA-F, HLA-DQA2, HLA-DRB1, HLA-DQA1, HLA-DPA1, TAPBP, HLA-E, HLA-DQB1	0.14	0.14
UP_SEQ_FEATURE	**region of interest:Connecting peptide**	11	0.55	PLAU, HLA-B, HLA-C, HLA-A, HLA-F, HLA-DQA2, HLA-DRB1, HLA-DQA1, HLA-DPA1, HLA-E, HLA-DQB1	0.22	0.22
UP_KEYWORDS	**MHC I**	6	0.30	HLA-B, HLA-C, HLA-A, HLA-F, HLA-E, HLA-DQB1	0.01	0.01
GOTERM_BP_DIRECT	**GO:0019882~antigen processing and presentation**	15	0.76	CD74, HLA-B, HLA-C, HLA-A, RELB, HLA-E, RAB10, CTSH, ULBP1, HLA-DQA2, HLA-DQA1, HLA-DRB1, HLA-DPA1, HLA-DQB1, RAB8B	0.11	0.11
KEGG_PATHWAY	**hsa05320:Autoimmune thyroid disease**	15	0.76	IL10, CD86, CD40, CD80, HLA-B, HLA-C, HLA-A, HLA-F, HLA-E, FAS, HLA-DQA2, HLA-DQA1, HLA-DRB1, HLA-DPA1, HLA-DQB1	0.03	0.02
GOTERM_CC_DIRECT	**GO:0042612~MHC class I protein complex**	6	0.30	HLA-B, HLA-C, HLA-A, HLA-F, HLA-E, HLA-DQB1	0.06	0.06

INTERPRO	**IPR011162:MHC classes I/II-like antigen recognition protein**	12	0.61	HLA-B, HLA-C, HLA-A, HLA-F, CD1C, ULBP1, HLA-DQA2, HLA-DRB1, HLA-DQA1, HLA-DPA1, HLA-E, HLA-DQB1	0.44	0.44
GOTERM_CC_DIRECT	**GO:0042613~MHC class II protein complex**	8	0.40	CD74, HLA-C, HLA-A, HLA-DQA2, HLA-DRB1, HLA-DQA1, HLA-DPA1, HLA-DQB1	0.08	0.08
INTERPRO	**IPR011161:MHC class I-like antigen recognition**	9	0.45	HLA-B, HLA-C, HLA-A, HLA-F, CD1C, ULBP1, HLA-DRB1, HLA-E, HLA-DQB1	0.51	0.51
GOTERM_BP_DIRECT	**GO:0002480~antigen processing and presentation of exogenous peptide antigen via MHC class I, TAP-independent**	5	0.25	HLA-B, HLA-C, HLA-A, HLA-F, HLA-E	0.43	0.43
GOTERM_BP_DIRECT	**GO:0042270~protection from natural killer cell mediated cytotoxicity**	4	0.20	HLA-B, SERPINB9, HLA-A, HLA-E	0.43	0.43
GOTERM_MF_DIRECT	**GO:0032395~MHC class II receptor activity**	6	0.30	HLA-C, HLA-DQA2, HLA-DRB1, HLA-DQA1, HLA-DPA1, HLA-DQB1	0.46	0.45
KEGG_PATHWAY	**hsa04514:Cell adhesion molecules (CAMs)**	27	1.36	CD86, CNTNAP1, CD40, CD80, NRXN2, PVR, PTPRF, ICAM1, SPN, ALCAM, CD58, TIGIT, HLA-DQA2, ICOSLG, HLA-DQA1, JAM2, HLA-DPA1, NTNG1, HLA-B, HLA-C, HLA-A, L1CAM, HLA-F, HLA-E, ESAM, HLA-DRB1, HLA-DQB1	0.09	0.08
GOTERM_CC_DIRECT	**GO:0030669~clathrin-coated endocytic vesicle membrane**	10	0.50	CD74, CLTC, AP1S1, AP2B1, AP1S3, HLA-DQA2, HLA-DRB1, HLA-DQA1, HLA-DPA1, HLA-DQB1	0.26	0.25
KEGG_PATHWAY	**hsa04672:Intestinal immune network for IgA production**	12	0.61	IL10, CD86, IL15RA, PIGR, CD40, CD80, HLA-DQA2, HLA-DRB1, ICOSLG, HLA-DQA1, HLA-DPA1, HLA-DQB1	0.11	0.09
GOTERM_CC_DIRECT	**GO:0030666~endocytic vesicle membrane**	13	0.66	CD74, CAV1, AP2B1, SMO, UBB, RPS27A, SCARF1, HLA-DQA2, HLA-DQA1, HLA-DRB1, HLA-DPA1, HLA-DQB1, WNT4	0.34	0.32
GOTERM_CC_DIRECT	**GO:0030670~phagocytic vesicle membrane**	12	0.61	RAB10, ATP6V0E1, HLA-B, ATP6V0A2, RAB39A, HLA-C, RAB9A, HLA-A, TLR6, HLA-F, RAB8B, HLA-E	0.34	0.32
KEGG_PATHWAY	**hsa05310:Asthma**	8	0.40	IL10, CD40, TNF, HLA-DQA2, HLA-DRB1, HLA-DQA1, HLA-DPA1, HLA-DQB1	0.24	0.20
UP_KEYWORDS	**MHC II**	5	0.25	HLA-DQA2, HLA-DRB1, HLA-DQA1, HLA-DPA1, HLA-DQB1	0.31	0.28

KEGG_PATHWAY	**hsa05323:Rheumatoid arthritis**	15	0.76	CD86, JUN, ATP6V0E1, CSF2, CSF1, CD80, TNF, ICAM1, IL1B, ATP6V0A2, HLA-DQA2, HLA-DQA1, HLA-DRB1, HLA-DPA1, HLA-DQB1	0.49	0.41
Annotation Cluster 16	**Enrichment Score: 2.0981289902802818**					
Category	**Term**	**Count**	**%**	**Genes**	**Benjamini**	**FDR**
UP_KEYWORDS	**Initiation factor**	14	0.71	EIF5B, EIF2S1, EIF1, EIF2S3, EIF6, EIF3I, TAF4B, EIF2D, EIF2B1, EIF4E2, EIF3A, EIF2A, EIF3B, EIF4G1	0.02	0.02
GOTERM_MF_DIRECT	**GO:0003743~translation initiation factor activity**	14	0.71	EIF5B, EIF2S1, EIF1, EIF2S3, EIF6, EIF3I, TAF4B, EIF2D, EIF2B1, EIF4E2, EIF3A, EIF2A, EIF3B, EIF4G1	0.32	0.32
Annotation Cluster 17	**Enrichment Score: 2.0353999429137897**					
Category	**Term**	**Count**	**%**	**Genes**	**Benjamini**	**FDR**
GOTERM_BP_DIRECT	**GO:0010803~regulation of tumor necrosis factor-mediated signaling pathway**	10	0.50	CYLD, UBB, TRADD, SPHK1, TNFAIP3, TRAF2, TRAF1, RPS27A, TNF, BIRC3	0.19	0.19
GOTERM_BP_DIRECT	**GO:0010939~regulation of necrotic cell death**	6	0.30	UBB, TRADD, PPIF, TRAF2, RPS27A, BIRC3	0.31	0.31
Annotation Cluster 18	**Enrichment Score: 2.025578607456214**					
Category	**Term**	**Count**	**%**	**Genes**	**Benjamini**	**FDR**
UP_KEYWORDS	**Sterol biosynthesis**	10	0.50	CYB5R2, NSDHL, HMGCS1, C14ORF1, CYP51A1, MSMO1, DHCR24, HMGCR, DHCR7, FDFT1	0.00	0.00
UP_KEYWORDS	**Steroid biosynthesis**	11	0.55	CYB5R2, NSDHL, HMGCS1, C14ORF1, CYP51A1, MSMO1, DHCR24, HMGCR, DHCR7, LSS, FDFT1	0.01	0.01
UP_KEYWORDS	**Cholesterol biosynthesis**	7	0.35	NSDHL, HMGCS1, CYP51A1, DHCR24, HMGCR, DHCR7, FDFT1	0.05	0.04
KEGG_PATHWAY	**hsa00100:Steroid biosynthesis**	8	0.40	SQLE, NSDHL, CYP51A1, MSMO1, DHCR24, DHCR7, LSS, FDFT1	0.05	0.04
UP_KEYWORDS	**Sterol metabolism**	14	0.71	CETP, HMGCS1, CYP51A1, LCAT, MSMO1, DHCR24, HMGCR, SREBF2, CYB5R2, NSDHL, C14ORF1, DHCR7, APOL1, FDFT1	0.06	0.05

UP_KEYWORDS	**Lipid biosynthesis**	25	1.26	LPCAT1, MSMO1, HMGCR, ACACA, AGPAT3, CYB5R2, NSDHL, FAM213B, C14ORF1, FDFT1, ELOVL1, CERS4, XBP1, DGAT2, HMGCS1, PTGES2, PTGES3, CYP51A1, DHCR24, LSS, PISD, SCD, FASN, DHCR7, MGLL	0.07	0.06
GOTERM_BP_DIRECT	**GO:0006695~cholesterol biosynthetic process**	10	0.50	SQLE, NSDHL, HMGCS1, CYP51A1, MSMO1, DHCR24, HMGCR, DHCR7, LSS, FDFT1	0.55	0.55
UP_KEYWORDS	**Cholesterol metabolism**	11	0.55	CETP, NSDHL, HMGCS1, CYP51A1, LCAT, DHCR24, HMGCR, DHCR7, APOL1, SREBF2, FDFT1	0.20	0.18
UP_KEYWORDS	**Steroid metabolism**	14	0.71	CETP, HMGCS1, CYP51A1, LCAT, MSMO1, DHCR24, HMGCR, SREBF2, CYB5R2, NSDHL, C14ORF1, DHCR7, APOL1, FDFT1	0.27	0.23
Annotation Cluster 20	**Enrichment Score: 1.8793235425526813**					
Category	**Term**	**Count**	**%**	**Genes**	**Benjamini**	**FDR**
GOTERM_BP_DIRECT	**GO:0046718~viral entry into host cell**	17	0.86	CD86, UVRAG, CR2, TFRC, CD80, RPSA, NUP153, SLC1A5, PVR, ICAM1, VAMP8, LAMP1, HYAL2, TNFRSF14, EPS15, TNFRSF4, SLAMF1	0.39	0.39
UP_KEYWORDS	**Host cell receptor for virus entry**	13	0.66	CD86, CR2, TFRC, CD80, RPSA, SLC1A5, PVR, ICAM1, LAMP1, TNFRSF14, TNFRSF4, HLA-DRB1, SLAMF1	0.09	0.08
Annotation Cluster 21	**Enrichment Score: 1.8165065971631997**					
Category	**Term**	**Count**	**%**	**Genes**	**Benjamini**	**FDR**
INTERPRO	**IPR009000:Translation elongation/initiation factor/Ribosomal, beta-barrel**	10	0.50	EEFSEC, EEF1A1, EFTUD2, EIF5B, MRPL3, HBS1L, GFM1, EIF2S3, GAR1, AARS	0.30	0.30
Annotation Cluster 22	**Enrichment Score: 1.77815791998743**					
Category	**Term**	**Count**	**%**	**Genes**	**Benjamini**	**FDR**
UP_KEYWORDS	**Viral nucleoprotein**	9	0.45	EFTUD2, SYNCRIP, HNRNPM, HNRNPK, SNRPD1, HNRNPF, HNRNPR, HNRNPC, HNRNPA1	0.03	0.02
GOTERM_CC_DIRECT	**GO:0019013~viral nucleocapsid**	9	0.45	EFTUD2, SYNCRIP, HNRNPM, HNRNPK, SNRPD1, HNRNPF, HNRNPR, HNRNPC, HNRNPA1	0.09	0.08
UP_KEYWORDS	**Spliceosome**	21	1.06	SF3B4, HSPA8, PPIL1, SF3B3, ALYREF, SRSF1, HNRNPU, HNRNPR, TTF2, PRPF19, EFTUD2, SYNCRIP, HNRNPM, LSM6, HNRNPK, SNRPD1, HNRNPF, SNRPD3, HNRNPC, HNRNPA1, TXNL4A	0.09	0.08

GOTERM_CC_DIRECT	**GO:0071013~catalytic step 2 spliceosome**	16	0.81	PPIL1, SF3B3, ALYREF, SRSF1, HNRNPU, HNRNPR, PRPF19, EFTUD2, SYNCRIP, HNRNPM, HNRNPK, SNRPD1, HNRNPF, SNRPD3, HNRNPC, HNRNPA1	0.40	0.38
Annotation Cluster 23	**Enrichment Score: 1.7609086846345918**					
Category	**Term**	**Count**	**%**	**Genes**	**Benjamini**	**FDR**
GOTERM_MF_DIRECT	**GO:0046978~TAP1 binding**	4	0.20	TAP2, TAP1, HLA-F, TAPBP	0.19	0.18
GOTERM_CC_DIRECT	**GO:0042825~TAP complex**	3	0.15	TAP2, TAP1, TAPBP	0.34	0.32
Annotation Cluster 24	**Enrichment Score: 1.7264944695550326**					
Category	**Term**	**Count**	**%**	**Genes**	**Benjamini**	**FDR**
GOTERM_BP_DIRECT	**GO:1900740~positive regulation of protein insertion into mitochondrial membrane involved in apoptotic signaling pathway**	10	0.50	YWHAE, TFDP1, YWHAQ, YWHAB, BCL2, TP53BP2, BID, TP53, TP63, YWHAG	0.19	0.19
Annotation Cluster 25	**Enrichment Score: 1.7211246028570963**					
Category	**Term**	**Count**	**%**	**Genes**	**Benjamini**	**FDR**
INTERPRO	**IPR013024:Butirosin biosynthesis, BtrG-like**	4	0.20	GGCT, CHAC2, CHAC1, GGACT	0.44	0.44
GOTERM_MF_DIRECT	**GO:0003839~gamma-glutamylcyclotransferase activity**	4	0.20	GGCT, CHAC2, CHAC1, GGACT	0.19	0.18
Annotation Cluster 26	**Enrichment Score: 1.676901228208052**					
Category	**Term**	**Count**	**%**	**Genes**	**Benjamini**	**FDR**

GOTERM_MF_DIRECT	**GO:0070034~telomerase RNA binding**	8	0.40	PINX1, GAR1, NHP2, HNRNPU, SNRPD3, HNRNPC, SMG7, NOP10	0.04	0.04
GOTERM_BP_DIRECT	**GO:0007004~telomere maintenance via telomerase**	7	0.35	RAD50, PINX1, GAR1, NHP2, TNKS1BP1, SMG7, NOP10	0.39	0.39
GOTERM_CC_DIRECT	**GO:0090661~box H/ACA telomerase RNP complex**	3	0.15	GAR1, NHP2, NOP10	0.47	0.45
GOTERM_CC_DIRECT	**GO:0031429~box H/ACA snoRNP complex**	3	0.15	GAR1, NHP2, NOP10	0.47	0.45
GOTERM_CC_DIRECT	**GO:0072589~box H/ACA scaRNP complex**	3	0.15	GAR1, NHP2, NOP10	0.47	0.45
Annotation Cluster 27	**Enrichment Score: 1.647855375363639**					
Category	**Term**	**Count**	**%**	**Genes**	**Benjamini**	**FDR**
UP_KEYWORDS	**Nucleotide-binding**	248	12.51	CLPB, VARS, RTCB, HNRNPU, SMC6, EPRS, ACTB, RPS6KA1, LONP2, KIF21B, EARS2, MCCC2, CSNK2A1, ACSL1, CSNK2A3, PRKCD, GTPBP6, ACSL4, PASK, GTPBP4, LARS2, PRKAR1B, RABL3, HPRT1, PRKDC, NOLC1, MST1R, ACTR3B, ATP5B, DHX33, LARS, DHX34, DHX37, TRPM7, DPH6, PCK2, CDK17, CDK18, XRCC6, XRCC5, RAB39A, ERAL1, PAICS, SRPK1, SMARCA4, EHD1, CCT6A, UCK2, EHD4, HYOU1, ALDH18A1, ITPA, AARS, FARSB, DDR1, ARF3, HBS1L, SMG1, GFM1, OLA1, NAT10, PFAS, IFIH1, TUBA1C, TUBA1B, TUBA1A, ACTR1B, RFK, NKIRAS2, KIF13A, KIF1C, RAC1, RIOK1, TK1, JAK3, IKBKE, RAB8B, CCT3, HELLS, RPS6KL1, WARS, RIPK2, SPHK1, TUBB, INSRR, RHOG, NME3, TYK2, RHOF, NME1, RAD51B, ITPKC, TUBB2B, RAD51D, RAP2A, TUBB2A, GARS, GART, DDR2, TOR4A, PKN3, GNAI3, ADCY3, ARFRP1, NRAS, PAK1, MTHFD1L, ASNA1, MFN2, C10ORF2, CKB, CCT7, CCT5, PAK4, CCT4, UBE2G2, TUBB4B, RAB11A, TTLL4, PSMC4, KIF26B, PSMC2, RAB9A, TRIP13, FRK, RTKN, TTF2, UBE2Z, YARS2, ACTG1, THG1L, EFTUD2, RAB44, PPIP5K1, FPGS, NARS2, RUVBL1, PIM1, MAP3K8, PIM3, PIM2, MB21D1, TOR3A, CSNK1G3, TAP2, UBE2E2, TAP1, LIG3, ATAD3A, EEF1A1, SLC27A4, BLK, VCP, NPR1, AK2, ARL1, TARS, ARL2, ACACA, HSP90B1, RAP1B, RAP1A, IRAK1, KIF3B, G3BP1, PGK1, MYH11, HSPA9, EEFSEC, YARS, DARS, NEK9, HSPA8, HSPA5, NEK6, UBE2A, GNL3L, EIF2S3, RHEB, CDK4, CDK2, UBE2N, IARS, MAP3K13, ABCD2, HSP90AB1, DDX47, PIK3CD, HK2, RND1, EEF2K, DNM1L, ACTR3, ABCC4, ACTR2, EIF5B, HSP90AA1, RFC2, MARS2, CAD, DARS2, CTPS1, PKM, PIK3CA, PEAK1, OAS3, BMP2K, MYH9, DCTPP1, HCN3, RALA, SRC, NLRC5, DDX21, NOD2, ATP2C1, ATAD2B, RAB21, CDC42, MAT2A, RPS6KC1, MKNK2, PTK2B, IARS2, CSK, ASCC3, ABCF2, GBP1, GBP4, ABCF1, MMAB, ATP2B1, WARS2, MAPK13, MYO1D, RAB10, MYO1E, MAPK11, CLCN5, RAD50, MYO1C, RAB13, APLF, KRAS, ABCE1, PFKM, RAN, MYO1G	0.00	0.00
UP_KEYWORDS	**ATP-binding**	188	9.49	CLPB, VARS, RTCB, HNRNPU, TTF2, SMC6, EPRS, UBE2Z, YARS2, ACTB, ACTG1, PPIP5K1, RPS6KA1, FPGS, NARS2, RUVBL1, PIM1, LONP2, MAP3K8, PIM3, KIF21B, PIM2, EARS2, MB21D1, MCCC2, CSNK1G3, TOR3A, CSNK2A1, ACSL1, CSNK2A3, PRKCD, TAP2, UBE2E2, TAP1, ACSL4, LIG3, PASK, ATAD3A, LARS2, BLK, VCP, PRKDC, AK2, NOLC1, TARS, MST1R, ACTR3B, ACACA, HSP90B1, ATP5B, IRAK1, DHX33, KIF3B, LARS, DHX34, G3BP1, DHX37, PGK1, MYH11, TRPM7, DPH6, CDK17, YARS, HSPA9, CDK18, DARS, NEK9, HSPA8, XRCC6, HSPA5, XRCC5, NEK6, UBE2A, PAICS, SRPK1, SMARCA4,	0.00	0.00

				CCT6A, EHD1, UCK2, EHD4, CDK4, CDK2, UBE2N, HYOU1, IARS, ALDH18A1, MAP3K13, AARS, FARSB, DDR1, SMG1, ABCD2, HSP90AB1, DDX47, OLA1, PIK3CD, NAT10, PFAS, HK2, IFIH1, ACTR1B, EEF2K, RFK, KIF13A, KIF1C, RIOK1, TK1, JAK3, IKBKE, CCT3, ACTR3, ABCC4, ACTR2, HELLS, RPS6KL1, HSP90AA1, WARS, RIPK2, RFC2, MARS2, SPHK1, CAD, INSRR, DARS2, NME3, CTPS1, TYK2, NME1, RAD51B, ITPKC, RAD51D, PKM, PIK3CA, PEAK1, OAS3, BMP2K, MYH9, GARS, GART, DDR2, TOR4A, SRC, PKN3, NLRC5, ADCY3, DDX21, NOD2, ATP2C1, ATAD2B, PAK1, MTHFD1L, MAT2A, RPS6KC1, ASNA1, MKNK2, C10ORF2, PTK2B, IARS2, CSK, CKB, ASCC3, ABCF2, CCT7, CCT5, ABCF1, PAK4, CCT4, MMAB, UBE2G2, ATP2B1, WARS2, MAPK13, MYO1D, MYO1E, MAPK11, RAD50, CLCN5, MYO1C, TTLL4, PSMC4, KIF26B, PSMC2, KRAS, TRIP13, ABCE1, PFKM, FRK, MYO1G		
GOTERM_MF_DIRECT	**GO:0005524~ATP binding**	201	10.14	CLPB, VARS, RTCB, HNRNPU, SMC6, EPRS, ACTB, RPS6KA1, LONP2, KIF21B, EARS2, MCCC2, CSNK2A1, ACSL1, CSNK2A3, PRKCD, ACSL4, PASK, RUNX3, LARS2, ALPK1, TP53, PRKDC, NOLC1, MST1R, ACTR3B, ATP5B, DHX33, LARS, DHX34, DHX37, TRPM7, DPH6, CDK17, CDK18, XRCC6, XRCC5, PAICS, SRPK1, SMARCA4, EHD1, CCT6A, UCK2, PPP5C, EHD4, HYOU1, ALDH18A1, AARS, FARSB, DDR1, SMG1, OLA1, NAT10, PFAS, IFIH1, ACTR1B, RFK, KIF13A, KIF1C, RIOK1, TK1, JAK3, IKBKE, CCT3, HELLS, RPS6KL1, WARS, RIPK2, SPHK1, INSRR, NME3, TYK2, NME1, RAD51B, ITPKC, RAD51D, GARS, GART, DDR2, TOR4A, PKN3, ADCY3, PAK1, MTHFD1L, ASNA1, C10ORF2, CKB, CCT7, CCT5, PAK4, CCT4, UBE2G2, MLH1, TTLL4, PSMC4, KIF26B, PSMC2, TRIP13, FRK, TTF2, UBE2Z, YARS2, ACTG1, THG1L, PPIP5K1, FPGS, NARS2, RUVBL1, PIM1, MAP3K8, PIM3, PIM2, MB21D1, TOR3A, CSNK1G3, SWAP70, TAP2, UBE2E2, TAP1, LIG3, ILF2, ATAD3A, TXLNB, BLK, VCP, NPR1, AK2, TARS, ACACA, HSP90B1, IRAK1, KIF3B, G3BP1, PGK1, MYH11, HSPA9, YARS, DARS, NEK9, HSPA8, HSPA5, NEK6, UBE2A, CDK4, CDK2, UBE2N, IARS, MAP3K13, ABCD2, HSP90AB1, DDX47, PIK3CD, HK2, HSP90B2P, EEF2K, ACTR3, ABCC4, ACTR2, HSP90AA1, RFC2, MARS2, CAD, DARS2, CTPS1, PKM, PIK3CA, PEAK1, OAS3, BMP2K, MYH9, SRC, NLRC5, DDX21, NOD2, ATP2C1, ATAD2B, MAT2A, RPS6KC1, MKNK2, PTK2B, IARS2, CSK, ASCC3, ABCF2, ABCF1, FDXACB1, MMAB, ATP2B1, WARS2, MAPK13, MYO1D, DNAJA1, MYO1E, MAPK11, CLCN5, RAD50, MYO1C, KRAS, ABCE1, PFKM, MYO1G	0.01	0.01
UP_KEYWORDS	**Kinase**	78	3.94	DDR1, MAPKBP1, CDKN1A, SMG1, SH3KBP1, PIK3CD, HK2, EEF2K, PPIP5K1, PLAU, RFK, RPS6KA1, PIM1, PIM3, MAP3K8, RIOK1, PIM2, TK1, JAK3, IKBKE, CSNK1G3, RPS6KL1, CSNK2A1, RIPK2, SPHK1, CSNK2A3, INSRR, PRKCD, NME3, TYK2, PASK, NME1, ITPKC, PKM, PIK3CA, PRKAR1B, PEAK1, CINP, BMP2K, ALPK1, DDR2, BLK, SRC, PRKDC, PKN3, MAPKAP1, AK2, MST1R, PAK1, IRAK1, RPS6KC1, MKNK2, PGK1, PTK2B, CSK, TRPM7, CKB, PAK4, PCK2, CDK17, CDK18, NEK9, CDKN2B, CDKN2A, NEK6, SRPK1, MAPK13, MAPK11, UCK2, CDK4, CDK2, CALM3, TAB2, ALDH18A1, PKIG, MAP3K13, PFKM, FRK	0.48	0.43
Annotation Cluster 29	**Enrichment Score: 1.625379549833877**					
Category	**Term**	**Count**	**%**	**Genes**	**Benjamini**	**FDR**
UP_KEYWORDS	**mRNA processing**	50	2.52	DDX47, TSEN15, HNRNPU, HNRNPR, TTF2, YBX1, PRPF19, EFTUD2, SYNCRIP, SNRPD1, C1QBP, SNRPD3, TXNL4A, NCBP2, PRPF40B, SFPQ, RBMXL1, GEMIN4, SRSF3, GEMIN5, RBM20, GEMIN8, NSRP1, SF3B4, KHDRBS1, SF3B3, SRSF1, CSTF2T, NOL3, IWS1, ZFP36L1, PUF60, SYMPK, HNRNPA1, DCPS, HSPA8, PPIL1, PNPT1, ZRANB2, ALYREF, NONO, CPSF2, SRPK1, HNRNPM, CPEB1, LSM6, HNRNPK, HNRNPF, HNRNPC, GRSF1	0.01	0.01
UP_KEYWORDS	**mRNA splicing**	41	2.07	SF3B4, SF3B3, DDX47, SRSF1, HNRNPU, HNRNPR, TTF2, YBX1, PRPF19, NOL3, IWS1, EFTUD2, SYNCRIP, PUF60, SNRPD1, C1QBP, SNRPD3, TXNL4A, HNRNPA1, DCPS, HSPA8, PPIL1, ZRANB2, NCBP2,	0.01	0.01

				ALYREF, NONO, PRPF40B, SRPK1, HNRNPM, SFPQ, LSM6, RBMXL1, HNRNPK, HNRNPF, GEMIN4, GEMIN5, SRSF3, RBM20, HNRNPC, GEMIN8, NSRP1		
UP_KEYWORDS	**Spliceosome**	21	1.06	SF3B4, HSPA8, PPIL1, SF3B3, ALYREF, SRSF1, HNRNPU, HNRNPR, TTF2, PRPF19, EFTUD2, SYNCRIP, HNRNPM, LSM6, HNRNPK, SNRPD1, HNRNPF, SNRPD3, HNRNPC, HNRNPA1, TXNL4A	0.09	0.08
GOTERM_CC_DIRECT	**GO:0071013~catalytic step 2 spliceosome**	16	0.81	PPIL1, SF3B3, ALYREF, SRSF1, HNRNPU, HNRNPR, PRPF19, EFTUD2, SYNCRIP, HNRNPM, HNRNPK, SNRPD1, HNRNPF, SNRPD3, HNRNPC, HNRNPA1	0.40	0.38
KEGG_PATHWAY	**hsa03040:Spliceosome**	23	1.16	SF3B4, HSPA8, PPIL1, SF3B3, CCDC12, NCBP2, ALYREF, SRSF1, PRPF40B, HNRNPU, PRPF19, EFTUD2, HNRNPM, RBMXL1, LSM6, HNRNPK, PUF60, SNRPD1, SRSF3, SNRPD3, HNRNPC, HNRNPA1, TXNL4A	0.27	0.23
Annotation Cluster 30	**Enrichment Score: 1.6134782118546154**					
Category	**Term**	**Count**	**%**	**Genes**	**Benjamini**	**FDR**
GOTERM_BP_DIRECT	**GO:0006413~translational initiation**	28	1.41	RPL4, RPL10, RPLP1, RPLP0, RPL10A, LARP1, RPL13, RPS2, RPS27A, EIF2B1, ABCF1, EIF2A, PAIP1, EIF5B, RPS6, RPL23A, RPSA, EIF2S1, EIF1, EIF2S3, EIF6, EIF3I, RPL29, ABCE1, EIF4E2, EIF3A, EIF3B, EIF4G1	0.09	0.09
GOTERM_CC_DIRECT	**GO:0022625~cytosolic large ribosomal subunit**	14	0.71	RPL4, RPL10, RPLP1, RPLP0, RPL23A, RPL10A, RSL1D1, RPL36AL, RPL7L1, MRTO4, NHP2, RPL13, RPL29, RSL24D1	0.25	0.24
Annotation Cluster 31	**Enrichment Score: 1.5504033280804272**					
Category	**Term**	**Count**	**%**	**Genes**	**Benjamini**	**FDR**
BIOCARTA	**h_cdc42racPathway:Role of PI3K subunit p85 in regulation of Actin Organization and Cell Migration**	9	0.45	ACTR3, CDC42, ACTR2, PAK1, PIK3CA, ARPC2, ARPC4, RAC1, ARPC5	0.27	0.27
GOTERM_CC_DIRECT	**GO:0005885~Arp2/3 protein complex**	6	0.30	ACTR3, ACTR2, ARPC2, ARPC4, ARPC5, ACTR3B	0.08	0.08
BIOCARTA	**h_salmonellaPathway:How does salmonella hijack a cell**	7	0.35	ACTR3, CDC42, ACTR2, ARPC2, ARPC4, RAC1, ARPC5	0.47	0.47
Annotation Cluster 32	**Enrichment Score: 1.5224422080928728**					
Category	**Term**	**Count**	**%**	**Genes**	**Benjamini**	**FDR**

GOTERM_MF_DIRECT	**GO:0042054~histone methyltransferase activity**	7	0.35	PRMT6, PRMT2, EED, PRMT1, CARM1, DOT1L, EZH2	0.03	0.03
GOTERM_MF_DIRECT	**GO:0016274~protein-arginine N-methyltransferase activity**	5	0.25	PRMT6, PRMT2, PRMT1, CARM1, WDR77	0.34	0.34
Annotation Cluster 33	**Enrichment Score: 1.521786493483401**					
Category	**Term**	**Count**	**%**	**Genes**	**Benjamini**	**FDR**
KEGG_PATHWAY	**hsa05130:Pathogenic Escherichia coli infection**	18	0.91	TUBB, ARPC4, ARPC5, TUBB4B, ACTB, ACTG1, CDC42, TUBA1C, TUBA1B, TUBB2B, TUBA1A, TUBB2A, CTTN, ARPC2, NCL, NCK2, HCLS1, ARHGEF2	0.00	0.00
GOTERM_BP_DIRECT	**GO:0030705~cytoskeleton-dependent intracellular transport**	7	0.35	TUBA1C, TUBA1B, TUBA1A, KIF26B, TUBB, KIF13A, KIF1C	0.39	0.39
KEGG_PATHWAY	**hsa04540:Gap junction**	15	0.76	SRC, TUBB, GNAI3, ITPR1, PDGFA, ADCY3, TUBB4B, TUBA1C, TUBA1B, TUBB2B, PLCB3, NRAS, TUBA1A, TUBB2A, KRAS	0.49	0.41
Annotation Cluster 34	**Enrichment Score: 1.5116366193545114**					
Category	**Term**	**Count**	**%**	**Genes**	**Benjamini**	**FDR**
GOTERM_CC_DIRECT	**GO:0034709~methylosome**	6	0.30	SNRPD1, PRMT1, CLNS1A, ERH, SNRPD3, WDR77	0.08	0.08
Annotation Cluster 35	**Enrichment Score: 1.493242602778786**					
Category	**Term**	**Count**	**%**	**Genes**	**Benjamini**	**FDR**
GOTERM_BP_DIRECT	**GO:1904874~positive regulation of telomerase RNA localization to Cajal body**	8	0.40	CCT3, CCT6A, RUVBL1, NHP2, CCT7, NOP10, CCT5, CCT4	0.06	0.06
GOTERM_BP_DIRECT	**GO:1904871~positive regulation of protein localization to Cajal body**	5	0.25	CCT3, CCT6A, CCT7, CCT5, CCT4	0.33	0.32
GOTERM_CC_DIRECT	**GO:0005832~chaperonin-containing T-complex**	5	0.25	CCT3, CCT6A, CCT7, CCT5, CCT4	0.14	0.13

GOTERM_CC_DIRECT	**GO:0002199~zona pellucida receptor complex**	4	0.20	CCT3, CCT7, CCT5, CCT4	0.47	0.45
Annotation Cluster 36	**Enrichment Score: 1.4743493080754415**					
Category	**Term**	**Count**	**%**	**Genes**	**Benjamini**	**FDR**
KEGG_PATHWAY	**hsa05161:Hepatitis B**	30	1.51	CDKN1A, YWHAB, SRC, PTEN, PIK3CD, ELK1, TNF, IFIH1, NRAS, CCND1, YWHAQ, MYC, PTK2B, E2F3, STAT6, IKBKE, STAT5A, JUN, STAT1, TICAM1, NFKB1, NFKBIA, PIK3CA, CDK4, CDK2, BCL2, FAS, CYCS, KRAS, TP53	0.04	0.03
KEGG_PATHWAY	**hsa05222:Small cell lung cancer**	20	1.01	CDKN2B, PTEN, PIK3CD, TRAF2, TRAF1, NFKB1, NFKBIA, PIK3CA, TRAF4, CCND1, TRAF3, CDK4, MYC, CDK2, BCL2, CYCS, E2F3, TP53, BIRC3, BCL2L1	0.04	0.04
KEGG_PATHWAY	**hsa05215:Prostate cancer**	20	1.01	CDKN1A, HSP90AA1, HSP90AB1, TCF7, INSRR, PTEN, PDGFA, PIK3CD, NFKB1, HSP90B1, NFKBIA, NRAS, PIK3CA, CCND1, CDK2, BCL2, KRAS, E2F3, TP53, NKX3-1	0.05	0.04
KEGG_PATHWAY	**hsa05221:Acute myeloid leukemia**	14	0.71	STAT5A, SPI1, TCF7, PIK3CD, NFKB1, PML, NRAS, PIK3CA, CCND1, MYC, PIM1, RARA, KRAS, PIM2	0.08	0.06
KEGG_PATHWAY	**hsa05219:Bladder cancer**	11	0.55	CDKN1A, NRAS, CCND1, CDKN2A, SRC, CDK4, MYC, KRAS, E2F3, TP53, TYMP	0.11	0.09
KEGG_PATHWAY	**hsa05220:Chronic myeloid leukemia**	16	0.81	STAT5A, CDKN1A, CDKN2A, PIK3CD, PTPN11, NFKB1, NFKBIA, NRAS, PIK3CA, CCND1, CDK4, MYC, KRAS, E2F3, TP53, BCL2L1	0.11	0.09
KEGG_PATHWAY	**hsa05212:Pancreatic cancer**	14	0.71	RALA, CDKN2A, STAT1, PIK3CD, NFKB1, CDC42, PIK3CA, CCND1, CDK4, KRAS, E2F3, RAC1, TP53, BCL2L1	0.19	0.16
KEGG_PATHWAY	**hsa05210:Colorectal cancer**	13	0.66	JUN, TCF7, PIK3CD, MLH1, PIK3CA, CCND1, MYC, BCL2, CYCS, KRAS, RAC1, TP53, APPL1	0.24	0.20
KEGG_PATHWAY	**hsa05214:Glioma**	13	0.66	CDKN1A, CDKN2A, PTEN, PDGFA, PIK3CD, NRAS, PIK3CA, CCND1, CDK4, KRAS, CALM3, E2F3, TP53	0.30	0.25
KEGG_PATHWAY	**hsa05213:Endometrial cancer**	11	0.55	NRAS, CCND1, PIK3CA, MYC, TCF7, PTEN, PIK3CD, KRAS, MLH1, ELK1, TP53	0.31	0.25
KEGG_PATHWAY	**hsa05216:Thyroid cancer**	7	0.35	NRAS, CCND1, TFG, MYC, TCF7, KRAS, TP53	0.40	0.34
KEGG_PATHWAY	**hsa05218:Melanoma**	13	0.66	CDKN1A, CDKN2A, PTEN, PDGFA, PIK3CD, FGF2, NRAS, PIK3CA, CCND1, CDK4, KRAS, E2F3, TP53	0.43	0.36
Annotation Cluster 37	**Enrichment Score: 1.4382135535663552**					

Category	Term	Count	%	Genes	Benjamini	FDR
UP_KEYWORDS	Immunity	70	3.53	CD86, CD84, CD40, CSF1, PIK3CD, RNF19B, OTUD7B, ETS1, PTMS, IFIH1, ALCAM, NUDCD1, C1QBP, MAP3K8, JAK3, ICOSLG, HLA-DPA1, MB21D1, JAGN1, CR2, DBNL, IL4R, RIPK2, TFEB, HLA-B, TAP2, HLA-C, TAP1, CTPS1, HLA-A, TICAM1, HLA-F, HLA-E, LAT2, PSMA1, TRAF3, OAS3, ORAI1, TLR10, IRF5, ARHGEF2, TLR6, HLA-DQB1, SRC, NLRC5, MST1R, NOD2, CD1C, CFP, SEC14L1, IRAK1, BTLA, PTK2B, SLAMF7, CSK, HLA-DQA2, GBP1, HLA-DQA1, SLAMF1, APOBEC3C, CD74, APOBEC3G, LILRB4, PML, BST2, CYLD, LOC102723996, POLR3H, HLA-DRB1, MYO1G	0.01	0.01
Annotation Cluster 38	Enrichment Score: 1.43661475320309					
Category	Term	Count	%	Genes	Benjamini	FDR
UP_KEYWORDS	Cell cycle	86	4.34	CDKN1A, STEAP3, ANKLE2, CETN2, CCDC124, CLTC, BCCIP, CLTA, IKZF1, CHAF1B, ZFYVE26, RASSF2, CCND2, CCND1, RASSF4, RUVBL1, RPS6KA1, KIF13A, ENSA, PIM1, ZNF207, PIM3, MAP3K8, PIM2, NBN, TXNL4A, TP63, APPL1, HELLS, NUDC, CSNK2A1, ANAPC7, DYNLT3, NSUN2, PRKCD, LIG3, KLHL42, TFDP1, PSME3, CINP, ERH, ARHGEF2, MAPRE1, TP53, KHDRBS1, RALA, SEH1L, TSG101, ANAPC16, SRC, PRCC, GNAI3, NEDD9, ARL2, ARPP19, CDC42, SYCE2, NPAT, ASUN, TP53BP2, E2F3, SNX9, CLSPN, PAK4, GADD45GIP1, NEK9, CDKN2B, CDKN2A, NEK6, NDE1, SIAH2, RCC2, MLH1, RAB11A, MAPK13, ZC3HC1, CYLD, NEDD1, RAD50, CDK4, PPP2R2D, CDK2, CDK2AP1, INSM1, MNAT1, RAN	0.01	0.01
UP_KEYWORDS	Cell division	44	2.22	RALA, ANKLE2, SEH1L, TSG101, ANAPC16, CETN2, CCDC124, CLTC, GNAI3, NEDD9, CLTA, ARPP19, CDC42, SYCE2, ZFYVE26, CCND2, CCND1, ASUN, RUVBL1, KIF13A, ENSA, ZNF207, SNX9, TXNL4A, NEK9, HELLS, NUDC, ANAPC7, DYNLT3, NEK6, NDE1, NSUN2, RCC2, LIG3, KLHL42, ZC3HC1, NEDD1, CDK4, CINP, PPP2R2D, CDK2, ARHGEF2, MAPRE1, RAN	0.46	0.41
UP_KEYWORDS	Mitosis	31	1.56	ANKLE2, SEH1L, ANAPC16, CETN2, CLTC, NEDD9, CLTA, ARPP19, ASUN, RUVBL1, ENSA, ZNF207, SNX9, TXNL4A, NEK9, HELLS, NUDC, ANAPC7, DYNLT3, NEK6, NDE1, NSUN2, RCC2, KLHL42, ZC3HC1, NEDD1, PPP2R2D, CDK2, ARHGEF2, MAPRE1, RAN	0.48	0.42
Annotation Cluster 39	Enrichment Score: 1.4049479776863307					
Category	Term	Count	%	Genes	Benjamini	FDR
GOTERM_MF_DIRECT	GO:0005164~tumor necrosis factor receptor binding	11	0.55	TRAF4, TNFSF14, TRAF3, STAT1, CD70, TNFSF4, TRADD, LTA, TRAF2, TRAF1, TNF	0.03	0.03
GOTERM_MF_DIRECT	GO:0031996~thioesterase binding	7	0.35	CDC42, TRAF4, TRAF3, TRAF2, CALM3, TRAF1, RAC1	0.10	0.09
Annotation Cluster 41	Enrichment Score: 1.3486146457569577					

Category	Term	Count	%	Genes	Benjamini	FDR
BIOCARTA	**h_tnfr2Pathway:TNFR2 Signaling Pathway**	9	0.45	NFKBIA, TRAF3, LTA, TNFAIP3, TRAF2, TRAF1, TNFRSF1B, TANK, NFKB1	0.35	0.35
Annotation Cluster 42	**Enrichment Score: 1.341177604232485**					
Category	**Term**	**Count**	**%**	**Genes**	**Benjamini**	**FDR**
GOTERM_BP_DIRECT	**GO:2000811~negative regulation of anoikis**	8	0.40	TLE1, PIK3CA, SRC, PTRH2, CAV1, BCL2, BCL2L1, MCL1	0.11	0.10
GOTERM_BP_DIRECT	**GO:0008630~intrinsic apoptotic signaling pathway in response to DNA damage**	12	0.61	BCL2A1, PRKDC, BCL2, HTRA2, MLH1, TNFRSF1B, CRIP1, TNF, IKBKE, PML, BCL2L1, MCL1	0.39	0.39
GOTERM_BP_DIRECT	**GO:0008637~apoptotic mitochondrial changes**	7	0.35	AIFM2, CDKN2A, PPIF, BID, HK2, BCL2L1, MCL1	0.44	0.44
Annotation Cluster 44	**Enrichment Score: 1.3257081957623664**					
Category	**Term**	**Count**	**%**	**Genes**	**Benjamini**	**FDR**
GOTERM_CC_DIRECT	**GO:0022624~proteasome accessory complex**	7	0.35	PSMD12, PSMD11, PSMD14, PSMC4, PSMC2, PSMD3, PSMD1	0.09	0.08
GOTERM_CC_DIRECT	**GO:0008541~proteasome regulatory particle, lid subcomplex**	5	0.25	PSMD12, PSMD11, PSMD14, SHFM1, PSMD3	0.09	0.09
Annotation Cluster 45	**Enrichment Score: 1.315336766320866**					
Category	**Term**	**Count**	**%**	**Genes**	**Benjamini**	**FDR**
UP_KEYWORDS	**Cell shape**	6	0.30	CDC42SE1, CYFIP1, CDC42EP5, CDC42EP3, CDC42EP2, MYH9	0.34	0.30
Annotation Cluster 46	**Enrichment Score: 1.2990599937024225**					
Category	**Term**	**Count**	**%**	**Genes**	**Benjamini**	**FDR**

BIOCARTA	**h_tnfr2Pathway:TNFR2 Signaling Pathway**	9	0.45	NFKBIA, TRAF3, LTA, TNFAIP3, TRAF2, TRAF1, TNFRSF1B, TANK, NFKB1	0.35	0.35
Annotation Cluster 47	**Enrichment Score: 1.295967412153615**					
Category	**Term**	**Count**	**%**	**Genes**	**Benjamini**	**FDR**
GOTERM_BP_DIRECT	**GO:0035338~long-chain fatty-acyl-CoA biosynthetic process**	11	0.55	ELOVL1, ACSL1, SCD, FASN, PPT1, THEM5, ACOT2, THEM4, ACSL4, ACOT4, ACACA	0.43	0.43
Annotation Cluster 52	**Enrichment Score: 1.2338459916976263**					
Category	**Term**	**Count**	**%**	**Genes**	**Benjamini**	**FDR**
GOTERM_MF_DIRECT	**GO:0005164~tumor necrosis factor receptor binding**	11	0.55	TRAF4, TNFSF14, TRAF3, STAT1, CD70, TNFSF4, TRADD, LTA, TRAF2, TRAF1, TNF	0.03	0.03
Annotation Cluster 53	**Enrichment Score: 1.1944566676434354**					
Category	**Term**	**Count**	**%**	**Genes**	**Benjamini**	**FDR**
KEGG_PATHWAY	**hsa00010:Glycolysis / Gluconeogenesis**	16	0.81	TPI1, PGAM1, AKR1A1, ENO1, HK2, LDHB, LDHA, G6PC3, PKM, ALDH2, ALDH1B1, PGK1, PGM2, DLD, PFKM, PCK2	0.07	0.06
UP_KEYWORDS	**Glycolysis**	8	0.40	PKM, TPI1, PGAM1, PGK1, ENO1, PFKM, HK2, DHTKD1	0.14	0.12
KEGG_PATHWAY	**hsa01230:Biosynthesis of amino acids**	15	0.76	TPI1, RPEL1, SHMT2, PGAM1, GOT2, PYCR1, ENO1, RPIA, PKM, MAT2A, PSAT1, PGK1, ALDH18A1, BCAT1, PFKM	0.19	0.16
KEGG_PATHWAY	**hsa01200:Carbon metabolism**	18	0.91	FH, H6PD, TPI1, RPEL1, SHMT2, MDH2, PGAM1, GOT2, ENO1, PGD, HK2, RPIA, PKM, PSAT1, PGK1, PGLS, DLD, PFKM	0.55	0.46
Annotation Cluster 54	**Enrichment Score: 1.1794535070379681**					
Category	**Term**	**Count**	**%**	**Genes**	**Benjamini**	**FDR**
UP_KEYWORDS	**S-adenosyl-L-methionine**	24	1.21	PRMT6, TRMT10C, PRMT2, NSUN4, METTL1, PRMT1, SMYD5, NSUN2, TYW3, DNMT3A, DOT1L, CDKAL1, TRMT2A, COMT, METTL21A, EMG1, TRMT5, CARM1, METTL10, LCMT2, TRMT61A, TRDMT1, TRMT61B, EZH2	0.26	0.23

UP_KEYWORDS	**Methyltransferase**	25	1.26	SHMT2, SMYD5, DOT1L, TRMT2A, ECE2, METTL21A, COMT, EMG1, METTL10, LCMT2, TRDMT1, PRMT6, TRMT10C, PRMT2, NSUN4, METTL1, PRMT1, TYW3, NSUN2, DNMT3A, CARM1, TRMT5, TRMT61A, TRMT61B, EZH2	0.35	0.31
Annotation Cluster 56	**Enrichment Score: 1.1595623764185663**					
Category	**Term**	**Count**	**%**	**Genes**	**Benjamini**	**FDR**
GOTERM_BP_DIRECT	**GO:0070911~global genome nucleotide-excision repair**	10	0.50	UBB, PARP1, SUMO3, CETN2, SUMO2, UBE2N, GTF2H3, RPS27A, RAD23B, GTF2H5	0.26	0.26
Annotation Cluster 57	**Enrichment Score: 1.128203662875693**					
Category	**Term**	**Count**	**%**	**Genes**	**Benjamini**	**FDR**
UP_KEYWORDS	**mRNA transport**	24	1.21	EIF5A, CHTOP, SEC13, SEH1L, NCBP2, POLDIP3, MVP, ALYREF, SRSF1, UPF3B, NUP153, NUTF2, LRPPRC, IWS1, ZFP36L1, NUP93, MYO1C, XPO1, NUP62, NUP35, SRSF3, IGF2BP3, HNRNPA1, AGFG1	0.00	0.00
UP_KEYWORDS	**Translocation**	15	0.76	EIF5A, SEC13, SEH1L, MVP, TIMM23, NUP153, NUTF2, TOMM22, SEC61A2, NUP93, MYO1C, ZMAT3, NUP62, NUP35, SEC61B	0.14	0.12
UP_KEYWORDS	**Nuclear pore complex**	10	0.50	EIF5A, NUP93, SEC13, MYO1C, SEH1L, MVP, NUP62, NUP35, NUP153, NUTF2	0.22	0.19
Annotation Cluster 58	**Enrichment Score: 1.128149589016034**					
Category	**Term**	**Count**	**%**	**Genes**	**Benjamini**	**FDR**
UP_KEYWORDS	**NAD**	25	1.26	H6PD, AHCY, MSMO1, HSD17B10, CYB5R2, LDHB, LDHA, NSDHL, ALDH2, ALDH1B1, SDR42E1, PARP1, MDH2, SIRT6, PARP14, PARP12, ALDH4A1, UEVLD, UGDH, MTHFD2, FASN, IMPDH2, DLD, BLVRA, GLYR1	0.20	0.17
Annotation Cluster 59	**Enrichment Score: 1.1082504029985456**					
Category	**Term**	**Count**	**%**	**Genes**	**Benjamini**	**FDR**
UP_KEYWORDS	**SH2 domain**	17	0.86	BLK, STAT5A, BCAR3, STAT1, SRC, SH2D3A, PTPN11, TYK2, SOCS2, SOCS1, NCK2, STAP2, CSK, STAT6, SH2B3, JAK3, FRK	0.22	0.20

Annotation Cluster 60	Enrichment Score: 1.0910837278359273					
Category	**Term**	**Count**	**%**	**Genes**	**Benjamini**	**FDR**
GOTERM_BP_DIRECT	GO:1902042~negative regulation of extrinsic apoptotic signaling pathway via death domain receptors	10	0.50	TRADD, PEA15, FAS, TNFAIP3, TNFRSF10B, TRAF2, CFLAR, ARHGEF2, RFFL, ICAM1	0.31	0.31
Annotation Cluster 62	Enrichment Score: 1.0800034797673121					
Category	**Term**	**Count**	**%**	**Genes**	**Benjamini**	**FDR**
GOTERM_CC_DIRECT	GO:0005885~Arp2/3 protein complex	6	0.30	ACTR3, ACTR2, ARPC2, ARPC4, ARPC5, ACTR3B	0.08	0.08
Annotation Cluster 63	Enrichment Score: 1.0645528096026518					
Category	**Term**	**Count**	**%**	**Genes**	**Benjamini**	**FDR**
KEGG_PATHWAY	hsa03450:Non-homologous end-joining	5	0.25	XRCC6, FEN1, RAD50, XRCC5, PRKDC	0.24	0.20
Annotation Cluster 64	Enrichment Score: 1.0630203681798411					
Category	**Term**	**Count**	**%**	**Genes**	**Benjamini**	**FDR**
UP_KEYWORDS	Threonine protease	6	0.30	PSMA4, PSMB5, PSMA1, PSMB2, PSMB1, PSMA7	0.20	0.17
GOTERM_CC_DIRECT	GO:0005839~proteasome core complex	6	0.30	PSMA4, PSMB5, PSMA1, PSMB2, PSMB1, PSMA7	0.47	0.45
Annotation Cluster 65	Enrichment Score: 1.0618894901227613					
Category	**Term**	**Count**	**%**	**Genes**	**Benjamini**	**FDR**

INTERPRO	**IPR020568:Ribosomal protein S5 domain 2-type fold**	12	0.61	EFTUD2, EXOSC5, GFM1, HSP90AA1, EXOSC4, HSP90B2P, PNPT1, HSP90AB1, LONP2, RPS2, MLH1, HSP90B1	0.41	0.41
Annotation Cluster 66	**Enrichment Score: 1.0568980699617907**					
Category	**Term**	**Count**	**%**	**Genes**	**Benjamini**	**FDR**
UP_KEYWORDS	**Flavoprotein**	18	0.91	GCDH, ACADVL, STEAP3, ACAD9, MICAL3, ETFDH, DHCR24, ETFA, SQRDL, CYB5R2, IL4I1, SQLE, POR, AIFM2, RFK, PNPO, DLD, PAOX	0.28	0.25
UP_KEYWORDS	**FAD**	16	0.81	GCDH, ACADVL, STEAP3, ACAD9, MICAL3, ETFDH, DHCR24, ETFA, SQRDL, CYB5R2, IL4I1, SQLE, POR, AIFM2, DLD, PAOX	0.35	0.31
Annotation Cluster 68	**Enrichment Score: 1.0370554549537905**					
Category	**Term**	**Count**	**%**	**Genes**	**Benjamini**	**FDR**
UP_KEYWORDS	**SH3-binding**	12	0.61	VASP, KHDRBS1, FUT8, CNTNAP1, SH3BP1, SH3KBP1, TP53BP2, RAPGEF1, SIRPA, ELMO2, ARHGAP17, EPS15	0.18	0.16
Annotation Cluster 70	**Enrichment Score: 1.0188668252887185**					
Category	**Term**	**Count**	**%**	**Genes**	**Benjamini**	**FDR**
GOTERM_BP_DIRECT	**GO:0006913~nucleocytoplasmic transport**	10	0.50	EIF5A, NPM1, SET, MYBBP1A, ANP32A, ANP32E, ANP32C, NSRP1, FBXO22, RAN	0.08	0.08
Annotation Cluster 71	**Enrichment Score: 1.0180232713363642**					
Category	**Term**	**Count**	**%**	**Genes**	**Benjamini**	**FDR**
KEGG_PATHWAY	**hsa03060:Protein export**	7	0.35	SEC61A2, SRP72, HSPA5, SEC61B, SRP14, SRP9, SEC11C	0.21	0.17
UP_KEYWORDS	**Signal recognition particle**	3	0.15	SRP72, SRP14, SRP9	0.40	0.35
Annotation Cluster 72	**Enrichment Score: 0.9983305188966244**					
Category	**Term**	**Count**	**%**	**Genes**	**Benjamini**	**FDR**

GOTERM_MF_DIRECT	**GO:0015186~L-glutamine transmembrane transporter activity**	4	0.20	SLC38A1, SLC38A7, SLC1A4, SLC1A5	0.34	0.34
GOTERM_BP_DIRECT	**GO:0006868~glutamine transport**	4	0.20	SLC38A1, SLC38A7, SLC1A4, SLC1A5	0.43	0.43
Annotation Cluster 74	**Enrichment Score: 0.9635861669841483**					
Category	**Term**	**Count**	**%**	**Genes**	**Benjamini**	**FDR**
UP_KEYWORDS	**Annexin**	5	0.25	ANXA2, ANXA5, ANXA6, ANXA7, ANXA2P2	0.20	0.18
UP_KEYWORDS	**Calcium/phospholipid-binding**	5	0.25	ANXA2, ANXA5, ANXA6, ANXA7, ANXA2P2	0.24	0.21
Annotation Cluster 75	**Enrichment Score: 0.9514427687046799**					
Category	**Term**	**Count**	**%**	**Genes**	**Benjamini**	**FDR**
BIOCARTA	**h_npcPathway:Mechanism of Protein Import into the Nucleus**	7	0.35	IL4I1, NUP62, NUP153, NUTF2, RANGAP1, RAN, SNHG3	0.47	0.47
Annotation Cluster 76	**Enrichment Score: 0.950280043875719**					
Category	**Term**	**Count**	**%**	**Genes**	**Benjamini**	**FDR**
GOTERM_BP_DIRECT	**GO:0035338~long-chain fatty-acyl-CoA biosynthetic process**	11	0.55	ELOVL1, ACSL1, SCD, FASN, PPT1, THEM5, ACOT2, THEM4, ACSL4, ACOT4, ACACA	0.43	0.43
KEGG_PATHWAY	**hsa00061:Fatty acid biosynthesis**	4	0.20	ACSL1, FASN, ACSL4, ACACA	0.55	0.46
Annotation Cluster 77	**Enrichment Score: 0.9311447229927665**					
Category	**Term**	**Count**	**%**	**Genes**	**Benjamini**	**FDR**
UP_KEYWORDS	**One-carbon metabolism**	6	0.30	AHCY, MAT2A, MTHFD1L, SHMT2, MTHFD2, FPGS	0.11	0.10

KEGG_PATHWAY	**hsa00670:One carbon pool by folate**	5	0.25	ATIC, MTHFD1L, SHMT2, MTHFD2, GART	0.55	0.46
Annotation Cluster 80	**Enrichment Score: 0.8964367227386555**					
Category	**Term**	**Count**	**%**	**Genes**	**Benjamini**	**FDR**
UP_SEQ_FEATURE	**domain:Leucine-zipper**	22	1.11	HOMEZ, XBP1, JUN, BATF3, XRCC5, PRKDC, API5, CEBPG, TFEB, FOXP4, SREBF2, BATF, FOXP1, RELB, MYC, MYB, GEMIN4, E2F3, ATF5, IKBKE, JUNB, NFE2L1	0.43	0.43
Annotation Cluster 81	**Enrichment Score: 0.8961961110575125**					
Category	**Term**	**Count**	**%**	**Genes**	**Benjamini**	**FDR**
KEGG_PATHWAY	**hsa04115:p53 signaling pathway**	15	0.76	CDKN1A, STEAP3, CD82, CDKN2A, PTEN, TP53I3, CCND2, CCND1, ZMAT3, CDK4, CDK2, FAS, CYCS, BID, TP53	0.13	0.11
GOTERM_CC_DIRECT	**GO:0000307~cyclin-dependent protein kinase holoenzyme complex**	5	0.25	CDKN1A, CCND2, CCND1, CDK4, CDK2	0.48	0.46
KEGG_PATHWAY	**hsa04110:Cell cycle**	19	0.96	YWHAE, ZBTB17, CDKN1A, CDKN2B, ANAPC7, CDKN2A, YWHAB, PRKDC, TFDP1, CCND2, ESPL1, CCND1, YWHAQ, CDK4, MYC, CDK2, E2F3, TP53, YWHAG	0.57	0.47
Annotation Cluster 90	**Enrichment Score: 0.851988787120894**					
Category	**Term**	**Count**	**%**	**Genes**	**Benjamini**	**FDR**
UP_KEYWORDS	**TPR repeat**	23	1.16	ANAPC7, ST13, NCF2, PRKDC, TOMM34, TRANK1, VPS13A, TTC1, TTC7A, SMG7, TTC27, RPAP3, TTC39A, PPP5C, KLC2, ZC3H7A, SRP72, ZC3H7B, TRAPPC12, NAA15, LONRF1, PPID, FKBP5	0.28	0.25
Annotation Cluster 94	**Enrichment Score: 0.806022155844504**					
Category	**Term**	**Count**	**%**	**Genes**	**Benjamini**	**FDR**
GOTERM_CC_DIRECT	**GO:0005874~microtubule**	42	2.12	MACF1, DYNC1I2, CNP, DCTN1, WDR43, TUBA1C, TUBA1B, KLC2, MTA1, TUBA1A, KIF3B, KIF13A, ZNF207, MAP6, KIF1C, KIF21B, MAP4, DNM1L, CCT7, CCDC50, SYBU, CCT5, CCT4, CCT3, NUDC, DYNLT3, NEK6, NDE1, RCC2, TUBB, TUBB4B, LRPPRC, CCT6A, CAMSAP3, CYLD, TUBB2B, TUBB2A, TTLL4, KIF26B, ARHGEF2, MAPRE1, EIF3A	0.40	0.38

Annotation Cluster 96	Enrichment Score: 0.7769479099774916					
Category	**Term**	**Count**	**%**	**Genes**	**Benjamini**	**FDR**
KEGG_PATHWAY	hsa03450:Non-homologous end-joining	5	0.25	XRCC6, FEN1, RAD50, XRCC5, PRKDC	0.24	0.20
Annotation Cluster 98	Enrichment Score: 0.7703258208165565					
Category	**Term**	**Count**	**%**	**Genes**	**Benjamini**	**FDR**
KEGG_PATHWAY	hsa04915:Estrogen signaling pathway	18	0.91	HSPA8, JUN, HSP90AA1, HSP90AB1, SRC, PRKCD, GNAI3, ITPR1, ADCY3, PIK3CD, ESR1, HSP90B1, PLCB3, NRAS, PIK3CA, KRAS, CALM3, FKBP5	0.29	0.24
KEGG_PATHWAY	hsa04912:GnRH signaling pathway	16	0.81	JUN, SRC, PRKCD, PLA2G4C, ITPR1, ADCY3, ELK1, MAPK13, PLD2, CDC42, MAPK11, PLCB3, NRAS, PTK2B, KRAS, CALM3	0.40	0.34
Annotation Cluster 103	Enrichment Score: 0.7374300957243186					
Category	**Term**	**Count**	**%**	**Genes**	**Benjamini**	**FDR**
KEGG_PATHWAY	hsa04660:T cell receptor signaling pathway	20	1.01	IL10, JUN, CSF2, PIK3CD, TNF, NFKB1, MAPK13, CDC42, NFKBIA, MAPK11, PAK1, PPP3CB, NRAS, PIK3CA, CDK4, NCK2, KRAS, MAP3K8, NFKBIE, PAK4	0.13	0.11
KEGG_PATHWAY	hsa04370:VEGF signaling pathway	12	0.61	CDC42, MAPK11, PPP3CB, NRAS, PIK3CA, SRC, SPHK1, PLA2G4C, PIK3CD, KRAS, RAC1, MAPK13	0.36	0.30
KEGG_PATHWAY	hsa04662:B cell receptor signaling pathway	12	0.61	NFKBIA, CR2, PPP3CB, NRAS, JUN, PIK3CA, PIK3CD, KRAS, RAC1, NFKBIE, NFKB1, RASGRP3	0.55	0.46
Annotation Cluster 109	Enrichment Score: 0.703326823755664					
Category	**Term**	**Count**	**%**	**Genes**	**Benjamini**	**FDR**
KEGG_PATHWAY	hsa00604:Glycosphingolipid biosynthesis - ganglio series	5	0.25	GLB1, ST3GAL5, B4GALNT1, ST3GAL1, ST3GAL2	0.33	0.27
Annotation Cluster 110	Enrichment Score: 0.69402331082437					
Category	**Term**	**Count**	**%**	**Genes**	**Benjamini**	**FDR**

UP_KEYWORDS	**Electron transport**	15	0.76	CYB5B, NDUFB9, CYB5A, ETFDH, CYBRD1, ETFA, TXN, HIGD1A, FDX1L, HIGD2A, NDUFS6, UQCRFS1, CYCS, CYC1, CYB561	0.47	0.41
Annotation Cluster 119	**Enrichment Score: 0.6328122055208907**					
Category	**Term**	**Count**	**%**	**Genes**	**Benjamini**	**FDR**
GOTERM_BP_DIRECT	**GO:0015908~fatty acid transport**	6	0.30	ACSL1, GOT2, ACSL4, PPARA, SLC27A4, MFSD2A	0.31	0.31
Annotation Cluster 121	**Enrichment Score: 0.6061715545259819**					
Category	**Term**	**Count**	**%**	**Genes**	**Benjamini**	**FDR**
UP_KEYWORDS	**Redox-active center**	10	0.50	PRDX3, VKORC1, PDIA3, PRDX4, PRDX1, TXN, FAM213A, DLD, TXNDC17, PDIA4	0.20	0.18
Annotation Cluster 129	**Enrichment Score: 0.5734602667191876**					
Category	**Term**	**Count**	**%**	**Genes**	**Benjamini**	**FDR**
GOTERM_CC_DIRECT	**GO:0031234~extrinsic component of cytoplasmic side of plasma membrane**	13	0.66	BLK, SRC, TYK2, CYLD, RGS1, S100A6, PTK2B, CSK, SNX9, KRAS, JAK3, FRK, CYTH1	0.39	0.37
Annotation Cluster 137	**Enrichment Score: 0.5406498980946017**					
Category	**Term**	**Count**	**%**	**Genes**	**Benjamini**	**FDR**
KEGG_PATHWAY	**hsa00330:Arginine and proline metabolism**	10	0.50	ALDH4A1, ALDH2, ALDH1B1, GOT2, SMS, PYCR1, CKB, ALDH18A1, SRM, AGMAT	0.43	0.36
Annotation Cluster 141	**Enrichment Score: 0.5300789591651532**					
Category	**Term**	**Count**	**%**	**Genes**	**Benjamini**	**FDR**
UP_KEYWORDS	**Cyclosporin**	3	0.15	PPIF, PPIA, PPID	0.48	0.43

UP_KEYWORDS	**Rotamase**	7	0.35	FKBP1A, PPIL1, FKBP2, PPIF, PPIA, PPID, FKBP5	0.48	0.43
Annotation Cluster 142	**Enrichment Score: 0.527742067957745**					
Category	**Term**	**Count**	**%**	**Genes**	**Benjamini**	**FDR**
UP_KEYWORDS	**Rotamase**	7	0.35	FKBP1A, PPIL1, FKBP2, PPIF, PPIA, PPID, FKBP5	0.48	0.43
Annotation Cluster 149	**Enrichment Score: 0.47231177905818716**					
Category	**Term**	**Count**	**%**	**Genes**	**Benjamini**	**FDR**
KEGG_PATHWAY	**hsa00512:Mucin type O-Glycan biosynthesis**	7	0.35	GALNT11, GALNT16, GALNT2, ST3GAL1, GALNT10, ST3GAL2, B4GALT5	0.49	0.40
Annotation Cluster 151	**Enrichment Score: 0.45685464120778946**					
Category	**Term**	**Count**	**%**	**Genes**	**Benjamini**	**FDR**
UP_KEYWORDS	**Transcription**	243	12.26	ZNF296, EHF, SPI1, MAML2, GFI1, ZNF292, IKZF1, ENO1, RBPJ, GABPB1, C14ORF166, ELK1, C14ORF169, IKZF4, ELK3, SPIB, MYC, ZMIZ2, SPATA24, MYB, JUNB, TP63, MED1, MEF2C, SMARCC1, CSNK2A1, ZNF282, ZNF281, HNF1B, RUNX3, SND1, HOXB9, ZNF717, SUB1, RFX5, VOPP1, TFAM, SRFBP1, ZNF710, ATF5, VPS25, TP53, ZNF154, CASZ1, ANP32A, AIRE, ZNF22, TXN, ZBTB5, HIVEP1, HIVEP3, NRBF2, ZNF267, STAT5A, BTF3, JUN, XBP1, XRCC6, XRCC5, ZNF260, IRF2BP2, SNF8, MINA, PARP14, ELL2, SMARCA4, HNRNPK, TRIP6, ZNF135, EZH2, GMEB1, ELL, ADIRF, MED19, LITAF, CHAF1B, MED14, C1QBP, PRMT6, HELLS, BATF3, PARP1, NCOA5, TFEB, COMMD1, BAZ1A, PAX5, PPRC1, CBFA2T3, SREBF2, SUPT3H, COMMD5, MED22, NR5A2, AEBP2, MDFIC, RARA, ZNF239, ZNF780B, PPARA, FOXC1, ZNF593, NFIX, NR1I2, ARNTL2, FSTL3, RELB, HIRA, TCEAL3, PLAGL1, TWISTNB, TCEB3, PLAGL2, STAT6, TCEB1, HSF5, TAF9B, CDKN2A, STAT1, MCRS1, GTF2H3, ELP6, GTF2H5, LRPPRC, BATF, ZNF33B, NR6A1, ZNF70, MYBBP1A, NFIC, APEX1, CRTC2, TTF2, ETS1, CHCHD3, CCND1, RUVBL1, ZNF563, SLC30A9, SUPT16H, TLE1, KDM2B, ARID5A, ZBTB32, POU3F1, FOXP4, ILF2, SAP30, FOXP1, EEF1A1, MORF4L1, TBL1XR1, ADNP, HOMEZ, KHDRBS1, TCF7, TAF5L, NPAT, ATXN1, ZNF788, ZNF544, ZBTB17, ZNF660, HSPA8, CBX6, ZFHX3, CHTOP, POU2F1, ZFHX2, DENND4A, NONO, HMGA1, ZBTB10, ESR1, NFKB1, NFKB2, COPRS, SP2, LHX2, CNOT11, BHLHE40, TAF4B, MNAT1, NFE2L1, ZSCAN2, ZNF770, YBX1, NFKBIZ, WDR5, MYBL2, NKX3-1, PELP1, MYOCD, TGIF2, EED, MKL1, ETV3, TRAF7, SFPQ, ETV3L, TFDP1, IRF4, POLR1B, ZNF878, IRF5, ZNF512, L3MBTL4, NFAT5, GTF3C4, GTF3C6, ZBTB46, CEBPG, TAF9, DDX21, HDAC9, IWS1, MTA1, PUF60, ZNF629, ZNF506, BAHD1, ATOH8, BEND3, E2F3, ZNF865, PCBD1, ASCC3, JAZF1, TCFL5, ATF7IP, SSRP1, PML, MAPK13, ASXL1, KLF7, MAPK11, KLF6, TNIP2, CARM1, ESF1, POLR3H, INSM1, NAA15	0.30	0.27
UP_KEYWORDS	**Transcription regulation**	236	11.91	ZNF296, EHF, SPI1, MAML2, GFI1, ZNF292, IKZF1, ENO1, RBPJ, GABPB1, C14ORF166, ELK1, C14ORF169, IKZF4, ELK3, SPIB, MYC, ZMIZ2, SPATA24, MYB, JUNB, TP63, MED1, MEF2C, SMARCC1, CSNK2A1, ZNF282, ZNF281, HNF1B, RUNX3, SND1, HOXB9, ZNF717, SUB1, RFX5, VOPP1, TFAM,	0.33	0.29

				SRFBP1, ZNF710, ATF5, VPS25, TP53, ZNF154, CASZ1, ANP32A, AIRE, ZNF22, TXN, ZBTB5, HIVEP1, HIVEP3, NRBF2, ZNF267, STAT5A, BTF3, JUN, XBP1, XRCC6, XRCC5, ZNF260, IRF2BP2, SNF8, MINA, PARP14, ELL2, SMARCA4, HNRNPK, TRIP6, ZNF135, EZH2, GMEB1, ELL, ADIRF, MED19, LITAF, CHAF1B, MED14, C1QBP, PRMT6, HELLS, BATF3, PARP1, NCOA5, TFEB, COMMD1, BAZ1A, PAX5, PPRC1, CBFA2T3, SREBF2, SUPT3H, COMMD5, MED22, NR5A2, AEBP2, MDFIC, RARA, ZNF239, ZNF780B, PPARA, FOXC1, ZNF593, NFIX, NR1I2, ARNTL2, FSTL3, RELB, HIRA, TCEAL3, PLAGL1, TCEB3, PLAGL2, STAT6, TCEB1, HSF5, TAF9B, CDKN2A, STAT1, MCRS1, GTF2H3, ELP6, GTF2H5, LRPPRC, BATF, ZNF33B, NR6A1, ZNF70, MYBBP1A, NFIC, APEX1, CRTC2, TTF2, ETS1, CHCHD3, CCND1, RUVBL1, ZNF563, SLC30A9, SUPT16H, TLE1, KDM2B, ARID5A, ZBTB32, POU3F1, FOXP4, ILF2, SAP30, FOXP1, EEF1A1, MORF4L1, TBL1XR1, ADNP, HOMEZ, KHDRBS1, TCF7, TAF5L, NPAT, ATXN1, ZNF788, ZNF544, ZBTB17, ZNF660, HSPA8, CBX6, ZFHX3, CHTOP, POU2F1, ZFHX2, DENND4A, NONO, HMGA1, ZBTB10, ESR1, NFKB1, NFKB2, COPRS, SP2, LHX2, CNOT11, BHLHE40, TAF4B, MNAT1, NFE2L1, ZSCAN2, ZNF770, YBX1, NFKBIZ, WDR5, MYBL2, NKX3-1, MYOCD, TGIF2, EED, MKL1, ETV3, TRAF7, SFPQ, ETV3L, TFDP1, IRF4, ZNF878, IRF5, ZNF512, L3MBTL4, NFAT5, ZBTB46, CEBPG, TAF9, HDAC9, IWS1, MTA1, PUF60, ZNF629, ZNF506, BAHD1, ATOH8, BEND3, E2F3, ZNF865, PCBD1, ASCC3, JAZF1, TCFL5, ATF7IP, SSRP1, PML, MAPK13, ASXL1, KLF7, MAPK11, KLF6, TNIP2, CARM1, ESF1, INSM1, NAA15		
Annotation Cluster 161	**Enrichment Score: 0.38761206591537545**					
Category	**Term**	**Count**	**%**	**Genes**	**Benjamini**	**FDR**
GOTERM_CC_DIRECT	**GO:0000776~kinetochore**	14	0.71	SEC13, SEH1L, ANAPC16, DCTN1, NDE1, DYNLT3, PINX1, RANGAP1, WDR43, RASSF2, XPO1, SUMO3, TRAPPC12, ZNF207	0.48	0.46

Appendix 11. The DAVID functional annotation categories (with FDR<0.5) of the 1986 statistically significantly down-regulated gene induced by CD40 stimulation in primary CLL cells at 24h time point

Annotation Cluster 1	Enrichment Score: 12.054096618540708					
Category	**Term**	**Count**	**%**	**Genes**	**Benjamini**	**FDR**
INTERPRO	**IPR001849:Pleckstrin homology domain**	66	3.48	ARHGAP9, ITK, DGKD, IRS1, PLEKHB1, IRS2, OSBPL11, SYNGAP1, MPRIP, AKT2, PSD3, AKT1, SBF1, PHLDA1, RALGPS2, GAB2, ARAP1, VAV1, BCR, ACAP3, TBC1D2, DOK2, ACAP2, ACAP1, DOK3, OBSCN, RASA3, PRKD3, RASA2, SPATA13, ARHGEF3, PRKD2, ARHGEF1, SOS1, SOS2, OSBP2, ARHGEF6, GRB7, SPTBN5, RASAL1, FGD1, FAM129C, ARHGAP12, FGD3, ABR, CYTH2, PLCG2, STAP1, SPTBN1, OSBPL8, AFAP1L2, OSBPL7, IQSEC2, OSBPL5, PLEKHA2, CDC42BPG, OSBPL3, PLCL2, DAB2IP, PLEKHA3, ARHGAP27, DEF6, PLEKHM1, PLCH2, PLCD1, SNTB2	0.00	0.00
INTERPRO	**IPR011993:Pleckstrin homology-like domain**	88	4.64	ARHGAP9, ITK, DGKD, PID1, IRS1, PLEKHB1, IRS2, ARHGEF10L, OSBPL11, CMIP, RGS3, SYNGAP1, MPRIP, AKT2, PSD3, AKT1, LDLRAP1, SBF1, PHLDA1, TNS3, RALGPS2, GAB2, ARAP1, VAV1, BCR, TBC1D1, ACAP3, TBC1D2, DOK2, ACAP2, ACAP1, DOK3, OBSCN, RASA3, PRKD3, RASA2, SPATA13, ARHGEF3, PRKD2, EVL, ARHGEF1, EZR, SOS1, PLCB2, WDFY4, SOS2, OSBP2, ARHGEF6, GRB7, SPTBN5, NUMBL, MTMR3, WBP2, EPB41, RASAL1, FGD1, FAM129C, ARHGAP12, FGD3, ABR, CYTH2, EPB41L3, PLCG2, STAP1, EPS8L2, APBB2, FAM43A, SPTBN1, OSBPL8, AFAP1L2, OSBPL7, IQSEC2, OSBPL5, PLEKHA2, HOMER2, CDC42BPG, OSBPL3, PLCL2, DAB2IP, PLEKHA3, ARHGAP27, DEF6, PLEKHM1, CCM2, PLCH2, PTPN4, PLCD1, SNTB2	0.00	0.00
SMART	**SM00233:PH**	66	3.48	ARHGAP9, ITK, DGKD, IRS1, PLEKHB1, IRS2, OSBPL11, SYNGAP1, MPRIP, AKT2, PSD3, AKT1, SBF1, PHLDA1, RALGPS2, GAB2, ARAP1, VAV1, BCR, ACAP3, TBC1D2, DOK2, ACAP2, ACAP1, DOK3, OBSCN, RASA3, PRKD3, RASA2, SPATA13, ARHGEF3, PRKD2, ARHGEF1, SOS1, SOS2, OSBP2, ARHGEF6, GRB7, SPTBN5, RASAL1, FGD1, FAM129C, ARHGAP12, FGD3, ABR, CYTH2, PLCG2, STAP1, SPTBN1, OSBPL8, AFAP1L2, OSBPL7, IQSEC2, OSBPL5, PLEKHA2, CDC42BPG, OSBPL3, PLCL2, DAB2IP, PLEKHA3, ARHGAP27, DEF6, PLEKHM1, PLCH2, PLCD1, SNTB2	0.00	0.00
UP_SEQ_FEATURE	**domain:PH**	58	3.06	ARHGAP9, ITK, DGKD, IRS1, PLEKHB1, IRS2, OSBPL11, CMIP, SYNGAP1, AKT2, PSD3, AKT1, SBF1, PHLDA1, RALGPS2, GAB2, VAV1, BCR, ACAP3, TBC1D2, DOK2, ACAP2, ACAP1, DOK3, OBSCN, RASA3, PRKD3, RASA2, SPATA13, ARHGEF3, PRKD2, ARHGEF1, SOS1, SOS2, OSBP2, ARHGEF6, GRB7, SPTBN5, RASAL1, ARHGAP12, ABR, CYTH2, PLCG2, STAP1, SPTBN1, OSBPL8, OSBPL7, IQSEC2, OSBPL5, CDC42BPG, OSBPL3, PLCL2, DAB2IP, PLEKHA3, ARHGAP27, DEF6, PLCH2, PLCD1	0.00	0.00
Annotation Cluster 2	**Enrichment Score: 8.66536030056708**					
Category	**Term**	**Count**	**%**	**Genes**	**Benjamini**	**FDR**
UP_KEYWORDS	**Zinc**	295	15.54	ZMYND8, EHMT2, JMJD1C, EHMT1, CBLB, ADARB2, IKZF3, IKZF5, ZFYVE28, RASSF1, PEG10, ANPEP, TNFSF10, ZNF721, TNS3, TRIM22, AGFG2, TRIM23, PRKCH, SP110, PRKCB, PRKCE, ZNF10, PRKCA, OVOL1, ZNF14, RUNX1, RNF125, PRKD3, ZC3H11A, TRIM14, PRKD2, ZNF831, FLYWCH1, ADPRM, ZNF395, ZNF273, MTMR3, TSHZ1, SP140, TSHZ2, ZBTB1, ZBTB4, ZBTB2, HELZ2, RNF213, ZNF704, ZNF703, ZNF823, AMZ2, ZNF821, ZNF700, ZBED6, ZNF266, ZSCAN18, BCL11A, TIPARP, SNAI3, SETDB2, NR1D2, NR1D1, ZNF34, PHC3, THAP11, RPS27, ZNF30, SLC2A4RG, PHF3, ITK, PHF2, COL18A1, ZCCHC11, GMEB2, ZNF250, ZNF490, PHF1, ZFAND2B, ZCCHC18, GLI1, LIMD1, PHF7, ING1, ZCCHC14, TRIM8, ING4, PPP3CA, ING2, TRIM7, ZMYM3, SMPD1, ZMYM6, REV3L, TIMP2, ZNF248, ZNF367,	0.00	0.00

				ZNF487, ZIK1, ZCCHC24, ZHX2, ZHX3, KCND1, SLC39A10, SIRT5, CBFA2T2, SIRT1, VAV1, SIRT2, NAALADL1, MBLAC2, NFX1, MMP17, RNF166, PPARD, ZNF595, SP100, RNASEL, ELOF1, PRICKLE1, FGD1, FGD3, RNF135, ADAM28, ZFP14, STAMBPL1, ZNF107, ZSWIM6, MBNL3, RNF130, ZNF224, ANKMY1, ZNF101, EGLN1, GIT2, NQO2, MAP3K1, MIB2, SYVN1, MYO9B, DEF8, RNF149, ZNF219, TTC3, YPEL1, TCEA2, ZNF699, ZNF335, YPEL5, YPEL4, ZNF575, YPEL3, ZNF211, YPEL2, LIMS1, ZNF331, DGKE, DGKD, DGKA, ZBTB20, PRDM2, NR3C1, NR3C2, RNF19A, ENPP2, ZNF569, EP300, SLC39A8, ZNF566, CA14, WHSC1L1, SLC39A3, ZNF441, RNF44, MORC3, LMO4, ZBTB38, ADAM10, SLC30A1, LMO7, RNF41, ACAP3, ACAP2, ACAP1, ZNF92, KAT6B, ZNF318, ZNF439, DPEP2, UTRN, CARS2, S100A8, KMT2E, ZNF671, ZNF791, MAZ, RASAL1, UBR2, RASGRP2, LPP, ZFP36L2, RAI1, MAN2A2, MAN2A1, DEAF1, ZKSCAN8, TMEM129, ZNF548, ZNF667, ZNF304, ANKZF1, BPTF, ZBTB18, ZNF540, SMAD3, ZBTB14, PHF10, PHF12, ZBTB11, NR4A2, GH1, SP4, MKRN1, ZFP64, PLEKHM1, PHF13, XAF1, ZNF654, ZCCHC2, ZNF652, PHF19, ZMYND15, RERE, RNF13, THRA, ZC3H3, AKAP8L, NGLY1, ZC3H6, SOBP, IRF2BPL, ALAD, TRPS1, GATAD1, WHSC1, TRIM65, UNKL, ADAMTS6, RBM5, KLF10, MSL2, ARAP1, KSR2, KLF16, RASA3, TRAF5, RASA2, ZNF516, ZMYND10, KDM7A, RNFT2, HDAC5, KDM3A, PDXK, TRIM52, UHRF2, RNF38, CXXC1, ZBTB44, CXXC5, ZBTB41, U2AF1L4, ZBTB40, HDAC7, CECR1, PDLIM1, RNF113A, ABLIM1, TNKS2, ZNF627, RNF39, ZNF862, USP20, RNF24, USP21, QPCTL, CDC42BPG, AMFR, LIMK2, KLF3, KLF2, REST, TRIM39, KLF9, ZNF615, TRIM38, ZNF853		
UP_KEYWORDS	**Zinc-finger**	233	12.28	ZMYND8, JMJD1C, CBLB, IKZF3, IKZF5, ZFYVE28, RASSF1, PEG10, ZNF721, TRIM22, AGFG2, TRIM23, PRKCH, SP110, PRKCB, PRKCE, ZNF10, PRKCA, OVOL1, ZNF14, RUNX1, RNF125, PRKD3, ZC3H11A, TRIM14, PRKD2, ZNF831, FLYWCH1, ZNF395, ZNF273, MTMR3, TSHZ1, SP140, TSHZ2, ZBTB1, ZBTB4, ZBTB2, HELZ2, RNF213, ZNF704, ZNF703, ZNF823, ZNF821, ZNF700, ZBED6, ZNF266, ZSCAN18, BCL11A, TIPARP, SNAI3, NR1D2, NR1D1, ZNF34, PHC3, THAP11, RPS27, ZNF30, SLC2A4RG, PHF3, ITK, PHF2, ZCCHC11, ZNF250, ZNF490, PHF1, ZFAND2B, ZCCHC18, GLI1, PHF7, ING1, ZCCHC14, TRIM8, ING4, ING2, TRIM7, ZMYM3, ZMYM6, REV3L, ZNF248, ZNF367, ZNF487, ZIK1, ZCCHC24, ZHX2, ZHX3, CBFA2T2, VAV1, NFX1, RNF166, PPARD, ZNF595, SP100, RNASEL, ELOF1, FGD1, FGD3, RNF135, ZFP14, ZNF107, ZSWIM6, MBNL3, RNF130, ZNF224, ANKMY1, ZNF101, EGLN1, GIT2, MAP3K1, MIB2, SYVN1, MYO9B, DEF8, RNF149, ZNF219, TTC3, TCEA2, ZNF699, ZNF335, ZNF575, ZNF211, ZNF331, DGKE, DGKD, DGKA, ZBTB20, PRDM2, NR3C1, NR3C2, RNF19A, ZNF569, EP300, ZNF566, WHSC1L1, ZNF441, RNF44, MORC3, ZBTB38, RNF41, ACAP3, ACAP2, ACAP1, ZNF92, KAT6B, ZNF318, ZNF439, UTRN, KMT2E, ZNF671, ZNF791, MAZ, RASAL1, UBR2, RASGRP2, ZFP36L2, RAI1, DEAF1, ZKSCAN8, TMEM129, ZNF548, ZNF667, ZNF304, ANKZF1, BPTF, ZBTB18, ZNF540, ZBTB14, PHF10, PHF12, ZBTB11, NR4A2, SP4, MKRN1, ZFP64, PLEKHM1, PHF13, XAF1, ZNF654, ZCCHC2, ZNF652, PHF19, ZMYND15, RERE, RNF13, THRA, ZC3H3, AKAP8L, ZC3H6, SOBP, IRF2BPL, TRPS1, GATAD1, WHSC1, TRIM65, UNKL, RBM5, KLF10, MSL2, ARAP1, KSR2, KLF16, RASA3, TRAF5, RASA2, ZNF516, ZMYND10, KDM7A, RNFT2, KDM3A, TRIM52, UHRF2, RNF38, CXXC1, ZBTB44, CXXC5, ZBTB41, U2AF1L4, ZBTB40, RNF113A, ZNF627, RNF39, ZNF862, USP20, RNF24, CDC42BPG, AMFR, KLF3, KLF2, REST, TRIM39, KLF9, ZNF615, TRIM38, ZNF853	0.00	0.00
UP_KEYWORDS	**Metal-binding**	410	21.60	EHMT2, EHMT1, ADARB2, ALKBH6, ZFYVE28, ALKBH5, ALKBH4, PRKCH, PRKCB, PRKCE, HPCAL1, CACNA2D2, ZNF10, PRKCA, HSPG2, ZNF14, RNF125, PRKD3, ZC3H11A, PRKD2, MPPE1, ADPRM, ZNF395, ZNF273, MTMR3, SAR1B, RNF213, HMOX1, AMZ2, ZSCAN18, ZNF266, LHPP, DMPK, TIPARP, SNAI3, NR1D2, NR1D1, ZNF34, PHC3, THAP11, EHD3, ZNF30, PLCH2, PHF3, PHF2, ITK, GMEB2, ZNF250, ZNF490, PHF1, PHF7, GLI1, ING1, TRIM8, ING4, ING2, TRIM7, IMPA2, SMPD1, TIMP2, ZNF248, ZNF367, ZNF487, ZIK1, HAVCR2, CNOT6L, KCND1, SIRT5, EPS15L1, SIRT1, SUMF2, SIRT2, PGM2L1, MBLAC2, MMP17, PLCB2, RNF166, PPARD, ZNF595, RNASEL, ELOF1, ADCY4, FGD1, RNF135, FGD3, ADAM28, ALOX5, CARNS1, ZNF107, ZSWIM6, MBNL3, P4HTM, RNF130, ZNF224, ZNF101, EGLN1, SYVN1, DEF8, RNF149, ZNF219, YPEL1, ZNF699, ZNF335, YPEL5, YPEL4, PLCD1, ZNF575,	0.00	0.00

				YPEL3, ZNF211, YPEL2, LIMS1, ZNF331, DGKE, DGKD, DGKA, GUCA1B, ZBTB20, SLC8A1, RNF19A, ZNF569, ZNF566, WHSC1L1, ZNF441, RNF44, ZBTB38, RNF41, ACAP3, ACAP2, OBSCN, ACAP1, STIM1, STIM2, KAT6B, ZNF439, ZNF318, TSSK6, TSSK3, UTRN, S100A8, TRABD2A, FTL, KMT2E, ZNF671, ZNF791, ARL3, MAZ, RASAL1, UBR2, AMDHD2, ZKSCAN8, ZNF548, ZNF667, ZNF304, NADK, ZBTB18, ZNF540, ZBTB14, TNK2, NEK7, ZBTB11, STK24, SP4, ZFP64, PLEKHM1, TPP1, CNOT8, XAF1, ZNF654, ZNF652, ITGB1, BMPR2, RNF13, ADPGK, ZC3H3, AKAP8L, ZC3H6, EFCAB12, ITGAL, ALAD, ITGB7, ATP7A, UNKL, TRIM65, ADAMTS6, MSL2, KSR2, NT5C3A, RRM2B, PAPD7, CTDSP2, TRAF5, ZNF516, DAGLB, RNFT2, HDAC5, TRIM52, UHRF2, LRP1, RNF38, CXXC1, PPM1K, ZBTB44, PPM1D, CXXC5, ZBTB41, HDAC7, ZBTB40, CECR1, ABLIM1, ZNF627, RNF39, ZNF862, RNF24, CDC42BPG, AMFR, KLF3, KLF2, TRIM39, KLF9, ZNF615, TRIM38, ZNF853, ISCA1, ACSM3, ZMYND8, ACSM1, GDE1, JMJD1C, CBLB, ANTXR2, IKZF3, IKZF5, RASSF1, ANPEP, PEG10, OGFOD2, TNFSF10, ZNF721, TNS3, TRIM22, AGFG2, TRIM23, SP110, OVOL1, RUNX1, CYP27A1, SIK3, TRIM14, FLYWCH1, ZNF831, PDE1B, TSHZ1, SP140, TSHZ2, ZBTB1, ZBTB4, ZBTB2, HELZ2, NUAK2, ZNF704, ARSK, ZNF703, ZNF823, ZNF821, ZNF700, ZBED6, RAB11FIP4, BCL11A, SETDB2, RPS27, CALM1, SLC2A4RG, COL18A1, ZCCHC11, ZFAND2B, ZCCHC18, LIMD1, ZCCHC14, PPP3CA, ZMYM3, NMRK1, ZMYM6, REV3L, IDS, SPTAN1, ZCCHC24, ZHX2, ZHX3, CBFA2T2, VAV1, NAALADL1, PITPNM1, NFX1, PITPNM2, SP100, GDPD1, GDPD3, PRICKLE1, NKD1, ZFP14, STAMBPL1, MGAT1, ANKMY1, MAP3K2, MAP3K3, GIT2, NQO2, MAP3K1, MIB2, MYO9B, PDP1, TTC3, TCEA2, ESYT1, CAPS, CIB1, PRDM2, NR3C1, NR3C2, GNPTAB, ENPP2, CAPN3, EP300, CA14, MORC3, LIG1, LMO4, ADAM10, CYBA, LMO7, ZNF92, DPEP2, CARS2, GNAZ, CABP4, RASGRP2, ACACB, LPP, ZFP36L2, RAI1, MAN2A2, MAN2A1, DEAF1, TMEM129, ANKZF1, BPTF, SMAD3, PHF10, PHF12, TRPV1, GNAO1, NR4A2, GH1, MKRN1, PHF13, ZCCHC2, PHF19, ZMYND15, RERE, B4GALT3, B4GALT1, MAST4, THRA, PRKCSH, NGLY1, ATP2A3, ATP2A1, SOBP, SGSH, IRF2BPL, TRPS1, CYP4V2, GATAD1, PDE4B, PDE4A, WHSC1, RBM5, KLF10, PLA2G4B, ARAP1, KLF16, RCN3, LATS2, RASA3, OAS2, RASA2, ZMYND10, MAN1B1, KDM7A, PDXK, KDM3A, NT5C2, U2AF1L4, GNA13, PDLIM1, RNF113A, TNKS2, MAN1C1, GALNT3, USP20, USP21, POLM, ATP13A1, QPCTL, LIMK2, ATP2B4, GALNS, REST, CHPT1, PDE7B		
GOTERM_MF_DIRECT	**GO:0046872~metal ion binding**	241	12.70	ACSM3, ACSM1, GDE1, JMJD1C, ADARB2, ANTXR2, IKZF3, IKZF5, ZFYVE28, ALKBH5, RASSF1, ALKBH4, TNFSF10, ZNF721, TNS3, AGFG2, PRKCH, PRKCE, CACNA2D2, ZNF10, PRKCA, OVOL1, ZNF14, RUNX1, PRKD3, ZC3H11A, PRKD2, ZNF831, FLYWCH1, ADPRM, ZNF395, ZNF273, MTMR3, PDE1B, SAR1B, TSHZ1, TSHZ2, ZBTB1, ZBTB4, ZBTB2, HELZ2, ZNF704, ARSK, ZNF703, ZNF823, HMOX1, ZNF821, ZNF700, ZBED6, ZNF266, ZSCAN18, DMPK, BCL11A, TIPARP, ADHFE1, ZNF34, ZNF30, SLC2A4RG, ITK, COL18A1, GMEB2, ZNF250, ZNF490, GLI1, NMRK1, REV3L, TIMP2, IDS, ZNF248, ZNF367, ZNF487, ZIK1, HAVCR2, ZHX2, ZHX3, KCND1, CNOT6L, CBFA2T2, SIRT1, PGM2L1, VAV1, SUMF2, NAALADL1, MBLAC2, PITPNM1, PITPNM2, ZNF595, RNASEL, ELOF1, GDPD1, ADCY4, GDPD3, FGD1, FGD3, ADAM28, ZFP14, STAMBPL1, CARNS1, ZNF107, MGAT1, MBNL3, ZNF224, ANKMY1, ZNF101, MAP3K2, GIT2, MAP3K3, NQO2, MIB2, MYO9B, DEF8, PDP1, ZNF219, YPEL1, ZNF699, ESYT1, ZNF335, YPEL5, YPEL4, ZNF575, YPEL3, ZNF211, YPEL2, ZNF331, DGKE, DGKD, ZBTB20, PRDM2, ENPP2, ZNF569, ZNF566, CA14, ZNF441, LIG1, ZBTB38, ADAM10, CYBA, ACAP3, ACAP2, ACAP1, OBSCN, ZNF92, ZNF439, DPEP2, CARS2, TRABD2A, ZNF671, GNAZ, ZNF791, ARL3, MAZ, RASAL1, ACACB, ZFP36L2, DEAF1, AMDHD2, ZKSCAN8, TMEM129, ZNF548, ZNF667, ZNF304, NADK, ANKZF1, ZBTB18, ZNF540, ZBTB14, TNK2, NEK7, TRPV1, ZBTB11, GNAO1, GH1, STK24, SP4, MKRN1, ZFP64, PLEKHM1, TPP1, CNOT8, ZNF654, ZNF652, ITGB1, ZMYND15, B4GALT3, BMPR2, ADPGK, ZC3H3, AKAP8L, NGLY1, ATP2A3, ATP2A1, ZC3H6, ITGAL, SOBP, IRF2BPL, SGSH, ALAD, TRPS1, PDE4B, PDE4A, ITGB7, KLF10, ARAP1, KSR2, KLF16, LATS2, PAPD7, RASA3, RRM2B, OAS2, CTDSP2, RASA2, ZNF516, ZMYND10, DAGLB, HDAC5, PPM1K, ZBTB44, PPM1D, NT5C2, ZBTB41, U2AF1L4, ZBTB40, HDAC7, GNA13, TNKS2,	0.03	0.03

				ZNF627, ZNF862, POLM, ATP13A1, USP21, ATP2B4, KLF3, KLF2, GALNS, REST, KLF9, ZNF615, CHPT1, ZNF853, PDE7B		
Annotation Cluster 3	**Enrichment Score: 5.344948459512079**					
Category	**Term**	**Count**	**%**	**Genes**	**Benjamini**	**FDR**
UP_KEYWORDS	**GTPase activation**	41	2.16	ARHGAP9, USP6NL, RGS14, FAM13B, NPRL2, LRRK2, ARHGAP18, RASAL1, ARHGAP6, SIPA1L3, ARHGAP4, ARHGAP12, ABR, RGS2, SIPA1L1, SYNGAP1, TBC1D10C, SRGAP3, TBC1D22A, RAP1GAP2, GIT2, DAB2IP, TBC1D9, MYO9B, ARHGAP27, ARAP1, BCR, TBC1D1, ACAP3, ACAP2, TBC1D2, ACAP1, RASA3, TBC1D20, RASA2, SGSM2, RAPGEF2, RIN3, ARHGEF1, DEPDC5, RIN2	0.00	0.00
GOTERM_MF_DIRECT	**GO:0005096~GTPase activator activity**	50	2.63	ARHGAP9, USP6NL, FAM13B, LRRK2, ARHGEF10L, ARHGAP6, SIPA1L3, ARHGAP4, RGS2, SIPA1L1, RGS3, SYNGAP1, TBC1D10C, TBC1D22A, AGFG2, AXIN1, TBC1D9, ARAP1, BCR, TBC1D1, ACAP3, TBC1D2, ACAP2, ACAP1, RABEP2, RASA3, TBC1D20, RASA2, RAPGEF2, RIN3, ARHGEF1, DEPDC5, SOS1, RIN2, ARHGEF6, RGS14, NPRL2, ARHGAP18, RASAL1, ARHGAP12, ABR, SRGAP3, RAP1GAP2, GIT2, DAB2IP, MYO9B, ARHGAP27, SGSM2, RUNDC1, GNB5	0.01	0.01
GOTERM_BP_DIRECT	**GO:0043547~positive regulation of GTPase activity**	83	4.37	ARHGAP9, ITGB1, FAM13B, DENND5B, IRS1, LRRK2, IRS2, ARHGEF10L, ARHGAP6, SIPA1L3, ARHGAP4, RCBTB2, RGS2, RGS3, SYNGAP1, PSD3, SBF1, SPTAN1, AGFG2, RALGPS2, AXIN1, ARAP1, VAV1, BCR, ACAP3, TBC1D2, ACAP2, ACAP1, OBSCN, RABEP2, RASA3, TBC1D20, AKAP9, RASA2, MADD, SPATA13, ARHGEF3, RAPGEF2, RIN3, ARHGEF1, DENND6B, DENND6A, DEPDC5, SOS1, RIN2, SOS2, RAPGEF3, ARHGEF6, SPTBN5, RGS14, NPRL2, ARHGAP18, RASAL1, RASGRP2, FGD1, ARHGAP12, FGD3, ABR, CYTH2, TBXA2R, CCL5, S1PR1, EPS8L2, SRGAP3, RALGDS, SPTBN1, RAP1GAP2, GIT2, SEMA4D, IQSEC2, DAB2IP, MYO9B, ARHGAP27, GNAO1, DNMBP, SGSM2, IL2RB, GNB5, RGL4, CALM1, RGL2, LIMS1, FGFR1	0.04	0.04
Annotation Cluster 4	**Enrichment Score: 4.558931193192469**					
Category	**Term**	**Count**	**%**	**Genes**	**Benjamini**	**FDR**
UP_KEYWORDS	**Kinase**	115	6.06	DGKE, DGKD, CERK, PANK1, DGKA, IGF1R, AKT2, PDK4, PDK3, AKT1, PIP4K2B, MAP3K9, SEPHS2, MAP2K3, PRKCH, PRKCB, DAPK2, PRKCE, LMTK2, DYRK1B, PRKCA, MAPK8IP3, BCR, DOK2, OBSCN, PRKD3, AKAP9, SIK3, TSSK6, PRKD2, ROR1, ULK1, TSSK3, PI4K2A, CSNK1G2, CDKL1, PXK, PFKFB3, AK1, PIK3R1, NUAK2, GRK5, PRKAR2A, GRK6, NADK, PACSIN1, MAP2K6, IP6K2, SRPK2, FN3K, CDK19, SRMS, DMPK, TNK2, TNK1, NEK7, PHKB, UCKL1, CLK1, ADCK2, STK24, GKAP1, PKIA, PI4KA, ATM, CALM1, MAP3K12, FGFR1, CDKN1C, ITK, CDKN1B, FLT1, BMPR2, DYRK2, MAST4, PRKCSH, ADPGK, MAST3, LRRK2, AKAP8L, AATK, DSTYK, PIP5KL1, NMRK1, TK2, MAP4K1, MAP4K2, SYK, MINK1, KSR2, IRAK4, GAK, SGK223, LATS2, LCK, PDXK, PRKX, CAMKK1, PAPSS2, PHKG2, MAPK1, CDKN2D, MAP3K2, GIT2, MAP3K3, CDK11A, MAP3K1, TPK1, CDC42BPG, LIMK2, MERTK, SBK1, TAOK2, PKN2, TAF1	0.00	0.00
UP_SEQ_FEATURE	**domain:Protein kinase**	76	4.00	EPHB6, ITK, FLT1, BMPR2, DYRK2, MAST4, MAST3, LRRK2, AATK, IGF1R, DSTYK, AKT2, AKT1, MAP3K9, MAP4K1, MAP2K3, MAP4K2, PRKCH, SYK, PRKCB, DAPK2, PRKCE, MINK1, DYRK1B, LMTK2, PRKCA, KSR2, IRAK4, GAK, SGK223, LATS2, PRKD3, LCK, SIK3, TSSK6, PRKD2, ROR1, ULK1, TSSK3, TRIB1, CSNK1G2, CDKL1, GUCY2C, RNASEL, PXK, PRKX, CAMKK1, NUAK2, GRK5, PHKG2, GRK6, MAPK1, MAP2K6, SRPK2, MAP3K2, MAP3K3, CDK19, CDK11A, SRMS, MAP3K1, MLKL, DMPK, CDC42BPG, LIMK2, TNK2, TNK1, NEK7, MERTK, CLK1, SBK1, ADCK2, STK24, TAOK2, PKN2, FGFR1, MAP3K12	0.00	0.00

INTERPRO	**IPR000719:Protein kinase, catalytic domain**	77	4.06	EPHB6, ITK, FLT1, BMPR2, DYRK2, MAST4, MAST3, LRRK2, AATK, IGF1R, DSTYK, AKT2, AKT1, MAP3K9, MAP4K1, MAP2K3, MAP4K2, PRKCH, SYK, PRKCB, DAPK2, PRKCE, MINK1, DYRK1B, LMTK2, PRKCA, KSR2, IRAK4, GAK, SGK223, LATS2, OBSCN, PRKD3, LCK, SIK3, TSSK6, PRKD2, ROR1, ULK1, TSSK3, TRIB1, CSNK1G2, CDKL1, GUCY2C, RNASEL, PXK, PRKX, CAMKK1, NUAK2, GRK5, PHKG2, GRK6, MAPK1, MAP2K6, SRPK2, MAP3K2, MAP3K3, CDK19, CDK11A, SRMS, MAP3K1, MLKL, DMPK, CDC42BPG, LIMK2, TNK2, TNK1, NEK7, MERTK, CLK1, SBK1, ADCK2, STK24, TAOK2, PKN2, FGFR1, MAP3K12	0.00	0.00
UP_KEYWORDS	**Serine/threonine-protein kinase**	63	3.32	BMPR2, DYRK2, MAST4, MAST3, LRRK2, AATK, DSTYK, AKT2, AKT1, MAP3K9, MAP4K1, MAP2K3, MAP4K2, PRKCH, PRKCB, DAPK2, PRKCE, MINK1, DYRK1B, LMTK2, PRKCA, KSR2, IRAK4, GAK, BCR, LATS2, OBSCN, PRKD3, SIK3, TSSK6, PRKD2, ULK1, TSSK3, CSNK1G2, CDKL1, PRKX, CAMKK1, NUAK2, GRK5, PHKG2, GRK6, MAPK1, MAP2K6, SRPK2, MAP3K2, MAP3K3, CDK19, CDK11A, MAP3K1, DMPK, CDC42BPG, LIMK2, TNK2, NEK7, CLK1, SBK1, ADCK2, STK24, TAOK2, PKN2, ATM, TAF1, MAP3K12	0.00	0.00
INTERPRO	**IPR011009:Protein kinase-like domain**	80	4.21	EPHB6, ITK, FLT1, BMPR2, DYRK2, MAST4, MAST3, LRRK2, AATK, IGF1R, DSTYK, AKT2, AKT1, MAP3K9, MAP4K1, MAP2K3, MAP4K2, PRKCH, SYK, PRKCB, DAPK2, PRKCE, MINK1, DYRK1B, LMTK2, PRKCA, KSR2, IRAK4, GAK, SGK223, LATS2, OBSCN, PRKD3, LCK, SIK3, TSSK6, PRKD2, ROR1, ULK1, TSSK3, TRIB1, CSNK1G2, CDKL1, GUCY2C, RNASEL, PXK, PRKX, CAMKK1, NUAK2, GRK5, PHKG2, GRK6, MAPK1, MAP2K6, SRPK2, MAP3K2, FN3K, MAP3K3, CDK19, CDK11A, SRMS, MAP3K1, MLKL, DMPK, CDC42BPG, LIMK2, TNK2, TNK1, NEK7, MERTK, CLK1, SBK1, ADCK2, STK24, TAOK2, PI4KA, PKN2, ATM, FGFR1, MAP3K12	0.00	0.00
GOTERM_BP_DIRECT	**GO:0006468~protein phosphorylation**	72	3.79	EPHB6, DYRK2, LRRK2, GMFG, AATK, PDK4, AKT1, MAP3K9, MAP4K1, MAP4K2, MORC3, PRKCH, SYK, PRKCB, DAPK2, PRKCE, MINK1, DYRK1B, LMTK2, ADAM10, PRKCA, KSR2, CDC25B, GAK, BCR, LATS2, OBSCN, PRKD3, LCK, SIK3, TSSK6, PRKD2, ULK1, TSSK3, TRIB1, CSNK1G2, CDKL1, GUCY2C, RNASEL, PXK, CTBP1, NPRL2, TAF1L, PIK3R1, CAMKK1, FYB, NUAK2, PHKG2, GRK6, MAPK1, C19ORF35, SRPK2, MAP3K2, CDK19, CDK11A, MAP3K1, MLKL, DMPK, CDC42BPG, LIMK2, TNK1, NEK7, PHKB, MERTK, SBK1, ADCK2, STK24, PKN2, ATM, FGFR1, TAF1, MAP3K12	0.02	0.02
GOTERM_MF_DIRECT	**GO:0004674~protein serine/threonine kinase activity**	62	3.27	DYRK2, MAST4, MAST3, LRRK2, AATK, DSTYK, AKT2, PDK3, AKT1, MAP3K9, MAP4K1, MAP2K3, MAP4K2, PRKCH, SYK, PRKCB, DAPK2, PRKCE, MINK1, DYRK1B, LMTK2, PRKCA, KSR2, IRAK4, GAK, BCR, LATS2, OBSCN, SIK3, TSSK6, PRKD2, ULK1, TSSK3, CSNK1G2, CDKL1, TAF1L, PRKX, CAMKK1, NUAK2, GRK5, PHKG2, MAPK1, MAP2K6, SRPK2, MAP3K2, CDK19, CDK11A, MAP3K1, DMPK, CDC42BPG, LIMK2, TNK2, NEK7, CLK1, SBK1, ADCK2, STK24, TAOK2, PKN2, ATM, TAF1, MAP3K12	0.01	0.01
UP_SEQ_FEATURE	**binding site:ATP**	79	4.16	ITK, FLT1, BMPR2, DYRK2, ACSM3, MAST4, MAST3, ACSM1, LRRK2, ATP2A3, AATK, IGF1R, DSTYK, NMRK1, AKT2, PDK4, PDK3, AKT1, MAP3K9, MAP4K1, MAP2K3, MAP4K2, PRKCH, LIG1, SYK, PRKCB, DAPK2, PRKCE, MINK1, DYRK1B, LMTK2, PRKCA, IRAK4, SGK223, LATS2, OBSCN, PRKD3, LCK, SIK3, TSSK6, PRKD2, ROR1, ULK1, TSSK3, CARS2, CSNK1G2, CDKL1, PRKX, CAMKK1, NUAK2, GRK5, PHKG2, GRK6, MAPK1, MAP2K6, SRPK2, MAP3K2, MAP3K3, CDK19, CDK11A, SRMS, MAP3K1, DMPK, CDC42BPG, LIMK2, TNK2, TNK1, NEK7, MERTK, ACSF2, CLK1, EHD3, SBK1, ADCK2, STK24, TAOK2, PKN2, FGFR1, MAP3K12	0.02	0.02
GOTERM_BP_DIRECT	**GO:0018105~peptidyl-serine phosphorylation**	28	1.48	MAST4, MAST3, LRRK2, PRKX, PKD1, AKT2, AKT1, MAPK1, PDK3, MAP4K1, MORC3, PRKCH, SYK, DMPK, PRKCB, PRKCE, LMTK2, PRKCA, CLK1, LATS2, PRKD3, PRKD2, PKN2, ULK1, ATM, CSNK1G2, TAF1, MAP3K12	0.04	0.04
INTERPRO	**IPR017441:Protein kinase, ATP binding site**	59	3.11	ITK, FLT1, BMPR2, DYRK2, LRRK2, AATK, IGF1R, DSTYK, AKT2, AKT1, MAP3K9, MAP4K1, MAP2K3, MAP4K2, PRKCH, SYK, PRKCB, DAPK2, PRKCE, MINK1, DYRK1B, LMTK2, PRKCA, LATS2, OBSCN, PRKD3, LCK, SIK3, TSSK6, PRKD2, ULK1, TSSK3, CSNK1G2, CDKL1, PRKX, CAMKK1, NUAK2, GRK5, PHKG2, GRK6, MAPK1, MAP2K6, SRPK2, MAP3K2, CDK19, SRMS, MAP3K1, DMPK, CDC42BPG, LIMK2, TNK2, TNK1, NEK7, MERTK, CLK1, STK24, TAOK2, PKN2, FGFR1	0.01	0.01

UP_KEYWORDS	**Transferase**	192	10.12	DPAGT1, DGKE, DGKD, CERK, PANK1, DGKA, EHMT2, XYLT2, XYLT1, EHMT1, SAT2, PRDM2, SAT1, IGF1R, NDST1, AS3MT, PTAR1, HERC3, POFUT2, GNPTAB, RNF19A, AKT2, PDK4, PDK3, AKT1, EP300, PIP4K2B, MAP3K9, SEPHS2, WHSC1L1, MAP2K3, ST6GAL1, PRKCH, PRKCB, DAPK2, PRKCE, GPT2, LMTK2, DYRK1B, PRKCA, MAPK8IP3, BCR, PLA2G15, DOK2, OBSCN, PRKD3, KAT6B, AKAP9, SIK3, TSSK6, PRKD2, ROR1, ULK1, TSSK3, PI4K2A, CSNK1G2, CDKL1, KMT2E, PXK, PFKFB3, AK1, PIK3R1, PTDSS1, NUAK2, GRK5, CHST11, CHST12, PRKAR2A, GRK6, CHST15, NADK, PACSIN1, MAP2K6, IP6K2, SRPK2, FN3K, GSTM4, CDK19, UBE2H, SRMS, DMPK, TIPARP, TNK2, TNK1, NEK7, SETDB2, PHKB, PARP16, UCKL1, CLK1, ADCK2, STK24, GKAP1, PKIA, PI4KA, NMT2, ATM, CALM1, OGT, CDS2, MAP3K12, FGFR1, CDKN1C, ITK, B4GALT3, ZCCHC11, CDKN1B, FLT1, B4GALT1, BMPR2, NAA40, DYRK2, MAST4, PRKCSH, ADPGK, MAST3, LRRK2, AKAP8L, SETD7, AATK, PYGM, HS2ST1, DSTYK, PIP5KL1, NMRK1, REV3L, TK2, WHSC1, COLGALT1, MAP4K1, MAP4K2, PARP4, SYK, NCOA3, MINK1, AMT, NSUN6, KSR2, NSUN7, IRAK4, PGM2L1, GAK, NT5C3A, SGK223, KAT2B, KAT2A, LATS2, PAPD7, OAS2, LCK, ST6GALNAC4, ST6GALNAC6, AGPAT5, PDXK, ZDHHC20, PRKX, CAMKK1, PAPSS2, TNKS2, MGAT5, PHKG2, GCNT2, HAS3, MAPK1, MGAT1, METTL7A, CDIPT, CDKN2D, MAP3K2, GIT2, MAP3K3, MAP3K1, GALNT3, POLM, TPK1, CDC42BPG, AMFR, QPCTL, MBOAT7, LIMK2, MBOAT1, UBE2G1, MERTK, HS3ST1, GATM, SBK1, LPCAT4, TAOK2, CHPT1, PKN2, CRAT, TAF1	0.00	0.00
GOTERM_MF_DIRECT	**GO:0004672~protein kinase activity**	57	3.00	EPHB6, LRRK2, AATK, AKT2, PDK4, PDK3, AKT1, MAP3K9, MAP4K1, MAP2K3, MAP4K2, PRKCH, SYK, PRKCB, DAPK2, PRKCE, MINK1, DYRK1B, PRKCA, KSR2, IRAK4, GAK, SGK223, OBSCN, SIK3, TSSK6, PRKD2, ROR1, AVP, TRIB1, CSNK1G2, CDKL1, GUCY2C, RNASEL, PXK, NPRL2, CCL5, PHKG2, C19ORF35, MAP2K6, SRPK2, MAP3K2, MAP3K3, CDK19, CDK11A, MAP3K1, MLKL, DMPK, LIMK2, TNK2, NEK7, CLK1, ADCK2, STK24, TAOK2, PKN2, MAP3K12	0.02	0.02
UP_KEYWORDS	**ATP-binding**	160	8.43	EPHB6, DGKE, DGKD, CERK, ACSM3, PANK1, ACSM1, DGKA, SMC4, IGF1R, AKT2, PDK4, PDK3, AKT1, PIP4K2B, MAP3K9, SEPHS2, MAP2K3, PRKCH, LIG1, FBXO18, PRKCB, DAPK2, PRKCE, STARD9, LMTK2, DYRK1B, PRKCA, BCR, OBSCN, SLFN11, PRKD3, SIK3, TSSK6, PRKD2, ROR1, ULK1, TSSK3, KIF20B, CARS2, PI4K2A, ABCG1, CSNK1G2, CDKL1, PFKFB3, ABCB1, UBA7, TARSL2, AK1, ABCB8, ACACB, HELZ2, NUAK2, GRK5, NLRP6, GRK6, EP400, NLRP1, KIF3C, N4BP2, NADK, MAP2K6, IP6K2, ABCA1, SRPK2, ABCA2, MYH7B, CDK19, UBE2H, DNAH10, SRMS, MLKL, DMPK, TNK2, HSPA7, TNK1, NEK7, HSPA6, ABCA9, ABCA7, TRPV1, ACSF2, UCKL1, CLK1, EHD3, GCLC, ADCK2, STK24, PI4KA, ATM, MAP3K12, FGFR1, ITK, FLT1, BMPR2, DYRK2, MAST4, CHD9, MAST3, LRRK2, DDX12P, ATP2A3, AATK, ATP2A1, DSTYK, PIP5KL1, NMRK1, TK2, ATP7A, ABCD1, MAP4K1, MAP4K2, ABCC2, APAF1, SYK, ABCC5, MINK1, KSR2, PEX1, IRAK4, KIF22, QRSL1, GAK, SGK223, LATS2, KIFC2, OAS2, LCK, PEX6, MCM6, PDXK, RNASEL, ACSS2, ADCY4, NLRC3, PRKX, CAMKK1, PAPSS2, PHKG2, CARNS1, MAPK1, ACSS1, MAP3K2, MAP3K3, CDK11A, MAP3K1, ATP13A1, TPK1, CDC42BPG, LIMK2, ATP2B4, MYO9B, UBE2G1, MERTK, SBK1, TAOK2, PKN2, ERCC6, MYO1F, TAF1	0.00	0.00
UP_KEYWORDS	**Nucleotide-binding**	197	10.38	EPHB6, ACSM3, CERK, PANK1, ACSM1, SMC4, AKT2, PDK4, PDK3, AKT1, PIP4K2B, SEPHS2, TRIM23, PRKCH, ARL15, PRKCB, DAPK2, PRKCE, STARD9, PRKCA, GTPBP1, BCR, PRKD3, SIK3, ULK1, PRKD2, KIF20B, PI4K2A, ABCB1, RRAD, TARSL2, SAR1B, ABCB8, HELZ2, NUAK2, PRKAR2A, N4BP2, ABCA1, SRPK2, ABCA2, MYH7B, CDK19, SRMS, DNAH10, DMPK, ABCA9, ABCA7, EHD3, ADCK2, ATM, ITK, DIRAS1, DDX12P, AATK, PYGM, DSTYK, NMRK1, TK2, MAP4K1, MAP4K2, SYK, MINK1, RHOH, TUBG2, KIF22, GNL1, RHOB, RAB33B, GAK, KIFC2, RAPGEF3, GUCY2C, RNASEL, ATL1, ADCY4, PRKX, CAMKK1, PAPSS2, CARNS1, MFN1, REM2, MAP3K2, MAP3K3, MAP3K1, TPK1, MYO9B, UBE2G1, TAOK2, PKN2, SLC27A1, DGKE, DGKD, DGKA, IGF1R, MAP3K9, MAP2K3, LIG1, FBXO18, LMTK2, DYRK1B, TUBA4A, RAB30, OBSCN, SLFN11, RAB37, TSSK6, TSSK3, ROR1, SLC27A3, CARS2, ABCG1, CSNK1G2, CDKL1, GNAZ, PFKFB3, UBA7, ARL3, AK1, ACACB, GRK5, NLRP6, GRK6, EP400, KIF3C, NLRP1, RAB6A, NADK, IP6K2, MAP2K6, UBE2H, MLKL, HSPA7, TNK2, TNK1, HSPA6, NEK7, TRPV1, ACSF2, UCKL1, CLK1,	0.00	0.00

				GNAO1, GCLC, STK24, PI4KA, MAFK, MAP3K12, FGFR1, BMPR2, DYRK2, FLT1, MAST4, CHD9, MAST3, LRRK2, ATP2A3, ATP2A1, PIP5KL1, ATP7A, ABCD1, ABCC2, APAF1, ABCC5, PEX1, KSR2, IRAK4, QRSL1, NT5C3A, ARL4C, SGK223, LATS2, OAS2, LCK, PEX6, MCM6, PDXK, ACSS2, RALB, NLRC3, NT5C2, GNA13, RAB40B, PHKG2, RAB24, MAPK1, ACSS1, CDK11A, ATP13A1, CDC42BPG, LIMK2, MX2, ATP2B4, MERTK, SBK1, ERCC6, HCN2, MYO1F, TAF1		
UP_SEQ_FEATURE	**active site:Proton acceptor**	87	4.58	ITK, FLT1, BMPR2, DYRK2, MAST4, ADPGK, MAST3, LRRK2, AATK, IGF1R, DSTYK, NMRK1, AKT2, AKT1, MAP3K9, L3HYPDH, ACAD8, MAP4K1, MAP2K3, MAP4K2, PRKCH, SYK, PRKCB, DAPK2, PRKCE, MINK1, RNASE6, DYRK1B, LMTK2, SIRT5, RNASE4, PRKCA, IRAK4, RNASE1, SIRT1, SIRT2, GAK, SGK223, LATS2, OBSCN, ALDH5A1, PRKD3, LCK, SIK3, TSSK6, PRKD2, ROR1, ULK1, TSSK3, CSNK1G2, ALDH9A1, CDKL1, HSD17B13, PRKX, HSD17B11, CAMKK1, NUAK2, GRK5, RDH10, PHKG2, GRK6, MAPK1, MAP2K6, SRPK2, MAP3K2, MAP3K3, CDK19, CDK11A, SRMS, MAP3K1, DMPK, CDC42BPG, QPCTL, TNK2, TNK1, NEK7, MERTK, CLK1, SBK1, ADCK2, STK24, TAOK2, GALM, PKN2, CRAT, FGFR1, MAP3K12	0.08	0.08
SMART	**SM00220:S_TKc**	57	3.00	DYRK2, MAST4, MAST3, LRRK2, DSTYK, AKT2, AKT1, MAP3K9, MAP4K1, MAP2K3, MAP4K2, PRKCH, PRKCB, DAPK2, PRKCE, MINK1, DYRK1B, PRKCA, KSR2, IRAK4, GAK, SGK223, LATS2, OBSCN, PRKD3, SIK3, TSSK6, PRKD2, ULK1, TSSK3, TRIB1, CSNK1G2, CDKL1, RNASEL, PRKX, CAMKK1, NUAK2, GRK5, PHKG2, GRK6, MAPK1, MAP2K6, SRPK2, MAP3K2, MAP3K3, CDK19, CDK11A, MAP3K1, DMPK, CDC42BPG, NEK7, CLK1, SBK1, STK24, TAOK2, PKN2, MAP3K12	0.07	0.07
INTERPRO	**IPR008271:Serine/threonine-protein kinase, active site**	46	2.42	DYRK2, MAST4, MAST3, LRRK2, PRKX, CAMKK1, DSTYK, NUAK2, AKT2, PHKG2, GRK6, AKT1, MAPK1, MAP3K9, MAP2K6, SRPK2, MAP2K3, CDK11A, CDK19, PRKCH, MAP3K1, DMPK, PRKCB, CDC42BPG, PRKCE, DAPK2, NEK7, MINK1, DYRK1B, PRKCA, KSR2, GAK, CLK1, OBSCN, SBK1, LATS2, PRKD3, TAOK2, SIK3, TSSK6, PRKD2, PKN2, ULK1, CSNK1G2, MAP3K12, CDKL1	0.12	0.11
UP_SEQ_FEATURE	**nucleotide phosphate-binding region:ATP**	113	5.95	EPHB6, ACSM3, ACSM1, SMC4, IGF1R, AKT2, PDK4, PDK3, AKT1, MAP3K9, SEPHS2, MAP2K3, PRKCH, PRKCB, DAPK2, PRKCE, STARD9, LMTK2, DYRK1B, PRKCA, OBSCN, SLFN11, PRKD3, SIK3, TSSK6, PRKD2, ROR1, ULK1, TSSK3, KIF20B, ABCG1, CSNK1G2, CDKL1, PFKFB3, UBA7, AK1, ABCB8, ACACB, HELZ2, NUAK2, GRK5, NLRP6, GRK6, EP400, NLRP1, KIF3C, N4BP2, MAP2K6, SRPK2, MYH7B, CDK19, DNAH10, SRMS, DMPK, TNK2, TNK1, NEK7, ACSF2, UCKL1, CLK1, EHD3, ADCK2, STK24, MAP3K12, FGFR1, ITK, FLT1, BMPR2, DYRK2, MAST4, CHD9, MAST3, LRRK2, DDX12P, AATK, DSTYK, NMRK1, ABCD1, MAP4K1, MAP4K2, APAF1, SYK, MINK1, PEX1, IRAK4, KIF22, SGK223, LATS2, KIFC2, LCK, PEX6, MCM6, PDXK, NLRC3, PRKX, CAMKK1, PAPSS2, PHKG2, CARNS1, MAPK1, MAP3K2, MAP3K3, CDK11A, MAP3K1, CDC42BPG, LIMK2, MYO9B, MERTK, SBK1, TAOK2, PKN2, ERCC6, MYO1F	0.49	0.49
GOTERM_MF_DIRECT	**GO:0005524~ATP binding**	171	9.01	EPHB6, DGKE, DGKD, CERK, ACSM3, PANK1, ACSM1, DGKA, SMC4, IGF1R, SMCHD1, AKT2, PDK4, PDK3, AKT1, PIP4K2B, MAP3K9, SEPHS2, MAP2K3, PRKCH, LIG1, FBXO18, PRKCB, DAPK2, PRKCE, STARD9, LMTK2, DYRK1B, PRKCA, RUNX1, BCR, OBSCN, SLFN11, PRKD3, SIK3, TSSK6, PRKD2, ROR1, ULK1, TSSK3, KIF20B, TRIB1, CARS2, PI4K2A, ABCG1, CSNK1G2, CDKL1, PXK, PFKFB3, ABCB1, UBA7, TARSL2, AK1, ABCB8, ACACB, HELZ2, NUAK2, GRK5, NLRP6, GRK6, EP400, NLRP1, KIF3C, N4BP2, NADK, MAP2K6, IP6K2, ABCA1, SRPK2, ABCA2, MYH7B, CDK19, UBE2H, DNAH10, SRMS, MLKL, DMPK, TNK2, HSPA7, TNK1, NEK7, HSPA6, ABCA9, ABCA7, TRPV1, ACSF2, UCKL1, CLK1, EHD3, GCLC, ADCK2, STK24, PI4KA, ATM, ITM2B, MAP3K12, FGFR1, ITK, FLT1, BMPR2, DYRK2, MAST4, CHD9, MAST3, LRRK2, DDX12P, ATP2A3, AATK, ATP2A1, DSTYK, PIP5KL1, NMRK1, TK2, ATP7A, ABCD1, MAP4K1, MAP4K2, ABCC2, APAF1, SYK, ABCC5, MINK1, KSR2, PEX1, IRAK4, KIF22, QRSL1, GAK, SGK223, LATS2, KIFC2, OAS2, LCK, PEX6, MCM6, GUCY2C, PDXK, RNASEL, ACSS2, ADCY4, NLRC3, PRKX, CAMKK1, PAPSS2, PHKG2, CARNS1, MAPK1, ACSS1, MAP3K2, MAP3K3, CDK11A, MAP3K1, KCNJ11, ATP13A1, TPK1, PNPLA8, CDC42BPG, LIMK2, ATP2B4, MYO9B, UBE2G1, MERTK, P2RX5, SBK1, MYO15B, P2RX1, TAOK2, PKN2, ERCC6, MYO1F, TAF1	0.28	0.27

Annotation Cluster 5	Enrichment Score: 4.486682889295296					
Category	**Term**	**Count**	**%**	**Genes**	**Benjamini**	**FDR**
INTERPRO	**IPR019787:Zinc finger, PHD-finger**	23	1.21	KMT2E, PHF3, PHF2, SP100, UHRF2, PHF10, SP110, PHF1, PHF12, ZMYND8, SP140, CXXC1, ING1, ING4, ING2, KAT6B, NFX1, PHF13, WHSC1, KDM7A, WHSC1L1, PHF19, BPTF	0.00	0.00
INTERPRO	**IPR001965:Zinc finger, PHD-type**	24	1.26	KMT2E, PHF3, PHF2, SP100, UHRF2, PHF10, SP110, PHF1, PHF12, ZMYND8, SP140, CXXC1, PHF7, ING1, ING4, RAI1, ING2, KAT6B, PHF13, WHSC1, KDM7A, WHSC1L1, PHF19, BPTF	0.00	0.00
SMART	**SM00249:PHD**	24	1.26	KMT2E, PHF3, PHF2, SP100, UHRF2, PHF10, SP110, PHF1, PHF12, ZMYND8, SP140, CXXC1, PHF7, ING1, ING4, RAI1, ING2, KAT6B, PHF13, WHSC1, KDM7A, WHSC1L1, PHF19, BPTF	0.00	0.00
INTERPRO	**IPR019786:Zinc finger, PHD-type, conserved site**	19	1.00	KMT2E, PHF3, PHF2, SP100, SP110, PHF1, PHF12, ZMYND8, SP140, CXXC1, ING1, ING4, ING2, NFX1, WHSC1, KDM7A, WHSC1L1, PHF19, BPTF	0.01	0.01
INTERPRO	**IPR011011:Zinc finger, FYVE/PHD-type**	28	1.48	KMT2E, PHF3, PHF2, SP100, MTMR3, UHRF2, PHF1, ZMYND8, SP140, CXXC1, PHF7, ING1, ZFYVE28, ING4, FGD3, ING2, WHSC1, WHSC1L1, BPTF, PHF10, SP110, PHF12, SYTL1, SYTL3, KAT6B, PHF13, KDM7A, PHF19	0.02	0.02
UP_SEQ_FEATURE	**zinc finger region:PHD-type**	14	0.74	KMT2E, PHF3, PHF2, UHRF2, SP110, ZMYND8, SP140, CXXC1, ING1, ING4, RAI1, ING2, PHF13, KDM7A	0.12	0.12
INTERPRO	**IPR013083:Zinc finger, RING/FYVE/PHD-type**	62	3.27	PHF3, PHF2, RNF13, PHF1, ZMYND8, CBLB, PHF7, ING1, ZFYVE28, TRIM8, ING4, ING2, TRIM7, RNF19A, WHSC1, TRIM65, TRIM22, WHSC1L1, TRIM23, RNF44, SP110, SYTL1, NOSIP, SYTL3, RNF41, RNF125, KAT6B, TRAF5, RNF166, KDM7A, RNFT2, KMT2E, SP100, MTMR3, TRIM52, UHRF2, SP140, RNF38, CXXC1, FGD1, RNF135, FGD3, RNF113A, RNF213, RNF39, RNF130, BPTF, MAP3K1, RNF24, PHF10, USP20, AMFR, PHF12, MIB2, SYVN1, TRIM39, RNF149, MKRN1, TTC3, PHF13, TRIM38, PHF19	0.11	0.11
Annotation Cluster 6	**Enrichment Score: 4.340064082533207**					
Category	**Term**	**Count**	**%**	**Genes**	**Benjamini**	**FDR**
UP_KEYWORDS	**SH3 domain**	40	2.11	ARHGAP9, ITK, NCF4, SLA, MIA3, PIK3R1, SLA2, FYB, ARHGAP4, CRKL, ARHGAP12, SH3TC1, PLCG2, EPS8L2, MAP3K9, SRGAP3, SPTAN1, PACSIN1, MPP1, SRMS, TNK2, TNK1, ARHGAP27, SORBS3, VAV1, MPP7, FCHSD1, CACNB2, AHI1, OBSCN, DLG2, DNMBP, MYO15B, BIN1, ABI3, LCK, SPATA13, GRAP, MYO1F, ARHGEF6	0.00	0.00
UP_SEQ_FEATURE	**domain:SH3**	34	1.79	ARHGAP9, ITK, NCF4, SLA, MIA3, PIK3R1, SLA2, FYB, ARHGAP4, ARHGAP12, SH3TC1, PLCG2, EPS8L2, MAP3K9, SRGAP3, SPTAN1, PACSIN1, MPP1, LOC440461, SRMS, TNK2, TNK1, ARHGAP27, MPP7, CACNB2, AHI1, OBSCN, DLG2, BIN1, ABI3, LCK, SPATA13, MYO1F, ARHGEF6	0.02	0.02
INTERPRO	**IPR001452:Src homology-3 domain**	40	2.11	ARHGAP9, ITK, NCF4, SLA, MIA3, PIK3R1, SLA2, FYB, ARHGAP4, CRKL, ARHGAP12, SH3TC1, PLCG2, EPS8L2, MAP3K9, SRGAP3, SPTAN1, PACSIN1, MPP1, SRMS, TNK2, TNK1, ARHGAP27, SORBS3, VAV1, MPP7, FCHSD1, CACNB2, AHI1, OBSCN, DLG2, DNMBP, MYO15B, BIN1, ABI3, LCK, SPATA13, GRAP, MYO1F, ARHGEF6	0.01	0.01
SMART	**SM00326:SH3**	36	1.90	ITK, NCF4, SLA, PIK3R1, SLA2, FYB, ARHGAP4, CRKL, ARHGAP12, SH3TC1, PLCG2, EPS8L2, MAP3K9, SRGAP3, SPTAN1, PACSIN1, MPP1, SRMS, TNK2, TNK1, SORBS3, VAV1, MPP7, FCHSD1, CACNB2, AHI1, DLG2, DNMBP, MYO15B, BIN1, ABI3, LCK, SPATA13, GRAP, MYO1F, ARHGEF6	0.13	0.12

Annotation Cluster 7	Enrichment Score: 3.185942275128096					
Category	**Term**	**Count**	**%**	**Genes**	**Benjamini**	**FDR**
UP_KEYWORDS	**Transcription regulation**	265	13.96	HDAC10, JMJD1C, IKZF3, IKZF5, ALKBH4, CREB3L2, CPNE1, BBX, CCNL2, ZNF721, CCNL1, TRIM22, TSPYL2, SFMBT1, SP110, PRKCB, ZNF10, SOX12, RFX1, OVOL1, ZNF14, RUNX1, EID2, TXNIP, HOXB2, MAML3, ASF1A, ZNF395, ZNF273, CTBP1, TSHZ1, TSHZ2, ZBTB1, ZBTB4, DEDD2, ZBTB2, HELZ2, ZNF703, ZNF823, ZNF821, ZNF700, ZBED6, SCAI, ZNF266, BANP, ZSCAN18, JUND, BCL11A, SNAI3, SS18L1, NFATC3, NFATC1, NR1D2, NR1D1, ZNF34, FLI1, FOSL2, THAP11, ZNF30, CREBRF, ID3, HBP1, RCOR1, SLC2A4RG, PHF2, BTG2, GMEB2, ZNF250, CITED2, TCF25, ZNF490, PHF1, SETD7, GLI1, LIMD1, MECP2, ING2, ZNF248, ZNF367, ZNF487, ZIK1, ACAD8, ZHX2, ZHX3, CNOT6L, TSC22D1, NCOA3, IL16, CBFA2T2, SIRT1, SIRT2, AES, KAT2B, MN1, KAT2A, NFX1, JDP2, VGLL4, PPARD, ZNF595, KANK2, KANK1, SP100, ELOF1, TMF1, SATB1, CIPC, PURA, MNT, ZFP14, TCEAL1, ZNF107, TBL1X, ZNF224, ZNF101, STAT2, PER1, TFAP4, ZNF219, TCEA2, PKN2, ZNF699, ZNF335, MPHOSPH8, ZNF575, ZNF211, ZNF331, KDM1A, CRTC1, NAB2, ZBTB20, ARID4A, PRDM2, NR3C1, CARF, NR3C2, ZNF569, EP300, MAP3K9, ZNF566, WHSC1L1, MEN1, ZNF441, EOMES, LMO4, ZBTB38, ARID5B, ZNF92, MAF, SAP25, KAT6B, ZNF318, ZNF439, ERF, KMT2E, ZNF671, ZNF791, AKNA, MAX, MAZ, CREM, FOXO4, FOXO3, DEAF1, ZKSCAN8, ZNF548, SAFB2, ZNF667, ZNF304, BPTF, MAP2K6, ZBTB18, ZNF540, CBX8, SMAD3, CBX4, ZBTB14, PHF10, PHF12, ZBTB11, FOXN2, NR4A2, MAFB, SP4, ZFP64, TCF4, MAFK, TCF3, CNOT8, BRWD1, ZNF654, MXD1, MXD3, ZNF652, PHF19, FGFR1, MXD4, CREBZF, ZMYND15, RERE, CALCOCO1, THRA, CHD9, CDCA7L, AKAP8L, HMGB2, AFF3, AFF4, LYL1, HHEX, DBP, TRPS1, RB1CC1, WHSC1, IFT57, MYBL1, KLF10, MSL3, KLF16, RBL2, ELF1, ELF2, IRF3, ZNF516, TERF2IP, IRF8, LCORL, KDM7A, HDAC5, KDM3A, SMARCD3, CEBPD, CEBPE, CXXC1, TAF1L, ZBTB44, ZBTB41, ZBTB40, HDAC7, IFI16, ELMSAN1, ZNF627, TBX21, ATXN1L, MXI1, MAPK1, E2F5, ZNF862, STOX1, MLXIP, SKOR1, USP21, FOXJ2, KLF3, TBX19, KLF2, PNRC1, USF1, REST, KLF9, ZNF615, ERCC6, TAF5, LPIN2, TAF1	0.00	0.00
UP_KEYWORDS	**Transcription**	266	14.01	HDAC10, JMJD1C, IKZF3, IKZF5, ALKBH4, CREB3L2, CPNE1, BBX, CCNL2, ZNF721, CCNL1, TRIM22, TSPYL2, SFMBT1, SP110, PRKCB, ZNF10, SOX12, RFX1, OVOL1, ZNF14, RUNX1, EID2, TXNIP, HOXB2, MAML3, ASF1A, ZNF395, ZNF273, CTBP1, TSHZ1, TSHZ2, ZBTB1, ZBTB4, DEDD2, ZBTB2, HELZ2, ZNF703, ZNF823, ZNF821, ZNF700, ZBED6, SCAI, ZNF266, BANP, ZSCAN18, JUND, BCL11A, SNAI3, SS18L1, NFATC3, NFATC1, NR1D2, NR1D1, ZNF34, FLI1, FOSL2, THAP11, ZNF30, CREBRF, ID3, HBP1, RCOR1, SLC2A4RG, PHF2, BTG2, GMEB2, ZNF250, CITED2, TCF25, ZNF490, PHF1, SETD7, GLI1, LIMD1, MECP2, ING2, ZNF248, ZNF367, ZNF487, ZIK1, ACAD8, ZHX2, ZHX3, CNOT6L, TSC22D1, NCOA3, IL16, CBFA2T2, SIRT1, SIRT2, AES, KAT2B, MN1, KAT2A, NFX1, JDP2, VGLL4, PPARD, ZNF595, KANK2, KANK1, SP100, ELOF1, TMF1, SATB1, CIPC, PURA, MNT, ZFP14, TCEAL1, ZNF107, TBL1X, ZNF224, ZNF101, STAT2, PER1, TFAP4, ZNF219, TCEA2, PKN2, ZNF699, ZNF335, MPHOSPH8, ZNF575, ZNF211, ZNF331, KDM1A, CRTC1, NAB2, ZBTB20, ARID4A, PRDM2, NR3C1, CARF, NR3C2, ZNF569, EP300, MAP3K9, ZNF566, WHSC1L1, MEN1, ZNF441, EOMES, LMO4, ZBTB38, ARID5B, ZNF92, MAF, SAP25, KAT6B, ZNF318, ZNF439, ERF, KMT2E, ZNF671, ZNF791, AKNA, MAX, MAZ, CREM, FOXO4, FOXO3, DEAF1, ZKSCAN8, ZNF548, SAFB2, ZNF667, ZNF304, BPTF, MAP2K6, ZBTB18, ZNF540, CBX8, SMAD3, CBX4, ZBTB14, PHF10, PHF12, ZBTB11, FOXN2, NR4A2, MAFB, SP4, ZFP64, TCF4, MAFK, TCF3, CNOT8, BRWD1, ZNF654, MXD1, MXD3, ZNF652, PHF19, FGFR1, MXD4, CREBZF, ZMYND15, RERE, CALCOCO1, THRA, CHD9, CDCA7L, AKAP8L, HMGB2, AFF3, AFF4, LYL1, HHEX, DBP, TRPS1, RB1CC1, WHSC1, IFT57, MYBL1, KLF10, MSL3, KLF16, RBL2, ELF1, ELF2, IRF3, ZNF516, TERF2IP, IRF8, LCORL, KDM7A, HDAC5, KDM3A, SMARCD3, CEBPD, CEBPE, CXXC1, TAF1L, ZBTB44, CXXC5, ZBTB41, ZBTB40, HDAC7, IFI16,	0.00	0.00

				ELMSAN1, ZNF627, TBX21, ATXN1L, MXI1, MAPK1, E2F5, ZNF862, STOX1, MLXIP, SKOR1, USP21, FOXJ2, KLF3, TBX19, KLF2, PNRC1, USF1, REST, KLF9, ZNF615, ERCC6, TAF5, LPIN2, TAF1		
UP_KEYWORDS	**Nucleus**	513	27.03	CYFIP2, EHMT2, EHMT1, ADARB2, SMC4, ALKBH6, TSEN54, ALKBH5, ALKBH4, AKT2, CREB3L2, AKT1, BBX, PIP4K2B, TSPYL2, PRKCB, PRKCE, STARD9, WDR74, ZNF10, PRKCA, SOX12, RFX1, ZNF14, EID2, BIN1, HOXB2, PRKD2, MAML3, ASF1A, SLBP, ZNF395, ZNF273, CTBP1, XPC, C9ORF72, DEDD2, NUP85, ZSCAN18, ZNF266, LHPP, ACD, JUND, DMPK, SNAI3, NFATC3, UPF3A, NFATC1, NR1D2, NR1D1, ZNF34, PHC3, FLI1, FOSL2, THAP11, FAM220A, FAM111A, ZNF30, HBP1, CDKN1C, PHF2, CDKN1B, GMEB2, ZNF250, TCF25, ZNF490, PHF1, DDX12P, SETD7, PHF7, GLI1, ING1, HIST2H2AC, MECP2, ING4, ING2, SH3BGRL2, ZNF248, ZNF367, ZNF487, ZIK1, TIGD3, DFFB, CNOT6L, SIRT5, EPS15L1, FOS, SIRT1, SIRT2, AES, GCHFR, KAT2B, KAT2A, JDP2, PPARD, ZNF595, KANK1, ELOF1, TMF1, CIPC, CCNDBP1, ALOX5, UBN1, ZNF107, MBNL3, ZNF224, ZNF101, CDKN2D, CENPT, EGLN1, MBD4, CARD8, STAT2, DEF6, ZNF219, TAOK2, YPEL1, CENPM, FOSB, PKN2, NCAPD2, ZNF699, ZNF335, YPEL4, ZNF575, YPEL3, ZNF211, YPEL2, ZNF331, GHDC, FMR1, CLSTN1, NAB2, ZBTB20, PYCARD, SESN1, ZNF569, ZNF566, PHLDA1, WHSC1L1, MEN1, ZNF441, BNIP3L, USP8, FBXO18, ZBTB38, CTNNBIP1, DYRK1B, MAF, SAP25, KAT6B, ZNF439, ZNF318, ERF, PHIP, MAD1L1, SRSF8, CDKL1, KMT2E, ZNF671, ZNF791, CBFB, MAX, ARL3, MAZ, CREM, MRI1, UBR2, FOXO4, FOXO3, BAG1, ZKSCAN8, ZNF548, SAFB2, MBP, ZNF667, ZNF304, IP6K2, MAP2K6, ZBTB18, ZNF540, OSBPL8, TIA1, ZBTB14, OSBPL3, TNK2, NEK7, RITA1, ZBTB11, FBXO32, FOXN2, LSM4, UCKL1, RGCC, MAFB, STK24, SP4, ZFP64, MAFK, CNOT8, XAF1, ZNF654, OGT, ZNF652, RAD9A, CALCOCO1, RNF13, NUMA1, CDCA7L, ZC3H3, AKAP8L, CELF6, LRMP, ARRB2, SYNE2, HHEX, UNKL, LBR, MSL3, DUSP26, PATL2, DNAJC1, RRM2B, PAPD7, CTDSP2, ZNF516, MCM6, LCORL, CERS2, HDAC5, SMARCD3, CEBPD, UHRF2, LRP1, CEBPE, RNF38, CXXC1, PBXIP1, ZBTB44, CXXC5, ACRC, FYB, ZBTB41, HDAC7, ZBTB40, HIRIP3, IFI16, ELMSAN1, ZNF627, RSBN1L, ATXN1L, E2F5, ZNF862, STOX1, MLXIP, PTPN18, SKOR1, FOXJ2, CABLES1, KLF3, KLF2, PNRC1, PRC1, KLF9, ZNF615, SYCP3, CUL4B, HDAC10, JMJD1C, IKZF3, IKZF5, TIAL1, RASSF1, TCL1A, PEG10, CPNE1, CCNL2, ZNF721, CCNL1, TRIM22, SRRM2, SFMBT1, SP110, OVOL1, MIF4GD, CDC40, RUNX1, FAM76B, FLYWCH1, KIF20B, EPB41, TSHZ1, SP140, TSHZ2, ZBTB1, ZBTB4, CDKN2AIP, GMCL1, ZBTB2, HELZ2, DPH1, ZNF703, ZNF823, ZNF821, ZNF700, ZBED6, RALGDS, SCAI, BANP, SRPK2, MAGEE1, BCL11A, PYHIN1, SS18L1, SETDB2, RANBP10, CREBRF, ID3, ATM, FBXL3, SLC2A4RG, RCOR1, ZCCHC11, USPL1, CITED2, LIMD1, PPP3CA, ZMYM3, MIS18BP1, PCF11, SUFU, ENC1, PRX, ZMYM6, REV3L, QSOX2, ZHX2, PARP4, ZHX3, TSC22D1, NCOA3, TSC22D3, IL16, KIF22, CBFA2T2, GLTSCR2, RHOB, NFX1, FAM193B, VGLL4, SP100, SATB1, PRKX, PRICKLE1, CAMKK1, PURA, MNT, ZFP14, TCEAL1, TBL1X, MAP3K2, PNPLA7, PLEKHA2, SORBS3, PER1, HIST3H2A, TFAP4, TTC3, TCEA2, MPHOSPH8, MIDN, DCLRE1C, KDM1A, CRTC1, ARID4A, CIB1, PRDM2, NR3C1, CARF, CMIP, NR3C2, RGS2, CCND3, RGS3, CAPN7, COTL1, EP300, TMEM38A, SBF1, HIST1H2AC, EOMES, MORC3, LIG1, SHISA5, ARID5B, NOSIP, ZNF92, SLFN11, HIST1H2BD, AKNA, MRO, ACACB, NDRG1, LPP, ZFP36L2, RAI1, NLRP6, GRK5, DEAF1, EP400, STAP1, NLRP1, BPTF, CBX8, MGEA5, SMAD3, CBX4, PHF10, PHF12, CLK1, PAN2, NR4A2, PHF13, TCF4, TCF3, CLASRP, BRWD1, MXD1, MXD3, FGFR1, MXD4, PHF19, CREBZF, ZMYND15, RERE, DYRK2, LDB1, THRA, CHD9, HMGB2, ATP2A3, HMGB1, AFF3, AFF4, AFF1, IRF2BPL, LMNB1, CABIN1, LYL1, DBP, TRPS1, RB1CC1, GATAD1, TMEM109, WHSC1, MYBL1, RBM5, DACT1, HIST1H1C, KLF10, SUN2, RBM15, AXIN1, PPP2R5C, ETV5, KLF16, RBL2, TBC1D1, HSH2D, ELF1, LATS2, ELF2, SETBP1, IRF3, OAS2, TERF2IP, IRF8, LUC7L3, RBMS2, KDM7A, AGPAT5, HIST1H2BN, KDM3A, RGS14, USP11, HIST1H2BK, TAF1L, TOB1, U2AF1L4, GNA13, NXF1, TNKS2, TBX21, MXI1, MAPK1, RBM38, CDK11A, USP21, POLM, MX2, LIMK2, LRWD1, USP28, TBX19, USF1, REST, KANSL2, ALOX5AP, ERCC6, TAF5, SSBP2, LPIN2, TAF1	0.01	0.01

GOTERM_MF_DIRECT	**GO:0003700~transcription factor activity, sequence-specific DNA binding**	120	6.32	KDM1A, ARID4A, PRDM2, NR3C1, IKZF3, CARF, IKZF5, NR3C2, CREB3L2, TRIM22, EOMES, LMO4, ZBTB38, OVOL1, RUNX1, ZNF92, MAF, ERF, HOXB2, ZNF831, CBFB, MAX, CTBP1, SP140, CREM, FOXO4, FOXO3, ZFP36L2, RAI1, DEAF1, ZKSCAN8, ZNF548, ZNF821, ZNF304, ZBED6, ZSCAN18, ZNF540, ZBTB18, JUND, SMAD3, ZBTB14, NFATC3, NFATC1, NR1D2, NR1D1, ZBTB11, FOXN2, FLI1, FOSL2, SP4, ZNF30, CREBRF, ID3, TCF4, MAFK, TCF3, CNOT8, MXD1, SLC2A4RG, CREBZF, RERE, ZNF250, THRA, CITED2, TCF25, ZNF490, PHF1, HMGB2, HMGB1, AFF4, AFF1, MECP2, DBP, TRPS1, GATAD1, ZNF367, ZIK1, KLF10, ZHX2, ZHX3, TSC22D1, TSC22D3, FOS, CBFA2T2, ETV5, VAV1, ELF1, ELF2, IRF3, NFX1, ZNF516, IRF8, JDP2, PPARD, ZNF595, KDM3A, CEBPD, TULP4, PURA, ZFP14, MNT, ELMSAN1, TBX21, TCEAL1, UBN1, E2F5, ZNF224, MLXIP, STAT2, KLF3, TBX19, KLF2, REST, ZNF219, KLF9, ZNF615, FOSB, ZNF699, TAF5, ZNF211	0.10	0.10
GOTERM_BP_DIRECT	**GO:0006351~transcription, DNA-templated**	222	11.70	HDAC10, JMJD1C, IKZF5, ALKBH4, CPNE1, BBX, CCNL2, ZNF721, CCNL1, TRIM22, TSPYL2, SFMBT1, SP110, PRKCB, ZNF10, RFX1, OVOL1, ZNF14, EID2, TXNIP, HOXB2, ASF1A, ZNF395, ZNF273, CTBP1, TSHZ1, TSHZ2, ZBTB4, DEDD2, ZBTB2, HELZ2, ZNF703, ZNF823, ZNF821, ZNF700, ZBED6, SCAI, ZNF266, BANP, ZSCAN18, BCL11A, SNAI3, SS18L1, NR1D2, NR1D1, ZNF34, FOSL2, THAP11, ZNF30, CREBRF, ID3, HBP1, RCOR1, SLC2A4RG, PHF3, PHF2, BTG2, ZNF250, CITED2, TCF25, ZNF490, PHF1, SETD7, GLI1, LIMD1, MECP2, ING2, ZNF248, ZNF367, ZNF487, ZIK1, ACAD8, ZHX2, ZHX3, CNOT6L, NCOA3, IL16, CBFA2T2, SIRT1, SIRT2, AES, MN1, JDP2, VGLL4, PPARD, ZNF595, KANK2, KANK1, SP100, SATB1, CIPC, PURA, ZFP14, TCEAL1, ZNF107, TBL1X, ZNF224, ZNF101, STAT2, PER1, ZNF219, TCEA2, PKN2, ZNF699, ZNF335, MPHOSPH8, ZNF575, ZNF211, ZNF331, KDM1A, CRTC1, NAB2, ZBTB20, PRDM2, NR3C1, NR3C2, ZNF569, MAP3K9, ZNF566, WHSC1L1, MEN1, ZNF441, EOMES, ZBTB38, ARID5B, ZNF92, MAF, SAP25, KAT6B, ZNF318, ZNF439, ERF, KMT2E, ZNF671, ZNF791, CREM, ZKSCAN8, ZNF548, SAFB2, ZNF667, ZNF304, BPTF, MAP2K6, ZBTB18, ZNF540, CBX8, SMAD3, CBX4, ZBTB14, PHF10, PHF12, ZBTB11, FOXN2, NR4A2, SP4, ZFP64, MAFK, TCF3, CNOT8, BRWD1, ZNF654, MXD1, MXD3, ZNF652, PHF19, FGFR1, MXD4, CREBZF, ZMYND15, RERE, CALCOCO1, LDB1, THRA, CHD9, CDCA7L, AKAP8L, HMGB2, AFF3, LYL1, HHEX, RB1CC1, WHSC1, IFT57, KLF10, MSL3, KLF16, RBL2, ELF2, TERF2IP, IRF8, KDM7A, HDAC5, KDM3A, SMARCD3, CEBPD, CXXC1, ZBTB44, CXXC5, ZBTB41, ZBTB40, HDAC7, IFI16, ELMSAN1, ZNF627, TBX21, ATXN1L, MXI1, MAPK1, E2F5, ZNF862, STOX1, MLXIP, SKOR1, USP21, KLF3, TBX19, KLF2, PNRC1, REST, KLF9, ZNF615, LPIN2	0.37	0.37
UP_KEYWORDS	**DNA-binding**	215	11.33	IKZF3, IKZF5, PEG10, CREB3L2, BBX, ZNF721, SP110, ZNF10, SOX12, RFX1, OVOL1, ZNF14, RUNX1, HOXB2, FLYWCH1, ZNF395, ZNF273, TSHZ1, SP140, TSHZ2, ZBTB1, XPC, ZBTB4, DEDD2, ZBTB2, HELZ2, ZNF823, ZNF821, ZNF700, ZBED6, ZNF266, BANP, ZSCAN18, ACD, JUND, SNAI3, NFATC3, NFATC1, NR1D2, NR1D1, ZNF34, PHC3, FLI1, FOSL2, THAP11, ZNF30, HBP1, ATM, SLC2A4RG, GMEB2, ZNF250, TCF25, ZNF490, DDX12P, GLI1, HIST2H2AC, MECP2, MIS18BP1, REV3L, ZNF248, ZNF367, ZNF487, ZIK1, TIGD3, ZHX2, ZHX3, KIF22, FOS, NFX1, JDP2, PPARD, ZNF595, SP100, TMF1, SATB1, PURA, MNT, ZFP14, UBN1, ZNF107, ZNF224, ZNF101, CENPT, MBD4, STAT2, HIST3H2A, TFAP4, ZNF219, TCEA2, FOSB, ZNF699, ZNF335, ZNF575, ZNF211, ZNF331, ZBTB20, PRDM2, NR3C1, CARF, NR3C2, HMCES, ZNF569, ZNF566, HIST1H2AC, MEN1, ZNF441, EOMES, ZBP1, FBXO18, ZBTB38, ARID5B, ZNF92, MAF, ZNF439, ERF, HIST1H2BD, ZNF671, ZNF791, AKNA, MAX, MAZ, CREM, FOXO4, FOXO3, ZFP36L2, DEAF1, ZKSCAN8, ZNF548, EP400, SAFB2, ZNF667, ZNF304, ZBTB18, ZNF540, SMAD3, ZBTB14, ZBTB11, FOXN2, NR4A2, MAFB, SP4, ZFP64, TCF4, MAFK, TCF3, ZNF654, MXD1, MXD3, ZNF652, MXD4, THRA, CHD9, ZC3H3, HMGB2, HMGB1, AFF3, LYL1, HHEX, DBP, TRPS1, TOP1MT, WHSC1, IFT57, LBR, MYBL1, HIST1H1C, KLF10, MSL3, ETV5, KLF16, RBL2, DNAJC1, ELF1, ELF2, IRF3, PAPD7, SETBP1, ZNF516, LUC7L3, IRF8, MCM6, LCORL, AHDC1, CERS2, HIST1H2BN, CEBPD, UHRF2, CEBPE, HIST1H2BK, CXXC1, TAF1L, ZBTB44, ZBTB41, ZBTB40, IFI16, ELMSAN1, ZNF627, TBX21, ATXN1L, MXI1, MAPK1, E2F5, STOX1, MLXIP, FOXJ2, KLF3, TBX19, KLF2, USF1, KLF9, ZNF615, ERCC6, SYCP3, SSBP2, TAF1	0.02	0.02

GOTERM_CC_DIRECT	**GO:0005634~nucleus**	523	27.56	CYFIP2, EHMT2, EHMT1, ADARB2, SMC4, ALKBH6, ALKBH5, ALKBH4, AKT2, CREB3L2, AKT1, TSPYL2, PRKCB, PRKCE, STARD9, WDR74, ZNF10, RFX1, ZNF14, PRKD3, CDIP1, TXNIP, HOXB2, PRKD2, MAML3, ASF1A, SLBP, ZNF395, ZNF273, CTBP1, SDR39U1, XPC, ABCB8, C9ORF72, RDH10, HMOX1, ZSCAN18, ZNF266, LHPP, ACD, CDK19, JUND, HOMER2, TIPARP, SNAI3, NFATC3, UPF3A, NFATC1, NR1D2, NR1D1, ZNF34, PHC3, FLI1, FOSL2, FAM220A, FAM111A, EHD3, PKIA, ZNF30, CPEB2, CDKN1C, PHF2, CDKN1B, GMEB2, ZNF250, TCF25, ZNF490, PHF1, DDX12P, PHF7, GLI1, ING1, HIST2H2AC, MECP2, ING4, ING2, TRIM7, ZNF248, ZNF367, ZNF487, ZIK1, TIGD3, DFFB, CNTD2, CNOT6L, SLC2A11, PGAM2, SIRT5, EPS15L1, FOS, DYNLL2, GNL1, SIRT1, SIRT2, AES, GCHFR, KAT2B, KAT2A, JDP2, PPARD, ZNF595, KANK1, TMF1, CIPC, CCNDBP1, UBN2, UBN1, ZNF107, MBNL3, RNF130, ZNF224, ZNF101, CDKN2D, CENPT, EGLN1, MBD4, CARD8, STAT2, DEF6, ZNF219, TAOK2, YPEL1, FOSB, PKN2, NCAPD2, ZNF699, ZNF335, ZNF575, ZNF211, ZNF331, DGKD, IRS1, FMR1, CLSTN1, NAB2, MAP3K7CL, ZBTB20, PYCARD, SESN3, SESN1, ZNF569, SLC25A42, ZNF566, WHSC1L1, MEN1, ZNF441, FBXO18, ZBTB38, CTNNBIP1, DYRK1B, MAF, SAP25, KAT6B, ZNF439, ERF, TSSK6, TSSK3, PHIP, S100A8, MAD1L1, CSNK1G2, SRSF8, CDKL1, ZNF671, ZNF791, CBFB, MAX, ARL3, MAZ, CREM, FOXO4, FOXO3, SLC9A3R1, AMDHD2, BAG1, ZKSCAN8, ZNF548, SAFB2, MBP, ZNF667, ZNF304, SKIL, IP6K2, ZBTB18, ZNF540, ZBTB14, TNK2, RITA1, FBXO32, FOXN2, UCKL1, PTPRE, RGCC, MAFB, STK24, SP4, ZFP64, FGFR1OP, MAFK, CNOT8, XAF1, ZNF654, OGT, ZNF652, RAD9A, CALCOCO1, NUMA1, CDCA7L, ZC3H3, AKAP8L, EFCAB13, CELF6, PTPN22, ARRB2, SYNE2, ALAD, HHEX, UNKL, APAF1, MSL3, DUSP26, PATL2, PTP4A1, ARL4C, DNAJC1, PAPD7, ZNF516, MCM6, LCORL, HDAC5, SMARCD3, CEBPD, UHRF2, RNF38, CXXC1, PBXIP1, ZBTB44, PPM1D, ACRC, FYB, ZBTB41, HDAC7, ZBTB40, HIRIP3, PARD6A, IFI16, ELMSAN1, ZNF627, RSBN1L, ATXN1L, TNNI2, E2F5, ZNF862, STOX1, MLXIP, PTPN18, SKOR1, AMFR, FOXJ2, CABLES1, KIAA1683, KLF3, KLF2, PNRC1, PRC1, KLF9, ZNF615, SYCP3, HDAC10, PANK1, ZMYND8, JMJD1C, CBLB, IKZF3, AQP3, IKZF5, TIAL1, HERC3, RASSF1, TCL1A, PEG10, CPNE1, CCNL2, ZNF721, CCNL1, TRIM22, TRIM23, SFMBT1, SP110, OVOL1, ANK1, RUNX1, FAM76B, HECA, ZNF831, KIF20B, ANKRA2, TRIB1, EPB41, TSHZ1, SP140, TSHZ2, DCUN1D4, ZBTB1, PIK3R1, ZBTB4, GMCL1, ZBTB2, NUAK2, DPH1, ZNF704, ZNF703, ZNF823, ZNF821, ZNF700, APOE, ZBED6, RALGDS, SCAI, SPTBN1, SRPK2, MAGEE1, BCL11A, SS18L1, SETDB2, RPS27, RANBP10, ID3, CD27, ATM, FBXL3, CALM1, SLC2A4RG, RCOR1, ZCCHC11, CITED2, TECR, LIMD1, PPP3CA, SUFU, ENC1, PRX, REV3L, ZHX2, PARP4, ZHX3, TSC22D1, SYK, NCOA3, TSC22D3, IL16, KIF22, CBFA2T2, RHOB, NFX1, FAM193B, VGLL4, SP100, SATB1, PRKX, PRICKLE1, CAMKK1, PURA, MNT, ZFP14, TCEAL1, APBB2, TBL1X, PLEKHA2, SORBS3, PER1, TFAP4, THEMIS2, TTC3, TCEA2, MPHOSPH8, CAPS, KDM1A, CRTC1, ARID4A, CIB1, PRDM2, NR3C1, ACRBP, CARF, CMIP, NR3C2, RGS2, CCND3, COTL1, CAPN3, EP300, SBF1, HIST1H2AC, EOMES, ZBP1, LIG1, ADAM10, ARID5B, NOSIP, TSC1, CYBA, LMO7, ZNF92, SLFN11, HIST1H2BD, PXK, AKNA, UBA7, PLD4, ADRB2, ACACB, NDRG1, LPP, ZFP36L2, SEL1L3, RAI1, GRK5, DEAF1, STAP1, FOPNL, NLRP1, BPTF, CBX8, MGEA5, SMAD3, CBX4, PHF10, PHF12, ARHGAP27, CLK1, PAN2, NR4A2, CAPRIN2, PHF13, TCF4, GNB5, TCF3, CLASRP, BRWD1, MXD1, MXD3, FGFR1, MXD4, CREBZF, ZMYND15, RERE, DYRK2, LDB1, THRA, CHD9, NGLY1, HMGB2, HMGB1, TAZ, SOBP, AFF3, PKD1, IRF2BPL, CABIN1, CASP9, LYL1, SENP7, DBP, TRPS1, TOP1MT, GATAD1, WHSC1, MYBL1, RBM5, DACT1, HIST1H1C, KLF10, AXIN1, PPP2R5C, IRAK4, ETV5, KLF16, RBL2, TBC1D1, HSH2D, ELF1, LATS2, ELF2, SETBP1, IRF3, OAS2, TERF2IP, LUC7L3, RBMS2, KDM7A, HIST1H2BN, LAMA5, PDXK, KDM3A, RGS14, USP11, HIST1H2BK, TOB1, GNA13, NXF1, TNKS2, FAM120C, TBX21, MXI1, MAPK1, CRYM, RBM38, CDK11A, POLM, MX2, LIMK2, LRWD1, USP28, TBX19, USF1, REST, NAA16, ERCC6, TAF5, SSBP2, LPIN2, TAF1	1.00	0.99
GOTERM_BP_DIRECT	**GO:0006355~regulation of transcription, DNA-templated**	149	7.85	ZNF331, HDAC10, ZMYND8, JMJD1C, PRDM2, NR3C1, IKZF5, NR3C2, ALKBH4, CPNE1, ZNF569, BBX, EP300, CCNL2, MAP3K9, ZNF721, ZNF566, TRIM22, WHSC1L1, TSPYL2, ZNF441, RNF44, SFMBT1, SP110, ZNF10, ZNF14, CARHSP1, ZNF92, SAP25, KAT6B, ZNF318, ZNF439, HOXB2, ZNF831, ABCG1, ZNF395, ZNF791, ZNF273, MAX, SP140, MAZ, CREM, FOXO4, CDKN2AIP, GMCL1, ZFP36L2, ZBTB2,	1.00	1.00

				SBNO1, ZNF703, ZKSCAN8, ZNF823, ZNF548, ZNF667, ZNF700, ZNF304, SCAI, ZNF266, BPTF, MAP2K6, ZNF540, SMAD3, PHF10, NR1D2, ZNF34, ZBTB11, THAP11, ZFP64, ZNF30, CREBRF, HBP1, TCF3, CNOT8, ZNF654, ZNF652, SLC2A4RG, PHF19, ZNF250, THRA, LDB1, CHD9, CITED2, ZNF490, PHF1, CDCA7L, SETD7, HMGB2, LIMD1, AFF3, AFF4, AFF1, LYL1, ING2, RB1CC1, SUFU, GATAD1, ZNF248, IFT57, MYBL1, ZNF487, ZIK1, ACAD8, CNOT6L, TSC22D1, NCOA3, TSC22D3, RHOH, MSL3, IL16, VAV1, MN1, KAT2A, IRF3, TERF2IP, VGLL4, ZNF595, KANK1, TMF1, SATB1, RNF38, CXXC1, TULP4, ZBTB44, ZBTB41, HDAC7, ZBTB40, PDLIM1, ZFP14, ZNF627, TBX21, MXI1, ZNF107, APBB2, ZNF862, ZNF224, ZNF101, CDK11A, SKOR1, KLF3, PNRC1, REST, ZNF219, ZNF615, PKN2, ZNF699, TAF5, SSBP2, ZNF335, ZNF575, ZNF211		
Annotation Cluster 8	**Enrichment Score: 3.1642482566826033**					
Category	**Term**	**Count**	**%**	**Genes**	**Benjamini**	**FDR**
UP_SEQ_FEATURE	**domain:PDZ**	25	1.32	MAST4, MAST3, HTRA3, HTRA4, LIN7B, SIPA1L3, PDLIM1, PARD6A, RGS3, SIPA1L1, SNX27, PRX, RHPN1, RHPN2, CYTIP, MPP1, LIMK2, LMO7, MPP7, GORASP1, RAPGEF2, PTPN4, CARD14, CARD11, SNTB2	0.02	0.02
INTERPRO	**IPR001478:PDZ domain**	28	1.48	MAST4, MAST3, HTRA3, HTRA4, LIN7B, SIPA1L3, PDLIM1, SLC9A3R1, PARD6A, RGS3, SIPA1L1, SNX27, PRX, RHPN1, RHPN2, CYTIP, MPP1, LIMK2, IL16, LMO7, MPP7, DLG2, GORASP1, RAPGEF2, PTPN4, CARD14, CARD11, SNTB2	0.08	0.08
SMART	**SM00228:PDZ**	25	1.32	MAST4, MAST3, HTRA3, HTRA4, LIN7B, SIPA1L3, PDLIM1, SLC9A3R1, PARD6A, RGS3, SIPA1L1, SNX27, PRX, RHPN1, RHPN2, CYTIP, MPP1, LIMK2, IL16, LMO7, MPP7, DLG2, RAPGEF2, PTPN4, SNTB2	0.39	0.39
Annotation Cluster 9	**Enrichment Score: 3.129072657924711**					
Category	**Term**	**Count**	**%**	**Genes**	**Benjamini**	**FDR**
UP_KEYWORDS	**Immunity**	72	3.79	ITK, IFITM1, DCLRE1C, TNFRSF13B, HMGB2, LRMP, PTPN22, TNFRSF13C, HMGB1, IL1RAP, CD3E, IFIT2, PYCARD, SIT1, CTLA4, HAVCR2, EOMES, ZBP1, MAP4K2, SYK, BTN3A1, CD300A, PRKCB, PRKCE, IRAK4, BTN3A2, LIME1, MR1, LAX1, SIRT2, TIRAP, ATG12, CLEC4C, RNF125, SLFN11, IRF3, CD8A, OAS2, TLR9, CD300E, PRKD2, TLR7, TLR4, S100A8, UNC93B1, ZBTB1, CD1D, LY9, RNF135, CD79B, CD79A, HLA-DMA, C5, IFI16, NLRP6, INPP5D, SLAMF6, CD14, NLRP1, LAIR1, MX2, DAB2IP, SCART1, THEMIS2, CD6, CD7, TBKBP1, TRIM38, SERINC3, CD244, LGR4, SERINC5	0.00	0.00
UP_KEYWORDS	**Innate immunity**	42	2.21	IFITM1, UNC93B1, HMGB2, ZBTB1, HMGB1, CD1D, IL1RAP, LY9, IFIT2, PYCARD, RNF135, C5, IFI16, NLRP6, SLAMF6, NLRP1, CD14, HAVCR2, ZBP1, MAP4K2, SYK, MX2, DAB2IP, IRAK4, MR1, SIRT2, TIRAP, ATG12, CLEC4C, IRF3, CD6, OAS2, TLR9, TLR7, TBKBP1, TRIM38, SERINC3, TLR4, LGR4, S100A8, SERINC5, CD244	0.00	0.00
Annotation Cluster 10	**Enrichment Score: 3.0734691002175567**					
Category	**Term**	**Count**	**%**	**Genes**	**Benjamini**	**FDR**

INTERPRO	**IPR004827:Basic-leucine zipper domain**	15	0.79	CREBZF, JUND, CEBPD, CEBPE, CREM, FOS, FOSL2, MAFB, DBP, MAF, CREB3L2, CREBRF, FOSB, MAFK, JDP2	0.04	0.04
UP_SEQ_FEATURE	**domain:Leucine-zipper**	23	1.21	CREBZF, MLXIP, JUND, TSC22D1, CEBPD, MAX, CEBPE, TSC22D3, CREM, FOS, USF1, FOSL2, MNT, MAFB, DBP, MAF, CREB3L2, FOSB, MAFK, TCF4, TCF3, E2F5, JDP2	0.09	0.09
UP_SEQ_FEATURE	**DNA-binding region:Basic motif**	27	1.42	CREBZF, CEBPD, CEBPE, MAX, CREM, LYL1, MNT, DBP, MXI1, CREB3L2, MLXIP, JUND, NCOA3, FOS, USF1, FOSL2, MAFB, TFAP4, MAF, FOSB, TCF4, MAFK, TCF3, MXD1, MXD3, JDP2, MXD4	0.41	0.41
SMART	**SM00338:BRLZ**	13	0.68	JUND, CEBPD, CEBPE, CREM, FOS, FOSL2, MAFB, DBP, MAF, CREB3L2, FOSB, MAFK, JDP2	0.20	0.20
Annotation Cluster 11	**Enrichment Score: 2.889988188784797**					
Category	**Term**	**Count**	**%**	**Genes**	**Benjamini**	**FDR**
UP_SEQ_FEATURE	**zinc finger region:Phorbol-ester/DAG-type 1**	10	0.53	DGKE, DGKD, PRKCH, PRKD3, PRKCB, DGKA, PRKCE, PRKD2, PRKCA, DEF8	0.02	0.02
UP_SEQ_FEATURE	**zinc finger region:Phorbol-ester/DAG-type 2**	10	0.53	DGKE, DGKD, PRKCH, PRKD3, PRKCB, DGKA, PRKCE, PRKD2, PRKCA, DEF8	0.02	0.02
INTERPRO	**IPR002219:Protein kinase C-like, phorbol ester/diacylglycerol binding**	18	0.95	DGKE, DGKD, PRKCH, PRKCB, DGKA, CDC42BPG, PRKCE, MYO9B, PRKCA, KSR2, DEF8, RASGRP2, VAV1, RASSF1, PRKD3, PLEKHM1, PRKD2, TNS3	0.01	0.01
SMART	**SM00109:C1**	18	0.95	DGKE, DGKD, PRKCH, PRKCB, DGKA, CDC42BPG, PRKCE, MYO9B, PRKCA, KSR2, DEF8, RASGRP2, VAV1, RASSF1, PRKD3, PLEKHM1, PRKD2, TNS3	0.03	0.03
GOTERM_MF_DIRECT	**GO:0004697~protein kinase C activity**	7	0.37	PRKCH, PRKD3, PRKCB, PRKCE, PKN2, PRKD2, PRKCA	0.17	0.17
Annotation Cluster 12	**Enrichment Score: 2.7156459013605057**					
Category	**Term**	**Count**	**%**	**Genes**	**Benjamini**	**FDR**
UP_SEQ_FEATURE	**domain:AGC-kinase C-terminal**	15	0.79	PRKCH, DMPK, MAST4, PRKCB, MAST3, CDC42BPG, PRKCE, PRKCA, PRKX, LATS2, GRK5, AKT2, GRK6, AKT1, PKN2	0.08	0.08
INTERPRO	**IPR000961:AGC-kinase, C-terminal**	15	0.79	PRKCH, DMPK, MAST4, PRKCB, MAST3, CDC42BPG, PRKCE, PRKCA, PRKX, LATS2, GRK5, AKT2, GRK6, AKT1, PKN2	0.05	0.05
SMART	**SM00133:S_TK_X**	13	0.68	PRKCH, DMPK, PRKCB, CDC42BPG, PRKCE, PRKCA, PRKX, LATS2, GRK5, AKT2, GRK6, AKT1, PKN2	0.20	0.20

Annotation Cluster 13	Enrichment Score: 2.6245928426171954					
Category	**Term**	**Count**	**%**	**Genes**	**Benjamini**	**FDR**
GOTERM_BP_DIRECT	GO:0008654~phospholipid biosynthetic process	13	0.68	AGPAT5, DGKE, ISYNA1, MBOAT7, MBOAT1, PTDSS1, LPCAT4, CHPT1, SERINC1, CDIPT, SERINC5, PPARD, SERINC4	0.12	0.12
UP_KEYWORDS	Phospholipid metabolism	13	0.68	AGPAT5, ISYNA1, ABHD3, MBOAT7, MBOAT1, PTDSS1, LPCAT4, CHPT1, SERINC1, CDIPT, SERINC5, CDS2, SERINC4	0.01	0.01
UP_KEYWORDS	Phospholipid biosynthesis	12	0.63	AGPAT5, ISYNA1, PTDSS1, LPCAT4, MBOAT7, MBOAT1, CHPT1, SERINC1, CDIPT, SERINC5, CDS2, SERINC4	0.02	0.02
Annotation Cluster 14	Enrichment Score: 2.540982212931622					
Category	**Term**	**Count**	**%**	**Genes**	**Benjamini**	**FDR**
UP_SEQ_FEATURE	domain:C2	17	0.90	PRKCH, PRKCB, PRKCE, PLA2G4B, PLCL2, DAB2IP, PRKCA, JMJD7, BCR, ABR, RGS3, SYNGAP1, PLCG2, PKN2, PLCH2, PLCB2, PLCD1	0.39	0.39
INTERPRO	IPR000008:C2 calcium-dependent membrane targeting	27	1.42	RASAL1, ABR, RGS3, SYNGAP1, CPNE1, PLCG2, TNS3, PRKCH, PRKCB, PRKCE, PLA2G4B, PLCL2, DAB2IP, SYTL1, PRKCA, SYTL3, BAIAP3, GAK, BCR, RASA3, RASA2, PKN2, ESYT1, PLCH2, PLCB2, PLCD1, C2CD2L	0.23	0.23
SMART	SM00239:C2	24	1.26	PRKCH, PRKCB, PRKCE, PLA2G4B, PLCL2, DAB2IP, SYTL1, PRKCA, RASAL1, SYTL3, BAIAP3, BCR, ABR, RGS3, SYNGAP1, RASA3, RASA2, CPNE1, PLCG2, PKN2, ESYT1, PLCH2, PLCB2, PLCD1	0.20	0.20
Annotation Cluster 15	Enrichment Score: 2.5356295748876923					
Category	**Term**	**Count**	**%**	**Genes**	**Benjamini**	**FDR**
UP_SEQ_FEATURE	domain:Ras-associating	11	0.58	GRB7, RASSF1, SNX27, RASSF7, RAPGEF2, RIN3, MYO9B, ARAP1, RIN2, RGL2, RALGDS	0.12	0.12
INTERPRO	IPR000159:Ras-association	11	0.58	GRB7, RASSF1, SNX27, RASSF7, RAPGEF2, RIN3, MYO9B, ARAP1, RIN2, RGL2, RALGDS	0.22	0.22
Annotation Cluster 16	Enrichment Score: 2.5058073926715876					
Category	**Term**	**Count**	**%**	**Genes**	**Benjamini**	**FDR**
UP_KEYWORDS	SH2 domain	21	1.11	GRB7, ITK, SRMS, SYK, STAT2, SLA, PIK3R1, SLA2, VAV1, CRKL, HSH2D, LCK, INPP5D, BLNK, PLCG2, STAP1, LCP2, RIN3, GRAP, RIN2, TNS3	0.01	0.01

INTERPRO	**IPR000980:SH2 domain**	22	1.16	GRB7, ITK, SRMS, SYK, STAT2, SLA, CBLB, PIK3R1, SLA2, VAV1, CRKL, HSH2D, LCK, INPP5D, BLNK, PLCG2, STAP1, LCP2, RIN3, GRAP, RIN2, TNS3	0.12	0.11
SMART	**SM00252:SH2**	20	1.05	GRB7, ITK, SRMS, SYK, STAT2, SLA, PIK3R1, SLA2, VAV1, CRKL, HSH2D, LCK, INPP5D, BLNK, PLCG2, STAP1, LCP2, RIN3, GRAP, TNS3	0.27	0.27
Annotation Cluster 17	**Enrichment Score: 2.228162721245955**					
Category	**Term**	**Count**	**%**	**Genes**	**Benjamini**	**FDR**
INTERPRO	**IPR008936:Rho GTPase activation protein**	20	1.05	ARHGAP9, FAM13B, PLXND1, DAB2IP, ARHGAP18, MYO9B, RASAL1, PIK3R1, ARAP1, ARHGAP27, IQGAP2, ARHGAP6, ARHGAP4, ARHGAP12, BCR, ABR, SYNGAP1, RASA3, RASA2, SRGAP3	0.06	0.06
Annotation Cluster 18	**Enrichment Score: 2.1929213236150047**					
Category	**Term**	**Count**	**%**	**Genes**	**Benjamini**	**FDR**
INTERPRO	**IPR010919:SAND domain-like**	7	0.37	SP100, SKOR1, GMEB2, SP110, DEAF1, SP140, SKIL	0.05	0.05
UP_SEQ_FEATURE	**domain:SAND**	5	0.26	SP100, GMEB2, SP110, DEAF1, SP140	0.49	0.49
INTERPRO	**IPR000770:SAND domain**	5	0.26	SP100, GMEB2, SP110, DEAF1, SP140	0.23	0.23
SMART	**SM00258:SAND**	5	0.26	SP100, GMEB2, SP110, DEAF1, SP140	0.23	0.23
Annotation Cluster 19	**Enrichment Score: 2.1201242349819474**					
Category	**Term**	**Count**	**%**	**Genes**	**Benjamini**	**FDR**
UP_KEYWORDS	**Guanine-nucleotide releasing factor**	26	1.37	DENND5B, ARHGEF10L, RASGRP2, FGD1, FGD3, ABR, CYTH2, PSD3, SBF1, RALGDS, RALGPS2, VAV1, BCR, MADD, SPATA13, ARHGEF3, RAPGEF2, DENND6B, ARHGEF1, DENND6A, RGL4, SOS1, RGL2, SOS2, RAPGEF3, ARHGEF6	0.01	0.01
UP_SEQ_FEATURE	**domain:Ras-GEF**	9	0.47	RAPGEF2, RGL4, RASGRP2, SOS1, RGL2, RALGDS, SOS2, RAPGEF3, RALGPS2	0.48	0.48
INTERPRO	**IPR001895:Guanine-nucleotide dissociation stimulator CDC25**	9	0.47	RAPGEF2, RGL4, RASGRP2, SOS1, RGL2, RALGDS, SOS2, RAPGEF3, RALGPS2	0.26	0.26
INTERPRO	**IPR023578:Ras guanine nucleotide exchange factor, domain**	9	0.47	RAPGEF2, RGL4, RASGRP2, SOS1, RGL2, RALGDS, SOS2, RAPGEF3, RALGPS2	0.26	0.26

SMART	**SM00147:RasGEF**	9	0.47	RAPGEF2, RGL4, RASGRP2, SOS1, RGL2, RALGDS, SOS2, RAPGEF3, RALGPS2	0.30	0.30
SMART	**SM00229:RasGEFN**	7	0.37	RAPGEF2, RASGRP2, SOS1, RGL2, RALGDS, SOS2, RAPGEF3	0.35	0.34
Annotation Cluster 20	**Enrichment Score: 2.082623531533771**					
Category	**Term**	**Count**	**%**	**Genes**	**Benjamini**	**FDR**
UP_KEYWORDS	**Guanine-nucleotide releasing factor**	26	1.37	DENND5B, ARHGEF10L, RASGRP2, FGD1, FGD3, ABR, CYTH2, PSD3, SBF1, RALGDS, RALGPS2, VAV1, BCR, MADD, SPATA13, ARHGEF3, RAPGEF2, DENND6B, ARHGEF1, DENND6A, RGL4, SOS1, RGL2, SOS2, RAPGEF3, ARHGEF6	0.01	0.01
GOTERM_MF_DIRECT	**GO:0005089~Rho guanyl-nucleotide exchange factor activity**	17	0.90	ARHGEF10L, FGD1, VAV1, ARHGAP4, BCR, FGD3, ABR, OBSCN, DNMBP, SPATA13, ARHGEF3, ARHGEF1, EPS8L2, SOS1, RGL2, SOS2, ARHGEF6	0.17	0.17
SMART	**SM00325:RhoGEF**	14	0.74	ARHGEF10L, FGD1, VAV1, BCR, FGD3, ABR, OBSCN, DNMBP, SPATA13, ARHGEF3, ARHGEF1, SOS1, SOS2, ARHGEF6	0.42	0.42
Annotation Cluster 21	**Enrichment Score: 1.9646590923423788**					
Category	**Term**	**Count**	**%**	**Genes**	**Benjamini**	**FDR**
KEGG_PATHWAY	**hsa04070:Phosphatidylinositol signaling system**	21	1.11	DGKE, MTMR3, DGKD, PRKCB, DGKA, ITPR2, PRKCA, PIK3R1, INPP5A, IMPA2, INPP5D, PI4KA, PLCG2, PIP4K2B, CALM1, CDIPT, PLCB2, PI4K2A, PLCD1, IP6K2, CDS2	0.02	0.02
KEGG_PATHWAY	**hsa00562:Inositol phosphate metabolism**	14	0.74	ISYNA1, MTMR3, INPP5A, IMPA2, INPP5D, PIP5KL1, PI4KA, PLCG2, PIP4K2B, PLCH2, CDIPT, PLCB2, PI4K2A, PLCD1	0.21	0.20
Annotation Cluster 22	**Enrichment Score: 1.8566638287743147**					
Category	**Term**	**Count**	**%**	**Genes**	**Benjamini**	**FDR**
INTERPRO	**IPR001487:Bromodomain**	12	0.63	KAT2B, SP100, KAT2A, SP110, ZMYND8, SP140, EP300, TAF1L, PHIP, BRWD1, TAF1, BPTF	0.12	0.12
UP_KEYWORDS	**Bromodomain**	11	0.58	KAT2B, KAT2A, SP110, ZMYND8, SP140, EP300, TAF1L, PHIP, BRWD1, TAF1, BPTF	0.02	0.02
SMART	**SM00297:BROMO**	12	0.63	KAT2B, SP100, KAT2A, SP110, ZMYND8, SP140, EP300, TAF1L, PHIP, BRWD1, TAF1, BPTF	0.18	0.17
INTERPRO	**IPR018359:Bromodomain, conserved site**	8	0.42	KAT2B, KAT2A, EP300, TAF1L, PHIP, BRWD1, TAF1, BPTF	0.37	0.37

Annotation Cluster 23	Enrichment Score: 1.8043454946613842					
Category	**Term**	**Count**	**%**	**Genes**	**Benjamini**	**FDR**
INTERPRO	**IPR017946:PLC-like phosphodiesterase, TIM beta/alpha-barrel domain**	9	0.47	PLCL2, GDPD1, GDE1, PLCG2, GDPD3, PLCH2, GPCPD1, PLCB2, PLCD1	0.12	0.12
Annotation Cluster 24	**Enrichment Score: 1.7576802253602772**					
Category	**Term**	**Count**	**%**	**Genes**	**Benjamini**	**FDR**
INTERPRO	**IPR018494:Oxysterol-binding protein, conserved site**	6	0.32	OSBPL8, OSBPL7, OSBPL5, OSBPL3, OSBPL11, OSBP2	0.23	0.23
INTERPRO	**IPR000648:Oxysterol-binding protein**	6	0.32	OSBPL8, OSBPL7, OSBPL5, OSBPL3, OSBPL11, OSBP2	0.23	0.23
Annotation Cluster 26	**Enrichment Score: 1.4542508576542912**					
Category	**Term**	**Count**	**%**	**Genes**	**Benjamini**	**FDR**
UP_KEYWORDS	**Calmodulin-binding**	23	1.21	PDE1B, EPB41, RRAD, DAPK2, ATP2B4, PHKB, MYO9B, TRPV1, IQGAP2, ADD3, SLC8A1, CAMKK1, SLC9A1, PPP3CA, OBSCN, KCNQ1, PHKG2, STRN, CEP97, SPTAN1, SPTBN1, MYO1F, SNTB2	0.12	0.11
Annotation Cluster 27	**Enrichment Score: 1.4401948725310674**					
Category	**Term**	**Count**	**%**	**Genes**	**Benjamini**	**FDR**
UP_SEQ_FEATURE	**domain:BTB**	25	1.32	KLHL14, KLHL15, KLHL32, ZBTB1, ZBTB20, ZBTB44, ZBTB4, GMCL1, ZBTB41, ZBTB40, ZBTB2, BTBD2, ENC1, ZBTB18, ZBTB14, ZBTB38, KLHL2, KLHL3, KLHL24, BTBD6, ZBTB11, KCTD7, KBTBD6, KLHL8, KBTBD7	0.37	0.37
INTERPRO	**IPR000210:BTB/POZ-like**	29	1.53	KLHL14, KLHL15, KCNA3, KLHL32, ZBTB1, ZBTB20, ZBTB44, ZBTB4, GMCL1, ZBTB41, ZBTB40, RCBTB2, ZBTB2, BTBD2, ENC1, ZBTB18, KCND1, ZBTB14, ZBTB38, KLHL2, KLHL3, KLHL24, BTBD6, ZBTB11, KCTD7, KBTBD6, KLHL8, KCTD12, KBTBD7	0.23	0.23
INTERPRO	**IPR011705:BTB/Kelch-associated**	14	0.74	KLHL14, KLHL15, KLHL32, KLHL2, KLHL3, KLHL24, BTBD6, GMCL1, RCBTB2, KBTBD6, KLHL8, ENC1, BTBD2, KBTBD7	0.23	0.23
INTERPRO	**IPR011333:BTB/POZ fold**	29	1.53	KLHL14, KLHL15, KCNA3, KLHL32, ZBTB1, ZBTB20, ZBTB44, ZBTB4, GMCL1, ZBTB41, ZBTB40, RCBTB2, ZBTB2, BTBD2, ENC1, ZBTB18, KCND1, ZBTB14, ZBTB38, KLHL2, KLHL3, KLHL24, BTBD6, ZBTB11, KCTD7, KBTBD6, KLHL8, KCTD12, KBTBD7	0.36	0.36

SMART	**SM00225:BTB**	29	1.53	KLHL14, KLHL15, KCNA3, KLHL32, ZBTB1, ZBTB20, ZBTB44, ZBTB4, GMCL1, ZBTB41, ZBTB40, RCBTB2, ZBTB2, BTBD2, ENC1, ZBTB18, KCND1, ZBTB14, ZBTB38, KLHL2, KLHL3, KLHL24, BTBD6, ZBTB11, KCTD7, KBTBD6, KLHL8, KCTD12, KBTBD7	0.32	0.31
SMART	**SM00875:SM00875**	13	0.68	KLHL14, KLHL15, KLHL32, KLHL2, KLHL3, KLHL24, BTBD6, GMCL1, KBTBD6, KLHL8, ENC1, BTBD2, KBTBD7	0.40	0.39
UP_KEYWORDS	**Kelch repeat**	12	0.63	ATRN, KLHDC3, KBTBD6, KLHL14, KLHL15, KLHL8, ENC1, KLHL32, KLHL2, KLHL3, KLHL24, KBTBD7	0.32	0.29
Annotation Cluster 28	**Enrichment Score: 1.4232636450580167**					
Category	**Term**	**Count**	**%**	**Genes**	**Benjamini**	**FDR**
KEGG_PATHWAY	**hsa04750:Inflammatory mediator regulation of TRP channels**	18	0.95	MAP2K3, PRKCH, IL1R1, PRKCB, PTGER2, PRKCE, PLA2G4B, ADCY4, ITPR2, PRKCA, IL1RAP, PIK3R1, TRPV1, PLCG2, CALM1, PLCB2, ASIC3, MAP2K6	0.16	0.15
KEGG_PATHWAY	**hsa04912:GnRH signaling pathway**	16	0.84	MAP2K3, MAP3K2, MAP3K3, MAP3K1, PRKCB, PLA2G4B, LHB, ADCY4, ITPR2, PRKCA, MAPK1, CALM1, SOS1, PLCB2, SOS2, MAP2K6	0.27	0.26
Annotation Cluster 29	**Enrichment Score: 1.4134361940678333**					
Category	**Term**	**Count**	**%**	**Genes**	**Benjamini**	**FDR**
INTERPRO	**IPR017946:PLC-like phosphodiesterase, TIM beta/alpha-barrel domain**	9	0.47	PLCL2, GDPD1, GDE1, PLCG2, GDPD3, PLCH2, GPCPD1, PLCB2, PLCD1	0.12	0.12
GOTERM_BP_DIRECT	**GO:0043647~inositol phosphate metabolic process**	11	0.58	ISYNA1, INPP5A, IMPA2, INPP5D, PLCG2, PLD4, PLCH2, CALM1, PLCB2, PLCD1, IP6K2	0.92	0.92
UP_KEYWORDS	**Lipid degradation**	17	0.90	ABHD4, RARRES3, PNPLA8, PLA2G4B, PLCL2, PLD4, PLD3, PLA2G15, BSCL2, NCEH1, ENPP2, PLCG2, PLCH2, DAGLB, PLCB2, PLCD1, PNPLA2	0.18	0.16
Annotation Cluster 30	**Enrichment Score: 1.3927018413296675**					
Category	**Term**	**Count**	**%**	**Genes**	**Benjamini**	**FDR**
UP_SEQ_FEATURE	**repeat:LRR 11**	19	1.00	LRRC37A3, DNAH10, LINGO3, LRRN2, LRRK2, NLRC3, SYNE2, FBXL20, MFHAS1, CHAD, CNTRL, LRIG1, LRRC8C, TLR9, LRRC8A, TLR7, CD14, TLR4, LGR4	0.48	0.48

UP_KEYWORDS	**Leucine-rich repeat**	40	2.11	LRRC58, LRRC56, LRRC34, LRRK2, LRRC6, NLRC3, ELFN2, PKD1, CMIP, FBXL20, NXF1, NLRP6, CHAD, CNTRL, LRRC8C, LRIG1, LRRC8A, NLRP1, CD14, CEP97, LRRC25, LRRC37A3, LRRC45, ZER1, LINGO3, CNOT6L, LRRN2, LRWD1, FBXL16, FBXL14, LRRC37B, NISCH, MFHAS1, LRFN1, TLR9, TLR7, FBXL3, LRCH4, TLR4, LGR4	0.12	0.11
Annotation Cluster 31	**Enrichment Score: 1.387162290812207**					
Category	**Term**	**Count**	**%**	**Genes**	**Benjamini**	**FDR**
INTERPRO	**IPR023152:Ras GTPase-activating protein, conserved site**	6	0.32	SYNGAP1, RASA3, RASA2, DAB2IP, RASAL1, IQGAP2	0.35	0.35
SMART	**SM00323:RasGAP**	6	0.32	SYNGAP1, RASA3, RASA2, DAB2IP, RASAL1, IQGAP2	0.32	0.31
Annotation Cluster 32	**Enrichment Score: 1.3698741959328966**					
Category	**Term**	**Count**	**%**	**Genes**	**Benjamini**	**FDR**
INTERPRO	**IPR005016:TMS membrane protein/tumour differentially expressed protein**	4	0.21	SERINC1, SERINC3, SERINC5, SERINC4	0.36	0.36
Annotation Cluster 34	**Enrichment Score: 1.323712597280405**					
Category	**Term**	**Count**	**%**	**Genes**	**Benjamini**	**FDR**
INTERPRO	**IPR025110:Domain of unknown function DUF4009**	7	0.37	SLC27A1, ACSS2, ACSM3, ACSM1, ACSS1, SLC27A3, ACSF2	0.32	0.31
Annotation Cluster 35	**Enrichment Score: 1.3123341382336493**					
Category	**Term**	**Count**	**%**	**Genes**	**Benjamini**	**FDR**
KEGG_PATHWAY	**hsa04620:Toll-like receptor signaling pathway**	18	0.95	MAP2K3, IFNAR2, PIK3R1, FOS, IRAK4, TIRAP, CASP8, IRF3, CTSK, AKT2, CCL5, TLR9, AKT1, MAPK1, TLR7, CD14, TLR4, MAP2K6	0.26	0.24

KEGG_PATHWAY	**hsa05164:Influenza A**	24	1.26	MAP2K3, IFNAR2, RNASEL, PRKCB, STAT2, HSPA6, PRKCA, PIK3R1, IRAK4, CASP9, PYCARD, NXF1, HLA-DMA, IRF3, OAS2, AKT2, CCL5, TNFSF10, AKT1, EP300, MAPK1, TLR7, TLR4, MAP2K6	0.48	0.45
Annotation Cluster 36	**Enrichment Score: 1.2883151249422808**					
Category	**Term**	**Count**	**%**	**Genes**	**Benjamini**	**FDR**
INTERPRO	**IPR013083:Zinc finger, RING/FYVE/PHD-type**	62	3.27	PHF3, PHF2, RNF13, PHF1, ZMYND8, CBLB, PHF7, ING1, ZFYVE28, TRIM8, ING4, ING2, TRIM7, RNF19A, WHSC1, TRIM65, TRIM22, WHSC1L1, TRIM23, RNF44, SP110, SYTL1, NOSIP, SYTL3, RNF41, RNF125, KAT6B, TRAF5, RNF166, KDM7A, RNFT2, KMT2E, SP100, MTMR3, TRIM52, UHRF2, SP140, RNF38, CXXC1, FGD1, RNF135, FGD3, RNF113A, RNF213, RNF39, RNF130, BPTF, MAP3K1, RNF24, PHF10, USP20, AMFR, PHF12, MIB2, SYVN1, TRIM39, RNF149, MKRN1, TTC3, PHF13, TRIM38, PHF19	0.11	0.11
UP_KEYWORDS	**Ligase**	42	2.21	SLC27A1, ACSS2, RNF13, UBA7, ACSM3, UHRF2, TARSL2, ACSM1, RNF38, PELI2, UBR2, CBLB, ACACB, TRIM8, RNF135, RNF213, TMEM129, CARNS1, ACSS1, RNF130, UNKL, TRIM22, TRIM23, LIG1, CBX4, MIB2, SYVN1, MSL2, NOSIP, QRSL1, ACSF2, RNF41, GCLC, RNF125, TRIM39, RNF149, NFX1, TTC3, MKRN1, TRIM38, SLC27A3, CARS2	0.20	0.18
Annotation Cluster 37	**Enrichment Score: 1.287816573199845**					
Category	**Term**	**Count**	**%**	**Genes**	**Benjamini**	**FDR**
UP_KEYWORDS	**cAMP**	8	0.42	PDE1B, PRKAR2A, PDE4B, PDE4A, PRKX, PDE7B, HCN2, RAPGEF3	0.24	0.22
Annotation Cluster 43	**Enrichment Score: 1.1669934747797173**					
Category	**Term**	**Count**	**%**	**Genes**	**Benjamini**	**FDR**
UP_KEYWORDS	**Ubl conjugation pathway**	70	3.69	DYRK2, RNF13, CBLB, AUP1, FBXO21, TRIM8, SENP7, HERC3, MAP1LC3B, RNF19A, UNKL, TRIM22, FBXO9, TRIM23, USP8, WSB1, ZER1, FBXO18, MSL2, FBXO15, NOSIP, FBXO10, ATG12, RNF41, RNF125, NFX1, NUMBL, UBA7, UHRF2, KLHL15, USP11, RNF38, PELI2, TULP4, UBR2, FBXO44, DCAF15, RNF135, FBXL20, RNF213, RAB40B, STAMBPL1, TMEM129, FAM63B, TBL1X, RNF130, UBE2H, CBX4, MAGEE1, USP20, USP21, AMFR, MIB2, SYVN1, KLHL2, KLHL3, UBE2G1, FBXL16, USP28, FBXO32, FBXL14, TRIM39, RNF149, MKRN1, KLHL8, TTC3, FBXL3, TRIM38, OTUD1, CUL4B	0.52	0.48
Annotation Cluster 52	**Enrichment Score: 1.0723931866878693**					
Category	**Term**	**Count**	**%**	**Genes**	**Benjamini**	**FDR**

INTERPRO	**IPR001245:Serine-threonine/tyrosine-protein kinase catalytic domain**	24	1.26	EPHB6, GUCY2C, ITK, SRMS, FLT1, SYK, MLKL, TNK2, LIMK2, NEK7, TNK1, LMTK2, AATK, KSR2, IRAK4, MERTK, IGF1R, GAK, DSTYK, LCK, ROR1, MAP3K9, MAP3K12, FGFR1	0.23	0.23
UP_KEYWORDS	**Tyrosine-protein kinase**	17	0.90	MAP2K3, ITK, SRMS, FLT1, DYRK2, SYK, TNK2, TNK1, DYRK1B, MERTK, IGF1R, CLK1, SGK223, DSTYK, LCK, MAP2K6, FGFR1	0.23	0.21
Annotation Cluster 53	**Enrichment Score: 1.060789865736934**					
Category	**Term**	**Count**	**%**	**Genes**	**Benjamini**	**FDR**
GOTERM_BP_DIRECT	**GO:0010875~positive regulation of cholesterol efflux**	7	0.37	ABCA1, LRP1, PTCH1, ABCA7, APOE, SIRT1, ABCG1	0.37	0.37
Annotation Cluster 54	**Enrichment Score: 1.0537908615806293**					
Category	**Term**	**Count**	**%**	**Genes**	**Benjamini**	**FDR**
UP_KEYWORDS	**Membrane**	746	39.30	XYLT2, XYLT1, EHMT1, NPIPB11, SLA2, FAM159A, ZFYVE28, FAM134C, NDST1, FAM134A, AKT2, CREB3L2, C3AR1, AKT1, PIP4K2B, CEP95, CMKLR1, GABARAPL3, GABARAPL1, PRKCB, DAPK2, PRKCE, HPCAL1, SYTL1, CACNA2D2, PRKCA, SCAMP1, TMEM80, TMEM81, SYTL3, ATG12, LRRC37B, BCR, SIGIRR, NISCH, RNF125, PRKD3, TMEM79, GPR160, ORAI2, PRKD2, MPPE1, ADPRM, PI4K2A, ABCB1, MTMR3, TTYH3, SAR1B, FAXDC2, FPR3, LYPD3, ABCB8, VPS26B, LY9, KIAA0040, XKRX, CHST11, NUP85, CHST12, PRKAR2A, RDH10, EPB41L3, CHST15, HMOX1, SSR1, C19ORF38, RHBDL1, ABCA1, LRRC37A3, ABCA2, MYH7B, GSDMB, FZD3, DNAH10, DMPK, HOMER2, ABCA9, ABCA7, EHD3, FXYD1, SFXN3, NMT2, TNFSF9, FXYD7, STRN, TNFSF8, PLCH2, FXYD5, GPR18, GAPT, ATG2B, HRK, GABRB2, OSBPL11, TMEM187, DSTYK, JPH3, C1QTNF6, SMPD1, CTLA4, AP3S1, EMB, GPR135, C11ORF24, HAVCR2, FCRL1, FCRL2, KCND1, SLC2A11, SLC39A10, EPS15L1, TMEM175, SIRT2, COQ10A, FAM210B, GCHFR, BACE2, SLC7A7, SLC7A8, MMP17, RAPGEF2, VAMP1, SLC18B1, VAMP4, RAPGEF3, VAMP2, KANK1, ASAH1, CLDND2, TP53I13, TMF1, ATL1, PELI2, ADCY4, KCNA3, APOLD1, TMEM71, GPR152, GGA2, ADAM29, HLA-DMA, ADAM28, GGA3, GPNMB, SLC17A9, TMEM65, SNX27, UCP3, ALOX5, SNX25, MFN1, GCNT2, SLC17A5, HAS3, METTL7A, RABAC1, GPR155, P4HTM, RNF130, NKTR, LRRC25, COLCA1, IL10RB, SYVN1, DAB2IP, LAPTM5, TMEM62, CRYM-AS1, SLC8B1, BLCAP, DEF6, TMEM154, TMEM156, TMEM59, GATM, TMEM159, RNF149, LPCAT4, TMEM56, TAOK2, PKN2, PLP2, CRLF3, CRAT, LGR4, TMEM229B, LIMS1, DGKE, SLC27A1, DGKD, ANKRD13D, PLXND1, CLSTN3, FMR1, CLSTN1, NCF4, GUCA1B, IL1RAP, AUP1, SLC8A1, CXCL16, TM7SF2, BEST4, LAPTM4A, CYSLTR1, SMCHD1, FCGRT, RNF19A, TOM1, SLC16A7, SLC26A11, SLC39A8, MAP3K9, SLC25A42, ZNF566, ANKRD13A, SLC16A4, SLC39A3, SEMA6B, IFNAR2, KCNH2, BNIP3L, USP8, LAG3, FBXO18, BTN1A1, F2R, STX7, DISP1, ARMCX3, BSCL2, CACNB2, CLEC4C, RAB30, ACAP2, ACAP1, STIM1, SYPL1, STIM2, MADD, ROR1, SLC25A53, PTPRCAP, UTRN, SLC27A3, FAM8A1, S100A8, OSBP2, TRABD2A, KMT2E, LCN8, UQCRB, ABHD3, INSIG2, ARL3, ITPR2, LIN7B, SLC9A1, SLC9A3R1, ITPRIPL1, TBXA2R, MBP,	0.00	0.00

				RAB6A, OSBPL8, SLC14A1, CD163, OSBPL7, SLC37A2, OSBPL5, OSBPL3, TNK2, TNK1, PHKB, PTPRE, BFSP2, PTPRC, STK24, REEP5, LRFN1, PLEKHM1, SERINC1, FAM26F, OR13A1, SERINC3, LRCH4, OGT, SLC26A6, SERINC5, MAP3K12, SERINC4, SLC48A1, ITGB1, FLT1, BMPR2, RNF13, ADPGK, LRRK2, CDCA7L, LRMP, ARRB2, ELFN2, ITGAL, NAGPA, SYNE2, FCGR3A, PIP5KL1, PSD3, ITGB7, ATP7A, LBR, TAPT1, DGCR2, AMN, APAF1, PVRIG, AVPR2, NDUFC1, KCNAB1, C1ORF162, KSR2, BET1L, TIRAP, PTP4A1, ARL4C, ATRN, DNAJC1, RRM2B, SNPH, LCK, DNAJC4, PECAM1, PPP1R12B, DAGLB, ST6GALNAC4, ST6GALNAC6, CERS2, RNFT2, LRP1, UNC93B1, PBXIP1, SLC25A29, P2RY6, PARD6A, SLC25A28, RAB24, FCHO2, LRRC8C, CEACAM21, LRRC8A, SLC13A5, E2F5, CNNM3, SEC11A, CNNM4, MLXIP, SLC35A1, LINGO3, SEMA4D, KCNJ11, RNF24, PCDH9, AMFR, SEMA4B, MBOAT7, SPAG4, MBOAT1, HIP1R, MERTK, TPCN1, SCART1, P2RX5, CLEC2B, P2RX1, IL2RB, SLC25A30, CD248, FCGR2B, FOLR2, PTPN4, FCGR2C, CD244, SLC25A36, EPHB6, VIPR1, IFITM1, SLC46A1, TRAF3IP3, AHCYL1, CERK, ACSM1, SLC23A1, PLEKHB1, GDE1, GCC2, LDLRAD4, ANTXR2, AQP3, TXNDC15, OR52N4, ANPEP, GOLGA1, TNFSF10, CPNE1, FAM65B, SLC12A6, SEC62, BRICD5, TRIM23, ARL6IP6, PAQR6, ST6GAL1, SLC6A16, IL1R1, COG4, BROX, ARRDC3, AP1B1, ANK1, RUNX1, CYP27A1, KCNQ1, SPATA13, FAM76B, KCTD12, EZR, ANKRA2, CUTA, IGSF8, GPM6A, GRB7, TMEM63A, SLC35D1, RRAD, GIPR, EPB41, CD1D, APCDD1, CD79B, CD79A, PTDSS1, SNX2, INPP5A, INPP5D, ARSK, SLAMF6, CD14, SEC31B, RAB11FIP4, SCAI, SPTBN1, BANP, VAT1, BBS2, TMEM86B, MAGEE1, LRRN2, SYNRG, TNFSF12, SIGLEC10, PARP16, UBAC2, MC1R, NCEH1, PARVG, VNN2, LPAR5, ADCK2, CD27, CD24, ITM2B, C2CD2L, CD320, CDS2, TNFRSF13B, SLC44A2, DIRAS1, TECR, GRIK3, AATK, MIA3, TNFRSF13C, PCSK7, CD3E, TRAM2, SIPA1L3, PPP3CA, MAP1LC3B, GLIPR1, SIPA1L1, SLC22A17, CHMP1B, SLC22A18, PRX, STAB1, CLDN23, QSOX1, CCR6, QSOX2, CD36, DIRC2, TMED5, RALGPS2, CD53, CD52, MAP4K2, SYK, BTN3A1, GAA, MINK1, ANO8, RHOH, GAB2, BTN3A2, RGMB, LIME1, IL17RA, RHOB, RAB33B, NAALADL1, PITPNM1, CLDN15, PITPNM2, TLR9, TLR7, ARHGEF1, CD48, CD47, ATP6V0C, TLR4, GUCY2C, SELPLG, STX16, ZDHHC20, DERL3, PTGER2, GDPD1, CXCR4, GDPD3, PRICKLE1, NKD1, STX10, DCST2, ZFP14, MGAT5, KISS1R, SUSD3, MGAT1, ATP6V0E2, REM2, LAIR1, MPP1, PNPLA7, PNPLA8, PLEKHA2, KLHL2, ORMDL1, PLEKHA3, LHFPL2, MPP7, KBTBD6, ESYT1, RAMP1, PNPLA2, DPAGT1, SCARB2, ITPRIP, DENND5B, SPPL2B, CIB1, TMEM140, NR3C2, IGF1R, TMEM143, RGS2, CCND3, RGS3, GNPTAB, SIT1, MPZ, FAM198B, ENPP2, TMEM38A, CA14, CD96, UNC5CL, CD300A, IL11RA, ATG9A, SHISA5, ADAM10, LMTK2, TSC1, DNAJB14, CYBA, SLC30A1, LMO7, MR1, LAX1, ERMN, MPEG1, KCTD7, PLA2G15, ALDH3A2, TMEM134, DPM3, TMX4, DOK3, TBC1D20, TMEM259, CD8A, SIDT1, DPEP2, CD300E, WDFY4, ABCG1, CARD11, SIDT2, RTN3, PMEL, GNAZ, PXK, KLHL14, PLD4, ADRB2, NDRG2, RASGRP2, ACACB, NDRG1, LPP, PLD3, SEL1L3, TMEM123, CALHM2, MAN2A2, NLRP6, GRK5, MAN2A1, TMEM127, ALDH3B1, TMEM129, GRK6, ASIC3, C16ORF54, PACSIN1, ACBD4, MLKL, RARRES3, RHBDD1, PTCH1, EPHX1, NKG7, TRPV1, ARHGAP27, BTNL2, TMEM110, GNAO1, GCLC, EFNA3, DLG2, TMEM236, CCPG1, PI4KA, DEGS2, GNB5, LRP10, MUC20, SDK2, SLC35E2B, FGFR1, B4GALT3, DYRK2, B4GALT1, MS4A7, ATP2A3, SLC2A3, ATP2A1, HMGB1, TMEM191A, TAZ, PKD1, HS2ST1, LMNB1, MFSD8, CYP4V2, TMEM107, BLNK, PDE4A, TMEM109, MAN1A1, SCARF2, ABCD1, SUN2, ABCC2, RBM15, PLA2G4B, ABCC5, AXIN1, ABHD14A, PEX1, ARAP1, SSTR3, CKAP4, TMEM2, RASA3, CDHR1, PEX6, GORASP1, TMEM219, SCN4A, MAN1B1, AGPAT5, RALB, RGS14, ADD3, DLL1, GNA13, CYTH2, RAB40B, CNR2, TNKS2, CLMN, GNG7, LEPROTL1, LRIG1, MAN1C1, S1PR1, CDIPT, S1PR4, TAS1R3, MBTPS1, GALNT3, ATP13A1, QPCTL, ATP2B4, SCIMP, SGPP1, PIK3IP1, CD6, CD5, ALOX5AP, CD7, CHPT1, CMTM1, LPIN2, HCN2, SNTB2		
UP_KEYWORDS	**Transmembrane helix**	526	27.71	XYLT2, XYLT1, EHMT1, NPIPB11, FAM159A, FAM134C, NDST1, FAM134A, CREB3L2, C3AR1, CEP95, CMKLR1, DAPK2, CACNA2D2, SCAMP1, TMEM80, TMEM81, LRRC37B, SIGIRR, TMEM79, GPR160, ORAI2, MPPE1, ADPRM, ABCB1, TTYH3, FAXDC2, FPR3, ABCB8, VPS26B, LY9, KIAA0040, XKRX, CHST11, CHST12, RDH10, EPB41L3, CHST15, HMOX1, SSR1, C19ORF38, RHBDL1, ABCA1, LRRC37A3,	0.14	0.13

				ABCA2, FZD3, DNAH10, DMPK, ABCA9, ABCA7, FXYD1, SFXN3, TNFSF9, FXYD7, TNFSF8, FXYD5, GPR18, GAPT, HRK, GABRB2, TMEM187, JPH3, C1QTNF6, SMPD1, CTLA4, EMB, GPR135, C11ORF24, HAVCR2, FCRL1, FCRL2, KCND1, SLC2A11, SLC39A10, TMEM175, FAM210B, BACE2, SLC7A7, SLC7A8, VAMP1, SLC18B1, VAMP4, VAMP2, ASAH1, CLDND2, TP53I13, ATL1, PELI2, ADCY4, KCNA3, APOLD1, TMEM71, GPR152, ADAM29, HLA-DMA, ADAM28, GPNMB, SLC17A9, TMEM65, UCP3, MFN1, GCNT2, SLC17A5, HAS3, METTL7A, RABAC1, GPR155, P4HTM, RNF130, LRRC25, COLCA1, IL10RB, SYVN1, LAPTM5, TMEM62, CRYM-AS1, SLC8B1, BLCAP, TMEM154, TMEM156, TMEM59, TMEM159, RNF149, LPCAT4, TMEM56, TAOK2, PKN2, PLP2, CRLF3, LGR4, TMEM229B, DGKE, SLC27A1, PLXND1, CLSTN3, CLSTN1, IL1RAP, AUP1, SLC8A1, CXCL16, TM7SF2, BEST4, LAPTM4A, CYSLTR1, SMCHD1, FCGRT, RNF19A, SLC16A7, SLC26A11, SLC39A8, MAP3K9, SLC25A42, ZNF566, SLC16A4, SLC39A3, SEMA6B, IFNAR2, KCNH2, BNIP3L, LAG3, FBXO18, BTN1A1, F2R, STX7, DISP1, ARMCX3, BSCL2, CLEC4C, STIM1, SYPL1, STIM2, ROR1, SLC25A53, PTPRCAP, SLC27A3, FAM8A1, TRABD2A, LCN8, ABHD3, INSIG2, ITPR2, SLC9A1, ITPRIPL1, TBXA2R, OSBPL8, SLC14A1, CD163, SLC37A2, OSBPL5, PTPRE, PTPRC, REEP5, LRFN1, SERINC1, FAM26F, OR13A1, SERINC3, LRCH4, SLC26A6, SERINC5, SERINC4, SLC48A1, ITGB1, FLT1, BMPR2, RNF13, ADPGK, CDCA7L, LRMP, ELFN2, ITGAL, NAGPA, SYNE2, FCGR3A, ITGB7, ATP7A, LBR, TAPT1, DGCR2, AMN, APAF1, PVRIG, AVPR2, NDUFC1, C1ORF162, BET1L, ATRN, DNAJC1, RRM2B, SNPH, DNAJC4, PECAM1, PPP1R12B, DAGLB, ST6GALNAC4, ST6GALNAC6, CERS2, RNFT2, LRP1, UNC93B1, PBXIP1, SLC25A29, P2RY6, SLC25A28, LRRC8C, CEACAM21, LRRC8A, SLC13A5, E2F5, CNNM3, SEC11A, CNNM4, SLC35A1, LINGO3, SEMA4D, KCNJ11, RNF24, PCDH9, AMFR, SEMA4B, MBOAT7, SPAG4, MBOAT1, MERTK, TPCN1, SCART1, P2RX5, CLEC2B, P2RX1, IL2RB, SLC25A30, CD248, FCGR2B, FCGR2C, CD244, SLC25A36, EPHB6, VIPR1, IFITM1, SLC46A1, TRAF3IP3, ACSM1, SLC23A1, GDE1, LDLRAD4, ANTXR2, AQP3, TXNDC15, OR52N4, ANPEP, TNFSF10, SLC12A6, SEC62, BRICD5, ARL6IP6, PAQR6, ST6GAL1, SLC6A16, IL1R1, KCNQ1, FAM76B, CUTA, IGSF8, GPM6A, TMEM63A, SLC35D1, GIPR, EPB41, CD1D, APCDD1, CD79B, CD79A, PTDSS1, ARSK, SLAMF6, SCAI, BANP, TMEM86B, LRRN2, TNFSF12, SIGLEC10, PARP16, UBAC2, MC1R, NCEH1, LPAR5, ADCK2, CD27, ITM2B, C2CD2L, CD320, CDS2, TNFRSF13B, SLC44A2, TECR, GRIK3, AATK, MIA3, TNFRSF13C, PCSK7, CD3E, TRAM2, GLIPR1, SLC22A17, SLC22A18, STAB1, CLDN23, QSOX1, CCR6, QSOX2, CD36, DIRC2, TMED5, CD53, CD52, MAP4K2, BTN3A1, GAA, ANO8, BTN3A2, LIME1, IL17RA, NAALADL1, CLDN15, TLR9, TLR7, CD48, CD47, ATP6V0C, TLR4, GUCY2C, SELPLG, STX16, ZDHHC20, DERL3, PTGER2, GDPD1, CXCR4, GDPD3, STX10, DCST2, ZFP14, MGAT5, KISS1R, SUSD3, MGAT1, ATP6V0E2, LAIR1, PNPLA7, PNPLA8, KLHL2, ORMDL1, LHFPL2, KBTBD6, ESYT1, RAMP1, PNPLA2, DPAGT1, SCARB2, DENND5B, SPPL2B, TMEM140, IGF1R, TMEM143, GNPTAB, SIT1, MPZ, FAM198B, ENPP2, TMEM38A, CA14, CD96, UNC5CL, CD300A, IL11RA, ATG9A, SHISA5, ADAM10, LMTK2, DNAJB14, CYBA, SLC30A1, LMO7, MR1, LAX1, ERMN, MPEG1, ALDH3A2, TMEM134, DPM3, TMX4, TBC1D20, TMEM259, CD8A, SIDT1, CD300E, WDFY4, ABCG1, SIDT2, RTN3, PMEL, PLD4, ADRB2, NDRG2, PLD3, SEL1L3, TMEM123, CALHM2, MAN2A2, MAN2A1, TMEM127, TMEM129, ASIC3, C16ORF54, ACBD4, RARRES3, RHBDD1, PTCH1, EPHX1, NKG7, TRPV1, BTNL2, TMEM110, GCLC, TMEM236, CCPG1, DEGS2, LRP10, SDK2, SLC35E2B, FGFR1, B4GALT3, DYRK2, B4GALT1, MS4A7, ATP2A3, SLC2A3, ATP2A1, TMEM191A, TAZ, PKD1, HS2ST1, MFSD8, CYP4V2, TMEM107, TMEM109, MAN1A1, SCARF2, ABCD1, SUN2, ABCC2, ABCC5, ABHD14A, SSTR3, CKAP4, TMEM2, CDHR1, TMEM219, SCN4A, MAN1B1, AGPAT5, DLL1, CNR2, CLMN, LEPROTL1, LRIG1, MAN1C1, S1PR1, CDIPT, S1PR4, TAS1R3, MBTPS1, GALNT3, ATP13A1, QPCTL, ATP2B4, SCIMP, SGPP1, PIK3IP1, CD6, CD5, ALOX5AP, CD7, CHPT1, CMTM1, HCN2		
UP_KEYWORDS	**Transmembrane**	527	27.77	XYLT2, XYLT1, EHMT1, NPIPB11, FAM159A, FAM134C, NDST1, FAM134A, CREB3L2, C3AR1, CEP95, CMKLR1, DAPK2, CACNA2D2, SCAMP1, TMEM80, TMEM81, LRRC37B, SIGIRR, TMEM79, GPR160, ORAI2, MPPE1, ADPRM, ABCB1, TTYH3, FAXDC2, FPR3, ABCB8, VPS26B, LY9, KIAA0040, XKRX, CHST11, CHST12, RDH10, EPB41L3, CHST15, HMOX1, SSR1, C19ORF38, RHBDL1, ABCA1, LRRC37A3,	0.14	0.13

				ABCA2, FZD3, DNAH10, DMPK, ABCA9, ABCA7, FXYD1, SFXN3, TNFSF9, FXYD7, TNFSF8, FXYD5, GPR18, GAPT, HRK, GABRB2, TMEM187, JPH3, C1QTNF6, SMPD1, CTLA4, EMB, GPR135, C11ORF24, HAVCR2, FCRL1, FCRL2, KCND1, SLC2A11, SLC39A10, TMEM175, FAM210B, BACE2, SLC7A7, SLC7A8, VAMP1, SLC18B1, VAMP4, VAMP2, ASAH1, CLDND2, TP53I13, ATL1, PELI2, ADCY4, KCNA3, APOLD1, TMEM71, GPR152, ADAM29, HLA-DMA, ADAM28, GPNMB, SLC17A9, TMEM65, UCP3, MFN1, GCNT2, SLC17A5, HAS3, METTL7A, RABAC1, GPR155, P4HTM, RNF130, LRRC25, COLCA1, IL10RB, SYVN1, LAPTM5, TMEM62, CRYM-AS1, SLC8B1, BLCAP, TMEM154, TMEM156, TMEM59, TMEM159, RNF149, LPCAT4, TMEM56, TAOK2, PKN2, PLP2, CRLF3, LGR4, TMEM229B, DGKE, SLC27A1, PLXND1, CLSTN3, CLSTN1, IL1RAP, AUP1, SLC8A1, CXCL16, TM7SF2, BEST4, LAPTM4A, CYSLTR1, SMCHD1, FCGRT, RNF19A, SLC16A7, SLC26A11, SLC39A8, MAP3K9, SLC25A42, ZNF566, SLC16A4, SLC39A3, SEMA6B, IFNAR2, KCNH2, BNIP3L, LAG3, FBXO18, BTN1A1, F2R, STX7, DISP1, ARMCX3, BSCL2, CLEC4C, STIM1, SYPL1, STIM2, ROR1, SLC25A53, PTPRCAP, SLC27A3, FAM8A1, TRABD2A, LCN8, ABHD3, INSIG2, ITPR2, SLC9A1, ITPRIPL1, TBXA2R, OSBPL8, SLC14A1, CD163, SLC37A2, OSBPL5, PTPRE, PTPRC, REEP5, LRFN1, SERINC1, FAM26F, OR13A1, SERINC3, LRCH4, SLC26A6, SERINC5, SERINC4, SLC48A1, ITGB1, FLT1, BMPR2, RNF13, ADPGK, CDCA7L, LRMP, ELFN2, ITGAL, NAGPA, SYNE2, FCGR3A, ITGB7, ATP7A, LBR, TAPT1, DGCR2, AMN, APAF1, PVRIG, AVPR2, NDUFC1, C1ORF162, BET1L, ATRN, DNAJC1, RRM2B, SNPH, DNAJC4, PECAM1, PPP1R12B, DAGLB, ST6GALNAC4, ST6GALNAC6, CERS2, RNFT2, LRP1, UNC93B1, PBXIP1, SLC25A29, P2RY6, SLC25A28, LRRC8C, CEACAM21, LRRC8A, SLC13A5, E2F5, CNNM3, SEC11A, CNNM4, SLC35A1, LINGO3, SEMA4D, KCNJ11, RNF24, PCDH9, AMFR, SEMA4B, MBOAT7, SPAG4, MBOAT1, MERTK, TPCN1, SCART1, P2RX5, CLEC2B, P2RX1, IL2RB, SLC25A30, CD248, FCGR2B, FCGR2C, CD244, SLC25A36, EPHB6, VIPR1, IFITM1, SLC46A1, TRAF3IP3, ACSM1, SLC23A1, GDE1, LDLRAD4, ANTXR2, AQP3, TXNDC15, OR52N4, ANPEP, TNFSF10, SLC12A6, SEC62, BRICD5, ARL6IP6, PAQR6, ST6GAL1, SLC6A16, IL1R1, RUNX1, KCNQ1, FAM76B, CUTA, IGSF8, GPM6A, TMEM63A, SLC35D1, GIPR, EPB41, CD1D, APCDD1, CD79B, CD79A, PTDSS1, ARSK, SLAMF6, SCAI, BANP, TMEM86B, LRRN2, TNFSF12, SIGLEC10, PARP16, UBAC2, MC1R, NCEH1, LPAR5, ADCK2, CD27, ITM2B, C2CD2L, CD320, CDS2, TNFRSF13B, SLC44A2, TECR, GRIK3, AATK, MIA3, TNFRSF13C, PCSK7, CD3E, TRAM2, GLIPR1, SLC22A17, SLC22A18, STAB1, CLDN23, QSOX1, CCR6, QSOX2, CD36, DIRC2, TMED5, CD53, CD52, MAP4K2, BTN3A1, GAA, ANO8, BTN3A2, LIME1, IL17RA, NAALADL1, CLDN15, TLR9, TLR7, CD48, CD47, ATP6V0C, TLR4, GUCY2C, SELPLG, STX16, ZDHHC20, DERL3, PTGER2, GDPD1, CXCR4, GDPD3, STX10, DCST2, ZFP14, MGAT5, KISS1R, SUSD3, MGAT1, ATP6V0E2, LAIR1, PNPLA7, PNPLA8, KLHL2, ORMDL1, LHFPL2, KBTBD6, ESYT1, RAMP1, PNPLA2, DPAGT1, SCARB2, DENND5B, SPPL2B, TMEM140, IGF1R, TMEM143, GNPTAB, SIT1, MPZ, FAM198B, ENPP2, TMEM38A, CA14, CD96, UNC5CL, CD300A, IL11RA, ATG9A, SHISA5, ADAM10, LMTK2, DNAJB14, CYBA, SLC30A1, LMO7, MR1, LAX1, ERMN, MPEG1, ALDH3A2, TMEM134, DPM3, TMX4, TBC1D20, TMEM259, CD8A, SIDT1, CD300E, WDFY4, ABCG1, SIDT2, RTN3, PMEL, PLD4, ADRB2, NDRG2, PLD3, SEL1L3, TMEM123, CALHM2, MAN2A2, MAN2A1, TMEM127, TMEM129, ASIC3, C16ORF54, ACBD4, RARRES3, RHBDD1, PTCH1, EPHX1, NKG7, TRPV1, BTNL2, TMEM110, GCLC, TMEM236, CCPG1, DEGS2, LRP10, SDK2, SLC35E2B, FGFR1, B4GALT3, DYRK2, B4GALT1, MS4A7, ATP2A3, SLC2A3, ATP2A1, TMEM191A, TAZ, PKD1, HS2ST1, MFSD8, CYP4V2, TMEM107, TMEM109, MAN1A1, SCARF2, ABCD1, SUN2, ABCC2, ABCC5, ABHD14A, SSTR3, CKAP4, TMEM2, CDHR1, TMEM219, SCN4A, MAN1B1, AGPAT5, DLL1, CNR2, CLMN, LEPROTL1, LRIG1, MAN1C1, S1PR1, CDIPT, S1PR4, TAS1R3, MBTPS1, GALNT3, ATP13A1, QPCTL, ATP2B4, SCIMP, SGPP1, PIK3IP1, CD6, CD5, ALOX5AP, CD7, CHPT1, CMTM1, HCN2		
Annotation Cluster 58	**Enrichment Score: 1.008131035580014**					

Category	Term	Count	%	Genes	Benjamini	FDR
KEGG_PATHWAY	hsa04662:B cell receptor signaling pathway	19	1.00	SYK, NFATC3, NFATC1, PIK3R1, FOS, VAV1, CD79B, CD79A, PPP3CA, AKT2, INPP5D, BLNK, PLCG2, AKT1, MAPK1, FCGR2B, SOS1, SOS2, CARD11	0.01	0.01
BIOCARTA	h_bcrPathway:BCR Signaling Pathway	14	0.74	MAP3K1, SYK, PRKCB, NFATC3, NFATC1, PRKCA, FOS, VAV1, CD79B, CD79A, PPP3CA, BLNK, CALM1, SOS1	0.02	0.02
BIOCARTA	h_tcrPathway:T Cell Receptor Signaling Pathway	14	0.74	MAP3K1, PRKCB, NFATC3, NFATC1, PRKCA, PIK3R1, FOS, CD3E, VAV1, PPP3CA, LCK, PTPN7, CALM1, SOS1	0.18	0.18
KEGG_PATHWAY	hsa04660:T cell receptor signaling pathway	19	1.00	ITK, NFATC3, NFATC1, PIK3R1, FOS, CD3E, VAV1, PPP3CA, PTPRC, LCK, CD8A, AKT2, AKT1, CTLA4, MAPK1, LCP2, SOS1, SOS2, CARD11	0.10	0.10
BIOCARTA	h_fcer1Pathway:Fc Epsilon Receptor I Signaling in Mast Cells	12	0.63	PPP3CA, MAP3K1, SYK, PRKCB, NFATC3, MAPK1, NFATC1, FOS, PIK3R1, CALM1, SOS1, VAV1	0.34	0.34
KEGG_PATHWAY	hsa04650:Natural killer cell mediated cytotoxicity	19	1.00	IFNAR2, SYK, PRKCB, NFATC1, PRKCA, PIK3R1, ITGAL, VAV1, PPP3CA, FCGR3A, LCK, TNFSF10, PLCG2, MAPK1, LCP2, CD48, SOS1, SOS2, CD244	0.39	0.37
Annotation Cluster 66	Enrichment Score: 0.8676199831544475					
Category	Term	Count	%	Genes	Benjamini	FDR
KEGG_PATHWAY	hsa02010:ABC transporters	10	0.53	ABCA1, ABCA2, ABCB1, ABCC2, ABCC5, ABCA9, ABCB8, ABCA7, ABCD1, ABCG1	0.26	0.24
Annotation Cluster 67	Enrichment Score: 0.852508098081019					
Category	Term	Count	%	Genes	Benjamini	FDR
KEGG_PATHWAY	hsa00310:Lysine degradation	10	0.53	ALDH3A2, KMT2E, EHMT2, SETD7, SETDB2, EHMT1, WHSC1, COLGALT1, WHSC1L1, ALDH9A1	0.48	0.45
Annotation Cluster 69	Enrichment Score: 0.8384899790210326					
Category	Term	Count	%	Genes	Benjamini	FDR
UP_KEYWORDS	Glycogen metabolism	6	0.32	AKT2, PPP1R3E, PHKG2, AKT1, PHKB, PYGM	0.44	0.41

Annotation Cluster 75	Enrichment Score: 0.7880464075002529					
Category	**Term**	**Count**	**%**	**Genes**	**Benjamini**	**FDR**
UP_KEYWORDS	Protein phosphatase	18	0.95	PTPN18, MTMR3, PPM1J, PTPN22, PTPN12, PPM1K, DUSP26, PPM1D, SSH2, CDC25B, PDP1, PTP4A1, PPP3CA, PTPRE, PTPRC, CTDSP2, PTPN7, PTPN4	0.43	0.40
Annotation Cluster 77	Enrichment Score: 0.7789672120039376					
Category	**Term**	**Count**	**%**	**Genes**	**Benjamini**	**FDR**
KEGG_PATHWAY	hsa04664:Fc epsilon RI signaling pathway	17	0.90	MAP2K3, SYK, PRKCB, PLA2G4B, PRKCA, PIK3R1, GAB2, VAV1, AKT2, INPP5D, PLCG2, AKT1, MAPK1, LCP2, SOS1, SOS2, MAP2K6	0.02	0.02
KEGG_PATHWAY	hsa04666:Fc gamma R-mediated phagocytosis	17	0.90	SYK, PRKCB, PRKCE, LIMK2, PRKCA, PIK3R1, GAB2, VAV1, CRKL, PTPRC, BIN1, AKT2, INPP5D, PLCG2, AKT1, MAPK1, FCGR2B	0.10	0.10
KEGG_PATHWAY	hsa05223:Non-small cell lung cancer	13	0.68	PRKCB, PRKCA, PIK3R1, FOXO3, CASP9, EML4, RASSF1, AKT2, PLCG2, AKT1, MAPK1, SOS1, SOS2	0.10	0.10
KEGG_PATHWAY	hsa05231:Choline metabolism in cancer	19	1.00	DGKE, DGKD, SLC44A2, PRKCB, DGKA, PLA2G4B, PRKCA, TSC1, PIK3R1, FOS, GPCPD1, AKT2, PDGFD, AKT1, MAPK1, CHPT1, SOS1, RALGDS, SOS2	0.10	0.10
KEGG_PATHWAY	hsa05220:Chronic myeloid leukemia	13	0.68	CDKN1B, CTBP1, CBLB, PIK3R1, GAB2, CRKL, RUNX1, BCR, AKT2, AKT1, MAPK1, SOS1, SOS2	0.39	0.37
KEGG_PATHWAY	hsa04066:HIF-1 signaling pathway	15	0.79	EGLN1, CDKN1B, FLT1, PFKFB3, PRKCB, PRKCA, PIK3R1, IGF1R, AKT2, PLCG2, AKT1, EP300, MAPK1, HMOX1, TLR4	0.48	0.45
Annotation Cluster 102	Enrichment Score: 0.5686677723894924					
Category	**Term**	**Count**	**%**	**Genes**	**Benjamini**	**FDR**
UP_KEYWORDS	Biological rhythms	17	0.90	KLF10, CRTC1, CIPC, CREM, NR1D2, NR1D1, SIRT1, PER1, KAT2B, RAI1, DBP, KLF9, ID3, EP300, FBXL3, OGT, LGR4	0.46	0.42
Annotation Cluster 107	Enrichment Score: 0.5574629406289565					
Category	**Term**	**Count**	**%**	**Genes**	**Benjamini**	**FDR**
UP_KEYWORDS	Cell cycle	75	3.95	CDKN1C, CDKN1B, NUMA1, CDCA7L, DDX12P, CIB1, NR3C1, ING1, SMC4, ING4, CCND3, RASSF1, RGS2, MIS18BP1, CHMP1B, RB1CC1, CNTRL, EP300, LZTS2, TSPYL2, USP8, LIG1, PRKCE, CKAP2, VASH1, SIRT2, CDC40, CDC25B, GAK, RBL2, PTP4A1, KAT2B, LATS2, PAPD7, TXNIP, MCM6, KIF20B, MAPRE2, MAD1L1, AVPI1, KMT2E, SDCCAG3, RALB, RGS14, UHRF2, ARL3, TAF1L, FOXO4, CCNDBP1,	0.09	0.08

				PPM1D, PARD6A, MAPK1, STOX1, BANP, CDKN2D, CENPT, RBM38, CDK19, CDK11A, PYHIN1, SETDB2, DAB2IP, CABLES1, BLCAP, RGCC, CCPG1, PRC1, TACC3, PHF13, NCAPD2, PKN2, ATM, SYCP3, CUL4B, TAF1		
Annotation Cluster 148	**Enrichment Score: 0.34713063185874105**					
Category	**Term**	**Count**	**%**	**Genes**	**Benjamini**	**FDR**
UP_KEYWORDS	**Immunoglobulin domain**	59	3.11	MYOM1, FLT1, WFIKKN1, IL1RAP, CD3E, FCRLA, VPREB3, FCRLB, FCGR3A, FCGRT, MPZ, CTLA4, EMB, HAVCR2, FCRL1, FCRL2, CD96, LAG3, BTN3A1, IL11RA, CD300A, IL1R1, BTN1A1, BTN3A2, HSPG2, MR1, TMEM81, SIGIRR, OBSCN, CD8A, PECAM1, CD300E, ROR1, CD48, CD47, IGSF8, CD1D, LY9, CD79B, CD79A, HLA-DMA, LRIG1, CEACAM21, SLAMF6, LAIR1, LINGO3, SEMA4D, LRRN2, SEMA4B, SIGLEC10, BTNL2, MERTK, LRFN1, CD7, FCGR2B, FCGR2C, SDK2, CD244, FGFR1	0.39	0.36